TECHNISCHE UNIVERSITÄT MÜNCHEN

WACKER-Lehrstuhl für Makromolekulare Chemie

Rare Earth Metal-Mediated Group Transfer Polymerization of Vinylphosphonates: Initiation, Propagation, and Stereoregularity

Benedikt Simon Soller

Vollständiger Abdruck der von der Fakultät für Chemie der Technischen Universität München zur Erlangung des akademischen Grades eines

Doktors der Naturwissenschaften

genehmigten Dissertation.

Vorsitzender: Prof. Dr. Shigeyoshi Inoue

Prüfer der Dissertation:

1. Prof. Dr. Dr. h.c. Bernhard Rieger
2. apl. Prof. Dr. Wolfgang Eisenreich
3. Prof. Dr. Tom Nilges

Die Dissertation wurde am 31.05.2016 bei der Technischen Universität München eingereicht und durch die Fakultät für Chemie am 14.07.2016 angenommen.

TECHNISCHE UNIVERSITÄT MÜNCHEN

WACKER LEHRSTUHL FÜR MAKROMOLEKULARE CHEMIE

Rare Earth Metal-Mediated Group Transfer Polymerization of Vinylphosphonates: Initiation, Propagation, and Stereoregularity

Seltenerdmetall mediierte Gruppentransferpolymerisation von Vinylphosphonaten: Initiation, Propagation und Stereoregularität

Dissertation

Zur Erlangung des akademischen Grades eines

Doktors der Naturwissenschaften

vorgelegt von

Benedikt Simon Soller

München, Mai 2016

Dedicated it to whomever makes it past this page

"A Chemist is a person who develops a general theory from a string of diverse formulae derived from micromatic precision from vague assumptions based on debatable tables of results extracted from inconclusive experiments carried out with inaccurate equipment of doubtful reliability and questionably mentality."

W. Brostow in *Science of Materials* 1979

Acknowledgments

Prof. Dr. Dr. h.c. Bernhard Rieger is thanked for giving me the opportunity to work on such an exciting and fruitful project, his complete trust in me, and the freedom to explore, learn, and develop during the past years. I gratefully thank Carsten Troll for his continued technical and organizational support and his efforts to provide a positive working atmosphere at the WACKER-Chair of Macromolecular Chemistry. Ms. Bauer and Ms. Saul-Hubrich are thanked for reducing the bureaucratic workload and their skillful help in various university processes.

I furthermore want to thank my colleagues in no particular order: Peter T. Altenbuchner is thanked for our scientific exchange on rare earth metal-mediated ring-opening polymerization and rare earth metal-mediated group transfer polymerization, our collaborations, the dinners in Munich or around the ISHC conference in Ottawa, and for sharing the laboratory at weekends or late working hours. Furthermore, thank you for your help with proof reading this manuscript and application letters. My labmate, Patrick D. L. Werz is thanked for being a great host - almost flatmate -, his insights on various software products and free tech support, his help to understand our universities' business travel application forms, and our attendance at the static light scattering course at Wyatt Europe in Dernbach. Unfortunately, we two were the only one left to clean up the mess in 56 402, shutting down this laboratory.

I would like to thank Alexander Kronast for the opportunity to give a presentation at Pacifichem conference in Honolulu as the only PhD among other prominent researchers being a part of the inorganic polymerization catalysis symposium. Furthermore, I am grateful for not being the only one left at the WACKER-Chair of Macromolecular Chemistry who stayed in the old laboratories. Furthermore, Stefan Kissling needs to be thanked to welcome me in his laboratory during my Master's thesis and together with Richard O. Reithmeier, both are thanked for completing our great group. All of my colleagues mentioned above is also thanked for our shared trips within Europe to Istanbul, Budapest, or Amsterdam.

Many thanks to Johannes Kainz for his knowhow on vinylphosphonate monomer syntheses as well as his kind help during my graduate studies. I would like to thank Qian Sun for her continued hard work in our laboratory, from the beginning after she transferred to TU Munich to her Master's thesis on free-standing photoluminescent hybrid materials. Furthermore, beyond her scientific expertise, I need to thank Qian Sun for her kindness, positive mind, friendship, and introducing me to Qingdao. All the best for your future in China. Philipp Pahl is thanked for further developing the topic of rare earth metal-mediated vinylphosphonate polymerization. I hope this topic will offer you with the same compensation, rewards, and enthusiasm as me.

Ulrike Ammari and the members of the microanalytical lab are thanked for their patient help in enabling the measurement of highly air sensitive compounds and preparing numerous elemental analyses. Special thank goes to Prof. Dr. Wolfgang Eisenreich for assisting with the laborious signal attribution to learn about the microstructure of poly(vinylphosphonate)s and all the given NMR measurement time.

I would like to thank not a person, but my *alma mater* TU Munich for the education and hopefully good preparation for future positions. Most part of my studies were made in Garching, but were not limited to Germany; my studies at TU Munich took me to Ludwigshafen am Rhein, and exotic locations such as the King Abdullah University of Science and Technology (KAUST) in Saudi Arabia, or Ateneo de Manila University in the Philippines. I want to thank my internship and Bachelor students Felix Geitner, Qingqi Zhao, Szu-Hao Cho, Dan Qu, Yeseul Park, Alexander Sigg, and Raphaela Grassl for their support and great work in my laboratory and for giving me the opportunity to work with such a diverse and international team. Fabian Herz is thanked for his contributions as a Master's thesis student and I wish you all the best at our chair on your new topic in the future.

I am grateful for the great guidance and training, I received at the WACKER-Chair of Macromolecular Chemistry. Especially, Robert Reichardt and Stephan Salzinger have been an undeniable stimulus during my first research attempts at TU Munich and gave me the impulse to challenge myself and to go beyond. Without your input and training during my undergraduate and master studies, I would not have become the scientist I am today. Words fail to express my gratitude for your assistance and friendship.

I would like to gratefully and sincerely thank my parents for their continued love and support. My sister Anna Soller is thanked for being one of the most important parts in my life; the past years made us separate geographically, but we can never be fully away from each other; let's see when I can follow you in the opposite direction. Jihyun Han is thanked in many aspects; you let me grow to be the person I am today. Mario F. Ellwart, Maximilian von Wedelstaedt, and Johannes Elferich are thanked for their persistent friendship and support.

Abbreviations

2VP	2-Vinylpyridine
b.p.	Boiling Point
bdsa	Bis(dimethylsilyl)amide
btsa	Bis(trimethylsilyl)amide
Bu	Butyl–
CN	Coordination Number
conc.	Concentrated
DAVP	Dialkyl Vinylphosphonate
DEEP	Diethyl Ethylphosphonate
DEMVP	Diethyl-1-methyl Vinylphosphonate
DEVP	Diethyl Vinylphosphonate
DIVP	Diisopropyl Vinylphosphonate
DMAA	*N,N*-Dimethylacrylamide
DMMA	*N,N*-Dimethylmethacrylamide
DMVP	Dimethyl Vinylphosphonate
eq.	Equivalents
Et	Ethyl–
ESI	Electrospray Ionization
GPC	Gel Permeation Chromatography
GTP	Group Transfer Polymerization
HPLC	High Performance Liquid Chromatography
i	Iso
*i*POx	2-Isopropyl-2-oxazoline
IPOx	2-Isopropenyl-2-oxazoline
IR	Infrared

kDa	kDalton (1 kDa = 1000 g·mol^{-1})
LCROP	Living Cationic Ring-opening Polymerization
LCST	Lower Critical Solution Temperature
LDA	Lithium Diisopropylamide
Ln	Element of the Rare Earth Metals (Sc, Y, and La – Lu; in Figures)
M	Metal
MALS	Multi Angle Light Scattering
Me	Methyl–
min	Minute
ml	Milliliter
MMA	Methyl Methacrylate
MS	Mass Spectrometry
NIPAM	*N*-Isopropyl Acrylamide
NMR	Nuclear Magnetic Resonance
PDI	Polydispersity Index
PE	Polyethylene
Ph	Phenyl–
Pr	Propyl– or Praseodymium
RE	Element of the Rare Earth Metals (Sc, Y, and La – Lu; in Text)
REM-GTP	Rare Earth Metal-mediated Group Transfer Polymerization
rt	Room Temperature
SI-GTP	Surface-initiated Group Transfer Polymerization
t	Tertiary
TBAB	Tetrabutylammonium Bromide
TGA	Thermogravimetric Analysis
THF	Tetrahydrofuran

TMS	Trimethylsilyl–
TOF	Turnover Frequency
TON	Turnover Number
VE	Valence Electron
v/v	Volume Ratio
w/w	Mass Ratio
X	Initiating Ligand

Table of Contents

1 Introduction

1.1 On the Importance of Chemistry to Society

"Chemistry, pure and applied, is a science and an industry".[1] Chemistry is the only natural science that extends from fundamental and applied research to a whole industry worshipping the composition, structure, properties and change of matter.[1] The most unique characteristic of chemistry as matter is its omnipresence in everyone's life with regard to food, machines, electronic gadgets, and materials. Chemistry is in a humble view the only science being able to bridge between physics and the general laws of the universe on one hand and biology, understanding the origin of life, thought, and intelligence.[1-2] By its expressions of matter, chemistry is also an art and enables human creativity on the small atomic dimension people will never be able to see at a glance.[3] The combination of atoms and structures is infinite and does therefore match the endless creativity of human mind.

This unique expression of chemistry does not accord to the general understanding of chemistry in society today. In fact, chemistry, as being present everywhere, is often neglected, tends to be forgotten, and chemical achievements often go unnoticed in the public view.[4-5] Modern comforts are all linked with chemistry and those achievements we nowadays consider spectacular would not have seen the light of day without chemistry and scientific progress. As most influential people in history, societies remember powerful emperors, political leaders, or social activists. However, these rankings and criteria diminish if compared to breakthroughs of chemistry and chemists and to emphasize it even more, modern societies could not flourish without the "all-embracing and beneficial influence of chemistry".[4] In the following, a few selected examples will be presented illustrating the general essential role of chemistry in our lives.

Without the discoveries of Louis Pasteur on the principles of vaccination, infectious diseases microbial fermentation, or pasteurization, modern day medicine and effective therapies would not exist or only to a lesser degree. Prior to Pasteur's work, the possible immunization against smallpox by vaccination with cowpox was already studied and tested by the physician Edward Jenner. However, primarily by the activities of the chemist and microbiologist Pasteur, a modern scientific understanding of infectious diseases was developed and vaccinations became a general principle for the control or even extinction of infectious diseases. Without the original discoveries of Pasteur and a subsequently steadily improvement of scientific understanding in medicine, the high life expectancy of humans in modern societies would be significantly lowered.

Whereas, aging societies are a problem in industrialized and emerging nations, overpopulation and a rampant population growth is one of the main factors for poverty in many developing countries. Methods for birth control existed since the early days of humanity, however, first the use of contraceptive pills gave

people a reliable tool for contraception and enabled families to control their family size. The origin of modern oral contraceptive pills dates back to the 1950s and the research on norethisterone conducted by Carl Djerassi and Luis E. Miramontes for Syntex (today Roche). The impact of this field of work upon society was described as "equal to or even surpassing that of the discovery of penicillin".[6] Still today, around 220 million people do not have access to modern contraception methods due to economic or social/religious reasons and improvements in this field is considered as one of the most cost-effective ways to achieve development goals.[7] Oral contraceptive pills act by the combination of synthetically produced hormones inhibiting fertility and are only one example for the tremendously important discoveries of pharmaceutical chemistry and synthetic organic chemistry to human society in the past decades.

Justus von Liebig, a pioneer of organic and agricultural chemistry, already recognized in the 19th century that traditional food production and a growing food consumption cannot match. Liebig's work also included contributions to biological chemistry and modern chemistry teaching methods. He strongly advised the use of inorganic fertilizer instead of humus and first described the importance of nitrogen sources and other elements in mineral form as essential plant nutrients in his formulation of the "law of the minimum".[8] Justus von Liebig was furthermore a strong advocate of an effective use of resources and can therefore be seen as a first mentor of sustainability. It is almost an irony of history that a century later sustainability gained awareness in the general public and Liebig's and general chemistry thoughts became readapted. However, in return, chemistry became a synonym for the environmental pollution caused by companies and an unregulated consumption of chemicals by consumers. This negative thinking about chemistry is unfortunately still present in society until today. Liebig's research laid the foundation for the modern industrialized agriculture, matching production and human population increase in the 19th century. Not only was Liebig a successful scientist, but also a successful business man; his insight on agricultural chemistry and nutrition also led to the establishment of the Liebig's Extract of Meat Company, producing meat extract overseas for the European market.[8]

The limited sources for chemical fertilizers according to Liebig, naturally occurring nitrogen-containing minerals, were foreseeable to deplete at the turn of the 20th century or almost completely relied on deposits in the Atacama Desert in Chile. Therefore, to ensure a steady food supply for the population of 1.5 billion people around 1900, an alternative access to nitrogen sources such as nitrates or ammonia was needed. The most obvious nitrogen source on earth is atmospheric nitrogen, however, the conversion of molecular nitrogen is challenging as it does not readily react with other chemicals.[9] The chemists Fritz Haber and Carl Bosch invented and commercialized the first efficient artificial nitrogen fixation based on preliminary studies conducted by Wilhelm Ostwald. Consequently, the process was named after them as Haber-Bosch process and both chemists were awarded with Nobel prizes in chemistry in 1918 and 1931. Even almost a century later, since Haber successfully fixed atmospheric nitrogen on laboratory scale, a

Nobel Prize in chemistry was awarded to Gerhard Ertl in 2007 for his contributions in catalysis and elucidating the mechanism of the Haber-Bosch ammonia synthesis.[10-11]

The Haber-Bosch process converts one molecule of nitrogen with three equivalents of hydrogen to ammonia using a catalyst under high temperatures and pressures. It was Bosch who led Haber's early laboratory discovery from expensive osmium catalysts to a world scale ammonia synthesis using feasible iron catalysts and to the presumably most important industrial chemical reaction since then. Bosch not only developed a new catalyst, he also had to find new ways to overcome process limitations, and setbacks due to an occurring decarbonization of the used steel reactors and bursting at high pressures. Roughly 1.4% of the overall worldwide energy consumption is used for the production of ammonia.[12] The ammonia production is directly related to the economic growth and financial crises can be seen in a reduced ammonia output.[12] Modest estimations attribute the food supply of around half of the human world population to the production of fertilizers to the direct synthesis of ammonia from its elements;[13] for 2016 this accounts worldwide for more than three billion people whose food supply directly relies on this single chemical reaction. Which other invention in the field of medicine, physics or biology can claim such an impact on society? Despite all this benefit for humanity, the life of Haber is also fulfilled with tragedy. Haber, being a contemporary scientist of early 20th century Europe and Germany, planned the chemical warfare during the First World War in Belgium and lost his wife, the chemist Clara Immerwahr, to suicide over a dispute on his military commitment. Furthermore, he was later being forced to repatriate his mother country Germany due to his Jewish origin and died on his way to exile in Basel in 1934.

Today's trends demanding "green", "organic", or "environmental" friendly foods that are grown without the use of artificial fertilizers or pesticides should not be condemned and "green" or conventionally produced food should not be seen in a simple black and white way. Artificial fertilizers and pesticides are readily available and unfortunately often overused in modern industrial societies and their application can be improved. Yet, we need to keep in mind that the production of non-conventional food is a luxury for a few middle and upper income households in developed nations. If the nutrition of low income households, being the majority of the world population, would solely rely on crops produced without artificial fertilizers or pesticides, their food supply would significantly decrease or even cause famine.

People see materials as granted since we use paper or advanced electronical gadgets in our daily lives. Yet, the process of developing and improving materials especially for the preservation of knowledge and information had been one of the most cost intensive and laborious task for mankind throughout the history. For example, the simple material paper, as we know it today, is a result of numerous modifications, different process steps, and added compounds to enhance stability, printability, or durability. The materials transformed significantly from ancient Egypt's papyrus, parchment, and early paper to the modern material

used today and by technological progress printed matter became a commodity product in the 20th century. In the 21st century, digitalization will further replace common materials and the production of memory chips, processors, or displays itself include chemical understanding in most processing steps such as Müller-Rochow Process, liquid crystals, or chemical-mechanical planarization (CMP) for the wet-etching of copper circuits. The improvement of materials for the information technology and data storage is still ongoing today and remains a challenge for future generations. To date, new materials can only be provided and improved by a molecular understanding of its structure and the development of materials translates to materials that help in our daily life.

In three centuries, chemistry improved the lives of humans, gave new materials, fed billions by promoting the acquisition of scientific knowledge in agriculture, led to significant improvement of medicine by the development of pharmaceuticals, and enabled mankind to overcome drastic challenges in the past. It is therefore not surprising that chemistry is permanently called upon to face important socioeconomic questions often connected to geopolitical phenomena. At the beginning of the 21st century, humanity is facing a series of problems attributed to overpopulation, urban living, aging societies, environmental pollution, unsustainable processes, malnutrition, climate change, and an unstopped consumption of limited resources.[14-16] As chemists, we often have to face a lack of knowledge encountering people being non-chemists. Considering all the benefits and positive changes initiated by chemistry chemists should proudly answer similar questions to: "What do Chemists do?" in a way according to Whitesides: "We change how people live and die", as chemists have continuously contributed to the development and progress of society and changed this planet and human life unmatched by any other profession in the modern era of humanity.[17]

1.2 Macromolecular Chemistry and the Importance for the Chemical Industry

The history of chemistry is a history of discoveries, innovations, and bringing together the practical and conceptual. Scientific assumptions can be directly converted to compounds and molecules as chemistry is the science that deals with the composition, structure, properties, and change of matter. Chemical research (in academia or industry) is therefore the manifestation of scientific thoughts in materials. We have seen that the past 100 years were driven by the successful partnership of universities and chemical companies being "one of the most beneficial partnerships our technologically sophisticated society has seen".[17] A glimpse of some of the tremendous scientific breakthroughs was given in the previous chapter. This chapter covers the perception and use of polymeric materials and their impact in our daily life, the importance of plastics for chemical companies and for employees, future challenges, and/or trends for the chemical industry.

For the past 150 years, plastics have been key enablers for innovations and to date, plastics are used in various fields and have replaced other typical materials such as metals, ceramics, wool, or wood owing to their superior properties. Polymers can easily be prepared on large scale from cheap starting materials; possess low densities, easy processability, and high availability; and are resistant to corrosion. Given these reasons, engineering applications of plastics are widespread and accordingly, our modern consumer-based societies are hard to imagine without synthetic materials. However, the year 2015 still turned out to be a rough year for European plastic producers and the overall plastics production in Europe still did not recover from the global financial crisis with a turnover of 350 billion €.[18] During the global financial crisis, stock products were shortened, production facilities were temporarily closed, and labor time was adjusted in Germany, leading to a significant setback in adding value and production. In return, the European plastic production is continuously losing its market shares (see Figure 1).

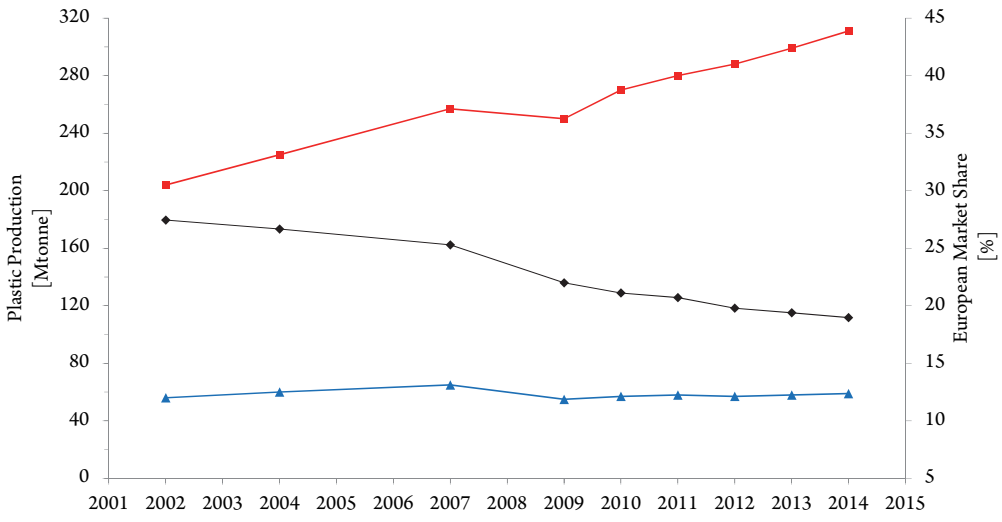

Figure 1. Plastic Production (Worldwide: red, squares; Europe: blue, triangles) and market share of European producers (black, diamonds).[18-21]

This is in sharp contrast to the rampant development of chemical companies in past decades. Since the mid-1980s, the global chemical industry has grown by 7 percent annually and the chemical industry was the fourth best performing sector out of 21 industries from 2006 to 2012.[22-24] After the global financial crisis, the total shareholder return more than halved in the chemical industry, however, was in average 4.7% per year and well ahead of most other industry sectors, which returned only 2.4% overall.[25]

The last decades have shown a strong shift in the global value-added chain for the large plastics and chemical companies on the market. In the 1980s, Western Europe and the German companies Bayer, BASF, and Hoechst, and US competitors dominated the global market for plastics and chemicals.[22] In 2010, the ten largest chemical companies were predominantly from Europe and the US (7 out of 10) and one competitor was from China, Japan, and Saudi Arabia respectively (see Table 1).[22] In late 2015, Dow Chemical and DuPont announced a 130 billion USD merge of both companies followed by a breakup of the (new) firm into three companies (agriculture, materials, and specialty products).[26-27] The merger is expected to deliver 3 billion USD in cost savings through synergies and save 1 billion USD in growth synergies.[28] Mergers are one approach to compete and improve the own market position and are expected to increase for large companies in the future. However, if cost reductions and "synergies" result in short term gains and blindfolded cost cuts to ease the shareholder's pressure, future innovations or new products can be affected limiting the long-term financial success of the merged company.[29] The tremendous challenges in the chemical industry and the permanent change of the main sales markets shifting east will result in further reorganizations and by 2030, five to eight of the largest ten chemical are expected to be from Asia and the Middle East (see Table 1).[22]

Table 1. Top Ten of the Worldwide Largest Chemical Companies and Foreseeable Regional Shift until 2030 (Sales in Billion €, Market Share in %)

1985				2010			2030 estimated
1	Bayer	14	2.8	BASF SE	48	2.0	
2	BASF SE	13	2.8	Dow Chemical	41	1.7	Europe 2–3
3	Hoechst	13	2.6	Exxon Mobil	40	1.7	
4	ICI	10	2.1	SABIC	35	1.5	NAFTA 1–2
5	Dow Chemical	8	1.7	Sinopec	35	1.4	
6	DuPont	8	1.7	Royal Dutch Shell	30	1.3	
7	Ciba-Geigy	7	1.5	DuPont	24	1.0	Middle East 2–3
8	Montedison	7	1.4	LyondellBasell	24	1.0	
9	Rhône-Poulenc	6	1.2	Ineos	21	0.9	Asia 3–5
10	Montanto	5	1.0	Mitsubishi Chemical	21	0.9	

This process is expected to facilitate in the next decades and the European plastic producers and chemical companies will face increased pressure on the market because of pricing (*i.e.*, cheap energy costs in the US and the Middle East) and need to strengthen their export business and/or be present on-site at the emerging markets outside of Europe to allow customer proximity and recruiting of talents/workforce (*i.e.*, China, Southeast Asia). The price of US natural gas has dropped more than 75% from 2008 to 2012; independently from the decline of the crude oil price since 2014.[30] Furthermore, to date, the global market for chemicals is roughly at parity between multinational companies and competitors from emerging markets in terms of revenues illustrating the advanced stage of global competition in this industry.[31] Almost half of the chemical sales today are based in Asia.[22] Projections for the next 20 years predict a diverging trend for Asia and Europe and if current global trends continue, the world market will grow by 3% over the next two decades, the Asian region is expected to grow by 5% annually, while Europe is expected to lag behind with only 1% growth per year.[22] A growth rate of the chemical sector in Europe of about 1% correlates to an estimated loss of jobs of about 30% by 2030.[22] Given this highly demanding, challenging and dynamic movements in the global chemical industry, the percentage of chemical- and pharmaceutical companies of the worldwide 50 most innovative companies in 2015 is stable at around 20% (BASF, Bayer, DuPont, 3M, etc., so-called traditional markets) versus predominant technology oriented companies.[32]

This is remarkable, hence, growth in the chemical industry is expected to be carried out by steadily improvements of existing products rather than by revolutionary discoveries, innovations, and new molecule classes. For polymers, this translates into (industrially preferred) innovations of existing materials derived from commodity monomers rather than completely new developments or new monomers for products and applications. However, not all future applications can likely be evolved from innovations of existing solutions. The use of polymeric materials is vast and polymers range in applications from simple packaging materials to high performance, and biodegradable materials. Specific properties in polymers are addressed by functional groups within the material and/or the polymerization technique (chain end-groups, graft structures, or block structures via sequential monomer addition). Interesting functional groups are introduced by heteroatom elements and oxygen, sulfur-, nitrogen, silicon-, halogen-containing materials are used in various commercial applications. One approach toward new material properties is the incorporation of phosphorus. In literature, functional groups featuring phosphorus are often introduced in a relatively significant distance from the polymerized functional group (*i.e.*, in most cases olefins for chain-growth-, and polar functional groups for step-growth polymerizations).[33] Therefore, the large absence of (simple) phosphorus-containing polymeric materials in academic research and industry processes is a scientific question to be tackled. Phosphorus-based materials are of specific interest due to their (attributed) high biocompatibility or flame-retarding properties. Especially the fact that nature chose phosphate groups for the world's most important storage material of biological information; DNA

and RNA, and the absence of (simple) phosphorus-containing artificial polymers for synthetic chemists make phosphorus-containing polymers an interesting field of research for new materials.

The change from structural materials to functional systems is one of the most prominent challenges in macromolecular chemistry and materials science in the next years.[34] At the beginning of the 21st century, new materials are needed for more and more efficient and resource-saving applications. Although common techniques are of great economic importance, they fail to address the change from 20th century structural materials to 21st century complex system polymers. Materials of the future, in combination with nanotechnology, medicine, or material science, offer solutions to these challenges. Furthermore, utilization and development of precision polymers will include fields such as tissue engineering, membranes, stimuli responsive materials, mobility, energy storage or engineering materials. Therefore, the need for new materials or an improvement in existing materials and processing techniques is essential. Living polymerizations are the most promising candidates to add specific functionalities to new materials. Over the last two decades living radical polymerization methods have developed rapidly, and for most cases, the living characteristics result from low radical concentrations giving rather low propagation rates and/or conversions. However, for feasible applications, methods with high precision of the macromolecular parameters in combination with rapid reaction velocities are required. Metal complex-catalyzed reaction sequences ideally fulfill these requirements.

1.3 Vinylphosphonates

Vinylphosphonates belong to one of the simplest and longest known phosphorus-containing monomers and the homopolymerization of vinylphosphonates leads to poly(vinylphosphonate)s consisting of saturated C-C bonds in the main chain only, which is one of the reason for their robustness and stability against main chain degradation (see Chart 1a). Another interesting feature of vinylphosphonates is the close proximity of the electron withdrawing group (EWG) and the vinylic double bond, which for vinylphosphonates results in an enol-type related delocalized resonance structure (see Chart 1b) being an important prerequisite for monomers suitable for anionic polymerizations as the negative charge at the growing chain end needs to be stabilized. However, classic anionic or free radical polymerization fail to produce high molecular weight poly(vinylphosphonate)s for different reasons (see Chapter 4.1).

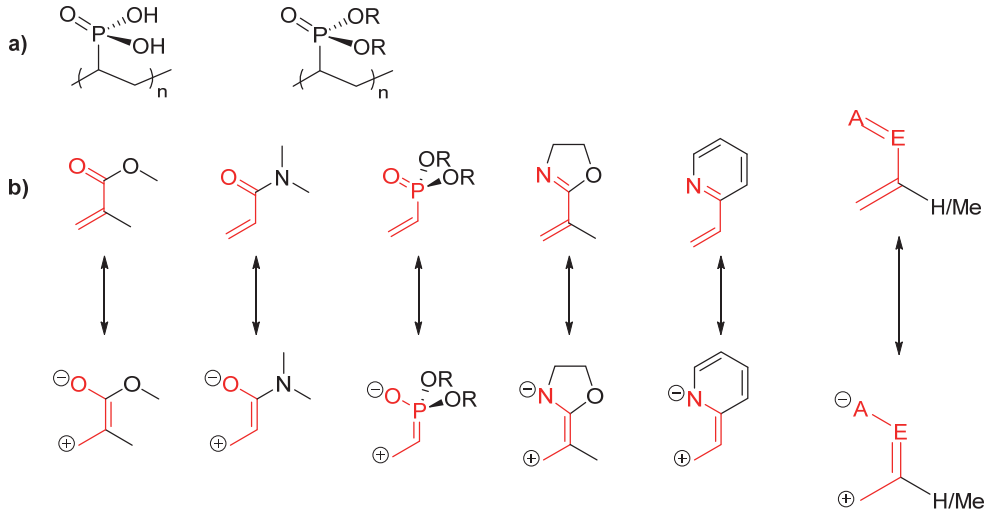

Chart 1. a) Poly(vinylphosphonic acid) (left) and poly(vinylphosphonate ester) (right). b) Overview of different Michael-type acceptor monomers (methyl methacrylate (MMA), *N,N*-Dimethylacrylamide (DMAA), dialkyl vinylphosphonate (DAVP), 2-isopropenyl-2-oxazoline (IPOx), 2-vinylpyridine (2VP), general structure of a Michael-type acceptor monomer (E = heteroatom, A = acceptor); from left to right.

Vinylphosphonates are Michael-type acceptor monomers and possess a sufficient π-overlap of the double bonds in an S-cis conformation. This important prerequisite for polymerization was confirmed at a rare earth (RE) metal center crystallographically (see Chapter 4.2).[35] For α-methyl substituted vinylphosphonates (*e.g.*, diethyl 1-methyl vinylphosphonate (DEMVP)) such a π-overlap is discussed to be hindered by steric repulsion between the methyl group and the methyl esters. For similar reasons, α-methyl substituted acrylamides are often not accessible for anionic polymerization reactions (DMMA, see Chart 2).[36] However, a computational study for a supposed insufficient π-overlap for α-methyl substituted vinylphosphonates is missing in literature. The polymerizability of different acrylamides was computed by DFT calculations.[37]

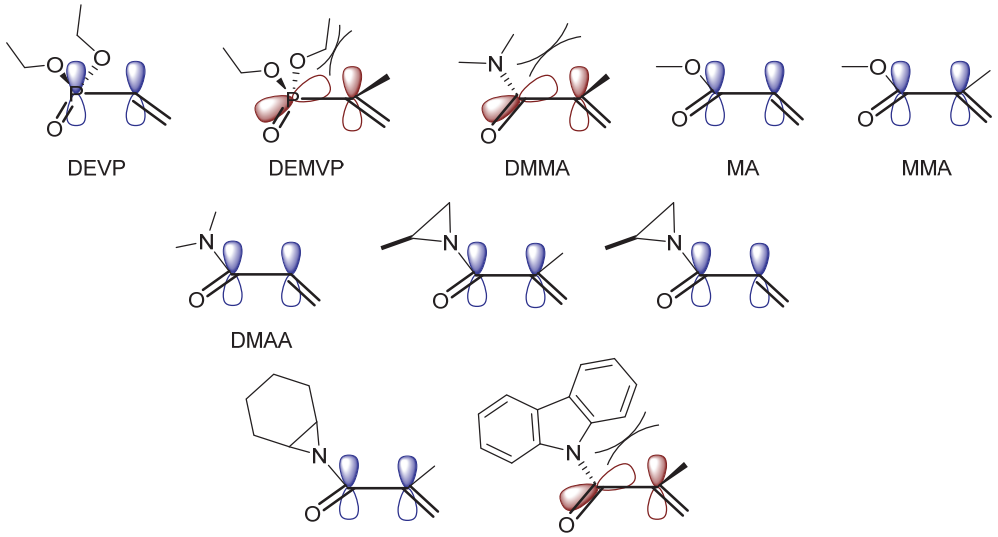

Chart 2. Comparison of different polar monomers and their (attributed) orbitals of the Michael system.

Phosphorus introduces interesting functional groups in polymers leading to specific material properties. Therefore, phosphorus-based plastics are getting increased attention for a variety of different applications from use in ion-exchange resins, fuel cells,[38-48] halogen-free flame retardants,[49-50] or due to their high biocompatibility[51-55] they can be used as dental adhesives or bone concrete.[56-60] The class of vinylphosphonates is discussed and compared to other phosphorus-containing monomers in detail in Chapter 4.1.

1.4 Terminology

In a broad sense, the propagation of all polymerization reactions can be seen as "catalytic" as multiple monomers are consumed per reactive initiating molecule. For a better distinction of those initiating compounds, the terms "initiators" and "catalysts" are used, depending on whether one or several polymer chains are produced by one reagent. The definition of initiator is precise for free radical, cationic, or anionic polymerization techniques, whereas for catalytic polymerizations, the catalyst can either relate to the initiating ligand or to the metal center activating and stabilizing the monomer and growing polymer chain end. To overcome this terminological conflict, according to previous literature, this article uses the term "catalyst" when referring to the catalyzed monomer addition. This thesis specifically deals with the repeated conjugate addition of Michael-type monomers via rare earth metal-mediated group transfer polymerization (REM-GTP) as a living polymerization initiated by rare earth metal complexes. Whereas complexes are often termed as catalysts, in fact only one polymer chain is formed per metal center and the turnover number (TON) is strictly one for living polymerizations in general. Therefore, the reader should be aware of this general misconception in literature due to a loose usage of the term catalyst for de facto non-catalytic living polymerizations.

The term rare earth metals is used for the group 3 elements scandium, yttrium, and the fourteen lanthanides (lanthanum – lutetium) excluding promethium (radioactive). The elements will be abbreviated by the term RE in text and Ln in chemical formula or figures. According to the IUPAC definition, a metallocene contains a transition metal and two cyclopentadienyl ligands ($(C_5H_5)^-$) coordinated in a η^5-C_5H_5 sandwich structure. In contrast to this more strict definition proposed by IUPAC, this thesis will use the term metallocene for all complexes containing at least one cyclopentadienyl ligand, substituted cyclopentadienyl ligands, or its (substituted) derivatives (indenyl, fluorenyl).

2 Theoretical Background and Aims of the Thesis

2.1 Rare Earth Metal-mediated Group Transfer Polymerization

There is no exact nomenclature on how lanthanide- or transition metal-mediated polymerizations of polar monomers following a repeated conjugate addition should be termed and the used terminologies in literature differ between the publications of several groups for the basically same polymerization mechanism. In literature, the term coordination polymerization (or coordinative anionic, or coordination addition polymerization) is often used for a zirconocene-mediated polymerizations of polar monomers.[36] For RE element-mediated polymerizations, the term rare earth metal-mediated group transfer polymerization (REM-GTP) became popular in the past years for the polymerization of vinylphosphonates.[61] A lot of confusion derived from the original dispute on the mechanism of silyl ketene acetal-initiated group transfer polymerization (SKA-GTP). The term GTP was originally used as the utilized silyl compounds were supposed to transfer from the initiator to the added monomer.[62-63] Since then, the mechanism of nucleophilic GTP has stimulated considerable scientific discussion.[62,64-72] The gist of this controversy was the contrast of associative or dissociative mechanism for SKA-GTP propagation taking place.[62,70-72] In further mechanistic studies the dissociative mechanism was supported by experimental results.[65-69] Therefore, the concept of SKA-GTP as an associative repeated transfer of the organosilyl-group might be misleading, but was kept in literature (see Chapter 4.1). This thesis will use the term REM-GTP for the polymerization of polar monomers by RE element complexes following a repeated conjugate addition and for REM-GTP only a GTP mechanism can take place in contrast to the name-giving SKA-GTP; therefore, the term GTP is correct to use for RE metal complexes for the polymerization of polar monomers. A short introduction for the first reports on MMA polymerization will be given here and the advantages of REM-GTP for vinylphosphonates over other polymerization methods (radical, or anionic) will be discussed in detail in Chapter 4.1.

REM-GTP enables the precise synthesis of high value materials and combines the advantages of both, living ionic- and coordinative polymerizations. The concept of "living polymerizations" was first introduced by Szwarc in 1956 (the term has nothing to do with living in the biological sense).[73-74] To avoid possible conflicts to the strict terminology an in theory ideal living polymerization, controlled polymerizations are in reality often referred as immortal, quasi-living, pseudo-living, or simply controlled polymerizations.[75-87] For the term immortal polymerization introduced by Inoue et al., chain transfer reactions between growing and dormant macromolecule cause the formation of more polymer molecules than catalyst molecules were originally used.[88]

The lack of a common language in the case of "living" polymerizations creates confusion, wastes time and journal space, and has the potential to inhibit computational literature searching. Therefore, a uniform

terminology was demanded by T. R. Darling,[89] creating an even more vivid scientific discussion without any decay of this controversy to be seen.[90] In a special issue of the Journal of Polymer Science Part A: Polymer Chemistry on the question: "Living or Controlled?" various reputable researchers including M. Szwarc, S. Inoue, K. Matyjaszewski, O. Nuyken, R. M. Waymouth, O. Webster, and H. Yasuda contributed their comments on this debate.[91-97]

Living polymerizations can be distinguished from free radical polymerization or from a condensation polymerization by plotting the molecular weight of the polymer versus the monomer conversion. In a living polymerization, the molecular weight is directly proportional to the conversion (see Figure 2, line A). In a free radical polymerization, high molecular weight polymer is formed in the initial stages of the reaction and a decrease of the molecular weight can be seen for higher monomer conversions in the case of a faster termination rate than the propagation rate and vice versa an increase of the molecular weight can be seen for higher monomer conversions in the case of a lower termination rate than the propagation rate (see Figure 2, line B). In a condensation polymerization, only dimers are formed until 50% conversion and high molecular weight polymers are only generated as the conversion reaches near quantitative conversion (see Figure 2, line C).

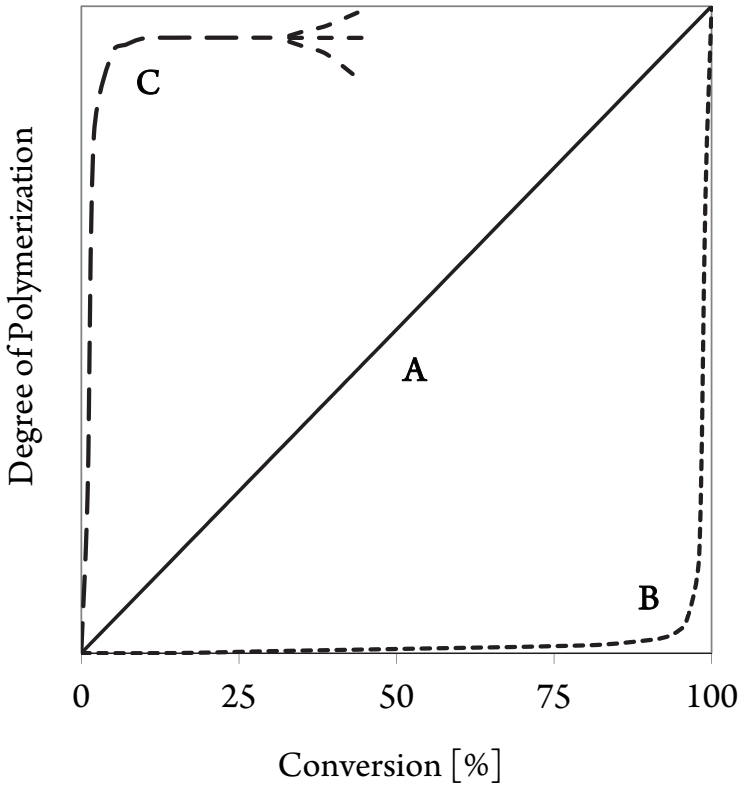

Figure 2. Plot of the (ideal) degree of polymerization vs. monomer conversion. a) Living polymerization. b) Step-growth polymerization with ideal stoichiometry. c) Free-radical polymerization (straight line: propagation rate = termination rate; increase: propagation rate > termination rate; decrease: propagation rate < termination rate).

According to its highly controlled character (to avoid the term living), REM-GTP leads to strictly linear polymers, with a very narrow molecular mass distribution (PDI < 1.1), exhibits a linear increase in the average molecular mass upon monomer conversion, and allows the synthesis of block copolymers as well as the introduction of chain-end functionalities. The coordination of the growing chain end at the catalyst suppresses side reactions and allows stereoregular polymerizations as well as tuning the activity by varying the metal center or ligand sphere.

In 1992, two independent publications reported on the living polymerization of MMA using transition- or lanthanide metal initiators: the neutral, single component samarocene $[(C_5Me_5)_2SmH]_2$ was presented by Yasuda et al. as well as the two-component zirconocene system ($(C_5H_5)_2ZrMe(thf)^+$, $(C_5H_5)_2ZrMe_2$) was reported by Collins and Ward.[98-99] The propagation proceeds in both cases via a repeated conjugate addition involving either one or two metal complexes.[100-102] This type of MMA polymerization is known as coordinative-anionic polymerization and due to its similarity to SKA-GTP, it was also termed as transition metal-mediated GTP by Collins and Ward.[99] $[(C_5Me_5)_2SmH]_2$ produces PMMA over a broad temperature range from as low as −95 °C up to 40 °C, with a controlled molecular mass (according to the $[MMA]_0/[Sm]_0$ ratio), low polydispersity (PDI < 1.05), and a high syndiotacticity of up to 95%.[98,103] The mechanism of initiation via nucleophilic transfer of a hydrido ligand and an eight-membered transition state was proven by the crystal structure of the MMA adduct $(C_5Me_5)_2Sm(MMA)_2H$. In the first step, the hydrido-bridged dimer has to be opened by coordination of one monomer molecule. The initiation follows a 1,4-addition of the hydrido ligand to MMA and an enolate is formed (see Scheme 1). The thus formed active species can further add to coordinating monomer through a repeated conjugated addition via the eight-membered transition state.

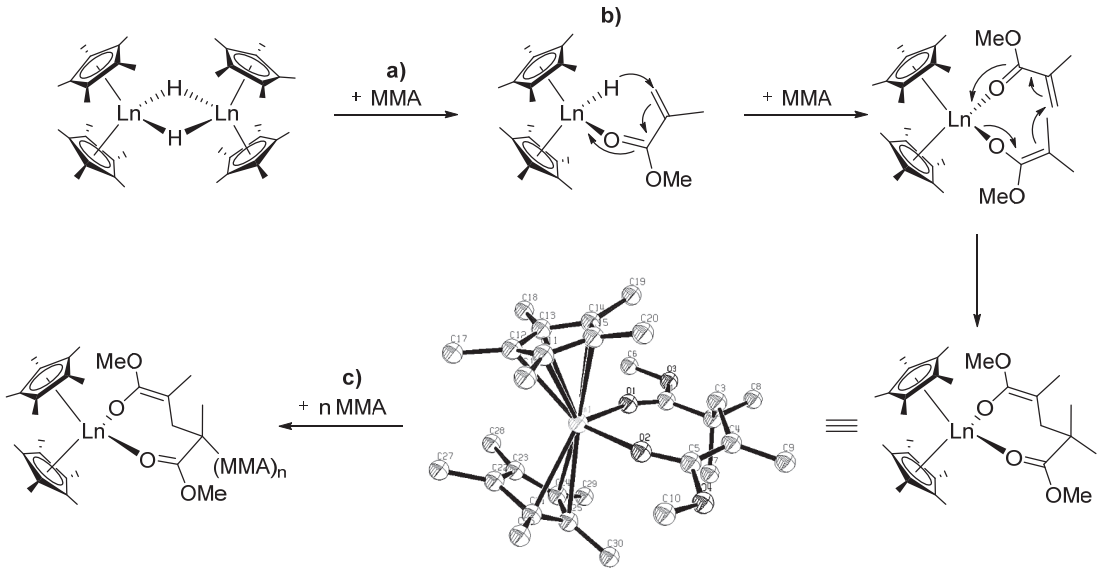

Scheme 1. Dimer opening by monomer a) coordination, b) initiation, and c) propagation of MMA REM-GTP by $[(C_5Me_5)_2SmH]_2$ (reprinted with permission from ref. 34. Copyright 2016 American Chemical Society).

2.1 Rare Earth Metal-mediated Group Transfer Polymerization

The advances of (meth)acrylates and (meth)acrylamide polymerizations since the first work in the early 1990s and the mechanism, application, and background of classic acrylic and polar monomer polymerization has been already covered in detail by Chen et al..[36] For reviews on the REM-GTP of vinylphosphonates, the reader is redirected to a review of Rieger et al. from 2012 and Chapter 4.1.[34,61]

In the beginning of this work on vinylphosphonate REM-GTP, our group had obtained a general understanding on the synthesis of simple organometallic RE complexes. The mechanism of vinylphosphonate REM-GTP was previously studied in detail by our group via kinetic studies using ^{31}P NMR and the polymerization process of vinylphosphonate REM-GTP was elucidated in depth.[35] However, several problems for the polymerization of vinylphosphonates were still unaddressed.[104] First of all, the traditionally used strongly basic initiators for the polymerization of (meth)acrylates and (meth)acrylamides were found to initiate vinylphosphonates via a deprotonation of the α-acidic C–H and the thus formed vinylphosphonate anion itself resulted in long initiation delays and low initiator efficiencies. In a first step, efficient initiators for REM-GTP of vinylphosphonates had to be evaluated. Furthermore, most published data of our group on vinylphosphonate REM-GTP were based on simple $(C_5H_5)^-$ based ligand systems. In a second step, a better understanding on ligand modifications was needed to be obtained for synthetically accessible RE metallocenes. Combining efficient initiators and suitable ligand structures, target complexes for a stereoregular polymerization of vinylphosphonates had to be identified and a signal assignment to quantify the tacticity needed to be performed. Therefore, for vinylphosphonate REM-GTP, novel initiators, ligand-induced steric crowding, and rigid, sterically crowded compounds had to be identified, synthesized, and evaluated for vinylphosphonate REM-GTP. Several approaches for these scientific problems are presented in the following chapters.

2.2 Novel Initiators for Vinylphosphonates

Suitable initiators need to have high initiator efficiencies, lead to a fast and uniform initiation reaction resulting in low PDI values, should be available via a feasible synthesis, poses a stable end-group, be a possible candidate for surface or particle modifications, can be modified for post polymerization reactions (*e.g.*, click chemistry), or allow the polymerization of block copolymers (sufficient nucleophilicity or low coordination strength).

Previously, our group had used alkyl- (*e.g.*, –Me, $-CH_2TMS$), thiol- (*i.e.*, –S*t*Bu), amide- (*e.g.*, bis(dimethylsilylamide), bdsa, $-N(SiHMe_2)_2$) and simple $(C_5H_5)^-$ ligands for the initiation of vinylphosphonates. Whereas, –Me or $-CH_2TMS$ initiators show long initiation periods (usually defined as the time until 3% conversion is reached) and low initiator efficiencies I^* ($I^* = M_{th}/M_n$, $M_{th} = eq._{Mon} \times M_{Mon}$) being less than 20% were found. For thiols (*e.g.*, –S*t*Bu) higher initiator efficiencies were determined, however, thiols are not a stable end ground for vinylphosphonate REM-GTP or might even eliminate from the polymer chain end during polymerization (determined via ESI-MS). The dimers $[(C_5H_5)_2YStBu]_2$ and $[(C_5H_5)_2LuStBu]_2$ both show a distinct initiation period of a few seconds for DEVP polymerization and PDEVPs with rather broad PDIs ≤ 1.30 are obtained.[35] Amide initiators (*i.e.*, bdsa) suffer from simultaneously occurring initiation processes and the corresponding oligomers showed either initiation by nucleophilic transfer of the amide, $(C_5H_5)^-$ transfer to the monomer, or even no end-group functionalization (olefinic chain ends presumably from an end-group elimination after polymerization) in ESI-MS measurements. Despite the different initiation reactions the obtained polymers had monomodal GPC distributions.[35] Only simple $(C_5H_5)_3Ln$ compounds were previously reported to initiate fast and efficiently.[105] In kinetic studies, it was found that $(C_5H_5)_3Lu$ was the only complex without any (observable) initiation period and $(C_5H_5)_3Yb$ already exhibits an initiation period of a few seconds and lower activities.[105] The activities of $(C_5H_5)_3Ln$ initiators strongly depends on the size of the used metal center and future developments of such complexes for example for surface modifications is hindered by the three statistic initiating ligands.

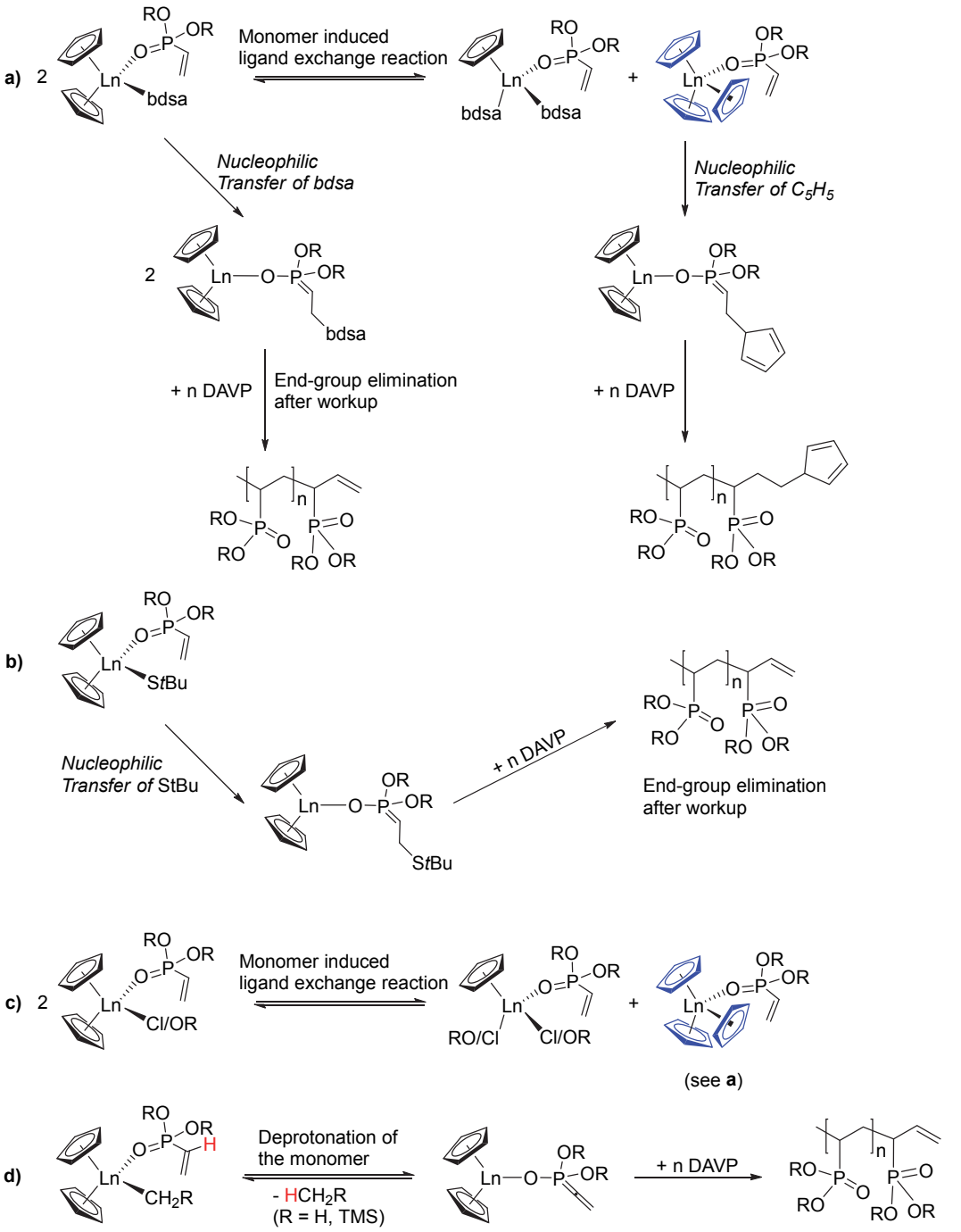

Scheme 2. a) Initiation of bdsa ligands can result in either nucleophilic transfer or ligand exchange reaction forming active Cp_3Ln. b) Initiation via thiols leads to end-group elimination and olefinic chain ends. c) Chloro or alkoxide ligands form active complexes after ligand exchange reaction. d) Alkyl initiators deprotonate vinylphosphonates resulting in olefinic chain ends.

Also the original publication of Collins and Ward on zirconocene-mediated MMA polymerization using alkyl initiators suffered from low initiator efficiencies ($I^* < 45\%$) and broad PDIs (1.19 – 1.40).[99] In later studies, enolate initiators were found to represent a significant development for the zirconocene-mediated GTP.[36,106-107] As previously described, the propagation of GTP takes place via an eight-membered ring transition state (see Chapter 2.1). An elegant approach to overcome initiation problems derived from deprotonation reactions or an insufficient nucleophilic transfer of a six electron process is therefore to have

a mechanistic match between the initiation reaction and the propagation. Zirconocene enolate complexes are an example for such a mechanistic match of initiation and propagation (both following an eight-electron process, see Scheme 3).

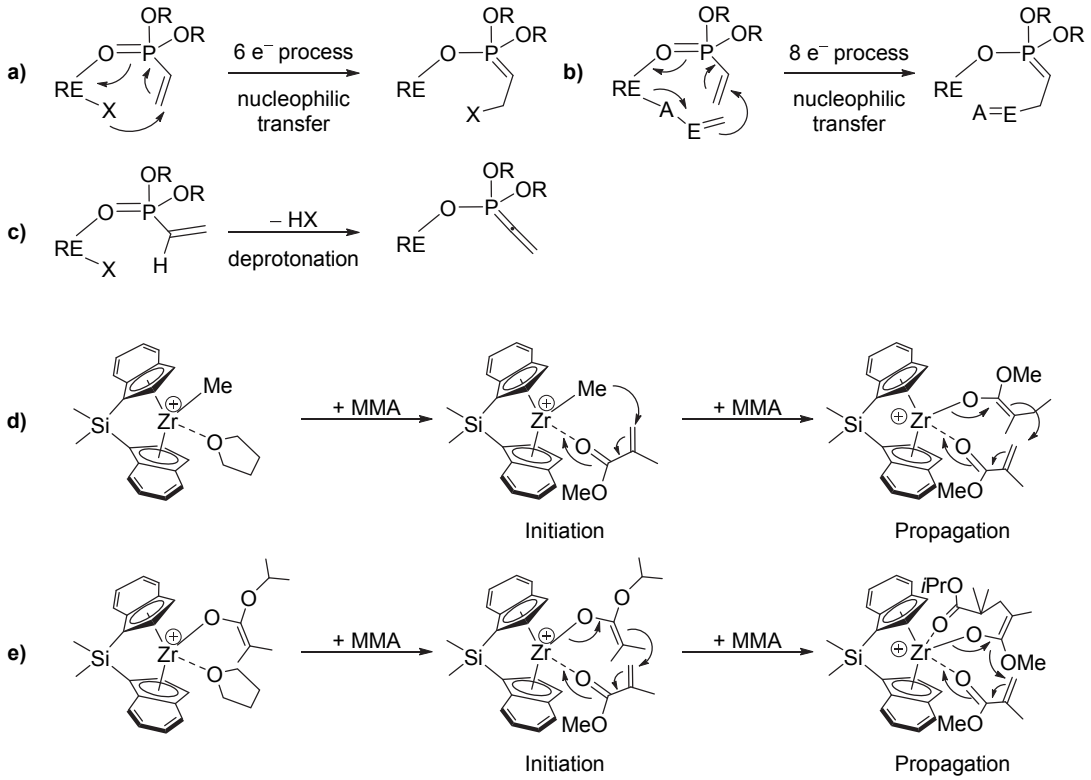

Scheme 3. Possible initiation reactions for REM-GTP of DAVP via a) 6e⁻ nucleophilic transfer of a ligand X, b) 8e⁻ nucleophilic transfer of a conjugated ligand, c) deprotonation of the acidic α-C–H. d) 6e⁻ Nucleophilic transfer of a methyl ligand of a zirconocene metal center. e) 8e⁻ Nucleophilic transfer of an enolate ligand of a zirconocene metal center.

To apply this approach to the REM-GTP of vinylphosphonates, the synthesis of RE enolate initiators (and similar structures) was attempted via simple deprotonation reactions in preliminary studies.[108] However, in this master's thesis only decomposition or unidentified mixtures of products were found for most substrates and no suitable initiators were obtained. The literature on RE enolate complexes is rare and limited to specific substrates only. In 1986, Evans et al. reported the synthesis of several RE enolate complexes via salt metathesis in low yields and for a thermolysis reaction a strong dependence of steric factors for the product formation or decomposition was observed (Scheme 4a).[109] The reactivity of early-lanthanide $(C_5Me_5)_2LnCH(SiMe_3)_2$ complexes (Ln = La, Ce) toward ketones was studied by Teuben et al..[110] For sterically less hindered ketones a coupling in an aldol fashion was found to be preferred and a selective product formation with one equivalent of ketone was not possible (see Scheme 4b, c).[110] However, for higher ketones (*e.g.*, 3-pentanone), no C–C bond formation was observed and enolate-ketone adducts were isolated (see Scheme 4d).[110] The insertion of the second equivalent 3-pentanone to produce the corresponding 4-hydroxy-4-methyl-2-pentanone does not take place. This lack of reactivity is not a result of steric reasons, because the reaction of $(C_5Me_5)_2LnCH(SiMe_3)_2$ and 4-hydroxy-4-methyl-2-

pentanone leads to the C–C bond cleavage (see Scheme 4e).[110] Cationic yttrium complexes were reported to form the corresponding alkoxide products with ketones.[111]

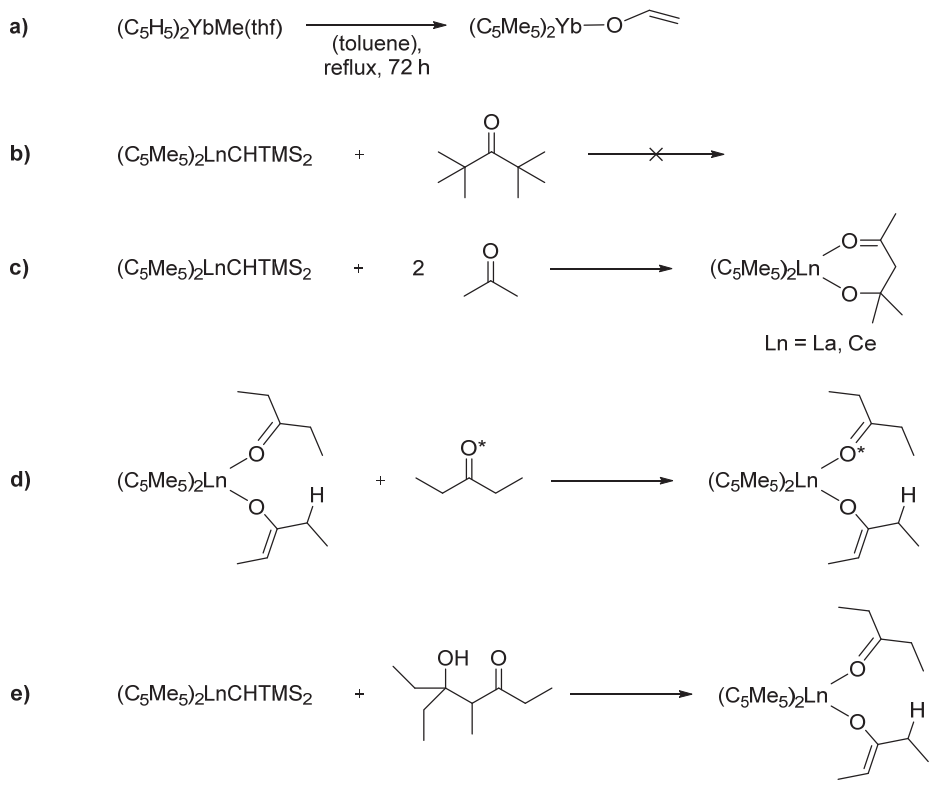

Scheme 4. Reactivity of different RE metal complexes with various oxygen containing substrates.

In summary and in agreement with previously obtained results in our group it was found that to date no simple synthetic access to RE enolate complexes exists. Therefore, instead of the deprotonation of acidic α-C–H ketone groups, σ-bond metathesis resulted in the formation of new activated hydrocarbyl ligands. This elegant approach to overcome initiation limitations for vinylphosphonate REM-GTP was applied by our group and published in *Organometallics*.[112] The *ortho*-methyl substituted pyridines are known for C–H bond activation at RE metal centers and the synthesis of (4,6-dimethylpyridin-2-yl)methyl initiators leads to enamide like ligands, which are supposed to initiate via an eight-membered ring transition state, and are discussed in Chapter 4.3.

2.3 Propagation of Vinylphosphonates

Since early publications in 2010, the REM-GTP of vinylphosphonates was restricted to selected ligand systems only.[61,113] In 2007, Leute and Dengler observed the oligomerization of vinylphosphonates using homoleptic RE precursor complexes.[114-115] In 2010, Rabe et al., published the utilization of the RE precursor complexes $Ln(bdsa)_3(thf)_2$ (Ln = La, Sm, Nd) for the polymerization of DEVP.[116] These catalysts suffered from incomplete monomer conversions and broad PDIs of the obtained polymer (PDI = 3.11 – 3.56) (see Figure 3a).[116] In a study published by Rieger et al. in 2010, the polymerization of DEVP by $(C_5H_5)_2YbMe$ and $(C_5H_5)_2YbCl$ complexes was reported and the successful block copolymerization of MMA and DEVP indicated a GTP mechanism taking place (see Figure 3b).[117] In a fully comprehensive mechanistic study, the initiation and propagation of several $(C_5H_5)_2Ln$-mediated DEVP and DIVP polymerizations were investigated.[35] In 2014, the scope of used ligands systems was extended from metallocene based compounds to bis(phenolate) yttrium catalysts for several Michael-type monomers such as 2-isopropenyl-2-ozaxoline, 2-vinylpyridine, or vinylphosphonates (see Figure 3c).[113] However, simple (C_5H_5)-based RE metallocenes possessed by far highest activities, but variations of the ligand systems remained scarce in literature and no modifications of the $(C_5H_5)^-$ ligand sphere were performed prior to this work.

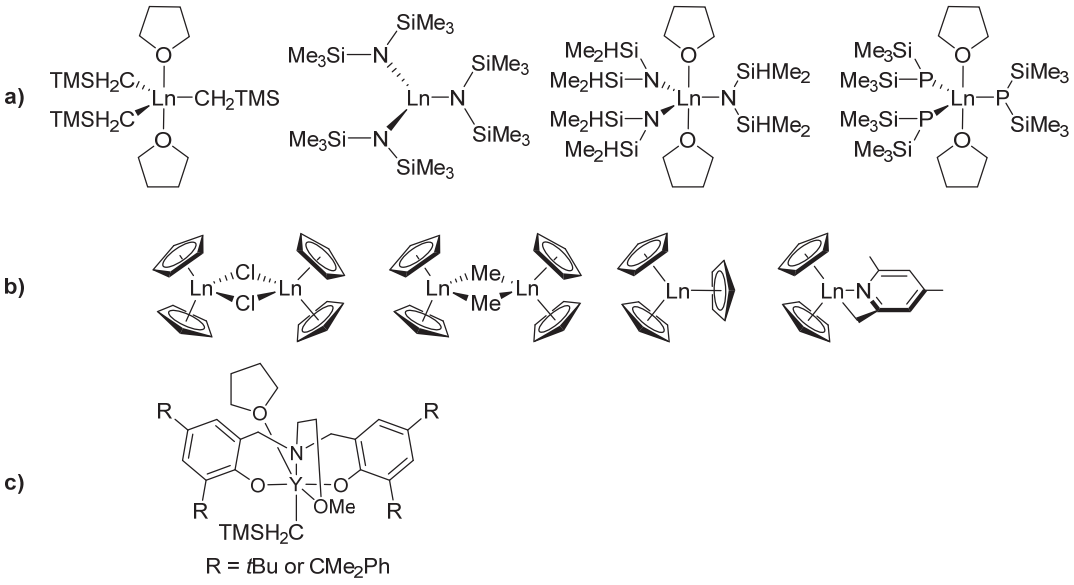

Figure 3. a) Early RE metal precursor complexes used for the polymerization of vinylphosphonates. b) RE metal metallocenes for the efficient polymerization of vinylphosphonates (in order of increasing activity and/or efficiency). c) 2-Methoxyethylamino-bis(phenolate)-yttrium catalysts with moderate activities for the polymerization of vinylphosphonates.

After synthetically accessible and efficient initiators from σ-bond metathesis were found (see Chapter 4.3) it was needed to conduct studies on $(C_5H_5)^-$ ligand modifications to examine the influence of ligand induced steric crowding. Therefore, a systematic stepwise increase of the steric bulk of the ligand sphere and a gradual change of the cation size (extending to early lanthanides) was needed to be performed

in a methodic study. The results and impact of the first metallocene ligand modifications for vinylphosphonate REM-GTP were published in *Macromolecules* and are discussed in Chapter 4.4. The insights of this study helped to evaluate promising candidates for a stereoregular polymerization of vinylphosphonates and will be briefly discussed in the next chapter.

2.4 Evaluation of Accessible, Rigid, and Sterically Crowded RE Catalysts for a Stereospecific Polymerization of Vinylphosphonates

The previous two Chapters 2.2 and 2.3 briefly illustrated the problems of low initiator efficiencies and/or activities for the initiation of vinylphosphonate via REM-GTP and the limitation to a few and mostly restricted to simple $(C_5H_5)^-$ ligands systems. Considering the notable amount of publications on vinylphosphonate REM-GTP the challenge of easily accessible and feasible RE metal catalysts for a stereospecific polymerization of vinylphosphonates was driving our research. The need for a stereospecific vinylphosphonate REM-GTP was further pointed out by the fact that REM-GTP was originally investigated as a polymerization method for the stereospecific polymerization of (meth)acrylates and (meth)acrylamides. Substituted, simple $(C_5H_5)^-$ RE metallocenes, and other ligand systems were previously found to produce atactic poly(vinylphosphonate)s (see Chart 3).

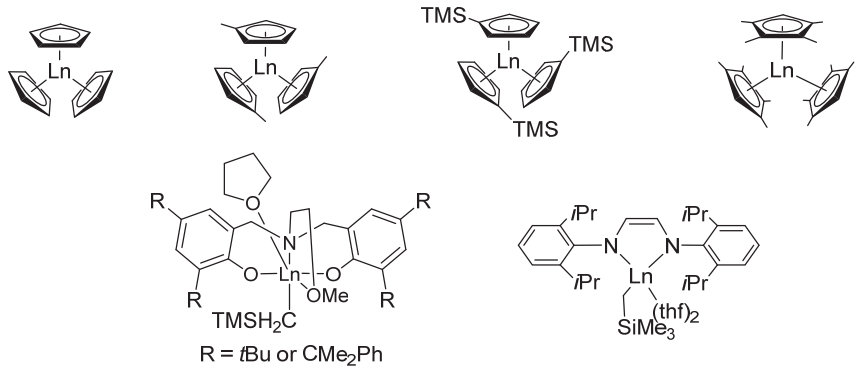

Chart 3. Comparison of different RE catalysts used for the REM-GTP of vinylphosphonates resulting in atactic poly(vinylphosphonate)s.

As a result of the previous studies on novel initiators and ligand induced steric crowding of vinylphosphonate REM-GTP, two main requirements for target complex structures were obtained:

I. The target systems should feature alkyl ligands (–Me, $-CH_2TMS$) and should be active for σ-bond metathesis to yield stable and efficient initiating ligands

II. Ligand induced steric crowding does not induce a control of the polymer microstructure, if the complexes and the sterically bulky substituents have a high flexibility. Therefore, rigidity between ligands and substituents needs to be introduced to the target structures

These insights from C–H bond activation and substituted tris(cyclopentadienyl) RE initiators lead to the synthesis and application of sterically crowded and ridged (*i.e.*, bridged) constrained geometry complexes (CGCs, see Figure 4). RE CGCs offer an outstanding access to tune the metal ligand interaction by in- or decreasing the steric demand of the metal cation or the ligand sphere. The ligand can be modified at the cyclopentadienyl or amide moiety and furthermore, the bridging unit can be changed (*e.g.,* $-CH_2CH_2-$, $-SiMe_2-$, or $-CMe_2-$) to give different cone angles shielding or deshielding the metal center.

2.4 Evaluation of Accessible, Rigid, and Sterically Crowded RE Catalysts for a Stereospecific Polymerization of Vinylphosphonates

Usually RE CGCs are synthesized using $Ln(CH_2TMS)_3(thf)_2$ precursors via alkane elimination reaction. The $-CH_2TMS$ ligand allows the further reaction and modification of the initiating ligands by C–H bond activation.

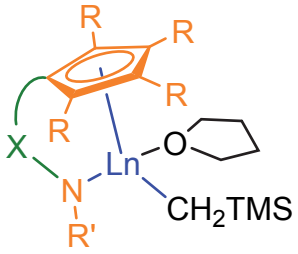

Figure 4. General representation of a RE CGC (green: bridge; orange: cyclopentadienyl and amide binding to the metal center; blue: RE cation).

The identification of possible target structures has been one goal studying a stereospecific vinylphosphonate REM-GTP. According to the definitions recommended by IUPAC, a stereospecific polymerization is the polymerization in which a tactic polymer is formed,[118] whereas a stereoselective polymerization is the polymerization in which a polymer is formed from a mixture of stereoisomeric monomer molecules by preferential incorporation of one stereoisomeric species.[36,119] However, a second problem was the limited knowledge about the microstructure of vinylphosphonates in literature and it was only investigated previously in few publications.[116,120] The contribution of Rabe et al. determined the microstructure of PDEVP on the triad level for [*mm*] triads, however, the signals were not quantified using isolated peaks due to overlapping or poorly resolved signals limiting the general insights of this study.[116] Usually, the microstructure of polymers is determined using ^{1}H and ^{13}C NMR. This leads to the following problems for poly(vinylphosphonate)s:

^{1}H NMR spectra of poly(vinylphosphonate)s give less information about the microstructure due to broad and overlapping methylene and methine signals, and high resolution ^{13}C measurements of the backbone area are difficult to obtain as a result of a low signal to noise ratio or due to thermoresponsive behavior of aqueous PDEVP solutions. The ester side chain signals do not show any stereoinformation. Therefore, methods to determine the microstructure of poly(vinylphosphonate)s using ^{31}P NMR seem to be the method of choice.

In ^{31}P NMR measurements, a splitting of the broad phosphorus signals in five domains is observed; however, the peaks cannot be separated without using peak deconvolution methods. As a tetrad sequence is excluded for phosphorus or methine proton signals in general, a splitting into pentads with several unresolved signals or simultaneous triad and pentad signals seems possible (see Figure 5).

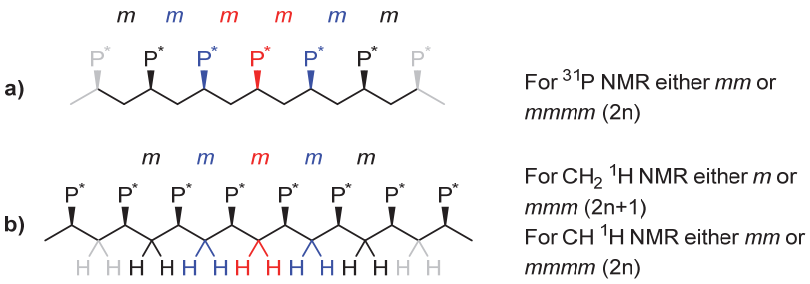

Figure 5. a) Triad or pentad (2n) sequence for phosphorus and methine proton signals. b) Diad or tetrad signals are expected for methylene signals of poly(vinylphosphonate)s.

Also for these RE CGCs, a high activity for C–H bond activation with activated substrates was observed and *sym*-collidine or alkenyl initiators from internal alkynes were synthesized. Furthermore these complexes have an overall high activity for the polymerization of DEVP and lead to (so far literature unknown) highly isotactic materials. The results and impact of CGC complexes for vinylphosphonate REM-GTP are presented and preliminary discussed in Chapter 4.5. However, further work is needed and a verification by multidimensional NMR studies is necessary prior to publication (see Chapter 4.5).

2.4 Evaluation of Accessible, Rigid, and Sterically Crowded RE Catalysts for a Stereospecific Polymerization of Vinylphosphonates

3 The Rare Earth Elements and General Principles in Lanthanide Chemistry

3.1 Rare Earth Metals

Despite its name, the elements of the rare earth metals are actually not uncommon within the lithosphere of the earth and some RE metals are more frequent than well-known elements such as lead, copper or lithium.[121] The unfortunate term "rare earth" elements for the lanthanides La-Lu and the group III elements Sc and Y origins from their naturally low concentrations in ores, their laborious mining and purification process, and the late discovery of the elements. RE elements are used in a variety of different fields. The luminescence of some elements is used in LEDs, lasers, lamps, or displays. Their magnetism can be used in data storage media or wind engines and they are used in metal alloys, light construction, batteries, and ceramics. Furthermore, RE elements are used in automotive catalysts and in many heterogeneous processes of the chemical, and oil and gas industry (see Figure 6).[122]

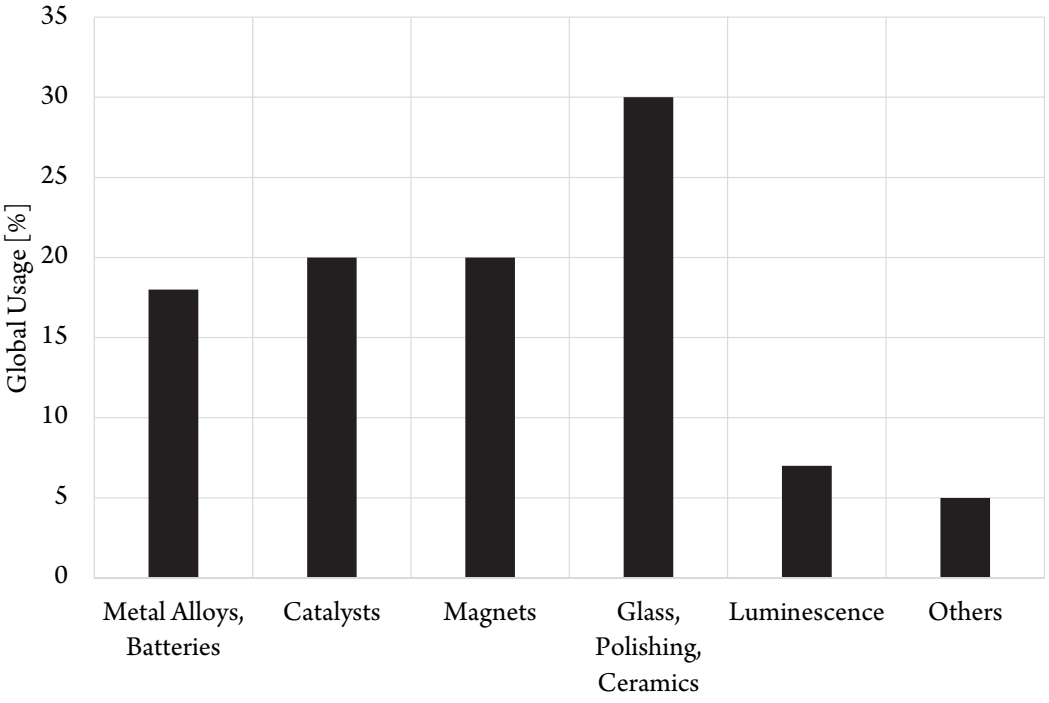

Figure 6. Global usage of RE elements in different markets.[122]

The partially occupied 4f orbitals of the RE elements have a limited radial extension and the 4f electrons are highly delocalized in the diffuse orbitals. Therefore, the positive charged nucleus is attracting the outer s-electrons, leading to more contracted orbitals and gradually smaller atomic radii with higher nuclear charge (see Figure 7). The 4f orbitals are shielded by the outer 5s- and p-orbitals and do not contribute to the chemical reactivity of the RE metals. As a results, the reactivity of RE complexes does not depend on the 4f orbital configuration and mostly relies on steric aspects.

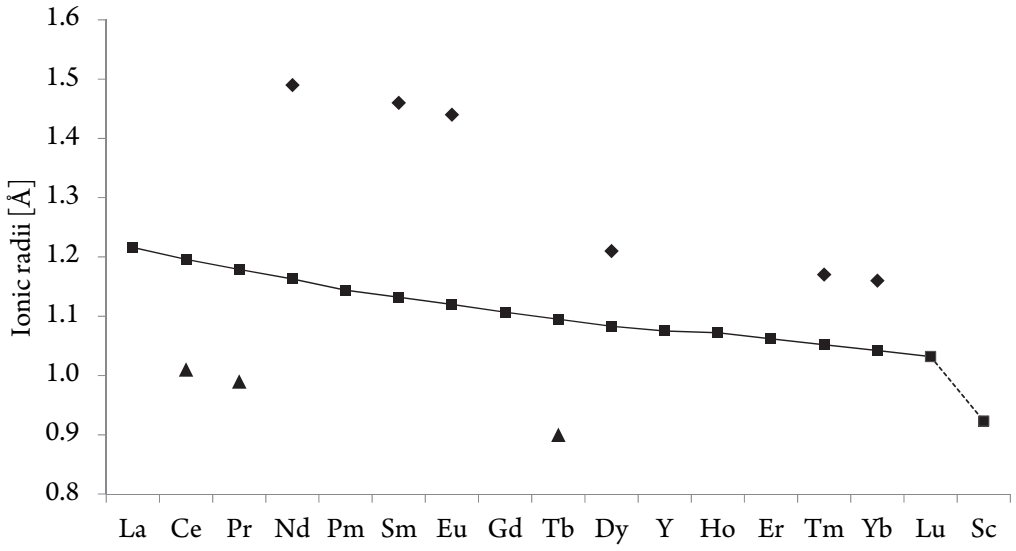

Figure 7. Decrease of the ionic radius with increase of the atomic number (squares - Ln^{3+} with the exception of scandium, dotted line; diamonds - Ln^{2+}; triangles - Ln^{4+}).

Around 10% of the lanthanide contraction is attributed to relativistic effects.[123] By the combination of organometallic ligand design and choice of the metal center, RE metal chemistry can be easily fine-tuned by steric controls. Within the periodic table, such a precise optimization based on metals is only possible for RE elements and the lanthanides are an ideal playground to study various metal ligand interactions or to control the coordination sites around the metal center. An exception to the gradual course of properties is Scandium with the lowest atomic number and being the smallest metal center of the REs (see Figure 7). Furthermore, Sc is the most Lewis-acidic elements and Sc complexes have a distinct behavior. For Sc compounds, the metal-ligand bond has a highly covalent character. Therefore, Sc is rather comparable to titanium than to the larger RE elements.[124-125]

Despite their redox stability and subsequent restricted reaction mechanisms, RE elements have high potential for catalytic transformations due to their strong Lewis acidity and overall high electrophilic and oxophilic interactions. The steric demand of different ligands for RE elements and the amount of steric crowding can be estimated using Marcalo's steric coordination number CN_S.[126] For recent trends in RE coordination chemistry, the reader is directed to the annually published reviews of Frank T. Edelmann.[127-128]

3.2 On the Importance of Questioning Scientific Assumptions

RE elements prefer the oxidation state +III and for RE elements changes to other oxidation states (*e.g.*, +IV, +II) are only possible under harsh conditions and lead to mostly highly reactive unstable compounds.[129-131] It is therefore not surprising that RE catalysts do not undergo the typical reaction pathways of d-block elements (*i.e.*, oxidative addition and reductive elimination). Thus, traditionally, only Yb^{2+}, Tm^{2+}, Dy^{2+}, Eu^{2+}, Sm^{2+}, and Nd^{2+} were known to be isolable in the oxidation state +II. However, the strict rule that most RE elements exist only in oxidation state +III was elucidated to be wrong within the past years, by the results of the group of William J. Evans among other scientists.

In 1988, Evans et al. presented the formation of the dinitrogen Sm complex $(C_5Me_5)_2Sm\text{-}(\mu\text{-}\eta^2\text{:}\eta^2\text{-}N_2)\text{-}Sm(C_5Me_5)_2$ from the reaction of a strongly reductive divalent $(C_5Me_5)_2Sm$ precursor and N_2.[132] The existence of other Ln^{2+} intermediates from trivalent precursors was proposed by the isolation of similar dinitrogen complexes (see Scheme 5).[133-138] A final evidence for a mononuclear Ln^{2+} species was reported by Lappert et al. via the isolation and verification of the first low valent species of stable La^{2+} and Ce^{2+} compounds.[139] The reduction of bulky $(C_4H_3TMS_2)_3Ln$ (Ln = La, Ce) complexes with K mirror in ethereal solvents resulted in the formation of a K^+ $(C_4H_3TMS_2)_3Ln^-$ complex with Ln^{2+} metals centers stabilized by crown ethers.[139] Based on this work, Evans et al. were able to synthesize the first crystallographically characterizable molecular complex of Y^{2+} in 2011.[140] Subsequently this approach was extended to the metal centers Ho^{2+} and Er^{2+}.[141] In 2013, the series of +2 ions (except the radioactive ^{61}Pm) was completed by Evans et al. for Pr^{2+}, Gd^{2+}, Tb^{2+}, and Lu^{2+}.[142]

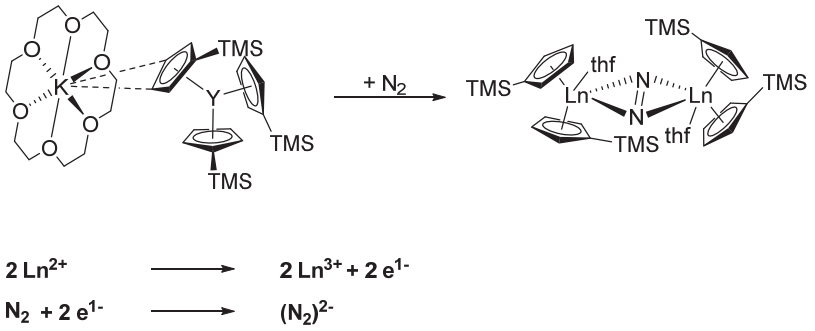

Scheme 5. Molecular Ln^{2+} complexes are strong reducing agents and reduce nitrogen forming dinitrogen complexes with $(N=N)^{2-}$ ligands.

In addition to new stable Ln^{2+} species, the group of Evans reported the first synthesis of a $(C_5Me_5)_3Ln$ (Ln = Sm) compound.[143] Previously, $(C_5Me_5)_3Ln$ complexes were believed to be sterically too crowded to exist due to the fact that one single $(C_5Me_5)^-$ ligand needs more than 120° at the metal center.[144-145] Therefore, three $(C_5Me_5)^-$ ligands would exceed 360° at the metal center; this simple statement was accepted to be true for many decades.[146] However, for $(C_5Me_5)_3Sm$, all $(C_5Me_5)^-$ ligands have a cone angle of 120° by moving further away from the metal center (see Figure 8).[143]

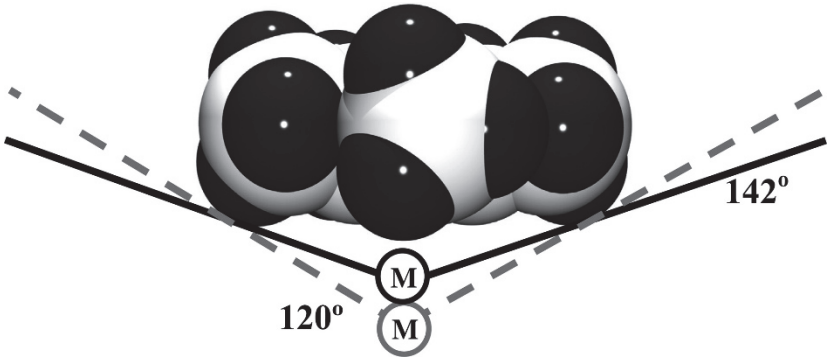

Figure 8. Expansion of the metal-ligand bond distance to accommodate three $(C_5Me_5)^-$ ligands around a metal center. The "normal" cone angle of 142° (solid line) results when the metal-ring centroid distance is of average bond distance. A smaller cone angle (dashed line) results when the metal is located further away from the ring (reprinted with permission from ref. 151. Copyright 2005 American Chemical Society).

Despite the Sm metal center being well shielded by its surrounding ligands, $(C_5Me_5)_3Sm$ has a high reactivity toward various substrates. In the presence of THF, $(C_5Me_5)_3Sm$ decomposes to form the ring-opening alkoxide adduct and with ethylene C_5Me_5 end capped poly(ethylene) is formed.[147-148] The general high reactivity is attributed to a $(\eta^5\text{-}C_5Me_5)_2Sm(\eta^1\text{-}C_5Me_5)$ transition state, allowing coordination of substrates.[148] Even redox chemistry, related to the redox chemistry of the divalent $(C_5Me_5)_2Sm$, was observed for the trivalent $(C_5Me_5)_3Sm$![144,147] In this case, Sm^{3+} cannot be the reducing agent and no Sm^{4+} compounds were observed during the reaction.[144] Therefore, the reduction process must originate from the ligand system and in fact $(C_5Me_5)^-$ is oxidized and $(C_5Me_5)_2$ is formed within the redox reaction.[149] $(C_5Me_5)_2$ was found previously as a byproduct for the reaction of $(C_5Me_5)_2Sm(thf)_2$ and cyclooctatetraene.[150] This interesting and surprising process was named sterically induced reduction.[151-152] Furthermore, the reaction of CO and $(C_5Me_5)_3Sm$ was reported by Evans et al..[153] With CO a thermally stable, nonclassical, 7-norbornadienyl carbocation is formed and was characterized crystallographically.[153] The sterically induced reduction of CO and $(C_5Me_5)_3Nd$ or $(C_5Me_5)_3U$ led to the formation of a nonclassical carbonium ion complex for neodymium, or in the case of uranium, an adduct complex was reported (see Scheme 6).[154]

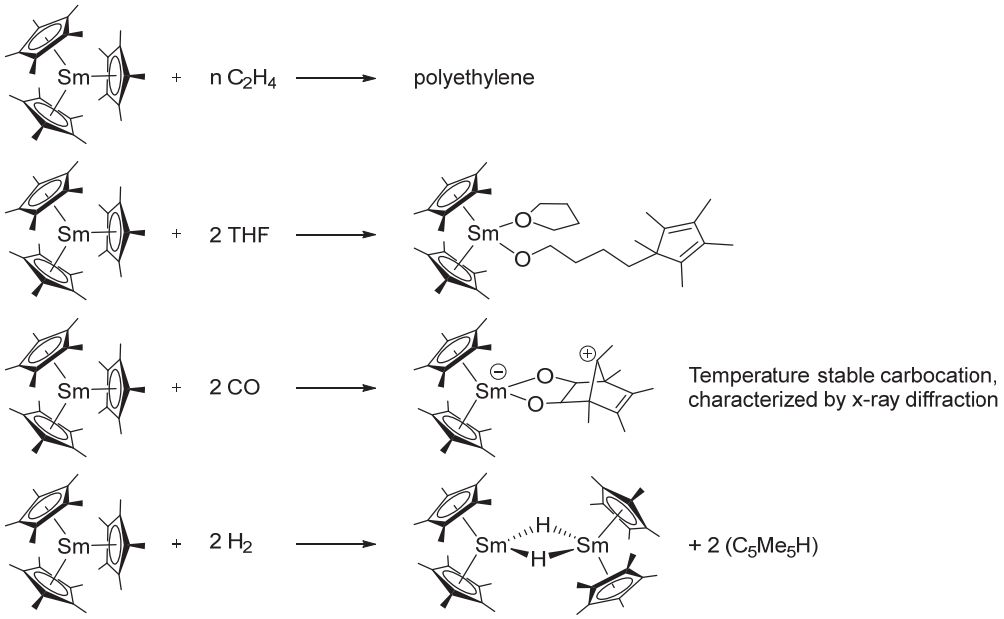

Scheme 6. Reactivity of $(C_5Me_5)_3Sm$ with various substrates.

Within a few years, fundamental areas in RE chemistry (such as oxidation state and maximum steric crowding) were changed and classic textbook chemistry became outdated. This shows that researcher need to be able to think beyond traditional mindsets and by questioning the barriers of conventional assumptions, new chemistry can become available.[144,155]

3.3 Synthetic Methods

The first step before studying new compounds with potentially intriguing properties is the synthesis of new substances, materials, and/or catalysts. Therefore, an ideally simple, convenient, and variable synthetic access is needed for preparative working chemists. Unfortunately, the synthesis of precursor molecules is often underappreciated in the development of a new chemistry.[144] In the case for RE element chemistry, the Ln–C bond has a strong ionic character and different routes were developed for the synthesis of interesting organometallic RE complexes. RE metal-based metallocenes were first synthesized in 1954 via salt metathesis.[156] Due to the similar reactivity of RE elements and alkali metals toward iron halides (formation of ferrocene), the RE metals appeared to be trivalent extensions of the ionic alkali metals.[156-157] Associated with this assumption, little interesting chemistry was expected for RE metals and in particular for $(C_5H_5)_3Ln$ metallocenes. Despite the variable electron counts and configurations for $(C_5H_5)_3Ln$ (Ln = La-Lu) complexes, all of the THF adducts have similar structures and reactivities.[158] This is in sharp contrast to the metals of the d-block, *e.g.*, ferrocene and cobaltocene displaying highly different reactivities and properties. The similar chemical behavior and lack of reactivity of $(C_5H_5)_3Ln$ compounds is in sharp contrast to the high activity of their $(C_5Me_5)_3Ln$ counterparts with various substrates (*vide supra*).

Previously to this work, our group mostly used the well-established salt metathesis and amide elimination from bdsa precursor systems for the preparation of RE metal complexes.[104,159] Also parts of this work are based on salt metathesis routes (see Chapter 4.4), however, for the previously presented challenges in the field of vinylphosphonate REM-GTP (see Chapter 2.1 – 2.3), those methods were found to be too specific or limited in their range of accessible substrates to tackle all scientific questions.[108] In this work, synthetic approaches to new initiators from C–H bond activation via σ-bond metathesis, ligand induced steric crowding in REM-GTP of vinylphosphonates, and finally the identification of suitable ligand systems for the stereospecific polymerization of vinylphosphonates were evaluated and conducted. Therefore, not only one synthetic route could be used and a wider approach was necessary. Taking this into account and for a better understanding, salt metathesis, amide elimination (*i.e.*, bdsa), and alkyl elimination (*i.e.*, $-CH_2TMS$) will be briefly presented in this chapter.

3.3.1 Rare Earth Metal Complexes Obtained via Salt Metathesis

Salt metathesis usually offers a direct access to RE metal compounds, is, however, very sensitive to impurities and often leads to the formation of ate-complexes (see Figure 9). The large size of the RE metal cations and their preference for high coordination numbers are a challenge to be met for RE catalysts. If the ligands do not sufficiently stabilize the metals center, electronic and steric saturation can be achieved by the formation of anionic RE halide and alkali halide ionic compounds. Such complexes are commonly observed from salt metathesis reactions and are also known as ate-complexes.[146,160-163] Removal of salts contaminations after the reaction is usually hindered or even impossible and in general the reactivity of ate-complexes is significantly lowered.[164]

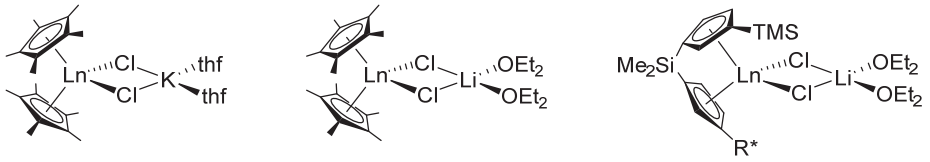

Figure 9. Overview on different ate-complexes as products from salt metathesis reaction.[160-163]

The simple synthetic protocol of salt metathesis was not notably modified for RE metal compounds since the first report of Wilkinson et al..[156-157] Usually the donor-free $LnCl_3$ salt is suspended in a donor solvent (*i.e.*, THF, Et_2O) and a deprotonated metal salt (usually alkali elements, in some cases alkaline earth elements) of the corresponding ligand is added subsequently. In terms of reactivity for RE metallocenes, potassium cyclopentadienyls have higher reactivities than the corresponding sodium or lithium salts and are often preferred for the synthesis of sterically crowded tris$(C_5R_xH_y)_3Ln$ compounds.[165]

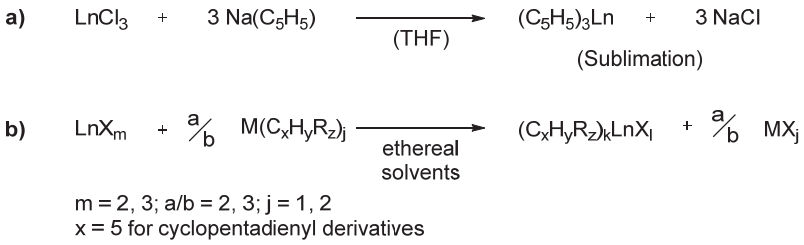

Scheme 7. Synthesis of RE metal complexes by salt metathesis reactions. a) Original synthesis route according to Wilkinson. b) General presentation.

The reaction of YCl_3 and an excess of Li(C_5H_4TMS) results in the formation of $(C_5H_4TMS)_2YCl$ and is unaffected by the yttrium to lithium salt ratio (3, 4, or 5 eq. Li(C_5H_4TMS)).[166] The reactivity of potassium cyclopentadienide is higher than sodium (> lithium) compounds and for the synthesis of sterically crowded (via ligand or metal center modifications) RE metal metallocenes the use of potassium precursors is advised if not mandatory (see Scheme 8).[166]

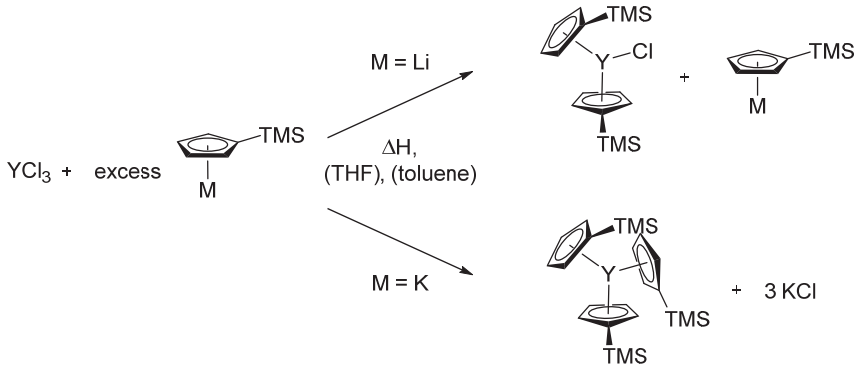

Scheme 8. Comparison of salt metathesis from lithium and potassium cyclopentadienyl precursors.[166]

Despite the simplicity of the salt metathesis route and the few needed reaction steps, the range of accessible structures is limited by low yields, solubility and purification issues, or lack of ligand modifications (*i.e.,* bridged structures).[124] An interesting approach for the synthesis of solvent-free highly sterically crowded RE metal compounds is followed by the group of Evans. The solvent-free isolation of highly sterically crowded RE metal complexes is a requirement for their synthesis. Donor molecules such as THF are likely to react with the sterically overcrowded metal centers resulting in stable decomposition products (*vide supra*, see Scheme 6).

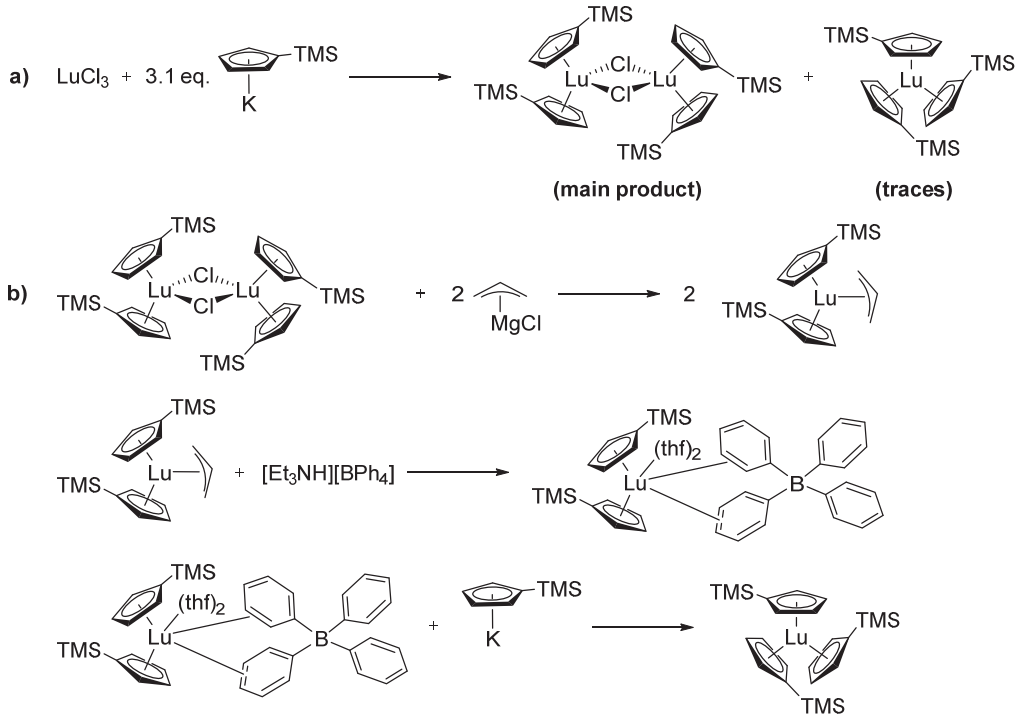

Scheme 9. a) The direct synthesis of sterically overcrowded RE complexes is often not possible. b) Cationic tetraphenylborate intermediates are a key step for the synthesis of many $(C_5Me_5)_3Ln$ or $(C_5H_4TMS)_3Ln$ complexes.

The synthesis route presented above was important for the synthesis of $(C_5H_4TMS)_3Lu$ and this compound was used for completing the series of Ln^{2+} ions also for the smallest Lu metal center (see Chapter 3.2).[167] Furthermore, the chloride/allyl/tetraphenylborate route was a significant development for the feasible synthesis of $(C_5Me_5)_3Sm$ from trivalent precursors.[160] Besides the significant work of Evans

on several challenging RE compounds obtained from salt metathesis reactions, the distinct drawbacks of this method (*vide supra*) limit the use of RE salt metathesis. Therefore, other methods involving the elimination of volatile compounds were consequently developed in the late 1980. The next chapter covers the process and changes in the field of amide elimination reactions.

3.3.2 Homoleptic Amide Precursors

A challenge to be met especially for homoleptic RE compounds is the formation of ate-salt complexes and their prevention. Therefore, sterically demanding amides are used and salt metathesis is often conducted in the first reactions steps in non-coordinating solvents to avoid ate-salt contaminations. Using this procedure, basic amide ligands such as (bis(trimethylsilylamide), btsa, $-N(SiMe_3)_2$, and bdsa, see Figure 10a) can be introduced at the metal center and the final complexes are obtained by amide elimination and deprotonation of an acidic ligand. The donor coordination allows the isolation of otherwise labile homoleptic compounds. If no stabilization of the RE cation is possible, RE complexes tend to form polymeric networks, resulting in a low solubility.[164]

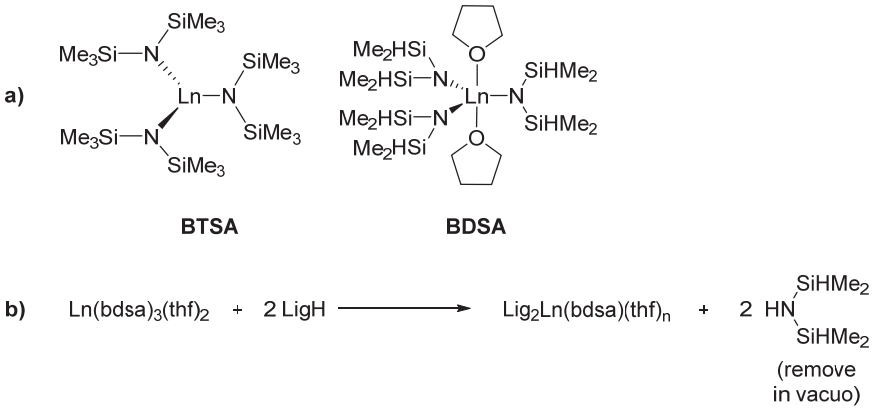

Figure 10. a) Comparison of btsa and bdsa RE complexes. b) Example for the formation of a RE bdsa complex via amide elimination.

Homoleptic group 4 complexes with σ-donor amide ligands were first prepared to introduce new binding motifs and to face some of the limitations of the salt metathesis route in 1959.[168-169] The binding motif and a possible nitrogen-metal π- bond and a sp^2 hybridization of the nitrogen was controversially discussed.[170] The planarity of the nitrogen is supported by crystal structures, ESR studies, and IR spectrometry.[171] In 1968, Lappert et al. studied the reactivity of tetrakis(amido) titanium, zirconium, and hafnium compounds with a broad scope of substrates including C_5H_6 and indenylH.[172] Simple amide precursors ($-NMe_2$, $-NEt_2$, $-NiPr_2$) were successfully used for the synthesis of a variety of group 4 *ansa*-metallocene complexes.[173-175] The advantages of the amine elimination route compared to simple salt metathesis were reported to be higher yields of the desired *rac*-isomer and an improved purification/better yields. The reaction of ethylene-bis(indenyl)H_2 and titanium amide complexes did not result in the formation of *ansa*-titanocene products.[173] The product ratio of *rac*- to *meso*-isomer is controlled for zirconocenes by the removal of the formed amine from the equilibrium and the final product formation is a result from various chemical reaction equilibria.[176-177] The kinetic product for the metallocene was reported to be exclusively the *rac*-isomer and the thermodynamic *rac*/*meso* ratio was 4/1.[176]

In the case of RE elements, the application of such bisalkylamides leads to the formation of oligomeric compounds or polymeric networks resulting in a decreased reactivity, low solubility, and challenging purification and/or characterization. The agglomeration is a result of both steric and electronic factors and may be attributed to the high basicity of bisalkylamides (*e.g.*, pKa($HNiPr_2$) = 36.0)[178] as well as to a steric undersaturation of the large RE metal center. The high basicity (*i.e.*, reactivity) also facilitates the formation of ate complexes.[104,124,164] For the utilization of the amine elimination reaction for RE metal centers, sterically demanding amides were needed to stabilize the large cations. Therefore, RE silylamides (*e.g.*, btsa) amide precursors were first synthesized by Bradley et al. in 1972 and reported to be solvent-free and monomeric.[179-181] In 1973, the crystal structures of $Ln(btsa)_3$ (Ln = Sc, Eu) were reported and the early results were summarized in a review article in 1977.[182-183] The reaction of $Ln(btsa)_3$ and $(C_5Me_5)H$ resulted in a mixture of products of $Ln(btsa)_3$, $(C_5Me_5)_2Ln(btsa)$, and $(C_5Me_5)Ln(btsa)_2$.[184] The reaction of $Ce(btsa)_3$ and 3 equivalents $(C_5H_3TMS_2)H$ was reported to yield $(C_5H_3TMS_2)_3Ce$.[185] Morawietz reported in his PhD thesis the synthesis of the bridged $Me_2Si(C_5H_4)_2Y(btsa)$ complex via amine elimination in THF in 90% yield (see Scheme 10).[171] The product yield is very sensitive toward the reaction conditions (starting temperature, solvent, concentrations) and in nonpolar solvents oligomeric or polymeric byproducts are obtained. The pKa value of btsa amides was reported to be 25.8 in thf.[186]

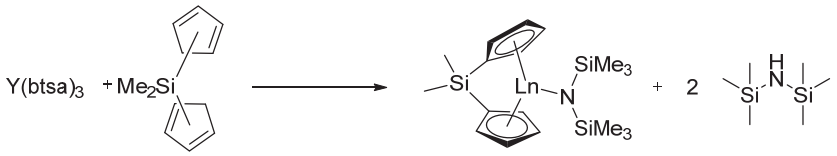

Scheme 10. Reaction of $Y(btsa)_3$ and $Me_2Si(C_5H_5)_2$ and formation of $Me_2Si(C_5H_4)_2Y(btsa)$ and Hbdsa.

The main disadvantages of btsa precursor complexes is their low reactivity against sterically demanding ligands such as substituted cyclopentadienyls due to steric oversaturation and a strong shielding of the metal center. Therefore, RE bdsa precursor systems were used since the 1990.[125,187-190] Contrary to $Ln(btsa)_3$ compounds, bdsa complexes are obtained as thf adduct of the formula $Ln(bdsa)_3(thf)_2$, have an expended trigonal bipyramidal molecular geometry with thf in the axial positions, and the thf coordination in the final complexes allows the metal center to be accessible for further modifications.[187-188] Using the extended bdsa silylamide route, a variety of *ansa*-RE metal metallocenes was synthesized from the corresponding protonated ligands, characterized, and studied by Eppinger and Anwander.[124,188,190] The RE metal center of bdsa complexes is stabilized by a strong β-Si–H "diagostic" interaction (see Figure 11).[188,191]

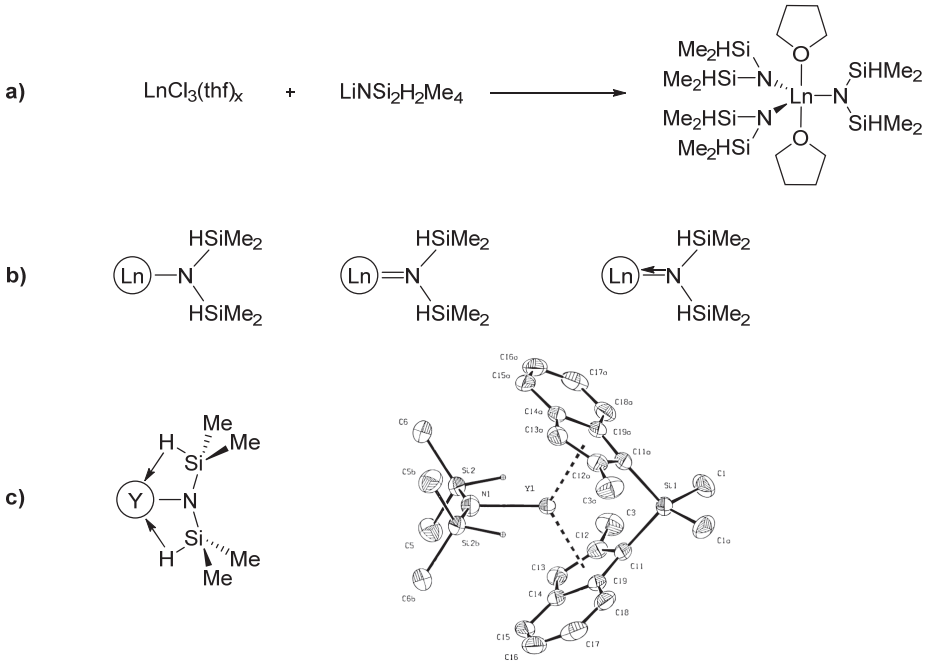

Figure 11. a) Synthesis of the $Ln(bdsa)_3(thf)_2$ precursor complex. b) Possible different coordination modes of bdsa to the RE metal center. c) β-Si–H diagostic interaction stabilizing the large RE metal center. Crystal structure of *rac*-(2-methylindenyl)$_2$SiMe$_2$Y(bdsa) (adapted with permission from ref. 188. Copyright 1997 American Chemical Society).

Bdsa compounds can be handled easily, their synthesis is facile, and the pKa of bdsa was determined to be 22.8 and is therefore sufficient for the deprotonation of most cyclopentadienyl compounds and its derivatives (*e.g.*, indenyl, fluorenyl).[190] A book review was published by Anwander on lanthanide amides.[192] However, the scope of ligands remains limited by the low pKa value of silylamides and the synthesis of modern post-metallocene compounds is hindered by simple amine elimination. Therefore, strong, basic homoleptic hydrocarbyl precursors were developed and will be presented in the next chapter.

3.3.3 Homoleptic Hydrocarbyl Precursors

The pKa values of RE hydrocarbyl compounds are not yet determined in literature, but can be estimated to be above 45 (pKa methane = 56 > pKa RE–CH_xR_y > 45 > pKa benzene = 43) and give access to the activation of a variety of functional groups and ligand systems.[193] Simple, soluble RE hydrocarbyl species can consists of bis(trimethylsilyl)methyl, (trimethylsilyl)methyl), or neopentyl ligands. In a pioneering study, Lappert et al. synthesized the first homoleptic $Ln(CH_2TMS)_3(thf)_2$ and $Ln(CH_2CMe_3)_3(thf)_2$ (Ln = Sc, Y) compounds in 1973.[194] The synthesis is usually performed in nonpolar solvents starting with one equivalent of the RE THF adduct and three equivalents $LiCH_2TMS$ under cooling (see Scheme 11).

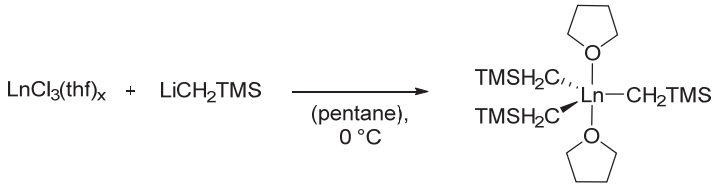

Scheme 11. Synthesis of $Ln(CH_2TMS)_3(thf)_2$.

LiCl and $Ln(CH_2TMS)_3(thf)_2$ are formed and $Ln(CH_2TMS)_3(thf)_2$ can be separated from suspended LiCl and oligomeric insoluble coordination polymers in moderate to high yields. For a successful synthesis of $Ln(CH_2TMS)_3(thf)_2$ it is essential to use nonpolar solvents and the RE thf adduct as the thf donor solvent coordination results in a steric saturation, stabilization of the RE metal center, reduction of the formation of coordination polymers, and an increased solubility. RE element hydrocarbyl compounds are only stable if the coordination sphere is saturated[195-196] and due to steric restrictions the synthesis of $Ln(CH_2TMS)_3(thf)_2$ is limited to the smaller RE cations as decomposition reactions accelerate with increasing RE meter center size. No $Ln(CH_2TMS)_3(thf)_2$ complexes of lanthanum, cerium, praseodymium, neodymium, and promethium (radioactive) are reported in literature and yields and literature references for all synthetically accessible $Ln(CH_2TMS)_3(thf)_2$ RE metal compounds are summarized in Table 2.

Table 2. $Ln(CH_2TMS)_3(thf)_x$: Synthesis, thf Coordination, Yield, and Characterization

RE metal center	$THF_{(coord.)}$	Yield [%]	Characterization	Reference
Sc	2	71	^1H, ^{13}C, IR, EA, mp,	ref. 194,197
Y	2, 3	69 – 82	^1H, ^{13}C, ^{29}Si, IR, EA, mp, x-ray	ref. 194,197-199
Lu	2	63 – 65	^1H, ^{13}C, IR, EA, x-ray	ref. 197,200-202
Yb	2	48	^1H, IR, EA, mp, x-ray	ref. 201-204
Tm	2	-	IR, EA	ref. 201,205
Er	2	29	IR, EA, mp, x-ray	ref. 201-202,204,206
Tb	2	-	IR, mp, x-ray	ref. 204
Sm	3	50	^1H, ^{13}C, IR, EA, mp, x-ray	ref. 202

Analog to organometallic transition metal compounds, the main decomposition pathway for RE metal hydrocarbyl complexes is the β-hydride elimination.[195] The use of alkyl ligands with alkyl substituents in the β-position (to the metal) prevents this side reaction.[207] However, contrary to this perception, $Ln(CH_2TMS)_3(thf)_2$ compounds decompose at ambient temperature as solid or in dissolved state within hours. Therefore, other decomposition pathways involving the formation of $SiMe_4$ must exist for such homoleptic compounds and an α-H elimination was first supposed,[206] but later disregarded for a more likely γ-H Elimination (see Scheme 12).[207]

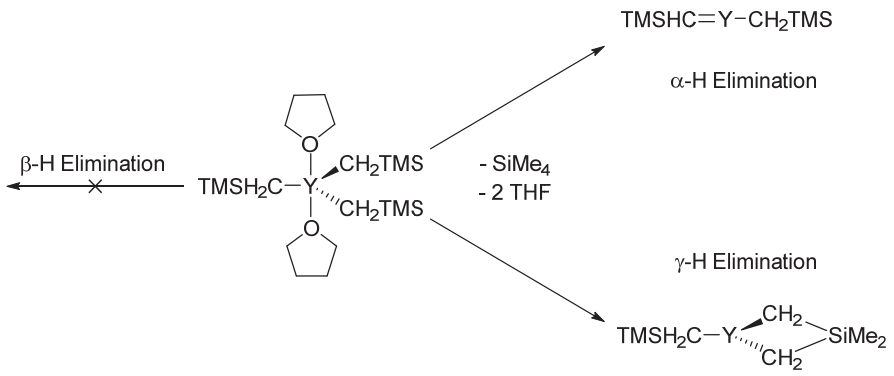

Scheme 12. Thermal decomposition pathways of $Lu(CH_2TMS)_3(thf)_2$.

The introduction of the $-CH_2TMS$ ligand gave access to numerous monoalkyl and dialkyl RE $-CH_2TMS$ complexes[164,208-209] and avoids the laborious purification steps and ate-complex formation from the reaction of RE halides and MeLi.[103,210] Although the synthesis of $Ln(CH_2TMS)_3(thf)_2$ precursor complexes was first reported by Lappert et al. for the RE metals scandium and yttrium as early as 1973, its chemistry remained dormant for decades.[164] Starting in the late 1990s, research and use of $Ln(CH_2TMS)_3(thf)_2$ compounds intensified and it remains the precursor route of choice for late RE metal cations to date. Until today, RE (trimethylsilyl)methyl derivatives are the most widely applied alkyl ligands in RE organometallic chemistry.[164]

Contrary to transition metal complexes, the neopentyl counterparts have never been widely used for the preparation of RE hydrocarbyl species due to their lower stability. The low thermal and light-stability of RE $-CH_2CMe_3$ compounds is attributed to the missing α-agostic interaction of the neopentyl ligand and the RE metal center.[164] The corresponding $Ln(CH_2CMe_3)_3(thf)_2$ precursors and other compounds consisting of RE$-CH_2CMe_3$ bonds decompose under exposure to light and are temperature sensitive due to a β-Me elimination decomposition limiting their use tremendously.[164,211]

The application of the bulky bis(trimethylsily)methyl ligand with RE metals leads to neutral, homoleptic, solvent-free precursor systems of the formula $Ln(CHTMS_2)_3$ and were first reported by Lappet et al. in 1974.[212] The structural characterization of $Ln(CHTMS_2)_3$ followed later for Ln = La and Sm.[213] The highly sterically demanding $-CHTMS_2$ ligands result in similar steric restrictions as btsa compounds having a lower reactivity for many substrates despite the high pKa value (~pKa > 45).

The reaction of bridged amine-cyclopentadienyl proligands and $Ln(CH_2TMS)_3(thf)_2$ leads to the formation of RE constrained geometry complexes (CGC, see Scheme 13a).[214] Group IV CGCs became prominent for the polymerization of sterically demanding α-olefins.[215] The introduction of an additional TMS group for the bis(trimethylsilyl)methyl ligand result in a significant higher shielding of the metal center and usually donor free (*i.e.*, THF free) and to some extend temperature stable complexes are obtained (see Scheme 13a).[216] The coordination sites at the metal are either less open or blocked and the bis(trimethylsilyl)methyl ligand is inert for the reaction with sterically demanding ligands (*e.g.*, CGC, and/or TMS substituted Cp ligands) and/or limited to early and middle $Ln(CHTMS_2)_3$ RE metals.[164,216] One report in literature describes the synthesis of donor free and stable in aromatic solvents (CGC)$Ln(CHTMS_2)_3$ compounds (Ln = Yb, Lu).[217] RE complexes based on tris(trimethylsilyl)methyl ligands ($-CTMS_3$) are only accessible for the divalent RE elements Yb, Eu, and Sm; limiting their applications (see Scheme 13b).[164,218-220]

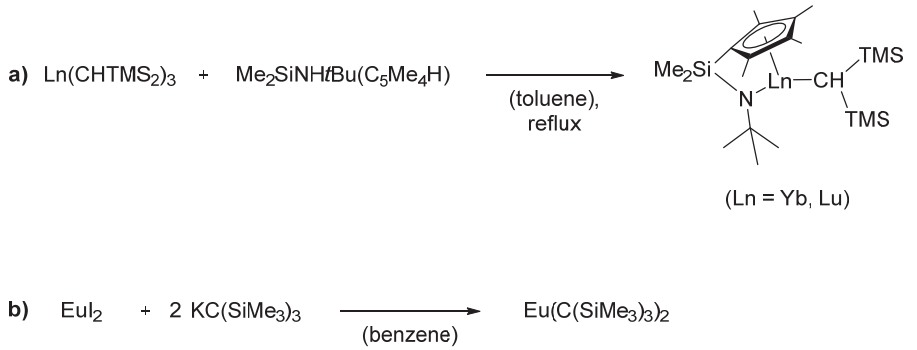

Scheme 13. a) Synthesis of donor solvent-free RE CGCs. b) Formation of the sterically crowded divalent europium hydrocarbyl complex $Eu(C(TMS)_3)_2$.

Despite their drawback (thermal stability, cation size restrictions), $Ln(CH_2TMS)_3(thf)_2$ compounds are nowadays widely used as precursors for RE alkyl complexes and the protonolysis of one, two, or three

$-CH_2TMS$ ligands under formation of $SiMe_4$ leads to a large variety of heteroleptic RE element complexes.[164] Particularly, the access to catalytically highly active cationic RE alkyl derivatives is currently an interesting research topic.[208-209]

3.3.4 Summary of the Different Synthetic Methods

The last chapters gave an overview about the most commonly applied synthesis and precursor routes for the organometallic chemistry of RE elements. Other, more "exotic" synthesis routes were previously described in other PhD theses.[104,124] Salt metathesis is the oldest method to prepare RE metallocenes, satisfies with its simplicity, and can usually be performed in few steps. It is, however, very sensitive to impurities and the yields, ligand design, and purification are often limited (*e.g.*, by ate-complex formation).

Therefore, amide elimination reactions were subsequently developed and applied for RE elements and btsa or bdsa precursor complexes usually avoid the formation of ate-complexes. The basicity is sufficient for many cyclopentadienyl derivatives and the Ln–N bond is stable enough to perform complex syntheses at elevated temperatures and room temperature stable catalysts are obtained. RE complexes with btsa ligands are obtained without coordinated thf donor molecules, however, the high steric demand limits this route. Sterically less demanding bdsa ligands avoid this problem, are more flexible to use, and represent the extended silylamide route.[124]

$Ln(CH_2TMS)_3(thf)_2$ complexes are the most successful applied RE metal alkyl precursor complexes. Compared to their neopentyl counterparts, the higher thermal and light stability of $Ln(CH_2TMS)_3(thf)_2$ precursors is attributed to an α-agostic interaction between the silicon and RE metal center. The donor-free $Ln(CHTMS_2)_3$ or $Ln(CTMS_3)_2$ complexes are limited to specific synthesis routes.

In view of the given synthetic background, the present study had the target to establish feasible synthetic methods for the synthesis of (novel) nucleophilic ligands for the initiation reaction of vinylphosphonate REM-GTP (ideally with mechanistic match between initiation and propagation, see Chapter 4.3). In first attempts, enolate ligands and related structures were studied to facilitate a fast uniform initiation of vinylphosphonates via an $8e^-$ process (see Scheme 14a). Alkyl ligand-containing metallocenes were chosen as possible target substrates due to the high pKa value of the alkyl ligand (pKa > 45, *vide supra*) and their synthesis was previously established at our chair via salt metathesis and alkane elimination reaction (see Scheme 14b).[35,117,221-222] Furthermore, to achieve a better understanding of the initiation and to obtain reliable data, the simple $(C_5H_5)^-$ metallocene ligand system had to be studied in order to compare the data to previously described $(C_5H_5)^-$ based catalysts. Therefore, $[(C_5H_5)_2YbMe]_2$ or $(C_5H_5)_2LnCH_2TMS(thf)$ (Ln = Y, Lu) turned out to be possible candidates. The synthesis of $[(C_5H_5)_2YbMe]_2$ includes two salt metathesis reactions, laborious purification steps, low yields, and ytterbium as a paramagnetic core prevents extended NMR studies. Therefore, simple $(C_5H_5)_2LnCH_2TMS(thf)$ complexes were obtained via alkane elimination reaction and used as starting material to test their reactivity with various substrates to form new initiating ligands.

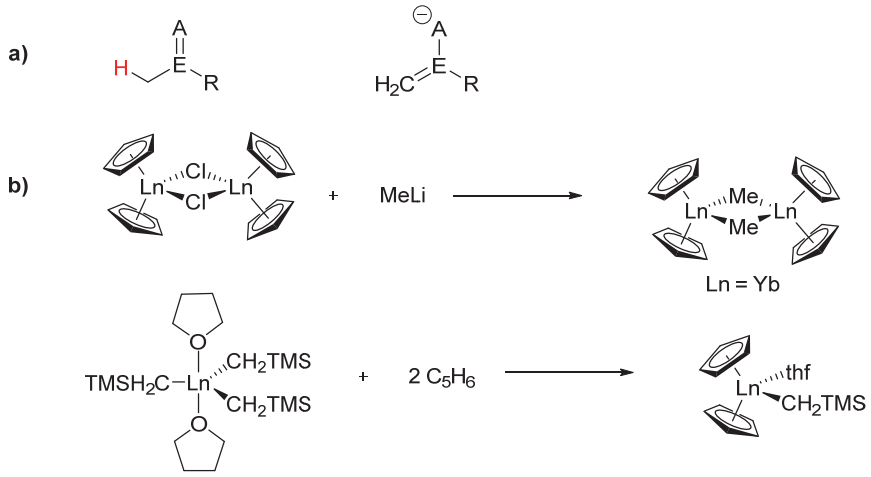

Scheme 14. a) General presentation of a conjugated system. b) Synthesis of RE alkyl metallocenes via salt metathesis (top) vs. alkane elimination (bottom).

After studying and optimizing the initiation reaction of vinylphosphonate REM-GTP, the propagation and the impact of metallocene ligand modification turned out to be an interesting scientific problem. Due to a better synthetic access, salt metathesis was chosen in this case above the $-CH_2TMS$ route to study the effect of ligand induced steric crowding for unbridged RE metallocenes.

To our knowledge, there are no reports in literature on the synthesis of substituted $(C_5H_yR_x)_2LnCH_2TMS(thf)_n$ complexes via alkane elimination reaction and the synthesis of these starting complexes might be hindered by the formation of unwanted byproducts (kinetic product formation instead of the desired thermodynamic product) or the catalysts can be unstable due to side reactions of the alkyl ligand and the stabilizing coordinated thf. A comparison of activities, initiator efficiencies, or PDI values of substituted $(C_5H_yR_x)_3Ln$ and $(C_5H_yR_x)_2LnCH_2TMS(thf)_n$ with different metals and/or ligand systems will lead to indecisive data and was therefore not conducted. Therefore, only substituted tris(cyclopentadienyl) RE complexes were used for the first study on ligand induced steric crowding for vinylphosphonates (see Chapter 4.4). Furthermore, RE metal complexes that are synthesized via salt metathesis such as $(C_5H_5)_3Ln$, $(C_5H_4Me)_3Ln$, or $(C_5Me_4H)_3Ln$ are in some cases also commercially available at a low price (see Chapter 4.4).

One main results of the conducted temperature dependent activity measurements was the high flexibility of single substituents and the resulting atactic poly(vinylphosphonate) microstructure. Therefore bridged ligand systems were brought into focus in the next step and within this work, it turned out that the limitations of salt metathesis were too substantial to use this method for the synthesis of sterically crowded, bridged, and highly active catalysts for the REM-GTP of vinylphosphonates. Therefore, $Ln(CH_2TMS)_3(thf)_2$ precursor complexes were used for the synthesis of RE CGCs to further study new ligand systems for a stereospecific vinylphosphonate polymerization. RE CGC are literature known and the $-CH_2TMS$ ligands assure access to efficient initiating ligands via σ-bond metathesis.

3.4 C–H Bond Activation

For the past 30 years, there has been continuous research by synthetic chemists to cleave and further functionalize the C–H bonds of hydrocarbons in a selective, catalytic manner. Already in 1985, Robert H. Crabtree dedicated a review article published in *Chem. Rev.* to this task.[223] The activation and conversion of natural gas (*i.e.*, methane), mineral oil, or paraffin (from Latin language meaning "barely reactive") is of both commercial and academic interest. Because of its lack of polarity, low acidity, low HOMO- and high LUMO σ-bonding orbitals,[223] and high bond dissociation energy (~410 kJ·mol^{-1}),[224] the C–H bond of hydrocarbons is among the most inert chemical bonds.[225-227] The strong and nonpolar nature of C–H bonds makes their selective C–H bond activation one of the most challenging tasks that chemists face today.[225-230] Some specialized bacteria use enzymes to provide energy and carbon from methane.[231] In chemistry, traditionally three different modes of action are discussed for C–H bond activation, namely, oxidative addition with electron rich late transition metals, electrophilic activation with electron-deficient late transition metals, and σ-bond metathesis with early transition metals and RE elements (see Figure 12).[232] Additionally, a 1,2-addition is discussed as a possible reaction pathway in the literature for some complexes (see Figure 12b).[233-234] The σ-bond metathesis mechanism is mostly accepted for d^0f^n metals and will be presented on the next pages (see Figure 12a). An oxidative addition and change of the metal's oxidation state is not possible for RE elements (see Figure 12c, Chapter 3.1).

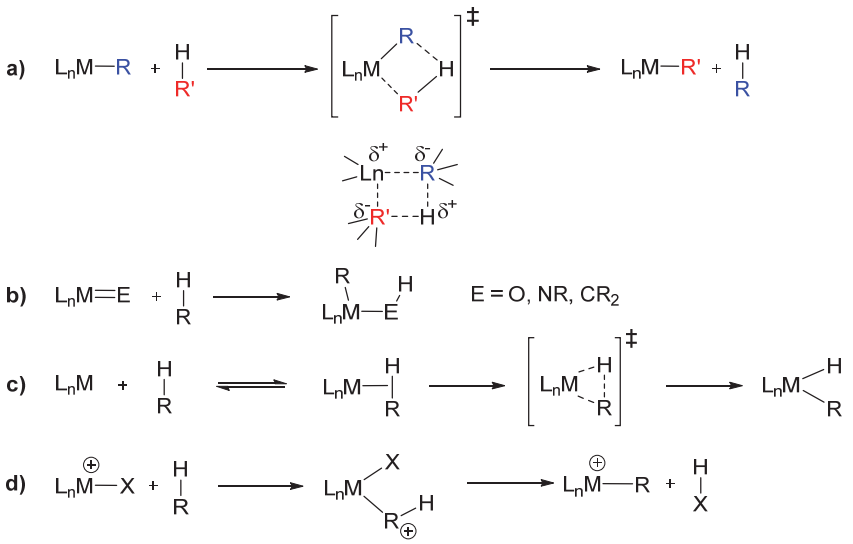

Figure 12. Four possible reaction pathways for C–H bond activation using metal-based catalysts: a) σ-bond metathesis. b) 1,2-Addition. c) Oxidative addition. d) Electrophilic substitution.

In a seminal study, Patricia L. Watson reported the exchange reaction of $(C_5Me_5)_2LnMe$ (Ln = Lu, Y) and ^{13}C-labeled methane (see Figure 13a).[235] The reaction rate increases with larger metal centers, however, this effect was not attributed to steric reasons in its original publication (higher accessibility of the metal center) and was explained by changes of the electrophilicity (see Figure 13b).[236] Mechanistic studies revealed, a concerted bimolecular reaction pathway following a most probable four-center transition state;[237] a mechanism that was later termed σ-bond metathesis.[238] Alternative tuck-in intermediates were originally discussed and later disregarded, however, they are still object of a controversial scientific discussion (see Scheme 15a).[239-241] The ability of non-(C_5Me_5) ligand containing complexes to undergo C–H bond activation contradicts the general tuck-in mechanism pathway. Methane and ethane activation were computed for scandium compounds and the energetically unfavored activation of methane was attributed to a better stabilization by hyperconjugation.[242]

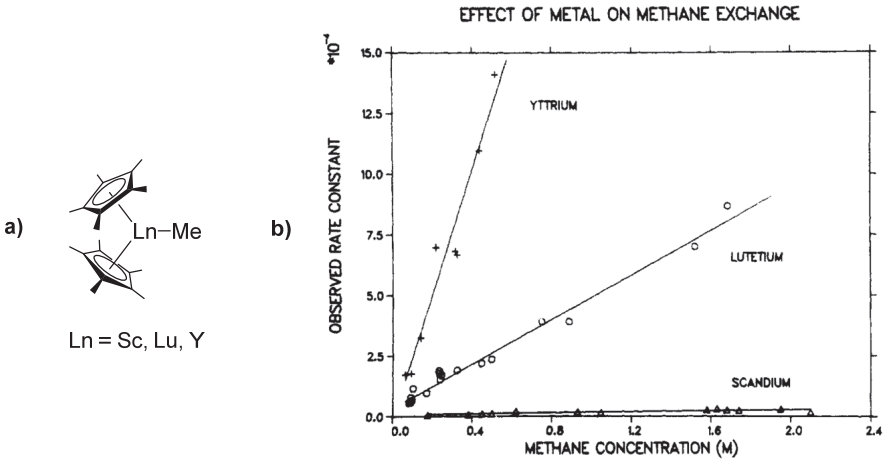

Figure 13. a) Complexes used for methane activation by Patricia L. Watson. b) Effect of RE metal center size on the methane exchange reaction rate (adapted with permission from ref. 236. Copyright 1985 American Chemical Society).

If $(C_5Me_5)_2ScMe$ is heated in cyclohexane at 80 °C for several days, methane is produced and the tuck-over Sc metallocene $(C_5Me_5)(C_5Me_4CH_2)Sc$ is formed (see Scheme 15b).[238] Contrary to the tuck-in structure, the tuck-over structure was later structurally characterized.[243] $(C_5Me_5)(C_5Me_4CH_2)Sc$ reacts with benzene-d_6 to afford a mixture of $(C_5Me_5)_2ScC_6D_5$ (Sc-d_5, major product) and $(C_5Me_5)(C_5Me_4CH_2D)ScC_6D_5$ (Sc-d_6, minor product).[238] Interestingly, if $(C_5Me_5)_2ScMe$ is reacted with benzene-d_6 at elevated temperature a competitive process is observed affecting the ratio of products, involving the bimolecular reaction of $(C_5Me_5)_2ScMe$ with benzene-d_6 to afford Sc-d_5 and CH_3D; and the unimolecular cyclometallation reaction to $(C_5Me_5)(C_5Me_4CH_2)Sc$ with concomitant loss of methane, followed by rapid reaction with benzene-d_6 to give Sc-d_6 (see Scheme 15b). The bimolecular pathway is favored at low temperatures (60 °C, ratio of 76:24), however, at 125 °C equal (50:50) preferences for both pathways were reported (see Scheme 15b).[238-239]

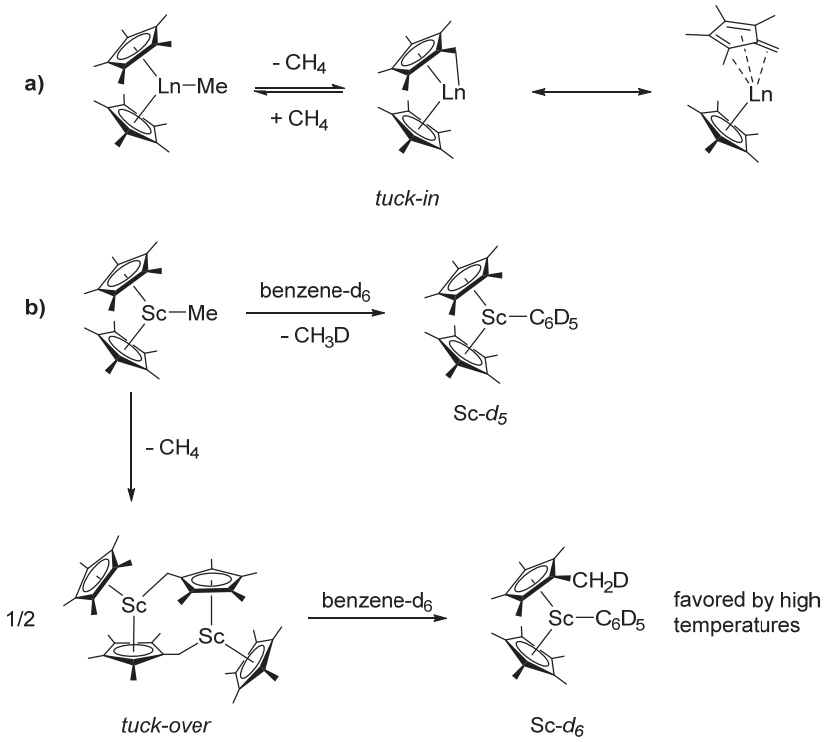

Scheme 15. a) Methane exchange reaction via a proposed tuck-in bridging. Two possible resonance structure of tuck-in or tetramethylfulvene bonding modes are discussed. b) Proposed oligomeric tuck-over structure.

Furthermore, the thermolysis of lanthanide hydride complexes $[(C_5Me_5)_2LnH]_2$ was found to result in the intermolecular C–H bond activation to generate hydride-bridged tuck-over complexes of the form $[(C_5Me_5)Ln(C_5Me_4CH_2)(\mu\text{-}H)Ln(C_5Me_5)_2]$ (Ln = Y,[244] Lu,[245] Sm,[246] La[247]) with simultaneous production of hydrogen gas. The structures of these complexes with a tetramethylfulvene motif were unambiguously characterized by single crystal X-ray diffraction experiments.[244-247] The reaction of $[(C_5Me_5)_2LuH]_2$ and tetramethylfulvene resulted in the formation of the tuck-over hydride bridged Lu compound $[(C_5Me_5)Ln(C_5Me_4CH_2)(\mu\text{-}H)Lu(C_5Me_5)_2]$, however, also $(C_5Me_5)_2Lu(CH{=}C_5Me_4)$, a rare example of a lanthanide vinyl complex, was obtained as the main product.[245]

Evans et al. reported the C–H bond activation of arenes for highly reactive $(C_5Me_5)_3Ln$ complexes for the smaller RE metal center Y.[248] The reaction of $(C_5Me_5)_3Y$ with benzene or toluene was unexpected, because for the larger RE metal centers including neodymium, samarium, and gadolinium the chloride/allyl/tetraphenylborate route using arene solvents did not result in the activation of benzene or toluene.[160,248] In the case of the reaction between $[(C_5Me_5)_2Y][BPh_4]$ and $K(C_5Me_5)$ in arene solvents the sp^2 and sp^3 C–H bond activation of benzene and toluene and no formation of $(C_5Me_5)_3Y$ was observed (see Figure 14a).[248] The analog reaction of $(C_5Me_5)_3Y$ with benzene and toluene (synthesized from $[(C_5Me_5)_2YH]_2$ and tetramethylfulvene) also resulted in the corresponding $(C_5Me_5)_2Y(C_6H_5)$ and $(C_5Me_5)_2Y(CH_2C_6H_5)$ compounds (see Figure 14b).[248]

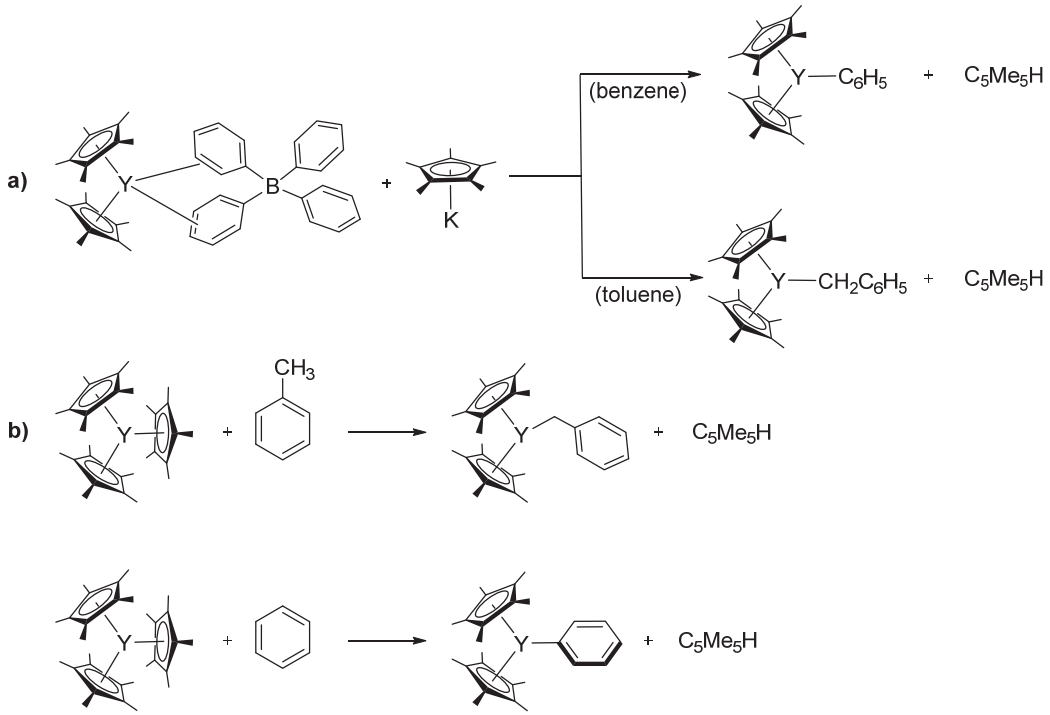

Figure 14. a) Unsuccessful preparation attempts for the synthesis of $(C_5Me_5)_3Y$ in aromatic substrates. b) Activation of benzene and toluene by $(C_5Me_5)_3Y$.

Based on the chloride/allyl/tetraphenylborate route, Evans et al. recently synthesized the extremely reactive unsolvated RE metallocene ethyl complex $(C_5Me_5)_2YEt$ (see Figure 15a).[249] The X-ray crystal structure of the yttrium ethyl complex shows an Y···H_3C agostic interaction and the reactivity of $(C_5Me_5)_2YEt$ was tested for olefin insertion, H_2 activation, C–H bond activation of arenes and methane, and β-H elimination processes.[249] The methane activation was studied with ^{13}C labeled methane and similar results to the work of Patricia L. Watson were obtained (see Figure 15b).

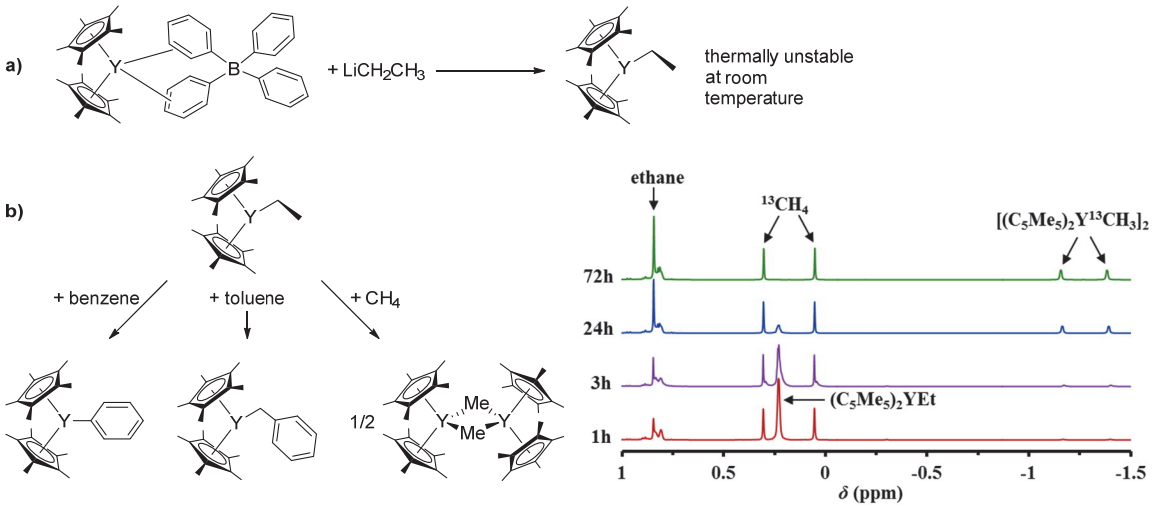

Figure 15. a) Synthesis and reactivity of $(C_5Me_5)_2YEt$ (adapted with permission from ref. 249. Copyright 2015 American Chemical Society).

To study such complexes in less reactive media, inert and deuterated solvents are often used. Especially deuterated cyclohexane (C_6D_{12}) features good properties and does not react with complexes due to steric (secondary and tertiary C–H bonds are less reactive) and isotopic reasons (the zero-point energy of C–D is considerably lower than of C–H bonds). The activation barrier of σ-bond metathesis is mostly controlled by negative $\Delta S^{\ddagger}$ values for the bimolecular process (solvation effect do not contribute to $\Delta S^{\ddagger}$ for the used nonpolar solvents). The strong $\Delta S^{\ddagger}$ terms are a result of significant loss of vibrational and rotational freedom in the transitions state and emphasize the "highly ordered" four centered transition state. An overview on experimentally determined entropy values is given in Table 3.

Table 3. Activation Entropy Data for Selected Examples of σ-Bond Metathesis of Various E–H Bonds

Bond	Reaction	$\Delta S^{\ddagger}$ [kJ·mol^{-1}·K^{-1}]	Reference
As–H	$(N_3N)ZrAsPh_2 + Ph_2AsH \rightarrow (N_3N)ZrH + Ph_4As_2$	−134	ref. 250
sp^2 C–H	$(C_5Me_5)_2ScMe + CH_2{=}CHPh \rightarrow (C_5Me_5)_2ScCH{=}CHPh + CH_4$	−151	ref. 238
sp^3 C–H	$(C_5Me_5)_2ScCH_2tBu + CH_4 \rightarrow (C_5Me_5)_2ScCH_3 + CMe_4$	−151	ref. 251
H–H	$(C_5Me_5)_2Th(CH_2tBu)OtBu + H_2 \rightarrow (C_5Me_5)_2Th(H)OtBu + CMe_4$	−213	ref. 252
P–H	$(N_3N)ZrPHPh + Ph_2PH \rightarrow (N_3N)ZrH + (PhPH)_2$	−151	ref. 253
Si–H	$(C_5H_5)(C_5Me_5)HfCl(SiH_2Ph) + PhSiH_3 \rightarrow (C_5H_5)(C_5Me_5)Hf(H)Cl + (PhSiH_2)_2$	−88	ref. 254
Sn–H	$(C_5H_5)(C_5Me_5)Hf(H)Cl + Mes_2SnH_2 \rightarrow (C_5H_5)(C_5Me_5)Hf(SnHMes_2)Cl + H_2$	−176	ref. 255

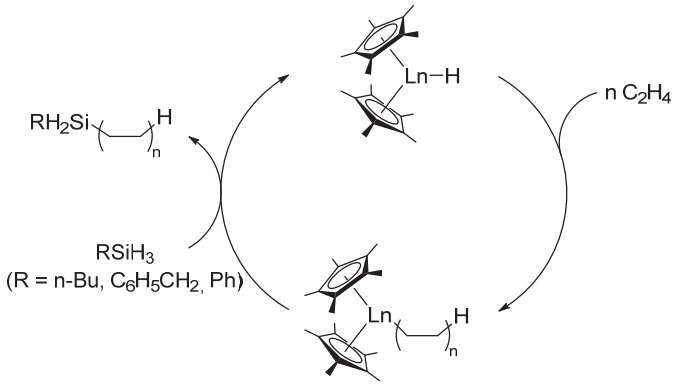

Scheme 16. Proposed catalytic cycle for the formation of silylated poly(ethylene) via σ-bond metathesis.

The in situ end-group functionalization of polyolefins with RE metallocenes was a scientific challenge in the 1990 and silanes were first used as a chain transfer reagent by Marks et al. in 1995.[256] In a detailed study, the polymerization of ethylene, and exchange reaction with silanes following a σ-bond metathesis pathway was published in 1999 (see Scheme 16).[257] The reaction of RE hydrides with silanes can proceed via two possible reaction pathways, one in which the silicon atom is in α-position to the metal center and a second in which silicon is in the β-position to the metal center (see Figure 16a). The first path results in an exchange of a hydride for a silyl ligand and in the latter path the metal hydride ligand is replaced with a hydride from a silane (degenerative exchange). This degenerative exchange mechanism is more likely for Si–H bonds than for analogue C–H bonds of alkanes (absent stabilization of the pentacoordinate carbon atom) and was elucidated in DFT studies for the reaction of $(C_5H_5)_2LaH$ and $H_3C–SiH_3$ (see Figure 16b).[258] The composition of silyl or hydride product from the σ-bond metathesis reaction of metal hydride and silane can be tuned by sterically demanding silane substituents.[259] In further studies, Tilley et al. applied this procedure to phosphine- and amine end capped PE.[260-263]

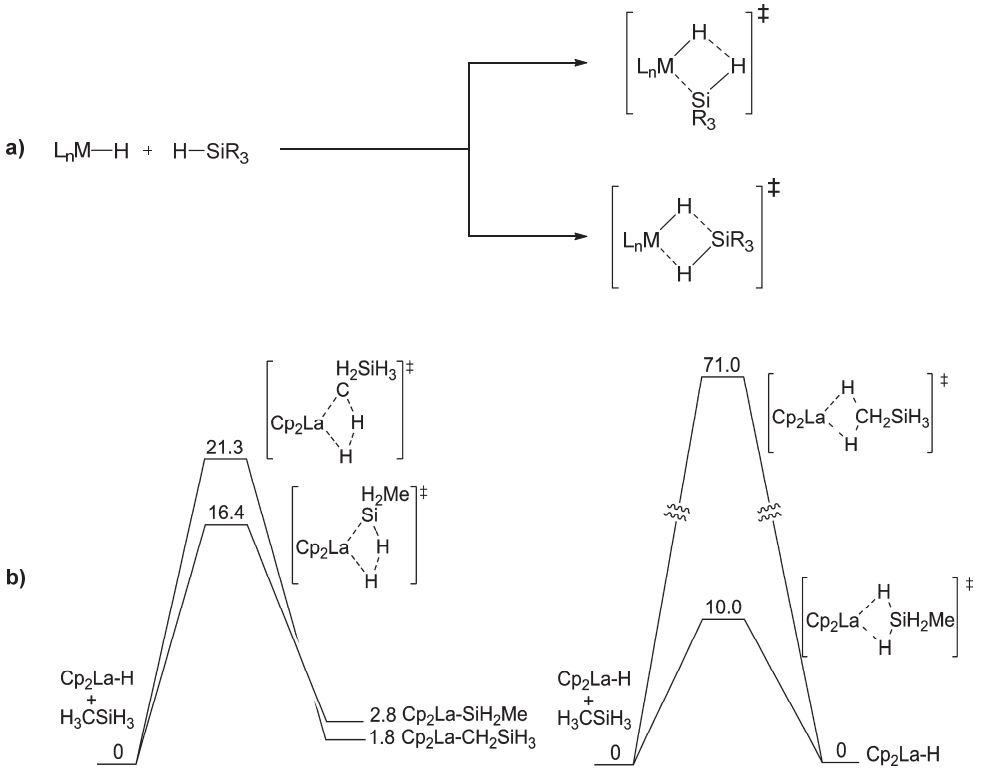

Figure 16. a) The reaction of a metal hydride with silane can either proceed via silicon exchange in the α-position (top) to yield a metal silyl product or with silicon in the β-position to result in a hydride ligand exchange. b) Simplified energy profiles (kcal mol^{-1}) calculated for the reaction of Cp_2LaH with $MeSiH_3$ (reprinted with permission from ref. 264; adapted from ref. 258)

In a report, published in a special issue dedicated to Gregory Hillhouse, Tilley et al. reported in 2015 the sp-, sp^2-, and sp^3-C–H bond activation (intramolecular in the latter case) of monoanionic, PNP-supported scandium dialkyl complexes.[265] C–H bond activation by f-block complexes (with focus on actinide elements) was covered in a review by Arnold et al.,[266] however, not all contributions, especially by Teuben et al., to the field of RE metal C–H bond activation were mentioned. Therefore, a quick overview on Teuben's work will be given here:

Several C–H bond activation reactions of $[(C_5Me_5)_2YH]_2$ and arenes were conducted by Teuben et al. in 1993.[244] The dimer $[(C_5Me_5)_2YH]_2$ reacted with benzene or toluene under the formation of $(C_5Me_5)_2Y(C_6H_5)$ and $(C_5Me_5)_2Y(CH_2C_6H_5)$.[244] In this contribution, the σ-bond metathesis for carbon substrates was also discussed for the carbon in the β-position to the metal center and termed "nonproductive" σ-bond metathesis (*vide supra*, see Figure 16b). For the substituted aromatic substrates PhX (X = –OMe, –SMe, $–NMe_2$, $–CH_2NMe_2$, $–PMe_2$), a strong preference for the ortho metallation at the sp^2 C–H bond and no activation of sp^3 C–H bonds or of substituted X was observed (see Scheme 17a).[244] In 1995, Teuben et al. reported the activation of ethers and sulfides by $[(C_5Me_5)_2LnH]_2$ (Ln = La, Ce, Y) forming alkoxides of the type $(C_5Me_5)_2LnOR$ or metallated compounds $(C_5Me_5)_2LnCH_2SR$ ($–SR_2$, R = –Me) and dihydrogen or thiolates of the type $(C_5Me_5)_2LnSR$ (SR_2, R = –Et) and ethylene (see Scheme 17b).[267] Also the ring-opening of THF and 1,4-dioxane was observed.[267] As opposed to THF and

dioxane, the aromatic substrates furan and thiophene were not opened by $[(C_5Me_5)_2YH]_2$ and a metallation at the α-position of the heteroaromatic substrate was observed instead (see Scheme 17b).[267] Other examples of RE complexes reacting with furan and/or thiophene heterocycles are reported in literature.[268-269]

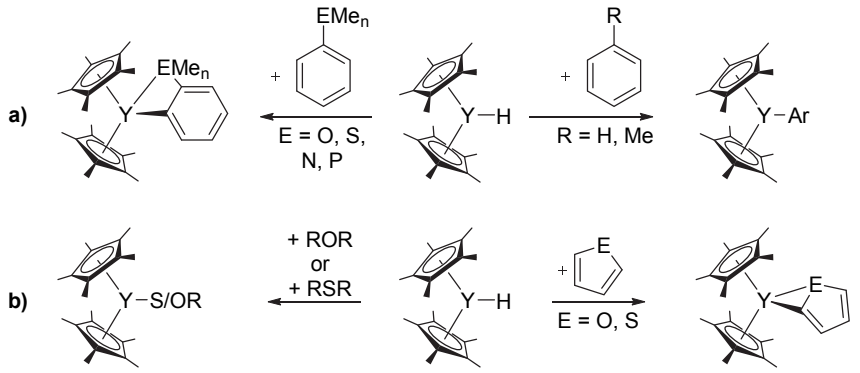

Scheme 17. a) Reaction of $[(C_5Me_5)_2YH]_2$ with aromatic substrates. b) Reaction of $[(C_5Me_5)_2YH]_2$ with heteroaromatic substrates and ethers.

Furthermore, $[(C_5Me_5)_2YH]_2$ was reported to metallate pyridine in the ortho-position forming $(C_5Me_5)_2Y$(2-pyridyl) (see Scheme 18a).[270] Ethylene or propylene can undergo insertion into the RE–carbon bond of $(C_5Me_5)_2Y$(2-pyridyl) and the monoinsertion products are obtained. This contribution is one of the first examples for a RE metal complex catalyzed alkylation of pyridines.[270] However, $(C_5Me_5)_2Y$(2-pyridyl) is not stable at higher temperatures and 2,2'-bipyridine was isolated as byproduct after workup.[270] After initial studies with pyridine and α-picoline both resulted in ortho-metallation,[271] for the reaction of yttrium compounds with pyridine the 1,2-insertion product was found instead.[272] However, the same yttrium complexes reacted with α-picoline to give the C–H bond activation product of the α-picoline methyl group instead of the ortho sp^2 C–H bond (see Scheme 18b).[272] Bis(alkoxysilylamido)yttrium compounds were reported to undergo the ortho metallation of pyridine or of ortho-alkyl substituted pyridine derivatives.[273] The reaction of ethylene and bis(alkoxysilylamido)yttrium(2-pyridyl) was conducted and no oligomerization of ethylene was observed; instead, α-methylpicolyl derivatives were obtained.[273] Other examples of RE complexes reacting with pyridine are reported in literature.[274-275]

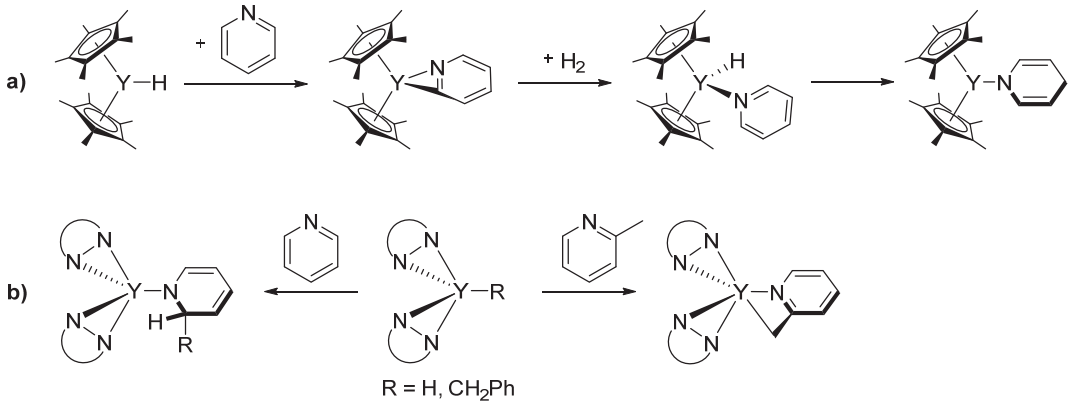

Scheme 18. a) C–H bond activation of pyridine by $[(C_5Me_5)_2YH]_2$. b) 1,2-Insertion of pyridine and ortho metallation of α-picoline by benzamidinate yttrium complexes.

Besides ortho-substituted pyridines, also 2-phenylpyridines can undergo C–H bond activation with RE metal complexes. Diaconescu et al. reported a two-step mechanism including hydrogen migration starting from a first ortho C–H bond activation product for the formation of the thermodynamically favored five-membered ring (see Scheme 19a).[276] Another interesting class of substrates for C–H bond activation are 2-propynyl derivatives. The activation of the methyl group of internal alkynes using $(C_5Me_5)_2LnCHTMS_2$ (Ln = La, Ce, Y) was reported by Teuben et al. in 2008.[277] The obtained complexes show a η^3-propargyl/allenyl structure with no preference for one binding motif. The reaction of such η^3-propargyl/allenyl compounds with (deuterated) alcohols results in the formation of allene and acetylene decomposition products (see Scheme 19b) and no influence of the steric demand of the alcohol (MeOD-d_4, $HOC_6H_2tBu_2Me$)) on the product distribution was observed.[277]

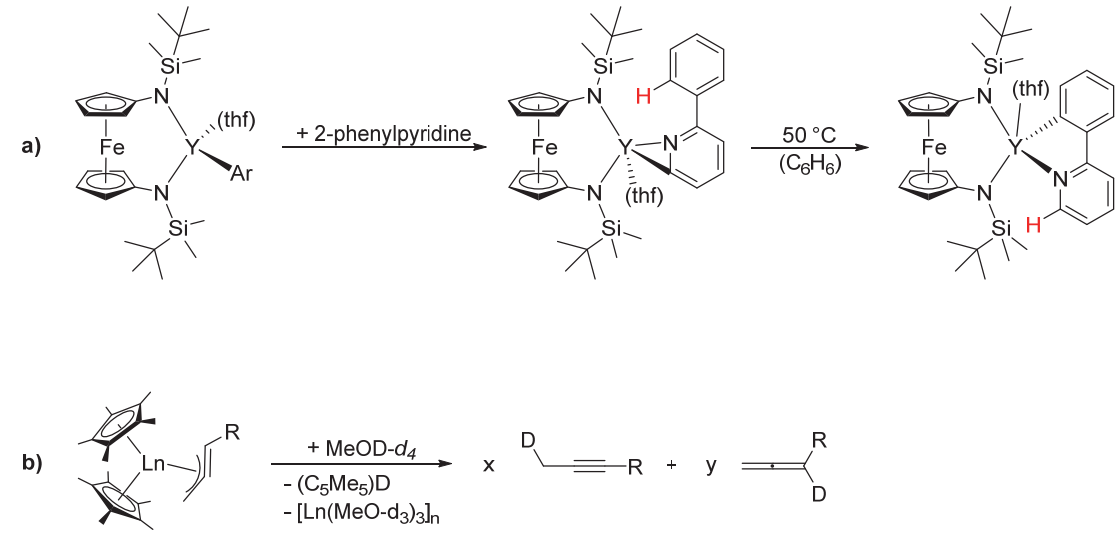

Scheme 19. a) Proton shift and formation of a 5-membered metallacycle. b) Mixture of isomers obtained from η^3-propargyl/allenyl yttrium complexes after the protonolysis with MeOD.

The first application of C–H bond activation for the initiation of polar monomers was performed by Mashima et at. in 2011.[278] In this study, an yttrium ene-diamido complex with $–CH_2TMS$ ligand was reacted with a variety of pyridine- or alkynyl derivatives, or used as an additive for the oligomerization (5 mol% cat.) and end-group functionalization of 2-vinylpyridine (2VP) (see Figure 17). The obtained oligomers had molecular masses below 5 kDa, low PDIs (≤ 1.2), and were reported with high tacticities ([*mmmm*] = 95%).[278] The high P2VP tacticities of the yttrium ene-diamido complex were found to depend on the used initiator/additive and were derived from ^{13}C NMR measurements in $CDCl_3$. However, the signal attribution was originally established in deuterated methanol,[278-279] therefore, supposedly wrong signals were assigned and the microstructure of P2VP obtained from the yttrium ene-diamido complex used by Mashima et al. was later found to be atactic.[280]

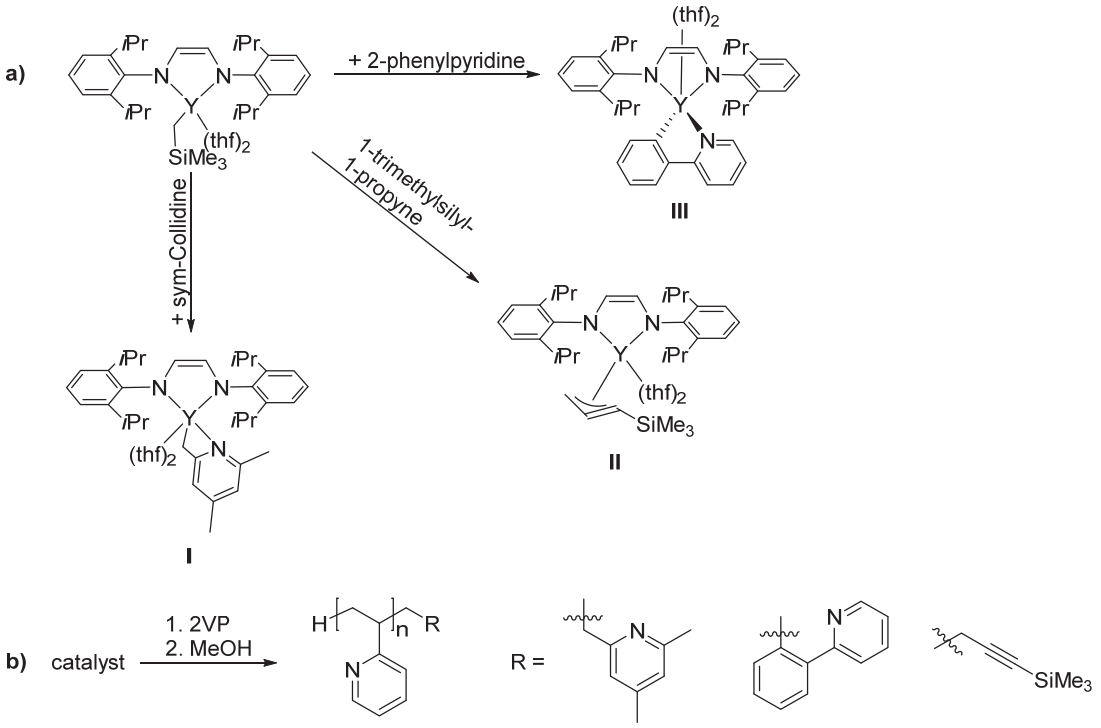

Figure 17. a) C–H activation of heteroaromatic compounds and internal alkynes by a yttrium ene diamido complex. b) Different end-group functionalized P2VPs.

The contribution and insights of Mashima et al. on the oligomerization of 2VP still proved to be very important for the initiation reaction of vinylphosphonates. Especially, the use of activated 2,4,6-trimethylpyridine (*sym*-collidine) ligands was later found to be applicable to $(C_5H_5)_2LnCH_2TMS(thf)$ (Ln = Y, Lu) complexes and to be an elegant approach to overcome initiation problems (low initiator efficiencies, long initiation delays) for vinylphosphonate REM-GTP (see Chapter 4.3). The substrate *sym*-collidine has two distinct advantages compared to other substrates for C–H bond activation. Firstly, the activated CH_2-methylene group and the aromatic pyridine ring represent a mesomeric enamide structure and can theoretically initiate polar monomers via an eight-membered ring transition state (see Scheme 20a). This aspect will be discussed in detail in Chapter 4.3. Furthermore,

besides the mechanistic match of initiation and propagation by the proposed enamide structure, the substitution of ortho- and para positions of pyridine also prevents the coupling of aromatic *N*-heterocycles at the RE metal center. The product of such coupling reactions under dearomatization are enamide complexes (see Scheme 20b).[270,272,281-282]

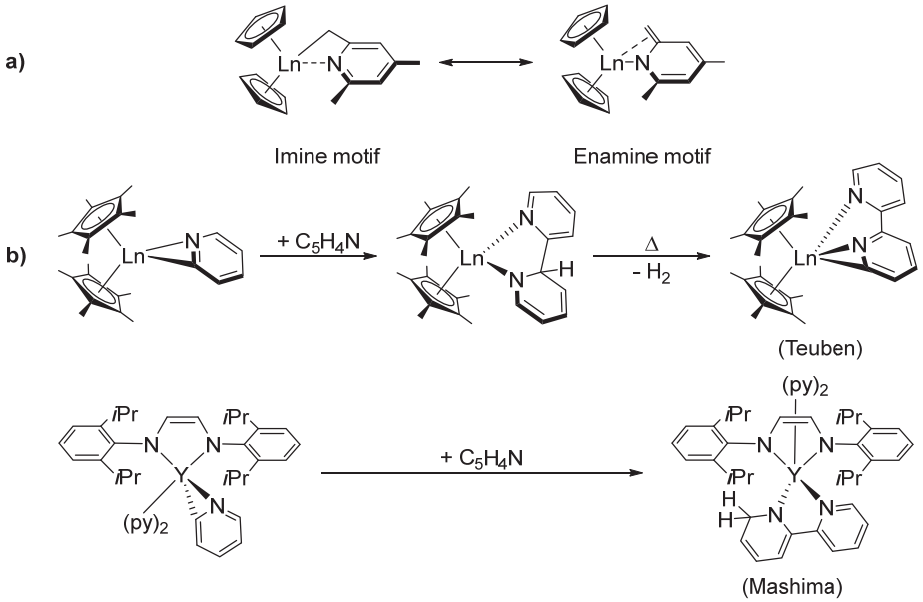

Scheme 20. a) Two different binding motives of activated *sym*-collidine to the RE metal center. b) Formation of a bipyridine (top) vs. dihydrobipyridine derivative (bottom).

Similar to the work of Marks et al. on silane, amine, or phosphine end-group functionalization of poly(ethylene) (*vide supra*), Teuben et al. reported the use of thiophene as a chain-transfer reagent for the polymerization of ethylene.[283] The ortho metallation of thiophene by $[(C_5Me_5)_2YH]_2$ was already reported in 1995 (*vide supra*).[267] In 1999, $[(C_5Me_5)_2YH]_2$, thiophene, and ethylene were used, and the oligomerization was reported to proceed slowly at 80 °C under 1 bar ethylene pressure.[283] Using the largest and sterically better accessible lanthanum metal center, the reaction of $[(C_5Me_5)_2LaH]_2$, thiophene, and ethylene resulted in clear solution containing a distribution of $H(CH_2CH_2)_n(2\text{-}C_4H_3S)$ oligomers with molecular masses below 4 kDa and a broad PDI.[283] The catalytic cycle of the reaction is depicted in Scheme 21.

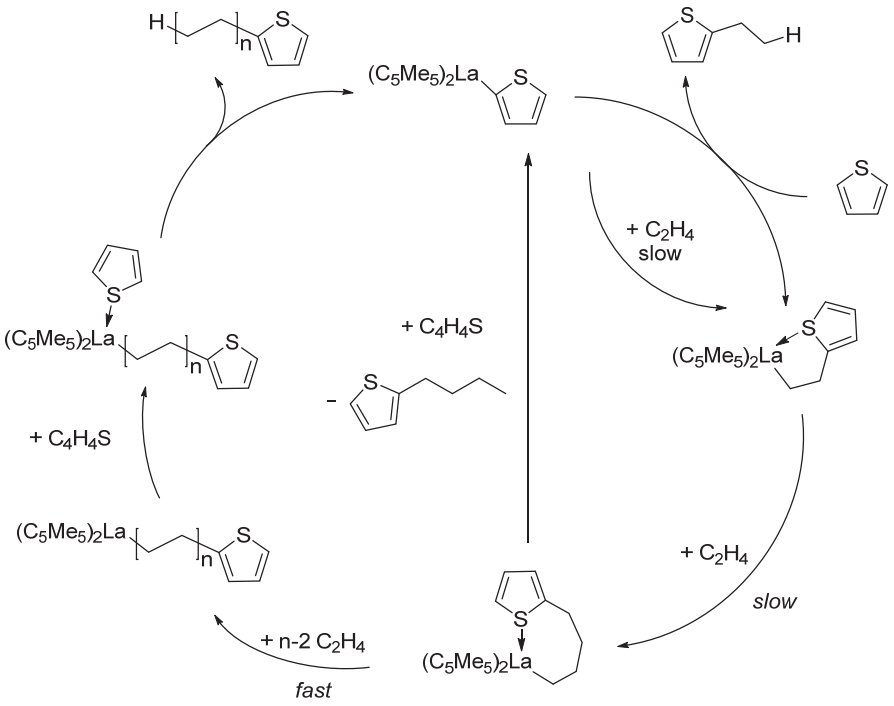

Scheme 21. Catalytic cycle for the thiophene end-group functionalization of ethylene. Thiophene is used in excess as a chain-transfer reagent.

Additionally to the C–H bond activation of heteroaromatic substrates, the ring-opening, and dearomatization of benzoxazole, benzthiazole, 1-methylimidazole, or 1-methylbenzimidazole substrates were observed and reported in literature for several RE metal compound.[284-288] In this chapter, C–H bond activation of various substrates was discussed (*vide supra*) and the literature results are summarized in Chart 4a and additionally, examples for the dearomatization of heteroaromatic substrates are also given there. In Chart 4b some examples for possible substrates are summarized that were to our knowledge not yet tested for the C–H bond activation with RE metal complexes. Furthermore, the initiation behavior of such novel ligands remains unknown for polar monomers and especially vinylphosphonates.

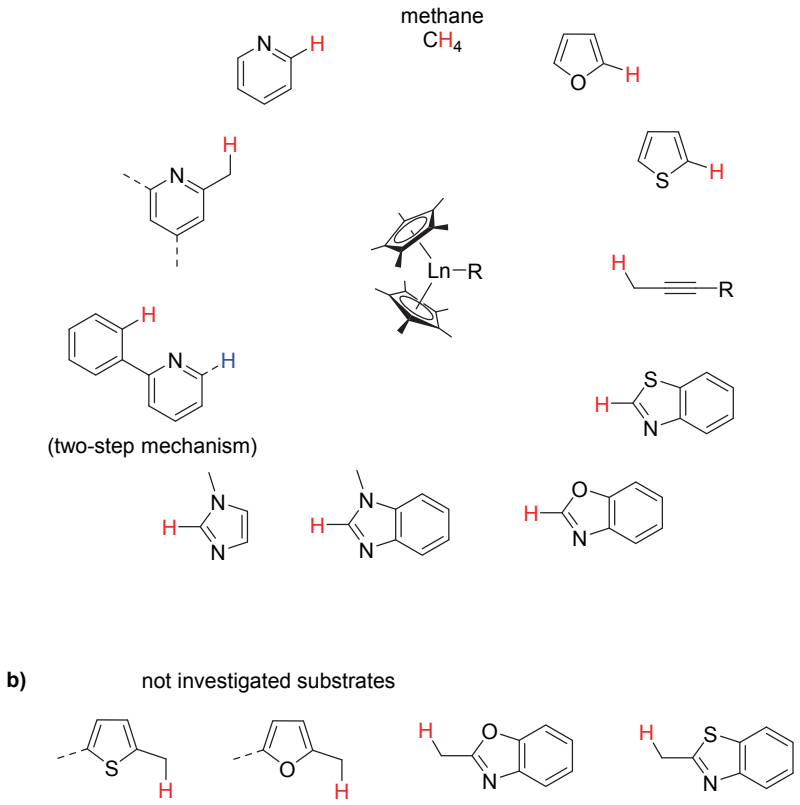

Chart 4. a) Overview of different substrates for the C–H bond activation at RE metal centers. b) Novel methyl-substituted compounds for the C–H bond activation of heteroaromatic substrates.

In distinct cases, an unexpected product formation for RE complexes has to be explained by C–H bond activation and a kinetic product control; the thermodynamically more stable compound from ligands deprotonation is not formed. One example was reported by Cui et al. in 2011, in which no reaction of an acidic cyclopentadienyl proton of (C_5Me_4HR) with $Ln(CH_2TMS)_3(THF)_2$ was observed.[289] Instead, the activation of the Cp–*Me* group was shown depending on the used ligand equivalents, coordinating to the metal center in a κ/η^3-allylic coordination mode (see Scheme 22). Other examples of unusual complex formation not following pka values and ligand acidities are discussed in the PhD thesis of Kai Carsten Hultzsch.[216]

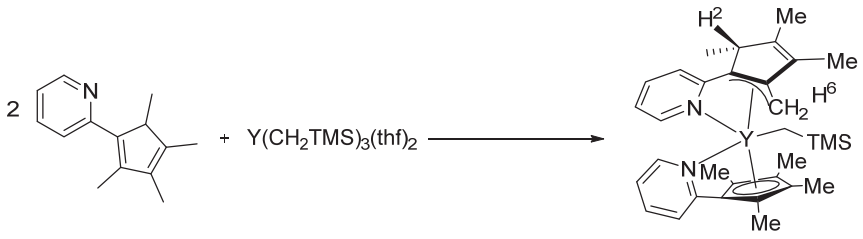

Scheme 22. Unusual complex formation by C–H bond activation of the kinetically favored product.

In general, scandium complexes show a higher selectivity for C–H bond activation - combined with lower activities (see Figure 13b) - than for α-olefin polymerization. This behavior was used in studies by Tilley et al. for a catalytic methane conversion and the formation of short chain alkanes from α-olefins. Hydromethylation reactions are distinct examples for the fully catalytic methane conversions catalyzed by

RE element complexes. The polymerization via RE complexes is a catalyzed reaction, however, not catalytic regarding the fact that the catalyst is not recovered after polymerization, and the TON is strictly one for living polymerizations (see Chapter 1.2). Other examples of RE-mediated C–H bond activation in catalytic processes include hydrosilylation, hydroamination, hydrophosphination, and dimerization of alkynes.[290-292]

The catalytic methane conversion based on a σ-bond metathesis process was first published in 2003 by Tilley et al..[251] Propylene inserts in the Ln–C σ-bond of $(C_5Me_5)_2ScMe$ without further polymerization of propylene and $(C_5Me_5)_2ScCH_2CHMe_2$ is formed (see Scheme 23). In a second step, the scandium alkyl ligand reacts in an exchange reaction with methane and isobutane is released and the thus formed $(C_5Me_5)_2ScMe$ can further react in the catalytic cycle. Over three days at room temperature, 3 eq. of isobutane are formed (30% conversion).[251] Heating of the reaction mixture to 80 °C overnight leads to a slightly higher conversion (4 eq. isobutane) and decomposition of the scandium catalyst.[251] Interestingly, β-hydride elimination from the scandium isobutyl complex does not occur, as isobutylene was not observed.[251] Furthermore, $(C_5Me_5)_2ScCH_2CHMe_2$ did not show any formation of tuck-over byproducts contrary to $(C_5Me_5)_2ScMe$ used by Bercaw et al. in 1987.[238,251] Other substrates, such as 2-butene, 1-hexene, 1-butene, 2-methylpropene, norbornylene, or 2-butyne did not produce methylated products over several days at room temperature or elevated temperatures (up to 70 °C) with this catalyst. Furthermore, the exchange reaction of $(C_5Me_5)_2ScCH_2CMe_3$ and methane under the stoichiometric formation of neopentane and $(C_5Me_5)_2ScMe$ was also reported in the same publication (see Scheme 23b).[251]

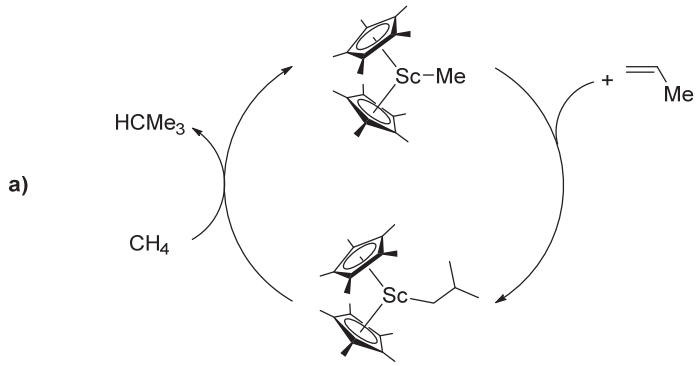

Scheme 23. a) Proposed catalytic cycle for the hydromethylation of propylene by $(C_5Me_5)_2ScMe$. b) Methane ligand exchange reaction of $(C_5Me_5)_2ScCH_2CMe_3$.

Using the bridged *ansa*-$Me_2Si(C_5Me_4)_2ScMe$ complex, the ligand exchange reaction with methane was found to be two orders of magnitude faster than for $(C_5Me_5)_2ScMe$.[293] Furthermore, the reaction of *ansa*-$Me_2Si(C_5Me_4)_2ScMe$ and propylene with the presence of methane was also found to be faster, however, showing far less selectivity for isobutane formation and side products such as isobutylene or 2-

methyl-1-pentene were found in the reaction mixture.[293] The authors explain this different reactivity by the possible activation of the C–H bond in propylene forming stable vinyl or/and allylic complexes. Also, β-H elimination from the isobutyl complex can form isobutylene and a Sc–H species, which may serve as a catalyst for the dimerization of propene to 2-methyl-1-pentene.[293] Therefore, isobutylene, a sterically hindered olefin with no hydrogen in the β position, was tested as a substrates for the hydromethylation reaction and TONs between 0.5 and 3.2 were observed for the formation of neopentane over several weeks.[293] The differences between unbridged scandium and lutetium complexes were computed for the hydromethylation of propylene resulting in a catalytic behavior of scandium and only stoichiometric results for lutetium.[294] The differences are explained by both electronic and steric effects with electronic reasons being more significant.[294] In a different study, the bridged *ansa*-$Me_2Si(C_5Me_4)_2ScMe$ complex was investigated in theoretical calculations and the strong binding of propene was found to hinder the catalytic cycle.[295] This was not found for the more bulky isobutylene, which is a weaker olefin ligand and thus allows competitive access of methane to the metal center for a catalytic cycle.[295]

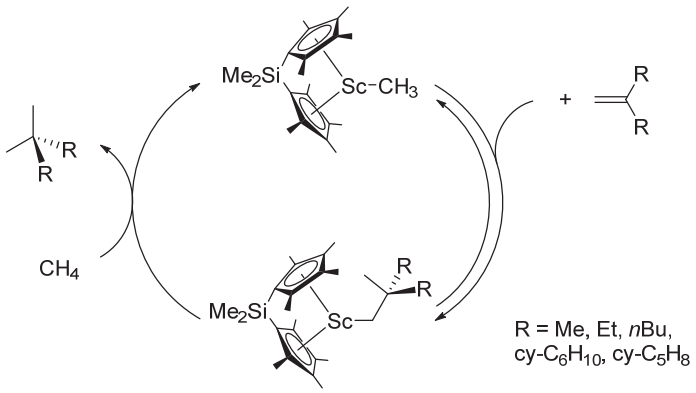

Scheme 24. Proposed catalytic cycle for the hydromethylation of sterically hindered secondary terminal olefins by $Me_2Si(C_5Me_4)_2ScMe$.

$(C_5Me_5)_2ScMe$ can catalyze the reaction of 10 eq. diphenylsilane and methane under harsh reaction conditions and $MePh_2SiH$ is formed with overall low TONs (150 atm, 80 °C, 7 days).[296] Recently, methane activation was reported for niobium complexes (see Figure 18) with similar drawbacks compared to the work of Watson et al. (low activities, complex decomposition).[297]

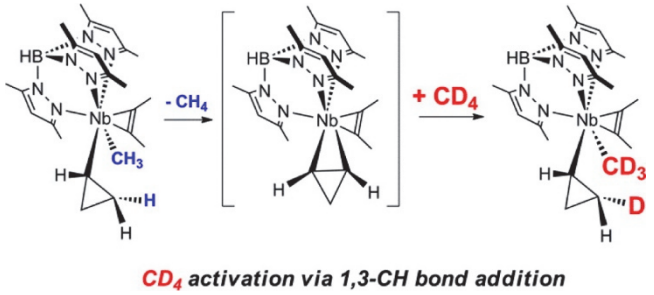

Figure 18. Stoichiometric methane activation by a niobium metallabicyclobutane complex (reprinted with permission from ref. 297. Copyright 2015 American Chemical Society).

3.4 C–H Bond Activation

In 2007, σ-bond metathesis was suggested to be extended or renamed to σ-CAM (complex assisted metathesis) to cover also special reaction pathways of high-valent late transition metal complexes.[298] For an overview on C–H bond activation in homogeneous organometallic chemistry, for example RE elements, the reader is directed toward a review by Rory Waterman.[264] The application of (different) C–H bond activation reactions for the synthesis of organic compounds was covered in recent reviews.[232,299] Furthermore, reviews focusing on the C–H bond activation from a computational perspective were published.[300-303]

4 Publications

In the following chapters all first and coauthor publications on the REM-GTP of polar monomers related to the work on this thesis are first briefly summarized and then reprinted.

The introduction to REM-GTP of vinylphosphonates is given in Chapter 4.1 published in *Chemical Reviews*. In Chapter 4.2, a detailed study on the mechanism of vinylphosphonate REM-GTP is shown and was published in the *Journal of the American Chemical Society*. In Chapter 4.3 novel initiating ligands obtained from the σ-bond metathesis reaction of $-CH_2TMS$ and *sym*-collidine is presented. The highly active and efficient initiation is attributed to a mechanistic match between initiation and propagation and the results were published in *Organometallics*. Chapter 4.4 gives the first results of ligand induced steric crowding for the REM-GTP of vinylphosphonates by various RE metallocenes and was published in *Macromolecules*. Chapter 4.5 shows a draft in preparation on the stereoregular polymerization of vinylphosphonates by RE CGCs. In Chapter 4.6, the material properties and flame retardant behavior of various poly(vinylphosphonate ester)s are shown for polycarbonate and the results were published in *Industrial & Engineering Chemistry Research*. Chapter 4.7 gives an overview on one of the first reports on REM-GTP of nitrogen-containing monomers, the synthesis of block copolymers, the resulting coordination strength, and the synthesis of nano-scaled objects. The manuscript was published in the *Journal of the American Chemical Society*. In Chapter 4.8, the development and application of post metallocene 2-methoxyethylaminobis(phenolate) RE catalysts for the polymerization of polar monomers is given and was published in *Macromolecules*. The main part of this thesis ends with Chapter 4.9 giving an overview on the precise synthesis of homopolymers, block copolymers, polymer brushes, and chain end functionalized materials by the catalyzed monomer insertion via RE and cationic group IV complexes.

Helpful for the general process of writing a paper are the guidelines published by Whitesides et al..[304] Before printing or sending manuscripts it is helpful to remove hyperlinks or raw data (Excel, ChemDraw) within the file by using CTRL + SHIFT + F9.

4.1 Rare Earth Metal-Mediated Precision Polymerization of Vinylphosphonates and Conjugated Nitrogen-Containing Vinyl Monomers

Status: Published online: December 31, 2015

Journal: Chemical Reviews

Volume 116, issue 4, pages 1993–2022

Publisher: American Chemical Society

Article Type: Review

DOI: 10.1021/acs.chemrev.5b00313

Authors: Benedikt S. Soller, Stephan Salzinger, and Bernhard Rieger

4.1.1 Abstract

This review summarizes recent trends in the field of REM-GTP of polar monomers; in particular vinylphosphonates and *N*-coordinating monomers such as IPOx and 2VP are discussed. In the first part, preliminary studies on radical, anionic, and SKA-GTP of vinylphosphonates are presented and the disadvantages of these methods are compared. In the main part, the mechanism of vinylphosphonate REM-GTP and the properties of poly(vinylphosphonate)s are presented in detail. The discussion of SI-GTP for the decoration of surfaces and particles leads to the recent development and application of REM-GTP for *N*-coordinating monomers.

The first author Benedikt S. Soller was supported by second author Stephan Salzinger in writing the manuscript.

CHEMICAL REVIEWS

Review

pubs.acs.org/CR

Rare Earth Metal-Mediated Precision Polymerization of Vinylphosphonates and Conjugated Nitrogen-Containing Vinyl Monomers

Benedikt S. Soller,[†] Stephan Salzinger,[‡] and Bernhard Rieger*[,†]

[†]WACKER-Lehrstuhl für Makromolekulare Chemie, Technische Universität München, Lichtenbergstraße 4, 85748 Garching bei München, Germany

[‡]Advanced Materials & Systems Research, BASF SE, GME/D-B001, 67056 Ludwigshafen am Rhein, Germany

ABSTRACT: This review focuses on introducing and explaining the rare earth metal-mediated group transfer polymerization (REM-GTP) of polar monomers and is composed of three main sections: poly(vinylphosphonate)s, surface-initiated group transfer polymerization (SI-GTP), and extension to *N*-coordinating Michael-type monomers (2-vinylpridine (2VP), 2-isopropenyl-2-oxazoline (IPOx)). The poly(vinylphosphonate)s section is divided into two parts: radical, anionic, and silyl ketene acetal group transfer polymerization (SKA-GTP) of vinylphosphonates in comparison to REM-GTP, and properties of poly(vinylphosphonate)s. The mechanism of vinylphosphonate REM-GTP is discussed in detail for initiation and propagation including activation enthalpies $\Delta H^{\ddagger}$ and entropies $\Delta S^{\ddagger}$ according to the Eyring equation. SI-GTP is presented as a method for surface functionalization, and recent trends for 2VP and IPOx polymerization are summarized. This review will serve as a good resource or guideline for researchers who are currently working in the field of rare earth metal mediated polymerization catalysis as well as for those who are interested in beginning to employ rare earth metal complexes for the synthesis of new materials from polar monomers.

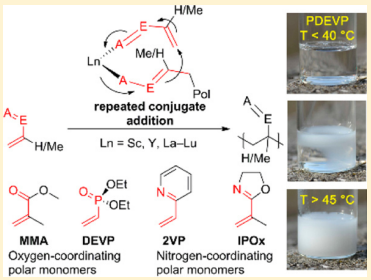

CONTENTS

1. INTRODUCTION

The field of polymer chemistry, associated with materials science, already has a long history of research, but development in this field is by no means slowing down. Since its recognition in the 1920s by Hermann Staudinger, macromolecular chemistry has steadily developed, and by the late 1980s, the production of polymers had already surpassed the world annual steel production by volume.[1−3] Following the tradition of naming eras in human history according to the predominantly used materials, we now live in the Polymer Age. Artificial compounds

Special Issue: Frontiers in Macromolecular and Supramolecular Science

Received: May 25, 2015
Published: December 31, 2015

DOI: 10.1021/acs.chemrev.5b00313
Chem. Rev. 2016, 116, 1993−2022

today represent more than just simple packaging materials. Plastics are used in various fields and have replaced other typical materials such as metals, ceramics, or wood owing to their superior properties. Polymers can easily be prepared on a large scale from cheap starting materials; possess low densities, easy processability, and high availability; and are resistant to corrosion. Accordingly, our modern consumer-based societies are hard to imagine without synthetic materials. At the beginning of the 21st century, humanity is facing a series of challenges due to overpopulation, urban living, aging societies, environmental pollution, unsustainable processes, malnutrition, climate change, and an unrestrained consumption of limited resources.[4−6] For an article on the future of chemistry and the need to reinvent chemical research and industry from molecules to systems in order to help solve increasingly multidisciplinary tasks, the reader is directed to an essay by Whitesides.[7] The growth in plastic production in the early 20th century was driven by commodity polymers and their polymerization methods (i.e., step polymerization or chain polymerization). The expansion of macromolecular chemistry in the second half of the 20th century was mostly determined by the discovery of highly active Ziegler−Natta polymerization catalysts for the polymerization of ethylene, propylene, and other α-olefins, resulting in the Nobel Prize in chemistry in 1963.[8−12] At the beginning of the 21st century, new materials are now needed for specific applications, and though common techniques are still of great importance, they fail to address the change from 20th century structural materials to 21st century complex system polymers. Materials of the future, in combination with nanotechnology, medicine, or materials science, offer solutions to these challenges. Furthermore, utilization and development of precision polymers will include fields such as tissue engineering, membranes, stimuli responsive materials, mobility, energy storage, or engineering materials. Therefore, the need for new materials or an improvement in existing materials and processing techniques is essential. Living polymerizations are the most promising candidates to add specific functionalities to new materials. Over the past two decades living radical polymerization methods have developed rapidly, and for most cases, the living characteristics result from low radical concentrations giving rather low propagation rates and/or conversions. However, for feasible applications, methods with high precision of the macromolecular parameters in combination with rapid reaction velocities are required. Catalytic reaction sequences ideally fulfill these requirements.

1.1. Phosphorus-Containing Polymers

Specific properties in polymers are addressed by functional groups within the material. The functionality can be part of the main chain or introduced as side groups, chain ends, graft structures, or block structures. Most polymers are built from monomers consisting of carbon, hydrogen (e.g., polyolefins), oxygen, nitrogen, silicon, sulfur, or halogens. Each of the listed elements can add specific functional groups and therefore particular properties to the materials. Therefore, it is surprising that fewer examples for polymers containing phosphorus groups exist. DNA and RNA are well-known examples in nature, and organisms store biological information efficiently in phosphate polymers.[13,14] Synthetic polymers based on phosphates are prone to hydrolysis, and many examples of phosphorus-containing polymers are reported in the literature. However, the functional group featuring phosphorus is often at a relatively significant distance from the polymerized functional group (i.e., in most cases these are olefins for chain growth and polar functional groups for step-growth polymerizations). Phosphorus-containing polymers show high biocompatibility[15−19] and find use in dental adhesives, bone concrete,[20−24] ion-exchange resins, fuel cells,[25−35] and halogen-free flame retardants,[36,37] to name just a few of the more common applications.[38,39] The most prominent examples of phosphorus-containing synthetic polymers are shown in Scheme 1, and a variety of other polymers with phosphorus are presented in the literature.[38,40−46]

Scheme 1. Different Types of Phosphorus-Containing Monomers and Their Corresponding Polymers: (a) Poly(phosphazene), (b) Poly(vinylphosphonate) and PVPA, (c) Poly(phosphonate), and (d) Poly(phosphate)

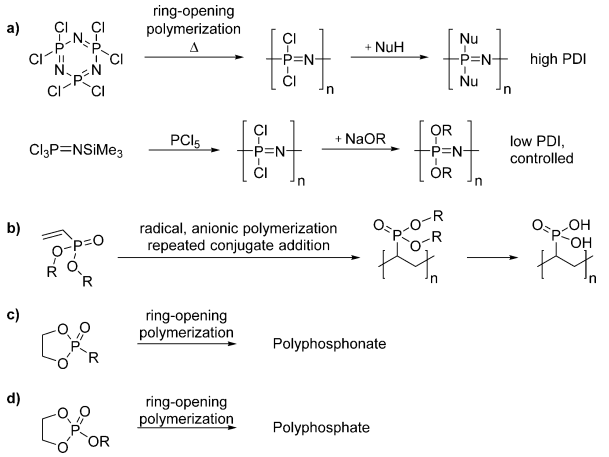

Poly(phosphazene)s represent an interesting and well-studied class of organic or inorganic phosphorus-containing polymers.[47−58] Highly flexible poly(phosphazene)s are also known as inorganic rubbers, and the substituents can be tuned to hydrolyze in water to give biologically nontoxic harmless products, important for biomedical applications.[48,59,60] Another class of phosphorus-containing macromolecules is poly(phosphoester)s (PPEs). PPEs consist of repeated phosphoester units in the main chain and have been receiving increased attention due to their biocompatibility and biodegradability via hydrolysis or enzymatic cleavage and structural similarity to naturally occurring biopolymers.[61−63]

However, this degradation does not limit the use of PPEs, as indicated by many reports on biomedical applications.[64,65] Since the phosphorus atom is pentavalent, reactive pendant groups including hydroxyl, carboxyl, and alkynyl may be introduced as side-chain functionalities, allowing PPEs to be structurally versatile.[66−71] Ring-opening polymerization (ROP) of cyclic phosphoesters is one of the most common processes, and attributed to the variety of cyclic phosphoesters from the condensation of alcohols and the chloro-substituted 1,3,2-dioxaphospholane diverse structures for PPEs are obtained (Scheme 1).[69,72−75] Biodegradable PPE-based polymeric micelles and shell cross-linked sphere-like nanoparticles have been prepared from amphiphilic block-graft terpolymers, and drug release studies demonstrate the use of PPE nanotherapeutics.[76] Recently, ROP,[77] olefin metathesis,[78−81] and ring-opening metathesis polymerization (ROMP)[82] were used for the polymerization of cyclic phosphates and phosphonates by the group of Wurm. Hyperbranched unsaturated PPEs can act as a protective matrix and allow the efficient scavenging of singlet

DOI: 10.1021/acs.chemrev.5b00313
Chem. Rev. 2016, 116, 1993−2022

oxygen, but do not react with molecular oxygen for the long-term photon upconversion in air.[83]

Vinylphosphonates belong to one of the simplest and longest known phosphorus-containing monomers. Since the 1940s, several synthetic pathways for the synthesis of dialkyl vinylphosphonate (DAVP) monomers exist, and DAVPs are obtained in good yields from simple starting materials.[84,85] Among them, the Michaelis–Arbuzov reaction is commonly used to obtain ethyl or isopropyl substituted vinylphosphonate esters in a two-step reaction (Scheme 2a).[84−88] Aryl- and vinyl-substituted

Scheme 2. Synthesis of Phosphonates via (a) Michaelis–Arbuzov and (b) Pd-Catalyzed Cross-Coupling Reactions

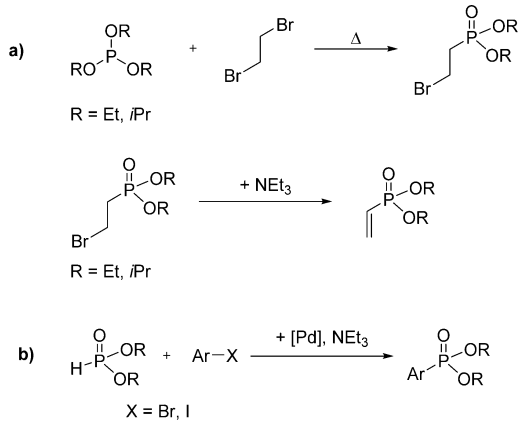

phosphonates can be synthesized in larger variety via palladium-catalyzed cross-coupling reactions from dialkyl phosphites (Scheme 2b).[89−91] Other reactions of vinylphosphonates, besides polymerization reactions, include Diels–Alder cyclization, thiol–ene click reaction, or 1,4-addition.[92−96] Recently, the coordination polymerization of vinylphosphonic acid (VPA) and diethyl vinylphosphonate (DEVP) for the synthesis of functionalized PE-*co*-PVPA and PE-*co*-PDEVP CdSe quantum dots has been published using phosphinesulfonato palladium catalysts tolerating a wide range of functional groups.[97] The obtained molecular masses with low phosphorus incorporation were estimated from ^{1}H NMR spectra and found to be below 8 kDa for PE-*co*-PVPA. In the case of PE-*co*-PDEVP, the molecular mass drops significantly to 1.1–2.5 kDa; however, no gel permeation chromatography (GPC) data was shown in the paper.[97]

The homopolymerization of vinylphosphonates leads to poly(vinylphosphonate)s consisting of saturated C–C bonds in the main chain only, which is the reason for their stability against hydrolysis. Therefore, backbone degradation of poly(vinylphosphonate)s is only possible under harsh conditions (in contrast to other phosphorus-containing polymers (vide supra)), and generally stable polymeric materials are obtained. However, the poor polymerizability of vinylphosphonates via classic polymerization methods has had limited studies on material properties and applications.

1.2. Terminology

In a broad sense, the propagation of all polymerization reactions can be seen as "catalytic" as multiple monomers are consumed per reactive initiating molecule. For a better distinction of those initiating compounds, the terms "initiators" and "catalysts" are used, depending on whether one or several polymer chains are produced by one reagent. The definition of initiator is precise for free radical, cationic, or anionic polymerization techniques, whereas for catalytic polymerizations the catalysts can either relate to the initiating ligand or to the metal center activating and stabilizing the monomer and growing polymer chain end. To overcome this terminological conflict, according to previous literature, this article uses the term "catalyst" when referring to the catalyzed monomer addition. This review deals specifically with the repeated conjugate addition of Michael-type monomers via rare earth metal-mediated group transfer polymerization (REM-GTP) as a living polymerization initiated by rare earth metal complexes. It uses the term "molecular mass" for polymer characterization, instead of "molecular weight", to concur with the physical unit of mass in kilograms and to avoid confusion with the dependence of weight and the physical unit in newtons (N).

1.3. Scope of Review

This review covers the progress in REM-GTP of vinylphosphonates and shows advantages of this method in comparison to classical anionic and radical vinylphosphonate polymerizations. We provide insights into early stage metal ligand interaction, the influence of steric crowding, the complex reaction pathway for unbridged rare earth metallocenes, optimization of initiation for the C–H acidic vinylphosphonates, and determination of the polymer microstructure, looking toward new possibilities for surface modification via surface-initiated group transfer polymerization (SI-GTP). Other monomer classes such as (meth)acrylates and (meth)acrylamides have been highlighted in previous reviews.[98−102] However, a novel perspective on *N*-coordinating Michael-type monomers, extending the scope of REM-GTP to new materials beyond *O*-coordinating (meth)acrylates, (meth)acrylamides, and vinylphosphonates, is included at the end of this review.

For clarity, the scope of this review is to show recent advances in the field of vinylphosphonate REM-GTP. However, considering the decades of effort by chemists to polymerize this specific class of monomers, a brief overview about radical and classic anionic polymerization is given. For further studies on radical vinylphosphonate polymerization, the reader is directed to a comprehensive review by Macarie and Ilia.[103]

2. RADICAL AND ANIONIC POLYMERIZATION OF VINYLPHOSPHONATES

Relatively few investigations on the radical homopolymerization of DAVPs have been reported. Given the good accessibility of vinylphosphonates (vide supra), the first unsuccessful polymerization attempts were made soon after their synthesis, resulting in poorly described oligomeric materials. A major drawback of the radical polymerization of vinylphosphonates is the low propagation rate, which is a result of the pronounced stability of the formed radical species. In combination with the frequent appearance of chain transfer reactions either to the monomer or to formed polymer, only materials with low molecular masses and low conversions are produced (Scheme 3). Instead, of propagating the generated phosphonate radicals transfer predominantly via an intramolecular hydrogen transfer of the phosphonate ester moiety. Thus, the formed radical in the side chain inserts into a new monomer unit and a P–O–C bond is formed in the main chain. This P–O–C bond is thermally unstable and leads to chain scission (Scheme 3).[104] The formation of low molecular mass PDAVPs via radical polymerization has also been observed in other studies.[105] An approach to overcome these limitations has not been achieved yet despite numerous attempts by researchers over the past deca-

DOI: 10.1021/acs.chemrev.5b00313
Chem. Rev. 2016, 116, 1993–2022

Scheme 3. Intramolecular Chain Scission of PDIVP via Hydrogen Transfer from the Backbone to the Ester under Formation of a Labile P−O−C Bond and the Resulting Polymer Cleavage

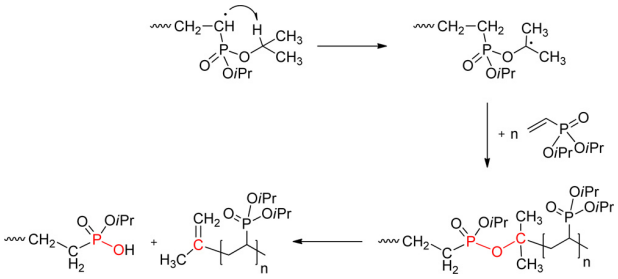

Scheme 4. Different Reaction Pathways for Anionic Vinylphosphonate Polymerization: (a) Deprotonation of α-CH Acidic Vinylphosphonates, (b) Nucleophilic Attack at the Phosphorus Atom and Elimination of an Alcoholate, and (c) Nucleophilic Attack at the Double Bond (Redrawn with Permission from Ref 127. Copyright 2012 John Wiley and Sons.)

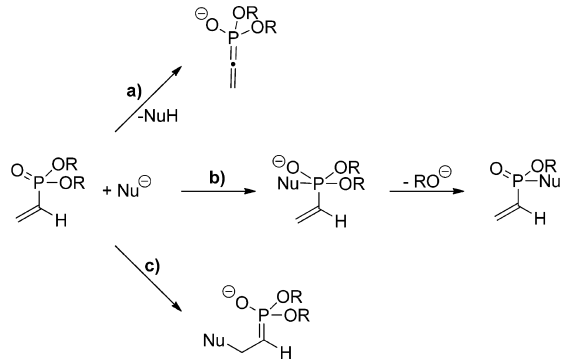

des.[84,106−110] Copolymers of DEVP and styrene, methyl methacrylate, butadiene, acrylonitrile, and other monomers are readily obtained by free radical polymerization.[107,110−116] However, conversions and phosphonate contents were found to be low and the influence of the phosphonate groups on the material properties was comparatively weak. Recently, the free radical copolymerization of DEVP and 2-chloroethyl methacrylate (CEMA) for the formation of spherical nanoparticles in water has been reported.[117] The reactivity ratios for the free radical copolymerization initiated via benzoyl peroxide of CEMA (M_1) and DEVP (M_2) were reported as $r_1 = 19.45$ and $r_2 = 0.11$, respectively, and the obtained homo- and copolymers were purified through precipitation fractionation.[117]

Contrary to the poor polymerizability of DAVPs, PVPA can be synthesized via free radical polymerization from vinylphosphonic acid dichloride and its subsequent hydrolysis or directly from VPA.[118−121] Therefore, this is the only vinylphosphonate-based product that has commercial applications, for example, as binder in bone and dental concrete.[21−24,122] However, the resulting products are poorly defined, with low-to-moderate molecular masses (<62 kDa), irregular chain structures, and high polydispersities; they also contain a high percentage of the remaining monomer, this being detrimental to biomedical applications.[103,120,123]

The anionic polymerization of vinylphosphonates generally exhibits higher activities and yields materials of overall higher molecular masses. However, anionic vinylphosphonate polymerization is by no means without limitations, and early attempts, using lithium, magnesium, or aluminum alkyls only resulted in low molecular mass oligomers. The resulting materials are briefly discussed but without determining molecular masses.[124−126] The main drawback of anionic DAVP polymerization is the existence of an acidic proton of the vinylic group in the α-position and the resulting termination reactions that occur as side reactions with the initiator (Scheme 4a).[127] The α-methyl-substituted dimethyl 1-methylvinylphosphonate was reported to be inaccessible for anionic styrene copolymerization with catalytic amounts of *n*-butyllithium (Scheme 4b).[128] However, using sodium naphthalene as anionic initiator a higher incorporation of phosphorus was achieved in the polystyrene (PS) copolymers.[128] In 2008, Jannasch and co-workers successfully grafted PDEVP onto poly(sulfone)s (PSU) by activation with *n*-butyllithium and 1,1-diphenylethylene (DPE). They also tested several PSU-*g*-PVPA copolymers of the free phosphonic acid for their application as highly proton-conducting membranes for fuel cells.[129] The usage of DPE as a co-initiator proved to be essential, as demonstrated by the poor polymerization results in the study of Leute and Bingöl in 2007 (without the use of DPE).[130,131] While Bingöl stated that anionic polymerization of vinylphosphonic esters was hampered, Leute could isolate oligomeric materials, obtaining best results by polymerization in toluene using *n*- or *sec*-butyllithium as the initiator.[130,131] An initiation by the abstraction of an acidic α-CH proton was observed to be competing with an initiation by nucleophilic addition to the double bond (Scheme 4a,c).[131] DPE was also used for the preparation of PS-*b*-PDEVP block copolymers via sequential anionic polymerization of styrene and DEVP in THF at −78 °C.[132] Without DPE, neither copolymerization with styrene nor efficient homopolymerization of DEVP is possible.[132] In the same year, Meyer and co-workers independently made identical observations for the block copolymerization of styrene and dimethyl or diisopropyl vinylphosphonate (DIVP) with block compositions ranging from approximately 9:2 to 3:7.[133] Again, DPE was used to reduce the reactivity and nucleophilicity of the macroinitiator anion before the second monomer was added. These results are in line with the lower reactivity and higher stability of DPE from the second phenyl substituent, which is commonly used as a co-initiator for anionic (meth)acrylate polymerizations.[134−136] DPE, although being an α-substituted styrene derivative, suppresses the nucleophilic attack of the macroinitiator at the phosphorus atom of DEVP, which results in a substitution reaction and therefore leads to either chain transfer or termination (Scheme 4b).[132] The higher stability of the DPE anion may also inhibit deprotonation of the acidic α-CH, as observed by Leute.[131] The addition of DPE is not necessary if the initiating species is not reactive enough to undergo the described side reactions, as observed by Jannasch and co-workers in 2010, who used a benzyllithium macroinitiator during a study on grafting PDEVP onto poly(phenylene oxide).[137] Following this general strategy of lithiated DPE macroinitiators, structurally designed water-soluble alternating aromatic multiblock copolymers with grafted DEVP units were produced and used for applications in electrolyte membranes.[138]

Despite recent developments, classical anionic polymerization of vinylphosphonates is limited to low degrees of polymerization and high polydispersities, even if the polymerization is carried out at −78 °C.[133] The broad molecular mass distribution may be attributed to a rather slow and therefore nonuniform initiation, as

DOI: 10.1021/acs.chemrev.5b00313
Chem. Rev. 2016, 116, 1993−2022

Scheme 5. (a) Associative and (b) Dissociative Mechanisms for SKA-GTP[a]

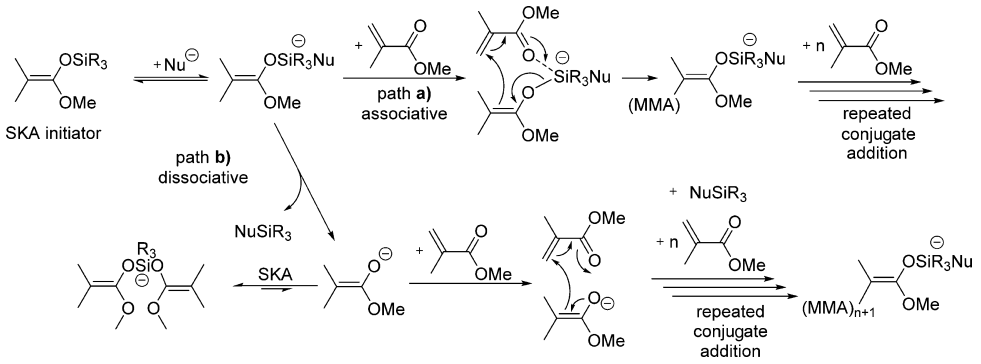

[a]Nu = HF_2^-, F_2^{2-}, cyanide, azide, oxyanions, or bioxyanions.

even after 4 h reaction time at elevated temperature, the *n*-BuLi DPE initiator complex was found coexisting in solution with the growing homopolymer.[133] At temperatures above −78 °C, oligomers or polymeric materials with broad M_w/M_n are produced (PDI > 3), indicating side and termination reactions.[131] The polymerization rates were not determined; however, indicated by long reaction times until full monomer conversion, the activities for anionic vinylphosphonate polymerization are low. This may be attributed to a resonance stabilization of the anionic chain end through the phosphonate moiety, decreasing the chain end reactivity and a poor activation of the monomer by the used metal salts.[131]

3. SILYL KETENE ACETAL-INITIATED GROUP TRANSFER POLYMERIZATION

A special case of a living-type polymerization method is the so-called silyl ketene acetal initiated group transfer polymerization (SKA-GTP). The concept of GTP was developed at the Central Research & Development Department of DuPont in the 1980s and is mostly attributed to the work of Owen W. Webster.[139] GTP uses SKA initiators as nucleophiles and Lewis acids to activate the monomer. Lewis bases are used as catalysts and SKA-GTP represents a living polymerization, follows a repeated conjugate addition to Michael-type monomers, and can be performed at elevated temperatures, giving access to commercial dispersion or rheology additives.[140,141] The molecular mass increases linearly with the conversion, and by sequential monomer addition, block copolymers are obtained. The term "GTP" was originally used as the utilized silyl compounds were supposed to transfer from the initiator to the added monomer.[139] Since then, the mechanism of nucleophilic GTP has stimulated considerable scientific discussion.[139,140,142−149] The gist of this controversy was the contrast of associative or dissociative mechanism for SKA-GTP propagation taking place (Scheme 5).[139,147−149] In further mechanistic studies the dissociative mechanism was supported by experimental results.[142−146] Therefore, the concept of SKA-GTP as an associative repeated transfer of the organosilyl group might be misleading, but remains in the literature.

Since its recognition, SKA-GTP has been applied to a variety of (meth)acrylates or (meth)acrylamides and many examples of copolymers with specific functionalities have been obtained. SKA-GTP is important for commercial and academic purposes.[150−158] Even attempts of a sequential copolymerization of methyl methacrylate (MMA) and DEVP using SKA initiators were conducted but resulted in the end-capping of PMMA by one DEVP unit, indicating a suppressed homopropagation of DEVP by an insufficient activation of the monomer.[159] Using SKA-GTP, the copolymerization of MMA and DEVP is possible; however, the incorporation of DEVP remains low (<2 mol %).[159]

4. RARE EARTH METAL-MEDIATED GROUP TRANSFER POLYMERIZATION

REM-GTP enables the precise synthesis of tailor-made functional materials, as this polymerization method combines the advantages of both living ionic and coordinative polymerizations. According to its highly controlled character, REM-GTP leads to strictly linear polymers, with a very narrow molecular mass distribution (PDI < 1.1), exhibits a linear increase in the average molecular mass upon monomer conversion, and allows the synthesis of block copolymers as well as the introduction of chain-end functionalities. The coordination of the growing chain end at the catalyst suppresses side reactions and allows stereoregular polymerization as well as tuning the activity by varying the metal center or ligand sphere. The advances in (meth)acrylates and (meth)acrylamides since the first work in the early 1990s and the mechanism, application, and background of classic acrylic and polar monomer polymerization have been already covered in detail by Chen.[102] Therefore, in this section, only a basic introduction to group 3 and group 4 GTP will be given.

In 1992, two independent communications reported on the living polymerization of MMA using metallocene catalysts. The neutral samarocene $[(C_5Me_5)_2SmH]_2$ was used by the group of Yasuda, whereas Collins and Ward presented an isoelectronic cationic zirconocene initiator.[160,161] The polymerization by $[(C_5Me_5)_2SmH]_2$ occurs over a broad temperature range from as low as −95 °C up to 40 °C, producing PMMA with a controlled molecular mass (according to the $[MMA]_0/[Sm]_0$ ratio), low polydispersities (PDI < 1.05), and a high syndiotacticity of up to 95% (Table 1).[160,162] Already in the beginning, a similar mechanism via a repeated conjugate addition of an ester enolate has been discussed for $[(C_5Me_5)_2SmH]_2$ and SKA initiators.[160] Based on the crystal structure of the $[(C_5Me_5)_2Sm(MMA)_2H]$ adduct, the propagation via an ester enolate is evident.[160] In the first step, the hydrido-bridged dimer is opened by coordination of MMA, and subsequently, an enolate is formed by the 1,4-addition of the hydrido ligand to MMA (Scheme 6). This active species can further insert into coordinated and activated monomer via an eight-membered-ring transition state. The polymerization of MMA via cationic zirconocenes follows the same mechanism. Initiation starts by

DOI: 10.1021/acs.chemrev.5b00313
Chem. Rev. 2016, 116, 1993−2022

Table 1. Polymerization Results for MMA in Toluene Synthesized by $[(C_5Me_5)_2SmH]_2$

temp [°C]	$[M]_0/[Sm]_0$	M_n [kDa]	PDI	tacticity rr [%]	conv [%], reaction time [h]
−95	1000	187	1.05	95.3	82 (60)
−78	500	82	1.04	93.1	97 (17)
0	3000	563	1.04	82.3	98 (3)
0	500	58	1.02	82.4	99 (1)
25	500	57	1.02	79.9	99 (1)
40	500	55	1.03	77.3	99 (1)

transfer of the initiating methyl ligand to the chain end, forming an ester enolate. The mechanism was identified by ^{13}C-labeled initiators and methyl end groups in the final PMMA polymer, respectively.[161] Group 4 complexes require a cocatalyst for activation, and therefore, the corresponding counterions can affect the stereoregularity or polymerization activity.[102,163] The mechanism of group 4 GTP is either mono- or bimetallic.[102,164−166]

In most cases, trivalent rare earth (RE) metal complexes are used for the polymerization of MMA and other (meth)acrylates, as they are highly active, they initiate via nucleophilic transfer, and the oxidation state Ln^{3+} leads to stable compounds. Divalent RE metals (Ln^{2+}) are known to be strong reducing agents and are easily oxidized via a single-electron transfer (SET) to other substrates. In an early study, Yasuda and co-workers discovered that divalent lanthanocenes also promote the living polymerization of MMA in the absence of an initiating ligand.[162] However, the observed molecular masses are significantly higher than expected, resulting in lower initiator efficiencies ($I^* < 30\%$). In later studies, Boffa and Novak revealed that the active species is trivalent dinuclear.[167] The actual active propagating species is formed by the combination of two rare earth MMA radical adducts, and structures of ABA block copolymers can be obtained from such bisinitiators.[167−170]

Readers interested in further studies on the GTP of polar monomers are referred to the excellent review by Chen from 2009.[102] The use of cationic rare earth metal complexes for the polymerization of conjugated dienes is now receiving increased attention.[171−182] For detailed studies on this topic, the reader is directed toward the reviews written by Hou and Okuda.[183,184]

5. REM-GTP OF VINYLPHOSPHONATES

5.1. Preliminary Studies

Motivated by the interesting properties of phosphorus-containing polymers and insufficient classic polymerization techniques for producing poly(vinylphosphonate)s, our group investigated the suitability of rare earth metal complexes for a catalyzed polymerization of DMVP and DIVP. Our research was inspired by the electronic and structural similarity between Michael-type acceptor vinylphosphonate esters and (meth)-acrylates. In initial studies, simple rare earth metal alkyl precursor systems were found to be active for the oligomerization of DMVP and DIVP.[131,185] The polymerization of DMVP is hampered by the poor solubility of PDMVP in suitable solvents (e.g., toluene, tetrahydrofuran (thf)). For $Ln(bdsa)_3(thf)_2$ compounds, the activities and yields increase with the decreasing ionic radius of the corresponding metal. For the smaller yttrium cation, an exchange reaction of axial coordinated tetrahydrofuran with DMVP was observed instead of polymerization under the used reaction conditions (Scheme 7).[185] DMVP coordinates to

Scheme 7. First Used Rare Earth Metal Precursors for the Oligomerization of DMVP and DIVP; Quantitative Exchange Reaction of Donor Solvent and DMVP in Axial Position (Redrawn with Permission from Ref 127. Copyright 2012 John Wiley and Sons.)

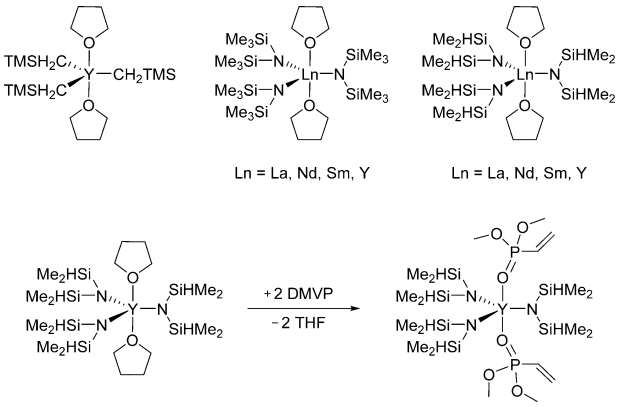

Scheme 6. Dimer Opening by Monomer (a) Coordination, (b) Initiation, and (c) Propagation of MMA REM-GTP by $[(C_5Me_5)_2SmH]_2$

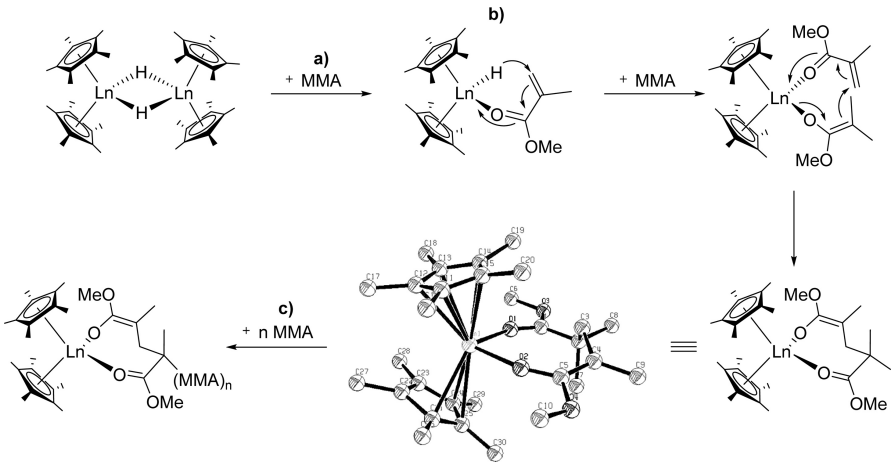

DOI: 10.1021/acs.chemrev.5b00313
Chem. Rev. 2016, 116, 1993−2022

the metal center via the oxygen and not the vinylic double bond as determined via NMR spectroscopy. Therefore, a GTP mechanism was proposed (Scheme 7).[185] These early studies demonstrated that poly(vinylphosphonate)s can be obtained via rare earth metal compounds.

A breakthrough in the polymerization of vinylphosphonates was achieved in 2010.[186] Using simple late rare earth metallocenes (Cp_2YbMe, Cp_2YbCl), the first polymerization of high molecular PDEVP above 1000 kDa was reported.[186] Contrary to a living REM-GTP, the obtained degree of polymerization was inconsistent with the initial $[M]_0$ to initiator ratio. Increasing the polymerization temperature led to an increase in not only the activity but also the initiator efficiencies (Table 2).[187,188] Back

Table 2. Polymerization of DEVP with Cp_2LnCl[a]

element	T_p[b] [°C]	M_w[c] [kg mol^{-1}]	M_n[c] [kg mol^{-1}]	PDI[c]	I^*[d] [%]	yield[e] [%]
Lu	30	1000	930	1.10	3.5	93
Yb	30	1000	830	1.20	4.0	98
Tm	30	890	810	1.10	4.0	85
Er	30	590	460	1.30	7.1	92
Ho	30	840	700	1.20	*f*	43
Dy	30	780	670	1.20	*f*	49
Lu	70	470	380	1.25	8.6	99
Yb	70	480	370	1.30	8.9	90
Tm	70	400	335	1.20	9.8	98
Er	70	470	390	1.20	8.4	96
Ho	70	375	300	1.25	10.9	93
Dy	70	310	210	1.45	15.6	99
Tb	70	155	105	1.50	31.2	84

[a]Toluene, monomer-to-catalyst ratio 200:1. [b]Polymerization temperature. [c]Determined by GPC-MALS. [d]$I^* = M_{exp}/M_n$, I^* = initiator efficiency, M_{exp} = expected molecular weight, based on living polymerization calculation. [e]Determined by weighing of the components. [f]Not calculated due to incomplete conversion.

then, a GTP-type mechanism had already been proposed and supported by the sequential block copolymerization of MMA and DEVP (Table 3).[186] The first synthesis of high molecular mass poly(vinylphosphonate)s started focused research activities investigating REM-GTP of vinylphosphonates and PDAVP material properties.

Table 3. Sequential Copolymerization of MMA and DEVP with Cp_2YbMe[a]

MMA[b]	DEVP[c]	M_w[d] [kDa]	M_n[d] [kDa]	PDI[c]	I^*[e] [%]	MMA/DEVP[f]	yield[g] [%]
100	–	14	12	1.1	83	–	98
100	100	24	22	1.2	120	1.15:1	94
100	–	15	13	1.2	77	–	97
200	200	60	52	1.1	82	*h*	96
200	–	23	20	1.1	100	–	99
200	100	44	42	1.1	87	2.1:1	98
400	–	53	27	2.0	148	–	99
400	400	150	98	1.5	108	*h*	99

[a]Toluene, 30 °C. [b]MMA-to-catalyst ratio. [c]DEVP-to-catalyst ratio. [d]Determined by GPC-MALS. [e]$I^* = M_{exp}/M_n$, I^* = initiator efficiency, M_{exp} = expected molecular weight, based on living polymerization calculation. [f]MMA/DEVP ratio in polymer product, determined by ^{1}H NMR spectroscopy. [g]Determined by weighing of the components. [h]Not determined.

5.2. Mechanism of DAVP REM-GTP

Given the structural and electronic similarity between MMA and vinylphosphonates, a group transfer mechanism had already been proposed for the successful synthesis of P(PMMA-*b*-PDEVP) block copolymers (Table 3, vide supra).[186] Contrary to results for the polymerization of MMA reported by Yasuda et al. (activity: Sm > Y > Yb > Lu),[162] the polymerization velocity of vinylphosphonates accelerates with decreasing ionic radius of the metal center, and late lanthanide initiators exhibit higher initiator efficiencies I^* and low PDIs (Table 4).[188] However, a deeper insight into the mechanism was lacking after the first preliminary results, until a comprehensive study of DAVP REM-GTP was published in 2013.[189] The determination of the monomer and catalyst orders of vinylphosphonate REM-GTP using a normalization method for living polymerizations was shown to follow a Yasuda-type monometallic propagation mechanism with a S_N2-type associative displacement of the polymer phosphonate ester by a monomer as the rate-determining step.[189] The normalization of activity results was necessary due to a significantly changing initiator efficiency and long initiation delays (Figure 1).

However, contrary to the nucleophilic transfer of a ligand to the coordinated (meth)acrylate monomer, the initiation of vinylphosphonates via lanthanide metallocenes follows a complex reaction pathway. This is mainly attributed to the α-acidic proton and consequent side reaction due to monomer deprotonation by strongly basic ligands instead of a nucleophilic transfer. An overview of different possibilities for DAVP initiation is given in Scheme 8. Initiation can proceed either via abstraction of the acidic α-CH of the vinylphosphonate (e.g., for X = Me, CH_2TMS), via nucleophilic transfer of X to a coordinated monomer (e.g., for X = Cp, SR), or via a monomer (i.e., donor)-induced ligand-exchange reaction forming Cp_3Ln in equilibrium (e.g., for X = Cl, OR), which serves as the active initiating species. An overview of the polymerization results of different initiators and metals is given in Table 5.

Chloro ligands are known as initiators for ROPs.[190−195] However, in the case of REM-GTP, chloro ligands do not initiate the polymerization of Michael-type monomers due to an insufficient nucleophilicity.[102] Alkoxides are used as effective chain transfer reagents for lactone ROP,[196−198] and theoretical calculations for the initiation of MMA via alkoxides resulted in an unlikely endothermic formation of an MMA isopropyloxide adduct.[199] However, contrary to expectation and after a distinct initiation period, bis(cyclopentadienyl) chloro rare earth metal complexes were found to initiate the polymerization of DAVPs, but further investigations were absent (Table 2).[127,186,187] To create a deeper understanding of the fundamental initiation mechanism of DAVP REM-GTP with these complexes, NMR spectroscopic studies of phosphonate coordination at the used complexes were conducted.[189] Diethyl ethylphosphonate (DEEP) was used due to its similar steric demand in comparison to DEVP as it excludes both initiation and subsequent polymerization. Addition of varying amounts of DEEP revealed a monomer (i.e., donor)-induced ligand exchange reaction forming $Cp_3Ln(DEEP)$ and $CpLnX_2(DEEP)_n$ in equilibrium with the adduct $Cp_2LnX(DEEP)$. Line broadening of the DEEP ^{1}H and ^{31}P NMR spectroscopic resonances indicates a fast exchange (on the NMR time scale) of coordinated and free DEEP. Larger metal centers and higher phosphonate concentrations accelerate the exchange reaction and shift the equilibrium toward the $Cp_3Ln/CpLnX_2$ side.[189] To elucidate the identity of the $Cp_3Ln(DEEP)$ adduct from the exchange

DOI: 10.1021/acs.chemrev.5b00313
Chem. Rev. 2016, 116, 1993−2022

Table 4. Catalytic Activity of Cp_3Ln Complexes for the Polymerization of DEVP[a]

Cp_3Ln	reaction time	conv[b] [%]	init period[c]	M_n [kDa]	I^*[d] [%]	TOF[b] [h^{-1}]	TOF/I^* [h^{-1}]
Lu	5 min	100	–	210	47	>125000	>265000
Yb	10 min	100	20 s	310	32	59400	185000
Tm	10 min	100	60 s	280	35	25200	72000
Er	32 min	100	6 min	530	19	5200	28000
Ho	2 h	99.5	30 min	670	15	1200	8000
Dy	5 h	85	100 min	710	12	270	2300

[a]Toluene, 30 °C, monomer-to-catalyst ratio 600:1. TOF, turnover frequency. [b]Determined by ^{31}P NMR spectroscopic measurement. [c]Initiation period, reaction time until 3% conversion is reached. [d]$I^* = M_{th}/M_n$, $M_{th} = 600M_{Mon}$·conversion.

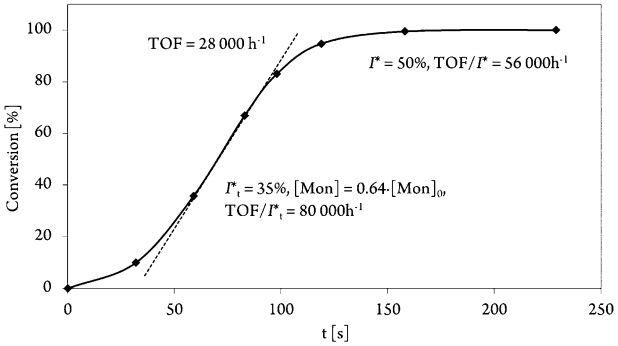

Figure 1. Conversion–time plot for the polymerization of DEVP showing a distinct initiation period and a strong dependency on the initiator efficiency I (I^*_t at the maximum rate, I^*, at the end of the reaction; [Mon] monomer concentration).

reaction, single crystals of Cp_3Y(DEEP) were obtained (Figure 2). Furthermore, the crystal structures of Cp_2LnCl(DEVP) (Ln = Ho, Yb) were obtained, by overlaying a toluene solution with pentane and cooling to −30 °C (Figure 3, Figure 4).

All crystal structures show the coordination of the monomer via the oxygen and not by coordination of the double bond. Importantly, the crystal structures of the DEVP adduct show that the Michael system of the coordinated vinylphosphonate is retained in an S-cis conformation with a pronounced π-overlap (torsion angles O═P—C═C of −10.14 and 10.47°); this is a key prerequisite for the polymerizability of a monomer by a repeated conjugate addition polymerization, i.e., a GTP.[102,186]

The investigations on the initiation mechanism revealed that all Cp_2LnX- and Cp_3Ln-initiated vinylphosphonate polymerizations are generally mediated by a Cp_2Ln unit.[189] Nevertheless, the observed normalized activities TOF/I^* of several bis(cyclopentadienyl) complexes with identical metal centers differ significantly, and there is no explanation for the large influence on the activity of the used vinylphosphonate, given by a monomer and catalyst order of 1. Therefore, temperature-dependent kinetic measurements were performed to determine activation enthalpies $\Delta H^{\ddagger}$ and entropies $\Delta S^{\ddagger}$ according to the Eyring equation.[189] These experiments were conducted for the metal centers Lu, Tm, Y, and Tb (in order of increasing metal ionic radius) as well as the monomers DEVP and DIVP (Figure 5).

Surprisingly, for both monomers, the enthalpy was found to not be affected by the metal ionic radius (Table 6). Thus, enthalpic effects, e.g., the Ln—(O═P) bond strength as a function of Lewis acidity and the metallacycle ring strain as a function of the radius of the metal center, do not determine the activity of different rare earth metals for vinylphosphonate REM-GTP. In fact, different activation barriers $\Delta G^{\ddagger}$ were found to be a result of a change of $-T\Delta S^{\ddagger}$, which was found to decrease linearly with decreasing metal ionic radius (Figure 6).

Consequently, the propagation rate of Cp_2LnX vinylphosphonate GTP is mainly determined by the activation entropy, i.e., the change of rotational and vibrational restrictions within the eight-membered metallacycle of the pentacoordinated intermediate in the rate-determining step, as a function of the steric demand of the metallacycle side chains and the steric crowding at the metal center.[189] Furthermore, the coordinated monomer shows only a minor influence on the polymerization

Scheme 8. Initiation of Vinylphosphonate GTP Using Unbridged Rare Earth Metallocenes (Cp_2LnX) via Deprotonation of the Acidic α-CH, Nucleophilic Transfer of X, or a Monomer-Induced Ligand-Exchange Reaction Forming Cp_3Ln(DAVP) (Redrawn from Ref 189. Copyright 2013 American Chemical Society.)

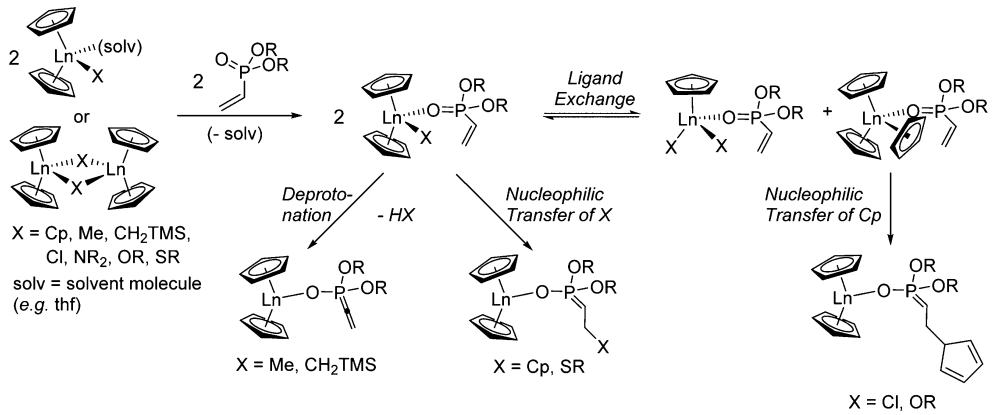

DOI: 10.1021/acs.chemrev.5b00313
Chem. Rev. 2016, 116, 1993–2022

Table 5. DEVP Polymerization Results for Cp_2LnX Catalysts[a]

catalyst	reaction time	conv[b] [%]	init period[c]	M_n[d] [kDa]	I^*[d] [%]	TOF[b]/I^* [h^{-1}]	end group[e]	extent of ligand exchange[f] [%]
$[Cp_2YCl]_2$	6 h	70	100 min	740	9.3	3700	Cp	15
$Cp_2Y(bdsa)(thf)$	3 h	95	15 min	1040	9.0	7200	Cp, bdsa (olefinic)[g]	3
$[Cp_2Y(OiPr)]_2$	30 h	26	2.5 h	1070	2.4	2000	Cp	<0.5 (10)[h]
$Cp_2Y(OAr)(thf)$	30 h	–	–	–	–	–	–	<0.5
$[Cp_2Y(StBu)]_2$	3 min	100	5 s	150	65	69000	StBu (olefinic)[g]	4
$Cp_2Y(CH_2TMS)(thf)$	40 min	88	5 min	510	17	10000	olefinic	5
$[Cp_2LuCl]_2$	1.5 h	93	7 min	780	11.7	20500	Cp	3
$Cp_2Lu(bdsa)(thf)$	3 h	96	20 min	1350	7.0	21000	Cp, bdsa (olefinic)[g]	1
$[Cp_2Lu(OiPr)]_2$	30 h	52	9 h	1270	4.0	600	Cp	<0.5 (<1)[h]
$Cp_2Lu(OAr)(thf)$	30 h	<1	–	–	–	–	–	<0.5
$[Cp_2Lu(StBu)]_2$	1.5 min	100	15 s	210	47	220000	StBu (olefinic)[g]	2
$Cp_2Lu(CH_2TMS)(thf)$	30 min	92	5 min	1130	8.0	39000	olefinic	1

[a]Toluene, 30 °C, monomer-to-catalyst ratio 600:1. [b]Determined by ^{31}P NMR spectroscopic measurement. [c]Initiation period, reaction time until 3% conversion is reached. [d]Determined by GPC-MALS, $I^* = M_{th}/M_n$, $M_{th} = 600M_{Mon}$·conversion. [e]Determined by ESI MS. [f]Conversion of Cp_2LnX for addition of 5 equiv of DEEP, determined from ^1H NMR spectroscopic signals of Cp_2LnX(DEEP) and Cp_3Ln(DEEP). [g]Olefinic chain ends formed by end group elimination. [h]Number in parentheses: extent of dimer opening for addition of 5 equiv of DEEP, determined from ^1H NMR spectroscopic signals of $Cp_2Ln(OiPr)$(DEEP) and DEEP.

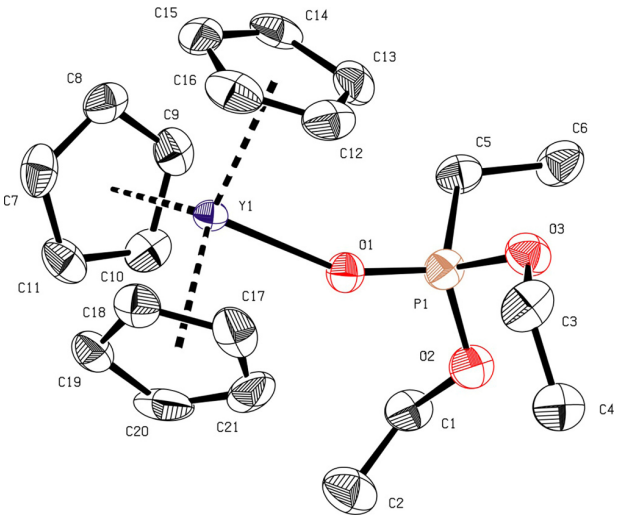

Figure 2. Crystal structure of the Cp_3Y(DEEP) adduct (50% thermal ellipsoids; hydrogen atoms omitted for clarity). Selected interatomic distances (Å) and bond angles (deg): Y—O(1), 2.294; P═O(1), 1.495; Y—O(1)═P, 7.24. (Reprinted from ref 189. Copyright 2013 American Chemical Society.)

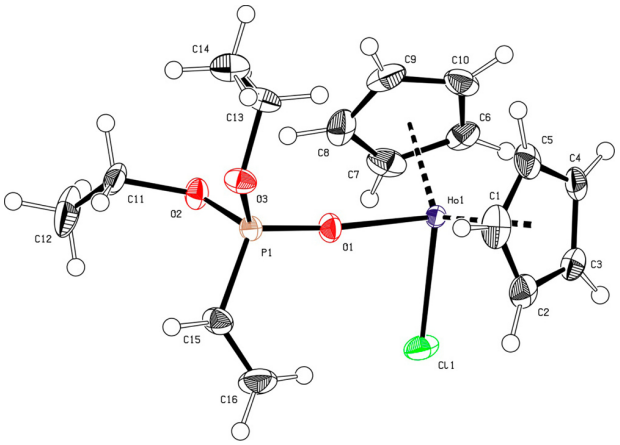

Figure 3. Crystal structure of the Cp_2HoCl(DEVP) adduct (50% thermal ellipsoids; hydrogen atoms omitted for clarity). Selected interatomic distances (Å), bond angles (deg), and torsion angles (deg): Ho—Cl, 2.582; Ho—O(1), 2.227; P═O(1), 1.485; P—C(15), 1.779; C(15)═C(16), 1.314; P═O(1)—Ho, 167.0; O(1)═P—C(15)═C(16), 10.14. (Reprinted from ref 189. Copyright 2013 American Chemical Society.)

rate of vinylphosphonate GTP as the activity is mainly determined by the steric demand of the growing polymer chain end and not by the added monomer.[189,200]

According to these experimental observations, the following mechanistic conclusions on REM-GTP of vinylphosphonates were drawn:

1. REM-GTP of DAVP proceeds via an S_N2-type associative displacement of the polymer phosphonate ester by a vinylphosphonate monomer with a pentacoordinated intermediate (Scheme 9). The first transition state, i.e., the monomer coordination, represents the rate-determining step. In this transition state, the metal—(O═P) bond to the activated monomer is much longer than the metal—(O—P) bond to the polymer ester. The longer Ln—(O═P) bond leads to a relatively small steric demand of the added vinylphosphonate in comparison with the growing chain end. The resulting minor effect of the steric demand of the added monomer on the propagation rate is in accordance with previous observations (vide supra), thus providing evidence for the proposed existence of a pentacoordinated intermediate.

2. Smaller metal centers destabilize the propagation ground state by a more confined arrangement of the eight-membered metallacycle according to the higher steric constraints caused by shorter Ln—Cp, Ln—(O—P), and Ln—(O═P) bonds. The destabilization of the ground state is not enthalpic (i.e., ring strain or the Ln—(O═P) bond strength), but entropic in nature (i.e., rotational and vibrational limitations in the eight-membered metallacycle). In the transition state, the Ln—(O═P) polymer phosphonate ester bond is lengthened, thus compensating for part of the steric stress induced by the coordination of a vinylphosphonate monomer. This effect is larger for a stronger destabilization of the ground state, i.e., for smaller metal centers.

3. Higher steric demand of the growing polymer chain end (i.e., sterically more demanding side chains) leads to a relative destabilization of the transition state by both enthalpic and

DOI: 10.1021/acs.chemrev.5b00313
Chem. Rev. 2016, 116, 1993–2022

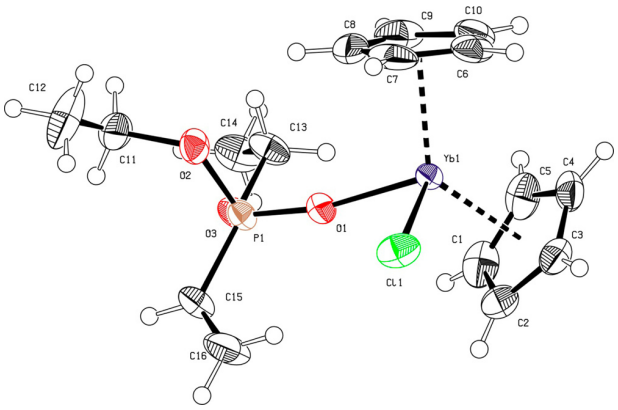

Figure 4. Crystal structure of the $Cp_2YbCl(DEVP)$ adduct (50% thermal ellipsoids; hydrogen atoms omitted for clarity). Selected interatomic distances (Å), bond angles (deg), and torsion angles (deg): Yb−Cl, 2.549; Yb−O(1), 2.196; P═O(1), 1.480; P−C(15), 1.769; C(15)═C(16), 1.311; P═O(1)—Yb, 168.2; O(1)═P—C(15)═C(16), 10.47. (Reprinted from ref 189. Copyright 2013 American Chemical Society.)

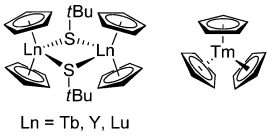

Figure 5. Used catalysts for the performed metal radius dependent Eyring plots.

Table 6. Activation Enthalpy $\Delta H^{\ddagger}$ and Entropy $\Delta S^{\ddagger}$ Dependence on Ionic Radius and Monomer Steric Demand

		DEVP		DIVP	
metal center	radius[a] [pm]	$\Delta H^{\ddagger}$ [kJ mol^{-1}]	$\Delta S^{\ddagger}$ [J (K mol)$^{-1}$]	$\Delta H^{\ddagger}$ [kJ mol^{-1}]	$\Delta S^{\ddagger}$ [J (K mol)$^{-1}$]
Tb	106.3	38.5	−102	41.3	−124
Y	104.0	38.3	−88.6	40.7	−112
Tm	102.0	39.1	−82.8	–	–
Lu	100.1	38.7	−73.6	42.0	−99.1

[a] Ln^{3+} ionic radii taken from *Lehrbuch der Anorganischen Chemie* (*Textbook of Inorganic Chemistry*, Engl. Transl.); Hollemann, A. F., Wiberg, E., Wiberg, N., Eds.; Walter de Gruyter & Co.: Berlin, 2007.

entropic effects, with the latter having the larger impact on the activation barrier. Compared to the propagation ground state, the coordinated monomer increases the steric crowding at the metal center, resulting in higher steric constraints within the eight-membered metallacycle; however, the actual monomer size plays only a minor role (vide supra). In contrast, larger metallacycle side chains induce a stronger increase in rotational and vibrational restrictions in the rate-determining step, thus destabilizing the transition state.

For the detailed mechanistic study on vinylphosphonate REM-GTP, a variety of catalysts with different initiators and metal centers were synthesized and tested for their activity in REM-GTP (vide supra). The highest activities and efficiencies for DAVPs were found for thiolato compounds; however, these exhibit distinct drawbacks such as end group elimination and smell, and the formation of $[Cp_2LnStBu]_2$ dimers prevents the polymerization of weaker coordinating monomers. Therefore,

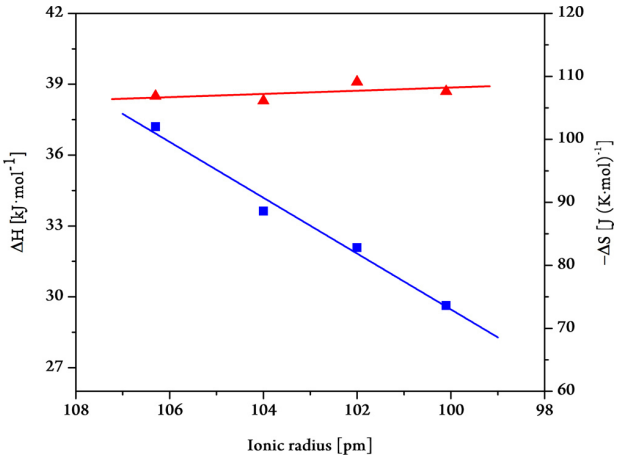

Figure 6. Activation enthalpy (red triangles) and entropy (blue squares) for DEVP polymerization using Cp_2LnX catalysts as a function of the metal ionic radius.

alternative highly active and efficient initiators are needed for REM-GTP.

5.3. Pyridine Initiators from C−H Bond Activation via σ-Bond Metathesis

The initiation for rare earth metal catalyzed polymerization of (meth)acrylates usually proceeds via the nucleophilic transfer of a strongly basic ligand, e.g., hydride, methyl, or trimethylsilylmethyl, to a coordinated monomer.[160] However, alkyl initiators were found to be poor initiators for vinylphosphonates and initiate via abstraction of the α-acidic proton (Scheme 8).[189] The thus-formed allenyl phosphonate anion is the actual initiator, but despite the chemical similarity, the nucleophilic attack of the phosphonate anion at the double bond of a second activated phosphonate monomer is inhibited and leads to low initiator efficiencies and long initiation times. Strategies to overcome the limitations of alkyl initiators were developed for zirconocene catalysts using ester enolates.[164,201] Enolate ligands simulate the active propagating species and initiate via an eight electron process. For rare earth metals, the literature on enolate compounds is limited and restricted to a few examples for selected systems only.[202,203] A similar approach to simulate the fast initiating species via an enolate is therefore not possible for REM-GTP. However, rare earth metals show a high tendency to form stable compounds from σ-bond metathesis and rare earth metal complexes are known in the literature for the C−H bond activation of methane,[204−206] hydrocarbons,[207−209] heteroaromatic substrates,[210−215] and internal alkynes.[216] A comprehensive review of C−H bond activation was recently published.[217] The first study in using activated yttrium ene−diamido complexes as initiators for the oligomerization of 2VP was carried out by Mashima et al.[218]

A successful strategy to overcome the initiation limitations for the REM-GTP of vinylphosphonates was achieved by using 2,4,6-trimethylpyridine as an activated heteroaromatic substrate for the reaction with $Cp_2YCH_2TMS(thf)$.[219] The resulting $Cp_2Y(CH_2(C_5H_2Me_2N))$ complex was used for the polymerization of DEVP; for the first time using a Cp_2LnX complex no initiation period was observed (Figure 7).[219]

The absence of any measurable initiation period for the $Cp_2Ln(CH_2(C_5H_2Me_2N))$ catalyst is attributed to a nucleophilic transfer of the $CH_2(C_5H_2Me_2N)$ ligand to DEVP via an eight-membered ring of an enamide in the transition state, simulating

DOI: 10.1021/acs.chemrev.5b00313
Chem. Rev. 2016, 116, 1993−2022

Scheme 9. Elemental Steps of Vinylphosphonate REM-GTP (Reprinted from Ref 189. Copyright 2013 American Chemical Society.)[a]

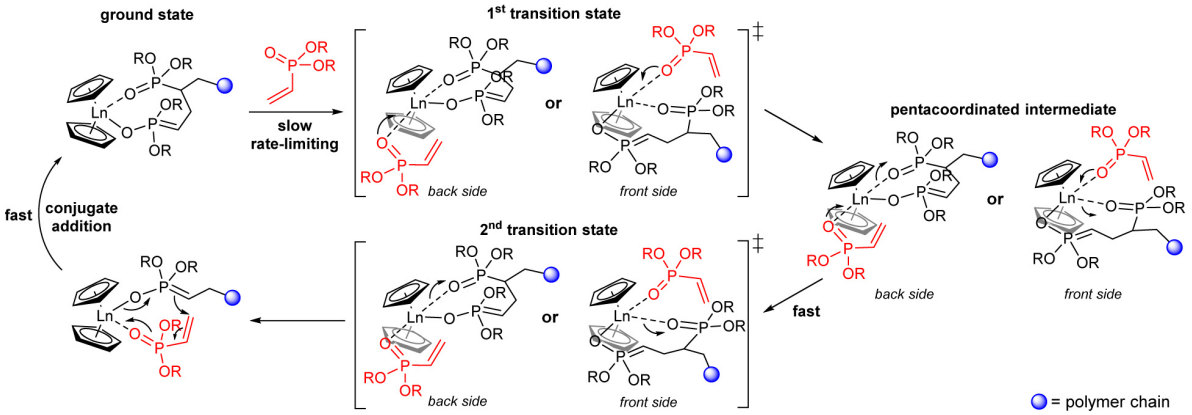

[a]The rate-limiting step is an S_N2-type associative displacement of the polymer phosphonate ester by a vinylphosphonate monomer, presumably via a pentacoordinated intermediate.

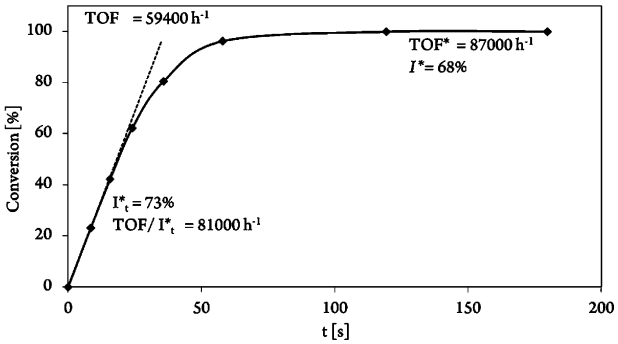

Figure 7. Conversion−reaction time plot for the polymerization of DEVP using $Cp_2Y(CH_2(C_5H_2Me_2N))$ (7.4 mg of catalyst, 10 vol % DEVP in 20 mL of toluene, 30 °C). (Reprinted from ref 219. Copyright 2015 American Chemical Society.)

the active propagating species. This assumption is further supported by the partial double-bond character of the activated methylene group (Figure 8).

From experimental data, initiation by nucleophilic transfer is evident; if it proceeds via a six- or eight-membered-ring transition

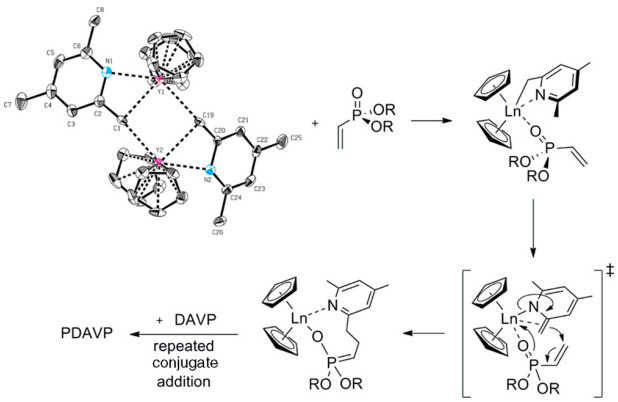

Figure 8. Dimer opening by monomer coordination and proposed initiation via an eight-membered ring of an enamide in the transition state.

state may only revealed by theoretical calculations. Interestingly, the formation of the corresponding $(CH_2(C_5H_2Me_2N))$ ligands was found to depend largely on the size of the used metal.[219]

A similar approach to overcome the initiation problems with alkyl initiators was made by Chen et al. for the polymerization of DMAA using cationic zirconocene ester enolate initiators.[220−222] Also the dependency of C_s- or C_2-symmetric *ansa*-zirconocenes in correlation with the used initiators for the polymerization of MMA was investigated.[223] The σ-bond metathesis of activated substrates is a very clean and easy way to obtain rare earth metal hydrocarbyl species, which differ in their initiation behavior from alkyl ligands and give access to end group functionalized materials. The living character (PDI = 1.02 at 30 °C, Figure 9,

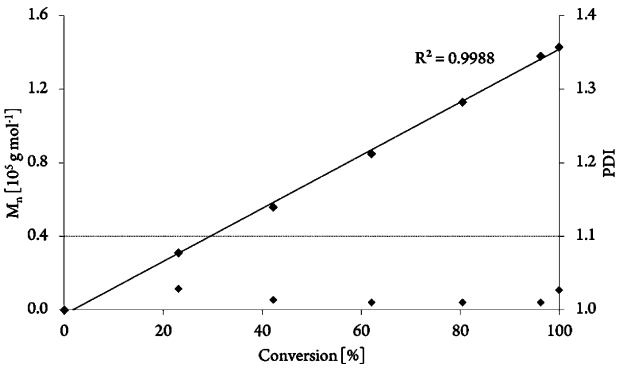

Figure 9. Linear increase of the number-averaged molecular weight during DEVP polymerization using $Cp_2Y(CH_2(C_5H_2Me_2N))$ and corresponding polydispersity (7.4 mg of catalyst, 10 vol % DEVP in 20 mL of toluene, 30 °C). (Reprinted from ref 219. Copyright 2015 American Chemical Society.)

Table 7), high initiator efficiencies, and lack of initiation period for DEVP are attributed to the proposed mechanistic match between initiation and propagation, where both follow an eight-membered-ring transition state (Figure 8). The formation of a stable C−C bond in particular opens up new areas for surface polymer modification applications.

In polymer chemistry, substrates for σ-bond metathesis have been mainly used, so far, to introduce polar end groups into nonpolar (i.e., polyolefins) materials as chain transfer

DOI: 10.1021/acs.chemrev.5b00313
Chem. Rev. 2016, 116, 1993−2022

Table 7. Comparison of $Cp_2Ln(CH_2(C_5H_2Me_2N))$ Initiators for the REM-GTP of DEVP, IPOx, and 2VP[a]

catalyst	monomer	$[Mon]_0/[Cat]_0$	init period[b]	M_n[c] [kDa]	PDI[c]	I^*_t[c] [%]	I^*[c] [%]	TOF[d] [h^{-1}]	TOF/I^*_t [h^{-1}]
$Cp_2Y(CH_2(C_5H_2Me_2N))$	DEVP	600	–	140	1.02	73	68	59400	81000
$[Cp_2Y(StBu)]_2$	DEVP	600	5 s	150	1.18	46	65	44000	96000
$Cp_2Lu(CH_2(C_5H_2Me_2N))$	DEVP	600	–	480	1.13	16	21	46000	300000
$[Cp_2Lu(StBu)]_2$	DEVP	600	15 s	210	1.27	35	47	103000	290000
$[Cp_2YbMe]_2$	DEVP	600	80 s	910	1.52	54	11	4300	8000
$Cp_2Y(CH_2(C_5H_2Me_2N))$	IPOx	200	*e*	20	1.26	*e*	89	*e*	*e*
$Cp_2Lu(CH_2(C_5H_2Me_2N))$	IPOx	200	*e*	38	1.39	*e*	59	*e*	*e*
$[Cp_2YbMe]_2$	IPOx	200	–	21	1.04	*f*	95	380	*f*
$Cp_2Y(CH_2(C_5H_2Me_2N)$	2VP	100	*f*	13	1.01	*f*	80	*f*	*f*
$Cp_2Lu(CH_2(C_5H_2Me_2N)$	2VP	100	*f*	38	1.08	*f*	28	*f*	*f*
$[Cp_2YbMe]_2$	2VP	100	*f*	14	1.01	*f*	75	44	*f*

[a]Toluene, 30 °C. [b]Initiation period, reaction time until 3% conversion is reached. [c]Determined by GPC-MALS, $I^*_t = M_{th}/M_n$, $M_{th} = ([Mon]_0/[Cat]_0)M_{Mon}$·conversion ($I^*_t$ at the maximum rate, I^* at the end of the reaction). [d]Determined by ^{31}P (DEVP) or ^1H (IPOx) NMR spectroscopic measurement. [e]Not determined due to incomplete conversion (yield = 80% (Y), 75% (Lu)). [f]Not determined.

reagents.[213,224−228] The method of using activated heteroaromatic substrates or internal alkynes as new initiators opens up new applications for REM-GTP of polar monomers, having initiation problems with hydride or alkyl ligands.[218,219]

6. PROPERTIES OF POLY(VINYLPHOSPHONATE)S

6.1. Thermoresponsive Behavior of Aqueous PDAVP Solutions

Polymers that change their properties according to their surroundings are considered smart polymers, and several examples for self-healing, photoresponsive, pH-responsive, or temperature-responsive polymers exist.[229−231] In macromolecular chemistry, temperature-dependent solubility is a prominent and well-studied field. Here, two cases can be distinguished: the lower critical solution temperature (LCST) represents the temperature below which a polymer solution is a one-phase system for all possible compositions; correspondingly the upper critical solution temperature (UCST) is the temperature above which a one-phase system is present.[232] Poly(vinylphosphonate)s show varying solubility depending on the nature of the ester side chain. Hydrophilic PDMVP is distinctly soluble in water and poorly soluble in organic solvents, whereas hydrophobic PDIVP is soluble in organic solvents. Therefore, it is not surprising that PDEVP shows amphiphilic behavior and is soluble in water and most common organic solvents. Aqueous solutions of PDEVP exhibit a thermoresponsive behavior and show an LCST close to the physiological range (T_{LCST} = 40−46 °C, Figure 10, Figure 11).[188] The LCST depends on the molecular mass and concentration of PDEVP, and generally, sharp and fully reversible phase transitions are observed over a narrow temperature range. With increasing molecular mass, aqueous solutions of PDEVP were found to precipitate at lower temperatures and lower concentrations, resulting in a broadened phase transition (Figure 11, Figure 12).[188]

REM-GTP gives access to a precise synthesis of homopolymers (vide supra). Furthermore, random copolymerization, block copolymers of polar monomers, copolymerization of polar monomers, and nonpolar olefins or ROP were successfully prepared by mechanistic crossovers using rare earth metal initiators.[98,99,101,167,179,233,234] Novel random DAVP copolymers were synthesized by varying their comonomer ratios via the easily accessible tris(cyclopentadienyl)ytterbium.[200] The copolymerization parameters were determined by activity measurements according to the Finemann−Ross method,[235] showing the formation of almost perfectly random copolymers (r_1, $r_2 \sim 1$).

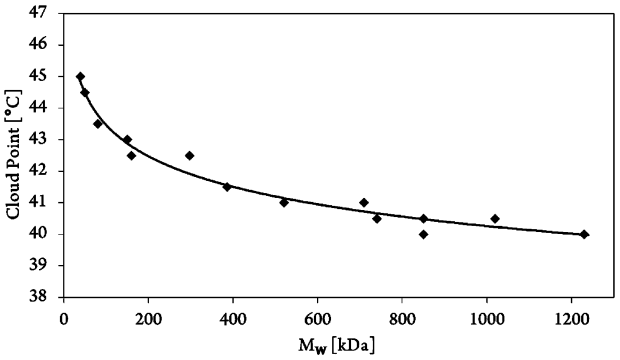

Figure 10. Cloud point vs mass-average M_w for aqueous PDEVP (5 mg mL^{-1}). (Redrawn from ref 188. Copyright 2011 American Chemical Society.)

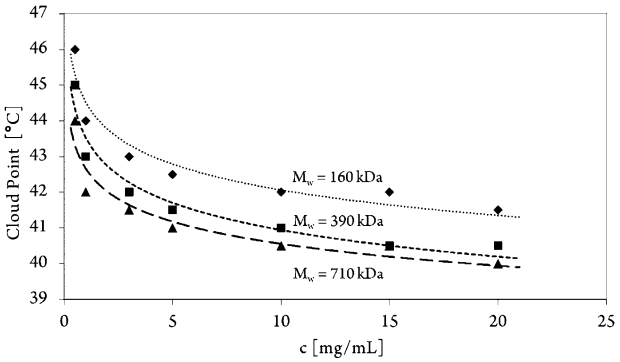

Figure 11. Cloud point vs concentration for aqueous PDEVP solutions with different molecular masses: 160 kDa (diamonds, dotted), 390 kDa (squares, short dashed), and 710 kDa (triangles, long dashed). (Redrawn from ref 188. Copyright 2011 American Chemical Society.)

The obtained copolymers from DEVP and dimethyl or di-*n*-propyl vinylphosphonate (DMVP, DPVP) are water-soluble and show thermoresponsive properties, exhibiting a tunable LCST between 5 and 92 °C (Figure 13). Hence, the LCST can be precisely adjusted by varying the comonomer composition and correlates linearly with the hydrophilic to hydrophobic comonomer ratio (Figure 14).

The phase transition of poly(vinylphosphonate)s follows a coil−globule transition mechanism, and the differential scanning calorimetric (DSC) experiment for 30 wt % aqueous PDEVP

DOI: 10.1021/acs.chemrev.5b00313
Chem. Rev. 2016, 116, 1993−2022

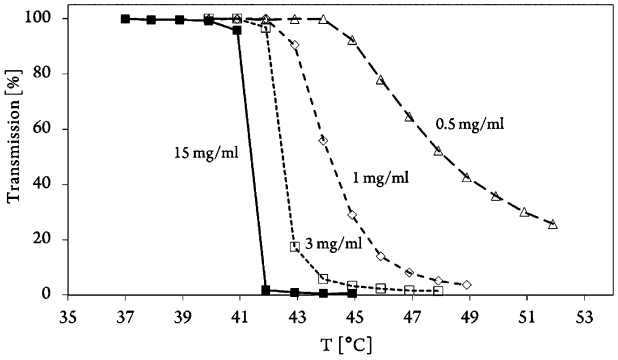

Figure 12. Change in transmittance at λ = 550 nm for PDEVP with 160 kDa at different concentrations: 15 mg mL^{-1} (squares, plain), 3 mg mL^{-1} (squares, short dashed), 1 mg mL^{-1} (diamonds, dashed), and 0.5 mg mL^{-1} (triangles, long dashed). The LCST was determined at a transmission rate of 85%. (Redrawn from ref 188. Copyright 2011 American Chemical Society.)

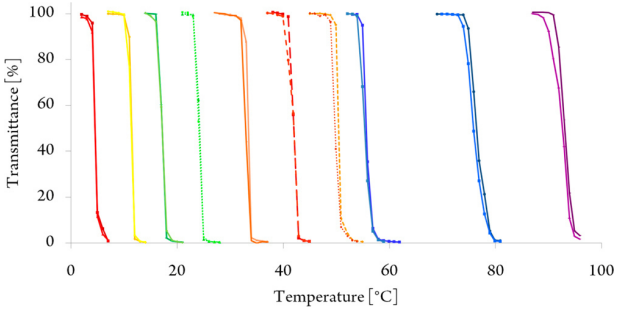

Figure 13. Determination of cloud points of DEVP–DPVP (0–35 °C), PDEVP (42 °C), and DEVP–DMVP (50–95 °C) homo/copolymers. The cloud point was determined at 10% decrease in transmittance for 1.0 wt % aqueous polymer solutions.

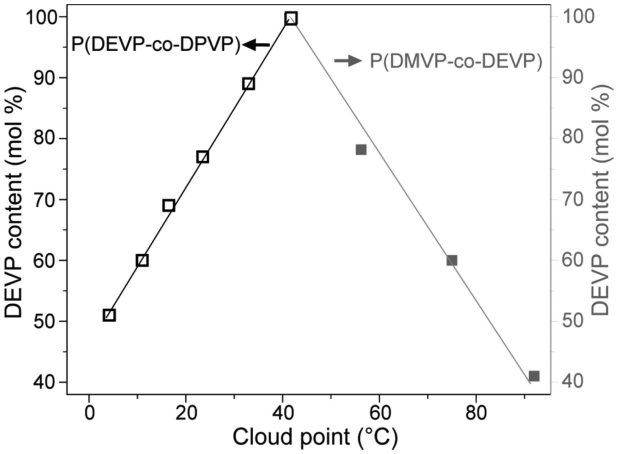

Figure 14. Linear dependence of the LCST on the comonomer content of DEVP and DPVP/DMVP copolymers. (Reprinted from ref 200. Copyright 2012 American Chemical Society.)

solutions revealed an endothermic process upon heating as a very sharp transition with an onset at 46 °C or an exothermic phase transition at 45 °C while cooling. The values from DSC measurements are in good agreement with the corresponding cloud point determined by turbidimetry.

For biomedical applications, the influence of salts and other complex media in which biological processes take place is an important parameter for the thermal behavior of polymers.[236] Therefore, the thermoresponsive properties of PDAVP copolymers were investigated in the presence of additives such as sodium chloride, calcium chloride, phosphate buffered saline (PBS), and fetal calf serum (FCS).[200] Typical salting-out effects were observed, but they were found to be smaller than those for PEG or PNIPAM.[237] The formation of perfectly random PDAVP copolymers with a uniform composition is highly desirable as gradient copolymers tend to assemble into complex nanostructures[238] or micelles and therefore often exhibit a prolonged or irreversible phase transition.[239−241] Therefore, PDEVP homopolymers or random poly(vinylphosphonate) copolymers are promising candidates for thermoresponsive smart polymers for biomedical applications.

6.2. Transformation of High Molecular Mass Poly(vinylphosphonate Esters) to Poly(vinylphosphonic Acid)

A direct GTP synthesis of VPA is not possible because group transfer (metal-mediated or SKA) and anionic polymerizations are highly sensitive toward protic impurities. Furthermore, an easy and mild transformation of vinylphosphonate esters to a free acid is necessary to evaluate the material properties of high molecular mass PVPA. Procedures in the literature often use harsh reaction conditions, concentrated acids, or prolonged reaction times, which can lead to degradation of high molecular mass PDAVP.[112,113,120,129,132,136,137,242] Therefore, a conversion of PDAVPs to PVPA was established via thermal treatment or a mild hydrolysis (Scheme 10). Wagner et al. reported the

Scheme 10. Transesterification of Poly(vinylphosphonate)s: (a and b) Chemical, (c) Thermal, and (d) Hydrolysis to PVPA (Redrawn with Permission from Ref 127. Copyright 2012 John Wiley and Sons.)

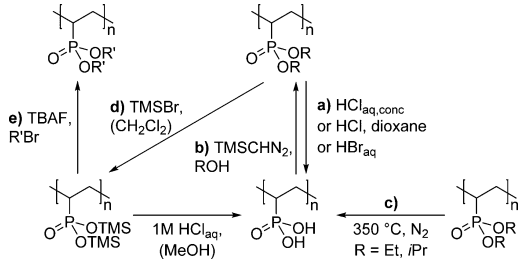

hydrolysis of PDIVPs (M_n < 40 kDa) obtained via anionic polymerization under mild conditions via treatment with trimethylsilyl bromide in refluxing dichloromethane.[133] Independently, a similar approach was used by Wagener et al. for the synthesis of phosphonic acid functionalized polyethylene.[243] Following this general procedure, complete hydrolysis was obtained for PDEVP, and for the corresponding PDIVP, a mixture of phosphonic acid, starting material, and silylester was observed.[188] The incomplete conversion of PDIVP is attributed to the stronger steric hindrance of the isopropyl group, to a hampered cleavage, and to a higher boiling point of the side product 2-bromopropane, which therefore cannot be removed from equilibrium. The mild hydrolysis proceeds via a two-step reaction. First, a transesterification of the corresponding poly(vinylphosphonate) was carried out with TMSBr, followed by hydrolysis in MeOH under acidic conditions. The

DOI: 10.1021/acs.chemrev.5b00313
Chem. Rev. 2016, 116, 1993−2022

intermediate poly(bis(trimethylsilyl) vinylphosphonate) was isolated and further reacted with benzyl bromide, but is very sensitive toward water (Scheme 10d).[188]

The above-presented transesterification is a mild method, but it fails to quantitatively produce PVPA from PDIVP and requires stoichiometric amounts of reagents and purification. A convenient alternative exists, by using the first thermal polymer degradation point of PDAVPs. At elevated temperatures, side group cleavage is observed leaving the main chain intact: in the case of PDEVP, ethylene is formed as the main product (280−340 °C; minor product Et_2O, EtOH) and for PDIVP, only propylene is observed at 245−270 °C. For both starting materials, the remaining polymeric material is free PVPA, as confirmed by NMR and elemental analysis.[188] This method follows a very easy preparative procedure and has the advantage that no other reactants are needed as it is solvent-free and highly atom efficient. Possible polymer degradation by thermal treatment was examined by determination of the M_w by static light scattering, using a Zimm plot. No indication of main chain scission was observed within the accuracy of the given light scattering setup.[188] PVPA decomposes to $P_xO_yC_z$ at temperatures above 460 °C in a second thermal polymer degradation point.[188]

6.3. Poly(vinylphosphonate)s as Flame Retardants

The interest in flame-retarding polymers as functional materials is steadily increasing as they find use as insulators in electronic applications[244−247] or in the aerospace and automotive industries as structural and functional composites.[248] There are two approaches for preparing flame-retarding materials. One is to synthesize structural polymers with intrinsic flame-retarding properties,[249−252] and the other is to add flame retardants as small molecules to the polymers.[253,254] In industrial and academic applications, phosphorus-containing compounds play a crucial role in polymer flame retardants (FRs), as they are less harmful to the environment compared to the persistent and possibly bioaccumulating halogen-based FRs.[255] Phosphorus flame-retardant additives (FRAs) can act in the condensed phase by enhancing charring and intumescence, or via inorganic glass formation and flame inhibition. Furthermore, P═O radicals can lead to flame inhibition in the gas phase by reacting in the flame zone with more reactive radicals.[256−259] Sterically hindered diaryl arylphosphonates such as dimesityl phenylphosphonate (DMPP) are reported to be effective FRAs in polycarbonates (PC) at low loadings of 3−5 wt %.[260] The use of low molecular mass FR can affect the material properties and lead to an undesired lower applicability of the final product (e.g., influencing glass transition temperature, melt viscosity, or tensile strength). Therefore, the use of oligomeric and polymeric phosphate or phosphonate additives is getting increased attention for flame-retardant applications.[261−266]

High molecular mass poly(vinylphosphonate)s synthesized via REM-GTP were recently used as halogen-free FRAs for polycarbonates (PC).[267] The aromatic di-*p*-tolyl vinylphosphonate (DTVP) was synthesized as the first example of an aromatic diaryl vinylphosphonate (DArVP).[267] However, contrary to DAVP polymerization, the activities and yields are significantly lower. This was attributed to the low flexibility of the rigid aromatic ester side chain hindering monomer coordination at the sterically demanding eight-membered-ring propagation transition state.[160] PC/PDTVP blends with PDTVP contents of up to 20 wt % were produced and no dripping during combustion occurred, showing advantages over low-molecular-weight phosphorus-based FRAs that drip when burning.[267] Furthermore, PDAVP/PC coatings were tested for their use as flame retardant coatings (FRCs), and PDIVP/PC FRCs were found to form a protective intumescent layer of free PVPA by exposure to heat (Figure 15c).[267] Poly(vinylphosphonate)s are promising

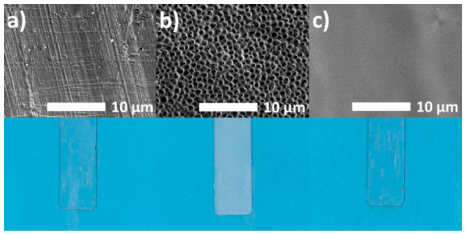

Figure 15. SEM micrographs of PDIVP coatings from MeOH solutions with concentrations of (a) 0.01, (b) 0.05, and (c) 0.1 g(PDIVP)/mL. (Reprinted from ref 267. Copyright 2015 American Chemical Society.)

compounds as additives for flame retardant applications, as they act mostly in the condensed phase. Aromatic PDArVP decompose in a one-step mechanism at higher temperatures compared to their flexible aliphatic counterparts (two-step mechanism) and show distinguished features in PC blends.

6.4. Poly(vinylphosphonate)s as Kinetic Hydrate Inhibitors

The PDAVPs PDIVP, PDEVP, and PDMVP were recently investigated as non-amide kinetic hydrate inhibitors (KHIs).[268] KHIs are frequently used in the offshore oil and gas production to prevent the formation of gas hydrates under high pressure and low temperatures. In the study by Kelland et al., the KHI performance of PDAVPs was found to increase with decreasing hydrophilicity from PDMVP, to PDEVP to PDIVP and the evaluated PDAVPs were produced via free radical or frustrated Lewis pairs (FLPs) polymerization (PDI = 1.3−2.5).[268] PDIVP homopolymer gave an average onset temperature of T_o of 8.3 °C compared to 17.3 °C with deionized water and no additive. The good performance is likely related to the low cloud point (1 wt % solution in deionized water), which was measured to be 18 °C. Three ethylated PDEVPs, with molecular weights in the range 30−60 kDa, were tested for KHI performances.[268] The two higher molecular weight samples gave the best performance, which is attributed to the lower cloud point of these samples than the molecular weight. A PDMVP-*co*-PDIVP copolymer with a high cloud point showed weak KHI effect (T_o = 13.1 °C).[268] Besides PDAVPs, poly(2-alkyl-2-oxazoline)s have been studied as KHIs.[269]

6.5. Microstructure of Poly(vinylphosphonate)s

Compared to other vinyl polymers and considering the broad scope of applications for PVPA and its esters, knowledge of the microstructure of poly(vinylphosphonate)s is limited due to their poor polymerizability via classic polymerization methods. In the literature, only a single publication by Komber, Steinert, and Voit deals with the microstructure of PVPA and PDMVP in-depth using ^1H, ^{13}C, and ^{31}P NMR studies.[123] PVPA synthesized by free radical polymerization was found to be atactic, and a large amount of head-to-head (H−H) and tail-to-tail (T−T) regioerrors of up to 17% were observed (Figure 16).[123] The misconfiguration and formation of H−H and T−T links are attributed to a cyclopolymerization under the formation of five- and six-membered rings of a VPA anhydride intermediate.[120,123]

PDMVP was prepared using two different synthetic procedures. One was to polymerize DMVP via free radical

DOI: 10.1021/acs.chemrev.5b00313
Chem. Rev. 2016, 116, 1993−2022

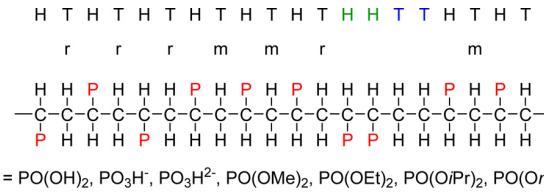

Figure 16. Microstructure of poly(vinylphosphonate)s with examples for H−H and T−T regioirregular structures.

polymerization, and as an alternative approach, PVPA was converted to PDMVP using a postpolymerization modification (Scheme 10).[123] Simultaneously, PVPA obtained via hydrolysis from PDMVP was further elucidated and compared to its counterpart. Interestingly, PDMVP obtained via free radical polymerization of DMVP consists of fewer regioirregular linkages than PVPA (8 ± 2%) and is isotactic-rich ([*m*] = 59%).[123] The ratio of PDMVP diads was calculated from the ^{1}H NMR backbone signals in D_2O and MeOD, and in principle, the signal assignment corresponds for both solvents. The assignment of the ^{1}H NMR signals for PVPA and PDMVP was assisted by two-dimensional HMQC and TOCSY measurements, and in combination with one- and two-dimensional (1D and 2D) methods the methylene (high field) and methine (low field) regions were allocated (Figure 17). A spectral line deconvolution was possible for neither PVPA nor PDMVP due to the high amount of H−H and T−T linkages in the polymers, and compared to ^{1}H NMR the ^{13}C and ^{31}P NMR spectra were found to give less stereochemical information.[123]

In 2010, Takeichi et al. reported an isotactic (*it*)-rich anionic polymerization of DMVP using organolithium initiators in combination with the Lewis acid tri-*n*-butylaluminum (*n*-Bu_3Al) in toluene. They produced *it*-rich PDMVP with molecular masses up to 11 kDa (Table 8).[270] Atactic PDMVP (prepared via free radical polymerization) was found to be soluble in acetone, chloroform, and water, whereas *it*-rich PDMVP was insoluble in organic solvents.[270] Depending on the used polymerization temperature, the percentage of [*m*] diads ranged between 60 and 67%. The tacticities were calculated from ^{1}H NMR data for [*m*] and [*r*] diads using an algorithm based on a peak deconvolution

Table 8. Polymerization Results of DMVP in Toluene

initiator	$[M]_0/[I]_0$	temp [°C]	yield[a] [%]	M_n[b] [kDa]	PDI	tacticity [%] *m*	*r*
AIBA	400	60	46	5	1.43	52	48
t-BuMgBr	50	−78	trace	–	–	–	–
t-BuLi	50	−78	29	7.5	2.65	65	35
t-BuLi, *n*-Bu_3Al	50	−78	76	5.5	1.30	67	33
t-BuLi, *n*-Bu_3Al	50	0	100	11	3.97	60	40
n-Bu_3Al	10	−78	trace	–	–	–	–

[a]Determined by weighing. [b]Determined by SEC using aqueous 0.2 M NaCl as eluant.

method for overlapping signals (Figure 18).[270] For the signal assignment, the previously published results of Komber, Steinert, and Voit were used.[123]

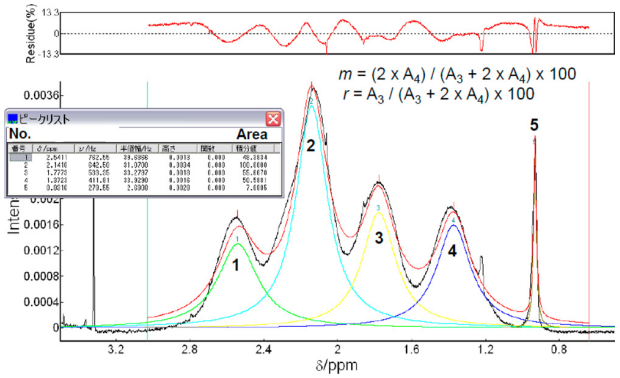

Figure 18. Algorithm-based ^{1}H NMR peak deconvolution of PDMVP obtained from anionic polymerization. (Reprinted with permission from ref 270. Copyright 2010 John Wiley and Sons.)

Up to now, a controlled stereoregular polymerization of vinylphosphonates via REM-GTP is an unmet challenge.

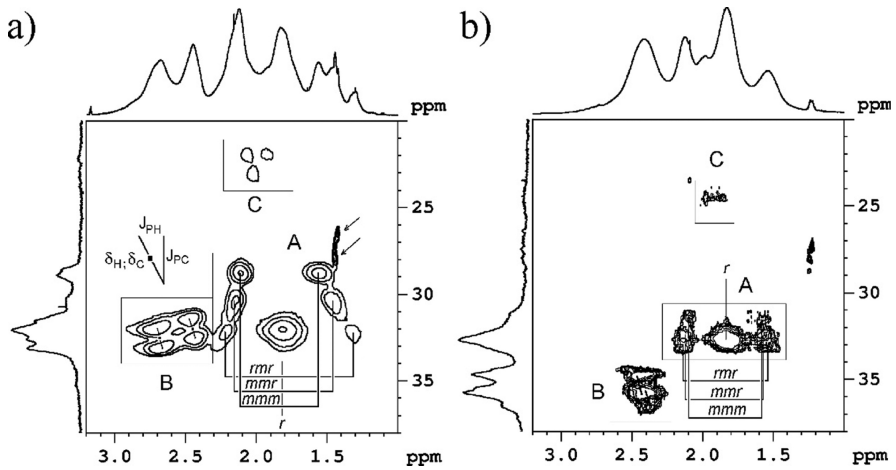

Figure 17. ^{1}H−^{13}C HMQC spectra (CH and CH_2 region) of PDMVP (a, MeOD) and PVPA (b, D_2O). The assignment to tetrads is given for the methylene signals. The inset in (a) explains the characteristic methine group signal pattern caused by the passive $^{1}J_{PC}$ (vertical axis) and $^{2}J_{PC}$ (horizontal axis) couplings; the filled square gives the position defining the ^{1}H and ^{13}C chemical shifts of the cross-peak. The arrows point at signals due to AIBN-based end groups. (Reprinted from ref 123. Copyright 2008 American Chemical Society.)

DOI: 10.1021/acs.chemrev.5b00313
Chem. Rev. 2016, 116, 1993−2022

Investigations on the initiation mechanism revealed that all Cp_2LnX- and Cp_3Ln-catalyzed vinylphosphonate polymerizations are generally mediated by a Cp_2Ln unit and that polymers with essentially the same (atactic) microstructure are produced (Figure 19).[189]

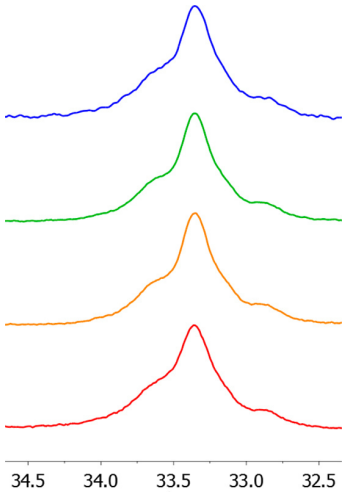

Figure 19. ^{31}P NMR spectra of PDEVP (in D_2O) produced with different catalysts (from top to bottom: $[Cp_2LuCl]_2$ (blue), Cp_3Lu (green), $Cp_2Lu(bdsa)(thf)$ (orange), and $[Cp_2YbMe]_2$ (red). For all catalysts, polymers with (nearly) identical atactic microstructure are obtained. (Redrawn from ref 189. Copyright 2013 American Chemical Society.)

Therefore, the commonly used, simple, unbridged, and sterically nondemanding Cp-based metallocene catalysts do not induce any tacticity for the polymerization of DEVP or DIVP, and only atactic polymers are formed.[189] In the literature, only one article reports on the isotactic polymerization of DEVP for REM-GTP using readily available $Ln(bdsa)_3(thf)_2$ (Ln = La, Nd, Sm) precursors.[271] PDEVPs with molecular masses between 65 and 84 kDa have been produced, and [*mm*] contents of up to 79% and conversions below 80% were reported.[271] The values of corresponding triads were calculated, from the methine proton region and the oxymethylene carbon signals, by line-fitting.[271] The methine and methylene signal regions were assigned based on HMQC measurements (Figure 20). The inadequate suitability of bdsa initiators has already been discussed in section 5.2 (vide supra).[189] Therefore, the resulting *it*-PDEVP samples show very high polydispersities (PDI = 3.11−3.56) possibly due to three possible initiating amide ligands; the used catalysts do not benefit from the advantages of REM-GTP (i.e., usual suppression of side or termination reactions and low polydispersities).

In summary, the assignment of PVPA and PDAVP triads and tetrads was realized using 2D HMQC and TOCSY measurements.[123,271] Due to overlapping signals in ^1H NMR, peak deconvolution, as performed by Takeichi et al., is an elegant method to quantify the microstructure based on simple ^1H NMR experiments.[270] However, a determination of the tacticity using ^1H NMR spectroscopy is only possible for PVPA or PDMVP; the other vinylphosphonate monomers (e.g., PDEVP, PDIVP) show overlapping signals of the ester side chain and in the area of the backbone methine and methylene signals. As for the corresponding signals in the ^{31}P NMR spectra, an attribution was so far not conducted, despite the advantages of the ^{31}P nuclei when compared to ^1H (overlapping signals, solvent and impurity proton peaks) and ^{13}C (low natural abundance and long relaxation times).

7. SURFACE-INITIATED GROUP TRANSFER POLYMERIZATION

The modification of surfaces with polymer layers, to provide protection and/or a specific functionality, is widely used and attracts significant commercial interest. Surface modifications and coatings need to be attached via a stable (preferably covalent) bond on a substrate, and radical, cationic, or anionic polymerizations can be applied.[272−279] Ideally, the polymerization process should control the material properties, the molecular mass, and the formation of copolymers. Thus, investigations on catalytic polymerization techniques were

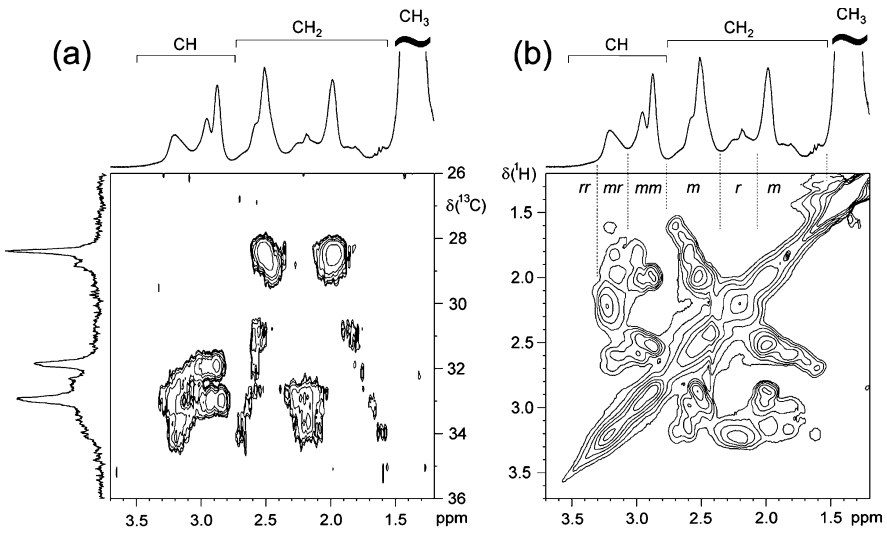

Figure 20. Regions of the $^1H-^{13}C$ HMQC spectrum (a) and $^1H-^1H$ TOCSY spectrum (b, mixing time 20 ms) of PDEVP (solvent C_6D_6; T = 70 °C). (Reprinted from ref 271. Copyright 2010 American Chemical Society.)

DOI: 10.1021/acs.chemrev.5b00313
Chem. Rev. 2016, 116, 1993−2022

Scheme 11. Preparation of Precoating Layer, Ytterbocene Catalyst Immobilization, and Subsequent SI-GTP of MMA or DAVP for (a) a 3-(Trimethoxysilyl)propyl Methacrylate (TMSPM) Monolayer, (b) a PEGDM Film on Silicon Wafer, and (c) Molecular Structure of MMA and DAVP, and SI-GTP Reaction Mechanism for Initiation and Chain Growth (Reprinted from Ref 285. Copyright 2012 American Chemical Society.)

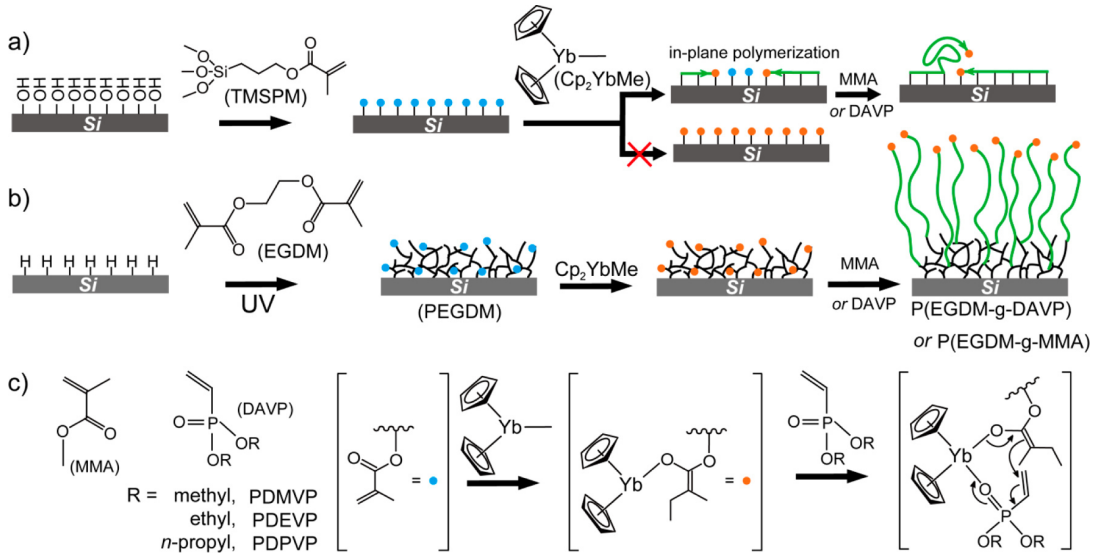

carried out.[280−284] Not only are the material properties of poly(vinylphosphonate)s of interest, but also the application of REM-GTP in combination with new monomers, resulting in hybrid or tailored materials, is an important fields for REM-GTP development. Based on the REM-GTP of vinylphosphonates, SI-GTP was developed, allowing the covalent modification of surfaces or particles with dense polymer brushes.[285,286] Stable poly(vinylphosphonate) coatings are of particular interest for applications in the biomedical field such as nonfouling coatings or cell proliferation surfaces.

SI-GTP on silicon surfaces was inspired by earlier work on P(MMA-*b*-DEVP) block copolymerization via Cp_2YbMe initiators.[186] As a first step, a hydrogen-terminated silicon surface, obtained via etching with 48% HF,[287−291] is topped with a layer of poly(ethylene glycol dimethacrylate) (PEGDM) via radical self-initiated photografting and photopolymerization (SIPGP).[292−295] The catalyst Cp_2YbMe is immobilized on the PEGDM layer, resulting in an active methacrylate enolate as the initiating species (Scheme 11). Upon monomer addition (MMA, DMVP, DEVP, or DPVP), a covalent bond between the enolate and coordinated monomer is formed. The propagation proceeds within minutes and growth rates of 57.0 and 26.5 nm min^{-1} for MMA and DEVP, respectively, were observed.[285] The formation of poly(vinylphosphonate) brushes was confirmed via X-ray photoelectron spectroscopy (XPS) and IR measurements, the latter exhibiting the characteristic P═O and P−O stretching modes at 1228 and 1027/1052 cm^{-1}, respectively. Atomic force microscopy (AFM) results, in combination with the XPS measurements, prove the homogeneity of the polymer brushes and a linear layer increase over the polymerization time (Figure 21).

Furthermore, polymer brushes prepared from different monomers show significant differences in their material properties. Contact angle measurements reveal a change in polarity for PDMVP-, PDEVP-, or PDPVP-modified silicon surfaces. A static water contact angle of 17 ± 3° was found for hydrophilic PDMVP surfaces and an angle of 76 ± 2° was found

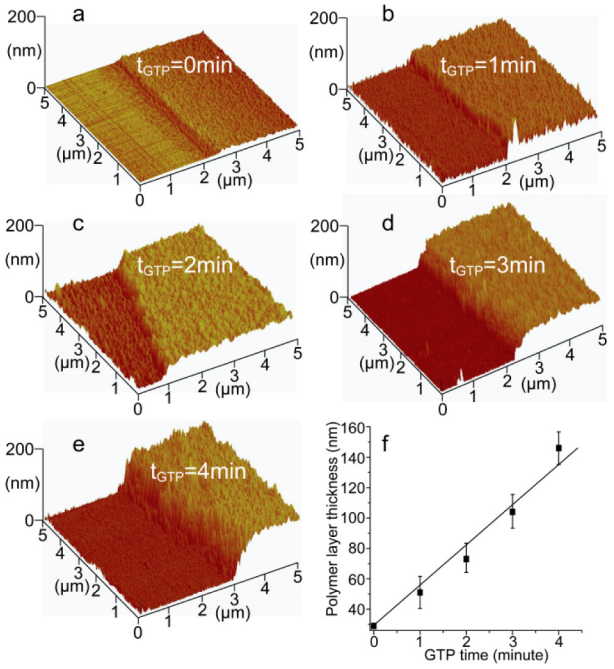

Figure 21. Three-dimensional representation of AFM scans of a PEGDM film on silicon wafer and polymer brushes after SI-GTP of DEVP. (a) SIPGP of EGDM for 30 min gives a PEGDM film with a thickness of 29 ± 6 nm. (b)−(e) SI-GTP of DEVP on the same substrate after 1, 2, 3, and 4 min results in 51 ± 11, 73 ± 9, 104 ± 11, and 146 ± 12 nm thick polymer brush layers, respectively. (f) P(EGDM-*g*-DEVP) layer thickness as a function of SI-GTP time. (Reprinted from ref 285. Copyright 2012 American Chemical Society.)

for the hydrophobic PDPVP, respectively (Figure 22).[285] PDEVP exhibits thermoresponsive behavior in water (vide supra), and at room temperature, a contact angle of 44 ± 2° was measured for the PDEVP brushes. At elevated temperatures, the contact angle increased to 66 ± 2° following a coil−globule

DOI: 10.1021/acs.chemrev.5b00313
Chem. Rev. 2016, 116, 1993−2022

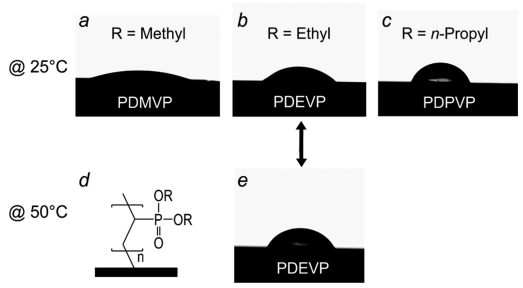

Figure 22. Molecular structure of PDAVP (d) and static water contact angle (CA) on different PDAVP coatings on silicon substrates at different temperatures. (a–c) CA of PDMVP, PDEVP, and PDPVP brushes at 25 °C. (e) CA of PDEVP brush at 50 °C. (Reprinted from ref 285. Copyright 2012 American Chemical Society.)

transition mechanism, decreasing the hydrophilicity of the surface (Figure 22). SI-GTP gives access to both thermoresponsive (PDEVP) and proton-conducting (PVPA) brush layers and allows the synthesis of perfectly decorated substrates.[285]

Using a similar procedure, SI-GTP was applied not only to silicon surfaces but also to poly(styrene) microspheres.[296] Rupture of the PS microspheres, due to polymerization inside the sphere or peeling as a result of the high surface tension of the formed brushes, was observed during REM-GTP with DAVPs (Figure 23).[296]

In addition, SI-GTP was used to modify silicon nanocrystals (SiNCs).[297] The optoelectronic behavior of SINCs is tunable by size and surface functionality. Hydrogen-terminated SINCs (size 3 nm) were reacted with EGDM, following the SI-GTP procedure.[297] However, after SIPGP, the free-standing hydrogen-terminated SiNCs formed larger aggregates, up to 177 ± 81 nm, due to cross-linking with the PEGDM layer (Figure 24a).[297] When $Cp_2YCH_2TMS(thf)$ was used as a catalyst for the polymerization of DEVP, photoluminescent-thermoresponsive hybrid materials were obtained.[297] SI-GTP adds well to other surface modification methods. However, the advantages of a catalytic living polymerization have not yet been addressed (i.e., copolymerization, stereoregular polymerization, or application to a wider variety of monomers). When combined with the unique properties of nanomaterials, SI-GTP can be a particularly useful tool for future materials and their modification over a wide range of applications.

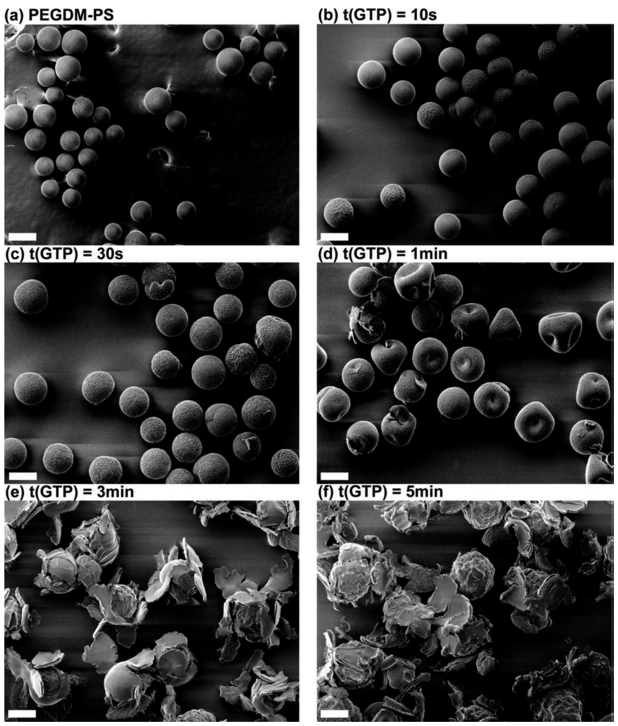

Figure 23. SEM scans of PDEVP modified PS microspheres after SI-GTP for different reaction times: (a) 0 s, (b) 10 s, (c) 30 s, (d) 1 min, (e) 3 min, and (f) 5 min. Scale bar: 200 μm. (Reprinted with permission from ref 296. Copyright 2014 John Wiley and Sons.)

8. APPLICATION OF REM-GTP TO NITROGEN-COORDINATING MONOMERS

In early studies, rare earth metallocene initiators were found to be inactive for the polymerization of 4-vinylpyridine or 2-vinylpyridine (2VP), the latter showing a Michael system.[162] However, in recent years, REM-GTP has been established for 2VP and 2-isopropenyl-2-oxazoline (IPOx), both proceeding via N–rare earth metal coordination (Figure 25).[218,298] The polymerization of 2VP is not limited to REM-GTP or coordinative–anionic procedures, as P2VP can be obtained at elevated temperatures via radical polymerization or by organolithium initiators at low temperatures using classic anionic polymerization methods. However, for IPOx, these methods lead to incomplete conversion or high polydispersities (Table 9).[299−302]

Recently, the polymerization of IPOx featuring FLPs as catalysts have been reported.[303,304] A crystal structure from the reaction of FLP and IPOx (ratio 1:1) of the corresponding zwitterionic imidazolium oxazolinylaluminate $IMes^+—CH_2C(Me)=(C_3H_4NO)Al(C_6F_5)_3^-$ was obtained and represents the active propagating species for this Lewis pair polymerization and a structural proof for the conjugated conformation of the vinyl and imine double bonds (Figure 26).[303]

Using the simple ytterbocene Cp_2YbMe as a catalyst, polymerization of IPOx proceeded smoothly at room temperature, exhibiting a high reaction rate; i.e., monomer conversion reached 95% within 2 h at room temperature, as monitored by in situ ^1H NMR (Table 9). To elucidate the living character of the polymerization, aliquots were taken at regular time intervals and analyzed by gel permeation chromatography multiangle light scattering (GPC-MALS) to estimate the absolute number-averaged molar mass (M_n) and the polydispersity of PIPOx. A plot of the M_n (from 2 to 21 kDa) vs monomer (IPOx) conversion (from 2.1 to 95%) reveals a linear relationship between these two parameters; the PDI remains extremely low (PDI < 1.07) for polymers obtained at all conversions (Figure 27).

On one hand, REM-GTP of the IPOx vinylidene functionality leads to poly-2-isopropenyl-2-oxazoline with a remarkably narrow polydispersity, and on the other hand, IPOx can undergo living cationic ring-opening polymerization (LCROP) of the heterocyclic motif; this results in defined poly-2-oxazolines suitable for a variety of applications in biomedicine.[299,305−312] Methyl triflate transfers PIPOx to a polyoxazolinium salt macroinitiator, and P(IPOx-*g*-EtOx) brushes with a narrow contour length distribution are formed via LCROP with 2-ethyl-2-oxazoline (EtOx) (Figure 28).[298]

In REM-GTP copolymerizations, the addition sequence of the comonomers is crucial for monomers with different reactivities and metal center coordination strength. On one hand,

DOI: 10.1021/acs.chemrev.5b00313
Chem. Rev. 2016, 116, 1993–2022

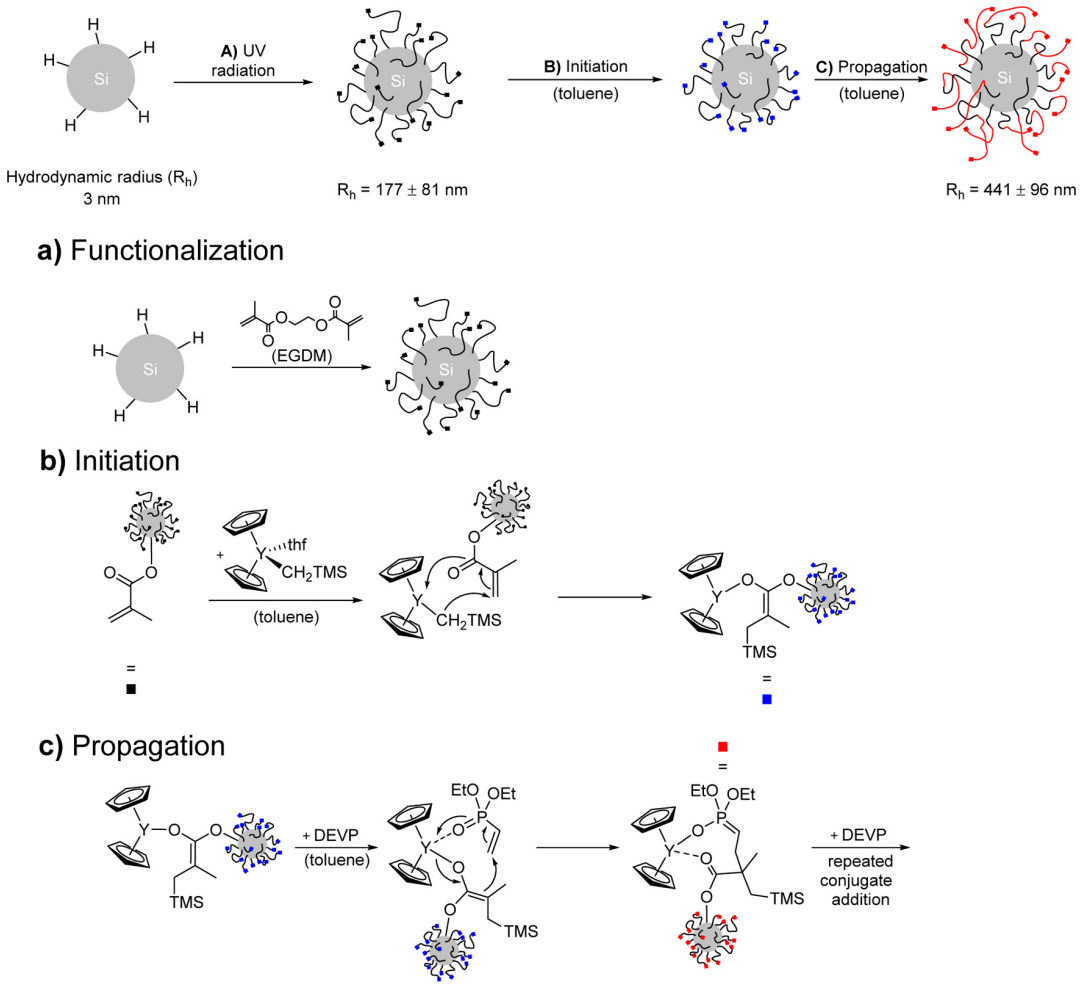

Figure 24. SI-GTP on hydrogen-terminated SiNC. Synthesis of free methyl methacrylate terminated binding sites: (a) functionalization, (b) initiation via nucleophilic attack of the alkyl ligand, and (c) propagation via eight-membered ring in the transition state.

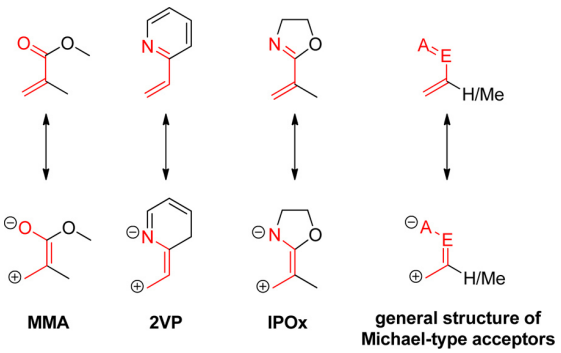

Figure 25. General structure of MMA and *N*-coordinating Michael-type acceptors suitable for REM-GTP.

monomers can only be polymerized in order of increasing coordination strength.[186,221,234] On the other hand, the reactivity is determined by the pK_a values of the corresponding monomers. Therefore, the resulting nucleophilicity or bond strength to the metal center determines if the monomer is active enough to undergo cross-propagation. In order to examine the relative reactivities of DEVP, MMA, IPOx, and 2VP, random copolymerizations with Cp_2YbMe were conducted. Consistently

Table 9. Comparison of IPOx Polymerizations Using Different Initiators[a]

initiator	T [°C]	TOF[b,c] [h^{-1}]	PDI	M_n[d] [kDa]	I^*[e] [%]	reaction time [h], conv [%]
Cp_3Yb	25	–	–	–	–	10, trace
Cp_2YbMe	25	380	1.04	21	95	1.5, 92
n-BuLi	25	3100	1.5	40	53	0.2, 95
n-BuLi	−78	18	1.2	2.5	–	2, 18
AIBN	60	–	2	18	–	8, 59

[a]Monomer:initiator = 200:1. [b]The turnover frequency (TOF) was defined as the maximum slope of the conversion vs reaction time plot. [c]Determined by ^{1}H NMR. [d]Determined by GPC-MALS. [e]$I^* = M_{th}/M_n$, $M_{th} = 200M_{Mon}$·conversion + $M_{end\ group}$.

only the corresponding homopolymers of the stronger coordinating comonomer were produced, as observed via ^{1}H NMR spectroscopy, revealing a monomer reactivity order to the ytterbium center of DEVP > MMA > IPOx > 2VP. Accordingly, sequential copolymerization yielded diblock copolymers in sequences of PMMA-*b*-PDEVP, PIPOx-*b*-PMMA, and PIPOx-*b*-PDEVP as well as P2VP-*b*-PIPOx and P2VP-*b*-PDEVP, while copolymerization in the reverse sequence only afforded homopolymers of PDEVP, PMMA, and PIPOx.[298]

DOI: 10.1021/acs.chemrev.5b00313
Chem. Rev. 2016, 116, 1993−2022

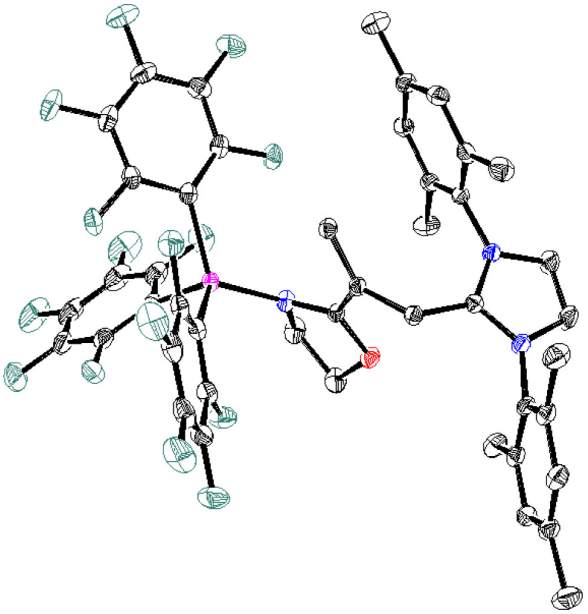

Figure 26. Crystal structure of a zwitterionic conjugated FLP IPOx conjugate. (Redrawn from ref 303. Copyright 2014 American Chemical Society.)

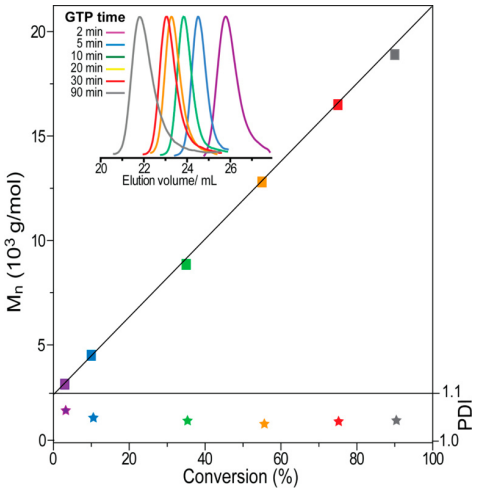

Figure 27. Linear growth of the absolute molecular weight (M_n) determined by multiangle laser light scattering as a function of IPOx conversion (determined by ^{1}H NMR). Inset: GPC traces as detected by elution volume. (Reprinted from ref 298. Copyright 2013 American Chemical Society.)

A highly active non-metallocene based catalyst for the controlled polymerization of 2VP has been presented in the literature.[313] Catalysts such as 2-methoxyethylaminobis-(phenolate)yttrium trimethylsilylmethyl were found to polymerize 2VP, exhibiting activities up to 1100 h^{-1} and low polydispersities (PDI = 1.01−1.04, M_n 22−112 kDa). The determination of the monomer and catalyst reaction order of 1 correlates to a Yasuda-type mechanism for the rare earth metal catalyzed polymerization of 2VP, and suggests that a GTP mechanism is taking place. The activation enthalpies $\Delta H^{\ddagger}$ and entropies $\Delta S^{\ddagger}$ were determined for 2VP according to the Eyring equation using in situ IR measurements. Therefore, normalization following an aliquot method was not possible, but the

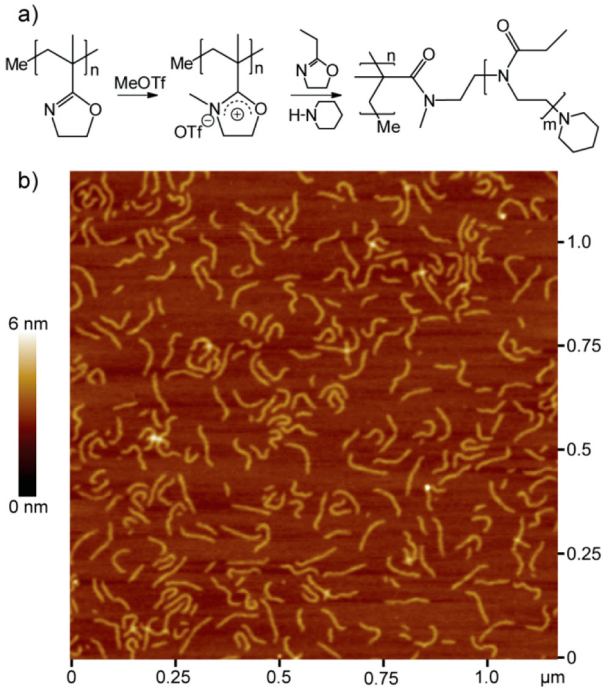

Figure 28. AFM scan of the molecular brush P(IPOx-*g*-EtOx). The polymer was deposited by dip-coating from a dilute chloroform solution onto freshly cleaved mica substrates. (Reprinted from ref 298. Copyright 2013 American Chemical Society.)

obtained values were in good agreement due to the high initiator efficiencies (I^* = 72−99%). Furthermore, the vinylphosphonates DEVP and DIVP, IPOx, and dimethylacrylamide (DMAA) were tested for their activities. DEVP and DIVP were found to polymerize slowly compared to 2VP, and only low activities were observed (TOF = 480 h^{-1} (DEVP), TOF = 42 h^{-1} (DIVP)). The produced P2VP, PIPOx, PDMAA, PDEVP and PDIVP were all found to be atactic.[313] C_1-symmetric 2-methoxyethylaminobis-(phenolate)yttrium trimethylsilylmethyl catalysts were recently reported to produce atactic to isotactic (P_m = 54−74%) P2VP with moderate activities (TOF = 360 h^{-1}) and found to follow an enantiomorphic site control mechanism.[314]

9. CONCLUSION

As a result of their versatility and superior, dominant material properties, polymers have been used as substitutes for classic raw materials for many decades. At the beginning of the 21st century, modern societies rely on further development of macromolecules as smart, resource-saving, and environmentally friendly materials for diverse applications. As stated at the beginning of this review, classic polymerization methods fail to address new monomers or specific functionalities from a precise polymer synthesis. New functionalities in polymers are indisputably needed, and living polymerization methods are the most promising candidates for precision polymer synthesis. Vinylphosphonates belong to the simplest phosphorus-containing vinyl monomers and have attracted great research interest due to a wide range of possible applications, from proton conducting membranes to smart polymers. Yet their polymerizability remained a challenge for decades. This review illustrates that the well-developed field of group 3 and cationic group 4 (meth)acrylate as well as (meth)acrylamide coordinative−anionic polymerization chemistry from the early 1990s

DOI: 10.1021/acs.chemrev.5b00313
Chem. Rev. 2016, 116, 1993−2022

experienced a revival during the past decade, being a method for the precise polymerization of new monomers unattainable via classical polymerization methods. The initiation and propagation of DAVP REM-GTP follows a complex mechanism pathway for simple Cp_2LnX systems, and further studies to apply more complex metallocene and non-metallocene structures are currently at an early stage of development.

In previous studies, the initiation of vinylphosphonates from strongly basic ligands (Me, CH_2TMS) via deprotonation, from nucleophilic transfer via ligand exchange (chloride, alkoxides), or via thiols (unstable end group, elimination reactions, odor) all lead to unsatisfactory results. Using C−H bond activation at rare earth metal centers, hydrocarbyls, which differ significantly from their corresponding alkyl precursor compounds, are generated. The procedure of σ-bond metathesis should be expanded to other monomer classes in the future to aid polymerization reactions or surface modification sequences.

For vinylphosphonates, the precise stereoregular polymerization and the influence of tacticity on the material properties is unknown. Furthermore, the extension of coordinative−anionic polymerization from commercially available (meth)acrylates and (meth)acrylamides to new monomers has developed significantly over the past years, but comprehensive studies on new Michael-type acceptor monomers and their polymerizability are still missing. In particular, the functionality of other untried elements (e.g., sulfur) or moieties (e.g., furfuryl, benzoxazolyl, or thiophenyl) in REM-GTP combined with a precise catalytic polymerization could add value to future polymeric materials.

Using an extended REM-GTP, precise two- and three-dimensional polymer and polymer-hybrid materials can be obtained. SI-GTP is experimentally facile, and at room temperature, stable polymer layers of thicknesses up to 300 nm can be achieved within a short polymerization time of a few minutes.

No single polymerization method or catalytic system can meet all requirements, demands, and needs. However, the authors want to state that rare earth metal catalyzed polymerization reactions can be one approach to help facing future challenges in materials science. Rare earth metal polymerization catalysis is a research topic that has faded in past years after two initial decades of extensive research into (meth)acrylates or (meth)acrylamides; recently it has again started to attract attention as a solution to specific scientific questions. In combination with macromolecular organization and self-assembly principles, an expanded REM-GTP should provide access to a wide range of new functional materials.

AUTHOR INFORMATION

Corresponding Author

*Tel.: +49 (0)89 289-13571. E-mail: rieger@tum.de.

Author Contributions

The manuscript was written through contributions of all authors. All authors have given approval to the final version of the manuscript.

Notes

The authors declare no competing financial interest.

Biographies

Benedikt S. Soller received his B.Sc. (2010) and his M.Sc. degree (2013) in chemistry from the Technische Universität München under the guidance of Prof. Bernhard Rieger. In 2011, he carried out research on emulsion polymerization at BASF SE in Ludwigshafen. During his master's studies, he spent two months at King Abdullah University of Science and Technology in Saudi Arabia as part of a research stay and six months at Ateneo de Manila University in the Philippines. He is currently a Ph.D. candidate with the group of Prof. Rieger. His research interests include the polymerization of vinylic monomers, further development of REM-GTP catalysts, stereoregular polymerization, and the application of SI-GTP on SiNCs for the preparation of hybrid materials. Besides his academic research interests, he is improving his knowledge of the Korean language and photography.

Stephan Salzinger studied chemistry at the Technische Universität München and received his M.Sc. in 2010. In 2009, he carried out research on self-assembling peptide nanotubes under the guidance of M. Amorín and J. R. Granja at the Universidad de Santiago de Compostela. In his master's thesis in the group of Bernhard Rieger, he investigated the stereoregularity and thermoresponsive behavior of vinylphosphonates. His Ph.D. work was focused on the extension of REM-GTP to new monomer classes and the elucidation of the mechanism of vinylphosphonate REM-GTP, for which he received a scholarship from the Fonds der Chemischen Industrie. After graduating in 2013, he joined the Advanced Materials & Systems Research laboratories of BASF SE in Ludwigshafen as a research engineer in polymer process development.

DOI: 10.1021/acs.chemrev.5b00313
Chem. Rev. 2016, 116, 1993−2022

Bernhard Rieger studied chemistry at the Ludwig-Maximilians-Universität München (LMU) and received his Ph.D. in 1988. After research at the University of Massachusetts at Amherst and in the plastics laboratory of BASF SE, he received his habilitation in 1995 at the University of Tübingen. In 1996, he became professor at the Department Materials and Catalysis at the University of Ulm. Since 2006, he has been professor at the Technische Universität München at the WACKER-Chair of Macromolecular Chemistry and director of the Institute of Silicon Chemistry. He is a fellow of the National Academy of Science and Engineering "acatech" (2013), a member of the European Academy of Science (2011), a member of the Finnish Academy of Science and Letters (2008), and an Honorary Doctor Dr. h.c. phil. of the University of Helsinki (2007). In 2013, he was awarded the Wöhler Prize for Sustainable Chemistry and holds a Philip Morris Award.

ACKNOWLEDGMENTS

The authors thank Peter T. Altenbuchner, Alexander Kronast, Johannes Kainz, and Patrick D. L. Werz for valuable discussions. Stephan Salzinger is grateful for a generous scholarship from the Fonds der Chemischen Industrie.

ABBREVIATIONS

bdsa	bis(dimethylsilyl)amide, $N(SiHMe_2)_2$
btsa	bis(trimethylsilyl)amide, $N(SiMe_3)_2$
DEMVP	diethyl 1-methylvinylphosphonate
DEVP	diethyl vinylphosphonate
DIVP	diisopropyl vinylphosphonate
DMAA	*N*,*N*-dimethylacrylamide
DMVP	dimethyl vinylphosphonate
DPE	1,1-diphenylethylene
DPVP	di-*n*-propyl vinylphosphonate
EGDM	ethylene glycol dimethacrylate
GTP	group transfer polymerization
*I**	initiator efficiency
MALS	multiangle (static) light scattering
MMA	methyl methacrylate
PDI	polydispersity index
SI-GTP	surface-initiated group transfer polymerization
SIPGP	self-initiated photografting and photopolymerization
SKA-GTP	silyl ketene acetal initiated group transfer polymerization
VPA	vinylphosphonic acid

REFERENCES

(1) Mülhaupt, R. Hermann Staudinger and the Origin of Macromolecular Chemistry. *Angew. Chem., Int. Ed.* **2004**, *43*, 1054−1063.
(2) Hapke, D. W. *Plastics—the Facts 2013*; 2013, Plastics Europe.
(3) Mordashov, A. In *Worldsteel Association, Crude Steel Production*; www.worldsteel.org (accessed May 2015).
(4) United Nations. In *Global Challenges for Humanity*. www.millennium-project.org (accessed 2015).
(5) Kreimeyer, A.; Eckes, P.; Fischer, C.; Lauke, H.; Schuhmacher, P. "We Create Chemistry for a Sustainable Future": Chemistry Creates Sustainable Solutions for a Growing World Population. *Angew. Chem., Int. Ed.* **2015**, *54*, 3178−3195.
(6) Iwata, T. Biodegradable and Bio-Based Polymers: Future Prospects of Eco-Friendly Plastics. *Angew. Chem., Int. Ed.* **2015**, *54*, 3210−3215.
(7) Whitesides, G. M. Reinventing Chemistry. *Angew. Chem., Int. Ed.* **2015**, *54*, 3196−3209.
(8) Ziegler, K.; Holzkamp, E.; Breil, H.; Martin, H. Das Mülheimer Normaldruck-Polyäthylen-Verfahren. *Angew. Chem.* **1955**, *67*, 541−547.
(9) Natta, G. Stereospezifische Katalysen und isotaktische Polymere. *Angew. Chem.* **1956**, *68*, 393−403.
(10) Natta, G.; Pasquon, I.; Giachetti, E. Kinetik der stereospezifischen Polymerisation des Propylens zu isotaktischen Polymeren. *Angew. Chem.* **1957**, *69*, 213−219.
(11) Eisch, J. J. Fifty Years of Ziegler−Natta Polymerization: From Serendipity to Science. A Personal Account. *Organometallics* **2012**, *31*, 4917−4932.
(12) Claverie, J. P.; Schaper, F. Ziegler-Natta catalysis: 50 years after the Nobel Prize. *MRS Bull.* **2013**, *38*, 213−218.
(13) Westheimer, F. Why nature chose phosphates. *Science* **1987**, *235*, 1173−1178.
(14) Kamerlin, S. C. L.; Sharma, P. K.; Prasad, R. B.; Warshel, A. Why nature really chose phosphate. *Q. Rev. Biophys.* **2013**, *46*, 1−132.
(15) Abueva, C. D. G.; Lee, B.-T. Poly(vinylphosphonic acid) immobilized on chitosan: A glycosaminoglycan-inspired matrix for bone regeneration. *Int. J. Biol. Macromol.* **2014**, *64*, 294−301.
(16) Tan, J.; Gemeinhart, R. A.; Ma, M.; Mark Saltzman, W. Improved cell adhesion and proliferation on synthetic phosphonic acid-containing hydrogels. *Biomaterials* **2005**, *26*, 3663−3671.
(17) Seo, J.-H.; Matsuno, R.; Takai, M.; Ishihara, K. Cell adhesion on phase-separated surface of block copolymer composed of poly(2-methacryloyloxyethyl phosphorylcholine) and poly(dimethylsiloxane). *Biomaterials* **2009**, *30*, 5330−5340.
(18) Chirila, T. V.; Zainuddin. Calcification of synthetic polymers functionalized with negatively ionizable groups: A critical review. *React. Funct. Polym.* **2007**, *67*, 165−172.
(19) Dalas, E.; Kallitsis, J. K.; Koutsoukos, P. G. Crystallization of hydroxyapatite on polymers. *Langmuir* **1991**, *7*, 1822−1826.
(20) Anbar, M.; St John, G. A.; Elward, T. E. Organic Polymeric Polyphosphonates as Potential Preventive Agents of Dental Caries: In Vivo Experiments. *J. Dent. Res.* **1974**, *53*, 1240−1244.
(21) Ellis, J.; Anstice, M.; Wilson, A. D. The glass polyphosphonate cement: A novel glass-ionomer cement based on poly(vinyl phosphonic acid). *Clin. Mater.* **1991**, *7*, 341−346.
(22) Ellis, J.; Wilson, A. D. The formation and properties of metal oxide poly(vinylphosphonic acid) cements. *Dent. Mater.* **1992**, *8*, 79−84.
(23) Braybrook, J. H.; Nicholson, J. W. Incorporation of crosslinking agents into poly(vinyl phosphonic acid) as a route to glass-polyalkenoate cements of improved compressive strength. *J. Mater. Chem.* **1993**, *3*, 361−365.
(24) Khouw-Liu, V. H. W.; Anstice, H. M.; Pearson, G. J. An in vitro investigation of a poly(vinyl phosphonic acid) based cement with four conventional glass-ionomer cements. Part 1: flexural strength and fluoride release. *J. Dent.* **1999**, *27*, 351−357.
(25) Bock, T.; Möhwald, H.; Mülhaupt, R. Arylphosphonic Acid-Functionalized Polyelectrolytes as Fuel Cell Membrane Material. *Macromol. Chem. Phys.* **2007**, *208*, 1324−1340.
(26) Allcock, H. R.; Hofmann, M. A.; Ambler, C. M.; Lvov, S. N.; Zhou, X. Y.; Chalkova, E.; Weston, J. Phenyl phosphonic acid functionalized poly[aryloxyphosphazenes] as proton-conducting membranes for direct methanol fuel cells. *J. Membr. Sci.* **2002**, *201*, 47−54.
(27) Berber, M. R.; Fujigaya, T.; Nakashima, N. High-Temperature Polymer Electrolyte Fuel Cell Using Poly(vinylphosphonic acid) as an

DOI: 10.1021/acs.chemrev.5b00313
Chem. Rev. 2016, 116, 1993−2022

Electrolyte Shows a Remarkable Durability. *ChemCatChem* **2014**, *6*, 567−571.
(28) Berber, M. R.; Fujigaya, T.; Sasaki, K.; Nakashima, N. Remarkably Durable High Temperature Polymer Electrolyte Fuel Cell Based on Poly(vinylphosphonic acid)-doped Polybenzimidazole. *Sci. Rep.* **2013**, *3*, 1764.
(29) Yamada, M.; Honma, I. Anhydrous proton conducting polymer electrolytes based on poly(vinylphosphonic acid)-heterocycle composite material. *Polymer* **2005**, *46*, 2986−2992.
(30) Lee, S.-I.; Yoon, K.-H.; Song, M.; Peng, H.; Page, K. A.; Soles, C. L.; Yoon, D. Y. Structure and Properties of Polymer Electrolyte Membranes Containing Phosphonic Acids for Anhydrous Fuel Cells. *Chem. Mater.* **2012**, *24*, 115−122.
(31) Dimitrov, I.; Takamuku, S.; Jankova, K.; Jannasch, P.; Hvilsted, S. Polysulfone Functionalized With Phosphonated Poly(pentafluorostyrene) Grafts for Potential Fuel Cell Applications. *Macromol. Rapid Commun.* **2012**, *33*, 1368−1374.
(32) Dimitrov, I.; Takamuku, S.; Jankova, K.; Jannasch, P.; Hvilsted, S. Proton conducting graft copolymers with tunable length and density of phosphonated side chains for fuel cell membranes. *J. Membr. Sci.* **2014**, *450*, 362−368.
(33) Jiang, F.; Kaltbeitzel, A.; Zhang, J.; Meyer, W. H. Nano-spheres stabilized poly(vinyl phosphonic acid) as proton conducting membranes for PEMFCs. *Int. J. Hydrogen Energy* **2014**, *39*, 11157−11164.
(34) Sen, U.; Usta, H.; Acar, O.; Citir, M.; Canlier, A.; Bozkurt, A.; Ata, A. Enhancement of Anhydrous Proton Conductivity of Poly(vinylphosphonic acid)−Poly(2,5-benzimidazole) Membranes via In Situ Polymerization. *Macromol. Chem. Phys.* **2015**, *216*, 106−112.
(35) Mizuno, M.; Iwasaki, A.; Umiyama, T.; Ohashi, R.; Ida, T. Local Structure and Dynamics of Imidazole Molecules in Proton-Conducting Poly(vinylphosphonic acid)−Imidazole Composite Material. *Macromolecules* **2014**, *47*, 7469−7476.
(36) Ebdon, J. R.; Price, D.; Hunt, B. J.; Joseph, P.; Gao, F.; Milnes, G. J.; Cunliffe, L. K. Flame retardance in some polystyrenes and poly(methyl methacrylate)s with covalently bound phosphorus-containing groups: initial screening experiments and some laser pyrolysis mechanistic studies. *Polym. Degrad. Stab.* **2000**, *69*, 267−277.
(37) Banks, M.; Ebdon, J. R.; Johnson, M. Influence of covalently bound phosphorus-containing groups on the flammability of poly(vinyl alcohol), poly(ethylene-co-vinyl alcohol) and low-density polyethylene. *Polymer* **1993**, *34*, 4547−4556.
(38) Monge, S.; Canniccioni, B.; Graillot, A.; Robin, J.-J. Phosphorus-Containing Polymers: A Great Opportunity for the Biomedical Field. *Biomacromolecules* **2011**, *12*, 1973−1982.
(39) David, G.; Negrell-Guirao, C.; Iftene, F.; Boutevin, B.; Chougrani, K. Recent progress on phosphonate vinyl monomers and polymers therefore obtained by radical (co)polymerization. *Polym. Chem.* **2012**, *3*, 265−274.
(40) Moszner, N.; Salz, U.; Zimmermann, J. Chemical aspects of self-etching enamel−dentin adhesives: A systematic review. *Dent. Mater.* **2005**, *21*, 895−910.
(41) Avci, D.; Mathias, L. J. Synthesis and photopolymerizations of phosphate-containing acrylate/(di)methacrylate monomers from 3-(acryloyloxy)-2-hydroxypropyl methacrylate. *Polym. Bull.* **2005**, *54*, 11−19.
(42) Moszner, N.; Zeuner, F.; Fischer, U. K.; Rheinberger, V. Monomers for adhesive polymers, 2. Synthesis and radical polymerisation of hydrolytically stable acrylic phosphonic acids. *Macromol. Chem. Phys.* **1999**, *200*, 1062−1067.
(43) Yeniad, B.; Albayrak, A. Z.; Olcum, N. C.; Avci, D. Synthesis and photopolymerizations of new phosphonated monomers for dental applications. *J. Polym. Sci., Part A: Polym. Chem.* **2008**, *46*, 2290−2299.
(44) Sahin, G.; Avci, D.; Karahan, O.; Moszner, N. Synthesis and photopolymerizations of new phosphonated methacrylates from alkyl α-hydroxymethacrylates and glycidyl methacrylate. *J. Appl. Polym. Sci.* **2009**, *114*, 97−106.
(45) Su, Y.; Li, C.; Zhao, W.; Shi, Q.; Wang, H.; Jiang, Z.; Zhu, S. Modification of polyethersulfone ultrafiltration membranes with phosphorylcholine copolymer can remarkably improve the antifouling and permeation properties. *J. Membr. Sci.* **2008**, *322*, 171−177.
(46) Edizer, S.; Sahin, G.; Avci, D. Development of reactive phosphonated methacrylates. *J. Polym. Sci., Part A: Polym. Chem.* **2009**, *47*, 5737−5746.
(47) Allcock, H. R.; Kugel, R. L. Synthesis of High Polymeric Alkoxy- and Aryloxyphosphonitriles. *J. Am. Chem. Soc.* **1965**, *87*, 4216−4217.
(48) Allcock, H. R. A Perspective of Polyphosphazene Research. *J. Inorg. Organomet. Polym. Mater.* **2006**, *16*, 277−294.
(49) Allcock, H. R. Recent advances in phosphazene (phosphonitrilic) chemistry. *Chem. Rev.* **1972**, *72*, 315−356.
(50) Allcock, H. R. Polyphosphazenes: New Polymers with Inorganic Backbone Atoms. *Science* **1976**, *193*, 1214−1219.
(51) Allcock, H. R. Rational Design and Synthesis of New Polymeric Material. *Science* **1992**, *255*, 1106−1112.
(52) Allcock, H. R. Polyphosphazene elastomers, gels, and other soft materials. *Soft Matter* **2012**, *8*, 7521−7532.
(53) Beşli, S.; Mutlu, C.; İbişoğlu, H.; Yuksel, F.; Allen, C. W. Synthesis of a New Class of Fused Cyclotetraphosphazene Ring Systems. *Inorg. Chem.* **2015**, *54*, 334−341.
(54) Sun, J.; Yu, Z.; Wang, X.; Wu, D. Synthesis and Performance of Cyclomatrix Polyphosphazene Derived from Trispiro-Cyclotriphosphazene as a Halogen-Free Nonflammable Material. *ACS Sustainable Chem. Eng.* **2014**, *2*, 231−238.
(55) Sun, J.; Wang, X.; Wu, D. Novel Spirocyclic Phosphazene-Based Epoxy Resin for Halogen-Free Fire Resistance: Synthesis, Curing Behaviors, and Flammability Characteristics. *ACS Appl. Mater. Interfaces* **2012**, *4*, 4047−4061.
(56) Tian, Z.; Liu, X.; Chen, C.; Allcock, H. R. Synthesis and Micellar Behavior of Novel Amphiphilic Poly[bis(trifluoroethoxy)phosphazene]-co-poly[(dimethylamino)ethyl methacrylate] Block Copolymers. *Macromolecules* **2012**, *45*, 2502−2508.
(57) Honeyman, C. H.; Manners, I.; Morrissey, C. T.; Allcock, H. R. Ambient Temperature Synthesis of Poly(dichlorophosphazene) with Molecular Weight Control. *J. Am. Chem. Soc.* **1995**, *117*, 7035−7036.
(58) Allcock, H. R.; Morozowich, N. L. Bioerodible polyphosphazenes and their medical potential. *Polym. Chem.* **2012**, *3*, 578−590.
(59) Tian, Z.; Chen, C.; Allcock, H. R. Injectable and Biodegradable Supramolecular Hydrogels by Inclusion Complexation between Poly(organophosphazenes) and α-Cyclodextrin. *Macromolecules* **2013**, *46*, 2715−2724.
(60) Andrianov, A. K.; Svirkin, Y. Y.; LeGolvan, M. P. Synthesis and Biologically Relevant Properties of Polyphosphazene Polyacids. *Biomacromolecules* **2004**, *5*, 1999−2006.
(61) Chaubal, M. V.; Gupta, A. S.; Lopina, S. T.; Bruley, D. F. Polyphosphates and Other Phosphorus-Containing Polymers for Drug Delivery Applications. *Crit. Rev. Ther. Drug Carrier Syst.* **2003**, *20*, 295.
(62) Chen, D.-P.; Wang, J. Synthesis and Characterization of Block Copolymer of Polyphosphoester and Poly(ε-caprolactone). *Macromolecules* **2006**, *39*, 473−475.
(63) Xiao, C.-S.; Wang, Y.-C.; Du, J.-Z.; Chen, X.-S.; Wang, J. Kinetics and Mechanism of 2-Ethoxy-2-oxo-1,3,2-dioxaphospholane Polymerization Initiated by Stannous Octoate. *Macromolecules* **2006**, *39*, 6825−6831.
(64) Wu, Q.; Zhou, D.; Kang, R.; Tang, X.; Yang, Q.; Song, X.; Zhang, G. Synthesis and Self-Assembly of Thermoresponsive Amphiphilic Biodegradable Polypeptide/Poly(ethyl ethylene phosphate) Block Copolymers. *Chem. - Asian J.* **2014**, *9*, 2850−2858.
(65) Wang, Y.-C.; Yuan, Y.-Y.; Wang, F.; Wang, J. Syntheses and characterization of block copolymers of poly(aliphatic ester) with clickable polyphosphoester. *J. Polym. Sci., Part A: Polym. Chem.* **2011**, *49*, 487−494.
(66) Wang, Y.-C.; Li, Y.; Yang, X.-Z.; Yuan, Y.-Y.; Yan, L.-F.; Wang, J. Tunable Thermosensitivity of Biodegradable Polymer Micelles of Poly(ε-caprolactone) and Polyphosphoester Block Copolymers. *Macromolecules* **2009**, *42*, 3026−3032.
(67) Tian, H.; Tang, Z.; Zhuang, X.; Chen, X.; Jing, X. Biodegradable synthetic polymers: Preparation, functionalization and biomedical application. *Prog. Polym. Sci.* **2012**, *37*, 237−280.

DOI: 10.1021/acs.chemrev.5b00313
Chem. Rev. 2016, 116, 1993−2022

(68) Zhang, S.; Li, A.; Zou, J.; Lin, L. Y.; Wooley, K. L. Facile Synthesis of Clickable, Water-Soluble, and Degradable Polyphosphoesters. *ACS Macro Lett.* **2012**, *1*, 328−333.
(69) Zhang, S.; Zou, J.; Zhang, F.; Elsabahy, M.; Felder, S. E.; Zhu, J.; Pochan, D. J.; Wooley, K. L. Rapid and Versatile Construction of Diverse and Functional Nanostructures Derived from a Polyphosphoester-Based Biomimetic Block Copolymer System. *J. Am. Chem. Soc.* **2012**, *134*, 18467−18474.
(70) Sun, C.-Y.; Dou, S.; Du, J.-Z.; Yang, X.-Z.; Li, Y.-P.; Wang, J. Doxorubicin Conjugate of Poly(Ethylene Glycol)-Block-Polyphosphoester for Cancer Therapy. *Adv. Healthcare Mater.* **2014**, *3*, 261−272.
(71) Lim, Y. H.; Tiemann, K. M.; Heo, G. S.; Wagers, P. O.; Rezenom, Y. H.; Zhang, S.; Zhang, F.; Youngs, W. J.; Hunstad, D. A.; Wooley, K. L. Preparation and in Vitro Antimicrobial Activity of Silver-Bearing Degradable Polymeric Nanoparticles of Polyphosphoester-block-Poly(l-lactide). *ACS Nano* **2015**, *9*, 1995−2008.
(72) Iwasaki, Y.; Yamaguchi, E. Synthesis of Well-Defined Thermoresponsive Polyphosphoester Macroinitiators Using Organocatalysts. *Macromolecules* **2010**, *43*, 2664−2666.
(73) Lim, Y. H.; Heo, G. S.; Rezenom, Y. H.; Pollack, S.; Raymond, J. E.; Elsabahy, M.; Wooley, K. L. Development of a Vinyl Ether-Functionalized Polyphosphoester as a Template for Multiple Post-polymerization Conjugation Chemistries and Study of Core Degradable Polymeric Nanoparticles. *Macromolecules* **2014**, *47*, 4634−4644.
(74) Clément, B.; Grignard, B.; Koole, L.; Jérôme, C.; Lecomte, P. Metal-Free Strategies for the Synthesis of Functional and Well-Defined Polyphosphoesters. *Macromolecules* **2012**, *45*, 4476−4486.
(75) Lim, Y. H.; Heo, G. S.; Cho, S.; Wooley, K. L. Construction of a Reactive Diblock Copolymer, Polyphosphoester-block-Poly(l-lactide), as a Versatile Framework for Functional Materials That Are Capable of Full Degradation and Nanoscopic Assembly Formation. *ACS Macro Lett.* **2013**, *2*, 785−789.
(76) Zhang, F.; Zhang, S.; Pollack, S. F.; Li, R.; Gonzalez, A. M.; Fan, J.; Zou, J.; Leininger, S. E.; Pavía-Sanders, A.; Johnson, R.; et al. Improving Paclitaxel Delivery: In Vitro and In Vivo Characterization of PEGylated Polyphosphoester-Based Nanocarriers. *J. Am. Chem. Soc.* **2015**, *137*, 2056−2066.
(77) Steinbach, T.; Ritz, S.; Wurm, F. R. Water-Soluble Poly(phosphonate)s via Living Ring-Opening Polymerization. *ACS Macro Lett.* **2014**, *3*, 244−248.
(78) Marsico, F.; Wagner, M.; Landfester, K.; Wurm, F. R. Unsaturated Polyphosphoesters via Acyclic Diene Metathesis Polymerization. *Macromolecules* **2012**, *45*, 8511−8518.
(79) Steinbach, T.; Alexandrino, E. M.; Wahlen, C.; Landfester, K.; Wurm, F. R. Poly(phosphonate)s via Olefin Metathesis: Adjusting Hydrophobicity and Morphology. *Macromolecules* **2014**, *47*, 4884−4893.
(80) Steinmann, M.; Markwart, J.; Wurm, F. R. Poly(alkylidene chlorophosphate)s via Acyclic Diene Metathesis Polymerization: A General Platform for the Postpolymerization Modification of Poly(phosphoester)s. *Macromolecules* **2014**, *47*, 8506−8513.
(81) Tauber, K.; Marsico, F.; Wurm, F. R.; Schartel, B. Hyperbranched poly(phosphoester)s as flame retardants for technical and high performance polymers. *Polym. Chem.* **2014**, *5*, 7042−7053.
(82) Steinbach, T.; Alexandrino, E. M.; Wurm, F. R. Unsaturated poly(phosphoester)s via ring-opening metathesis polymerization. *Polym. Chem.* **2013**, *4*, 3800−3806.
(83) Marsico, F.; Turshatov, A.; Peköz, R.; Avlasevich, Y.; Wagner, M.; Weber, K.; Donadio, D.; Landfester, K.; Baluschev, S.; Wurm, F. R. Hyperbranched Unsaturated Polyphosphates as a Protective Matrix for Long-Term Photon Upconversion in Air. *J. Am. Chem. Soc.* **2014**, *136*, 11057−11064.
(84) Kosolapoff, G. M. Isomerization of Alkyl Phosphites. VII. Some Derivatives of 2-Bromoethane Phosphonic Acid. *J. Am. Chem. Soc.* **1948**, *70*, 1971−1972.
(85) Ford-Moore, A. H.; Williams, J. H. 278. The reaction between trialkyl phosphites and alkyl halides. *J. Chem. Soc.* **1947**, 1465−1467.
(86) Bhattacharya, A. K.; Thyagarajan, G. Michaelis-Arbuzov rearrangement. *Chem. Rev.* **1981**, *81*, 415−430.
(87) Michaelis, A.; Kaehne, R. Ueber das Verhalten der Jodalkyle gegen die sogen. Phosphorigsäureester oder O-Phosphine. *Ber. Dtsch. Chem. Ges.* **1898**, *31*, 1048−1055.
(88) Gerrard, W.; Green, W. J. 568. Mechanism of the formation of dialkyl alkylphosphonates. *J. Chem. Soc.* **1951**, 2550−2553.
(89) Hirao, T.; Masunaga, T.; Ohshiro, Y.; Agawa, T. A Novel Synthesis of Dialkyl Arenephosphonates. *Synthesis* **1981**, *1981*, 56−57.
(90) Kalek, M.; Stawinski, J. Pd(0)-Catalyzed Phosphorus−Carbon Bond Formation. Mechanistic and Synthetic Studies on the Role of the Palladium Sources and Anionic Additives. *Organometallics* **2007**, *26*, 5840−5847.
(91) Kalek, M.; Ziadi, A.; Stawinski, J. Microwave-Assisted Palladium-Catalyzed Cross-Coupling of Aryl and Vinyl Halides with H-Phosphonate Diesters. *Org. Lett.* **2008**, *10*, 4637−4640.
(92) Herpel, R. H.; Vedantham, P.; Flynn, D. L.; Hanson, P. R. High-load, oligomeric phosphonyl dichloride: facile generation via ROM polymerization and application to scavenging amines. *Tetrahedron Lett.* **2006**, *47*, 6429−6432.
(93) Essahli, M.; Asri, M. E.; Boulahna, A.; Zenkouar, M.; Viguier, M.; Hervaud, Y.; Boutevin, B. New alkylated and perfluoroalkylated phosphonic acids: Synthesis, adhesive and water-repellent properties on aluminum substrates. *J. Fluorine Chem.* **2006**, *127*, 854−860.
(94) Matveeva, E. V.; Shipov, A. E.; Petrovskii, P. V.; Odinets, I. L. Amino acids as suitable N-nucleophiles for the aza-Michael reaction of vinylphosphoryl compounds in water. *Tetrahedron Lett.* **2011**, *52*, 6562−6565.
(95) Bou Orm, N.; Dkhissi, Y.; Daniele, S.; Djakovitch, L. Synthesis of 2-(arylamino)ethyl phosphonic acids via the aza-Michael addition on diethyl vinylphosphonate. *Tetrahedron* **2013**, *69*, 115−121.
(96) Han, L.-B.; Zhao, C.-Q. Stereospecific Addition of H−P Bond to Alkenes: A Simple Method for the Preparation of (RP)-Phenylphosphinates. *J. Org. Chem.* **2005**, *70*, 10121−10123.
(97) Rünzi, T.; Baier, M. C.; Negele, C.; Krumova, M.; Mecking, S. Nanocomposites of Phosphonic-Acid-Functionalized Polyethylenes with Inorganic Quantum Dots. *Macromol. Rapid Commun.* **2015**, *36*, 165−173.
(98) Yasuda, H.; Ihara, E. Rare earth metal initiated polymerizations of polar and nonpolar monomers to give high molecular weight polymers with extremely narrow molecular weight distribution. *Macromol. Chem. Phys.* **1995**, *196*, 2417−2441.
(99) Desurmont, G.; Tanaka, M.; Li, Y.; Yasuda, H.; Tokimitsu, T.; Tone, S.; Yanagase, A. New approach to block copolymerization of ethylene with polar monomers by the unique catalytic function of organolanthanide complexes. *J. Polym. Sci., Part A: Polym. Chem.* **2000**, *38*, 4095−4109.
(100) Yasuda, H. Organo transition metal initiated living polymerizations. *Prog. Polym. Sci.* **2000**, *25*, 573−626.
(101) Yasuda, H. Rare-earth-metal-initiated polymerizations of (meth)acrylates and block copolymerizations of olefins with polar monomers. *J. Polym. Sci., Part A: Polym. Chem.* **2001**, *39*, 1955−1959.
(102) Chen, E. Y. X. Coordination Polymerization of Polar Vinyl Monomers by Single-Site Metal Catalysts. *Chem. Rev.* **2009**, *109*, 5157−5214.
(103) Macarie, L.; Ilia, G. Poly(vinylphosphonic acid) and its derivatives. *Prog. Polym. Sci.* **2010**, *35*, 1078−1092.
(104) Bingöl, B.; Hart-Smith, G.; Barner-Kowollik, C.; Wegner, G. Characterization of Oligo(vinyl phosphonate)s by High-Resolution Electrospray Ionization Mass Spectrometry: Implications for the Mechanism of Polymerization. *Macromolecules* **2008**, *41*, 1634−1639.
(105) Sato, T.; Hasegawa, M.; Seno, M.; Hirano, T. Radical polymerization behavior of dimethyl vinylphosphonate: Homopolymerization and copolymerization with trimethoxyvinylsilane. *J. Appl. Polym. Sci.* **2008**, *109*, 3746−3752.
(106) Pike, R. M.; Cohen, R. A. Organophosphorus polymers. I. Peroxide-initiated polymerization of diethyl and diisopropyl vinylphosphonate. *J. Polym. Sci.* **1960**, *44*, 531−538.
(107) Shulyndin, S. V.; Levin, Y. A.; Ivanov, B. E. Copolymerisation of Unsaturated Organophosphorus Monomers. *Russ. Chem. Rev.* **1981**, *50*, 865.

DOI: 10.1021/acs.chemrev.5b00313
Chem. Rev. 2016, 116, 1993−2022

(108) Kolesnikov, G. S.; Rodionova, Y. F.; Fedorova, L. S.; Medved, T. Y.; Kabachnik, M. I. Carbochain polymers and copolymers—XLII. Synthesis, polymerization and copolymerization of aromatic esters of vinylphosphonic and α-chlorovinylphosphonic acids. *Polym. Sci. U.S.S.R.* **1963**, *4*, 635−643.
(109) Harman, D.; Wheatstone, R. R. U.S. Patent US 2765331 A, 1956.
(110) Muray, B. J. Homo- and copolymerization of vinyl phosphates and phosphonates. *J. Polym. Sci., Part C: Polym. Symp.* **1967**, *16*, 1869−1886.
(111) Banks, M.; Ebdon, J. R.; Johnson, M. The flame-retardant effect of diethyl vinyl phosphonate in copolymers with styrene, methyl methacrylate, acrylonitrile and acrylamide. *Polymer* **1994**, *35*, 3470−3473.
(112) Wu, Q.; Weiss, R. A. Synthesis and characterization of poly(styrene-co-vinyl phosphonate) ionomers. *J. Polym. Sci., Part B: Polym. Phys.* **2004**, *42*, 3628−3641.
(113) Wu, Q.; Weiss, R. A. Viscoelastic properties of poly(styrene-co-vinylphosphonate) ionomers. *Polymer* **2007**, *48*, 7558−7566.
(114) Marvel, C. S.; Wright, J. C. Some copolymers of dimethyl 1-propene-2-phosphonate and of 1-phenylvinylphosphonic acid. *J. Polym. Sci.* **1952**, *8*, 255−256.
(115) Arcus, C. L.; Matthews, R. J. S. 883. Phosphonic polymers. Part I. The copolymerisation of diethyl vinylphosphonate and styrene. *J. Chem. Soc.* **1956**, 4607−4612.
(116) Jin, S.; Gonsalves, K. E. Synthesis and Characterization of Functionalized Poly(ε-caprolactone) Copolymers by Free-Radical Polymerization. *Macromolecules* **1998**, *31*, 1010−1015.
(117) Deng, N.; Ni, X.; Shen, Z. Syntheses and properties of amphiphilic poly (diethyl vinylphosphonate-co-2-chloroethyl methacrylate) copolymers. *Des. Monomers Polym.* **2015**, *18*, 470−478.
(118) David, G.; Boutevin, B.; Seabrook, S.; Destarac, M.; Woodward, G.; Otter, G. Radical Telomerisation of Vinyl Phosphonic Acid with a Series of Chain Transfer Agents. *Macromol. Chem. Phys.* **2007**, *208*, 635−642.
(119) David, G.; Boyer, C.; Tayouo, R.; Seabrook, S.; Ameduri, B.; Boutevin, B.; Woodward, G.; Destarac, M. A Process for Polymerizing Vinyl Phosphonic Acid with C6F13I Perfluoroalkyl Iodide Chain-Transfer Agent. *Macromol. Chem. Phys.* **2008**, *209*, 75−83.
(120) Bingöl, B.; Meyer, W. H.; Wagner, M.; Wegner, G. Synthesis, Microstructure, and Acidity of Poly(vinylphosphonic acid). *Macromol. Rapid Commun.* **2006**, *27*, 1719−1724.
(121) Strandberg, C.; Rosenauer, C.; Wegner, G. Poly(vinyl phosphonic acid): Hydrodynamic Properties and SEC-Calibration in Aqueous Solution. *Macromol. Rapid Commun.* **2010**, *31*, 374−379.
(122) Greish, Y. E.; Brown, P. W. Chemically formed HAp-Ca poly(vinyl phosphonate) composites. *Biomaterials* **2001**, *22*, 807−816.
(123) Komber, H.; Steinert, V.; Voit, B. 1H, 13C, and 31P NMR Study on Poly(vinylphosphonic acid) and Its Dimethyl Ester. *Macromolecules* **2008**, *41*, 2119−2125.
(124) Bride, M. H.; Cummings, W. A. W.; Pickles, W. Phosphorus-containing polymers. *J. Appl. Chem.* **1961**, *11*, 352−357.
(125) Blomberg, C. Magnesium: Annual survey covering the year 1971. *J. Organomet. Chem.* **1972**, *45*, 1−137.
(126) Levin, Y. A.; Gozman, I. P.; Gazizova, L. K.; Khristoforova, Y. I.; Yagfarova, T. A.; Bylyev, V. A.; Ivanov, B. Y. High molecular poly-α-alkenylphosphonates and phosphonamides. *Polym. Sci. U.S.S.R.* **1974**, *16*, 81−89.
(127) Salzinger, S.; Rieger, B. Rare Earth Metal-Mediated Group Transfer Polymerization of Vinylphosphonates. *Macromol. Rapid Commun.* **2012**, *33*, 1327−1345.
(128) Paisley, D. M.; Marvel, C. S. Some polymers and copolymers of vinyldiphenylphosphine. *J. Polym. Sci.* **1962**, *56*, 533−538.
(129) Parvole, J.; Jannasch, P. Polysulfones Grafted with Poly(vinylphosphonic acid) for Highly Proton Conducting Fuel Cell Membranes in the Hydrated and Nominally Dry State. *Macromolecules* **2008**, *41*, 3893−3903.
(130) Bingöl, B. Macromolecules with Phosphorus Functionalities. Ph.D. Thesis, Johannes-Gutenberg Universität Mainz, Germany, 2007.
(131) Leute, M. Macromolecules with Phosphorus Functionalities. Ph.D. Thesis, Universität Ulm, Germany, 2007.
(132) Perrin, R.; Elomaa, M.; Jannasch, P. Nanostructured Proton Conducting Polystyrene−Poly(vinylphosphonic acid) Block Copolymers Prepared via Sequential Anionic Polymerizations. *Macromolecules* **2009**, *42*, 5146−5154.
(133) Wagner, T.; Manhart, A.; Deniz, N.; Kaltbeitzel, A.; Wagner, M.; Brunklaus, G.; Meyer, W. H. Vinylphosphonic Acid Homo- and Block Copolymers. *Macromol. Chem. Phys.* **2009**, *210*, 1903−1914.
(134) Varshney, S. K.; Hautekeer, J. P.; Fayt, R.; Jerome, R.; Teyssie, P. Anionic polymerization of (meth)acrylic monomers. 4. Effect of lithium salts as ligands on the "living" polymerization of methyl methacrylate using monofunctional initiators. *Macromolecules* **1990**, *23*, 2618−2622.
(135) Baskaran, D.; Chakrapani, S.; Sivaram, S. Effect of Chelation of the Lithium Cation on the Anionic Polymerization of Methyl Methacrylate Using Organolithium Initiators. *Macromolecules* **1995**, *28*, 7315−7317.
(136) Quirk, R. P.; Yoo, T.; Lee, Y.; Kim, J.; Lee, B. Applications of 1,1-Diphenylethylene Chemistry in Anionic Synthesis of Polymers with Controlled Structures. *Adv. Polym. Sci.* **2000**, *153*, 67−162.
(137) Ingratta, M.; Elomaa, M.; Jannasch, P. Grafting poly(phenylene oxide) with poly(vinylphosphonic acid) for fuel cell membranes. *Polym. Chem.* **2010**, *1*, 739−746.
(138) Sannigrahi, A.; Takamuku, S.; Jannasch, P. Block selective grafting of poly(vinylphosphonic acid) from aromatic multiblock copolymers for nanostructured electrolyte membranes. *Polym. Chem.* **2013**, *4*, 4207−4218.
(139) Webster, O. W.; Hertler, W. R.; Sogah, D. Y.; Farnham, W. B.; RajanBabu, T. V. Group-transfer polymerization. 1. A new concept for addition polymerization with organosilicon initiators. *J. Am. Chem. Soc.* **1983**, *105*, 5706−5708.
(140) Webster, O. Group Transfer Polymerization: A Critical Review of Its Mechanism and Comparison with Other Methods for Controlled Polymerization of Acrylic Monomers. *Adv. Polym. Sci.* **2004**, *167*, 1−34.
(141) Webster, O. W. The discovery and commercialization of group transfer polymerization. *J. Polym. Sci., Part A: Polym. Chem.* **2000**, *38*, 2855−2860.
(142) Mai, P. M.; Müller, A. H. E. Kinetics of group transfer polymerization of methyl methacrylate in tetrahydrofuran, 1. Effect of concentrations of catalyst and initiator on reaction rates. *Makromol. Chem., Rapid Commun.* **1987**, *8*, 99−107.
(143) Mai, P. M.; Müller, A. H. E. Kinetics of group transfer polymerization of methyl methacrylate in tetrahydrofuran, 2. Effect of monomer concentration and temperature on reaction rates. *Makromol. Chem., Rapid Commun.* **1987**, *8*, 247−253.
(144) Müller, A. H. E. Kinetic Discrimination between Various Mechanisms in Group-Transfer Polymerization. *Macromolecules* **1994**, *27*, 1685−1690.
(145) Müller, A. H. E.; Litvinenko, G.; Yan, D. Kinetic Analysis of "Living" Polymerization Systems Exhibiting Slow Equilibria. 3. "Associative" Mechanism of Group Transfer Polymerization and Ion Pair Generation in Cationic Polymerization. *Macromolecules* **1996**, *29*, 2339−2345.
(146) Müller, A. H. E.; Litvinenko, G.; Yan, D. Kinetic Analysis of "Living" Polymerization Systems Exhibiting Slow Equilibria. 4. "Dissociative" Mechanism of Group Transfer Polymerization and Generation of Free Ions in Cationic Polymerization. *Macromolecules* **1996**, *29*, 2346−2353.
(147) Quirk, R. P.; Bidinger, G. P. Mechanistic role of enolate ions in "group transfer polymerization". *Polym. Bull.* **1989**, *22*, 63−70.
(148) Quirk, R. P.; Ren, J. Mechanistic studies of group transfer polymerization. Silyl group exchange studies. *Macromolecules* **1992**, *25*, 6612−6620.
(149) Jenkins, A. D. Enolate ions and the initiation of "group-transfer" polymerization. *Eur. Polym. J.* **1991**, *27*, 649.
(150) Fuchise, K.; Chen, Y.; Satoh, T.; Kakuchi, T. Recent progress in organocatalytic group transfer polymerization. *Polym. Chem.* **2013**, *4*, 4278−4291.

DOI: 10.1021/acs.chemrev.5b00313
Chem. Rev. 2016, 116, 1993−2022

(151) Zhang, Y.; Schmitt, M.; Falivene, L.; Caporaso, L.; Cavallo, L.; Chen, E. Y. X. Organocatalytic Conjugate-Addition Polymerization of Linear and Cyclic Acrylic Monomers by N-Heterocyclic Carbenes: Mechanisms of Chain Initiation, Propagation, and Termination. *J. Am. Chem. Soc.* **2013**, *135*, 17925−17942.
(152) Popescu, M.-T.; Tsitsilianis, C.; Papadakis, C. M.; Adelsberger, J.; Balog, S.; Busch, P.; Hadjiantoniou, N. A.; Patrickios, C. S. Stimuli-Responsive Amphiphilic Polyelectrolyte Heptablock Copolymer Physical Hydrogels: An Unusual pH-Response. *Macromolecules* **2012**, *45*, 3523−3530.
(153) Chen, Y.; Takada, K.; Kubota, N.; Eric, O.-T.; Ito, T.; Isono, T.; Satoh, T.; Kakuchi, T. Synthesis of end-functionalized poly(methyl methacrylate) by organocatalyzed group transfer polymerization using functional silyl ketene acetals and α-phenylacrylates. *Polym. Chem.* **2015**, *6*, 1830−1837.
(154) Fuchise, K.; Sakai, R.; Satoh, T.; Sato, S.-i.; Narumi, A.; Kawaguchi, S.; Kakuchi, T. Group Transfer Polymerization of N,N-Dimethylacrylamide Using Nobel Efficient System Consisting of Dialkylamino Silyl Enol Ether as an Initiator and Strong Brønsted Acid as an Organocatalyst. *Macromolecules* **2010**, *43*, 5589−5594.
(155) Fevre, M.; Vignolle, J.; Heroguez, V.; Taton, D. Tris(2,4,6-trimethoxyphenyl)phosphine (TTMPP) as Potent Organocatalyst for Group Transfer Polymerization of Alkyl (Meth)acrylates. *Macromolecules* **2012**, *45*, 7711−7718.
(156) Chen, Y.; Fuchise, K.; Narumi, A.; Kawaguchi, S.; Satoh, T.; Kakuchi, T. Core-First Synthesis of Three-, Four-, and Six-Armed Star-Shaped Poly(methyl methacrylate)s by Group Transfer Polymerization Using Phosphazene Base. *Macromolecules* **2011**, *44*, 9091−9098.
(157) Takada, K.; Fuchise, K.; Kubota, N.; Ito, T.; Chen, Y.; Satoh, T.; Kakuchi, T. Synthesis of α-, ω-, and α,ω-End-Functionalized Poly(n-butyl acrylate)s by Organocatalytic Group Transfer Polymerization Using Functional Initiator and Terminator. *Macromolecules* **2014**, *47*, 5514−5525.
(158) Takada, K.; Ito, T.; Kitano, K.; Tsuchida, S.; Takagi, Y.; Chen, Y.; Satoh, T.; Kakuchi, T. Synthesis of Homopolymers, Diblock Copolymers, and Multiblock Polymers by Organocatalyzed Group Transfer Polymerization of Various Acrylate Monomers. *Macromolecules* **2015**, *48*, 511−519.
(159) Hertler, W. R. Vinylphosphonic esters as end-capping agents in group transfer polymerization. *J. Polym. Sci., Part A: Polym. Chem.* **1991**, *29*, 869−873.
(160) Yasuda, H.; Yamamoto, H.; Yokota, K.; Miyake, S.; Nakamura, A. Synthesis of monodispersed high molecular weight polymers and isolation of an organolanthanide(III) intermediate coordinated by a penultimate poly(MMA) unit. *J. Am. Chem. Soc.* **1992**, *114*, 4908−4910.
(161) Collins, S.; Ward, D. G. Group-transfer polymerization using cationic zirconocene compounds. *J. Am. Chem. Soc.* **1992**, *114*, 5460−5462.
(162) Yasuda, H.; Yamamoto, H.; Yamashita, M.; Yokota, K.; Nakamura, A.; Miyake, S.; Kai, Y.; Kanehisa, N. Synthesis of high molecular weight poly(methyl methacrylate) with extremely low polydispersity by the unique function of organolanthanide(III) complexes. *Macromolecules* **1993**, *26*, 7134−7143.
(163) Nodono, M.; Tokimitsu, T.; Makino, T. Polymerization of Methyl Methacrylate Initiated by a Divalent Samarium Phenoxide Complex with an Alkyl Aluminium Compound. *Macromol. Chem. Phys.* **2003**, *204*, 877−884.
(164) Li, Y.; Ward, D. G.; Reddy, S. S.; Collins, S. Polymerization of Methyl Methacrylate Using Zirconocene Initiators: Polymerization Mechanisms and Applications. *Macromolecules* **1997**, *30*, 1875−1883.
(165) Sustmann, R.; Sicking, W.; Bandermann, F.; Ferenz, M. On the Mechanism of Polymerization of Acrylates by Zirconocene Complexes, an ab Initio and Density Functional Theory MO Study. *Macromolecules* **1999**, *32*, 4204−4213.
(166) Bandermann, F.; Ferenz, M.; Sustmann, R.; Sicking, W. Polymerization of methyl methacrylate with the neutral zirconocene enolate Cp2ZrMe[OC(Me)═CMe2]. *Macromol. Symp.* **2001**, *174*, 247−254.
(167) Boffa, L. S.; Novak, B. M. Bimetallic Samarium(III) Initiators for the Living Polymerization of Methacrylates and Lactones. A New Route into Telechelic, Triblock, and "Link-Functionalized" Polymers. *Macromolecules* **1994**, *27*, 6993−6995.
(168) Miyake, G. M.; Newton, S. E.; Mariott, W. R.; Chen, E. Y. X. Coordination polymerization of renewable butyrolactone-based vinyl monomers by lanthanide and early metal catalysts. *Dalton Transactions* **2010**, *39*, 6710−6718.
(169) Boffa, L. S.; Novak, B. M. Bimetallic samarium(III) catalysts via electron transfer initiation: The facile synthesis of well-defined (meth)acrylate triblock copolymers. *Tetrahedron* **1997**, *53*, 15367−15396.
(170) Boffa, L. S.; Novak, B. M. "Link-Functionalized" Polymers: An Unusual Macromolecular Architecture through Bifunctional Initiation. *Macromolecules* **1997**, *30*, 3494−3506.
(171) Hu, Y.; Miyake, G. M.; Wang, B.; Cui, D.; Chen, E. Y. X. ansa-Rare-Earth-Metal Catalysts for Rapid and Stereoselective Polymerization of Renewable Methylene Methylbutyrolactones. *Chem. - Eur. J.* **2012**, *18*, 3345−3354.
(172) Hu, Y.; Xu, X.; Zhang, Y.; Chen, Y.; Chen, E. Y. X. Polymerization of Naturally Renewable Methylene Butyrolactones by Half-Sandwich Indenyl Rare Earth Metal Dialkyls with Exceptional Activity. *Macromolecules* **2010**, *43*, 9328−9336.
(173) Hu, Y.; Wang, X.; Chen, Y.; Caporaso, L.; Cavallo, L.; Chen, E. Y. X. Rare-Earth Half-Sandwich Dialkyl and Homoleptic Trialkyl Complexes for Rapid and Stereoselective Polymerization of a Conjugated Polar Olefin. *Organometallics* **2013**, *32*, 1459−1465.
(174) Jende, L. N.; Hollfelder, C. O.; Maichle-Mössmer, C.; Anwander, R. Rare-Earth-Metal Allyl Complexes Supported by the [2-(N,N-Dimethylamino)ethyl]tetramethylcyclopentadienyl Ligand: Structural Characterization, Reactivity, and Isoprene Polymerization. *Organometallics* **2015**, *34*, 32−41.
(175) Jian, Z.; Cui, D.; Hou, Z.; Li, X. Living catalyzed-chain-growth polymerization and block copolymerization of isoprene by rare-earth metal allyl precursors bearing a constrained-geometry-conformation ligand. *Chem. Commun.* **2010**, *46*, 3022−3024.
(176) Jian, Z.; Tang, S.; Cui, D. Highly Regio- and Stereoselective Terpolymerization of Styrene, Isoprene and Butadiene with Lutetium-Based Coordination Catalyst. *Macromolecules* **2011**, *44*, 7675−7681.
(177) Jian, Z.; Petrov, A. R.; Hangaly, N. K.; Li, S.; Rong, W.; Mou, Z.; Rufanov, K. A.; Harms, K.; Sundermeyer, J.; Cui, D. Phosphazene-Functionalized Cyclopentadienyl and Its Derivatives Ligated Rare-Earth Metal Alkyl Complexes: Synthesis, Structures, and Catalysis on Ethylene Polymerization. *Organometallics* **2012**, *31*, 4267−4282.
(178) Chen, R.; Yao, C.; Wang, M.; Xie, H.; Wu, C.; Cui, D. Synthesis of Heterocyclic-Fused Cyclopentadienyl Scandium Complexes and the Catalysis for Copolymerization of Ethylene and Dicyclopentadiene. *Organometallics* **2015**, *34*, 455−461.
(179) Yao, C. G.; Liu, D. T.; Li, P.; Wu, C. J.; Li, S. H.; Liu, B.; Cui, D. M. Highly 3,4-Selective Living Polymerization of Isoprene and Copolymerization with epsilon-Caprolactone by an Amidino N-Heterocyclic Carbene Ligated Lutetium Bis(alkyl) Complex. *Organometallics* **2014**, *33*, 684−691.
(180) Li, L.; Wu, C.; Liu, D.; Li, S.; Cui, D. Binuclear Rare-Earth-Metal Alkyl Complexes Ligated by Phenylene-Bridged β-Diketiminate Ligands: Synthesis, Characterization, and Catalysis toward Isoprene Polymerization. *Organometallics* **2013**, *32*, 3203−3209.
(181) Yao, C.; Wu, C.; Wang, B.; Cui, D. Copolymerization of Ethylene with 1-Hexene and 1-Octene Catalyzed by Fluorenyl N-Heterocyclic Carbene Ligated Rare-Earth Metal Precursors. *Organometallics* **2013**, *32*, 2204−2209.
(182) Wang, L.; Liu, D.; Cui, D. NNN-Tridentate Pyrrolyl Rare-Earth Metal Complexes: Structure and Catalysis on Specific Selective Living Polymerization of Isoprene. *Organometallics* **2012**, *31*, 6014−6021.
(183) Nishiura, M.; Hou, Z. Novel polymerization catalysts and hydride clusters from rare-earth metal dialkyls. *Nat. Chem.* **2010**, *2*, 257−268.

DOI: 10.1021/acs.chemrev.5b00313
Chem. Rev. 2016, 116, 1993−2022

(184) Zeimentz, P. M.; Arndt, S.; Elvidge, B. R.; Okuda, J. Cationic Organometallic Complexes of Scandium, Yttrium, and the Lanthanoids. *Chem. Rev.* **2006**, *106*, 2404−2433.
(185) Dengler, J. Neue Homopolymere aus Vinylphosphonaten. Diploma Thesis, Technische Universität München, Germany, 2007.
(186) Seemann, U. B.; Dengler, J. E.; Rieger, B. High-Molecular-Weight Poly(vinylphosphonate)s by Single-Component Living Polymerization Initiated by Rare-Earth-Metal Complexes. *Angew. Chem.* **2010**, *122*, 3567−3569.
(187) Seemann, U. B. Polyvinylphosphonate und deren Copolymere durch Seltenerdmetall initiierte Gruppen-Transfer-Polymerisation. Ph.D. Thesis, Technische Universität München, Germany, 2010.
(188) Salzinger, S.; Seemann, U. B.; Plikhta, A.; Rieger, B. Poly(vinylphosphonate)s Synthesized by Trivalent Cyclopentadienyl Lanthanide-Induced Group Transfer Polymerization. *Macromolecules* **2011**, *44*, 5920−5927.
(189) Salzinger, S.; Soller, B. S.; Plikhta, A.; Seemann, U. B.; Herdtweck, E.; Rieger, B. Mechanistic Studies on Initiation and Propagation of Rare Earth Metal-Mediated Group Transfer Polymerization of Vinylphosphonates. *J. Am. Chem. Soc.* **2013**, *135*, 13030−13040.
(190) Darensbourg, D. J.; Mackiewicz, R. M.; Rodgers, J. L.; Fang, C. C.; Billodeaux, D. R.; Reibenspies, J. H. Cyclohexene Oxide/CO2 Copolymerization Catalyzed by Chromium(III) Salen Complexes and N-Methylimidazole: Effects of Varying Salen Ligand Substituents and Relative Cocatalyst Loading. *Inorg. Chem.* **2004**, *43*, 6024−6034.
(191) Darensbourg, D. J.; Moncada, A. I. Tuning the Selectivity of the Oxetane and CO2 Coupling Process Catalyzed by (Salen)CrCl/n-Bu4NX: Cyclic Carbonate Formation vs Aliphatic Polycarbonate Production. *Macromolecules* **2010**, *43*, 5996−6003.
(192) Anderson, C. E.; Vagin, S. I.; Xia, W.; Jin, H.; Rieger, B. Cobaltoporphyrin-Catalyzed CO2/Epoxide Copolymerization: Selectivity Control by Molecular Design. *Macromolecules* **2012**, *45*, 6840−6849.
(193) Darensbourg, D. J.; Chung, W.-C. Availability of Other Aliphatic Polycarbonates Derived from Geometric Isomers of Butene Oxide and Carbon Dioxide Coupling Reactions. *Macromolecules* **2014**, *47*, 4943−4948.
(194) Reichardt, R.; Vagin, S.; Reithmeier, R.; Ott, A. K.; Rieger, B. Factors Influencing the Ring-Opening Polymerization of Racemic β-Butyrolactone Using CrIII(salphen). *Macromolecules* **2010**, *43*, 9311−9317.
(195) Vagin, S. I.; Reichardt, R.; Klaus, S.; Rieger, B. Conformationally Flexible Dimeric Salphen Complexes for Bifunctional Catalysis. *J. Am. Chem. Soc.* **2010**, *132*, 14367−14369.
(196) Amgoune, A.; Thomas, C. M.; Ilinca, S.; Roisnel, T.; Carpentier, J.-F. Highly Active, Productive, and Syndiospecific Yttrium Initiators for the Polymerization of Racemic β-Butyrolactone. *Angew. Chem., Int. Ed.* **2006**, *45*, 2782−2784.
(197) Amgoune, A.; Thomas, C. M.; Roisnel, T.; Carpentier, J.-F. Ring-Opening Polymerization of Lactide with Group 3 Metal Complexes Supported by Dianionic Alkoxy-Amino-Bisphenolate Ligands: Combining High Activity, Productivity, and Selectivity. *Chem. - Eur. J.* **2006**, *12*, 169−179.
(198) Bouyahyi, M.; Ajellal, N.; Kirillov, E.; Thomas, C. M.; Carpentier, J.-F. Exploring Electronic versus Steric Effects in Stereoselective Ring-Opening Polymerization of Lactide and β-Butyrolactone with Amino-alkoxy-bis(phenolate)−Yttrium Complexes. *Chem. - Eur. J.* **2011**, *17*, 1872−1883.
(199) Fang, J.; Tschan, M. J. L.; Brule, E.; Robert, C.; Thomas, C. M.; Maron, L. A joint experimental/theoretical investigation of the MMA polymerization initiated by yttrium phenoxyamine complexes. *Dalton Transactions* **2013**, *42*, 9226−9232.
(200) Zhang, N.; Salzinger, S.; Rieger, B. Poly(vinylphosphonate)s with Widely Tunable LCST: A Promising Alternative to Conventional Thermoresponsive Polymers. *Macromolecules* **2012**, *45*, 9751−9758.
(201) Nguyen, H.; Jarvis, A. P.; Lesley, M. J. G.; Kelly, W. M.; Reddy, S. S.; Taylor, N. J.; Collins, S. Isotactic Polymerization of Methyl Methacrylate Using a Prochiral, Zirconium Enolate Initiator. *Macromolecules* **2000**, *33*, 1508−1510.
(202) Evans, W. J.; Dominguez, R.; Hanusa, T. P. Organolanthanide and organoyttrium enolate chemistry. Synthesis of [(C5H4R)2Ln(μ-OCH:CH2)]2 complexes and the molecular structure of [(CH3C5H4)2Y(μ-OCH:CH2)]2. *Organometallics* **1986**, *5*, 1291−1296.
(203) Heeres, H. J.; Maters, M.; Teuben, J. H.; Helgesson, G.; Jagner, S. Organolanthanide-induced carbon-carbon bond formation. Preparation and properties of monomeric lanthanide aldolates and enolates. *Organometallics* **1992**, *11*, 350−356.
(204) Watson, P. L. Methane exchange reactions of lanthanide and early-transition-metal methyl complexes. *J. Am. Chem. Soc.* **1983**, *105*, 6491−6493.
(205) Watson, P. L. Facile C−H activation by lutetium-methyl and lutetium-hydride complexes. *J. Chem. Soc., Chem. Commun.* **1983**, 276−277.
(206) MacDonald, M. R.; Langeslay, R. R.; Ziller, J. W.; Evans, W. J. Synthesis, Structure, and Reactivity of the Ethyl Yttrium Metallocene, (C5Me5)2Y(CH2CH3), Including Activation of Methane. *J. Am. Chem. Soc.* **2015**, *137*, 14716−14725.
(207) Sadow, A. D.; Tilley, T. D. Homogeneous Catalysis with Methane. A Strategy for the Hydromethylation of Olefins Based on the Nondegenerate Exchange of Alkyl Groups and σ-Bond Metathesis at Scandium. *J. Am. Chem. Soc.* **2003**, *125*, 7971−7977.
(208) Fontaine, F.-G.; Tilley, T. D. Control of Selectivity in the Hydromethylation of Olefins via Ligand Modification in Scandocene Catalysts. *Organometallics* **2005**, *24*, 4340−4342.
(209) Barros, N.; Eisenstein, O.; Maron, L.; Tilley, T. D. DFT Investigation of the Catalytic Hydromethylation of Olefins by Scandocenes. 2. Influence of the Ansa Ligand on Propene and Isobutene Hydromethylation. *Organometallics* **2008**, *27*, 2252−2257.
(210) Deelman, B.-J.; Booij, M.; Meetsma, A.; Teuben, J. H.; Kooijman, H.; Spek, A. L. Activation of Ethers and Sulfides by Organolanthanide Hydrides. Molecular Structures of (Cp*2Y)2(μ-OCH2CH2O) (THF)2 and (Cp*2Ce)2(μ-O) (THF)2. *Organometallics* **1995**, *14*, 2306−2317.
(211) Duchateau, R.; van Wee, C. T.; Teuben, J. H. Insertion and C−H Bond Activation of Unsaturated Substrates by Bis(benzamidinato)-yttrium Alkyl, [PhC(NSiMe3)2]2YR (R = CH2Ph·THF, CH(SiMe3)-2), and Hydrido, {[PhC(NSiMe3)2]2Y(μ-H)}2, Compounds. *Organometallics* **1996**, *15*, 2291−2302.
(212) Duchateau, R.; Brussee, E. A. C.; Meetsma, A.; Teuben, J. H. Synthesis and Reactivity of Bis(alkoxysilylamido)yttrium η2-Pyridyl and η2-α-Picolyl Compounds. *Organometallics* **1997**, *16*, 5506−5516.
(213) Ringelberg, S. N.; Meetsma, A.; Hessen, B.; Teuben, J. H. Thiophene C−H Activation as a Chain-Transfer Mechanism in Ethylene Polymerization: Catalytic Formation of Thienyl-Capped Polyethylene. *J. Am. Chem. Soc.* **1999**, *121*, 6082−6083.
(214) Ringelberg, S. N.; Meetsma, A.; Troyanov, S. I.; Hessen, B.; Teuben, J. H. Permethyl Yttrocene 2-Furyl Complexes: Synthesis and Ring-Opening Reactions of the Furyl Moiety. *Organometallics* **2002**, *21*, 1759−1765.
(215) Arndt, S.; Spaniol, T. P.; Okuda, J. Activation of C−H Bonds in Five-Membered Heterocycles by a Half-Sandwich Yttrium Alkyl Complex. *Eur. J. Inorg. Chem.* **2001**, *2001*, 73−75.
(216) Quiroga Norambuena, V. F.; Heeres, A.; Heeres, H. J.; Meetsma, A.; Teuben, J. H.; Hessen, B. Synthesis, Structure, and Reactivity of Rare-Earth Metallocene η3-Propargyl/Allenyl Complexes. *Organometallics* **2008**, *27*, 5672−5683.
(217) Waterman, R. σ-Bond Metathesis: A 30-Year Retrospective. *Organometallics* **2013**, *32*, 7249−7263.
(218) Kaneko, H.; Nagae, H.; Tsurugi, H.; Mashima, K. End-Functionalized Polymerization of 2-Vinylpyridine through Initial C−H Bond Activation of N-Heteroaromatics and Internal Alkynes by Yttrium Ene−Diamido Complexes. *J. Am. Chem. Soc.* **2011**, *133*, 19626−19629.
(219) Soller, B. S.; Salzinger, S.; Jandl, C.; Pöthig, A.; Rieger, B. C−H Bond Activation by σ-Bond Metathesis as a Versatile Route toward

DOI: 10.1021/acs.chemrev.5b00313
Chem. Rev. 2016, 116, 1993−2022

Highly Efficient Initiators for the Catalytic Precision Polymerization of Polar Monomers. *Organometallics* **2015**, *34*, 2703−2706.
(220) Mariott, W. R.; Chen, E. Y. X. Stereospecific, Coordination Polymerization of Acrylamides by Chiral ansa-Metallocenium Alkyl and Ester Enolate Cations. *Macromolecules* **2004**, *37*, 4741−4743.
(221) Mariott, W. R.; Chen, E. Y. X. Mechanism and Scope of Stereospecific, Coordinative-Anionic Polymerization of Acrylamides by Chiral Zirconocenium Ester and Amide Enolates. *Macromolecules* **2005**, *38*, 6822−6832.
(222) Rodriguez-Delgado, A.; Chen, E. Y. X. Mechanistic Studies of Stereospecific Polymerization of Methacrylates Using a Cationic, Chiral ansa-Zirconocene Ester Enolate. *Macromolecules* **2005**, *38*, 2587−2594.
(223) Rodriguez-Delgado, A.; Mariott, W. R.; Chen, E. Y. X. Synthesis and MMA polymerization of chiral ansa-zirconocene ester enolate complexes with C2- and Cs-ligation. *J. Organomet. Chem.* **2006**, *691*, 3490−3497.
(224) Koo, K.; Fu, P.-F.; Marks, T. J. Organolanthanide-Mediated Silanolytic Chain Transfer Processes. Scope and Mechanism of Single Reactor Catalytic Routes to Silapolyolefins. *Macromolecules* **1999**, *32*, 981−988.
(225) Kawaoka, A. M.; Marks, T. J. Organolanthanide-Catalyzed Synthesis of Phosphine-Terminated Polyethylenes. *J. Am. Chem. Soc.* **2004**, *126*, 12764−12765.
(226) Kawaoka, A. M.; Marks, T. J. Organolanthanide-Catalyzed Synthesis of Phosphine-Terminated Polyethylenes. Scope and Mechanism. *J. Am. Chem. Soc.* **2005**, *127*, 6311−6324.
(227) Amin, S. B.; Marks, T. J. Organolanthanide-Catalyzed Synthesis of Amine-Capped Polyethylenes. *J. Am. Chem. Soc.* **2007**, *129*, 10102−10103.
(228) Amin, S. B.; Seo, S.; Marks, T. J. Organo-fn,d0-Mediated Synthesis of Amine-Capped Polyethylenes. Scope and Mechanism. *Organometallics* **2008**, *27*, 2411−2420.
(229) Jochum, F. D.; Theato, P. Temperature- and light-responsive smart polymer materials. *Chem. Soc. Rev.* **2013**, *42*, 7468−7483.
(230) Roy, D.; Brooks, W. L. A.; Sumerlin, B. S. New directions in thermoresponsive polymers. *Chem. Soc. Rev.* **2013**, *42*, 7214−7243.
(231) Schattling, P.; Jochum, F. D.; Theato, P. Multi-stimuli responsive polymers - the all-in-one talents. *Polym. Chem.* **2014**, *5*, 25−36.
(232) *Compendium of Chemical Terminology - IUPAC Recommendations*, 2nd ed. (the "Gold Book"); McNaught, A. D., Wilkinson, A., compilers; Blackwell Scientific Publications, 1997.
(233) Ihara, E.; Morimoto, M.; Yasuda, H. Living Polymerizations and Copolymerizations of Alkyl Acrylates by the Unique Catalysis of Rare Earth Metal Complexes. *Macromolecules* **1995**, *28*, 7886−7892.
(234) Soller, B. S.; Zhang, N.; Rieger, B. Catalytic Precision Polymerization: Rare Earth Metal-Mediated Synthesis of Homopolymers, Block Copolymers, and Polymer Brushes. *Macromol. Chem. Phys.* **2014**, *215*, 1946−1962.
(235) Kelen, T.; Tudos, F. Analysis of the linear methods for determining copolymerization reactivity ratios. I. New improved linear graphic method. *J. Macromol. Sci., Chem.* **1975**, *A9*, 1−27.
(236) Ayano, E.; Kanazawa, H. Aqueous chromatography system using temperature-responsive polymer-modified stationary phases. *J. Sep. Sci.* **2006**, *29*, 738−749.
(237) Lutz, J.-F.; Akdemir, Ö.; Hoth, A. Point by Point Comparison of Two Thermosensitive Polymers Exhibiting a Similar LCST: Is the Age of Poly(NIPAM) Over? *J. Am. Chem. Soc.* **2006**, *128*, 13046−13047.
(238) Blanazs, A.; Warren, N. J.; Lewis, A. L.; Armes, S. P.; Ryan, A. J. Self-assembly of double hydrophilic block copolymers in concentrated aqueous solution. *Soft Matter* **2011**, *7*, 6399−6403.
(239) Lambermont-Thijs, H. M. L.; Hoogenboom, R.; Fustin, C.-A.; Bomal-D'Haese, C.; Gohy, J.-F.; Schubert, U. S. Solubility behavior of amphiphilic block and random copolymers based on 2-ethyl-2-oxazoline and 2-nonyl-2-oxazoline in binary water−ethanol mixtures. *J. Polym. Sci., Part A: Polym. Chem.* **2009**, *47*, 515−522.
(240) Trinh, L. T. T.; Lambermont-Thijs, H. M. L.; Schubert, U. S.; Hoogenboom, R.; Kjøniksen, A.-L. Thermoresponsive Poly(2-oxazoline) Block Copolymers Exhibiting Two Cloud Points: Complex Multistep Assembly Behavior. *Macromolecules* **2012**, *45*, 4337−4345.
(241) Salzinger, S.; Huber, S.; Jaksch, S.; Busch, P.; Jordan, R.; Papadakis, C. Aggregation behavior of thermo-responsive poly(2-oxazoline)s at the cloud point investigated by FCS and SANS. *Colloid Polym. Sci.* **2012**, *290*, 385−400.
(242) Hartmann, M.; Hipler, U. C.; Carlsohn, H. Synthese von Styrencopolymeren ungesättigter Phosphonsäuren und Phosphonsäureester. *Acta Polym.* **1980**, *31*, 165−168.
(243) Opper, K. L.; Fassbender, B.; Brunklaus, G.; Spiess, H. W.; Wagener, K. B. Polyethylene Functionalized with Precisely Spaced Phosphonic Acid Groups. *Macromolecules* **2009**, *42*, 4407−4409.
(244) Chang, H. C.; Lin, H. T.; Lin, C. H.; Su, W. C. Facile preparation of a phosphinated bisphenol and its low water-absorption epoxy resins for halogen-free copper clad laminates. *Polym. Degrad. Stab.* **2013**, *98*, 102−108.
(245) Jang, W.; Seo, M.; Seo, J.; Park, S.; Han, H. Correlation of residual stress and adhesion on copper by the effect of chemical structure of polyimides for copper-clad laminates. *Polym. Int.* **2008**, *57*, 350−358.
(246) Hasegawa, M.; Nomura, R. Thermal- and solution-processable polyimides based on mellophanic dianhydride and their applications as heat-resistant adhesives for copper-clad laminates. *React. Funct. Polym.* **2011**, *71*, 109−120.
(247) Tang, Z.; Li, Y.; Zhang, Y. J.; Jiang, P. Oligomeric siloxane containing triphenylphosphonium phosphate as a novel flame retardant for polycarbonate. *Polym. Degrad. Stab.* **2012**, *97*, 638−644.
(248) Wang, X.; Song, L.; Yang, H.; Xing, W.; Lu, H.; Hu, Y. Cobalt oxide/graphene composite for highly efficient CO oxidation and its application in reducing the fire hazards of aliphatic polyesters. *J. Mater. Chem.* **2012**, *22*, 3426−3431.
(249) Shieh, J.-Y.; Wang, C.-S. Synthesis of novel flame retardant epoxy hardeners and properties of cured products. *Polymer* **2001**, *42*, 7617−7625.
(250) Hoang, D.; Kim, J.; Jang, B. N. Synthesis and performance of cyclic phosphorus-containing flame retardants. *Polym. Degrad. Stab.* **2008**, *93*, 2042−2047.
(251) Lin, C. H.; Huang, C. M.; Wang, M. W.; Dai, S. A.; Chang, H. C.; Juang, T. Y. Synthesis of a phosphinated acetoxybenzoic acid and its application in enhancing Tg and flame retardancy of poly(ethylene terephthalate). *J. Polym. Sci., Part A: Polym. Chem.* **2014**, *52*, 424−434.
(252) Köppl, T.; Brehme, S.; Pospiech, D.; Fischer, O.; Wolff-Fabris, F.; Altstädt, V.; Schartel, B.; Döring, M. Influence of polymeric flame retardants based on phosphorus-containing polyesters on morphology and material characteristics of poly(butylene terephthalate). *J. Appl. Polym. Sci.* **2013**, *128*, 3315−3324.
(253) Pawelec, W.; Aubert, M.; Pfaendner, R.; Hoppe, H.; Wilén, C.-E. Triazene compounds as a novel and effective class of flame retardants for polypropylene. *Polym. Degrad. Stab.* **2012**, *97*, 948−954.
(254) Dumitrascu, A.; Howell, B. A. Flame-retarding vinyl polymers using phosphorus-functionalized styrene monomers. *Polym. Degrad. Stab.* **2011**, *96*, 342−349.
(255) de Wit, C. A. An overview of brominated flame retardants in the environment. *Chemosphere* **2002**, *46*, 583−624.
(256) Liang, S.; Hemberger, P.; Neisius, N. M.; Bodi, A.; Grützmacher, H.; Levalois-Grützmacher, J.; Gaan, S. Elucidating the Thermal Decomposition of Dimethyl Methylphosphonate by Vacuum Ultraviolet (VUV) Photoionization: Pathways to the PO Radical, a Key Species in Flame-Retardant Mechanisms. *Chem. - Eur. J.* **2015**, *21*, 1073−1080.
(257) Schartel, B. Phosphorus-based Flame Retardancy Mechanisms—Old Hat or a Starting Point for Future Development? *Materials* **2010**, *3*, 4710−4745.
(258) Price, D.; Pyrah, K.; Hull, T. R.; Milnes, G. J.; Ebdon, J. R.; Hunt, B. J.; Joseph, P.; Konkel, C. S. Flame retarding poly(methyl methacrylate) with phosphorus-containing compounds: comparison of an additive with a reactive approach. *Polym. Degrad. Stab.* **2001**, *74*, 441−447.
(259) Price, D.; Pyrah, K.; Hull, T. R.; Milnes, G. J.; Ebdon, J. R.; Hunt, B. J.; Joseph, P. Flame retardance of poly(methyl methacrylate)

DOI: 10.1021/acs.chemrev.5b00313
Chem. Rev. 2016, 116, 1993−2022

modified with phosphorus-containing compounds. *Polym. Degrad. Stab.* **2002**, *77*, 227−233.
(260) Joo, B. J.; Lee, M. S.; Lee, B. K. U.S. Patent US 2009149587 A1, 2009.
(261) Chen, X.; Ye, J.; Yuan, L.; Liang, G.; Gu, A. Multi-functional ladderlike polysiloxane: synthesis, characterization and its high performance flame retarding bismaleimide resins with simultaneously improved thermal resistance, dimensional stability and dielectric properties. *J. Mater. Chem. A* **2014**, *2*, 7491−7501.
(262) Shan Wang, C.; Yueh Shieh, J. Synthesis and flame retardancy of phosphorus containing polycarbonate. *J. Polym. Res.* **1999**, *6*, 149−154.
(263) Freitag, D.; Go, P.; Stahl, G. U.S. Patent US 20070203269 A1, 2007.
(264) Perez, R. M.; Sandler, J. K. W.; Altstädt, V.; Hoffmann, T.; Pospiech, D.; Artner, J.; Ciesielski, M.; Döring, M.; Balabanovich, A. I.; Knoll, U.; et al. Novel phosphorus-containing hardeners with tailored chemical structures for epoxy resins: Synthesis and cured resin properties. *J. Appl. Polym. Sci.* **2007**, *105*, 2744−2759.
(265) Ciesielski, M.; Schäfer, A.; Döring, M. Novel efficient DOPO-based flame-retardants for PWB relevant epoxy resins with high glass transition temperatures. *Polym. Adv. Technol.* **2008**, *19*, 507−515.
(266) Chen, L.; Wang, Y.-Z. Aryl Polyphosphonates: Useful Halogen-Free Flame Retardants for Polymers. *Materials* **2010**, *3*, 4746−4760.
(267) Lanzinger, D.; Salzinger, S.; Soller, B. S.; Rieger, B. Poly(vinylphosphonate)s as Macromolecular Flame Retardants for Polycarbonate. *Ind. Eng. Chem. Res.* **2015**, *54*, 1703−1712.
(268) Magnusson, C. D.; Liu, D.; Chen, E. Y. X.; Kelland, M. A. Non-Amide Kinetic Hydrate Inhibitors: Investigation of the Performance of a Series of Poly(vinylphosphonate) Diesters. *Energy Fuels* **2015**, *29*, 2336−2341.
(269) Villano, L. D.; Kommedal, R.; Fijten, M. W. M.; Schubert, U. S.; Hoogenboom, R.; Kelland, M. A. A Study of the Kinetic Hydrate Inhibitor Performance and Seawater Biodegradability of a Series of Poly(2-alkyl-2-oxazoline)s. *Energy Fuels* **2009**, *23*, 3665−3673.
(270) Kawauchi, T.; Ohara, M.; Udo, M.; Kawauchi, M.; Takeichi, T. Preparation of isotactic-rich poly(dimethyl vinylphosphonate) and poly(vinylphosphonic acid) via the anionic polymerization of dimethyl vinylphosphonate. *J. Polym. Sci., Part A: Polym. Chem.* **2010**, *48*, 1677−1682.
(271) Rabe, G. W.; Komber, H.; Häussler, L.; Kreger, K.; Lattermann, G. Polymerization of Diethyl Vinylphosphonate Mediated by Rare-Earth Tris(amide) Compounds. *Macromolecules* **2010**, *43*, 1178−1181.
(272) Barbey, R.; Lavanant, L.; Paripovic, D.; Schüwer, N.; Sugnaux, C.; Tugulu, S.; Klok, H.-A. Polymer Brushes via Surface-Initiated Controlled Radical Polymerization: Synthesis, Characterization, Properties, and Applications. *Chem. Rev.* **2009**, *109*, 5437−5527.
(273) Matyjaszewski, K.; Miller, P. J.; Shukla, N.; Immaraporn, B.; Gelman, A.; Luokala, B. B.; Siclovan, T. M.; Kickelbick, G.; Vallant, T.; Hoffmann, H.; et al. Polymers at Interfaces: Using Atom Transfer Radical Polymerization in the Controlled Growth of Homopolymers and Block Copolymers from Silicon Surfaces in the Absence of Untethered Sacrificial Initiator. *Macromolecules* **1999**, *32*, 8716−8724.
(274) Zhang, T.; Du, Y.; Müller, F.; Amin, I.; Jordan, R. Surface-initiated Cu(0) mediated controlled radical polymerization (SI-CuCRP) using a copper plate. *Polym. Chem.* **2015**, *6*, 2726−2733.
(275) Bao, Z.; Bruening, M. L.; Baker, G. L. Rapid Growth of Polymer Brushes from Immobilized Initiators. *J. Am. Chem. Soc.* **2006**, *128*, 9056−9060.
(276) Advincula, R. In *Surface-Initiated Polymerization I*; Jordan, R., Ed.; Springer: Berlin, 2006; Vol. *197*.
(277) Zhou, Q.; Wang, S.; Fan, X.; Advincula, R.; Mays, J. Living Anionic Surface-Initiated Polymerization (LASIP) of a Polymer on Silica Nanoparticles. *Langmuir* **2002**, *18*, 3324−3331.
(278) Jordan, R.; Ulman, A. Surface Initiated Living Cationic Polymerization of 2-Oxazolines. *J. Am. Chem. Soc.* **1998**, *120*, 243−247.
(279) Jordan, R.; Ulman, A.; Kang, J. F.; Rafailovich, M. H.; Sokolov, J. Surface-Initiated Anionic Polymerization of Styrene by Means of Self-Assembled Monolayers. *J. Am. Chem. Soc.* **1999**, *121*, 1016−1022.
(280) Zheng, J.; Wang, Y.; Ye, L.; Lin, Y.; Tang, T.; Zhang, J. Surface Coordination Polymerization of Ethylene by Hydrozirconation-Immobilized Metallocene. *Macromol. Rapid Commun.* **2014**, *35*, 1198−1203.
(281) Escudé, N. C.; Chen, E. Y. X. Stereoregular Methacrylate-POSS Hybrid Polymers: Syntheses and Nanostructured Assemblies. *Chem. Mater.* **2009**, *21*, 5743−5753.
(282) Priftis, D.; Petzetakis, N.; Sakellariou, G.; Pitsikalis, M.; Baskaran, D.; Mays, J. W.; Hadjichristidis, N. Surface-Initiated Titanium-Mediated Coordination Polymerization from Catalyst-Functionalized Single and Multiwalled Carbon Nanotubes. *Macromolecules* **2009**, *42*, 3340−3346.
(283) Ye, Q.; Wang, X.; Li, S.; Zhou, F. Surface-Initiated Ring-Opening Metathesis Polymerization of Pentadecafluorooctyl-5-norbornene-2-carboxylate from Variable Substrates Modified with Sticky Biomimic Initiator. *Macromolecules* **2010**, *43*, 5554−5560.
(284) Weck, M.; Jackiw, J. J.; Rossi, R. R.; Weiss, P. S.; Grubbs, R. H. Ring-Opening Metathesis Polymerization from Surfaces. *J. Am. Chem. Soc.* **1999**, *121*, 4088−4089.
(285) Zhang, N.; Salzinger, S.; Deubel, F.; Jordan, R.; Rieger, B. Surface-Initiated Group Transfer Polymerization Mediated by Rare Earth Metal Catalysts. *J. Am. Chem. Soc.* **2012**, *134*, 7333−7336.
(286) Deubel, F.; Rieger, B.; Salzinger, S.; Zhang, N. World Patent WO 2013072309 A1, 2013.
(287) Buriak, J. M. Organometallic Chemistry on Silicon and Germanium Surfaces. *Chem. Rev.* **2002**, *102*, 1271−1308.
(288) Hessel, C. M.; Henderson, E. J.; Veinot, J. G. C. Hydrogen Silsesquioxane: A Molecular Precursor for Nanocrystalline Si−SiO2 Composites and Freestanding Hydride-Surface-Terminated Silicon Nanoparticles. *Chem. Mater.* **2006**, *18*, 6139−6146.
(289) Veinot, J. G. C. Synthesis, surface functionalization, and properties of freestanding silicon nanocrystals. *Chem. Commun.* **2006**, 4160−4168.
(290) Li, X.; He, Y.; Swihart, M. T. Surface Functionalization of Silicon Nanoparticles Produced by Laser-Driven Pyrolysis of Silane followed by HF−HNO3 Etching. *Langmuir* **2004**, *20*, 4720−4727.
(291) Knotter, D. M. Etching Mechanism of Vitreous Silicon Dioxide in HF-Based Solutions. *J. Am. Chem. Soc.* **2000**, *122*, 4345−4351.
(292) Steenackers, M.; Lud, S. Q.; Niedermeier, M.; Bruno, P.; Gruen, D. M.; Feulner, P.; Stutzmann, M.; Garrido, J. A.; Jordan, R. Structured Polymer Grafts on Diamond. *J. Am. Chem. Soc.* **2007**, *129*, 15655−15661.
(293) Zhang, N.; Steenackers, M.; Luxenhofer, R.; Jordan, R. Bottle-Brush Brushes: Cylindrical Molecular Brushes of Poly(2-oxazoline) on Glassy Carbon. *Macromolecules* **2009**, *42*, 5345−5351.
(294) Steenackers, M.; Küller, A.; Stoycheva, S.; Grunze, M.; Jordan, R. Structured and Gradient Polymer Brushes from Biphenylthiol Self-Assembled Monolayers by Self-Initiated Photografting and Photopolymerization (SIPGP). *Langmuir* **2009**, *25*, 2225−2231.
(295) Chen, T.; Amin, I.; Jordan, R. Patterned polymer brushes. *Chem. Soc. Rev.* **2012**, *41*, 3280−3296.
(296) Yang, J.; Liang, Y.; Salzinger, S.; Zhang, N.; Dong, D.; Rieger, B. Poly(vinylphosphonate)s functionalized polymer microspheres via rare earth metal-mediated group transfer polymerization. *J. Polym. Sci., Part A: Polym. Chem.* **2014**, *52*, 2919−2925.
(297) Kehrle, J.; Höhlein, I. M. D.; Yang, Z.; Jochem, A.-R.; Helbich, T.; Kraus, T.; Veinot, J. G. C.; Rieger, B. Thermoresponsive and Photoluminescent Hybrid Silicon Nanoparticles by Surface-Initiated Group Transfer Polymerization of Diethyl Vinylphosphonate. *Angew. Chem.* **2014**, *126*, 12702−12705.
(298) Zhang, N.; Salzinger, S.; Soller, B. S.; Rieger, B. Rare Earth Metal-Mediated Group-Transfer Polymerization: From Defined Polymer Microstructures to High-Precision Nano-Scaled Objects. *J. Am. Chem. Soc.* **2013**, *135*, 8810−8813.
(299) Tomalia, D. A.; Thill, B. P.; Fazio, M. J. Ionic Oligomerization and Polymerization of 2-Alkenyl-2-oxazolines. *Polym. J.* **1980**, *12*, 661−675.

DOI: 10.1021/acs.chemrev.5b00313
Chem. Rev. 2016, 116, 1993−2022

(300) Zhang, N.; Huber, S.; Schulz, A.; Luxenhofer, R.; Jordan, R. Cylindrical Molecular Brushes of Poly(2-oxazoline)s from 2-Isopropenyl-2-oxazoline. *Macromolecules* **2009**, *42*, 2215−2221.
(301) Kagiya, T.; Matsuda, T.; Zushi, K. Radical Copolymerization of 2-lsopropenyl-2-oxazoline with Styrene in the Presence of Lewis Acids. *J. Macromol. Sci., Part A: Pure Appl.Chem.* **1972**, *6*, 1349−1372.
(302) Weber, C.; Neuwirth, T.; Kempe, K.; Ozkahraman, B.; Tamahkar, E.; Mert, H.; Becer, C. R.; Schubert, U. S. 2-Isopropenyl-2-oxazoline: A Versatile Monomer for Functionalization of Polymers Obtained via RAFT. *Macromolecules* **2012**, *45*, 20−27.
(303) He, J.; Zhang, Y.; Falivene, L.; Caporaso, L.; Cavallo, L.; Chen, E. Y. X. Chain Propagation and Termination Mechanisms for Polymerization of Conjugated Polar Alkenes by [Al]-Based Frustrated Lewis Pairs. *Macromolecules* **2014**, *47*, 7765−7774.
(304) He, J.; Zhang, Y.; Chen, E. Y. X. Synthesis of Pyridine- and 2-Oxazoline-Functionalized Vinyl Polymers by Alane-Based Frustrated Lewis Pairs. *Synlett* **2014**, *25*, 1534−1538.
(305) Hoogenboom, R. Poly(2-oxazoline)s: A Polymer Class with Numerous Potential Applications. *Angew. Chem., Int. Ed.* **2009**, *48*, 7978−7994.
(306) Schlaad, H.; Diehl, C.; Gress, A.; Meyer, M.; Demirel, A. L.; Nur, Y.; Bertin, A. Poly(2-oxazoline)s as Smart Bioinspired Polymers. *Macromol. Rapid Commun.* **2010**, *31*, 511−525.
(307) Luxenhofer, R.; Schulz, A.; Roques, C.; Li, S.; Bronich, T. K.; Batrakova, E. V.; Jordan, R.; Kabanov, A. V. Doubly amphiphilic poly(2-oxazoline)s as high-capacity delivery systems for hydrophobic drugs. *Biomaterials* **2010**, *31*, 4972−4979.
(308) Adams, N.; Schubert, U. S. Poly(2-oxazolines) in biological and biomedical application contexts. *Adv. Drug Delivery Rev.* **2007**, *59*, 1504−1520.
(309) Viegas, T. X.; Bentley, M. D.; Harris, J. M.; Fang, Z.; Yoon, K.; Dizman, B.; Weimer, R.; Mero, A.; Pasut, G.; Veronese, F. M. Polyoxazoline: Chemistry, Properties, and Applications in Drug Delivery. *Bioconjugate Chem.* **2011**, *22*, 976−986.
(310) Knop, K.; Hoogenboom, R.; Fischer, D.; Schubert, U. S. Poly(ethylene glycol) in Drug Delivery: Pros and Cons as Well as Potential Alternatives. *Angew. Chem., Int. Ed.* **2010**, *49*, 6288−6308.
(311) Luxenhofer, R.; Sahay, G.; Schulz, A.; Alakhova, D.; Bronich, T. K.; Jordan, R.; Kabanov, A. V. Structure-property relationship in cytotoxicity and cell uptake of poly(2-oxazoline) amphiphiles. *J. Controlled Release* **2011**, *153*, 73−82.
(312) Barz, M.; Luxenhofer, R.; Zentel, R.; Vicent, M. J. Overcoming the PEG-addiction: well-defined alternatives to PEG, from structure-property relationships to better defined therapeutics. *Polym. Chem.* **2011**, *2*, 1900−1918.
(313) Altenbuchner, P. T.; Soller, B. S.; Kissling, S.; Bachmann, T.; Kronast, A.; Vagin, S. I.; Rieger, B. Versatile 2-Methoxyethylaminobis-(phenolate)yttrium Catalysts: Catalytic Precision Polymerization of Polar Monomers via Rare Earth Metal-Mediated Group Transfer Polymerization. *Macromolecules* **2014**, *47*, 7742−7749.
(314) Altenbuchner, P. T.; Adams, F.; Kronast, A.; Herdtweck, E.; Pothig, A.; Rieger, B. Stereospecific catalytic precision polymerization of 2-vinylpyridine via rare earth metal-mediated group transfer polymerization with 2-methoxyethylamino-bis(phenolate)-yttrium complexes. *Polym. Chem.* **2015**, *6*, 6796−6801.

DOI: 10.1021/acs.chemrev.5b00313
Chem. Rev. 2016, 116, 1993−2022

4.2 Mechanistic Studies on Initiation and Propagation of Rare Earth Metal-Mediated Group Transfer Polymerization of Vinylphosphonates

Status: Published online: July 26, 2013

Journal: Journal of the American Chemical Society

Volume 135, issue 36, pages 13030–13040

Publisher: American Chemical Society

Article Type: Article

DOI: 10.1021/ja404457f

Authors: Stephan Salzinger, Benedikt S. Soller, Andriy Plikhta, Uwe B. Seemann, Eberhardt Herdtweck, and Bernhard Rieger

4.2.1 Abstract

In this chapter, the first detailed mechanistic studies on both initiation and propagation of REM-GTP of vinylphosphonates are presented. The reactive α-C–H group of vinylphosphonates and the use of unbridged RE metallocenes lead to a complex network for the initiation reaction. Depending on the nature of the initiating ligand, the initiation can either proceed via abstraction of the acidic α-C–H of the vinylphosphonate, via transfer of a nucleophilic ligand to a coordinated monomer, or via a monomer- (*i.e.*, donor-) induced ligand exchange reaction forming the active Cp_3Ln species in equilibrium. Isolated DEVP adducts Cp_2LnCl(DEVP) provide the first X-ray crystallographic proof for vinylphosphonate coordination at the active site via the oxygen of the phosphonate moiety. Kinetic studies including time-resolved analysis of monomer conversion and molecular weights of the formed polymers allows the determination of the initiator efficiency throughout the whole reaction. Using this normalization method, REM-GTP was shown to follow a monometallic Yasuda-type polymerization mechanism, with an S_N2-type associative displacement of the polymer phosphonate ester by a monomer as the rate-determining step. Temperature dependent activity measurements lead to the determination of the thermodynamic parameters $\Delta H^{\ddagger}$ and $\Delta S^{\ddagger}$ for the pentacoordinate intermediate. The activation entropy $\Delta S^{\ddagger}$ of the rate-determining step is strongly affected by the metal radius and the monomer size, whereas these parameters show only minor influence on the activation enthalpy $\Delta H^{\ddagger}$ for unsubstituted unbridged RE metallocenes. Accordingly, the propagation rate of vinylphosphonate REM-GTP is shown to be mainly determined by the change of rotational and vibrational restrictions within the eight-membered metallacycle in the rate-determining step.

The first author Stephan Salzinger was supported by second author Benedikt S. Soller in performing and interpreting the experimental results.

JACS
JOURNAL OF THE AMERICAN CHEMICAL SOCIETY

Article

pubs.acs.org/JACS

Mechanistic Studies on Initiation and Propagation of Rare Earth Metal-Mediated Group Transfer Polymerization of Vinylphosphonates

Stephan Salzinger, Benedikt S. Soller, Andriy Plikhta, Uwe B. Seemann, Eberhardt Herdtweck, and Bernhard Rieger*

WACKER-Lehrstuhl für Makromolekulare Chemie, Technische Universität München, Lichtenbergstraße 4, 85748 Garching bei München, Germany

Supporting Information

ABSTRACT: Initiation of rare earth metal-mediated vinylphosphonate polymerization with unbridged rare earth metallocenes (Cp_2LnX) follows a complex reaction pathway. Depending on the nature of X, initiation can proceed either *via* abstraction of the acidic α-CH of the vinylphosphonate (e.g., for X = Me, CH_2TMS), *via* nucleophilic transfer of X to a coordinated monomer (e.g., for X = Cp, SR) or *via* a monomer (i.e., donor)-induced ligand-exchange reaction forming Cp_3Ln in equilibrium (e.g., for X = Cl, OR), which serves as the active initiating species. As determined by mass spectrometric end group analysis, different initiations may also occur simultaneously (e.g., for X = $N(SiMe_2H)_2$). A general differential approach for the kinetic analysis of living polymerizations with fast propagation and comparatively slow initiation is presented. Time-resolved analysis of monomer conversion and molecular weights of the formed polymers allow the determination of the initiator efficiency throughout the whole reaction. Using this normalization method, rare earth metal-mediated vinylphosphonate GTP is shown to follow a Yasuda-type monometallic propagation mechanism, with an S_N2-type associative displacement of the polymer phosphonate ester by a monomer as the rate-determining step. The propagation rate of vinylphosphonate GTP is mainly determined by the activation entropy, i.e. the change of rotational and vibrational restrictions within the eight-membered metallacycle in the rate-determining step as a function of the steric demand of the metallacycle side chains and the steric crowding at the metal center.

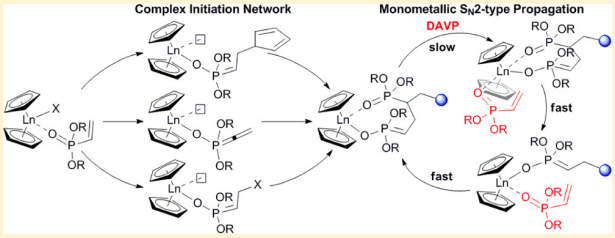

INTRODUCTION

Phosphorus-containing polymers, especially those comprising phosphonate moieties, have gained significant interest due to their potential utilization in a large variety of applications, ranging from polyelectrolytes in batteries and fuel cells over halogen-free flame retardants to diverse uses in the biomedical field.[1−10] However, a straightforward approach to these polymers *via* polymerization of vinylphosphonates has long been hard to establish, as radical and classical anionic synthesis routes often result in low yields of polymer with unsatisfying degrees of polymerization.[11] Recently, it could be shown that poly(vinylphosphonate)s with high molar mass and low polydispersity can be efficiently prepared in the presence of rare earth metal catalysts,[11−16] presumably following a group transfer polymerization (GTP) mechanism.[11]

Rare earth metal-mediated GTP (REM-GTP) of acrylic monomers was first reported by Yasuda et al.[17] in 1992 and is also referred to as coordinative-anionic or coordination-addition polymerization.[18] Over the past decades, intensive research has been carried out to optimize the reaction conditions and the initiator efficiency and to broaden the use of coordinative-anionic polymerizations for a variety of monomers, e.g. different (meth)acrylates and (meth)-acrylamides.[18−21] The initiation for this living-type of polymerization commonly occurs *via* 1,4-addition of a nucleophilic ligand from the metal complex to a coordinated monomer or, in the case of divalent lanthanide initiators, *via* redox initiation.[18,22] The propagation proceeds *via* repeated conjugate addition over an eight-membered ring intermediate (Scheme 1a),[18−21,23] which could be isolated and characterized by X-ray crystallography.[17,23] Hereby, the catalyst both stabilizes the anionic chain end and activates the coordinated monomer.[11,18] The coordination of the growing chain end at the catalyst suppresses side reactions and allows stereospecific polymerization as well as activity optimization by variation of both the metal center and the catalyst ligand sphere.[18−21] Besides this monometallic propagation, coordinative-anionic polymerizations may also follow a bimetallic mechanism, for which alternating one metal center activates the monomer, while the other stabilizes the growing chain end (e.g., for group 4 metal-mediated GTP, Scheme 1b).[24−28]

The mechanism taking place and the corresponding rate-determining step (RDS) are difficult to predict and were found

Received: May 13, 2013
Published: July 26, 2013

dx.doi.org/10.1021/ja404457f | J. Am. Chem. Soc. 2013, 135, 13030−13040

Scheme 1. Proposed Monometallic (a) and Bimetallic (b) Propagation Mechanism for Coordinative-Anionic Polymerization of Michael Acceptor-Type Monomers[a]

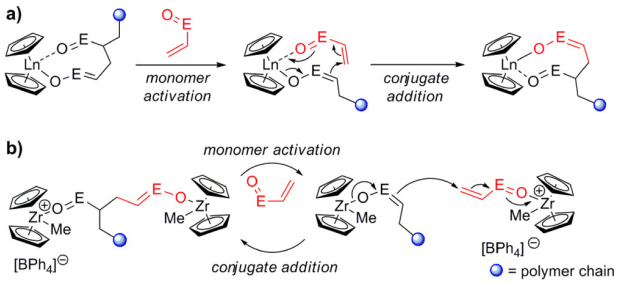

[a]E = C(OR), C(NR$_2$), P(OR)$_2$.

Scheme 2. Proposed S_N1-Type (a) and S_N2-Type (b) Polymer Ester Cleavage from/Monomer Addition to the Metal Center for REM-GTP[a]

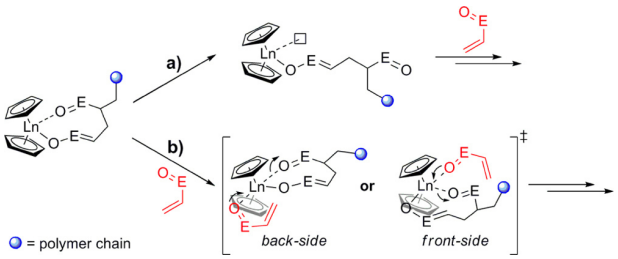

[a]E = C(OR), C(NR$_2$), P(OR)$_2$.

to be strongly dependent on the ligand architecture, the metal center, and the used monomer.[18,25−27,29−36] The influence of mechanism and RDS on the stereoregularity of the polymerization and, *vice versa*, the mechanistic conclusions drawn from obtained microstructures have been controversially discussed.[20,28−30,33,36−40] Besides the actual conjugate addition, the RDS can be cleavage of the polymer ester group from the metal center (S_N1-type reaction, Scheme 2a) or an associative displacement of this ester group by a monomer (S_N2-type reaction, Scheme 2b).[20,25−30,36,37,40−42] The latter is both described in a back-side manner or *via* an attack at the same site relative to the leaving polymer ester group (front-side), *i.e. via* a chain retention or a chain migratory mechanism.[28−30,33,37−40,42] In the case of monometallic coordinative-anionic polymerization, depending on the evident RDS, the monomer addition will occur either alternating at both sites of the catalyst or predominantly at only one site *via* site-retention.[29,30,33,36−40,42]

Recent publications have shown that REM-GTP is not only applicable to common acrylic monomers, but as well to several other monomer classes, i.e. dialkyl vinylphosphonates (DAVP), 2-isopropylene-2-oxazoline and 2-vinylpyridine.[11−16,43,44] In previous work, we have shown that late lanthanide metallocenes are efficient initiators and highly active catalysts for DAVP polymerization.[14,16] Initial investigations have proven the livingness of polymerization and suggest a GTP mechanism taking place,[11,12,14] however, detailed mechanistic studies on both initiation and propagation of REM-GTP of vinylphosphonates have not yet been conducted.

In this article, we show that initiation of vinylphosphonate GTP follows a complex reaction network. We present a general procedure for kinetic analysis of living polymerizations with fast propagation and comparatively slow initiation. A detailed study of the influence of metal radii, steric demand of the monomers and reaction temperature on the polymerization rate gives insight into the mechanism of REM-GTP, both for vinylphosphonates in particular as well as for its general understanding.

RESULTS AND DISCUSSION

We previously reported on the use of tris(cyclopentadienyl)-lanthanide complexes (Cp$_3$Ln) for the polymerization of diethyl and diisopropyl vinylphosphonate (DEVP and DIVP, respectively).[14] Whereas the rate of initiation was found to be accelerated by both decreasing metal radius and increasing steric demand of the monomer, i.e. by higher steric crowding of the intermediate Cp$_3$Ln(DAVP), the propagation rate was enhanced by smaller metal radii and decreasing steric demand of the monomer, contradicting previous work on (meth)-acrylate rare earth metal-mediated GTP.[18−20,23,45] Within the frame of this previous work, we could not address the origin of this faster propagation for late lanthanides, i.e. for higher Lewis acidity and *higher* steric crowding of the active species, in combination with an increased activity for smaller monomers, *i.e. lower* steric crowding of the active species.

In earlier work, we applied bis(cyclopentadienyl)-chloro, -amide, and -methyl complexes ([Cp$_2$LnCl]$_2$, Cp$_2$Ln(bdsa)-(thf), and [Cp$_2$YbMe]$_2$, respectively; bdsa = bis(dimethylsilyl)-amide, N(SiMe$_2$H)$_2$) for vinylphosphonate polymerization.[11,12,46] For the chloro and amide catalysts, a distinct initiation period was evident. In accordance with their previous use for MMA polymerization, the observed initiator efficiencies were low; however, the activity is considerably higher for

Table 1. DEVP Polymerization Results for Previously Applied Cp$_2$LnX Catalysts[a]

catalyst	reaction time	conversion[b]/%	init. period[c]	M_n[d]/kDa	PDI (M_w/M_n)	I^*[d]/%	TOF[b]/I^*/h^{-1}	TOF/I^* (Cp$_3$Ln)[e]/h^{-1}
[Cp$_2$HoCl]$_2$	24 h	76	180 min	810	1.32	9.6	1100	8000
[Cp$_2$YCl]$_2$	6 h	70	100 min	740	1.31	9.3	3700	23000
[Cp$_2$ErCl]$_2$	6 h	79	100 min	780	1.35	10.0	2800	28000
[Cp$_2$TmCl]$_2$	3.5 h	86	90 min	990	1.29	8.5	5900	72000
[Cp$_2$YbCl]$_2$	3 h	81	90 min	890	1.36	9.8	8400	185000
[Cp$_2$LuCl]$_2$	1.5 h	93	7 min	780	1.34	11.7	20500	>265000
Cp$_2$Y(bdsa)(thf)	3 h	95	15 min	1040	1.27	9.0	7200	23000
Cp$_2$Lu(bdsa)(thf)	3 h	96	20 min	1350	1.20	7.0	21000	>265000
[Cp$_2$YbMe]$_2$	30 min	99	80 s	900	1.52	10.8	49000	185000

[a]Toluene, 30 °C, monomer-to-catalyst ratio 600:1. [b]Determined by ^{31}P NMR spectroscopic measurement, [c]Initiation period, reaction time until 3% conversion is reached, [d]Determined by GPC-MALS, $I^* = M_{th}/M_n$, $M_{th} = 600 \times M_{Mon} \times$ conversion, [e]normalized activity for corresponding Cp$_3$Ln.[14]

dx.doi.org/10.1021/ja404457f | J. Am. Chem. Soc. 2013, 135, 13030−13040

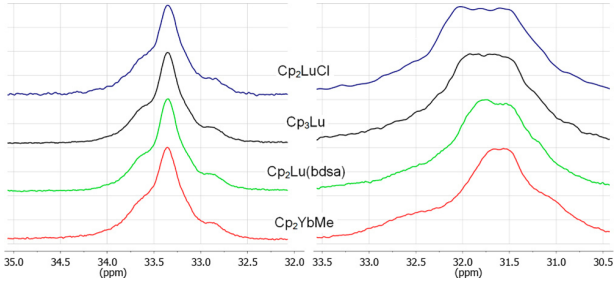

Figure 1. ^{31}P NMR spectra of PDEVP (left, in D_2O) and PDIVP (right, in $CDCl_3$) produced with different catalysts (from top to bottom: $[Cp_2LuCl]_2$ (blue), Cp_3Lu (black), $Cp_2Lu(bdsa)(thf)$, (green) and $[Cp_2YbMe]_2$ (red)). For all catalysts, polymers with (nearly) identical atactic polymer microstructure are obtained.

vinylphosphonate (Table 1) than for MMA polymerization (TOF = 7 h^{-1}).[18,47] According to our study on Cp_3Ln-initiated vinylphosphonate GTP, the normalized activity TOF/I*[14] was found to be strongly accelerated for later lanthanides, e.g. for $[Cp_2LnCl]_2$/DEVP from 1100 h^{-1} for Ho to 20500 h^{-1} for Lu (Table 1, entry 1−6).[14] At the same time, contradicting the polymerization with Cp_3Ln, the initiator efficiency was either unaffected by the metal size (Table 1) or found to decrease for smaller metal centers (see ref 11), depending on concentration and polymerization temperature. Hereby, all Cp_3Ln and Cp_2LnX complexes yielded polymers with the same (essentially) atactic polymer microstructure (Figure 1), indicating the active catalytic species consistently to be a Cp_2Ln unit. The normalized activity, however, was found to be strongly different for Cp_3Ln in comparison to that of $[Cp_2LnCl]_2$, $[Cp_2YbMe]_2$, and $Cp_2Ln(bdsa)(thf)$ (Table 1). In order to explain the observed differences between Cp_2LnX and Cp_3Ln complexes and the differences from (meth)acrylate polymerizations, we conducted detailed analyses of both initiation and propagation of vinylphosphonate GTP.

Initiation Mechanism. ESI MS analysis of vinylphosphonate oligomers produced with $[Cp_2YbMe]_2$ shows no apparent end group (Figure S1 in Supporting Information [SI]). As methanolic workup leads to chain termination by a proton, the exclusive observation of signals with $m/z = n \times M_{Mon} + M_{Na}$ is attributed to an initiation *via* deprotonation yielding CH_4 and an olefinic chain end. Similar to Cp_3Ln, for $[Cp_2LnCl]_2$, initiation was found to proceed *via* transfer of a cyclopentadienyl ligand to a coordinated monomer (Figure S2, S3 in SI).[14,48] These results clearly show that, depending on the ligand's basicity and nucleophilicity, initiation can generally either proceed *via* deprotonation of the acidic α-CH of the vinylphosphonate or *via* nucleophilic transfer (Scheme 3). This is in line with previous observations on classical anionic vinylphosphonate polymerizations.[11,49]

For the amide catalysts $Cp_2Ln(bdsa)(thf)$, on the other hand, two series of peaks were evident in the mass spectrometric end group analysis, one with a bdsa and one with a Cp end group (Figure 2). The ratio of these end groups

Scheme 3. Possible Initiation Reactions for Rare Earth Metal-Mediated Vinylphosphonate Polymerizations

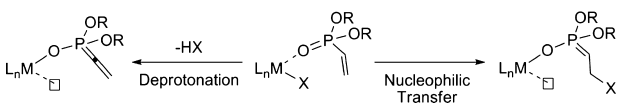

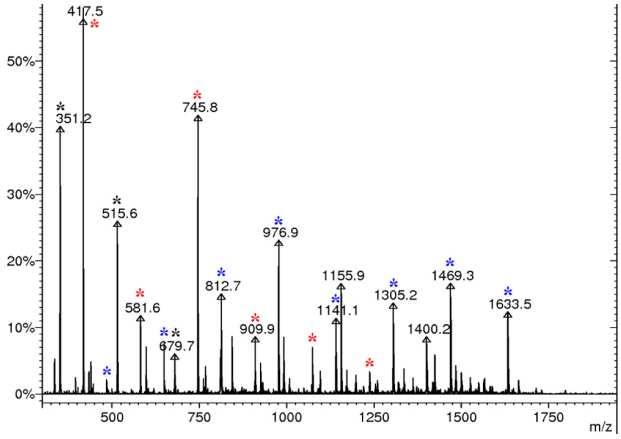

Figure 2. ESI MS spectrum of DEVP oligomers produced with $Cp_2Y(bdsa)(thf)$. Two major series of peaks are evident: $m/z = n \times M_{Mon} + 66 + M_{Na}$ (red), $m/z = n \times M_{Mon} + 133 + M_{Na}$ (blue); M_{Mon} = 164, end groups: $M_{Cp} + M_H$ = 66, $M_{bdsa} + M_H$ = 133. Peaks at m/z = 351, 515, and 679 are attributed to fragmentation (black).[48]

Scheme 4. Donor-Induced Ligand-Exchange Reaction Caused by Coordination of Phosphonates at Cp_2LnX Complexes for the Example DEEP

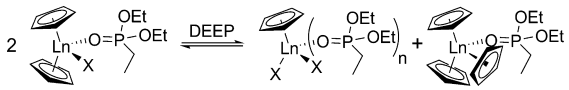

was found to be strongly dependent on the reaction conditions, and frequently, a peak series with olefinic chain ends was observed instead of bdsa end groups (Figures S4, S5 in SI). As in some cases, only olefinic chain ends were detected (Figure S5 in SI), this observation can be attributed to an elimination of the bdsa end group. Despite the simultaneous occurrence of two different initiation reactions, the obtained polymer shows a monomodal molecular weight distribution, indicating that both types of initiation produce the same active species.

To get deeper insight in the underlying initiation mechanism, an NMR spectroscopic study of phosphonate coordination at the used complexes was conducted. Diethyl ethylphosphonate (DEEP) was used due to its similar steric demand in comparison to DEVP and as it excludes both initiation and subsequent polymerization. Addition of varying amounts of DEEP (0.5, 1, 2, and 5 equiv with respect to the metal center, respectively) revealed a monomer (i.e., donor)-induced ligand exchange reaction forming $Cp_3Ln(DEEP)$ and $CpLnX_2(DEEP)_n$ in equilibrium with the adduct Cp_2LnX-(DEEP) (Scheme 4, Figure 3). Line broadening of the DEEP ^{1}H and ^{31}P NMR spectroscopic signals indicates a fast exchange (in the NMR time scale) of coordinated and free DEEP (Figure 3). Larger metal centers and higher phosphonate concentration accelerate this exchange reaction and shift the equilibrium to the $Cp_3Ln/CpLnX_2$ side.

To provide proof of the identity of the $Cp_3Ln(DEEP)$ adduct, the NMR samples of the corresponding Y complex were overlaid with pentane, yielding colorless crystals suitable for single-crystal X-ray crystallography (Figures 4 and S13 in SI). In attempts to crystallize a vinylphosphonate adduct, according to the prolonged initiation period, addition of 1 equiv of DEVP to a toluene solution of $[Cp_2LnCl]_2$ (Ln = Ho, Yb), subsequent overlaying with pentane, and cooling to −30 °C

dx.doi.org/10.1021/ja404457f | J. Am. Chem. Soc. 2013, 135, 13030−13040

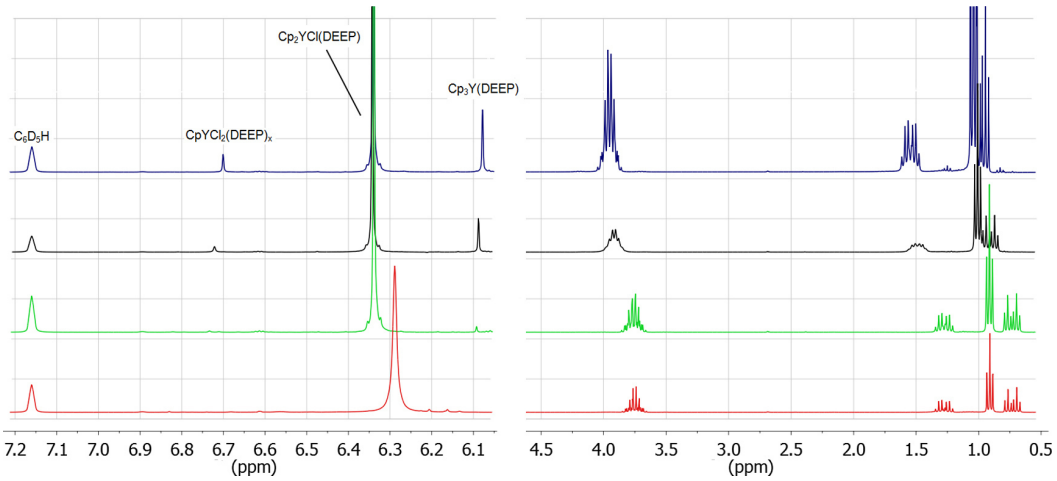

Figure 3. ^{1}H NMR spectra of DEEP coordination at the rare earth metal center for addition of 0.5 (red), 1 (green), 2 (black), and 5 equiv (blue) of DEEP (with respect to the metal center) to $[Cp_2YCl]_2$ in C_6D_6, respectively. A donor-induced ligand-exchange reaction forming $Cp_3Y(DEEP)$ and $CpYCl_2(DEEP)_n$ in equilibrium with the adduct $Cp_2YCl(DEEP)$ is evident. For addition of 2 equiv of DEEP, line broadening for the DEEP ^{1}H NMR spectroscopic signals shows an exchange of free and coordinated DEEP in the ^{1}H NMR time scale.

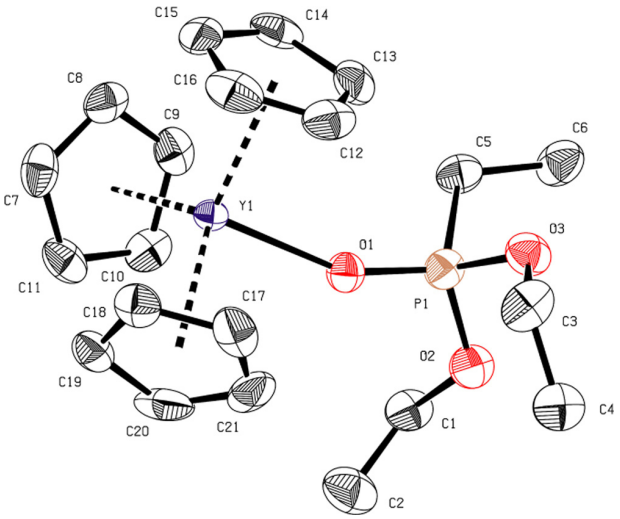

Figure 4. Crystal structure of the adduct $Cp_3Y(DEEP)$ (50% thermal ellipsoids; hydrogen atoms were omitted for clarity). Selected interatomic distances and bond angles: Y−O(1), 2.294 Å; P═O(1), 1.495 Å; Y−O(1)═P, 7.24°.

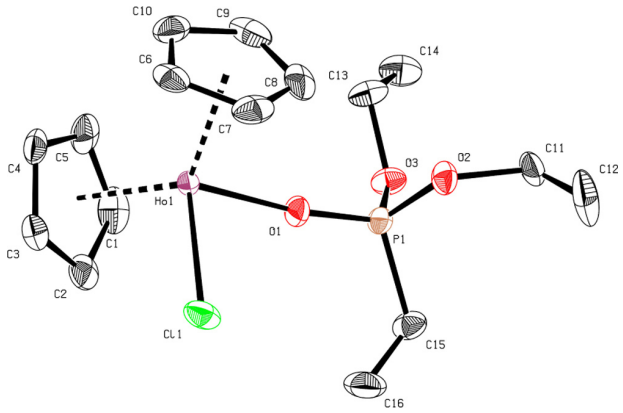

Figure 5. Crystal structure of the adduct $Cp_2HoCl(DEVP)$ (50% thermal ellipsoids; hydrogen atoms were omitted for clarity). Selected interatomic distances, bond angles, and torsion angles: Ho−Cl, 2.582 Å; Ho−O(1), 2.227 Å; P═O(1), 1.485 Å; P−C(15), 1.779 Å; C(15)═C(16), 1.314 Å; P═O(1)−Ho, 167.0°; O (1)═P−C(15)═C(16), −10.14°.

yielded the adduct $Cp_2LnCl(DEVP)$, as proven by X-ray crystallography. This way, we can provide first crystallographic proof of vinylphosphonate coordination at the active site *via* the oxygen of the phosphonate moiety (Figures 5 and S14, S15 in SI). Previously, this type of coordination was suggested by ^{1}H and ^{31}P NMR spectroscopies.[13,50] Importantly, the crystal structures show that the Michael system of the coordinated vinylphosphonate is retained in an S-cis conformation with a pronounced π-overlap (torsion angles O═P−C═C of −10.14 and 10.47°, Figures 5 and S14, S15 in SI), a key prerequisite for the polymerizability of a monomer by a repeated conjugate addition polymerization, i.e. a GTP.[11,18] When the isolated DEVP adducts are dissolved in toluene, vinylphosphonate oligomers are formed after a few hours at room temperature without the addition of further monomer. This inherent instability of the Cp_2LnCl (DEVP) adducts provides further evidence for the observed ligand-exchange reaction.

Different initiators, Cp_2LnX, were synthesized and tested for their vinylphosphonate polymerization behavior (Table 2). Except for the aryloxy-substituted complexes $Cp_2Ln(OAr)$-(thf), in all cases, the formation of $Cp_3Ln(DEEP)$ was observed. As previously shown, in the case of late lanthanides, $Cp_3Ln(DAVP)$ serves as an efficient initiator for DAVP polymerization.[14] If neither deprotonation of the acidic α-CH nor nucleophilic transfer is possible due to insufficient reactivity of the LnX bond (e.g., for X = Cl, O(Alk/Ar)), formed $Cp_3Ln(DAVP)$ will serve as the active initiating species (Scheme 5). This conclusion is corroborated by end group analysis of produced DEVP oligomers as well as by the inability of $Cp_2Ln(OAr)(thf)$ (which was found not to undergo a ligand-exchange reaction, but to decompose upon DEEP addition) and $Cp^*_2LuCl(thf)$ (for which formation of Cp^*_3Lu, and thus a ligand exchange is not possible[51]) to initiate polymerization (Table 2 and Figures S6−11 in SI).

Thiolato complexes $[Cp_2Ln(StBu)]_2$ were found to be well-suited for the initiation of vinylphosphonate GTP. However, for

dx.doi.org/10.1021/ja404457f | J. Am. Chem. Soc. 2013, 135, 13030−13040

Table 2. DEVP Polymerization Results for Cp_2LnX Catalysts[a]

catalyst	reaction time	conversion[b]/%	init. period[c]	M_n[d]/kDa	PDI (M_w/M_n)	I^*[d]/%	TOF[b]/I^* /h^{-1}	end group[e]	extent of ligand exchange[f]/%
$[Cp_2YCl]_2$	6 h	70	100 min	740	1.31	9.3	3700	Cp	15
$Cp_2Y(bdsa)(thf)$	3 h	95	15 min	1040	1.27	9.0	7200	Cp, bdsa (olefinic)[g]	3
$[Cp_2Y(OiPr)]_2$	30 h	26	2.5 h	1070	1.20	2.4	2000	Cp	<0.5 (10)[h]
$Cp_2Y(OAr)(thf)$	30 h	–	–	–	–	–	–	–	<0.5
$[Cp_2Y(StBu)]_2$	3 min	100	5 s	150	1.18	65	69000	StBu (olefinic)[g]	4
$Cp_2Y(CH_2TMS)(thf)$	40 min	88	5 min	510	1.45	17	10000	olefinic	5
$[Cp_2LuCl]_2$	1.5 h	93	7 min	780	1.34	11.7	20500	Cp	3
$Cp_2Lu(bdsa)(thf)$	3 h	96	20 min	1350	1.20	7.0	21000	Cp, bdsa (olefinic)[g]	1
$[Cp_2Lu(OiPr)]_2$	30 h	52	9 h	1270	1.18	4.0	600	Cp	<0.5 (<1)[h]
$Cp_2Lu(OAr)(thf)$	30 h	<1	–	–	–	–	–	–	<0.5
$[Cp_2Lu(StBu)]_2$	1.5 min	100	15 s	210	1.27	47	220000	StBu (olefinic)[g]	2
$Cp_2Lu(CH_2TMS)(thf)$	30 min	92	5 min	1130	1.38	8.0	39000	olefinic	1

[a]Toluene, 30 °C, monomer-to-catalyst ratio 600:1. [b]Determined by ^{31}P NMR spectroscopic measurement. [c]Initiation period, reaction time until 3% conversion is reached. [d]Determined by GPC-MALS, $I^* = M_{th}/M_n$, $M_{th} = 600 \times M_{Mon} \times$ conversion. [e]Determined by ESI MS. [f]Conversion of Cp_2LnX for addition of 5 equiv of DEEP, determined from ^1H NMR spectroscopic signals of Cp_2LnX(DEEP) and Cp_3Ln(DEEP). [g]Olefinic chain ends formed by end group elimination. [h]Number in brackets: extent of dimer opening for addition of 5 equiv of DEEP, determined from ^1H NMR spectroscopic signals of $Cp_2Ln(OiPr)$(DEEP) and DEEP.

Scheme 5. Initiation of Vinylphosphonate GTP Using Unbridged Rare Earth Metallocenes (Cp_2LnX) *via* Deprotonation of the Acidic α-CH, Nucleophilic Transfer of X, or a Monomer-Induced Ligand-Exchange Reaction Forming Cp_3Ln(DAVP)

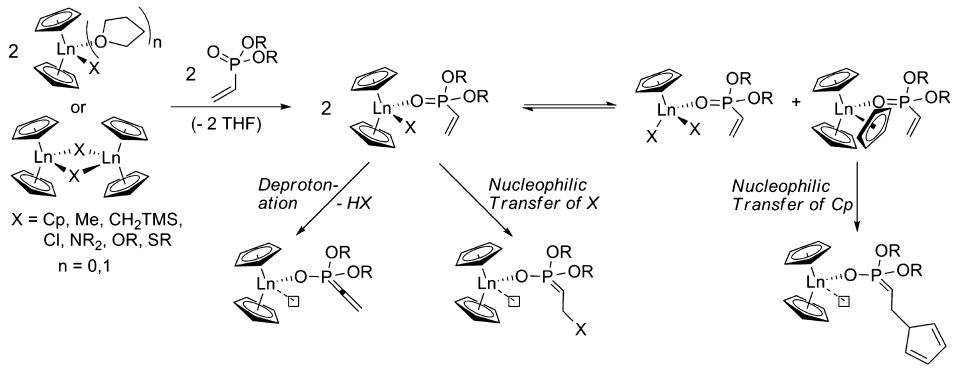

the observed fast transfer of thiolates to a coordinated monomer, the opening of dimers by coordination of a vinylphosphonate becomes rate-limiting (Scheme 5), as underlined by the lengthened initiation period and lower I^* of the more stable $[Cp_2Lu(StBu)]_2$ dimer in comparison to its Y analogue (Table 2, entries 5 and 11). For the more stable alkoxy dimers (e.g., $[Cp_2Ln(OiPr)]_2$), this limitation was observed also for the stronger coordinating vinylphosphonates as an incomplete reaction with DEEP to form $Cp_2Ln(OiPr)$(DEEP) (Table 2, entries 3 and 9)). Similar to bdsa, StBu end groups were found to be prone to elimination (Figures S8, S9 in SI). Steric repulsion is a major driving force of the elimination reaction, as larger monomers, e.g. DIVP, were found to facilitate this reaction, i.e. StBu end groups could not be found in ESI MS analysis of produced PDIVP oligomers (Figure S12 in SI). According to $[Cp_2YbMe]_2$, ESI MS analysis of DEVP oligomers produced with strongly basic CH_2TMS initiators revealed an initiation by deprotonation of the acidic α-CH of the vinylphosphonate. The low initiator efficiencies of both Me and CH_2TMS initiators (Tables 1 and 2) show that deprotonation of α-acidic monomers is a slow and thus unsuitable form of initiation for REM-GTP.

The above results show that the initiation of vinylphosphonate REM-GTP with unbridged rare earth metallocenes (Cp_2LnX) follows a complex reaction pathway (Scheme 5). Depending on the nature of X, initiation can either proceed *via* an abstraction of the acidic α-CH of the vinylphosphonate (e.g., for X = Me, CH_2TMS), *via* nucleophilic transfer of X to a coordinated momoner (e.g., for X = Cp, SR) or *via* a monomer (i.e., donor)-induced ligand-exchange reaction forming Cp_3Ln in equilibrium (e.g., for X = Cl, OR), which serves as the active initiating species. Each of the reaction steps (Scheme 5) can be rate-limiting, and different initiations may also occur simultaneously (e.g., for X = $N(SiMe_2H)_2$). Only nucleophilic transfer was found to ensure a homogeneous initiation of REM-GTP of vinylphosphonates, as the occurring initiation by deprotonation using the common strongly basic methyl, CH_2TMS, or hydride initiators[18−21] is rather slow.

Propagation Mechanism. The investigations on the initiation mechanism revealed that Cp_2LnX-initiated vinylphosphonate polymerizations are generally mediated by a Cp_2Ln unit. Nevertheless, the observed normalized activities TOF/I^* of different bis(cyclopentadienyl) complexes with identical metal centers are not the same (Tables 1 and 2). For

ideal living polymerizations, i.e. living polymerizations for which the initiation rate is considerably faster than the propagation rate, I^* is mainly determined by an initial initiator deactivation and therefore does not change during the course of polymerization. REM-GTP of vinylphosphonates is very fast and therefore primarily limited by an inefficient initiation reaction. Thus, the initiator efficiency I^* is significantly increasing during polymerization. Consequently, for a proper comparison of the catalytic activity, I^* has to be determined throughout the whole reaction. Better normalization results are yielded, if the initiator efficiency at the maximum rate of monomer conversion I^*_t is used instead of this efficiency at the end of the reaction (Figure 6).

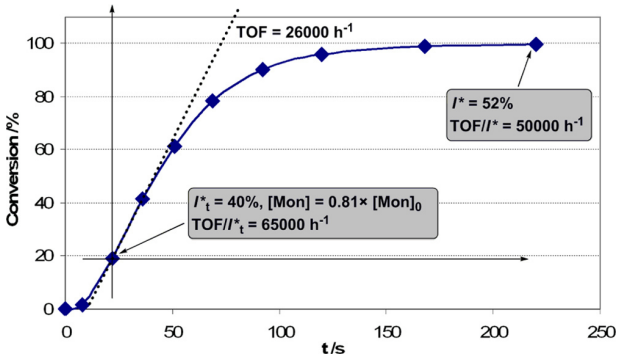

Figure 6. Conversion-reaction time plot for polymerization of DEVP, change of I^*_t during the reaction, and corresponding normalized TOFs (8.6 mg $[Cp_2Y(StBu)]_2$, 7.5 vol % DEVP in toluene (20 mL), 30 °C).

For the very fast polymerization of DEVP, the maximum rate is typically observed for a conversion of approximately 15−40% (Figure 6). Thus, temperature (it is not possible to completely remove the reaction heat from the system) and viscosity effects cannot be entirely excluded, especially for high monomer concentrations. As GTP is sensitive to protic impurities and since GPC analysis needs to be performed with the aliquots taken in order to determine I^*_t, there is also a lower concentration limit for reliable kinetic analysis. In our study, we found that 2.5−10 vol % monomer concentrations in toluene are ideal.

The general rate law for catalyzed polymerizations reads

$$r = k \times [\mathrm{Cat}]^m \times [\mathrm{Mon}]^n \quad (1)$$

For a meaningful kinetic analysis, we use the maximum rate of conversion, the present active catalyst concentration [Cat*], and the residual monomer concentration [Mon]. In accordance with a living-type polymerization, we calculate these concentrations following

$$[\mathrm{Cat}^*] = [\mathrm{Cat}]_0 \times I^*_t \quad (2)$$

and

$$[\mathrm{Mon}] = [\mathrm{Mon}]_0 \times (1 - C) \quad (3)$$

with the overall catalyst concentration $[\mathrm{Cat}]_0$, the initial monomer concentration $[\mathrm{Mon}]_0$, the conversion C, and

$$I^*_t = M_{\mathrm{Mon}} \times ([\mathrm{Mon}]_0/[\mathrm{Cat}]_0) \times C/M_n \quad (4)$$

with the monomer molar mass M_{Mon} and the number-averaged molecular weight M_n at the given reaction time t as determined *via* absolute analysis using GPC-MALS. This normalization with the initiator efficiency I^*_t addresses both inefficient initiation and catalyst deactivation due to (protic) impurities.

As the initiator efficiency depends on concentration and monomer-to-catalyst ratio, the active catalyst concentration cannot be exactly predicted. Thus, for the determination of the reaction orders, first, the initial monomer concentration is kept constant to determine the order in catalyst m. For different concentrations of the same catalyst at otherwise identical reaction conditions, the maximum rate is consistently reached at similar conversion. Therefore, the residual monomer concentration is also assumed to be constant, and $\ln(r)$ is plotted against $\ln([\mathrm{Cat}^*])$ yielding a reaction order of $m = 1$ for every evaluated catalyst (Figures 7 and S16 and Tables S1 and S2 in SI). Consequently, rare earth metal-mediated vinylphosphonate GTP follows a monometallic propagation according to the mechanism previously shown for (meth)acrylic monomers (Scheme 1a).

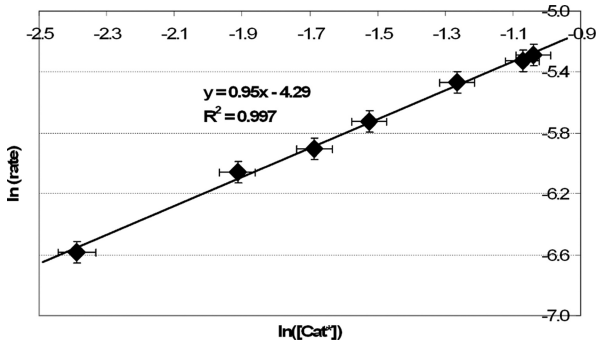

Figure 7. Determination of catalyst order (Cp_3Tm, 5 vol % DEVP in toluene, 30 °C).

In order to verify the corresponding RDS, the monomer order n is determined by the following:

$$r/[\mathrm{Cat}^*] = k \times [\mathrm{Mon}]^n \quad (5)$$

by plotting $\ln(r/[\mathrm{Cat}^*])$ against $\ln([\mathrm{Mon}])$.

The viscosity of the reaction mixture is strongly affected by the initial monomer concentration, thus making a reliable determination of the monomer reaction order difficult. Only catalysts with high initiator efficiency, I^*_t, allow kinetic analysis of the monomer order, as they both yield lower-molecular weight polymers and exhibit their maximum rate for rather low conversions (below 30%). Moreover, an initial heterogeneous polymerization is observed for fast initiating complexes with poor solubility in toluene, such as Cp_3Ln. Accordingly, Cp_3Tm allows determination of the catalyst order for DEVP polymerization, as it dissolves completely during an initiation period of approximately one minute, providing initiator efficiencies I^*_t of 13−21% (Figure 7 and Table S1 in SI). However, for these low initiator efficiencies, a reliable determination of monomer orders is not possible. In addition, catalyst orders for DIVP polymerization may not be obtained using Cp_3Ln due to an occurring initial heterogeneous polymerization.

For this purpose, a better soluble complex with higher initiator efficiency is necessary. $[Cp_2Y(StBu)]_2$ was used as it dissolves instantly upon monomer addition and reaches initiator efficiencies I^*_t of 35−54% and 57−86% in the case of DEVP and DIVP polymerization, respectively (Tables S2−S5 in SI). Using this thiolato yttrocene, the order in catalyst for DIVP polymerization could be determined as $m = 1$, showing

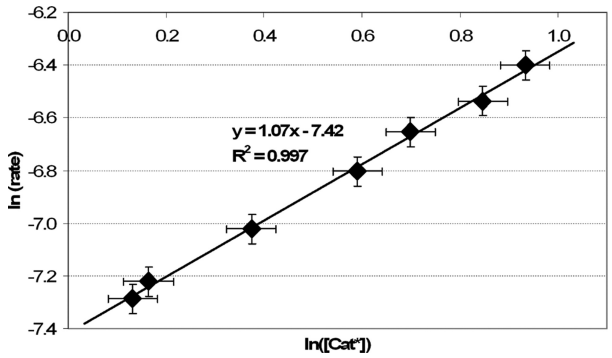

Figure 8. Determination of catalyst order ($[Cp_2Y(StBu)]_2$, 12.5 vol % DIVP in toluene, 30 °C.

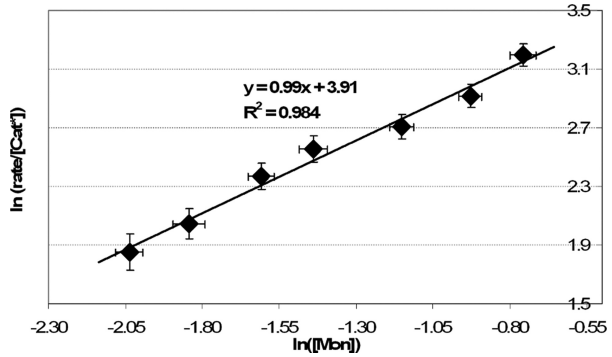

Figure 9. Determination of monomer order ($[Cp_2Y(StBu)]_2$, 2.5−10 vol % DEVP in toluene, 30 °C).

that increase of the monomer steric demand does not lead to a change of the propagation mechanism (Figure 8, Table S3 in SI). Determination of the monomer order according to equation (5) yields n = 1 for polymerization of both DEVP and DIVP (Figures 9, S17, Tables S4, S5 in SI). These results show that rare earth metal-mediated vinylphosphonate GTP follows a monometallic Yasuda-type polymerization mechanism, with an S_N2-type associative displacement of the polymer phosphonate ester by a monomer as the RDS as depicted in Scheme 2b. Whether the addition of vinylphosphonate occurs *via* a back-side or front-side attack, *i.e. via* chain-retention or chain migratory mechanism, may not be verified this way. For this purpose, studies on the stereospecifity of C_S- or C_1-symmetric catalysts and/or theoretical calculations need to be performed. Such studies are currently underway in our laboratories.

Still, these results provide no explanation of the origin of the influence of metal radii and steric demand of monomers on the catalytic activity. For this purpose, temperature-dependent kinetic analysis was performed to determine activation enthalpies $\Delta H^{\ddagger}$ and entropies $\Delta S^{\ddagger}$ according to the Eyring equation

$$\ln(k/T) = -\Delta H^{\ddagger}/R \times 1/T + \Delta S^{\ddagger}/R + \ln(k_B/h) \qquad (6)$$

with the rate constant k, the temperature T, the gas constant R, the Boltzmann constant k_B, and the Planck constant h. Plotting $\ln(k/T)$ against $1/T$ yields the activation enthalpy and entropy of the RDS (Figure 10).

These experiments were performed for the metal centers Lu, Tm, Y, and Tb (in order of increasing metal ionic radius[52]) as

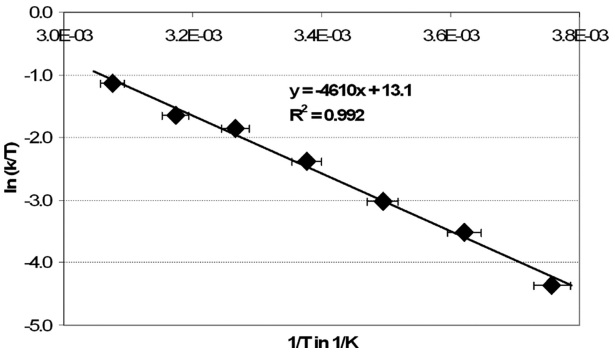

Figure 10. Eyring plot for $[Cp_2Y(StBu)]_2$-initiated DEVP (10 vol %) polymerization in toluene (−7 to 52 °C, $\Delta H^{\ddagger}$ = 38.3 kJ mol^{-1}, $\Delta S^{\ddagger}$ = −88.6 J (mol K)$^{-1}$).

Table 3. Activation Enthalpy $\Delta H^{\ddagger}$ and Entropy $\Delta S^{\ddagger}$ Dependence on Ionic Radius and Monomer Steric Demand

		DEVP		DIVP	
metal center	radius/ pm[a]	$\Delta H^{\ddagger}$/ kJ mol^{-1}	$\Delta S^{\ddagger}$/ J (K mol)$^{-1}$	$\Delta H^{\ddagger}$/ kJ mol^{-1}	$\Delta S^{\ddagger}$/ (J K mol)$^{-1}$
Tb	106.3	38.5	−102	41.3	−124
Y	104.0	38.3	−88.6	40.7	−112
Tm	102.0	39.1	−82.8	–	–
Lu	100.1	38.7	−73.6	42.0	−99.1

[a] Ln^{3+} ionic radius.[52]

well as for the monomers DEVP and DIVP (Table 3 and Figures S6−S12 in SI, Figures 10 and S18−S23 in SI). Contradicting the reactivity order of different rare earth metals for MMA polymerization previously reported by Yasuda et al. (Sm > Y > Yb > Lu),[23] vinylphosphonate GTP is accelerated by a decreasing ionic radius of the metal center (see also ref 14). Surprisingly, for both monomers, $\Delta H^{\ddagger}$ was found not to be affected by the metal ionic radius (within the limits of experimental accuracy of ∼1−2 kJ mol^{-1}). Thus, enthalpic effects, e.g. the Ln−(O═P) bond strength as a function of the Lewis acidity and the metallacycle ring strain as a function of the radius of the metal center, therefore do not determine the activity of different rare earth metals for vinylphosphonate GTP. In fact, different activation barriers $\Delta G^{\ddagger}$ were found to be a result of a change of $-T\Delta S^{\ddagger}$, which was found to decrease linearly with decreasing metal ionic radius (Table 3, Figure 11).

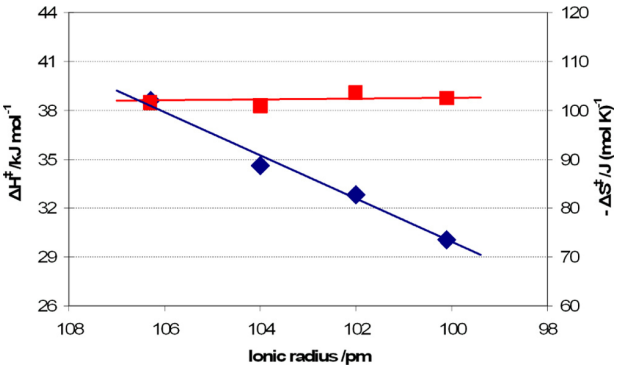

Figure 11. Activation enthalpy (red squares) and entropy (blue diamonds) for DEVP polymerization using Cp_2LnX catalysts in dependence of the metal ionic radius.

dx.doi.org/10.1021/ja404457f | J. Am. Chem. Soc. 2013, 135, 13030−13040

Scheme 6. Elemental Steps of Rare Earth-Mediated GTP of Vinylphosphonates[a]

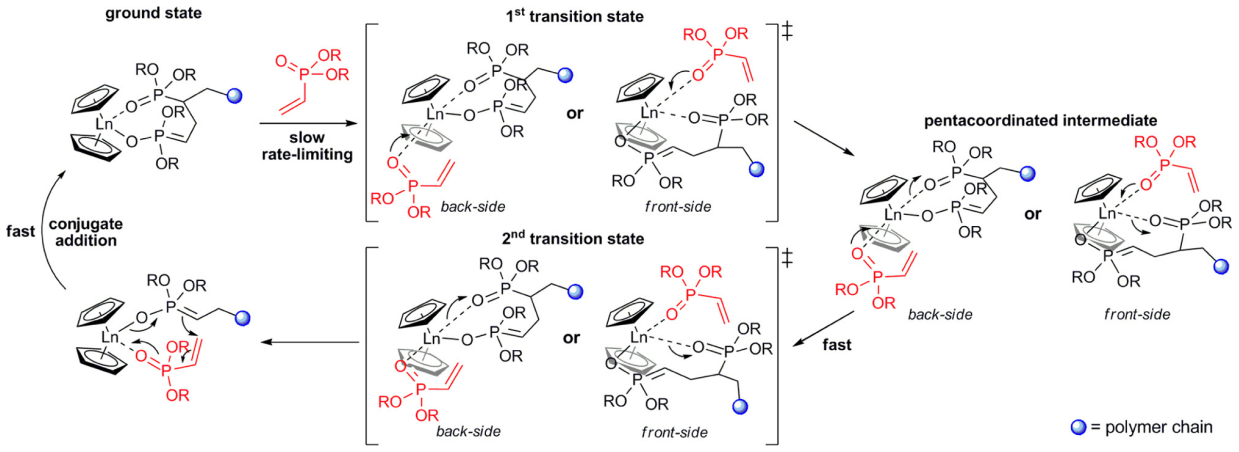

[a]The rate-limiting step is an S_N2-type associative displacement of the polymer phosphonate ester by a vinylphosphonate monomer, presumably *via* a pentacoordinated intermediate.

An increase of monomer steric demand leads to an increase of both $\Delta H^{\ddagger}$ and $-T\Delta S^{\ddagger}$ (Table 3). Hereby, at room temperature, the change of $\Delta S^{\ddagger}$ has a larger effect on the propagation rate ($\Delta\Delta H^{\ddagger} \approx 3$ kJ mol^{-1}, $-T\Delta\Delta S^{\ddagger} \approx 7$ kJ mol^{-1} for DEVP vs DIVP).

Importantly, a recent study on statistical copolymerization of different DAVPs revealed that the rate of vinylphosphonate GTP is mainly determined by the steric demand of the growing chain end, not by the added monomer.[16] Taking these considerations into account, the following mechanistic conclusions on rare earth metal-mediated GTP of vinylphosphonates can be drawn:

(1) The steric demand of the incoming monomer only shows minor influence on the propagation rate. Ziegler et al.[28] have shown coordinative-anionic polymerization of MA to proceed *via* a pentacoordinated intermediate with its formation by coordination of MA as the RDS. In the corresponding transition state, the metal−(O═C) bond to the incoming monomer is much longer than the metal−(O═C) bond to the polymer ester. In the present case, assuming REM-GTP of DAVP also proceeds over a pentacoordinated intermediate, the longer Ln−(O═P) bond in the corresponding transition state leads to a relatively small steric demand of the added vinylphosphonate in comparison to the growing chain end. The resulting minor effect of the steric demand of the added monomer on the propagation rate is in accordance with our observations (*vide supra*), thus providing initial evidence for the associative displacement to proceed over two transition states *via* a pentacoordinated intermediate (Scheme 6).

(2) Smaller metal centers destabilize the propagation ground state by a more confined arrangement of the eight-membered metallacycle according to the higher steric constraints caused by shorter Ln−Cp, Ln−(O−P) and Ln−(O═P) bonds. Contradicting to our expectation, the destabilization of the ground state is not of enthalpic (i.e., ring strain or the Ln−(O═P) bond strength), but of entropic nature (i.e., rotational and vibrational limitations in the eight-membered metallacycle). In the transition state, the Ln−(O═P) polymer phosphonate ester bond is lengthened, thus compensating part of the steric stress induced by the coordination of a vinylphosphonate monomer. This effect is larger for a stronger destabilization of the ground state, i.e. for smaller metal centers. Accordingly, we also expect an acceleration of vinylphosphonate REM-GTP by the introduction of sterically more demanding ligand systems (e.g., Cp*$_2$ instead of Cp$_2$). Such studies are currently underway in our laboratories

(3) Higher steric demand of the growing polymer chain end (i.e., sterically more demanding side chains) leads to a relative destabilization of the transition state by both enthalpic and entropic effects, with the latter having the larger impact on the activation barrier. In comparison to the propagation ground state, the incoming monomer increases the steric crowding at the metal center (Scheme 6), leading to higher steric constraints within the eight-membered metallacycle, however, with the actual monomer size playing only a minor role (*vide supra*). In contrast, larger metallacycle side chains induce a stronger increase of rotational and vibrational restrictions in the RDS, thus destabilizing the transition state.

In summary, the propagation rate of vinylphosphonate GTP is mainly determined by the change of rotational and vibrational restrictions within the eight-membered metallacycle in the RDS as a function of the steric demand of the metallacycle side chains and the steric crowding at the metal center. In previous mechanistic studies on coordinative-anionic polymerization of (meth)acrylates, entropic effects have been largely disregarded,[27,28,32,36−40] even if Eyring plots were conducted.[37] In contrast to (meth)acrylates, the constitution of DAVP is tetrahedral and DAVPs are sterically more demanding. Therefore, rotational limitations and thus entropic effects are believed to have a stronger effect on DAVP than for (meth)acrylate GTP. However, taking into account the drastic effect of the metal radius and the monomer size on the activation entropy for vinylphosphonate GTP, also for (meth)acrylic monomers, experimental studies on activation entropies and theoretical studies on the free energy surface with a separate investigation of enthalpic and entropic effects may provide useful insight into the mechanism of monometallic rare earth metal/group 4 metallocenium cation-mediated GTP.

In case of coordinative-anionic polymerizations, it is well-established that the metal center has to remain easily accessible in order to ensure high activities. The current study and the present activity trend for vinylphosphonate GTP (smaller metal centers yield highly active catalysts) questions the general applicability of this concept. This conclusion is in line with

previous observations by Chen et al.,[40] which have found that an increase of steric crowding at the active site not only yields higher stereospecifity and a suppression of side reactions but also an acceleration of the propagation. Hence, in order to obtain high activity, the steric crowding of the catalyst needs to be well-adjusted: high enough to ensure sufficient destabilization of the eight-membered metallacycle ground state and to prohibit unfavored side reactions (e.g., site epimerization) and small enough to still facilitate an S_N2-type associative displacement of the polymer ester by an incoming monomer.

CONCLUSION

In this contribution, the first detailed mechanistic studies on both initiation and propagation of rare earth metal-mediated GTP of vinylphosphonates have been presented. During the course of our study, we were able to isolate the DEVP adducts, Cp_2LnCl (DEVP), providing the first X-ray crystallographic proof for vinylphosphonate coordination at the active site *via* the oxygen of the phosphonate moiety, and thus further supporting the hypothesis of GTP mechanism taking place. We have shown that the reactive α-CH and the use of unbridged rare earth metallocenes lead to a complex initiation network for vinylphosphonate GTP. Depending on the nature of the initiating ligand, initiation can either proceed *via* abstraction of the acidic α-CH of the vinylphosphonate, *via* transfer of a nucleophilic ligand to a coordinated monomer, or *via* a monomer (i.e., donor)-induced ligand-exchange reaction forming Cp_3Ln in equilibrium. We found the applied initiators, especially traditionally used strongly basic methyl, CH_2TMS, or hydride initiators, to suffer from different limitations, thus restricting their efficient use to selected monomers only. Therefore, rare earth metal-based GTP catalysts still require further development of versatile initiating ligands for an efficient application to a variety of monomers.

A detailed kinetic analysis of DAVP REM-GTP has been complicated by a very fast polymerization reaction in combination with a comparatively slow initiation. Thus, the overall reaction rate is influenced by both initiation and propagation. In this contribution, we have shown a general differential approach to separately analyze the propagation reaction for such living polymerizations. Time-resolved analysis of monomer conversion and molecular weights of the formed polymers allows the determination of the initiator efficiency throughout the whole reaction. Using this normalization method, rare earth metal-mediated GTP was shown to follow a monometallic Yasuda-type polymerization mechanism, with an S_N2-type associative displacement of the polymer phosphonate ester by a monomer as the RDS. The activation entropy $\Delta S^{\ddagger}$ of the RDS is strongly affected by the metal radius and the monomer size, whereas these parameters show only minor influence on the activation enthalpy $\Delta H^{\ddagger}$. As the steric demand of the added monomer shows only a minor influence on the propagation rate, the associative displacement is very likely to proceed over two transition states *via* a pentacoordinated intermediate. In order to support the mechanistic conclusions drawn in this contribution, further studies with a modified ligand architecture (especially C_1- and C_s-symmetric complexes) as well as theoretical calculations are currently underway.

EXPERIMENTAL SECTION

General. All reactions were carried out under argon atmosphere using standard Schlenk or glovebox techniques. All glassware was heat dried under vacuum prior to use. Unless otherwise stated, all chemicals were purchased from Sigma-Aldrich, Acros Organics, or ABCR and used as received. Toluene, thf and pentane were dried using an MBraun SPS-800 solvent purification system. Hexane, isopropanol, *tert*-butylthiol and DEEP were dried over 3 Å molecular sieves. Cp_3Ln,[53] $[Cp_2LnCl]_2$,[54] $[Cp_2YbMe]_2$,[55] $Cp^*_2LuCl(thf)$,[56] NaCp,[57] Li(bdsa),[58] the precursor complexes $Ln(bdsa)_3(thf)_2$ and $Ln(CH_2TMS)_3(thf)_2$,[58,59] as well as the monomers DEVP and DIVP[49] were prepared according to literature procedures. Monomers were dried over calcium hydride and distilled prior to use.

NMR spectra were recorded on a Bruker AV-300 or AV-500C spectrometer. ^{1}H-, ^{13}C-, and ^{29}Si NMR spectroscopic chemical shifts δ are reported in ppm relative to tetramethylsilane. δ (^{1}H) is calibrated to the residual proton signal, δ (^{13}C) to the carbon signal, and δ (^{29}Si) to the deuterium signal of the solvent. ^{31}P NMR spectroscopic chemical shifts are reported in ppm relative to and calibrated to 85% aqueous H_3PO_4. Deuterated solvents were obtained from Deutero or Eurisotop and dried over 3 Å molecular sieves. Elemental analyses were measured at the Laboratory for Microanalytics at the Institute of Inorganic Chemistry at the Technische Universität München. ESI MS analytical measurements were performed with methanol solutions on a Varian 500-MS spectrometer, using 70 keV in the positive ionization mode. IR spectra were recorded under argon atmosphere on a Bruker Vertex 70 spectrometer with a Bruker Platinum ATR setup and the integrated MCT detector. Samples were applied as thf solution or Et_2O suspension and measured after evaporation of the solvent. GPC was carried out on a Varian LC-920 equipped with two analytical PL Polargel M columns. As eluent, a mixture of 50% thf, 50% water, and 9 g L^{-1} tetrabutylammonium bromide (TBAB) was used in the case of PDEVP; for PDIVP analysis, the eluent was thf with 6 g L^{-1} TBAB. Absolute molecular weights have been determined online by multiangle light-scattering (MALS) analysis using a Wyatt Dawn Heleos II in combination with a Wyatt Optilab rEX as concentration source.

Complex Synthesis. *General Procedure for Synthesis of $Cp_2Ln(bdsa)(thf)$.* Two equivalents of freshly distilled cyclopentadiene are added to a toluene solution of 1equiv of $Ln(bdsa)_3(thf)_2$ (~0.25 M). The resulting solution is stirred overnight at 110 °C in a pressure Schlenk vessel, the solvent and formed 1,1,3,3-tetramethyldisilazane are removed *in vacuo*, and the resulting solid is recrystallized from toluene at −35 °C.

General Procedure for Synthesis of $Cp_2Ln(CH_2TMS)(thf)$. Two equivalents of freshly distilled cyclopentadiene are added to a toluene solution of 1 equiv of $Ln(CH_2TMS)_3(thf)_2$ (~0.25 M). The resulting solution is stirred overnight at rt, the solvent and formed tetramethylsilane are removed *in vacuo*, and the resulting solid is recrystallized from toluene/hexane at −35 °C.

General Procedure for Synthesis of Cp_2LnX. One equivalent of a stem solution of XH in toluene (~5 wt %) is added dropwise to a toluene solution of 1 equiv of $Cp_2Ln(bdsa)(thf)$ (~0.1 M). The resulting mixture is stirred overnight at rt, and the solvent and formed 1,1,3,3-tetramethyldisilazane are removed *in vacuo*, yielding pure product in quantitative yield.

For characterization of the synthesized organometallic compounds, see the Supporting Information.

Single-Crystal X-ray Structure Determinations. *$Cp_3Y(DEEP)$:* crystal data: formula $C_{21}H_{30}O_3PY$; M_r = 450.33; crystal color and shape: colorless fragment, crystal dimensions: 0.18 mm × 0.41 mm × 0.51 mm; crystal system: monoclinic; space group: $P2_1/n$ (no. 14); a = 11.5091 Å (4), b = 8.2872 (3) Å, c = 22.6167 (8) Å, β = 101.516 (2)°; V = 2113.72 (13) Å^3; Z = 4; μ (Mo Kα) = 2.851 mm^{-1}; ρ_{calcd} = 1.415 g cm^{-3}; θ-range = 1.84−25.36°; data collected: 75310; independent data [$I_o > 2\sigma(I_o)$/all data/R_{int}]: 3531/3849/0.041; data/restraints/parameter: 3849/0/238; $R1[I_o > 2\sigma(I_o)$/all data]: 0.0446/0.0485; $wR2[I_o > 2\sigma(I_o)$/all data]: 0.1182/0.1211; GOF = 1.074; $\Delta\rho_{max/min}$: 2.98/−0.86 eÅ^{-3}.

$Cp_2HoCl(DEVP)$: crystal data: formula $C_{16}H_{23}ClHoO_3P$; M_r = 494.69; crystal color and shape: colorless fragment; crystal dimensions: 0.18 mm × 0.51 mm × 0.64 mm; crystal system: orthorhombic; space group: $Pna2_1$ (no. 33); a = 20.7465 (6) Å, b = 11.7265 (4) Å, c =

7.8125 (3) Å; V = 1900.66 (11) Å^3 ; Z = 4; μ (Mo Kα) = 4.395 mm^{-1}; ρ_{calcd} = 1.729 g cm^{-3}; θ-range = 1.96−25.42°; data collected: 51428; independent data [$I_o > 2\sigma(I_o)$/all data/R_{int}]: 3484/3487/0.044; data/restraints/parameter: 3487/1/202; $R1[I_o > 2\sigma(I_o)$/all data]: 0.0144/0.0145; $wR2[I_o > 2\sigma(I_o)$/all data]: 0.0369/0.0369; GOF=1.197; $\Delta\rho_{max/min}$: 0.91/−0.73 eÅ^{-3}.

$Cp_2YbCl(DEVP)$: crystal data: formula $C_{16}H_{23}ClO_3PYb$; M_r = 502.80; crystal color and shape: colorless fragment, crystal dimensions: 0.18 mm × 0.51 mm × 0.53 mm; crystal system: orthorhombic; space group: $Pna2_1$ (no. 33); a = 20.7504 (7) Å, b = 11.7361 (4) Å, c = 7.8075 (3) Å; V = 1901.35 (12) Å^3 ; Z = 4; μ (Mo Kα) = 5.151 mm^{-1}; ρ_{calcd} = 1.757 g cm^{-3}; θ-range =1.96−25.36°; data collected: 46215; independent data [$I_o > 2\sigma(I_o)$/all data/R_{int}]: 3449/3461/0.053; data/restraints/parameter: 3461/1/201; $R1[I_o > 2\sigma(I_o)$/all data]: 0.0142/0.0143; $wR2[I_o > 2\sigma(I_o)$/all data]: 0.0373/0.0374; GOF = 1.088; $\Delta\rho_{max/min}$: 0.70/−0.55 eÅ^{-3}.

For detailed information, see Supporting Information. CCDC 930675 (**$Cp_3Y(DEEP)$**), CCDC 930674 (**$Cp_2HoCl(DEVP)$**), and CCDC 930673 (**$Cp_2YbCl(DEVP)$**) contain the supplementary crystallographic data for this compound. These data can be obtained free of charge from The Cambridge Crystallographic Data Centre *via* www.ccdc.cam.ac.uk/data_request/cif or *via* https://www.ccdc.cam.ac.uk/services/structure_deposit/.

Oligomerization. Five equivalents of DEVP are added to 1 equiv of catalyst in toluene. The resulting mixture is stirred for 2 h at room temperature and quenched by addition of MeOH or acidified (37 wt % HCl_{aq}) MeOH. Volatiles were removed under reduced pressure, and the residue was extracted with MeOH. For end group analysis, ESI-MS measurements of the methanolic extract were performed.

Coordination of DEEP. To a solution/suspension of 1 equiv of Cp_2LnX or Cp_3Ln in C_6D_6 0.5, 1, 2, or 5 equiv of a stem solution of DEEP in C_6D_6 is added, respectively. The resulting mixture is transferred into an NMR tube. ^{1}H NMR spectroscopic shifts of the formed adducts (signals of Cp and X) are determined for addition of 5 equiv of DEEP. ^{1}H and ^{31}P NMR spectroscopic shifts of coordinated DEEP are determined for addition of 0.5 equiv of DEEP, respectively. The extent of ligand exchange (Table 2) is determined from the integral ratio of the ^{1}H NMR spectroscopic signals of the cyclopentadienyl protons of formed Cp_3Ln(DEEP) and Cp_2LnX-(DEEP) for addition of 5 equiv of DEEP. For NMR spectroscopic characterization of the formed phosphonate adducts, see Supporting Information.

Activity Measurements and Kinetic Analysis. For activity measurements, the stated amount of catalyst (15−50 μmol) is dissolved/suspended in 20 mL of toluene, and the reaction mixture is thermostatted to the desired temperature. Then, the stated amount of monomer (3.5−13 mmol) is added. During the course of the measurement, the temperature is monitored with a digital thermometer, and aliquots (0.5 mL) are taken and quenched by addition to deuterated methanol (0.2 mL). After the stated reaction time, the reaction is quenched by addition of MeOD (0.5 mL). The reaction is carried out in an MBraun Glovebox under argon atmosphere to take aliquots every 6−10 s at the beginning of the measurement. For each aliquot, the conversion is determined by ^{31}P NMR spectroscopy and the molecular weight of the formed polymer by GPC-MALS analysis.

For kinetic analysis, the maximum rate is determined from the maximum slope of the conversion-reaction time plot. I^*_t is defined as the given initiator efficiency at the inflection point of the conversion-reaction time plot. In case an aliquot was taken at or sufficiently close to the inflection point the initiator efficiency determined for this aliquot is used as I^*_t; if this is not the case, I^*_t is determined as the average of the initiator efficiencies of the aliquots taken directly before and after this inflection point. The conversion used for calculation of the residual monomer concentration is determined accordingly. Error bars are calculated from the following uncertainties: $\Delta[Cat]_0$ = 0.1 mg, $\Delta[Mon]_0$ = 0.05 mL (in case of DEVP) or 0.05 g (in case of DIVP), ΔC = 3%, ΔT = 2 K, and a 5% relative uncertainty for the determination of the maximum slope and I^*_t.

■ ASSOCIATED CONTENT

Supporting Information

Characterization of synthesized organometallic compounds, ESI MS analysis of DAVP oligomers, detailed information for single crystal X-ray structure determination, obtained data from activity measurements and kinetic analysis. This material is available free of charge via the Internet at http://pubs.acs.org.

■ AUTHOR INFORMATION

Corresponding Author

rieger@tum.de

Notes

The authors declare no competing financial interest.

■ ACKNOWLEDGMENTS

We thank Dr. Sergej Vagin, Dr. Ning Zhang, Markus Hammann, and Dominik Lanzinger for valuable discussions. S.S. is grateful for a generous scholarship from the Fonds der Chemischen Industrie.

■ REFERENCES

(1) Ellis, J.; Wilson, A. D. *Dent. Mater.* **1992**, *8*, 79.
(2) Ebdon, J. R.; Price, D.; Hunt, B. J.; Joseph, P.; Gao, F.; Milnes, G. J.; Cunliffe, L. K. *Polym. Degrad. Stab.* **2000**, *69*, 267.
(3) Greish, Y. E.; Brown, P. W. *Biomaterials* **2001**, *22*, 807.
(4) Gemeinhart, R. A.; Bare, C. M.; Haasch, R. T.; Gemeinhart, E. J. *J. Biomed. Mater. Res., Part A* **2006**, *78A*, 433.
(5) Bock, T.; Möhwald, H.; Mühlhaupt, R. *Macromol. Chem. Phys.* **2007**, *208*, 1324.
(6) Steininger, H.; Schuster, M.; Kreuer, K. D.; Kaltbeitzel, A.; Bingoel, B.; Meyer, W. H.; Schauff, S.; Brunklaus, G.; Maier, J.; Spiess, H. W. *Phys. Chem. Chem. Phys.* **2007**, *9*, 1764.
(7) Parvole, J.; Jannasch, P. *Macromolecules* **2008**, *41*, 3893.
(8) Macarie, L.; Ilia, G. *Prog. Polym. Sci.* **2010**, *35*, 1078.
(9) Atanasov, V.; Kerres, J. *Macromolecules* **2011**, *44*, 6416.
(10) Monge, S.; Canniccioni, B.; Graillot, A.; Robin, J. *Biomacromolecules* **2011**, *12*, 1973.
(11) Salzinger, S.; Rieger, B. *Macromol. Rapid Commun.* **2012**, *33*, 1327.
(12) Seemann, U. B.; Dengler, J. E.; Rieger, B. *Angew. Chem., Int. Ed.* **2010**, *49*, 3489.
(13) Rabe, G. W.; Komber, H.; Haeussler, L.; Kreger, K.; Lattermann, G. *Macromolecules* **2010**, *43*, 1178.
(14) Salzinger, S.; Seemann, U. B.; Plikhta, A.; Rieger, B. *Macromolecules* **2011**, *44*, 5920.
(15) Zhang, N.; Salzinger, S.; Deubel, F.; Jordan, R.; Rieger, B. *J. Am. Chem. Soc.* **2012**, *134*, 7333.
(16) Zhang, N.; Salzinger, S.; Rieger, B. *Macromolecules* **2012**, *45*, 9751.
(17) Yasuda, H.; Yamamoto, H.; Yokota, K.; Miyake, S.; Nakamura, A. *J. Am. Chem. Soc.* **1992**, *114*, 4908.
(18) Chen, E. Y.-X. *Chem. Rev.* **2009**, *109*, 5157.
(19) Yasuda, H.; Ihara, E. *Macromol. Chem. Phys.* **1995**, *196*, 2417.
(20) Yasuda, H.; Ihara, E. *Adv. Polym. Sci.* **1997**, *133*, 53.
(21) Yasuda, H. *Prog. Polym. Sci.* **2000**, *25*, 573.
(22) Boffa, L. S.; Novak, B. M. *Macromolecules* **1994**, *27*, 6993.
(23) Yasuda, H.; Yamamoto, H.; Yamashita, M.; Yokota, K.; Nakamura, A.; Miyake, S.; Kai, Y.; Kanehisa, N. *Macromolecules* **1993**, *26*, 7134.
(24) Collins, S.; Ward, D. G. *J. Am. Chem. Soc.* **1992**, *114*, 5460.
(25) Collins, S.; Ward, D. G.; Suddaby, K. H. *Macromolecules* **1994**, *27*, 7222.
(26) Li, Y.; Ward, D. G.; Reddy, S. S.; Collins, S. *Macromolecules* **1997**, *30*, 1875.
(27) Sustmann, R.; Sicking, W.; Bandermann, F.; Ferenz, M. *Macromolecules* **1999**, *32*, 4204.

(28) Tomasi, S.; Weiss, H.; Ziegler, T. *Organometallics* **2006**, *25*, 3619.
(29) Giardello, M. A.; Yamamoto, Y.; Brard, L.; Marks, T. J. *J. Am. Chem. Soc.* **1995**, *117*, 3276.
(30) Nguyen, H.; Jarvis, A. P.; Lesley, M. J. G.; Kelly, W. M.; Reddy, S. S.; Taylor, N. J.; Collins, S. *Macromolecules* **2000**, *33*, 1508.
(31) Cameron, P. A.; Gibson, V. C.; Graham, A. J. *Macromolecules* **2000**, *33*, 4329.
(32) Hölscher, M.; Keul, H.; Höcker, H. *Macromolecules* **2002**, *35*, 8194.
(33) Rodriguez-Delgado, A.; Mariott, W. R.; Chen, E. Y.-X. *Macromolecules* **2004**, *37*, 3092.
(34) Ning, Y.; Cooney, M. J.; Chen, E. Y.-X. *J. Organomet. Chem.* **2005**, *690*, 6263.
(35) Rodriguez-Delgado, A.; Mariott, W. R.; Chen, E. Y.-X. *J. Organomet. Chem.* **2006**, *691*, 3490.
(36) Ning, Y.; Caporaso, L.; Correa, A.; Gustafson, L. O.; Cavallo, L.; Chen, E. Y.-X. *Macromolecules* **2008**, *41*, 6910.
(37) Frauenrath, H.; Keul, H.; Höcker, H. *Macromolecules* **2001**, *34*, 14.
(38) Hölscher, M.; Keul, H.; Höcker, H. *Chem.—Eur. J.* **2001**, *7*, 5419.
(39) Caporaso, L.; Cavallo, L. *Macromolecules* **2008**, *41*, 3439.
(40) Zhang, Y.; Ning, Y.; Caporaso, L.; Cavallo, L.; Chen, E. Y.-X. *J. Am. Chem. Soc.* **2010**, *132*, 2695.
(41) Rodriguez-Delgado, A.; Chen, E. Y.-X. *Macromolecules* **2005**, *38*, 2587.
(42) Ning, Y.; Chen, E. Y.-X. *J. Am. Chem. Soc.* **2008**, *130*, 2463.
(43) Zhang, N.; Salzinger, S.; Soller, B. S.; Rieger, B. *J. Am. Chem. Soc.* **2013**, *135*, 8810.
(44) Kaneko, H.; Nagae, H.; Tsurugi, H.; Mashima, K. *J. Am. Chem. Soc.* **2011**, *133*, 19626.
(45) Ihara, E.; Morimoto, M.; Yasuda, H. *Macromolecules* **1995**, *28*, 7886.
(46) Seemann, U. B. Ph.D. Thesis, Technische Universität München, Garching bei München, October 2010.
(47) Qian, Y.; Bala, M. D.; Yousaf, M.; Zhang, H.; Huang, J.; Sun, J.; Liang, C. *J. Organomet. Chem.* **2002**, *188*, 1.
(48) Observation of lower molecular weight fragments with $m/z = n \times M_{Mon} + M_{Na}$ has been previously observed for initiation with Cp_3Ln, and can be attributed to chain scission during ESI MS analysis as these fragments are not observed for analysis by MALDI-ToF MS.
(49) Leute, M. Ph.D. Thesis, Universität Ulm, 2007.
(50) Dengler, J. E. Diploma Thesis, Technische Universität München, Garching bei München, August 2007.
(51) Demir, S.; Mueller, T. J.; Ziller, J. W.; Evans, W. J. *Angew. Chem., Int. Ed.* **2011**, *50*, 515.
(52) Hollemann, A. F., Wiberg, E., Wiberg, N., Eds. *Lehrbuch der Anorganischen Chemie (Textbook of Inorganic Chemistry, Engl. Transl.)*; Walter de Gruyter & Co: Berlin, 2007.
(53) Birmingham, J. M.; Wilkinson, G. *J. Am. Chem. Soc.* **1956**, *78*, 42.
(54) Maginn, R. E.; Manastyrskyj, S.; Dubeck, M. *J. Am. Chem. Soc.* **1963**, *85*, 672.
(55) Evans, W. J.; Dominguez, R.; Hanusa, T. P. *Organometallics* **1986**, *5*, 263.
(56) Tilley, T. D.; Andersen, A. R. *Inorg. Chem.* **1981**, *20*, 3267.
(57) Panda, T. K.; Gamer, M. T.; Roesky, P. W. *Organometallics* **2003**, *22*, 877.
(58) Eppinger, J. Ph.D. Thesis, Technische Universität München, Garching bei München, May1999.
(59) Hultzsch, K. C.; Voth, P.; Beckerle, K.; Spaniol, T. P.; Okuda, J. *Organometallics* **2000**, *19*, 228.

Supporting Information:

Mechanistic Studies on Initiation and Propagation of Rare Earth Metal-Mediated Group Transfer Polymerization of Vinylphosphonates

*Stephan Salzinger, Benedikt S. Soller, Andriy Plikhta, Uwe B. Seemann, Eberhardt Herdtweck, Bernhard Rieger**

WACKER-Lehrstuhl für Makromolekulare Chemie, Technische Universität München, Lichtenbergstraße 4, 85748 Garching

Characterization of Synthesized Organometallic Compounds

$Cp_2Y(bdsa)(thf)$: Yield: 15.5 g colorless crystals (36.8 mmol, 75%). ^{1}H NMR (C_6D_6, 298 K, 300 MHz): δ = 0.34 (d, 12H, ^3J(H-H) = 3.0 Hz, Si-CH_3), 1.15 (m, 4H, THF-H_I), 3.36 (m, 4H, THF-H_{II}), 4.28 (m, 2H, Si-*H*), 6.13 (s, 10H, Cp-*H*). ^{13}C NMR (C_6D_6, 300 K, 125 MHz): δ = 3.4 (s, Si-*C*H_3), 25.2 (s, THF-C_I), 71.9 (s, THF-C_{II}), 110.7 (s, Cp-*C*). ^{29}Si NMR (C_6D_6, 300K, 100 MHz): δ = -25.4 (s). IR (cm^{-1}): 3674, 3566, 3087, 2974, 2885, 2704, 2083, 2046, 1645, 1458, 1439, 1369, 1346, 1241, 1175, 1059, 1032, 1009, 913, 872, 778, 766, 699. EA: calculated: C 51.05, H 7.62, N 3.31; found: C 50.83, H 7.63, N 3.27.

$Cp_2Lu(bdsa)(thf)$: Yield: 9.5 g colorless crystals (18.6 mmol, 78%). ^{1}H NMR (C_6D_6, 298 K, 300 MHz): δ = 0.37 (d, 12H, ^3J(Si-H) = 3.1 Hz, Si-CH_3), 1.23 (m, 4H, THF-H_I), 3.35 (m, 4H, THF-H_{II}), 4.28 (m, 2H, Si-*H*), 6.11 (s, 10H, Cp-*H*). ^{13}C NMR (C_6D_6, 298 K, 75 MHz): δ = 3.5 (s, Si-*C*H_3), 25.3 (s, THF-C_I), 72.2 (s, THF-C_{II}), 110.3 (s, Cp-*C*). ^{29}Si NMR (C_6D_6, 298 K, 60 MHz): δ = -23.7 (s). IR (cm^{-1}): 3561, 3090, 2954, 2707, 2098, 2049, 1438, 1249, 1179, 1011, 906, 875, 779, 735. EA: calculated: C 42.42, H 6.33, N 2.75; found: C 41.90, H 6.29, N 2.91.

$Cp_2Tb(bdsa)(thf)$: Yield: 1.95 g colorless crystals (3.9 mmol, 70%). IR (cm^{-1}): 3666, 3085, 2974, 2886, 2705, 2107, 2045, 1636, 1458, 1439, 1369, 1346, 1243, 1175, 1059, 1033, 1010, 879, 777, 763, 688. EA: calculated: C 43.80, H 6.54, N 2.84; found: C 43.79, H 6.70, N 2.78.

$Cp_2Y(CH_2TMS)(thf)$: Yield: 5.4 g colorless needles (14.3 mmol, 65%). ^{1}H NMR (C_6D_6, 300 K, 500 MHz): δ = -0.67 (d, 2H, ^2J(Y-H) = 3.5 Hz, Si-CH_2), 0.43 (s, 9H, Si-CH_3), 0.92 (m, 4H, THF-H_I), 2.95 (m, 4H, THF-H_{II}), 6.12 (s, 10H, Cp-*H*). ^{13}C NMR (C_6D_6, 300 K, 125 MHz): δ = 4.8 (s, Si-CH$_3$), 24.9 (s, THF-C_I), 25.4 (d, ^1J(Y-C) = 42.5 Hz, Si-CH$_2$), 71.2 (s, THF-C_{II}), 110.4 (s, Cp-*C*). ^{29}Si NMR (C_6D_6, 300K, 100 MHz): δ = -3.0 (s). IR (cm^{-1}): 3674, 3559, 3087, 2955, 2893, 2707, 1638, 1459, 1438, 1422, 1368, 1345, 1287, 1248, 1011, 861, 766, 696. EA: calculated: C 57.13, H 7.72; found: C 57.21, H 7.85.

$Cp_2Lu(CH_2TMS)(thf)$: Yield: 5.5 g beige solid (11.9 mmol, 78%). ^{1}H NMR (C_6D_6, 300 K, 500 MHz): δ = -0.76 (s, 2H, Si-CH_2), 0.43 (s, 9H, Si-CH_3), 0.89 (m, 4H, THF-H_I), 2.91 (m, 4H, THF-H_{II}), 6.06 (s, 10H, Cp-*H*). ^{13}C NMR (C_6D_6, 300 K, 125 MHz): δ = 5.0 (s, Si-CH$_3$), 24.9 (s, THF-C_I), 27.3 (s, Si-CH$_2$), 71.5 (s, THF-C_{II}), 109.8 (s, Cp-*C*). ^{29}Si NMR (C_6D_6, 300K, 100 MHz): δ = -0.8 (s). IR (cm^{-1}): 3563, 3091, 2953, 2896, 2710, 1459, 1439, 1420, 1287, 1248, 1122, 1013, 859, 775, 695. EA: calculated: C 46.55, H 6.29; found: C 45.93, H 6.10.

$[Cp_2Y(O\textit{i}Pr)]_2$: Yield: 230 mg white powder (0.83 mmol). ^{1}H NMR (THF-d8, 298 K, 300 MHz): δ = 1.25 (d, 6H, ^3J(H-H) = 6.0 Hz, CH_3), 3.84 (sp, 1H, ^3J(H-H) = 6.0 Hz, O-CH(CH$_3$)$_2$), 6.20 (s, 10H, Cp-*H*). ^{13}C NMR (THF-d8, 298 K, 75 MHz): δ = 28.8 (s, CH$_3$), 68.6 (s, O-CH(CH$_3$)$_2$),), 112.1 (s, Cp-*C*). IR (cm^{-1}): 3092, 2960, 2926, 2836, 1653, 1459, 1379, 1368, 1329, 1254, 1157, 1118, 1011, 952, 811, 793, 782, 768, 752. EA: calculated: C 56.13, H 6.16; found: C 55.92, H 5.98.

$[Cp_2Lu(O\textit{i}Pr)]_2$: Yield: 150 mg beige powder (0.42 mmol). ^{1}H NMR (C_6D_6, 298 K, 300 MHz): δ = 0.87 (d, 6H, ^3J(H-H) = 6.1 Hz, CH_3), 3.49 (sp, 1H, ^3J(H-H) = 6.1 Hz, O-CH(CH$_3$)$_2$), 6.12 (s, 10H, Cp-*H*). ^{13}C NMR (C_6D_6, 300 K, 125 MHz): δ = 28.2 (s, CH$_3$), 68.3 (s, O-CH(CH$_3$)$_2$),), 110.8 (s, Cp-*C*). IR (cm^{-1}): 3096, 3071, 2965, 2926, 2842, 1662, 1459, 1381, 1367, 1331, 1257, 1158, 1117, 1010, 951, 818, 796, 786, 754, 676. EA: calculated: C 42.87, H 4.70; found: C 42.17, H 4.50.

$Cp_2Y(O(C_6H_2(CH_3)_3)(thf)$: Yield: 200 mg yellow crystals (0.47 mmol). ^{1}H NMR (C_6D_6, 300 K, 500 MHz): δ = 1.06 (m, 4H, THF-H_I), 2.29 (s, 6H, ortho-CH_3), 2.38 (s, 3H, para-CH_3), 3.24 (m, 4H, THF-H_{II}), 6.13 (s, 10H, Cp-*H*), 7.03 (s, 2H, Ar-*H*). ^{13}C NMR (THF-d8, 300 K, 125 MHz): δ = 18.9 (s, ortho-CH$_3$), 21.0 (s, para-CH$_3$), 26.7 (s, THF-C_I), 68.5 (s, THF-C_{II}), 111.2 (s, Cp-*C*), 123.8 (para-C_{Ar}-CH$_3$), 125.4 (ortho-C_{Ar}-CH$_3$), 129.4 (s, C_{Ar}H), 161.0 (d, ^2J(Y-C) = 5.2 Hz, C_Ar-O). IR (cm^{-1}): 3086, 2958, 2910, 2854, 1648, 1608, 1478, 1426, 1312, 1266, 1229, 1197, 1160, 1013, 856, 828, 772, 741. EA: calculated: C 64.79, H 6.86; found: C 64.75, H 6.99.

$Cp_2Lu(O(C_6H_2(CH_3)_3)(thf)$: Yield: 210 mg yellow crystals (0.42 mmol). ^{1}H NMR (C_6D_6, 298 K, 300 MHz): δ = 1.05 (m, 4H, THF-H_I), 2.27 (s, 6H, ortho-CH_3), 2.39 (s, 3H, para-CH_3), 3.25 (m, 4H, THF-H_{II}), 6.07 (s, 10H, Cp-*H*), 7.04 (s, 2H, Ar-*H*). ^{13}C NMR (THF-d8, 300 K, 125 MHz): δ = 19.0 (s, ortho-CH_3), 21.0 (s, para-CH_3), 26.7 (s, THF-C_I), 68.5 (s, THF-C_{II}), 110.9 (s, Cp-*C*), 124.1 (para-C_{Ar}-CH_3), 125.2 (ortho-C_{Ar}-CH_3), 129.5 (s, C_{Ar}H), 162.5 (s, C_{Ar}-O). IR (cm^{-1}): 3089, 2957, 2915, 2857, 1647, 1607, 1479, 1427, 1313, 1267, 1227, 1198, 1160, 1012, 856, 831, 778, 741. EA: calculated: C 53.91, H 5.70; found: C 53.29, H 5.55.

$[Cp_2Y(StBu)]_2$: Yield: 2.92 g white powder (9.45 mmol). ^{1}H NMR (THF-d8, 300 K, 500 MHz): δ = 1.41 (s, 9H, CH_3), 6.11 (s, 10H, Cp-*H*). ^{13}C NMR (THF-d8, 300 K, 125 MHz): δ = 38.8 (s, CH_3), 43.3 (s, S-$C(CH_3)_3$), 111.4 (s, Cp-*C*). IR (cm^{-1}): 3088, 2960, 2925, 2853, 1654, 1568, 1452, 1437, 1416, 1360, 1261, 1146, 1093, 1014, 793, 765. EA: calculated: C 54.55, H 6.21, S 10.40; found: C 54.89, H 6.38, S 9.84.

$[Cp_2Lu(StBu)]_2$: Yield: 1.25 g white powder (3.22 mmol). ^{1}H NMR (THF-d8, 300 K, 500 MHz): δ = 1.42 (s, 9H, CH_3), 6.06 (s, 10H, Cp-*H*). ^{13}C NMR (THF-d8, 300 K, 125 MHz): δ = 38.7 (s, CH_3), 43.5 (s, S-$C(CH_3)_3$), 110.5 (s, Cp-*C*). IR (cm^{-1}): 3084, 2955, 2924, 2854, 1655, 1577, 1458, 1376, 1360, 1261, 1096, 1013, 795, 768. EA: calculated: C 42.64, H 4.86, S 8.13; found: C 42.79, H 4.93, S 7.75.

$[Cp_2Tb(StBu)]_2$: Yield: 0.45 g bright yellow powder (1.20 mmol). IR (cm^{-1}): 3088, 2952, 2924, 2852, 1650, 1579, 1453, 1437, 1416, 1375, 1360, 1256, 1146, 1060, 1010, 806, 765. EA: calculated: C 44.45, H 5.06, S 8.48; found: C 44.21, H 4.94, S 7.95.

Cp_3Y(DEEP): ^{1}H NMR (C_6D_6, 298 K, 300 MHz): δ = 0.78 (dt, 3H, ^3J(P-H) = 20.8 Hz, ^3J(H-H) = 7.7 Hz, P-CH_2-CH_3), 0.92 (t, 6H, ^3J(H-H) = 7.1 Hz, P-O-CH_2-CH_3), 1.22 (dq, 2H, ^2J(P-H) = 17.6 Hz, ^3J(H-H) = 7.7 Hz, P-CH_2-CH_3), 3.68 (m, 4H, P-O-CH_2-CH_3), 6.07 (s, 15H, Cp-*H*). ^{31}P NMR (C_6D_6, 298 K, 121 MHz): δ = 35.3 (d, ^2J(Y-P) = 10.4 Hz).

Cp_3Lu(DEEP): ^{1}H NMR (C_6D_6, 298 K, 300 MHz): δ = 0.77 (dt, 3H, ^3J(P-H) = 20.8 Hz, ^3J(H-H) = 7.5 Hz, P-CH_2-CH_3), 0.91 (t, 6H, ^3J(H-H) = 7.0 Hz, P-O-CH_2-CH_3), 1.23 (dq, 2H, ^2J(P-H) = 17.9 Hz, ^3J(H-H) = 7.7 Hz, P-CH_2-CH_3), 3.69 (m, 4H, P-O-CH_2-CH_3), 6.05 (s, 15H, Cp-*H*). ^{31}P NMR (C_6D_6, 298 K, 121 MHz): δ = 35.8 (s).

Cp_2YCl(DEEP): ^{1}H NMR (C_6D_6, 298 K, 300 MHz): δ = 0.72 (dt, 3H, ^3J(P-H) = 21.1 Hz, ^3J(H-H) = 7.6 Hz, P-CH_2-CH_3), 0.90 (t, 6H, ^3J(H-H) = 7.1 Hz, P-O-CH_2-CH_3), 1.27 (dq, 2H, ^2J(P-H) = 18.3 Hz, ^3J(H-H) = 7.6 Hz, P-CH_2-CH_3), 3.74 (m, 4H, P-O-CH_2-CH_3), 6.33 (s, 10H, Cp-*H*). ^{31}P NMR (C_6D_6, 298 K, 121 MHz): δ = 36.0 (s).

Cp_2LuCl(DEEP): ^{1}H NMR (C_6D_6, 298 K, 300 MHz): δ = 0.70 (dt, 3H, ^3J(P-H) = 21.2 Hz, ^3J(H-H) = 7.7 Hz, P-CH_2-CH_3), 0.89 (t, 6H, ^3J(H-H) = 7.1 Hz, P-O-CH_2-CH_3), 1.27 (dq, 2H, ^2J(P-H) = 18.3 Hz, ^3J(H-H) = 7.7 Hz, P-CH_2-CH_3), 3.75 (m, 4H, P-O-CH_2-CH_3), 6.28 (s, 10H, Cp-*H*). ^{31}P NMR (C_6D_6, 298 K, 121 MHz): δ = 36.7 (s).

Cp_2Y(bdsa)(DEEP): ^{1}H NMR (C_6D_6, 298 K, 300 MHz): δ = 0.42 (d, 12H, ^3J(H-H) = 3.0 Hz, Si-CH_3), 0.76 (dt, 3H, ^3J(P-H) = 20.9 Hz, ^3J(H-H) = 7.6 Hz, P-CH_2-CH_3), 0.89 (t, 6H, ^3J(H-H) = 7.1 Hz, P-O-CH_2-CH_3), 1.34 (dq, 2H, ^2J(P-H) = 18.1 Hz, ^3J(H-H) = 7.7 Hz, P-CH_2-CH_3), 3.72 (m, 4H, P-O-CH_2-CH_3), 4.60 (m, 2H, Si-*H*), 6.28 (s, 10H, Cp-*H*). ^{31}P NMR (C_6D_6, 298 K, 121 MHz): δ = 33.8 (d, ^2J(Y-P) = 11.2 Hz).

Cp_2Lu(bdsa)(DEEP): ^{1}H NMR (C_6D_6, 298 K, 300 MHz): δ = 0.45 (d, 12H, ^3J(H-H) = 2.9 Hz, Si-CH_3), 0.74 (dt, 3H, ^3J(P-H) = 21.0 Hz, ^3J(H-H) = 7.6 Hz, P-CH_2-CH_3), 0.88 (t, 6H, ^3J(H-H) = 7.1 Hz, P-O-CH_2-CH_3), 1.33 (dq, 2H, ^2J(P-H) = 18.1 Hz, ^3J(H-H) = 7.6 Hz, P-CH_2-CH_3), 3.71 (m, 4H, P-O-CH_2-CH_3), 4.66 (m, 2H, Si-*H*), 6.26 (s, 10H, Cp-*H*). ^{31}P NMR (C_6D_6, 298 K, 121 MHz): δ = 34.8 (s).

$Cp_2Y(CH_2TMS)$(DEEP): ^{1}H NMR (C_6D_6, 300 K, 500 MHz): δ = -0.62 (d, 2H, ^2J(Y-H) = 3.4 Hz, Si-CH_2), 0.48 (s, 9H, Si-CH_3), 0.63 (dt, 3H, ^3J(P-H) = 21.0 Hz, ^3J(H-H) = 7.7 Hz, P-CH_2-CH_3), 0.81 (t, 6H, ^3J(H-H) = 7.1 Hz, P-O-CH_2-CH_3), 1.07 (dq, 2H, ^2J(P-H) = 18.1 Hz, ^3J(H-H) = 7.7 Hz, P-CH_2-CH_3), 3.51 (m, 4H, P-O-CH_2-CH_3), 6.28 (s, 10H, Cp-*H*). ^{31}P NMR (C_6D_6, 300 K, 202 MHz): δ = 34.7 (d, ^2J(Y-P) = 11.0 Hz).

$Cp_2Lu(CH_2TMS)$(DEEP): ^{1}H NMR (C_6D_6, 300 K, 500 MHz): δ = -0.72 (s, 2H, Si-CH_2), 0.50 (s, 9H, Si-CH_3), 0.63 (dt, 3H, ^3J(P-H) = 21.1 Hz, ^3J(H-H) = 7.6 Hz, P-CH_2-CH_3), 0.80 (t, 6H, ^3J(H-H) = 7.1 Hz, P-O-CH_2-CH_3), 1.07 (dq, 2H, ^2J(P-H) = 18.1 Hz, ^3J(H-H) = 7.6 Hz, P-CH_2-CH_3), 3.51 (m, 4H, P-O-CH_2-CH_3), 6.23 (s, 10H, Cp-*H*). ^{31}P NMR (C_6D_6, 300 K, 202 MHz): δ = 35.5 (s).

Cp_2Y(O*i*Pr)(DEEP): ^{1}H NMR (C_6D_6, 300 K, 500 MHz): δ = 1.28 (d, 6H, ^3J(H-H) = 5.9 Hz, CH_3), 4.28 (m, 1H, O-C*H*(CH_3)$_2$), 6.32 (s, 10H, Cp-*H*). Due to incomplete reaction of DEEP with [Cp_2Y(O*i*Pr)]$_2$ and exchange of free and coordinated DEEP, ^{1}H and ^{31}P NMR spectroscopic signals of coordinated DEEP could not be determined.

For addition of DEEP to **[Cp_2Lu(O*i*Pr)]$_2$**, no reaction was observed.

$Cp_2Y(O(C_6H_2(CH_3)_3)$(DEEP): ^{1}H NMR (C_6D_6, 300 K, 500 MHz): δ = 0.71 (dt, 3H, ^3J(P-H) = 21.0 Hz, ^3J(H-H) = 7.6 Hz, P-CH_2-CH_3), 0.82 (t, 6H, ^3J(H-H) = 7.1 Hz, P-O-CH_2-CH_3), 1.18 (dq, 2H, ^2J(P-H) = 17.9 Hz, ^3J(H-H) = 7.6 Hz, P-CH_2-CH_3), 2.39 (s, 6H, ortho-CH_3), 2.41 (s, 3H, para-CH_3), 3.61 (m, 4H, P-O-CH_2-CH_3), 6.28 (s, 10H, Cp-*H*), 7.07 (s, 2H, Ar-*H*). ^{31}P NMR (C_6D_6, 300 K, 202 MHz): δ = 35.2 (d, ^2J(Y-P) = 8.1 Hz).

$Cp_2Lu(O(C_6H_2(CH_3)_3)$(DEEP): ^{1}H NMR (C_6D_6, 300 K, 500 MHz): δ = 0.73 (dt, 3H, ^3J(P-H) = 20.9 Hz, ^3J(H-H) = 7.6 Hz, P-CH_2-CH_3), 0.84 (t, 6H, ^3J(H-H) = 7.1 Hz, P-O-CH_2-CH_3), 1.22 (dq, 2H, ^2J(P-H) = 17.9 Hz, ^3J(H-H) = 7.6 Hz, P-CH_2-CH_3), 2.39 (s, 6H, ortho-CH_3), 2.43 (s, 3H, para-CH_3), 3.65 (m, 4H, P-O-CH_2-CH_3), 6.23 (s, 10H, Cp-*H*), 7.09 (s, 2H, Ar-*H*). ^{31}P NMR (C_6D_6, 300 K, 202 MHz): δ = 35.9 (s).

Cp_2Y(S*t*Bu)(DEEP): ^{1}H NMR (C_6D_6, 300 K, 500 MHz): δ = 0.74 (dt, 3H, ^3J(P-H) = 20.9 Hz, ^3J(H-H) = 7.7 Hz, P-CH_2-CH_3), 0.90 (t, 6H, ^3J(H-H) = 7.1 Hz, P-O-CH_2-CH_3), 1.29 (dq, 2H, ^2J(P-H) = 18.1 Hz, ^3J(H-H) = 7.7 Hz, P-CH_2-CH_3), 1.81 (s, 9H, CH_3), 3.77 (m, 4H, P-O-CH_2-CH_3), 6.33 (s, 10H, Cp-*H*). ^{31}P NMR (C_6D_6, 300 K, 202 MHz): δ = 35.1 (s).

Cp_2Lu(S*t*Bu)(DEEP): ^{1}H NMR (C_6D_6, 300 K, 500 MHz): δ = 0.73 (dt, 3H, ^3J(P-H) = 21.1 Hz, ^3J(H-H) = 7.6 Hz, P-CH_2-CH_3), 0.89 (t, 6H, ^3J(H-H) = 7.1 Hz, P-O-CH_2-CH_3), 1.28 (dq, 2H, ^2J(P-H) = 18.1 Hz, ^3J(H-H) = 7.7 Hz, P-CH_2-CH_3), 1.79 (s, 9H, CH_3), 3.77 (m, 4H, P-O-CH_2-CH_3), 6.28 (s, 10H, Cp-*H*). ^{31}P NMR (C_6D_6, 300 K, 202 MHz): δ = 36.0 (s).

Oligomerization Experiments

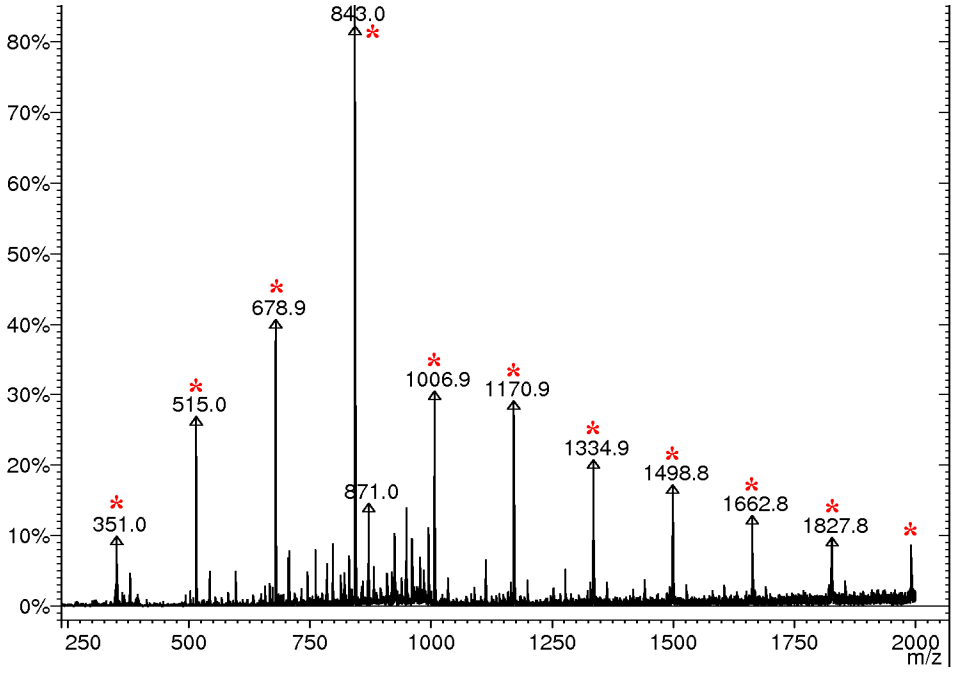

Figure S1. ESI MS spectrum of DEVP oligomers produced with $[Cp_2YbMe]_2$. One major series of peaks is evident: m/z = n × M_{Mon} + M_{Na} (red); M_{Mon} = 164, no apparent end group.

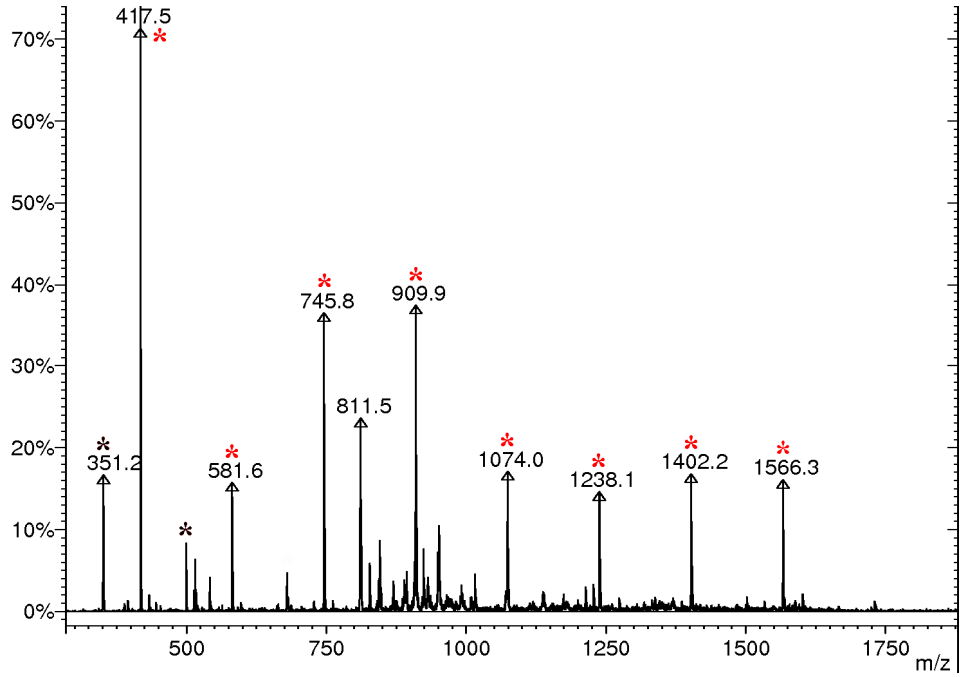

Figure S2. ESI MS spectrum of DEVP oligomers produced with $[Cp_2YCl]_2$. One major series of peaks is evident: m/z = n × M_{Mon} + 66 + M_{Na} (red); M_{Mon} = 164, end groups: M_{Cp} + M_H = 66. Peaks at m/z = 351 and 515 are attributed to fragmentation (black).

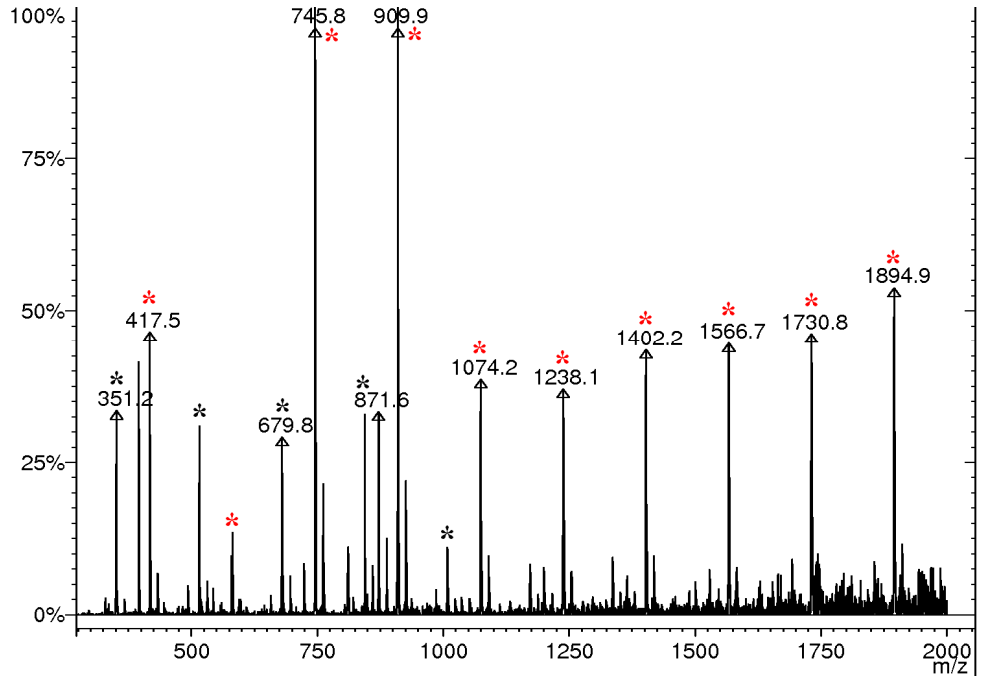

Figure S3. ESI MS spectrum of DEVP oligomers produced with $[Cp_2LuCl]_2$. One major series of peaks is evident: m/z = n × M_{Mon} + 66 + M_{Na} (red); M_{Mon} = 164, end groups: M_{Cp} + M_H = 66. Peaks at m/z = 351, 515, 679, 843 and 1007 are attributed to fragmentation (black).

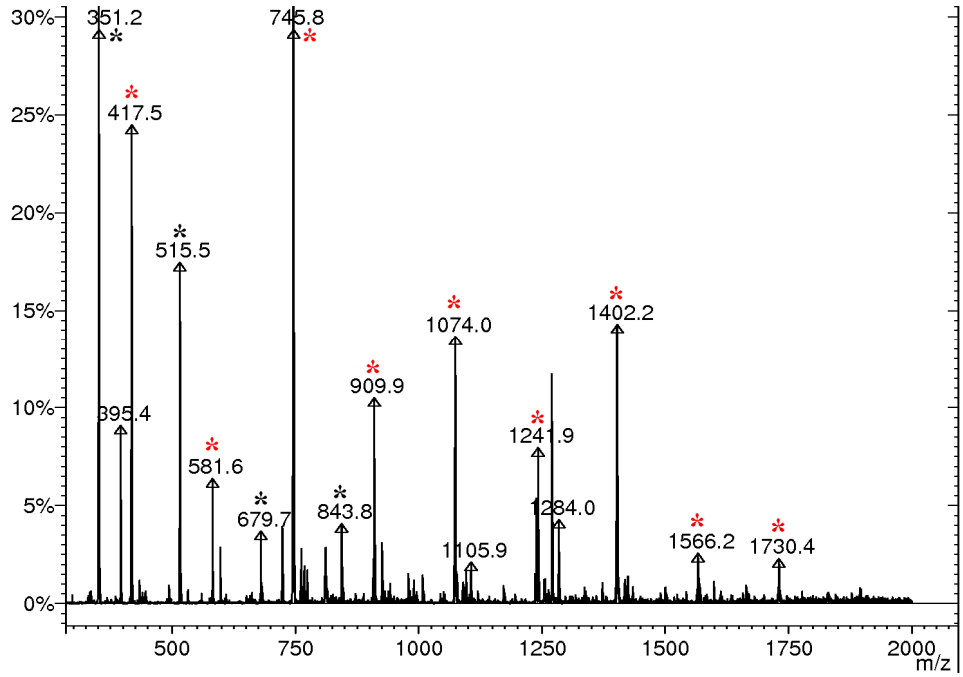

Figure S4. ESI MS spectrum of DEVP oligomers produced with $Cp_2Lu(bdsa)(thf)$. One major series of peaks is evident: m/z = n × M_{Mon} + 66 + M_{Na} (red); M_{Mon} = 164, end groups: M_{Cp} + M_H = 66. Peaks at m/z = 351, 515, 679 and 843 are attributed to fragmentation (black).

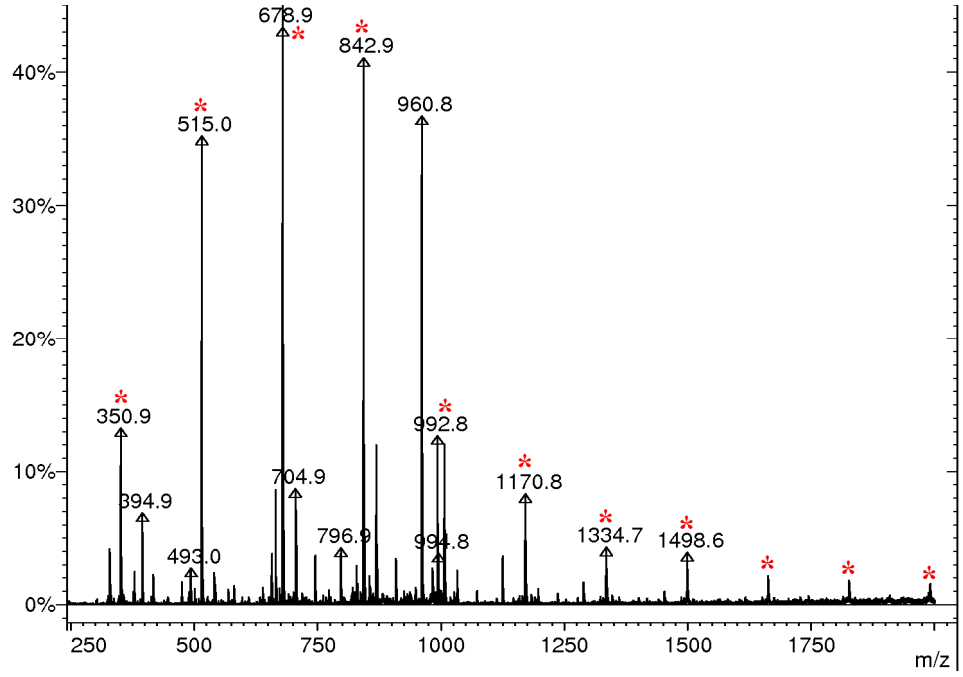

Figure S5. ESI MS spectrum of DEVP oligomers produced with $Cp_2Lu(bdsa)(thf)$. One major series of peaks is evident: m/z = n × M_{Mon} + M_{Na} (red); M_{Mon} = 164, no apparent end groups.

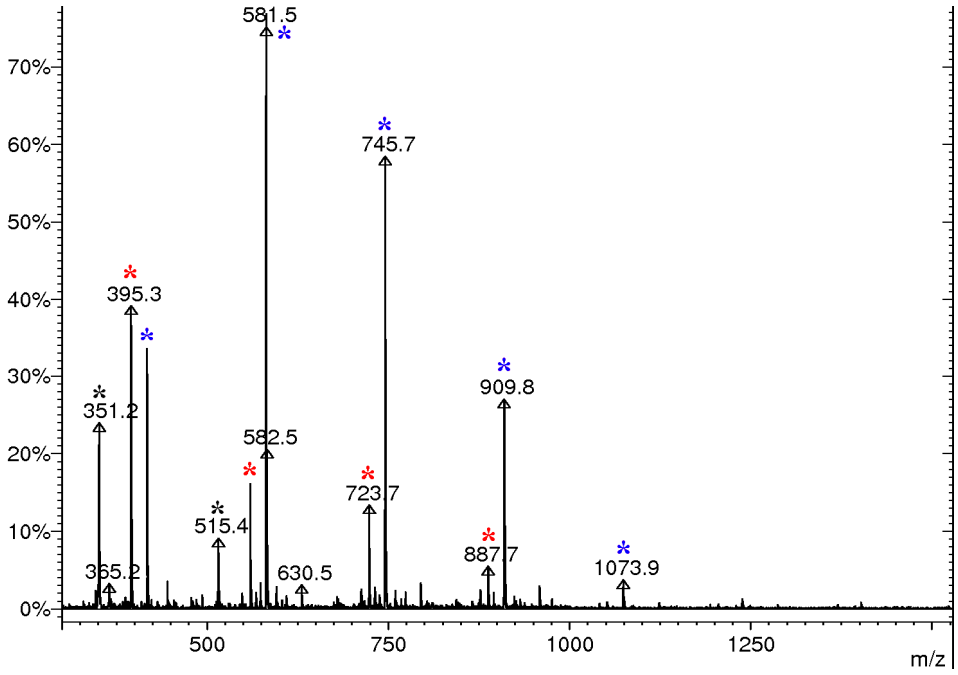

Figure S6. ESI MS spectrum of DEVP oligomers produced with $[Cp_2Y(O\mathit{i}Pr)]_2$. Two major series of peaks are evident: m/z = n × M_{Mon} + 66 + M_H (red), m/z = n × M_{Mon} + 66 + M_{Na} (blue); M_{Mon} = 164, end groups: M_{Cp} + M_H = 66. Peaks at m/z = 351 and 515 are attributed to fragmentation.

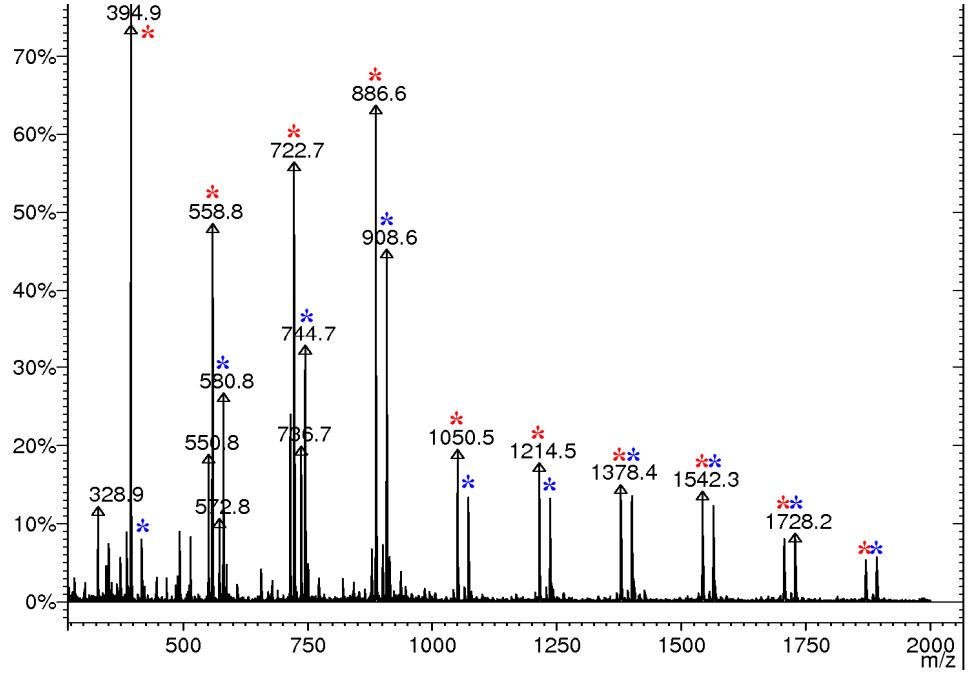

Figure S7. ESI MS spectrum of DEVP oligomers produced with $[Cp_2Lu(O\mathit{i}Pr)]_2$. Two major series of peaks are evident: m/z = n × M_{Mon} + 66 + M_H (red), m/z = n × M_{Mon} + 66 + M_{Na} (blue); M_{Mon} = 164, end groups: M_{Cp} + M_H = 66.

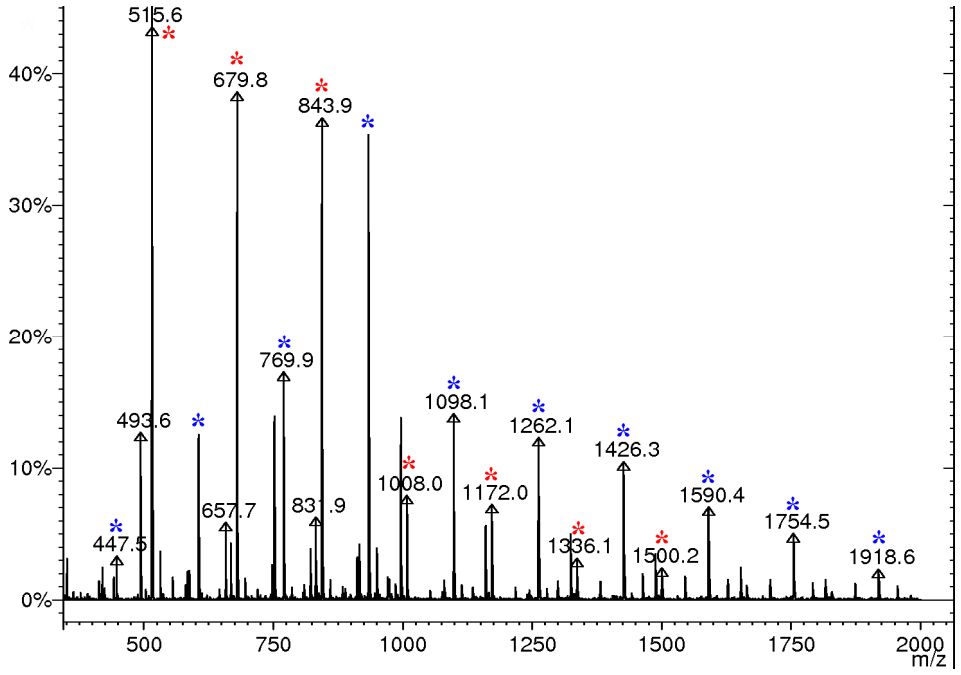

Figure S8. ESI MS spectrum of DEVP oligomers produced with $[Cp_2YS\mathit{t}Bu]_2$. Two major series of peaks are evident: m/z = n × M_{Mon} + M_{Na} (red), m/z = n × M_{Mon} + 90 + M_{Na} (blue); M_{Mon} = 164, end groups: $M_{S\mathit{t}Bu}$ + M_H = 90.

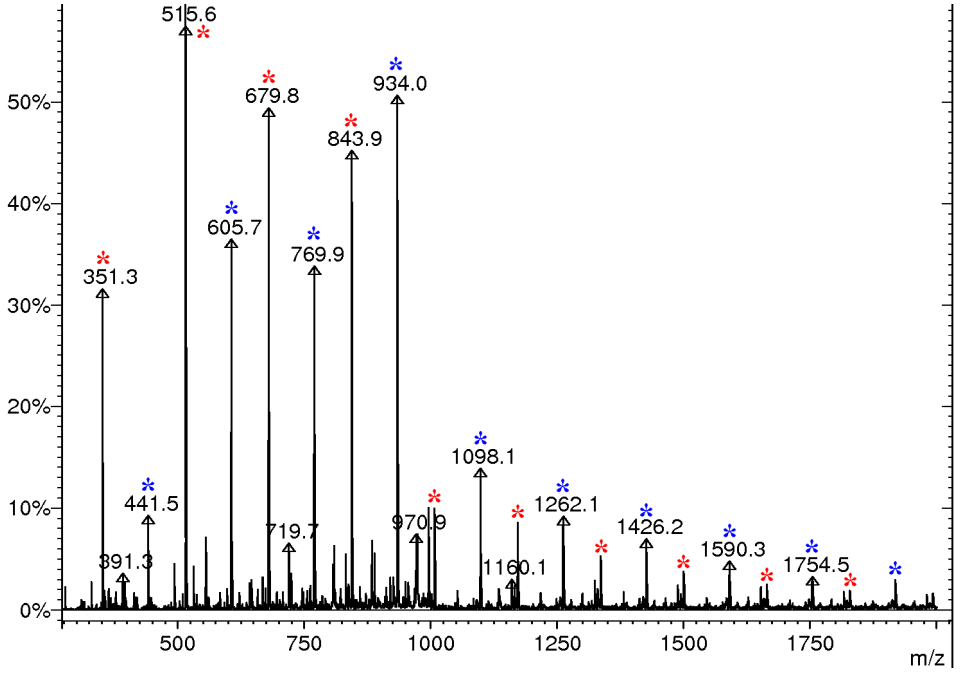

Figure S9. ESI MS spectrum of DEVP oligomers produced with $[Cp_2LuS\mathit{t}Bu]_2$. Two major series of peaks are evident: m/z = n × M_{Mon} + M_{Na} (red), m/z = n × M_{Mon} + 90 + M_{Na} (blue); M_{Mon} = 164, end groups: $M_{S\mathit{t}Bu}$ + M_H = 90.

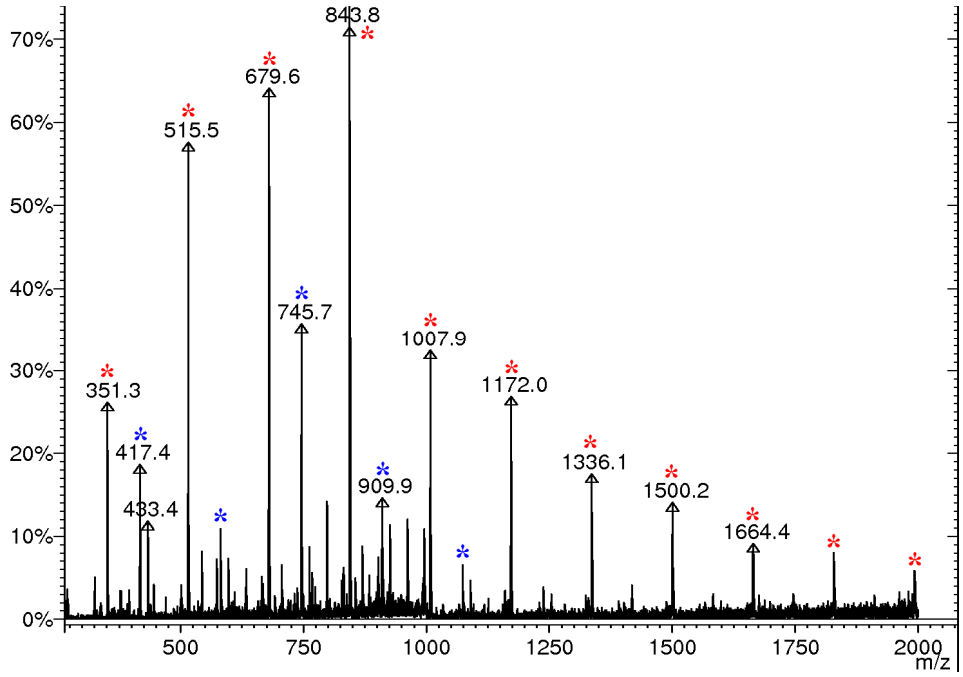

Figure S10. ESI MS spectrum of DEVP oligomers produced with $Cp_2Y(CH_2TMS)(thf)$. Two major series of peaks are evident: m/z = n × M_{Mon} + M_{Na} (red), m/z = n × M_{Mon} + 66 + M_{Na} (blue); M_{Mon} = 164, end groups: M_{Cp} + M_H = 66.

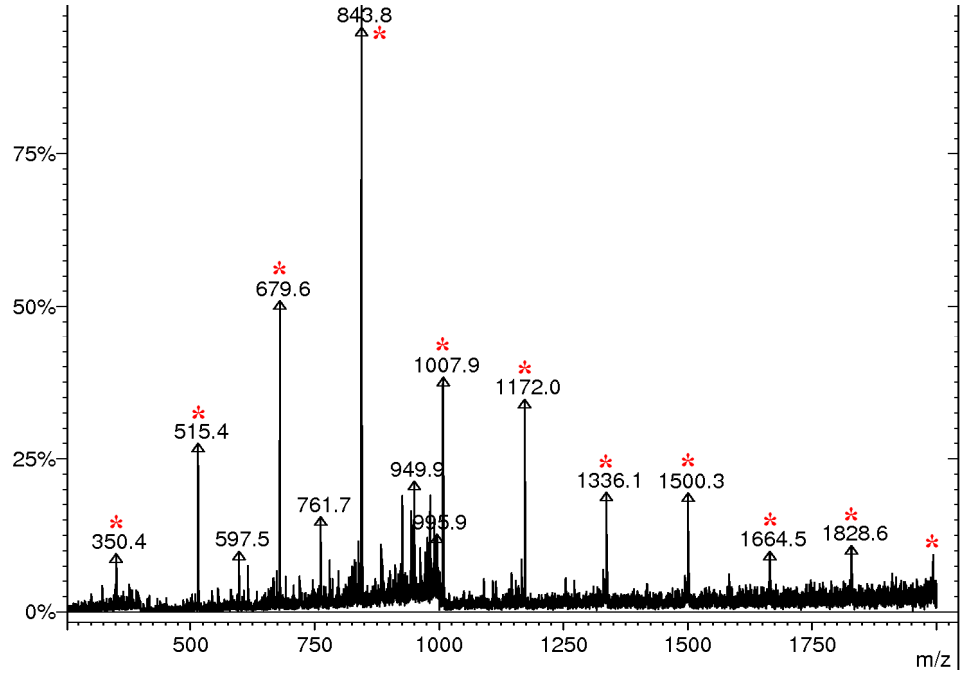

Figure S11. ESI MS spectrum of DEVP oligomers produced with $Cp_2Lu(CH_2TMS)(thf)$. One major series of peaks is evident: m/z = n × M_{Mon} + M_{Na} (red); M_{Mon} = 164, no apparent end group.

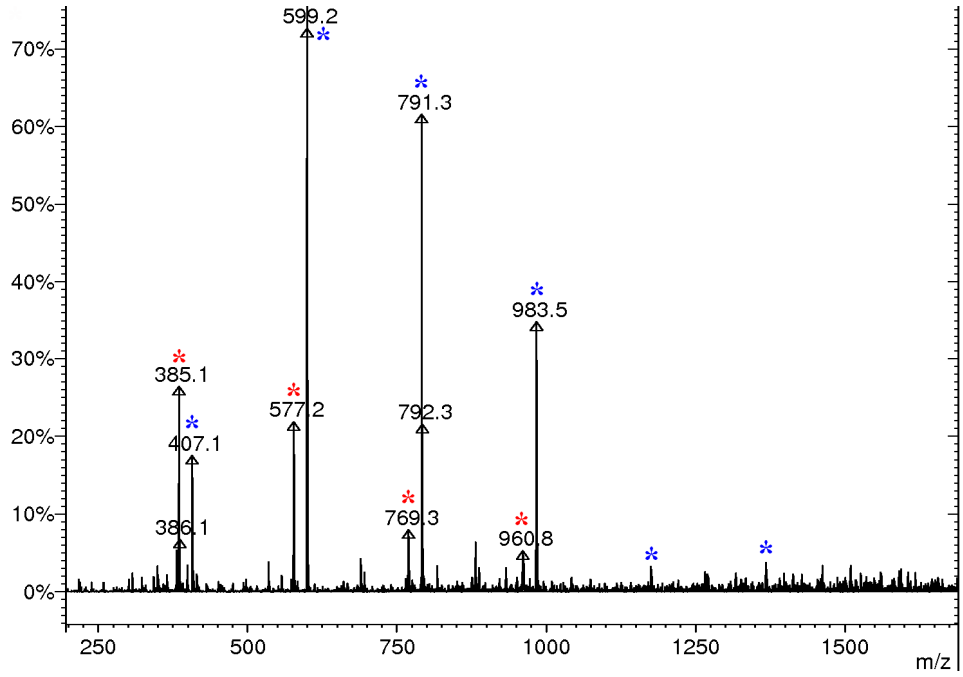

Figure S12. ESI MS spectrum of DIVP oligomers produced with $[Cp_2YS\mathit{t}Bu]_2$. Two major series of peaks are evident: m/z = n × M_{Mon} + M_H (red), m/z = n × M_{Mon} + M_{Na} (red); M_{Mon} = 192, no apparent end group.

Single Crystal X-Ray Structure Determination of Compounds $Cp_3Y(DEEP)$, $Cp_2HoCl(DEVP)$, and $Cp_2YbCl(DEVP)$

General:

Data were collected on an X-ray single crystal diffractometer equipped with a CCD detector (Bruker APEX II, κ–CCD), a rotating anode (Bruker AXS, FR591) with MoK_α radiation (λ = 0.71073 Å), and a graphite monochromator by using the SMART software package.[1] The measurements were performed on a single crystal coated with perfluorinated ether. The crystal was fixed on the top of a glass fiber and transferred to the diffractometer. The crystal was frozen under a stream of cold nitrogen. A matrix scan was used to determine the initial lattice parameters. Reflections were merged and corrected for Lorenz and polarization effects, scan speed, and background using SAINT.[2] Absorption corrections, including odd and even ordered spherical harmonics were performed using SADABS.[2] Space group assignments were based upon systematic absences, *E* statistics, and successful refinement of the structures. Structures were solved by direct methods with the aid of successive difference Fourier maps, and were refined against all data using WinGX[7] based on SIR-92.[3] If not mentioned otherwise, non-hydrogen atoms were refined with anisotropic displacement parameters. Methyl hydrogen atoms were refined as part of rigid rotating groups, with C–H = 0.98 Å and $U_{iso(H)} = 1.5U_{eq(C)}$. Other H atoms were placed in calculated positions and refined using a riding model, with methylene and aromatic C–H distances of 0.99 and 0.95 Å, respectively, and $U_{iso(H)} = 1.2 \cdot U_{eq(C)}$. Full-matrix least-squares refinements were carried out by minimizing $\Sigma w(F_o^2-F_c^2)^2$ with SHELXL-97[5] weighting scheme. Neutral atom scattering factors for all atoms and anomalous dispersion corrections for the non-hydrogen atoms were taken from *International Tables for Crystallography*.[4] Images of the crystal structures were generated by PLATON.[6]

Special:

$Cp_2HoCl(DEVP)$: Extinction Correction. The correct enantiomere is proved by Flack's Parameter.

$Cp_2YbCl(DEVP)$: The correct enantiomere is proved by Flack's Parameter.

$Cp_3Y(DEEP)$

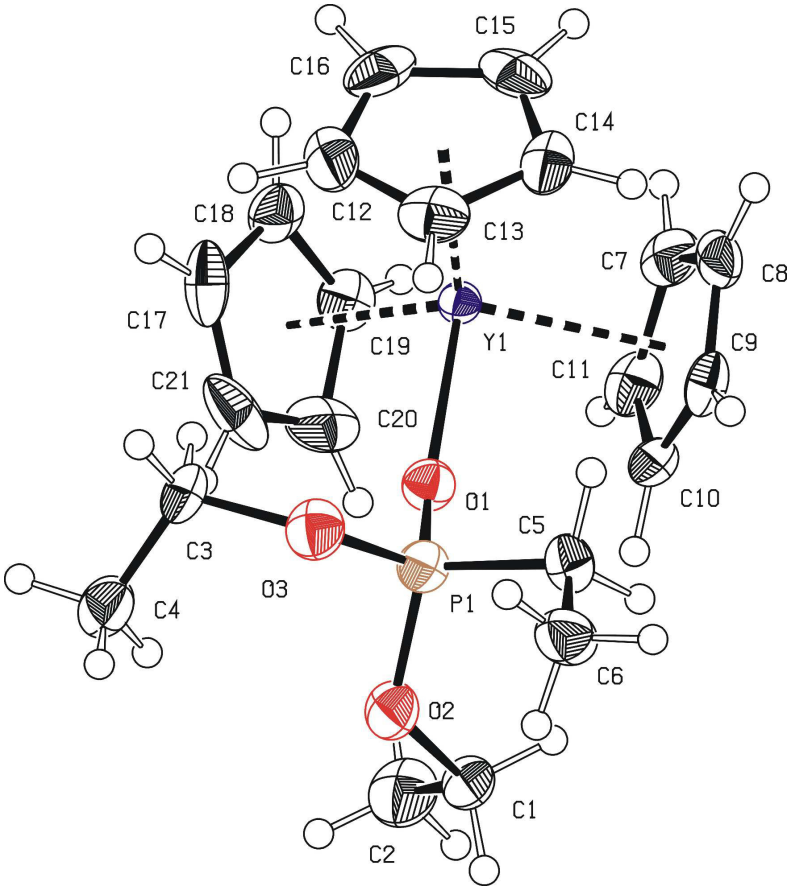

Figure S13. Ortep drawing drawing of compound $Cp_3Y(DEEP)$ with 50% ellipsoids.[6]

Operator:	*** Herdtweck ***
Molecular Formula:	$C_{21}\ H_{30}\ O_3\ P\ Y$
Crystal Color / Shape	Colorless fragment
Crystal Size	Approximate size of crystal fragment used for data collection: $0.18 \times 0.41 \times 0.51$ mm
Molecular Weight:	450.33 a.m.u.
F_{000}:	936
Systematic Absences:	h0l: h+l≠2n; 0k0: k≠2n
Space Group:	Monoclinic $P\ 2_1/n$ (I.T.-No.: 14)
Cell Constants:	Least-squares refinement of 9637 reflections with the programs "APEX suite" and "SAINT" [1,2]; theta range 1.84° < θ < 25.36°; Mo($K\bar{\alpha}$); λ = 71.073 pm a = 1150.91(4) pm b = 828.72(3) pm β = 101.516(2)° c = 2261.67(8) pm V = 2113.72(13)· 10^6 pm^3; Z = 4; D_{calc} = 1.415 g cm^{-3}; Mos. = 0.72
Diffractometer:	Kappa APEX II (Area Diffraction System; BRUKER AXS); rotating anode; graphite monochromator; 50 kV; 40 mA; λ = 71.073 pm; Mo($K\bar{\alpha}$)

Temperature:	(-150±1) °C;	(123±1) K
Measurement Range:	1.84° < θ < 25.36°; h: -13/13, k: -9/9, l: -27/27	
Measurement Time:	2 × 5 s per film	
Measurement Mode:	measured: 13 runs; 8565 films / scaled: 13 runs; 8565 films	
	φ– and ω–movement; Increment: $\Delta\varphi/\Delta\omega$ = 0.50°; dx = 55.0 mm	
LP - Correction:	Yes [2]	
Intensity Correction	No/Yes; during scaling [2]	
Absorption Correction:	Multi-scan; during scaling; μ = 2.851 mm^{-1} [2]	
	Correction Factors:	T_{min} = 0.3668 T_{max} = 0.7452
Reflection Data:	79021	reflections were integrated and scaled
	3711	reflections systematic absent and rejected
	75310	reflections to be merged
	3849	independent reflections
	0.041	R_{int}: (basis F_o^2)
	3849	independent reflections (all) were used in refinements
	3531	independent reflections with $I_o > 2\sigma(I_o)$
	99.7 %	completeness of the data set
	238	parameter full-matrix refinement
	16.2	reflections per parameter
Solution:	Direct Methods [3]; Difference Fourier syntheses	
Refinement Parameters:	In the asymmetric unit:	
	26	Non-hydrogen atoms with anisotropic displacement parameters
Hydrogen Atoms:	In the difference map(s) calculated from the model containing all non-hydrogen atoms, not all of the hydrogen positions could be determined from the highest peaks. For this reason, the hydrogen atoms were placed in calculated positions (d_{C-H} = 95, 98, 99 pm). Isotropic displacement parameters were calculated from the parent carbon atom (U_H = 1.2/1.5 U_C). The hydrogen atoms were included in the structure factor calculations but not refined.	
Atomic Form Factors:	For neutral atoms and anomalous dispersion [4]	
Extinction Correction:	no	
Weighting Scheme:	$w^{-1} = \sigma^2(F_o^2)+(a*P)^2+b*P$	
	with a: 0.0637; b: 5.8032; P: [Maximum(0 or F_o^2)+2$*F_c^2$]/3	
Shift/Err:	Less than 0.001 in the last cycle of refinement:	
Resid. Electron Density:	+2.98 $e_{0;}^-/Å^3$; -0.86 $e_{0;}^-/Å^3$	
R1:	$\Sigma(\|\|F_o\|-\|F_c\|\|)/\Sigma\|F_o\|$	
[$F_o > 4\sigma(F_o)$; N=3531]:		= 0.0446
[all reflctns; N=3849]:		= 0.0485
wR2:	$[\Sigma w(F_o^2-F_c^2)^2/\Sigma w(F_o^2)^2]^{1/2}$	
[$F_o > 4\sigma(F_o)$; N=3531]:		= 0.1182
[all reflctns; N=3849]:		= 0.1211
Goodness of fit:	$[\Sigma w(F_o^2-F_c^2)^2/(NO-NV)]^{1/2}$	= 1.074
Remarks:	Refinement expression $\Sigma w(F_o^2-F_c^2)^2$	

$Cp_2HoCl(DEVP)$

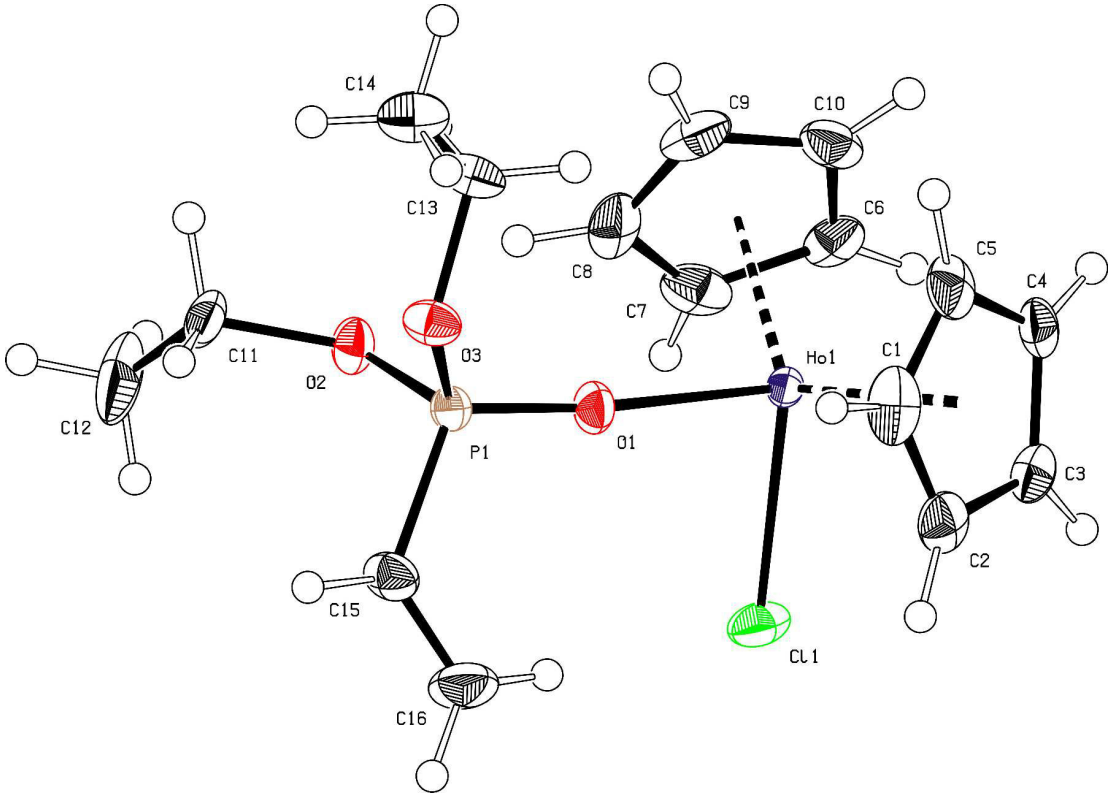

Figure S14. Ortep drawing drawing of compound $Cp_2HoCl(DEVP)$ with 50% ellipsoids.[6]

Operator:	*** Herdtweck ***
Molecular Formula:	C_{16} H_{23} Cl Ho O_3 P
Crystal Color / Shape	Colorless fragment
Crystal Size	Approximate size of crystal fragment used for data collection: 0.18 × 0.51 × 0.64 mm
Molecular Weight:	494.69 a.m.u.
F_{000}:	968
Systematic Absences:	0kl: k+l≠2n; h0l: h≠2n; 00l: l≠2n
Space Group:	Orthorhombic $P\,na2_1$ (I.T.-No.: 33)
Cell Constants:	Least-squares refinement of 9797 reflections with the programs "APEX suite" and "SAINT" [1,2]; theta range 1.96° < θ < 25.42°; Mo($K\bar{\alpha}$); λ = 71.073 pm a = 2074.65(6) pm b = 1172.65(4) pm c = 781.25(3) pm V = 1900.66(11)· 10^6 pm^3; Z = 4; D_{calc} = 1.729 g cm^{-3}; Mos. = 0.70
Diffractometer:	Kappa APEX II (Area Diffraction System; BRUKER AXS); rotating anode; graphite monochromator; 50 kV; 40 mA; λ = 71.073 pm; Mo($K\bar{\alpha}$)
Temperature:	(-150±1) °C; (123±1) K
Measurement Range:	1.96° < θ < 25.42°; h: -24/25, k: -14/14, l: -9/9
Measurement Time:	2 × 5 s per film

Measurement Mode:	measured: 11 runs; 4738 films / scaled: 11 runs; 4738 films φ– and ω–movement; Increment: $\Delta\varphi/\Delta\omega = 0.50°$; dx = 45.0 mm
LP - Correction:	Yes [2]
Intensity Correction	No/Yes; during scaling [2]
Absorption Correction:	Multi-scan; during scaling; $\mu = 4.395$ mm^{-1} [2] Correction Factors: $T_{min} = 0.2508$ $T_{max} = 0.7452$
Reflection Data:	53506 reflections were integrated and scaled 2077 reflections systematic absent and rejected 1 obvious wrong intensity and rejected 51428 reflections to be merged 3487 independent reflections 0.044 R_{int}: (basis F_o^2) 3487 independent reflections (all) were used in refinements 3484 independent reflections with $I_o > 2\sigma(I_o)$ 99.4 % completeness of the data set 202 parameter full-matrix refinement 17.3 reflections per parameter
Solution:	Direct Methods [3]; Difference Fourier syntheses
Refinement Parameters:	In the asymmetric unit: 22 Non-hydrogen atoms with anisotropic displacement parameters
Hydrogen Atoms:	In the difference map(s) calculated from the model containing all non-hydrogen atoms, not all of the hydrogen positions could be determined from the highest peaks. For this reason, the hydrogen atoms were placed in calculated positions (d_{C-H} = 95, 98, 99 pm). Isotropic displacement parameters were calculated from the parent carbon atom (U_H = 1.2/1.5 U_C). The hydrogen atoms were included in the structure factor calculations but not refined.
Atomic Form Factors:	For neutral atoms and anomalous dispersion [4]
Extinction Correction:	F_c (korr) = kF_c[1+ 0.001 · ε · F_c^2· λ^3/sin(2Θ)]$^{-1/4}$ SHELXL-97 [5] ε refined to $\varepsilon = 0.0024(2)$
Weighting Scheme:	$w^{-1} = \sigma^2(F_o^2)+(a*P)^2+b*P$ with a: 0.0091; b: 1.7395; P: [Maximum(0 or F_o^2)+2∗F_c^2]/3
Shift/Err:	Less than 0.001 in the last cycle of refinement:
Resid. Electron Density:	+0.91 $e_{0;}^-$/Å^3; -0.73 $e_{0;}^-$/Å^3
R1:	$\Sigma(\|\|F_o\|-\|F_c\|\|)/\Sigma\|F_o\|$
[$F_o > 4\sigma(F_o)$; N=3484]:	= 0.0144
[all reflctns; N=3487]:	= 0.0145
wR2:	$[\Sigma w(F_o^2-F_c^2)^2/\Sigma w(F_o^2)^2]^{1/2}$
[$F_o > 4\sigma(F_o)$; N=3484]:	= 0.0369
[all reflctns; N=3487]:	= 0.0369
Goodness of fit:	$[\Sigma w(F_o^2-F_c^2)^2/(NO-NV)]^{1/2}$ = 1.197
Flack's Parameter :	$x = 0.07(1)$
Remarks:	Refinement expression $\Sigma w(F_o^2-F_c^2)^2$

Compound $Cp_2YbCl(DEVP)$

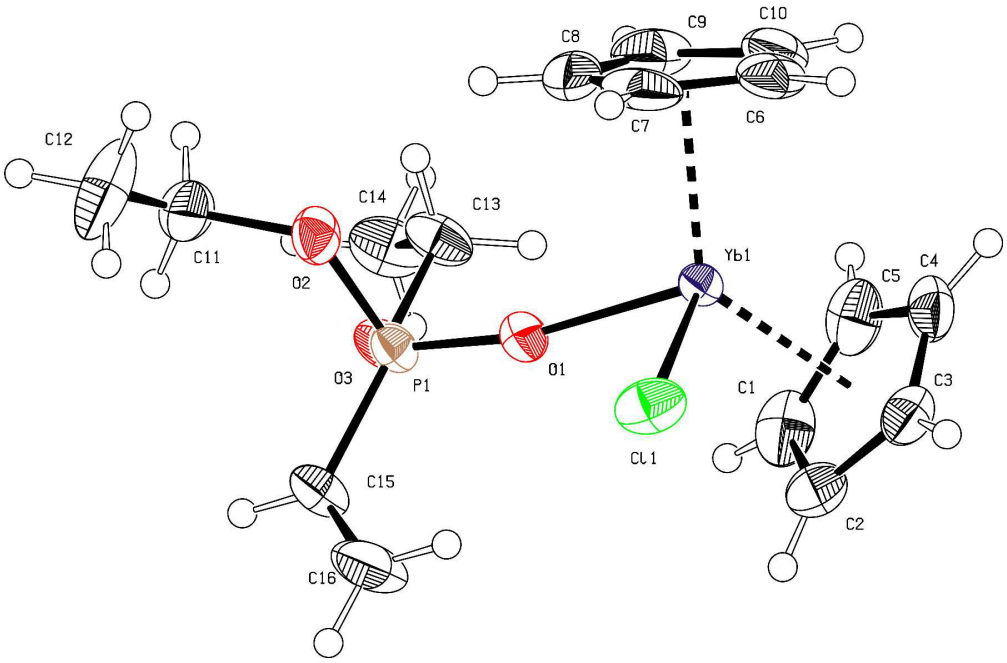

Figure S15. Ortep drawing drawing of compound $Cp_2YbCl(DEVP)$ with 50% ellipsoids.[6]

Operator:	*** Herdtweck ***
Molecular Formula:	$C_{16}\ H_{23}\ Cl\ O_3\ P\ Yb$
Crystal Color / Shape	Colorless fragment
Crystal Size	Approximate size of crystal fragment used for data collection: 0.18 × 0.51 × 0.53 mm
Molecular Weight:	502.80 a.m.u.
F_{000}:	980
Systematic Absences:	0kl: k+l≠2n; h0l: h≠2n; 00l: l≠2n
Space Group:	Orthorhombic $P\ na2_1$ (I.T.-No.: 33)
Cell Constants:	Least-squares refinement of 9735 reflections with the programs "APEX suite" and "SAINT" [1,2]; theta range 1.96° < θ < 25.36°; Mo($K\bar{\alpha}$); λ = 71.073 pm a = 2075.04(7) pm b = 1173.61(4) pm c = 780.75(3) pm V = 1901.35(12)· 10^6 pm^3; Z = 4; D_{calc} = 1.757 g cm^{-3}; Mos. = 0.40
Diffractometer:	Kappa APEX II (Area Diffraction System; BRUKER AXS); rotating anode; graphite monochromator; 50 kV; 40 mA; λ = 71.073 pm; Mo($K\bar{\alpha}$)
Temperature:	(-120±1) °C; (153±1) K
Measurement Range:	1.96° < θ < 25.36°; h: -24/24, k: -14/14, l: -9/9
Measurement Time:	2 × 5 s per film
Measurement Mode:	measured: 13 runs; 4857 films / scaled: 13 runs; 4857 films φ– and ω–movement; Increment: $\Delta\varphi/\Delta\omega$ = 0.50°; dx = 45.0 mm
LP - Correction:	Yes [2]
Intensity Correction	No/Yes; during scaling [2]

Absorption Correction:	Multi-scan; during scaling; μ = 5.151 mm^{-1} [2]	
	Correction Factors: T_{min} = 0.3291 T_{max} = 0.7452	
Reflection Data:	48470	reflections were integrated and scaled
	2255	reflections systematic absent and rejected
	46215	reflections to be merged
	3461	independent reflections
	0.053	R_{int}: (basis F_o^2)
	3461	independent reflections (all) were used in refinements
	3449	independent reflections with $I_o > 2\sigma(I_o)$
	99.3 %	completeness of the data set
	201	parameter full-matrix refinement
	17.2	reflections per parameter
Solution:	Direct Methods [3]; Difference Fourier syntheses	
Refinement Parameters:	In the asymmetric unit:	
	22 Non-hydrogen atoms with anisotropic displacement parameters	
Hydrogen Atoms:	In the difference map(s) calculated from the model containing all non-hydrogen atoms, not all of the hydrogen positions could be determined from the highest peaks. For this reason, the hydrogen atoms were placed in calculated positions (d_{C-H} = 95, 98, 99 pm). Isotropic displacement parameters were calculated from the parent carbon atom (U_H = 1.2/1.5 U_C). The hydrogen atoms were included in the structure factor calculations but not refined.	
Atomic Form Factors:	For neutral atoms and anomalous dispersion [4]	
Extinction Correction:	no	
Weighting Scheme:	$w^{-1} = \sigma^2(F_o^2)+(a*P)^2+b*P$	
	with a: 0.0125; b: 1.2304; P: [Maximum(0 or F_o^2)+2$*F_c^2$]/3	
Shift/Err:	Less than 0.002 in the last cycle of refinement:	
Resid. Electron Density:	+0.70 $e_{0;}^-/Å^3$; -0.55 $e_{0;}^-/Å^3$	
R1:	$\Sigma(\|\|F_o\|-\|F_c\|\|)/\Sigma\|F_o\|$	
[$F_o > 4\sigma(F_o)$; N=3449]:		= 0.0142
[all reflctns; N=3461]:		= 0.0143
wR2:	$[\Sigma w(F_o^2-F_c^2)^2/\Sigma w(F_o^2)^2]^{1/2}$	
[$F_o > 4\sigma(F_o)$; N=3449]:		= 0.0373
[all reflctns; N=3461]:		= 0.0374
Goodness of fit:	$[\Sigma w(F_o^2-F_c^2)^2/(NO-NV)]^{1/2}$	= 1.088
Flack's Parameter :	x = 0.08(1)	
Remarks:	Refinement expression $\Sigma w(F_o^2-F_c^2)^2$	

Kinetic Studies

Table S1. Determination of catalyst order (Cp_3Tm, 5vol% DEVP, toluene, 30 °C)

[Cat] /mmol L^{-1}	TOF /h^{-1}	I^*_t /%	TOF/I^*_t /h^{-1}	ln([Cat*])	rate /mol L^{-1} s^{-1}	ln(rate)
0.54	9100	17	54000	-2.39	1.38E-03	-6.59
0.82	10000	18	56000	-1.91	2.34E-03	-6.06
1.09	9000	17	53000	-1.69	2.73E-03	-5.90
1.36	8600	16	54000	-1.53	3.26E-03	-5.73
1.63	11000	21	52000	-1.07	4.87E-03	-5.32
2.17	7000	13	54000	-1.27	4.22E-03	-5.47
2.72	6700	13	52000	-1.04	5.04E-03	-5.29

Table S2. Determination of catalyst order ($[Cp_2Y(StBu)]_2$, 5vol% DEVP, toluene, 30 °C)

[Cat] /mmol L^{-1}	TOF /h^{-1}	I^*_t /%	TOF/I^*_t /h^{-1}	ln([Cat*])	rate /mol L^{-1} s^{-1}	ln(rate)
0.95	19900	44	45000	-0.87	5.29E-03	-5.24
1.09	20600	43	48000	-0.76	6.18E-03	-5.09
1.36	19700	41	48000	-0.58	7.43E-03	-4.90
1.63	19000	39	49000	-0.45	8.58E-03	-4.76
1.90	18000	39	46000	-0.30	9.55E-03	-4.65
2.17	16400	35	47000	-0.28	9.84E-03	-4.62
2.44	15400	35	44000	-0.16	1.07E-02	-4.54

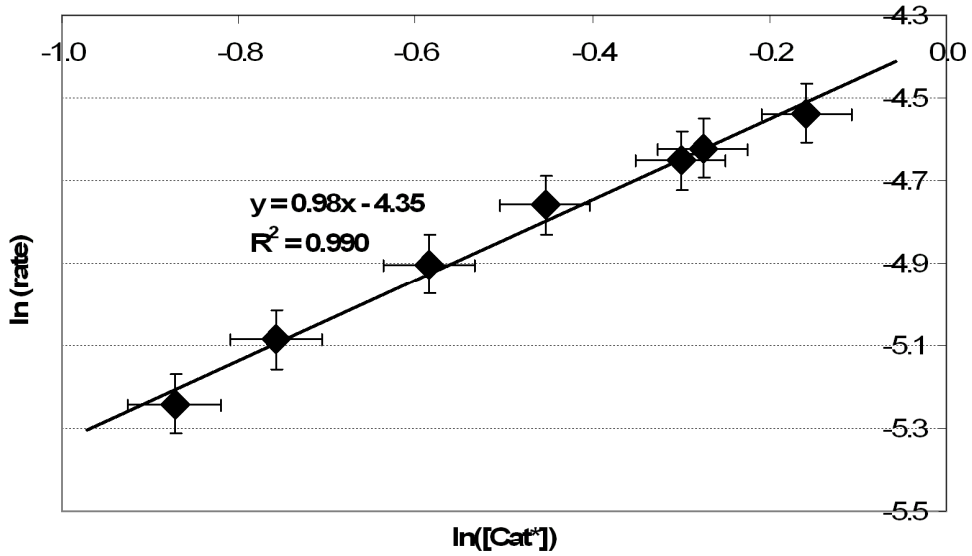

Figure S16. Determination of catalyst order ($[Cp_2Y(StBu)]_2$, 5vol% DEVP, toluene, 30 °C).

Table S3. Determination of catalyst order ([$Cp_2Y(StBu)]_2$, 12.5vol% DIVP, toluene, 30 °C)

[Cat] /mmol L^{-1}	TOF /h^{-1}	I^*_t /%	TOF/I^*_t /h^{-1}	ln([Cat*])	rate /mol L^{-1} s^{-1}	ln(rate)
1.63	1520	70	2170	0.13	6.85E-04	-7.29
1.90	1380	62	2230	0.16	7.31E-04	-7.22
2.17	1480	67	2210	0.37	8.93E-04	-7.02
2.44	1640	74	2220	0.59	1.11E-03	-6.80
2.72	1710	74	2310	0.70	1.29E-03	-6.65
2.99	1760	78	2260	0.85	1.45E-03	-6.54
3.26	1840	78	2360	0.93	1.66E-03	-6.40

Table S4. Determination of monomer order ([$Cp_2Y(StBu)]_2$, DEVP, toluene, 30 °C)

$[Mon]_0$ /mol L^{-1}	[Cat] /mmol L^{-1}	TOF /h^{-1}	I^*_t /%	TOF/I^*_t /h^{-1}	Conversion at max. rate /%	ln([Mon])	rate /mol L^{-1} s^{-1}	ln(rate/[Cat*])
0.163	1.09	8300	36	23000	20	0.130	2.50E-03	1.85
0.223	1.09	12900	45	29000	29	0.158	3.79E-03	2.04
0.260	1.09	14700	38	39000	23	0.200	4.43E-03	2.37
0.325	1.09	20600	44	47000	27	0.237	6.18E-03	2.56
0.390	1.09	32000	54	60000	19	0.316	8.80E-03	2.70
0.488	1.09	26700	40	67000	19	0.395	8.05E-03	2.92
0.651	1.09	45000	51	88000	28	0.469	1.36E-02	3.20

Table S5. Determination of monomer order ([$Cp_2Y(StBu)]_2$, DIVP, toluene, 30 °C)

$[Mon]_0$ /mol L^{-1}	[Cat] /mmol L^{-1}	TOF /h^{-1}	I^*_t /%	TOF/I^*_t /h^{-1}	Conversion at max. rate /%	ln([Mon])	rate /mol L^{-1} s^{-1}	ln(rate/[Cat*])
0.195	1.09	610	86	710	12.8	0.170	1.82E-04	-1.64
0.260	1.09	660	76	870	10.2	0.233	1.99E-04	-1.43
0.325	1.39	950	79	1200	12.3	0.285	3.66E-04	-1.10
0.390	1.09	760	57	1330	5.5	0.369	2.29E-04	-1.00
0.480	2.17	1230	68	1810	8.7	0.438	7.47E-04	-0.68
0.520	2.17	1230	69	1780	7.9	0.479	7.39E-04	-0.71
0.650	2.72	1710	74	2310	12.0	0.572	1.29E-03	-0.44

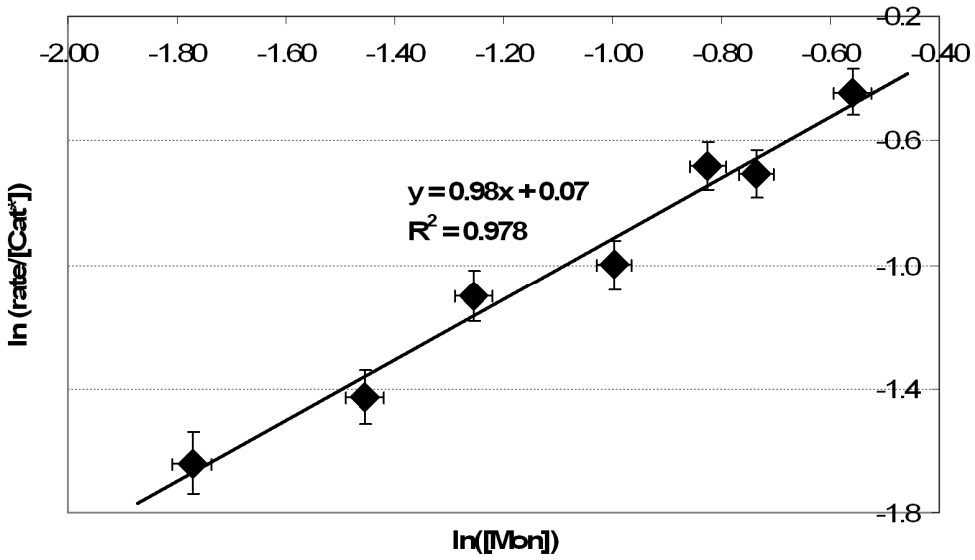

Figure S17. Determination of monomer order ($[Cp_2Y(StBu)]_2$, 3-12.5vol% DIVP, toluene, 30 °C).

Table S6. Temperature-dependent kinetics for Cp_2Y-catalyzed DEVP polymerization (1.09 mmol L^{-1} $[Cp_2Y(StBu)]_2$, 0.651 mol L^{-1} DEVP, toluene)

T /°C	TOF /h^{-1}	I^*_t /%	TOF/I^*_t /h^{-1}	Conversion at max. rate /%	rate /mol L^{-1} s^{-1}	1/T /K^{-1}	ln(k/T)
-7	3400	64	5300	34	1.02E-03	3.76E-03	-4.36
3	8950	67	13400	32	2.67E-03	3.62E-03	-3.51
13	14500	58	25000	24	4.37E-03	3.49E-03	-3.02
23	25900	54	48000	26	7.80E-03	3.38E-03	-2.38
33	44000	54	81000	28	1.33E-02	3.27E-03	-1.85
42	53000	47	110000	21	1.59E-02	3.17E-03	-1.65
52	90000	49	180000	25	2.72E-02	3.08E-03	-1.14

Table S7. Temperature-dependent kinetics for Cp_2Tb-catalyzed DEVP polymerization (1.09 mmol L^{-1} $[Cp_2Y(StBu)]_2$, 0.325 mol L^{-1} DEVP, toluene)

T /°C	TOF /h^{-1}	I^*_t /%	TOF/I^*_t /h^{-1}	Conversion at max. rate /%	rate /mol L^{-1} s^{-1}	1/T /K^{-1}	ln(k/T)
21	1640	40	4100	10	5.00E-04	3.40E-03	-4.32
33	6000	70	8570	18	1.81E-03	3.27E-03	-3.54
40	7920	61	13000	13	2.38E-03	3.19E-03	-3.21
51	12600	61	20700	12	3.78E-03	3.08E-03	-2.79
62	19600	69	28000	22	5.89E-03	2.98E-03	-2.38
71	26000	69	37700	36	7.83E-03	2.91E-03	-1.93

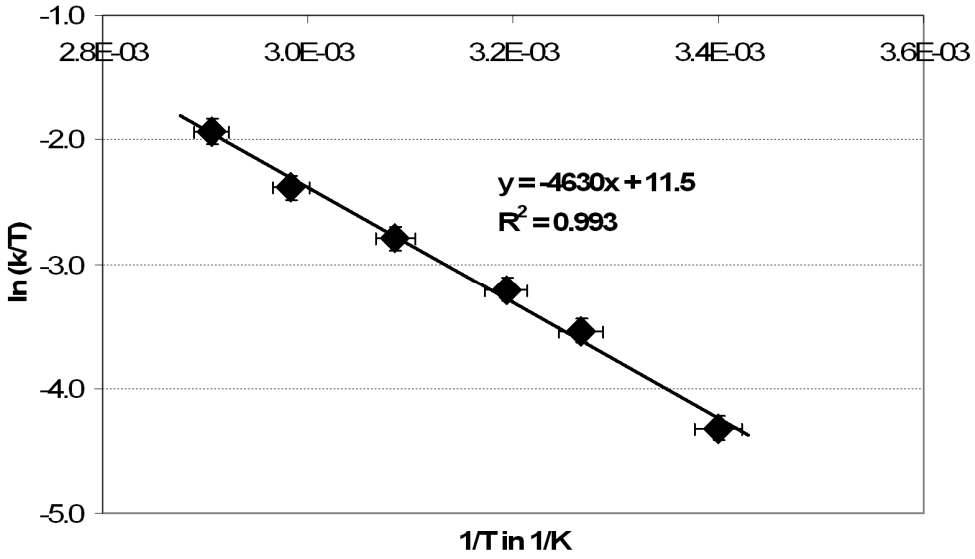

Figure S18. Eyring-plot for $[Cp_2Tb(StBu)]_2$-initiated DEVP (5vol%) polymerization in toluene (21 – 70 °C, $\Delta H^{\ddagger}$ = 38.0 kJ mol^{-1}, $\Delta S^{\ddagger}$ = -104 J $(mol\ K)^{-1}$).

Table S8. Temperature-dependent kinetics for Cp_2Tm-catalyzed DEVP polymerization (1.09 mmol L^{-1} Cp_3Tm, 0.325 mol L^{-1} DEVP, toluene)

T /°C	TOF /h^{-1}	I^*_t /%	TOF/I^*_t /h^{-1}	Conversion at max. rate /%	rate /mol L^{-1} s^{-1}	1/T /K^{-1}	ln(k/T)
-1	730	13	5600	41	2.21E-04	3.67E-03	-3.51
10	1900	15	13600	37	5.65E-04	3.53E-03	-2.82
21	4500	18	25000	34	1.34E-03	3.40E-03	-2.22
32	9000	19	47000	38	2.72E-03	3.28E-03	-1.54
42	15800	20	79000	40	4.75E-03	3.17E-03	-1.04
55	26400	26	100000	48	7.94E-03	3.05E-03	-0.68
61	51000	27	190000	39	1.53E-02	2.99E-03	-0.24

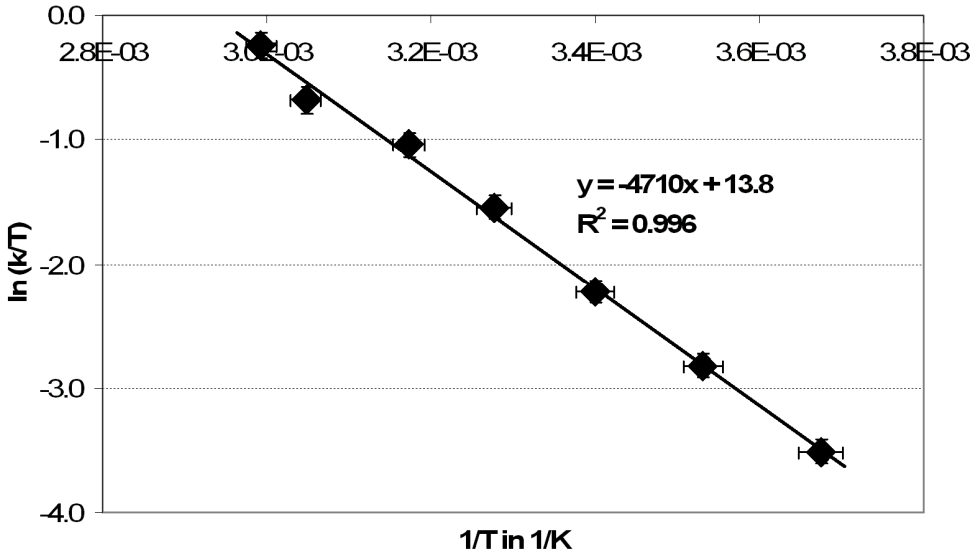

Figure S19. Eyring-plot for Cp_3Tm-initiated DEVP (5vol%) polymerization in toluene (-1 – 61 °C, $\Delta H^{\ddagger}$ = 39.1 kJ mol^{-1}, $\Delta S^{\ddagger}$ = -82.8 J $(mol\ K)^{-1}$).

Table S9. Temperature-dependent kinetics for Cp_2Lu-catalyzed DEVP polymerization (1.09 mmol L^{-1} $[Cp_2Lu(StBu)]_2$, 0.325 mol L^{-1} DEVP, toluene)

T /°C	TOF /h^{-1}	I^*_t /%	TOF/I^*_t /h^{-1}	Conversion at max. rate /%	rate /mol L^{-1} s^{-1}	1/T /K^{-1}	ln(k/T)
14	8500	15	61000	37	2.55E-03	3.48E-03	-1.33
23	16600	17	98000	29	4.99E-03	3.38E-03	-0.93
33	33000	19	165000	29	9.85E-03	3.27E-03	-0.40
43	67000	22	300000	30	2.02E-02	3.16E-03	0.16
53	84000	24	350000	49	2.53E-02	3.07E-03	0.58
63	141000	23	600000	42	4.25E-02	2.97E-03	0.98

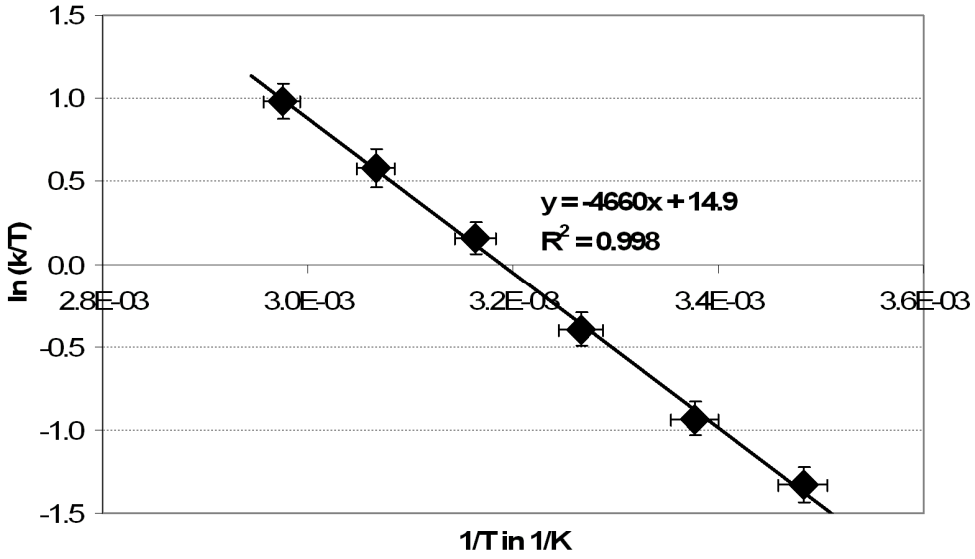

Figure S20. Eyring-plot for $[Cp_2Lu(StBu)]_2$-initiated DEVP (5vol%) polymerization in toluene (14 – 63 °C, $\Delta H^{\ddagger}$ = 38.7 kJ mol^{-1}, $\Delta S^{\ddagger}$ = -73.6 J $(mol\ K)^{-1}$).

Table S10. Temperature-dependent kinetics for Cp_2Tb-catalyzed DIVP polymerization (2.17 mmol L^{-1} $[Cp_2Y(S\textit{t}Bu)]_2$, 0.651 mol L^{-1} DIVP, toluene)

T /°C	TOF /h^{-1}	I^*_t /%	TOF/I^*_t /h^{-1}	Conversion at max. rate /%	rate /mol L^{-1} s^{-1}	1/T /K^{-1}	ln(k/T)
24	120	44	270	2.0	7.23E-05	3.37E-03	-7.83
31	250	62	400	2.7	1.49E-04	3.29E-03	-7.46
40	400	58	690	2.1	2.44E-04	3.19E-03	-6.94
47	500	52	960	2.5	3.01E-04	3.12E-03	-6.64
58	880	54	1630	2.8	5.29E-04	3.02E-03	-6.14
67	1380	54	2560	3.9	8.35E-04	2.94E-03	-5.70

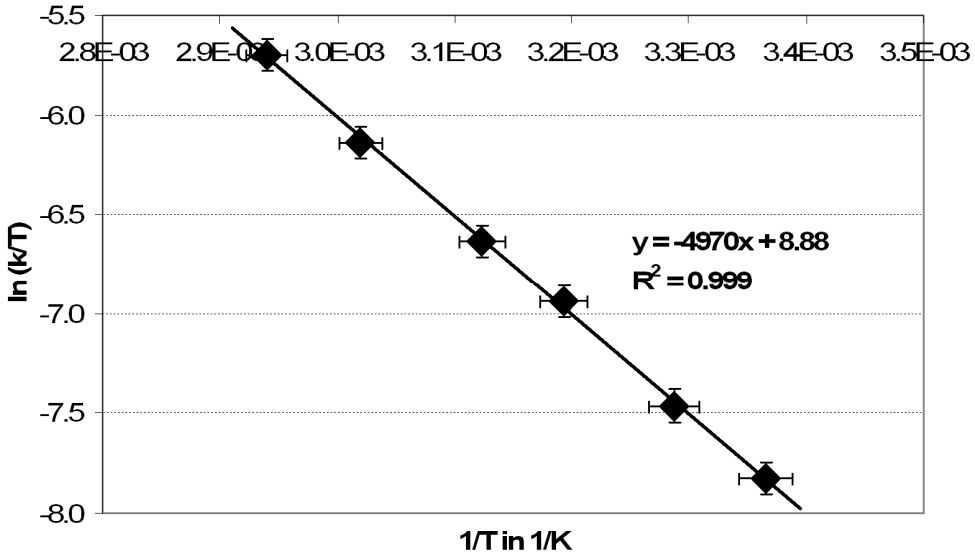

Figure S21. Eyring-plot for $[Cp_2Tb(S\textit{t}Bu)]_2$-initiated DIVP (12.5vol%) polymerization in toluene (23 – 67 °C, $\Delta H^{\ddagger}$ = 41.3 kJ mol^{-1}, $\Delta S^{\ddagger}$ = -124 J $(mol\ K)^{-1}$).

Table S11. Temperature-dependent kinetics for Cp_2Y-catalyzed DIVP polymerization (2.17 mmol L^{-1} $[Cp_2Y(StBu)]_2$, 0.651 mol L^{-1} DIVP, toluene)

T /°C	TOF /h^{-1}	I^*_t /%	TOF/I^*_t /h^{-1}	Conversion at max. rate /%	rate /mol L^{-1} s^{-1}	1/T /K^{-1}	ln(k/T)
10	350	65	530	9.9	2.09E-04	3.53E-03	-7.02
21	760	67	1130	8.2	4.59E-04	3.40E-03	-6.32
30	1460	71	2060	8.0	8.79E-04	3.30E-03	-5.76
41	2460	71	3460	9.4	1.48E-03	3.18E-03	-5.26
50	3530	73	4840	8.5	2.13E-03	3.09E-03	-4.96
59	5600	74	7570	11.9	3.36E-03	3.01E-03	-4.51
69	10600	74	14300	11.8	6.37E-03	2.92E-03	-3.90

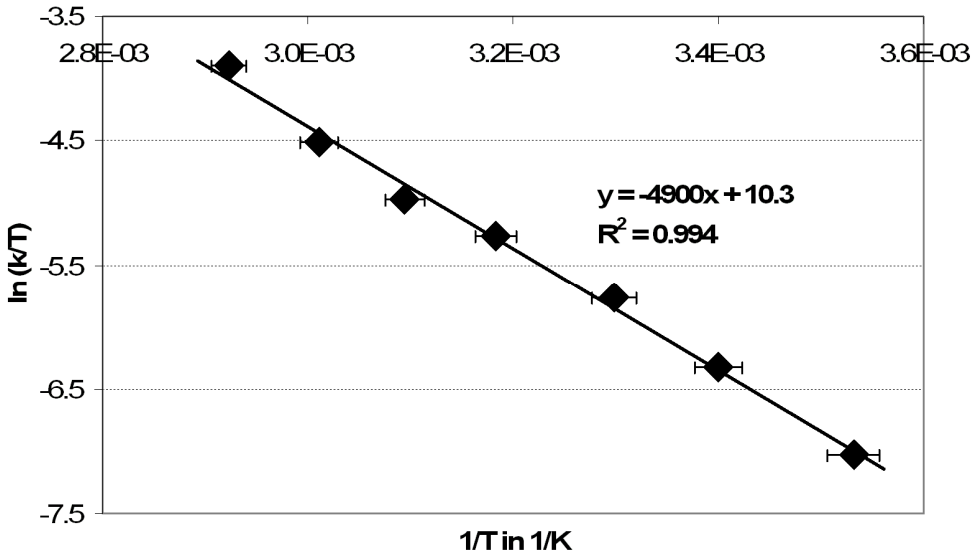

Figure S22. Eyring-plot for $[Cp_2Y(StBu)]_2$-initiated DIVP (12.5vol%) polymerization in toluene (10 – 69 °C, $\Delta H^{\ddagger}$ = 40.7 kJ mol^{-1}, $\Delta S^{\ddagger}$ = -112 J $(mol\ K)^{-1}$).

Table S12. Temperature-dependent kinetics for Cp_2Lu-catalyzed DIVP polymerization (1.09 mmol L^{-1} $[Cp_2Y(StBu)]_2$, 0.325 mol L^{-1} DIVP, toluene)

T /°C	TOF /h^{-1}	I^*_t /%	TOF/I^*_t /h^{-1}	Conversion at max. rate /%	rate /mol L^{-1} s^{-1}	1/T /K^{-1}	ln(k/T)
11	350	57	610	28	1.05E-04	3.52E-03	-5.97
21	560	46	1220	24	1.69E-04	3.40E-03	-5.38
32	2000	86	2330	25	6.01E-04	3.28E-03	-4.75
42	3100	65	4770	23	9.46E-04	3.17E-03	-4.08
51	4500	70	6430	23	1.34E-03	3.08E-03	-3.83
59	8400	89	9400	23	2.54E-03	3.01E-03	-3.46
70	14800	82	18000	21	4.45E-03	2.91E-03	-2.87

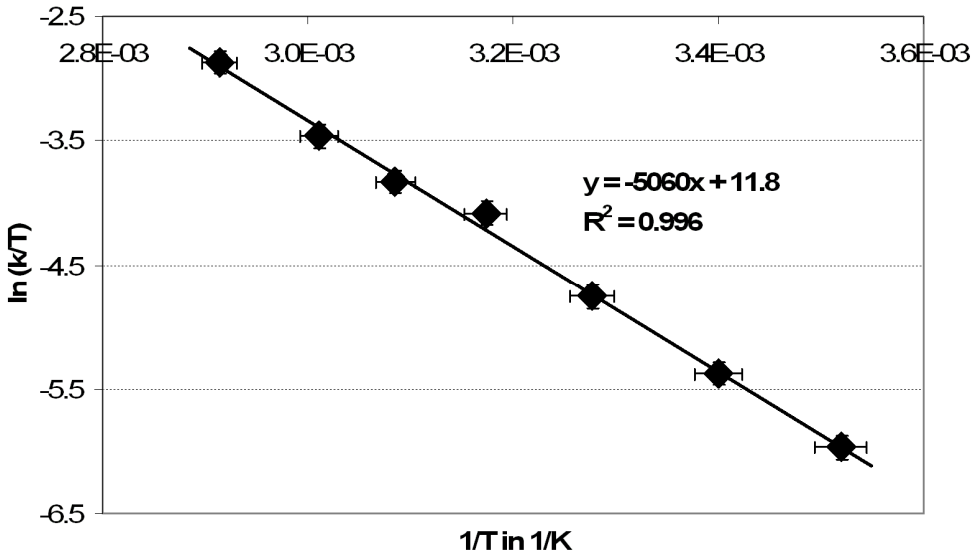

Figure S23. Eyring-plot for $[Cp_2Lu(StBu)]_2$-initiated DIVP (6.25vol%) polymerization in toluene (11 – 70 °C, $\Delta H^{\ddagger}$ = 42.0 kJ mol^{-1}, $\Delta S^{\ddagger}$ = -99.1 J $(mol\ K)^{-1}$).

References:

(1) APEX suite of crystallographic software. APEX 2 Version 2008.4. Bruker AXS Inc., Madison, Wisconsin, USA (2008).
(2) SAINT, Version 7.56a and SADABS Version 2008/1. Bruker AXS Inc., Madison, Wisconsin, USA (2008).
(3) Altomare, A.; Cascarano, G.; Giacovazzo, C.; Guagliardi, A.; Burla, M. C.; Polidori, G.; Camalli M. "**SIR92**", *J. Appl. Cryst.* **1994**, *27*, 435-436.
(4) International Tables for Crystallography, Vol. C, Tables 6.1.1.4 (pp. 500-502), 4.2.6.8 (pp. 219-222), and 4.2.4.2 (pp. 193-199), Wilson, A. J. C., Ed., Kluwer Academic Publishers, Dordrecht, The Netherlands, 1992.
(5) Sheldrick, G. M. "**SHELXL-97**", University of Göttingen, Göttingen, Germany, (1998).
(6) Spek, A. L. "**PLATON**", A Multipurpose Crystallographic Tool, Utrecht University, Utrecht, The Netherlands, (2010).
(7) L. J. Farrugia, "**WinGX** (Version 1.70.01 January 2005) ", *J. Appl. Cryst.* **1999**, *32*, 837-838.

4.3 C–H Bond Activation by σ-Bond Metathesis as a Versatile Route toward Highly Efficient Initiators for the Catalytic Precision Polymerization of Polar Monomers

Status: Published online: January 29, 2015

Journal: Organometallics

Volume 34, issue 11, pages 2703–2706

Publisher: American Chemical Society

Article Type: Note

DOI: 10.1021/om501173r

Authors: Benedikt S. Soller, Stephan Salzinger, Christian Jandl, Alexander Pöthig, and Bernhard Rieger

4.3.1 Abstract

Within the scope of this chapter it will be shown that the synthesis of RE conjugated enolate-type initiating ligands via protonolysis of classical α-C–H-acidic substrates is not a suitable preparative method due to decomposition and other side reactions. However, the σ-bond metathesis reaction of RE hydrocarbyls (–CH_2TMS) and *sym*-collidine was found to proceed rapidly (depending on the used RE metal center), gives stable metallocene derivatives, and established a route towards highly efficient and versatile initiators for the REM-GTP of vinylphosphonates. Accordingly, 2,4,6-trimethylpyridyl bis(cyclopentadienyl) RE metal complexes exhibit unprecedented initiation rates for RE metal-mediated dialkyl vinylphosphonate polymerization and facilitate an efficient initiation for a broad scope of Michael acceptor-type monomers. The high initiator efficiencies and activities are attributed to a mechanistic match between the initiation and propagation reaction mechanism and an obtained crystal structure of $(C_5H_5)_2Y(CH_2(C_5H_2Me_2N))$ indicates a partly conjugated system for the activated methylene group.

The first author Benedikt S. Soller was supported by second author Stephan Salzinger in performing and interpreting the experimental results, and the crystallographers Christian Jandl and Alexander Pöthig helped completing the complex characterization.

ORGANOMETALLICS

Note

pubs.acs.org/Organometallics

C–H Bond Activation by σ-Bond Metathesis as a Versatile Route toward Highly Efficient Initiators for the Catalytic Precision Polymerization of Polar Monomers

Benedikt S. Soller, Stephan Salzinger, Christian Jandl, Alexander Pöthig, and Bernhard Rieger*

WACKER-Lehrstuhl für Makromolekulare Chemie, Technische Universität München, Lichtenbergstraße 4, 85748 Garching bei München, Germany

Supporting Information

ABSTRACT: Rare earth metals show high activities toward C–H bond activation of heteroaromatic substrates and even methane. In this work, we demonstrate the suitability of this synthetic approach to rare earth metallocenes and show the applicability of the resulting complexes as highly efficient initiators for rare earth metal-mediated group transfer polymerization. Bis(cyclopentadienyl)(4,6-dimethylpyridin-2-yl)methyl lanthanide complexes exhibit unprecedented initiation rates for rare earth metal-mediated dialkyl vinylphosphonate polymerization and facilitate an efficient initiation for a broad scope of Michael acceptor-type monomers.

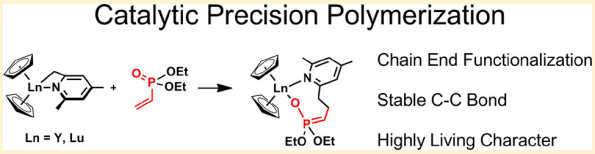

Since the first reports on living polymerizations of acrylic monomers using early transition metal initiators by Collins, Ward,[1] and Yasuda et al.[2] in 1992, researchers have devoted their efforts in the optimization of reaction conditions and initiator efficiency and the extension of this method to a variety of (meth)acrylates and (meth)acrylamides.[3] With respect to the propagation mechanism, this type of polymerization is recognized as coordinative-anionic or coordination–addition polymerization, and due to its similarity to silyl ketene acetal-initiated group transfer polymerization, it is also referred to as transition metal-mediated GTP.[3d,4] Rare earth metal-mediated group transfer polymerization (REM-GTP) is of particular interest, as recent publications have shown that its applicability is not limited to common acrylic monomers, but also facilitates the polymerization of several other monomer classes, i.e., dialkyl vinylphosphonates (DAVP), 2-isopropylene-2-oxazoline (IPOx), and 2-vinylpyridine (2VP).[4b,5] Moreover, our group reported on the development of a surface-initiated group transfer polymerization (SI-GTP) mediated by rare earth metal catalysts allowing the perfect decoration of substrates with polymer brushes of specific functionality.[6] Recently, the modification of silicon nanoparticles to form thermoresponsive and photoluminescent hybrid materials using SI-GTP was published.[7]

The applicability of REM-GTP to new monomers enables the precise synthesis of tailor-made functional materials, as this polymerization method combines the advantages of both living ionic and coordinative polymerizations. According to its highly living character, REM-GTP leads to strictly linear polymers with very narrow molecular weight distribution (PDI < 1.1), exhibits a linear increase of the average molar mass upon monomer conversion, and allows the synthesis of block copolymers as well as the introduction of chain end functionalities.[3] The coordination of the growing chain end at the catalyst suppresses side reactions and allows stereospecific polymerization as well as activity optimization by variation of both the metal center and the catalyst ligand sphere.[3,4b]

REM-GTP initiation usually proceeds via nucleophilic transfer of a strongly basic ligand, e.g., hydride, methyl, or CH_2TMS, to a coordinated monomer (Scheme 1a; this is not the case for divalent rare earth metal centers, for which redox initiation occurs).[3d,8]

Accordingly, for zirconocene systems, a variety of strategies for the synthesis of enolate initiators, which follow a faster initiation mechanism over an eight-electron process (Scheme 1b), has been presented.[3d,9] Surprisingly, only little effort was devoted to the development of new initiating species for rare

Scheme 1. Possible Initiation Reactions for REM-GTP of DAVP: Nucleophilic Transfer via a (a) 6e⁻ or (b) 8e⁻ Process and (c) Deprotonation of the Acidic α-CH

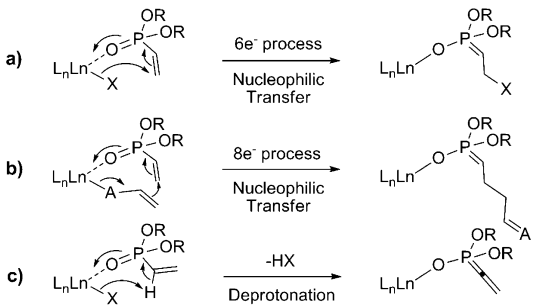

Special Issue: Mike Lappert Memorial Issue

Received: November 20, 2014
Published: January 29, 2015

DOI: 10.1021/om501173r
Organometallics 2015, 34, 2703–2706

earth metal-based catalysts, which would in turn allow the introduction of novel chain end functionalities.

In previous work, we have shown that late lanthanide metallocenes are highly active catalysts for DAVP polymerization.[5c] However, in detailed mechanistic studies we found that the traditionally used strongly basic methyl and CH_2TMS initiators lead to an inefficient, slow initiation by deprotonation of the acidic α-CH (Scheme 1c).[10] Other initiating groups, such as sterically crowded Cp_3Ln complexes and thiolato complexes $[Cp_2Ln(StBu)]_2$, were found to efficiently initiate DAVP polymerization; however, further development of Cp_3Ln complexes is limited and thiolate end groups were found to be prone to elimination.[10] Moreover, these complexes are not suitable initiators for sterically less demanding or weaker coordinating monomers such as IPOx or 2VP.[5f,10]

Accordingly, the development of new initiators for REM-GTP, which facilitate an efficient initiation for a broad scope of monomers and which lead to a stable end group functionalization via a C−C bond, is still of current interest. Inspired by the use of enolate-type initiators in zirconium-mediated GTP, our group focused on the development of enolate or enamide initiators (Scheme 2) in order to facilitate an initiation over an eight-electron process. Such initiators simulate the active propagating species and bypass the ineffective initiation step starting from the alkyl initiator.

Scheme 2. Attempted Synthesis of Enolate and Enamide Rare Earth Metallocene Initiators via Deprotonation of Classical α-CH-Acidic Substrates

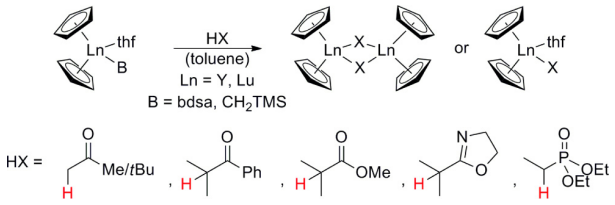

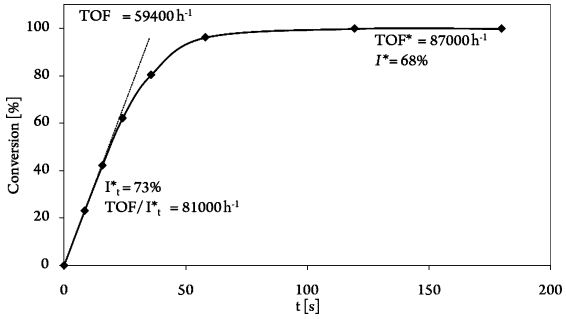

Figure 1. Conversion-reaction time plot for the polymerization of DEVP using $Cp_2Y(CH_2(C_5H_2Me_2N))$ (7.4 mg catalyst, 10 vol % DEVP in 20 mL of toluene, 30 °C).

As synthetic routes via salt metathesis from lithium enolates and rare earth metal chlorides and via thermolysis of alkyl complexes in the presence of tetrahydrofuran are restricted to selected systems only,[11] we decided to investigate the accessibility of rare earth enolates via α-CH-deprotonation of the respective carbonyls (or oxazoline/phosphonate) by amide and alkyl precursors $Cp_2Ln(bdsa)(thf)$ and $Cp_2Ln(CH_2TMS)$-

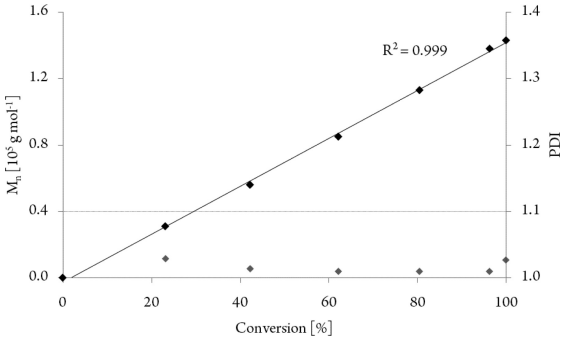

Figure 2. Linear increase of the number-averaged molecular weight during DEVP polymerization using $Cp_2Y(CH_2(C_5H_2Me_2N))$ and corresponding polydispersity (7.4 mg catalyst, 10 vol % DEVP in 20 mL of toluene, 30 °C).

(thf) (bdsa = bis(dimethylsilylamide, $N(SiMe_2H)_2$). We first evaluated the reaction between $Cp_2Ln(bdsa)(thf)$ and acetone resulting in the quantitative formation of $Cp_2Ln(N(SiMe_2OiPr)(SiMe_2H))$ by hydrosilylation of the carbonyl moiety.

Surprisingly, the more reactive $Cp_2Ln(CH_2TMS)(thf)$ precursor leads to no reaction with a large variety of substrates up to elevated reaction temperatures, at which decomposition was observed, revealing a pronounced kinetic limitation for the protonolysis reaction. Only with isobutyrophenone the formation of the corresponding alkoxide from the nucleophilic attack of the alkyl ligand was observed.

Despite numerous attempts and the use of different precursor complexes and substrates, the formation of enolate rare earth complexes by protonolysis of classical α-CH-acidic substrates could not be facilitated. This is in agreement with literature results, where full conversions for alkyl ligands were observed in NMR-scale reaction, but only low yields of the corresponding enolate were achieved, due to the formation of side products.[11,12] A similar approach to functionalize rare earth metal alkyl complexes is to use the high activity of group 3 elements for σ-bond metathesis.[13] The C−H activation of pyridines[14] and other heteronuclear[15] and also internal alkynes[16] was well studied by Teuben et al. Recently, Mashima et al. reported on the introduction of chain end functionality for 2VP polymerization by initial C−H bond activation of nonclassical CH-acidic substrates via alkyllyttrium-mediated σ-bond metathesis.[5d,17] In order to evaluate the applicability of this approach to rare earth metallocenes, we reacted $Cp_2Y(CH_2TMS)(thf)$ with 2,4,6-trimethylpyridine in toluene solution, yielding the desired $Cp_2Y(CH_2(C_5H_2Me_2N))$ after stirring at room temperature for 30 min (Scheme 3).

The synthesis of $Cp_2Y(CH_2(C_5H_2Me_2N))$ from $Cp_2YCH_2TMS(thf)$ and sym-collidine is quantitative within 30 min, and no difference in activity or molecular weight for the polymerization of DEVP was observed for the isolated complex or an *in situ* generated catalyst (see Figure S1). Interestingly, σ-bond metathesis and synthesis of the smaller lutetium cation was not nearly as active as for the larger yttrium analogon. $Cp_2Lu(CH_2(C_5H_2Me_2N))$ had to be stirred overnight for complete conversion and was recrystallized for purification. Therefore, an *in situ* activation is possible only for $Cp_2Y(CH_2(C_5H_2Me_2N))$.

The (4,6-dimethylpyridin-2-yl)methyl ligand can coordinate to the metal center in the form of both a carbanion and an

DOI: 10.1021/om501173r
Organometallics 2015, 34, 2703−2706

Table 1. Comparison of $Cp_2Ln(CH_2(C_5H_2Me_2N))$ Initiators for the REM-GTP of DEVP and IPOx (Toluene, 30 °C)[5f,10]

catalyst	monomer	$[Mon]_0/[Cat]_0$	init. period[a]	M_n[b] [kDa]	PDI[b]	I^*_t[b] [%]	I^*[b] [%]	TOF[c] [h^{-1}]	TOF/I^*_t [h^{-1}]
$Cp_2Y(CH_2(C_5H_2Me_2N))$	DEVP	600	–	140	1.02	73	68	59 400	81 000
$[Cp_2Y(StBu)]_2$	DEVP	600	5 s	150	1.18	46	65	44 000	96 000
$Cp_2Lu(CH_2(C_5H_2Me_2N))$	DEVP	600	–	480	1.13	16	21	46 000	300 000
$[Cp_2Lu(StBu)]_2$	DEVP	600	15 s	210	1.27	35	47	103 000	290 000
$[Cp_2YbMe]_2$	DEVP	600	80 s	910	1.52	54	11	4300	8000
$Cp_2Y(CH_2(C_5H_2Me_2N))$	IPOx	200	–[d]	20	1.26	–[d]	89	–[d]	–[d]
$Cp_2Lu(CH_2(C_5H_2Me_2N))$	IPOx	200	–[d]	38	1.39	–[d]	59	–[d]	–[d]
$[Cp_2YbMe]_2$	IPOx	200	–	21	1.04	–[e]	95	380	–[e]

[a]Initiation period, reaction time until 3% conversion is reached. [b]Determined by GPC-MALS, $I^*_t = M_{th}/M_n$, $M_{th} = [Mon]_0/[Cat]_0 \times M_{Mon} \times$ conversion (I^*_t at the maximum rate, I^* at the end of the reaction). [c]Determined by ^{31}P (DEVP) or ^1H (IPOx) NMR spectroscopic measurement. [d]Not determined due to incomplete conversion (Yield = 80% (Y), 75% (Lu)). [e]Not determined.

Scheme 3. Synthesis of $Cp_2Ln(CH_2(C_5H_2Me_2N))$ via C−H Bond Activation by σ-Bond Metathesis

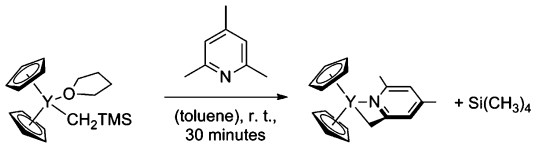

enamide (Figure 4). Accordingly, initiation of DAVP polymerization could occur via all three routes presented in Scheme 1. ESI-MS analysis of produced DEVP oligomers shows a chain end functionalization by (4,6-dimethylpyridin-2-yl)methyl and does not provide any evidence for initial deprotonation (Scheme 1, Figure S5), which is in accordance with the observed high initiation rates. The crystal structure of $Cp_2Y(CH_2(C_5H_2Me_2N))$ (Figure 3) shows the formation of

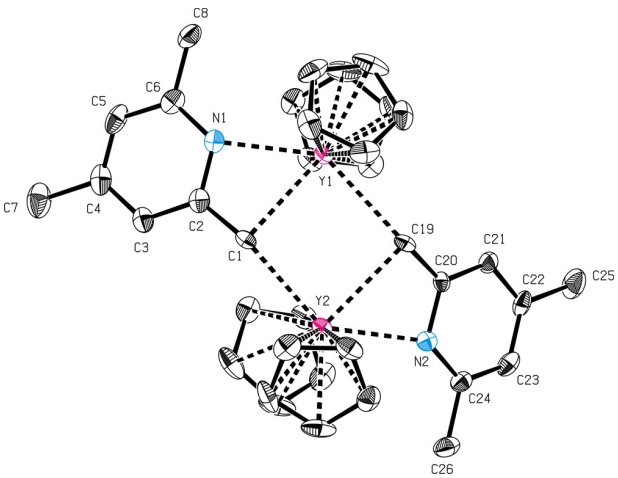

Figure 3. ORTEP drawing of $Cp_2Y(CH_2(C_5H_2Me_2N))$ with 50% ellipsoids. All H atoms have been omitted for clarity. Selected bond distances (Å) and angles (deg): C1—C2, 1.456(5); C6—C8, 1.504(5); Y1—C1, 2.641(4); Y1—C1—C2, 87.2(2); N1—C2—C1, 115.1(3).

dimers and indicates a partial double bond character of the C1−C2 bond (1.456(5) Å) compared to the nonactivated C6−C8 methyl group (1.504(5) Å). This is in agreement with crystal structure data of similar ortho-alkylpyridines.[18] From experimental data, initiation by nucleophilic transfer is evident; whether it proceeds via a six- or eight-electron process may be revealed only by theoretical calculations.

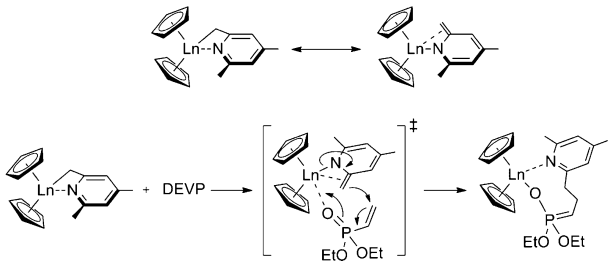

Figure 4. Coordination of the heteroaromatic initiator to the metal as carbanion or enamide and proposed eight-membered-ring transition state for the initiation of DEVP.

In order to verify the suitability of these complexes as initiators for REM-GTP, we carried out polymerization experiments with diethyl vinylphosphonate (DEVP). Hereby, for the first time using a Cp_2LnX initiator, polymerization of DEVP could be facilitated without observation of an initiation period (Figure 1, Table 1). Kinetic measurements revealed a linear increase of the number-averaged molecular weight upon conversion, narrow polydispersity throughout the whole reaction, and activities comparable to those observed for the corresponding thiolato complexes (Figure 2, Table 1).[10] In contrast to the previously applied thiolato complexes, the initiator efficiency of the yttrium complex remains constant throughout the whole polymerization (Figure 1), indicating the initiator efficiency of 68% to be mainly a result of an initial deactivation by impurities (e.g., water). Whereas thiolates are not stable and eliminate during vinylphosphonate polymerization, (4,6-dimethylpyridin-2-yl)methyl initiators form a stable C−C bond. The stable end group is important to prevent unwanted side reactions from olefinic chain ends and opens up new approaches for polymeric surface modifications. The formed dimer of $Cp_2Y(CH_2(C_5H_2Me_2N))$ does not hamper the initiation and facilitates the propagation with a high initiator efficiency. In the case of the lutetium compound a significant drop of I^* is observed. This is attributed to a more stable dimer and the general high polymerization activity. In such cases, the propagation rate surpasses the dissolving of the dimer by coordination and fewer complexes initiate. For thiolato compounds dimers prevent the coordination of IPOx or 2VP completely and no polymerization occurs. Moreover, (4,6-dimethylpyridin-2-yl)methyl complexes initiate the polymerization of not only vinyl phosphonates but also IPOx, even though only materials with rather broad polydispersity could be obtained, indicating a slow and nonuniform initiation (Table 1). Nevertheless, the described complexes are the first systems

DOI: 10.1021/om501173r
Organometallics 2015, 34, 2703−2706

exhibiting high initiator efficiencies for both DAVP and IPOx polymerization.

In conclusion, we have shown that σ-bond metathesis gives highly efficient initiators for REM-GTP via C–H bond activation of 2,4,6-trimethylpyridine. The rate of the σ-bond metathesis depends heavily on the size of the used metal, and in the case of yttrium also the *in situ* preparation of (4,6-dimethylpyridin-2-yl)methyl initiators is possible. The obtained catalysts show high activities and no initiation period. Accordingly, the molecular weight of PDEVP increases linearly with monomer conversion and the polydispersity remains remarkably narrow. We attribute the living character to a mechanistic match between initiation and propagation, both following an eight-electron process. Further studies to apply initiators from C–H activation to new catalysts for a stereospecific polymerization of polar monomers are currently under way.

■ ASSOCIATED CONTENT

Supporting Information

Detailed procedures for complex synthesis, polymerizations, and oligomerization reactions and detailed information for single-crystal X-ray structure determination (CCDC No. 1031228). This material is available free of charge via the Internet at http://pubs.acs.org.

■ AUTHOR INFORMATION

Corresponding Author

*E-mail: rieger@tum.de.

Notes

The authors declare no competing financial interest.

■ ACKNOWLEDGMENTS

The authors thank Peter T. Altenbuchner and Alexander Kronast for valuable discussions. S.S. is grateful for a generous scholarship from the Fonds der Chemischen Industrie.

■ REFERENCES

(1) Collins, S.; Ward, D. G. *J. Am. Chem. Soc.* **1992**, *114*, 5460–5462.
(2) Yasuda, H.; Yamamoto, H.; Yokota, K.; Miyake, S.; Nakamura, A. *J. Am. Chem. Soc.* **1992**, *114*, 4908–4910.
(3) (a) Yasuda, H.; Ihara, E. *Macromol. Chem. Phys.* **1995**, *196*, 2417–2441. (b) Yasuda, H.; Ihara, E. *Adv. Polym. Sci.* **1997**, *133*, 53–101. (c) Yasuda, H. *Prog. Polym. Sci.* **2000**, *25*, 573–626. (d) Chen, E. Y. X. *Chem. Rev.* **2009**, *109*, 5157–5214.
(4) (a) Webster, O. *Adv. Polym. Sci.* **2004**, *167*, 1–34. (b) Salzinger, S.; Rieger, B. *Macromol. Rapid Commun.* **2012**, *33*, 1327–1345.
(5) (a) Seemann, U. B.; Dengler, J. E.; Rieger, B. *Angew. Chem.* **2010**, *122*, 3567–3569. (b) Rabe, G. W.; Komber, H.; Häussler, L.; Kreger, K.; Lattermann, G. *Macromolecules* **2010**, *43*, 1178–1181. (c) Salzinger, S.; Seemann, U. B.; Plikhta, A.; Rieger, B. *Macromolecules* **2011**, *44*, 5920–5927. (d) Kaneko, H.; Nagae, H.; Tsurugi, H.; Mashima, K. *J. Am. Chem. Soc.* **2011**, *133*, 19626–19629. (e) Zhang, N.; Salzinger, S.; Rieger, B. *Macromolecules* **2012**, *45*, 9751–9758. (f) Zhang, N.; Salzinger, S.; Soller, B. S.; Rieger, B. *J. Am. Chem. Soc.* **2013**, *135*, 8810–8813. (g) Altenbuchner, P. T.; Soller, B. S.; Kissling, S.; Bachmann, T.; Kronast, A.; Vagin, S. I.; Rieger, B. *Macromolecules* **2014**, *47*, 7742–7749.
(6) (a) Zhang, N.; Salzinger, S.; Deubel, F.; Jordan, R.; Rieger, B. *J. Am. Chem. Soc.* **2012**, *134*, 7333–7336. (b) Yang, J.; Liang, Y.; Salzinger, S.; Zhang, N.; Dong, D.; Rieger, B. *J. Polym. Sci., Part A: Polym. Chem.* **2014**, *52*, 2919–2925.
(7) Kehrle, J.; Höhlein, I. M. D.; Yang, Z.; Jochem, A.-R.; Helbich, T.; Kraus, T.; Veinot, J. G. C.; Rieger, B. *Angew. Chem.* **2014**, *126*, 12702–12705.
(8) (a) Boffa, L. S.; Novak, B. M. *Macromolecules* **1994**, *27*, 6993–6995. (b) Boffa, L. S.; Novak, B. M. *Tetrahedron* **1997**, *53*, 15367–15396. (c) Soller, B. S.; Zhang, N.; Rieger, B. *Macromol. Chem. Phys.* **2014**, *215*, 1946–1962.
(9) (a) Mariott, W. R.; Chen, E. Y. X. *Macromolecules* **2004**, *37*, 4741–4743. (b) Mariott, W. R.; Chen, E. Y. X. *Macromolecules* **2005**, *38*, 6822–6832. (c) Rodriguez-Delgado, A.; Chen, E. Y. X. *Macromolecules* **2005**, *38*, 2587–2594. (d) Li, Y.; Ward, D. G.; Reddy, S. S.; Collins, S. *Macromolecules* **1997**, *30*, 1875–1883. (e) Nguyen, H.; Jarvis, A. P.; Lesley, M. J. G.; Kelly, W. M.; Reddy, S. S.; Taylor, N. J.; Collins, S. *Macromolecules* **2000**, *33*, 1508–1510.
(10) Salzinger, S.; Soller, B. S.; Plikhta, A.; Seemann, U. B.; Herdtweck, E.; Rieger, B. *J. Am. Chem. Soc.* **2013**, *135*, 13030–13040.
(11) Evans, W. J.; Dominguez, R.; Hanusa, T. P. *Organometallics* **1986**, *5*, 1291–1296.
(12) (a) Nakajima, Y.; Okuda, J. *Organometallics* **2007**, *26*, 1270–1278. (b) Heeres, H. J.; Maters, M.; Teuben, J. H.; Helgesson, G.; Jagner, S. *Organometallics* **1992**, *11*, 350–356.
(13) (a) Watson, P. L. *J. Am. Chem. Soc.* **1983**, *105*, 6491–6493. (b) Watson, P. L. *J. Chem. Soc., Chem. Commun.* **1983**, 276–277. (c) Waterman, R. *Organometallics* **2013**, *32*, 7249–7263.
(14) (a) Duchateau, R.; van Wee, C. T.; Teuben, J. H. *Organometallics* **1996**, *15*, 2291–2302. (b) Duchateau, R.; Brussee, E. A. C.; Meetsma, A.; Teuben, J. H. *Organometallics* **1997**, *16*, 5506–5516.
(15) (a) Deelman, B.-J.; Booij, M.; Meetsma, A.; Teuben, J. H.; Kooijman, H.; Spek, A. L. *Organometallics* **1995**, *14*, 2306–2317. (b) Ringelberg, S. N.; Meetsma, A.; Troyanov, S. I.; Hessen, B.; Teuben, J. H. *Organometallics* **2002**, *21*, 1759–1765.
(16) Quiroga Norambuena, V. F.; Heeres, A.; Heeres, H. J.; Meetsma, A.; Teuben, J. H.; Hessen, B. *Organometallics* **2008**, *27*, 5672–5683.
(17) Thompson, M. E.; Baxter, S. M.; Bulls, A. R.; Burger, B. J.; Nolan, M. C.; Santarsiero, B. D.; Schaefer, W. P.; Bercaw, J. E. *J. Am. Chem. Soc.* **1987**, *109*, 203–219.
(18) Guan, B.-T.; Wang, B.; Nishiura, M.; Hou, Z. *Angew. Chem., Int. Ed.* **2013**, *52*, 4418–4421.

DOI: 10.1021/om501173r
Organometallics 2015, 34, 2703–2706

Supporting Information:

C–H Bond Activation by σ-Bond Metathesis as a Versatile Route towards Highly Efficient Initiators for the Catalytic Precision Polymerization of Polar Monomers

*Benedikt S. Soller, Stephan Salzinger, Christian Jandl, Alexander Pöthig, Bernhard Rieger**

WACKER-Lehrstuhl für Makromolekulare Chemie, Technische Universität München, Lichtenbergstraße 4, 85748 Garching

Material and Methods

All reactions were carried out under argon atmosphere using standard Schlenk or glovebox techniques. All glassware was heat dried under vacuum prior to use. Unless otherwise stated, all chemicals were purchased from Sigma-Aldrich, Acros Organics or ABCR and used as received. Toluene, THF and pentane were dried using an MBraun SPS-800 solvent purification system. Hexane was dried over 3 Å molecular sieve. Li(bdsa),[1] the precursor complexes $Ln(bdsa)_3(thf)_2$,[1] $Ln(CH_2TMS)_3(thf)_2$,[2] $Cp_2Ln(bdsa)(thf)$[3] and $Cp_2Ln(CH_2TMS)(thf)$[3] as well as DEVP[4] were prepared according to literature procedures. Monomers were dried over calcium hydride and destilled prior to use. NMR spectra were recorded on a Bruker AVIII-300 or AV-500C spectrometer. ^1H, ^{13}C and ^{29}Si NMR spectroscopic chemical shifts δ are reported in ppm relative to tetramethylsilane. $\delta(^1H)$ is calibrated to the residual proton signal, $\delta(^{13}C)$ to the carbon signal and $\delta(^{29}Si)$ to the deuterium signal of the solvent. ^{31}P NMR spectroscopic chemical shifts are reported in ppm relative to and calibrated to 85% aqueous H_3PO_4. Deuterated solvents were obtained from Eurisotop or Sigma Aldrich and dried over 3Å molecular sieve. Elemental analyses were measured at the Laboratory for Microanalytics at the Institute of Inorganic Chemistry at the Technische Universität München. ESI MS analytical measurements were performed with methanol solutions on a Varian 500-MS spectrometer in positive ionization mode.

Complex Synthesis

General procedure for the synthesis of Cp_2LnX:

1 eq of a stem solution of XH in toluene (ca. 5 w%) is added dropwise to a toluene solution of 1 eq of $Cp_2Ln(bdsa)(thf)$ or $Cp_2Ln(CH_2TMS)(thf)$ (ca. 0.1 M) at room temperature. The resulting mixture is stirred for the stated reaction time, the solvent and formed 1,1,3,3-tetramethyldisilazane/$SiMe_4$ are removed *in vacuo.*

$Cp_2Lu(N(SiMe_2OiPr)(SiMe_2H))$: Following the general procedure, the reaction mixture was stirred over night. Yield: 190 mg white powder (0.39 mmol, quantitative). ^{1}H NMR (C_6D_6, 300 K, 500 MHz): δ = 0.08 (s, 6H, Si(O*i*Pr)(CH_3)$_2$), 0.27 (d, 6H, 3*J*(H-H) = 3.0 Hz, SiH(CH_3)$_2$), 0.73 (d, 6H, 3*J*(H-H) = 6.2 Hz, CH(CH_3)$_2$), 3.50 (sp, 1H, ^{3}*J*(H-H) = 6.2 Hz, O-C*H*(CH_3)$_2$), 4.89 (sp, 1H, ^{3}*J*(H-H) = 3.0 Hz, Si-*H*), 6.15 (s, 10H, Cp-*H*). ^{13}C NMR (C_6D_6, 300 K, 125 MHz): δ = 2.5 (s, Si(*C*H$_3$)$_2$), 3.2 (s, Si(*C*H$_3$)$_2$), 24.9 (s, CH(*C*H$_3$)$_2$), 68.7 (s, O*C*H(CH$_3$)$_2$), 111.6 (s, Cp-*C*). ^{29}Si NMR (C_6D_6, 300K, 100 MHz): δ = 24.5 (s), 45.7 (s).

$Cp_2Y(CH_2(C_5H_2Me_2N))$: Following the general procedure, the reaction mixture was stirred for 30 minutes. Yield: 320 mg yellow powder (0.9 mmol, quantitative). ^{1}H NMR (C_6D_6, 292 K, 300 MHz): δ = 1.79 (s, 3H, CH_3), 2.83 (s, 3H, CH_3), 2.44 (s, 2H, CH_2), 5.80 (s, 1H, Pyr-C*H*), 6.05 (s, 10H, Cp-*H*), 6.41 (s, 1H, Pyr-C*H*). ^{13}C NMR (C_6D_6, 298 K, 125 MHz): δ = 21.1 (s, *C*H$_3$), 23.9 (s, *C*H$_3$), 40.7 (d, *C*H$_2$, $^1J_{Y\text{-}C}$ = 12.5 Hz), 111.2 (s, Cp-*C*), 112.3 (s, Pyr-*C*H), 118.5 (s, Pyr-*C*H), 148.0 (s, Pyr-C_{qu}), 155.8 (s, Pyr-C_{qu}), 167.4 (s, Pyr-C_{qu}). Anal. Calcd for $YC_{20}H_{18}N$·0.2thf: C, 63.84; H, 6.16; N, 3.96. Found: C, 63.93; H, 6.08; N, 4.00.

$Cp_2Lu(CH_2(C_5H_2Me_2N))$: Following the general procedure, the reaction mixture was stirred over night. Yield: 174 mg yellow powder (0.4 mmol, 32 %, recrystallized from toluene/pentane). ^{1}H NMR (C_6D_6, 298 K, 300 MHz): δ = 1.74 (s, 3H, CH_3), 1.82 (s, 3H, CH_3), 2.39 (s, 2H, CH_2), 5.68 (s, 10H, Pyr-C*H*), 6.04 (s, 1H, Cp-*H*), 6.49 (s, 1H, Pyr-C*H*). ^{13}C NMR (C_6D_6, 298 K, 125 MHz): δ = 20.9 (s, *C*H$_3$), 23.7 (s, *C*H$_3$), 37.8 (s, *C*H$_2$), 110.7 (s, Cp-*C*), 114.7 (s, Pyr-*C*H), 120.2 (s, Pyr-*C*H), 149.5 (s, Pyr-C_{qu}), 156.1 (s, Pyr-C_{qu}), 168.5 (s, Pyr-C_{qu}). Anal. Calcd for $LuC_{20}H_{18}N$: C, 50.83; H, 4.74; N, 3.29. Found: C, 49.18; H, 4.86; N, 2.72.

Oligomerization

5 eq of the respective monomer are added to 1 eq of catalyst in toluene. The resulting mixture is stirred for 2 hours at room temperature and quenched by addition of MeOH. Volatiles were removed under reduced pressure and the residue is extracted with MeOH. For end group analysis, ESI-MS measurements of the methanolic extract are performed.

Activity measurements

For activity measurements, the stated amount of catalyst (15-50 μmol) is dissolved in 20mL of toluene and the reaction mixture is thermostated to the desired temperature. Then, the stated amount of DEVP (3.5-13 mmol) is added. During the course of the measurement, the temperature is monitored with a digital thermometer and aliquots (0.5 mL) are taken and quenched by addition to deuterated methanol (0.2 mL). After the stated reaction time, the reaction is quenched by addition of MeOD (0.5 mL). The reaction is carried out in an MBraun Glovebox under argon atmosphere to take aliquots every 6-10 seconds at the beginning of the measurement. For each aliquot, the conversion is determined by ^{31}P NMR spectroscopy, the molecular weight of the formed polymer by GPC-MALS analysis.

Molecular Weight Determination

GPC was carried out on a Varian LC-920 equipped with two PL Polargel columns. As eluent a mixture of 50% THF, 50% water, and 9 g L^{-1} tetrabutylammonium bromide (TBAB) was used. Absolute molecular weights have been determined online by multiangle light scattering (MALS) analysis using a Wyatt Dawn Heleos II in combination with a Wyatt Optilab rEX as concentration source.

Table S1. Polymerization results for the REM-GTP of 2VP (toluene, 30 °C)[5]

Catalyst	Monomer	$[Mon]_0/[Cat]_0$	Init. period[a]	M_n[b] [kDa]	PDI[b]	I^*_t[b] [%]	I^*[b] [%]	TOF[c] [h^{-1}]	TOF/I^*_t [h^{-1}]
$Cp_2Y(CH_2(C_5H_2Me_2N)$	2VP	100	-[e]	13	1.01	-[e]	80	-[e]	-[e]
$Cp_2Lu(CH_2(C_5H_2Me_2N)$	2VP	100	-[e]	38	1.08	-[e]	28	-[e]	-[e]
$[Cp_2YbMe]_2$	2VP	100	-[e]	14	1.01	-[e]	75	44	-[e]

[a]Initiation period, reaction time until 3% conversion is reached, [b]determined by GPC-MALS, $I^*_t = M_{th}/M_n$, $M_{th} = [Mon]_0/[Cat]_0 \times M_{Mon} \times$ conversion (I^*_t at the maximum rate, I * at the end of the reaction), [c]determined by ^{31}P (DEVP) or ^1H (IPOx) NMR spectroscopic measurement, [e]not determined.

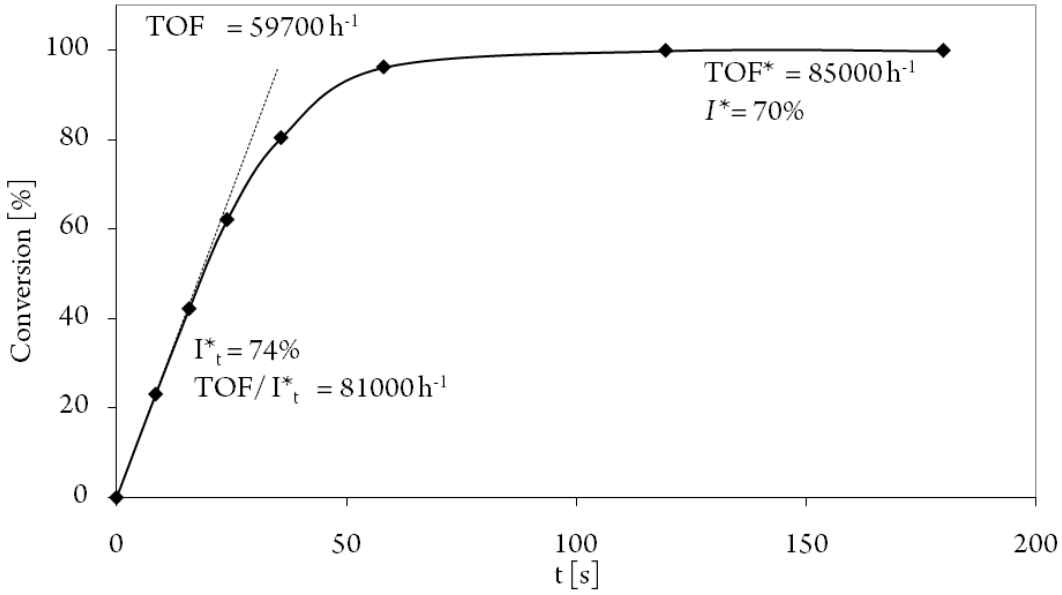

Figure S1: Conversion-reaction time plot for the polymerization of DEVP using *in situ* generated $Cp_2Y(CH_2(C_5H_2Me_2N))$, (7.4 mg catalyst, 10vol% DEVP in 20 mL toluene, 30 °C).

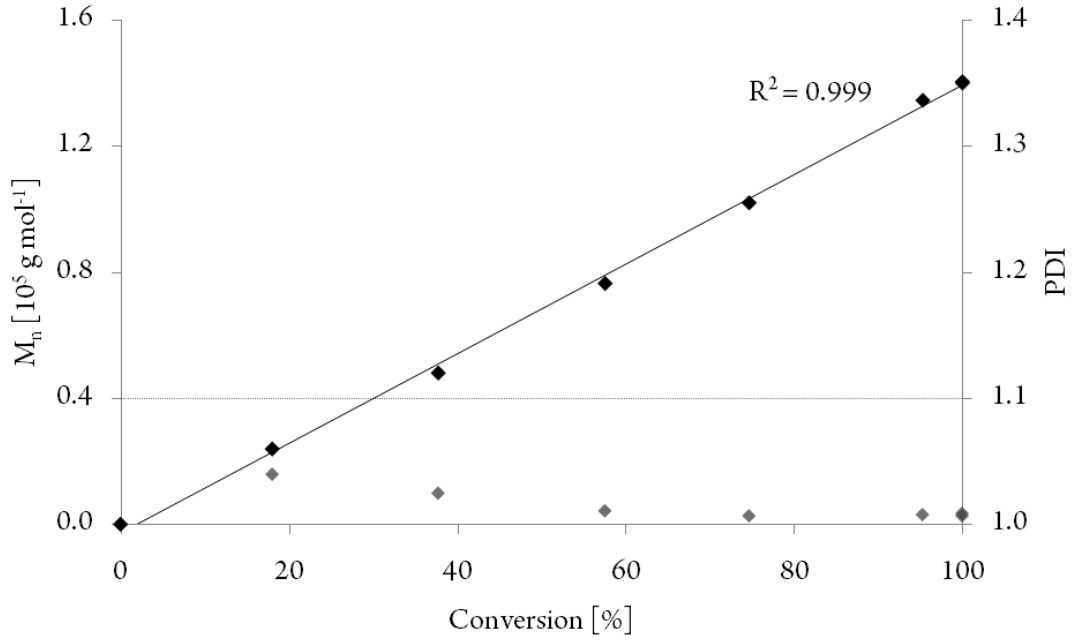

Figure S2: Conversion-reaction time plot for the polymerization of DEVP using *in situ* generated $Cp_2Y(CH_2(C_5H_2Me_2N))$, (7.4 mg catalyst, 10vol% DEVP in 20 mL toluene, 30 °C).

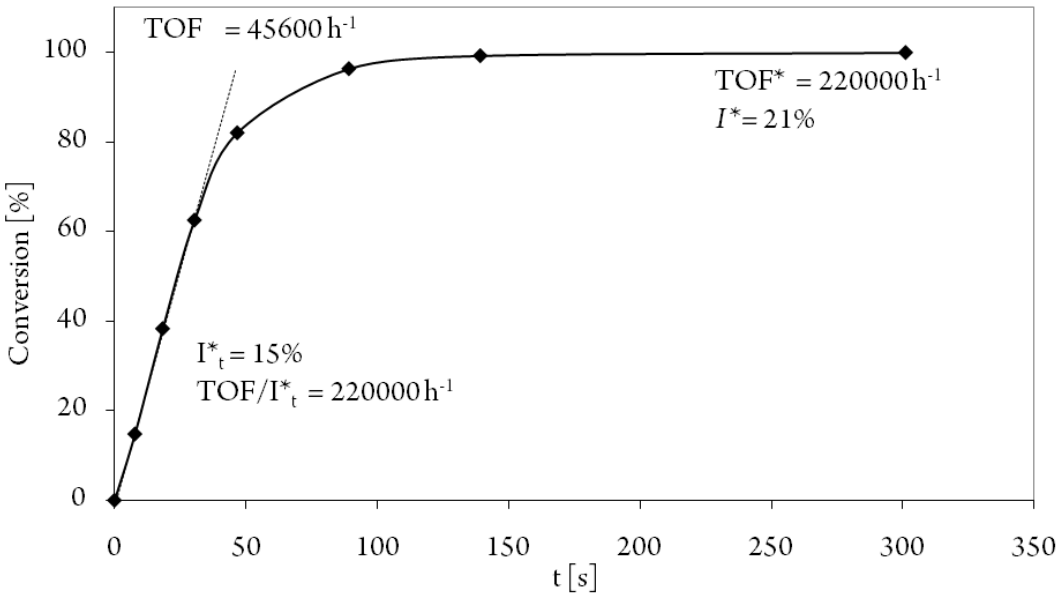

Figure S3. Conversion-reaction time plot for the polymerization of DEVP using $Cp_2Lu(CH_2(C_5H_2Me_2N))$, (9.2 mg catalyst, 10vol% DEVP in 20 mL toluene, 30 °C).

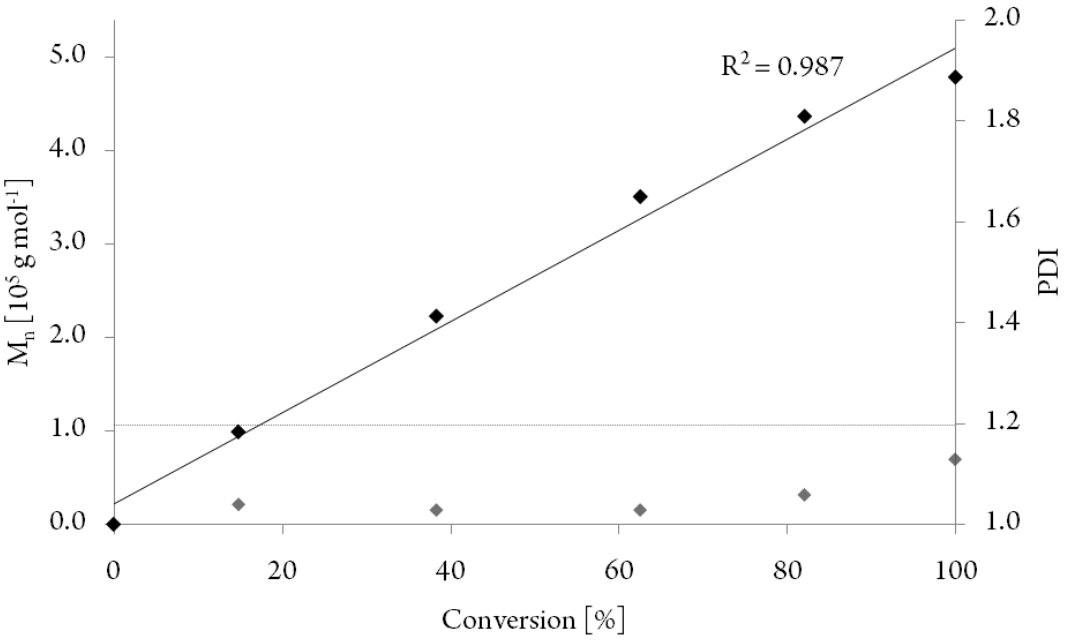

Figure S4: Conversion-reaction time plot for the polymerization of DEVP using $Cp_2Lu(CH_2(C_5H_2Me_2N))$, (9.2 mg catalyst, 10vol% DEVP in 20 mL toluene, 30 °C).

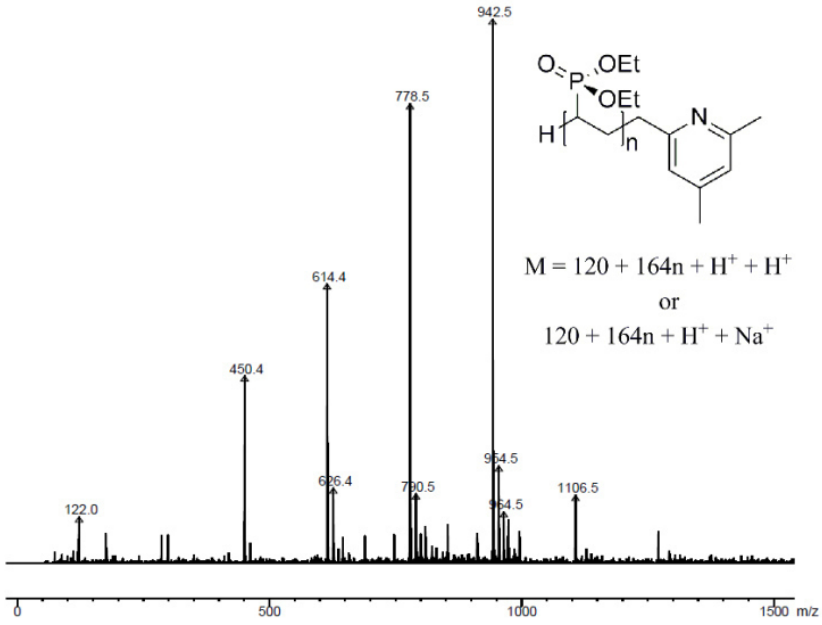

Figure S5. ESI MS spectrum of DEVP oligomers produced with $Cp_2Y(CH_2(C_5H_2Me_2N))$.

SC-XRD determination (CCDC 1031228)

A yellow fragment-like specimen of $C_{36}H_{40}N_2Y_2$, approximate dimensions 0.324 mm x 0.327 mm x 0.405 mm, was used for the X-ray crystallographic analysis. The X-ray intensity data were measured on a Bruker Kappa APEX II CCD system equipped with a graphite monochromator and a Mo fine-focus tube (λ = 0.71073 Å).

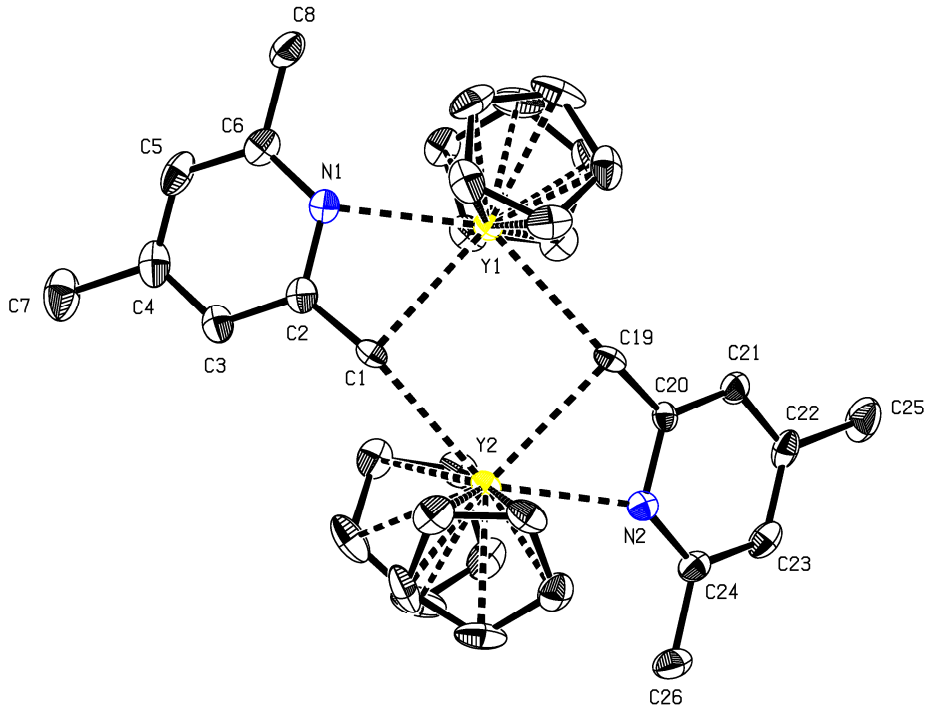

Figure S6. Ortep drawing with 50% ellipsoids for $Cp_2Y(CH_2(C_5H_2Me_2N))$.

A total of 1392 frames were collected. The total exposure time was 23.20 hours. The frames were integrated with the Bruker SAINT software package using a narrow-frame algorithm. The integration of the data using a monoclinic unit cell yielded a total of 34217 reflections to a maximum θ angle of 25.35° (0.83 Å resolution), of which 5737 were independent (average redundancy 5.964, completeness = 100.0%, R_{int} = 10.40%, R_{sig} = 8.18%) and 3937 (68.62%) were greater than $2\sigma(F^2)$. The final cell constants of a = 11.9223(4) Å, b = 22.3436(8) Å, c = 12.7820(4) Å, β = 113.273(2)°, volume = 3127.91(19) $Å^3$, are based upon the refinement of the XYZ-centroids of 3701 reflections above 20 σ(I) with 5.032° < 2θ < 46.07°. Data were corrected for absorption effects using the multi-scan method (SADABS). The ratio of minimum to maximum apparent transmission was 0.643. The calculated minimum and maximum transmission coefficients (based on crystal size) are 0.3140 and 0.3790.

The structure was solved and refined using the Bruker SHELXTL Software Package in conjunction with SHELXLE, using the space group P 1 21/n 1, with Z = 4 for the formula

unit, $C_{36}H_{40}N_2Y_2$. The final anisotropic full-matrix least-squares refinement on F^2 with 517 variables converged at R1 = 3.83%, for the observed data and wR2 = 7.00% for all data. The goodness-of-fit was 0.997. The largest peak in the final difference electron density synthesis was 0.381 $e^-/Å^3$ and the largest hole was -0.493 $e^-/Å^3$ with an RMS deviation of 0.090 $e^-/Å^3$. On the basis of the final model, the calculated density was 1.441 g/cm^3 and F(000), 1392 e^-.

Chemical formula	$C_{36}H_{40}N_2Y_2$	
Formula weight	678.52	
Temperature	123(2) K	
Wavelength	0.71073 Å	
Crystal size	0.324 x 0.327 x 0.405 mm	
Crystal habit	yellow fragment	
Crystal system	Monoclinic	
Space group	P 1 21/n 1	
Unit cell dimensions	a = 11.9223(4) Å	α = 90°
	b = 22.3436(8) Å	β = 113.273(2)°
	c = 12.7820(4) Å	γ = 90°
Volume	3127.91(19) $Å^3$	
Z	4	
Density (calculated)	1.441 g/cm^3	
Absorption coefficient	3.719 mm^{-1}	
F(000)	1392	

Diffractometer	Bruker Kappa APEX II CCD	
Radiation source	fine-focus tube, Mo	
Theta range for data collection	1.82 to 25.35°	
Index ranges	-14<=h<=14, -26<=k<=26, -15<=l<=15	
Reflections collected	34217	
Independent reflections	5737 [R(int) = 0.1040]	
Coverage of independent reflections	100.0%	
Absorption correction	multi-scan	
Max. and min. transmission	0.3790 and 0.3140	
Structure solution technique	direct methods	
Structure solution program	SHELXS-97 (Sheldrick, 2008)	
Refinement method	Full-matrix least-squares on F^2	
Refinement program	SHELXL-97 (Sheldrick, 2008) and SHELXLE (Huebschle. 2011)	
Function minimized	$\Sigma\, w(F_o^2 - F_c^2)^2$	
Data / restraints / parameters	5737 / 0 / 517	
Goodness-of-fit on F^2	0.997	
Final R indices	3937 data; I>2σ(I)	R1 = 0.0383, wR2 = 0.0609
	all data	R1 = 0.0802, wR2 = 0.0700
Weighting scheme	$w=1/[\sigma^2(F_o^2)+(0.0251P)^2]$ where $P=(F_o^2+2F_c^2)/3$	
Largest diff. peak and hole	0.381 and -0.493 $eÅ^{-3}$	
R.M.S. deviation from mean	0.090 $eÅ^{-3}$	

References

[1] J. Eppinger, *PhD Thesis*, Technische Universität München, **1999**.

[2] K. C. Hultzsch, P. Voth, K. Beckerle, T. P. Spaniol, J. Okuda, *Organometallics* **2000**, *19*, 228, K. C. Hultzsch, *PhD Thesis*, Universität Mainz, **1999**.

[3] S. Salzinger, B. S. Soller, A. Plikhta, U. B. Seemann, E. Herdtweck, B. Rieger, Journal of the American Chemical Society **2013**, *135*, 13030-13040.

[4] Leute, M. *PhD Thesis*, Universität Ulm, **2007**.

[5] Zhang, N.; Salzinger, S.; Soller, B. S.; Rieger, B. J. Am. Chem. Soc. **2013**, *135*, 8810.

4.3 C–H Bond Activation by σ-Bond Metathesis as a Versatile Route toward Highly Efficient Initiators for the Catalytic Precision Polymerization of Polar Monomers

4.4 Ligand Induced Steric Crowding in Rare Earth Metal-Mediated Group Transfer Polymerization of Vinylphosphonates: Does Enthalpy Matter?

Status: Published online: February 19, 2016

Journal: Macromolecules

Volume 49, issue 5, pages 1582–1589

Publisher: American Chemical Society

Article Type: Article

DOI: 10.1021/acs.macromol.5b01937

Authors: Benedikt S. Soller, Qian Sun, Stephan Salzinger, Christian Jandl, Alexander Pöthig, and Bernhard Rieger

4.4 Ligand Induced Steric Crowding in Rare Earth Metal-Mediated Group Transfer Polymerization of Vinylphosphonates: Does Enthalpy Matter?

4.4.1 Abstract

This chapter shows the first report on ligand induced steric crowding for the REM-GTP of vinylphosphonates. Several initiators with increased steric demand of the coordinated ligand sphere and decreased size of the catalytically active metal center are prepared using salt metathesis and the effects of the modifications on molecular mass, propagation rate, initiation delay, and molecular mass distribution are monitored via activity measurements using a normalization method for living polymerizations, and a correlation between steric crowding and activity is presented. In previous studies the thermodynamic parameters were determined for the REM-GTP of vinylphosphonates using simple $(C_5H_5)_2LnX$ complexes with different RE metal centers and changes in activity were found to be only determined by entropic effects (see Chapter 4.2). The thermodynamic parameters of 2VP polymerization by 2-methoxyethylaminobis(phenolate)yttrium catalysts are presented in Chapter 4.8 and recently Dongmei Cui et al. studied the influence of the cation size for the styrene polymerization via cationic RE complexes.[305] In the work of Cui et al., no normalization method was used due to occurring chain transfer reactions, however, the experimental thermodynamic results are supported by the calculated energy gaps of the HOMO of styrene and the LUMO of corresponding complexes.[305]

In this chapter, the temperature-dependent kinetic analyses are performed for several methyl-, trimethylsilyl-, and tetramethylcyclopentadienyl-substituted complexes to determine the activation enthalpies $\Delta H^{\ddagger}$ and entropies $\Delta S^{\ddagger}$ according to the Eyring equation. For $(C_5Me_4H)_3Ln$ complexes (Ln = Sm, Tb, Y), a change in the reaction enthalpy $\Delta H^{\ddagger}$ is observed compared to un- and monosubstituted compounds. The metal–monomer and metal–poly(phosphonate ester) bond distances are found to be prolonged for the pentacoordinated intermediate. Single sterically demanding groups such as –TMS were found to have a negative effect on the activity. This decrease of activity was addressed to a high energy barrier due to entropic effects and the high amount of rotation and vibration for such large and heavy substituents. In contrast to this result, the single methyl groups of $(C_5H_4Me)_3Y$ sufficiently destabilize the pentacoordinate intermediate and facilitate the propagation. $[(C_5H_4TMS)_2SmH]_2$ and $[(C_5H_3TMS_2)_2SmH]_2$ were previously reported to produce syndiotactic PMMA, however, in this study all obtained poly(vinylphosphonate)s were considered atactic.

The first author Benedikt S. Soller was supported by second authors Qian Sun in performing the temperature dependent kinetic measurements, Stephan Salzinger in interpreting the experimental results, and the crystallographers Christian Jandl and Alexander Pöthig in completing the complex characterization.

Macromolecules

Article

pubs.acs.org/Macromolecules

Ligand Induced Steric Crowding in Rare Earth Metal-Mediated Group Transfer Polymerization of Vinylphosphonates: Does Enthalpy Matter?

Benedikt S. Soller,[†] Qian Sun,[†] Stephan Salzinger,[§] Christian Jandl,[‡] Alexander Pöthig,[‡] and Bernhard Rieger*[,†]

[†]WACKER-Chair of Macromolecular Chemistry and [‡]Chair of Inorganic Chemistry, Catalysis Research Center, Technische Universität München, Lichtenbergstraße 4, 85748 Garching bei München, Germany

[§]Advanced Materials & Systems Research, BASF SE, GME/D-B001, 67056 Ludwigshafen am Rhein, Germany

Supporting Information

ABSTRACT: This contribution presents the first rare earth metal-mediated group transfer polymerization of vinylphosphonates from substituted cyclopentadienyl rare earth catalysts. Several initiators with increased steric demand of the coordinated ligand sphere and decreased size of the catalytically active metal center are prepared using salt metathesis. The effects of the modifications on molecular mass, propagation rate, initiation delay, and molecular mass distribution are monitored via activity measurements using a normalization method for living polymerizations, and the correlation between steric crowding and activity is presented. Temperature-dependent kinetic analyses are performed for several methyl-, trimethylsilyl-, and tetramethylcyclopentadienyl-substituted complexes to determine the activation enthalpies $\Delta H^{\ddagger}$ and entropies $\Delta S^{\ddagger}$ according to the Eyring equation. For $(C_5Me_4H)_3Ln$ complexes (Ln = Sm, Tb, Y), a change in the reaction enthalpy $\Delta H^{\ddagger}$ is observed compared to un- and monosubstituted compounds. The metal−monomer and metal−poly(phosphonate ester) bond distances are found to be prolonged for the pentacoordinated intermediate.

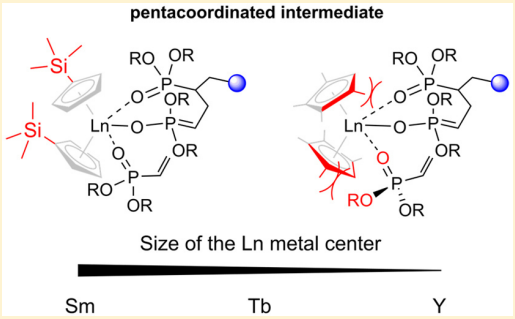

INTRODUCTION

Alterations of the ligand sphere and the metal−ligand interaction and the introduction of sterically demanding or less demanding groups are ubiquitous methods in homogeneous catalysis. Such modifications are able to tune the characteristics of catalytically active systems and change specific properties such as stability, activity, and/or selectivity.[1] Therefore, ligand design and changes of the metal center are one of the main techniques in organometallic chemistry, enabling researchers and companies to access a wide range of catalytic reactions.[2−5]

In addition to their use in organic synthesis, rare earth (RE) elements are well-known for their high activities in the polymerization catalysis of polar vinyl monomers.[6] The living polymerization of methyl methacrylate (MMA) using RE metals or group 4 initiators was first reported in 1992 by two independent groups.[7,8] Yasuda et al. used the neutral single component $[(C_5Me_5)_2SmH]_2$ samarocene.[7] The produced PMMA showed a high syndiotacticity of up to 95%, and the polymerization rate was found to increase with cation size (Sm > Y > Yb > Lu).[9] In the following years, RE metal-mediated group transfer polymerization (REM-GTP) was applied to a variety of (meth)acrylates, (meth)acrylamides, and the precise synthesis of block copolymer structures.[6,10−13]

The scope of monomers accessible for REM-GTP has recently been extended to *N*-coordinating monomers such as 2-vinylpyridine or 2-isopropenyl-2-oxazoline (Figure 1).[14−17] As functional groups provide interesting material properties, the application of polymerization techniques to new monomers is one of the main areas in polymer research. Phosphorus-containing materials, especially those comprising of phosphonate moieties, have gained significant interest in research and industry because of their wide range of possible applications from proton-conducting materials to the usage in the biomedical field.[18−23] Vinylphosphonates belong to the simplest phosphorus-containing monomers; however, studies on their corresponding material properties were hampered by their poor polymerizability using classic polymerization methods.[24,25]

Flame-retardant coating and additives of poly(dialkyl vinylphosphonate)s (PDAVP) and poly(ditolyl vinylphosphonate) have been tested for their use as halogen-free flame-retardants for polycarbonate.[26] Poly(diethyl vinylphosphonate) (PDEVP) shows amphiphilic behavior and is soluble in organic solvents and water. Therefore, upon heating, aqueous PDEVP

Received: September 3, 2015
Revised: January 19, 2016
Published: February 19, 2016

DOI: 10.1021/acs.macromol.5b01937
Macromolecules 2016, 49, 1582−1589

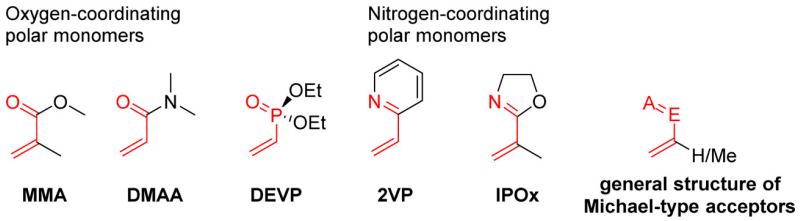

Figure 1. Overview of polar monomers accessible for the repeated conjugate addition polymerization via REM-GTP.

solutions have a lower critical solution temperature (LCST) close to the physiological range.[27] Furthermore, PDEVP copolymers with dimethyl vinylphosphonate or di-*n*-propyl vinylphosphonate show a highly tunable LCST over the entire temperature range of water from 5 to 92 °C.[28] Additionally, REM-GTP can be applied for the modification of silicon surfaces or polystyrene particles using a surface-initiated group transfer polymerization procedure.[29,30] Furthermore, the modification of silicon nanoparticles to form thermoresponsive and photoluminescent hybrid materials via surface-initiated group transfer polymerization was conducted.[31] Recently, $Cp_2Ln(CH_2(C_5H_2Me_2N))$ (Ln = Y, Lu) complexes with (4,6-dimethylpyridin-2-yl)methyl initiators have been reported as efficient catalysts without an initiation period.[32] The absence of an initiation delay is attributed to an eight-membered ring transition state for the initiation, mechanistically matching the propagation.[6,33−35]

Our group previously used simple ytterbium complexes (Cp_2YbMe and Cp_2YbCl) to prepare high molecular weight PDEVP and PDEVP-*b*-PMMA block copolymers, indicating a propagation via a repeated conjugate addition of the Michael-type monomer.[36] The mechanism of REM-GTP of vinylphosphonates was further elucidated in 2013; experimental results point toward a Yasuda-type polymerization mechanism with an S_N2-type associative displacement of the polymer phosphonate ester by a monomer as the rate-determining step.[37] The rate of vinylphosphonate REM-GTP accelerates as the size of the metal center for late lanthanides decreases.[27,37] The change in propagation rate has been elucidated via temperature-dependent activity measurements of unsubstituted Cp_3Ln or $Cp_2LnStBu$ (Ln = Tb, Y, Tm, Lu) catalysts using the Eyring equation; the propagation rate was found to be mainly determined by the activation entropy and not by the activation enthalpy.[37] Recently, higher activities with smaller RE metals were reported for syndioselective styrene polymerizations and supported by Eyring analyses and DFT simulation.[38] The observed influence of the metal cation radius was attributed to lower LUMO orbitals, facilitating monomer coordination to the metal center.[38]

Herein, we present the polymerization of DEVP from substituted tris(cyclopentadienyl) RE initiators resulting in high to moderate activities and high initiator efficiencies (Chart 1). To date, a systematic approach to sterically crowded lanthanide metallocenes for the polymerization of vinylphosphonates has not been reported. The presented complexes are obtained via salt metathesis reaction in tetrahydrofuran from 3 equiv of the corresponding potassium cyclopentadienide and the RE trichloride or a modification, as described in the Experimental Section.

Chart 1. Molecular Structure of Monosubstituted and Tetramethyl-Substituted Cp_3Ln Catalysts Used for the Polymerization of DEVP in This Study[a]

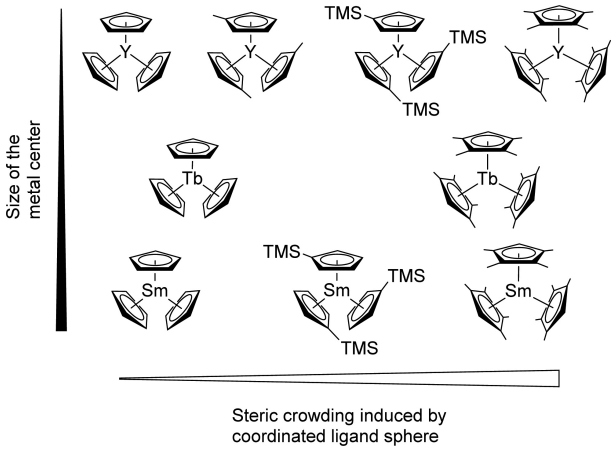

[a]For $(C_5H_4Me)_3Y(thf)$, the coordinated THF solvent molecule is omitted for clarity.

RESULTS AND DISCUSSION

In this study, the metals Sm, Tb, and Y (in order of decreasing ionic radii) were used to investigate early (Sm) and late (Tb) lanthanides. Furthermore, the RE yttrium was chosen as its cation size is in between the lanthanides dysprosium and holmium, the paramagnetic core allows NMR studies, and several substituted tris(cyclopentadienyl) yttrium complexes are accessible. The synthesis of substituted tris(cyclopentadienyl)lutetium compounds is hindered by steric effects or solubility restrictions as Lu is the smallest RE cation.[39−42]

Cyclopentadienyl ligands are not basic enough to deprotonate vinylphosphonate monomers; therefore, an initiation by nucleophilic transfer occurs either via six- or eight-membered ring transition state, the latter imitating the propagation transition state (Scheme 1). Cyclopentadienyl-based ligands are generally known as strong, stable, and often inert ligands; however, they show a variety of different coordination modes.[43] Phosphonate esters are two electron-donating species and are therefore supposed to strengthen the η^1-(σ)-character of the metal−Cp bond through coordination, resulting in a nucleophilic transfer to a coordinated monomer. This conclusion is supported by studies performed by Evans with sterically crowded $(C_5Me_5)_3Ln$ complexes (Ln = La, Ce, Pr, Nd, Sm), for which an equilibrium between η^5- and η^1-(C_5Me_5) metal bonding was proposed.[44−46]

Despite the various possible modifications of metallocene ligands used for RE elements in the literature,[47,48] to date only the influence of the metal center size has been investigated for the polymerization of vinylphosphonates, and no modifications

DOI: 10.1021/acs.macromol.5b01937
Macromolecules 2016, 49, 1582−1589

Scheme 1. Nucleophilic Transfer of a Cp Ligand to DEVP via a Six- or Eight-Membered Ring Intermediate Followed by a Propagation via Repeated Conjugate Addition of the Polymer Chain to the Coordinated DEVP

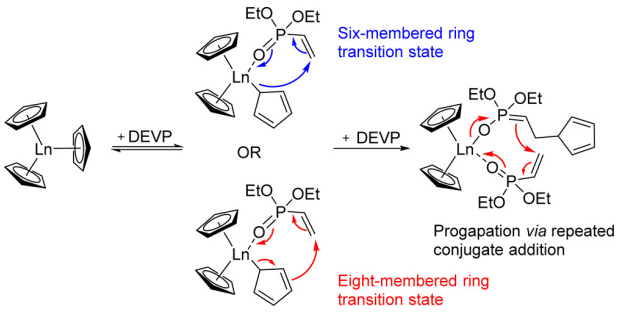

of the Cp ligand sphere have been reported.[27,37,49] Rabe et al. used nonmetallocene $Ln(NSiHMe_2)_3(thf)_2$ precursor systems for the REM-GTP of DEVP, resulting in very broad molecular mass distributions and incomplete conversions.[50] 2-Methoxyethylaminobis(phenolate)yttrium initiators are highly active catalysts for the polymerization of 2VP (TOF = 1100 h^{-1}).[16] However, for vinylphosphonates, such complexes show an inverted behavior resulting in significantly lower activities (TOF = 42 h^{-1} for DIVP, TOF = 480 h^{-1} for DEVP). Therefore, in this contribution, we wanted to investigate the influence of the metal ion radii of early lanthanides and the impact of sterically demanding substituents for several tris(cyclopentadienyl) RE metallocene initiators.

Impact of the Ligand Sphere. All polymerizations were conducted with 300 or 600 equiv of monomer at 30 °C in 5 or 10 vol % toluene solutions. All kinetic data were normalized using the initiator efficiency I^*_t at the maximum rate of monomer conversion as I^*_t changes for different conversions (Figure 2). The used normalization method also reduces the influence of protic impurities (e.g., water in the monomer) and gives consistent values for TOF/I^*_t (Table S6).[37]

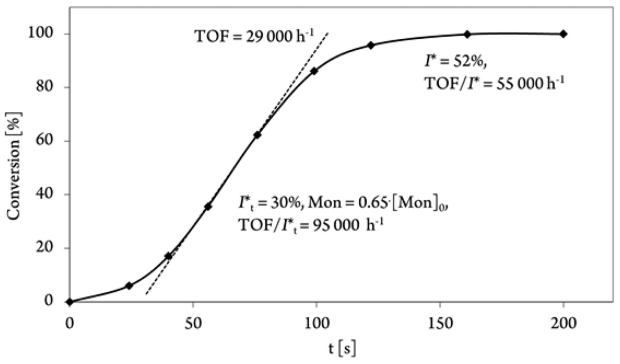

Figure 2. Conversion−reaction time plot for the polymerization of DEVP (10 vol %) in toluene with $(C_5H_4Me)_3Y(thf)$ as initiator. Change of the initiator efficiency I^*_t vs I^* over the reaction time and the corresponding normalized TOFs.

Unsubstituted Cp_3Ln initiators of the lanthanides Dy−Lu were previously used for the polymerization of DEVP.[27] The RE complex Cp_3Y has not been tested for the polymerization of vinylphosphonates; however, its properties are similar to those of the lanthanides Cp_3Dy and Cp_3Ho due to the similar cation radius (*vide supra*). Cp_3Y shows a long initiation period of 20 min, and quantitative conversion is reached after 60 min (Table 1). To our delight, the introduction of a single methyl substituent for $(C_5MeH_4)_3Y(thf)$ results in a significant reduction of the initiation period along with higher initiator efficiency and activity (Figure 2). The overall polymerization time of DEVP via $(C_5MeH_4)_3Y(thf)$ (2.5 min) is in fact faster than the overall initiation period of the unsubstituted Cp_3Y (20 min, Table 1).

Interestingly, the introduction of the sterically more demanding trimethylsilyl group for $(C_5H_4TMS)_3Y$ results in a significant decrease of the activity and an increase of the polymerization time with a narrow molecular mass distribution at room temperature. We attribute the lower activity of $(C_5H_4TMS)_3Y$ to a hindered coordination of the monomer due to steric repulsion, resulting in an overall slower propagation rate. However, DEVP polymerization via $(C_5H_4TMS)_3Y$ starts instantly and is the only example to date of a substituted Cp_3Ln complex without (measurable) initiation delay. Only the unsubstituted, highly active Cp_3Lu was previously reported with no initiation period, whereas the Cp_3Ln complex of the adjacent ytterbium shows a distinct initiation period of a few seconds.[27]

The yttrium catalysts used herein show a decrease in molecular mass attributed to an increased initiator efficiency for higher steric crowding of the ligand sphere. Furthermore, the obtained values for the polydispersity are also dependent on the used ligand and the molecular mass distribution decreases with increasing steric demand (PDI: Cp_3Y > $(C_5H_4Me)_3Y(thf)$ > $(C_5H_4TMS)_3Y \approx (C_5Me_4H)_3Y$).

Extension of Vinylphosphonate REM-GTP to Larger Metal Centers. The Cp_3Ln metallocenes of the early lanthanides (Sm−Gd) were previously found to be inactive for the polymerization of vinylphosphonates.[27,51] One of our goals was to create active early lanthanide complexes for the REM-GTP of vinylphosphonates via steric crowding of the ligand sphere because such complexes can be easily synthesized or, in some cases, are commercially available. In a first attempt, $(C_5H_4TMS)_3Sm$ was synthesized and tested for DEVP polymerization (Table 1). After stirring overnight at room temperature, polymeric materials were obtained and characterized via GPC-MALS. However, the values for I^* were drastically lower, and the activities were insufficient to perform further kinetic measurements. After a crystal structure was obtained (Figure S1), $(C_5H_4TMS)_3Sm$ was discarded for all activity measurements in this work. Nevertheless, $(C_5H_4TMS)_3Sm$ is one of the first early RE metallocenes shown to be active for vinylphosphonate polymerization.

Using the tetramethyl-substituted $(C_5Me_4H)_3Sm$ complex resulted in a significant increase in activity compared to $(C_5H_4TMS)_3Sm$. Instead, of stirring overnight, DEVP polymerization was nearly quantitative after 120 min (Table 1, Figures S65−S76), and the initiator efficiencies I^* and I^*_t were found to be adequate using a large early lanthanide metal center. Terbium belongs to the late lanthanides and its size is intermediate between Sm and Y; therefore, it was chosen for further investigations. The activities, initiator efficiencies, and molecular mass distribution were found to gradually improve from the Sm metal center to the Y metal center (Table 1). However, contrary to $(C_5H_4TMS)_3Y$ and in agreement with the results for Tb, the sterically crowded $(C_5Me_4H)_3Y$ catalyst shows an initiation period of a few seconds and remarkably high initiator efficiencies (Table 1, Figures S35−S48). The I^* of 86% (for Y) and 85% (for Tb) are the highest initiator

DOI: 10.1021/acs.macromol.5b01937
Macromolecules 2016, 49, 1582−1589

Table 1. DEVP Polymerization Results for Tris(cyclopentadienyl) RE Initiators[a]

catalyst	monomer	$[Mon]_0/[Cat]_0$	reaction time [min]	init. period[b]	conv[c] [%]	M_n[d] [kDa]	PDI[d]	I^*_t[c] [%]	I^*[d] [%]	TOF[b] [h^{-1}]	TOF/I^*_t [h^{-1}]
Cp_3Sm	DEVP	600	overnight		traces					inactive	inactive
$(C_5H_4TMS)_3Sm$	DEVP	300	overnight		95	385	1.51		13		
$(C_5Me_4H)_3Sm$	DEVP	600	120	5 min	99	210	1.17	14	46	700	4800
Cp_3Tb	DEVP	600	overnight		traces					inactive	inactive
$(C_5Me_4H)_3Tb$	DEVP	600	25	70 s	>99	116	1.06	47	85	5100	11000
Cp_3Y	DEVP	600	60	20 min	>97	720	1.26	12	14	2600	21000
$(C_5H_4Me)_3Y(thf)$	DEVP	600	2.5	10 s	>99	188	1.20	30	52	29000	95000
$(C_5H_4TMS)_3Y$	DEVP	600	9		>99	145	1.12	61	67	14000	21000
$(C_5Me_4H)_3Y$	DEVP	600	6	15 s	>99	115	1.05	66	86	13000	19000
Cp_3Lu	DEVP	600	0.5		>99	210	1.13	42	47	>125000	>265000

[a]Toluene, 30 °C, 10 vol % for monomer-to-catalyst ratio 600:1, 5 vol % for monomer-to-catalyst ratio 300:1. [b]Initiation period, reaction time until 3% conversion is reached. [c]Conversion, determined by ^{31}P NMR spectroscopic measurement. [d]Determined by GPC-MALS, $I^* = M_{th}/M_n$, $M_{th} = eq_{(monomer)} \times M_{Mon} \times$ conversion (I^*_t at the maximum rate, I^* at the end of the reaction).

efficiencies reported in the literature and are mostly a result of remaining water deactivating the catalyst during initiation. By cooling a concentrated toluene solution to −35 °C, single crystals of $(C_5Me_4H)_3Y$ were obtained and analyzed via X-ray diffraction (Figure 3).

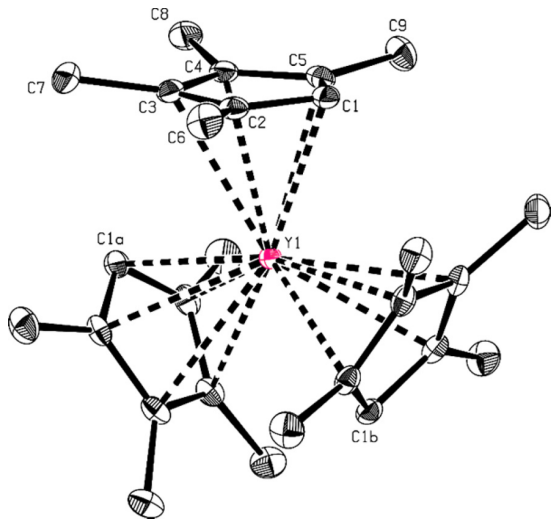

Figure 3. ORTEP drawing of $(C_5Me_4H)_3Y$ with 50% ellipsoids. All H atoms have been omitted for clarity. Selected bond distances (Å) and angles (deg): Y1—C1, 2.6350(17); C2—C6, 1.518(3); C1−Y1−C1a, 120.0.

The high solubilities of $(C_5Me_4H)_3Ln$ and $(C_5H_4TMS)_3Y$ complexes in aromatic solvents further facilitate a uniform initiation, whereas unsubstituted Cp_3Ln initiators only start dissolving in toluene *after* monomer addition. As already previously described for Cp_3Ln catalysts (*vide supra*), the activities and initiator efficiencies increase with decreasing size of the metal center for sterically demanding ligand systems. For $(C_5Me_4H)_3Ln$ complexes, the polymerization rates and initiator efficiencies increase with decreasing size of the metal center (Y > Tb > Sm, Table 1), and a correlation between the living character of the polymerization and the used metal center can be established by plotting the molecular weight M_n against the conversion (see Supporting Information). These results are contrary to those obtained for the polymerization of MMA via $(C_5Me_5)_2LnX$ initiators, in which the reaction velocity increased as the metal center size increased (Sm > Y > Yb > Lu).[9]

Microstructure of PDEVP. One goal of this work was to evaluate ligand systems for the stereoregular polymerization of vinylphosphonates. In the literature, $[(C_5H_4TMS)_2SmMe]_2$ and $[(C_5H_3TMS_2)_2SmMe]_2$ have been reported to produce highly syndiotactic PMMA ([*rr*] = 72%−90%) compared to PMMA obtained from $[(C_5Me_5)_2SmH]_2$ ([*rr*] = 80%−92%).[52] Interestingly, in this study, the microstructures of all PDEVP samples produced from substituted Cp ligands were found to be atactic (Figure S3). The methylene signal area of acrylic monomers can show either diad or tetrad sequences, whereas the corresponding methine region and ^{31}P NMR signals result in triads or pentads.[53] The splitting of the broad phosphorus signals in five domains is observed in Figure S3; however, the peaks cannot be separated without using peak deconvolution methods. As a tetrad sequence is excluded for phosphorus, a splitting into pentads with several unresolved signals seems possible. However, more measurements and a comparison with stereoregular poly(vinylphosphonate) samples are needed to further elucidate these assumptions and to establish a method to determine the tacticities of poly(vinylphosphonate)s via ^{31}P NMR. ^1H NMR spectra give less information due to broad and overlapping methylene and methine signals, and high-resolution ^{13}C measurements of the backbone area are difficult to obtain in D_2O due to the high viscosities and thermoresponsive behavior of aqueous PDEVP solutions.[49]

Rabe et al. reported the synthesis of PDEVPs with molecular masses between 65 and 84 kDa using readily available $Ln(bdsa)_3(thf)_2$ (Ln = La, Nd, Sm) precursor complexes, resulting in broad polydispersities, [*mm*] contents up to 79%, and conversions below 80%.[50] To date, this contribution is the only work on stereoregular PDEVP; however, [*mm*] triads were not quantified using isolated peaks due to overlapping or poorly resolved signals.[50] Despite our expectations, the herein obtained PDEVP samples must be considered atactic.[37,49]

Determination of Thermodynamic Parameters. To further understand the measured activities for substituted tris(cyclopentadienyl) RE complexes and the obtained (atactic) microstructures, temperature-dependent activity measurements were conducted according to the Eyring equation:

$$\ln(k/T) = -\Delta H^{\ddagger}/R \times 1/T + \Delta S^{\ddagger}/R + \ln(k_B/h) \quad (1)$$

Plotting $\ln(k/T)$ against $1/T$ results in the activation enthalpy ($\Delta H^{\ddagger}$) and entropy ($\Delta S^{\ddagger}$) of the rate-determining step of the

DOI: 10.1021/acs.macromol.5b01937
Macromolecules 2016, 49, 1582−1589

pentacoordinated transition state. These temperature-dependent activity measurements were conducted for all substituted tris(cyclopentadienyl) RE complexes with the exception of $(C_5H_4TMS)_3Sm$, which was not reactive enough for kinetic analyses. All activity measurements and the resulting TOFs were normalized using the initiator efficiency I^*_t to exclude inaccurate results due to changes in initiator efficiencies with longer polymerization times and higher conversions. These measurements were performed for all substituted RE metallocenes presented in this work and the results are summarized in Table 2.

Table 2. Dependence of the Activation Enthalpy $\Delta H^{\ddagger}$ and Entropy $\Delta S^{\ddagger}$ as a Function of Ionic Radius and Ligand Sphere

		DEVP	
catalyst	cation size[a] [pm]	$\Delta H^{\ddagger}$ [kJ mol^{-1}]	$\Delta S^{\ddagger}$ [J (mol K)$^{-1}$]
$(C_5H_4Me)_3Y(thf)$	104.0	38.6	−84.9
$(C_5H_4TMS)_3Y$	104.0	38.5	−99.0
$(C_5Me_4H)_3Y$	104.0	50.8	−56.8
$(C_5Me_4H)_3Tb$	106.3	50.6	−63.7
$(C_5Me_4H)_3Sm$	109.8	50.4	−74.1

[a] Ln^{3+} ionic radius taken from ref 54 for CN = 6. Hollemann, A. F., Wiberg, E., Wiberg, N., Eds.; *Lehrbuch der Anorganischen Chemie (Textbook of Inorganic Chemistry*, Engl. Transl.); Walter de Gruyter & Co.: Berlin, 2007.

To our surprise, the catalysts $(C_5H_4Me)_3Y(thf)$ and $(C_5H_4TMS)_3Y$ do not show a change of $\Delta H^{\ddagger}$ when compared to unsubstituted metallocenes.[37] Therefore, changes in activity between the differently un- and monosubstituted complexes are only a result of entropic reasons. In fact, $(C_5H_4Me)_3Y(thf)$ is similar in entropy and activity with the previously studied $[Cp_2YStBu]_2$.[37] We attribute the matching enthalpy $\Delta H^{\ddagger}$ for the monosubstituted complexes $(C_5H_4Me)_3Y(thf)$ and $(C_5H_4TMS)_3Y$ and unsubstituted RE metallocenes to the high flexibility of the single substituents and the large steric demand of the eight-membered ring transition state of the propagation. Therefore, a single substituent is unlikely to be found near the active center due to the sterically crowded pentacoordinated intermediate (Figure 4). An arrangement and conformation of the substituent in the largest spacious distance to the metallacycle and coordinated monomer appears favored (Figure 4).

Additionally, for the monosubstituted complexes, an increase of steric crowding does not result in higher activities for $(C_5H_4TMS)_3Y$. Detailed studies for other $(C_5H_4TMS)_3Ln$ catalysts are restricted due to low activities (i.e., Sm, Table 1) or the hindered synthesis of smaller metal centers (i.e., Lu, *vide supra*). Furthermore, no explanation was given for the significant differences in activity between $(C_5H_4TMS)_3Sm$ and $(C_5Me_4H)_3Sm$. Therefore, we conducted temperature-dependent activity measurements for the $(C_5Me_4H)_3Ln$ systems. The η^1 character of the $(C_5Me_4H)_3Ln$ monomer adduct is supposed to be further strengthened, facilitating a fast and efficient initiation (*vide supra*).

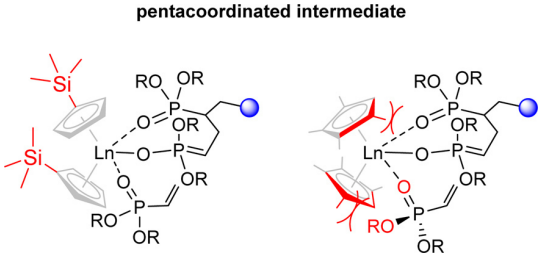

Figure 4. Differences in steric crowding for trimethylsilyl- or tetramethyl-substituted cyclopentadienyl RE catalysts, resulting in different bond distances.

For the first time, a change of the activation enthalpy term $\Delta H^{\ddagger}$ is observed for $(C_5Me_4H)_3Ln$ catalysts (Table 2). Contrary to single substituents, the methyl groups of the C_5Me_4H ligand cannot all rearrange in maximal distance from the active center, resulting in higher steric crowding. Therefore, in the transition state the Ln−(O−P) and Ln−(O═P) bond distances are lengthened to partly compensate the sterically demanding pentacoordinate intermediate. Despite the change of the enthalpy term $\Delta H^{\ddagger}$ for this ligand system, the changes of the activation barrier between the different $(C_5Me_4H)_3Ln$ metal centers are only determined by $\Delta S^{\ddagger}$ and are found to decrease linearly with decreasing cation size (Table 2 and Figure 5).

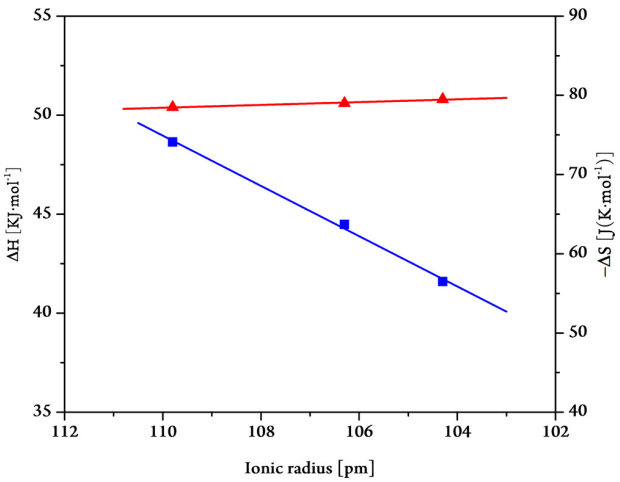

Figure 5. Activation enthalpy (red triangles) and entropy (blue squares) for DEVP polymerization using $(C_5Me_4H)_3Ln$ (Ln = Sm, Tb, Y) catalysts in dependence of the metal ionic radius.

According to results from the temperature-dependent activity measurements and the obtained changes in enthalpy and entropy, the following conclusions are drawn regarding REM-GTP of DEVP:

The increased steric demand induced by single substituents is compensated by rearranging the spacious groups in maximum distance from the active site. For $(C_5Me_4H)_3Ln$ complexes, such a rearrangement is not possible in the same extend; therefore, changes in enthalpy and bond lengths are observed.

Smaller metal centers destabilize the propagation ground state by a more confined arrangement of the eight-membered metallacycle according to the higher steric constraints caused by shorter Ln−Cp, Ln−(O−P), and Ln−(O═P) bonds. The destabilization of the ground state is not of enthalpic in origin (i.e., ring strain or the Ln−(O═P) bond strength) but instead is entropic in nature (i.e., rotational and vibrational limitations in the eight-membered metallacycle). In the transition state, the Ln−(O═P) polymer phosphonate ester bond is lengthened,

DOI: 10.1021/acs.macromol.5b01937
Macromolecules 2016, 49, 1582−1589

thus compensating part of the steric stress induced by the coordination of a vinylphosphonate monomer. This effect is larger for a stronger destabilization of the ground state, i.e., for smaller metal centers.

The performed temperature-dependent activity measurements also provide an explanation for the different DEVP polymerization behavior of $(C_5Me_4H)_3Sm$ and $(C_5H_4TMS)_3Sm$. For unsubstituted and monosubstituted Cp-based complexes, the enthalpic term $\Delta H^{\ddagger}$ is unaffected by the metal radius or substitution; therefore, changes in the activation energy are of entropic nature only. However, for $(C_5Me_4H)_3Ln$ initiators, the enthalpy term increases and entropic effects have a reduced impact on the overall activation energy barrier. Thus, for $(C_5Me_4H)_3Ln$ catalysts, in the transition state the Ln−(O═P) polymer bond distances are prolonged. The higher DEVP polymerization velocity for $(C_5Me_4H)_3Sm$ is therefore attributed to a smaller entropic contribution to the energy barrier. In contrast, for $(C_5H_4TMS)_3Sm$, the entropic contributions dominate the lower enthalpy term $\Delta H^{\ddagger}$ and rotational and vibrational degrees of freedom in the eight-membered metallacycle are restricted by the large TMS substituents and low activities are observed. On the other hand, the high enthalpy $\Delta H^{\ddagger}$ term for $(C_5Me_4H)_3Y$ is partly compensated by the low entropy term, resulting in a slightly higher activity for $(C_5H_4TMS)_3Y$.

For substituted cyclopentadienyl RE catalysts, an increased influence of the entropy term is seen for the activation energy barrier when compared to unsubstituted cyclopentadienyl systems. This is attributed to the higher entropic rotational and vibrational influence of large substituents (i.e., TMS) compared to single Cp-H protons. For the $(C_5Me_4H)_3Ln$ systems, the entropic impact of the four methyl substituents is neglected by the overall loss of rotational and vibrational degrees of freedom in the sterically constrained pentacoordinate intermediate, resulting in comparatively low $\Delta S^{\ddagger}$ entropy terms.

These results are in line with previous observations by Chen et al., which found an increased steric demand at the active metal center; this increased steric demand not only results in higher stereospecifities or the suppression of side reactions but also accelerates the propagation rate for MMA polymerizations.[55] Therefore, in order to obtain high polymerization velocities and conversions, the steric demand at the active site needs to be well-adjusted: enough sterically crowded to induce a sufficient destabilization of the eight-membered metallacycle ground state and adequate enough to allow the S_N2-type associative displacement of the polymer ester by an incoming monomer.[37,55]

CONCLUSION

In this work, we have shown that REM-GTP of vinylphosphonates is not restricted to late RE metal metallocenes and that DAVPs with narrow molecular mass distributions can be obtained from sterically crowded RE metal complexes. The elements of the RE metals offer an outstanding access for adjusting the ligand−metal interactions due to the similar behavior of RE elements and the steady, gradual course of the ionic radii of lanthanides within the sixth period. In this work, the steric demand of the active site was regulated by varying the metal center or by introducing substituents at the ligand with different sizes. As a result of the metal−ligand interactions, the herein studied catalysts vary in their properties ranging from inert (Cp_3Ln, Ln = Tb, Sm) to highly active ($(C_5H_4Me)_3Y(thf)$). $(C_5Me_4H)_3Sm$ is the first example for DAVP REM-GTP using early lanthanocenes, and in general the activities of DEVP REM-GTP accelerate with decreasing cation size. Furthermore, the polymerization behaviors of $(C_5Me_4H)_3Ln$ complexes differ from un- or monosubstituted RE metallocenes. The pentacoordinated intermediates of these complexes exhibit lengthened metal-monomer bond lengths, resulting in a higher enthalpy $\Delta H^{\ddagger}$ term and are partly compensated by lower $\Delta S^{\ddagger}$ contributions to the activation barrier. From the temperature-dependent experimental results and theoretical conclusions, the differences in reactivities between $(C_5Me_4H)_3Ln$ and $(C_5H_4TMS)_3Ln$ for Ln = Sm and Y can be explained.

No influence on the microstructure of PDEVP is seen from the used metal center or the coordinating ligand sphere. All polymers prepared in this study have the same (i.e., atactic) microstructure. The precise stereoregular polymerization of vinyl phosphonates is still an unmet challenge. Therefore, for a stereoregular polymerization of vinylphosphonates, other ligand systems need to be evaluated to investigate the material properties of stereoregular poly(vinylphosphonate ester)s or poly(vinylphosphonic acid). With respect to the results of this work, rigid (i.e., bridged and sterically crowded) catalyst systems need to be evaluated for the synthesis of stereoregular poly(vinylphosphonate)s.

EXPERIMENTAL SECTION

General. All reactions were carried out under an argon atmosphere using standard Schlenk or glovebox techniques. All glassware was heat dried under vacuum prior to use. Unless otherwise stated, all chemicals were purchased from Sigma-Aldrich or Alpha Aesar and used as received. Toluene, THF, and pentane were dried using an MBraun SPS-800 solvent purification system. Hexane was dried over 4 Å molecular sieve. Mesitylene was dried over activated aluminum oxide and stored under an argon atmosphere over 4 Å molecular sieve. $(C_5Me_4H)_3Tb$ and $(C_5Me_4H)_3Sm$ were obtained according to literature procedures or purchased from Sigma-Aldrich.[56,57] DEVP, KC_5H_4TMS, and $(C_5H_4TMS)_3Y$ were prepared according to literature procedures.[40,58,59] DEVP was dried over calcium hydride for several weeks and distilled prior to use. NMR spectra were recorded on a Bruker AVIII-300 or AV-500C spectrometer. ^1H, ^{13}C, and ^{29}Si NMR spectroscopic chemical shifts δ are reported in ppm relative to tetramethylsilane. $\delta(^1H)$ is calibrated to the residual proton signal, $\delta(^{13}C)$ to the carbon signal, and $\delta(^{29}Si)$ to the deuterium signal of the solvent. ^{31}P NMR spectroscopic chemical shifts are reported in ppm relative to and calibrated to 85% aqueous H_3PO_4. Deuterated solvents were obtained from Sigma-Aldrich and dried over 3 Å molecular sieve. Elemental analyses were measured at the Laboratory for Microanalytics at the Institute of Inorganic Chemistry at the Technische Universität München.

Activity Measurements. For activity measurements, the stated amount of catalyst (21.7 μmol) is dissolved in 20 mL of toluene, and the reaction mixture is thermostated to the desired temperature. Then, the stated amount of DEVP (13 mmol, 10 vol %) is added. During the course of the measurement, the temperature is monitored with a digital thermometer and aliquots (0.5 mL) are taken and quenched by addition to deuterated methanol (0.2 mL). After the stated reaction time, the reaction is quenched by addition of MeOD (0.5 mL). The reaction is carried out in an MBraun Glovebox under an argon atmosphere to take aliquots every 6−10 s at the beginning of the measurement. For each aliquot, the conversion is determined by ^{31}P NMR spectroscopy and the molecular weight of the formed polymer by GPC-MALS analysis.

Molecular Weight Determination. GPC was carried out on a Varian LC-920 equipped with two PL Polargel columns. As eluent a mixture of 50% THF, 50% water, and 9 g L^{-1} tetrabutylammonium bromide (TBAB) was used. Absolute molecular weights have been determined online by multiangle light scattering (MALS) analysis

DOI: 10.1021/acs.macromol.5b01937
Macromolecules 2016, 49, 1582−1589

using a Wyatt Dawn Heleos II in combination with a Wyatt Optilab rEX as concentration source.

Complex Synthesis. *KC_5H_4Me.* Commercial methylcyclopentadiene dimer contains up to 10% cyclopentadiene. If not purified, this will lead to major purity problems for derived organometallic compounds, particularly for those containing several C_5H_4Me ligands. Therefore, the crude methylcyclopentadiene dimer was purified by repeated cracking and distillation using a 40 cm Vigreux column. The first ∼10% of the distillate is discarded, and ∼70% of the remainder is collected. The methylcyclopentadiene is redistilled using the same experimental setup until a product purity of >99% is obtained.

Purified methylcyclopentadiene dimer (60 mL) is placed in a 250 mL Schlenk flask with a metal reflux condenser, potassium (3.31 g, 84.6 mmol) is added at room temperature, and the experimental setup is heated to 150 °C overnight. The produced hydrogen gas is released via an overpressure valve on top of the reflux condenser. The mixture is filtered using a Schlenk frit and washed two times with 50 mL of pentane. The product is obtained as a white pyrophoric solid (7 g, 59.2 mmol, 70%). ^{1}H NMR (300 MHz, 293 K, thf-d_8): δ 5.28 (m, 4H, C_5H_4Me), 2.08 (s, 3H, C_5H_4Me).

KC_5Me_4H. was synthesized following an adapted literature procedure.[40] In a 250 mL Schenk flask, tetramethylcyclopentadiene (4.75 g, 38.9 mmol) is dissolved at 0 °C in pentane. A 55 mL toluene solution of potassium bis(trimethylsilyl)amide (7.90 g, 39.6 mmol) is added dropwise, and the suspension is allowed to warm to room temperature overnight. The white suspension is filtered, and the residue is washed three times with 40 mL of pentane. The remaining solvents are removed under vacuum, and KC_5Me_4H is obtained as a white pyrophoric powder (5.80 g, 36.1 mmol, 93%). ^{1}H NMR (300 MHz, 293 K, thf-d_8): δ 4.88 (s, 1H, C_5Me_4H), 1.90 (s, 6H, C_5Me_4H), 1.84 (s, 6H, C_5Me_4H).

$(C_5H_4Me)_3Y(thf)$. was synthesized following an adapted literature procedure.[41] In an argon-filled glovebox, YCl_3 (0.44 g, 2.23 mmol) is suspended in 30 mL of THF and KC_5H_4Me (8.31 g, 7.03 mmol) is added stepwise. The colorless mixture is sealed in a 100 mL side arm Schlenk flask and stirred at room temperature overnight. The solvent is removed under vacuum from the resulting pale yellow mixture, and the obtained solids are stirred in 20 mL of toluene at 80 °C for 1 h. The mixture is filtered to remove gray-white insoluble material, presumably KCl and excess KC_5H_4Me. Removal of toluene under vacuum yields $(C_5H_4Me)_3Y(thf)$ as a pale yellow microcrystalline solid (533 mg, 1.34 mmol, 60%). ^{1}H NMR (300 MHz, 293 K, thf-d_8): δ 5.79 (t, 6H, C_5H_4Me), 5.63 (t, 6H, C_5H_4Me), 3.61 (m, 4H, α-thf), 2.16 (s, 9H, C_5H_4Me) 1.77 (m, 4H, β-thf). ^{13}C NMR (75 MHz, 293 K, thf-d_8): δ 118.1 (C_5H_4Me), 115.2 (C_5H_4Me), 108.3 (C_5H_4Me), 68.2 (α-thf), 26.4 (β-thf), 15.4 (C_5H_4Me). Anal. Calcd for $C_{22}H_{29}OY$: C, 66.33; H, 7.34. Found: C, 66.02; H 7.30.

$(C_5Me_4H)_3Y$. In an argon-filled glovebox, YCl_3 (344 mg, 1.76 mmol) is suspended in 15 mL of THF and KC_5Me_4H (890 mg, 5.55 mmol) is added stepwise. The colorless mixture is sealed in a 50 mL side arm Schlenk flask and stirred at room temperature overnight. The solvent is removed under vacuum from the resulting yellow mixture, and the obtained solids are stirred in 22 mL of mesitylene at 150 °C overnight. The solvent is removed under vacuum, and the mixture is filtered to remove gray-white insoluble material, presumably KCl and excess KC_5Me_4H. Removal of mesitylene under vacuum yields $(C_5Me_4H)_3Y$ as a pale yellow microcrystalline solid (580 mg, 1.28 mmol, 73%). Single crystals of $(C_5Me_4H)_3Y$ suitable for X-ray diffraction were grown from a 0.05 M toluene solution and cooling to −35 °C in a glovebox freezer. ^{1}H NMR (300 MHz, 293 K, C_6D_6): δ 6.04 (s, 3H, C_5Me_4H), 2.03 (s, 18H, C_5Me_4H), 1.83 (s, 18H, C_5Me_4H). ^{13}C NMR (75 MHz, 293 K, C_6D_6): δ 124.1 (C_5Me_4H), 114.4 (d, C_5Me_4H), 113.8 (d, C_5H_4Me), 26.4 (C_5Me_4H), 15.4 (C_5Me_4H). Anal. Calcd for $C_{27}H_{39}Y$: C, 71.67; H, 8.64. Found: C, 71.57; H 8.74.

$(C_5H_4TMS)_3Sm$. was synthesized following an adapted literature procedure.[60] In an argon-filled glovebox, $SmCl_3$ (128 mg, 0.50 mmol) is suspended in 7 mL of toluene and KC_5H_4TMS (273 mg, 1.55 mmol) is added stepwise. The colorless mixture is sealed in a 25 mL side arm Schlenk flask and heated to reflux overnight. The solvent is removed under vacuum from the resulting yellow mixture, and the obtained solids are stirred in hexane for 1 h under reflux. The mixture is filtered to remove gray-white insoluble material, presumably KCl and excess KC_5H_4TMS. Removal of hexane under vacuum yields $(C_5H_4TMS)_3Sm$ as an orange microcrystalline solid (194 mg, 0.36 mmol, 69%). Orange crystals of $(C_5H_4TMS)_3Sm$ suitable for X-ray diffraction were grown from a concentrated pentane solution at −35 °C by slowly evaporating the solvent to dryness. Anal. Calcd for $C_{24}H_{39}Si_3Sm$: C, 51.27; H, 6.99. Found: C, 51.38; H 7.08.

■ ASSOCIATED CONTENT

Supporting Information

The Supporting Information is available free of charge on the ACS Publications website at DOI: 10.1021/acs.macromol.5b01937.

Detailed procedures for activity measurements, polymerization results, and temperature-dependent kinetic studies along with detailed information for single crystal X-ray structure determination (CCDC No. 1421923 and 1421924) (PDF)

Structure of $(C_5Me_4H)_3Y$ (CIF)

Structure of $(C_5H_4TMS)_3Sm$ (CIF)

■ AUTHOR INFORMATION

Corresponding Author

*E-mail rieger@tum.de (B.R.).

Author Contributions

B.S.S. and S.S. conceived the idea and designed the experiments. B.S.S. performed the experiments. B.S.S. wrote the manuscript and participated in data analyses and discussions. B.R. directed the project. All authors have given approval to the final version of the manuscript.

Notes

The authors declare no competing financial interest.

■ ACKNOWLEDGMENTS

The authors thank Peter T. Altenbuchner and Alexander Kronast for valuable discussions. Dan Qu, Raphaela Graßl, Alexander Sigg, and Szu-Hao Cho are thanked for their help with activity measurements. Stephan Salzinger is grateful for a generous scholarship from the Fonds der Chemischen Industrie.

■ REFERENCES

(1) Crabtree, R. H. *The Organometallic Chemistry of the Transition Metals*; John Wiley & Sons: 2009.

(2) Riederer, S. K. U.; Gigler, P.; Högerl, M. P.; Herdtweck, E.; Bechlars, B.; Herrmann, W. A.; Kühn, F. E. *Organometallics* **2010**, *29*, 5681−5692.

(3) Amgoune, A.; Thomas, C. M.; Ilinca, S.; Roisnel, T.; Carpentier, J.-F. *Angew. Chem., Int. Ed.* **2006**, *45*, 2782−2784.

(4) Schöbel, A.; Herdtweck, E.; Parkinson, M.; Rieger, B. *Chem. - Eur. J.* **2012**, *18*, 4174−4178.

(5) Spaleck, W.; Antberg, M.; Rohrmann, J.; Winter, A.; Bachmann, B.; Kiprof, P.; Behm, J.; Herrmann, W. A. *Angew. Chem., Int. Ed. Engl.* **1992**, *31*, 1347−1350.

(6) Chen, E. Y. X. *Chem. Rev.* **2009**, *109*, 5157−5214.

(7) Yasuda, H.; Yamamoto, H.; Yokota, K.; Miyake, S.; Nakamura, A. *J. Am. Chem. Soc.* **1992**, *114*, 4908−4910.

(8) Collins, S.; Ward, D. G. *J. Am. Chem. Soc.* **1992**, *114*, 5460−5462.

(9) Yasuda, H.; Yamamoto, H.; Yamashita, M.; Yokota, K.; Nakamura, A.; Miyake, S.; Kai, Y.; Kanehisa, N. *Macromolecules* **1993**, *26*, 7134−7143.

(10) Yasuda, H.; Furo, M.; Yamamoto, H.; Nakamura, A.; Miyake, S.; Kibino, N. *Macromolecules* **1992**, *25*, 5115−5116.

DOI: 10.1021/acs.macromol.5b01937
Macromolecules 2016, 49, 1582−1589

(11) Ihara, E.; Morimoto, M.; Yasuda, H. *Macromolecules* **1995**, *28*, 7886−7892.
(12) Yasuda, H.; Ihara, E. *Macromol. Chem. Phys.* **1995**, *196*, 2417−2441.
(13) Soller, B. S.; Zhang, N.; Rieger, B. *Macromol. Chem. Phys.* **2014**, *215*, 1946−1962.
(14) Kaneko, H.; Nagae, H.; Tsurugi, H.; Mashima, K. *J. Am. Chem. Soc.* **2011**, *133*, 19626−19629.
(15) Zhang, N.; Salzinger, S.; Soller, B. S.; Rieger, B. *J. Am. Chem. Soc.* **2013**, *135*, 8810−8813.
(16) Altenbuchner, P. T.; Soller, B. S.; Kissling, S.; Bachmann, T.; Kronast, A.; Vagin, S. I.; Rieger, B. *Macromolecules* **2014**, *47*, 7742−7749.
(17) Altenbuchner, P. T.; Adams, F.; Kronast, A.; Herdtweck, E.; Pothig, A.; Rieger, B. *Polym. Chem.* **2015**, *6*, 6796−6801.
(18) Parvole, J.; Jannasch, P. *Macromolecules* **2008**, *41*, 3893−3903.
(19) Perrin, R.; Elomaa, M.; Jannasch, P. *Macromolecules* **2009**, *42*, 5146−5154.
(20) Sannigrahi, A.; Takamuku, S.; Jannasch, P. *Polym. Chem.* **2013**, *4*, 4207−4218.
(21) Monge, S.; Canniccioni, B.; Graillot, A.; Robin, J.-J. *Biomacromolecules* **2011**, *12*, 1973−1982.
(22) Ellis, J.; Anstice, M.; Wilson, A. D. *Clin. Mater.* **1991**, *7*, 341−346.
(23) Ellis, J.; Wilson, A. D. *Dent. Mater.* **1992**, *8*, 79−84.
(24) David, G.; Negrell-Guirao, C.; Iftene, F.; Boutevin, B.; Chougrani, K. *Polym. Chem.* **2012**, *3*, 265−274.
(25) Salzinger, S.; Rieger, B. *Macromol. Rapid Commun.* **2012**, *33*, 1327−1345.
(26) Lanzinger, D.; Salzinger, S.; Soller, B. S.; Rieger, B. *Ind. Eng. Chem. Res.* **2015**, *54*, 1703−1712.
(27) Salzinger, S.; Seemann, U. B.; Plikhta, A.; Rieger, B. *Macromolecules* **2011**, *44*, 5920−5927.
(28) Zhang, N.; Salzinger, S.; Rieger, B. *Macromolecules* **2012**, *45*, 9751−9758.
(29) Zhang, N.; Salzinger, S.; Deubel, F.; Jordan, R.; Rieger, B. *J. Am. Chem. Soc.* **2012**, *134*, 7333−7336.
(30) Yang, J.; Liang, Y.; Salzinger, S.; Zhang, N.; Dong, D.; Rieger, B. *J. Polym. Sci., Part A: Polym. Chem.* **2014**, *52*, 2919−2925.
(31) Kehrle, J.; Höhlein, I. M. D.; Yang, Z.; Jochem, A.-R.; Helbich, T.; Kraus, T.; Veinot, J. G. C.; Rieger, B. *Angew. Chem.* **2014**, *126*, 12702−12705.
(32) Soller, B. S.; Salzinger, S.; Jandl, C.; Pöthig, A.; Rieger, B. *Organometallics* **2015**, *34*, 2703−2706.
(33) Li, Y.; Ward, D. G.; Reddy, S. S.; Collins, S. *Macromolecules* **1997**, *30*, 1875−1883.
(34) Nguyen, H.; Jarvis, A. P.; Lesley, M. J. G.; Kelly, W. M.; Reddy, S. S.; Taylor, N. J.; Collins, S. *Macromolecules* **2000**, *33*, 1508−1510.
(35) Rodriguez-Delgado, A.; Chen, E. Y. X. *Macromolecules* **2005**, *38*, 2587−2594.
(36) Seemann, U. B.; Dengler, J. E.; Rieger, B. *Angew. Chem.* **2010**, *122*, 3567−3569.
(37) Salzinger, S.; Soller, B. S.; Plikhta, A.; Seemann, U. B.; Herdtweck, E.; Rieger, B. *J. Am. Chem. Soc.* **2013**, *135*, 13030−13040.
(38) Lin, F.; Wang, X.; Pan, Y.; Wang, M.; Liu, B.; Luo, Y.; Cui, D. *ACS Catal.* **2016**, *6*, 176−185.
(39) Evans, W. J.; Lee, D. S.; Johnston, M. A.; Ziller, J. W. *Organometallics* **2005**, *24*, 6393−6397.
(40) Peterson, J. K.; MacDonald, M. R.; Ziller, J. W.; Evans, W. J. *Organometallics* **2013**, *32*, 2625−2631.
(41) Evans, W. J.; Meadows, J. H.; Kostka, A. G.; Closs, G. L. *Organometallics* **1985**, *4*, 324−326.
(42) Coles, M. P.; Hitchcock, P. B.; Lappert, M. F.; Protchenko, A. V. *Organometallics* **2012**, *31*, 2682−2690.
(43) O'Connor, J. M.; Casey, C. P. *Chem. Rev.* **1987**, *87*, 307−318.
(44) Evans, W. J.; Forrestal, K. J.; Ziller, J. W. *Angew. Chem., Int. Ed. Engl.* **1997**, *36*, 774−776.
(45) Evans, W. J.; Perotti, J. M.; Kozimor, S. A.; Champagne, T. M.; Davis, B. L.; Nyce, G. W.; Fujimoto, C. H.; Clark, R. D.; Johnston, M. A.; Ziller, J. W. *Organometallics* **2005**, *24*, 3916−3931.
(46) Mueller, T. J.; Nyce, G. W.; Evans, W. J. *Organometallics* **2011**, *30*, 1231−1235.
(47) Edelmann, F. T. *Coord. Chem. Rev.* **2014**, *261*, 73−155.
(48) Edelmann, F. T. *Coord. Chem. Rev.* **2015**, *284*, 124−205.
(49) Soller, B. S.; Salzinger, S.; Rieger, B. *Chem. Rev.* **2016**, DOI: 10.1021/acs.chemrev.5b00313.
(50) Rabe, G. W.; Komber, H.; Häussler, L.; Kreger, K.; Lattermann, G. *Macromolecules* **2010**, *43*, 1178−1181.
(51) Seemann, U. B. PhD Thesis, TU München, 2010.
(52) Satoh, Y.; Ikitake, N.; Nakayama, Y.; Okuno, S.; Yasuda, H. *J. Organomet. Chem.* **2003**, *667*, 42−52.
(53) Komber, H.; Steinert, V.; Voit, B. *Macromolecules* **2008**, *41*, 2119−2125.
(54) Wiberg, E.; Holleman, A. F.; Wiberg, N. *Lehrbuch Der Anorganischen Chemie*; De Gruyter: 2007.
(55) Zhang, Y.; Ning, Y.; Caporaso, L.; Cavallo, L.; Chen, E. Y. X. *J. Am. Chem. Soc.* **2010**, *132*, 2695−2709.
(56) Schumann, H.; Glanz, M.; Hemling, H. *J. Organomet. Chem.* **1993**, *445*, C1−C3.
(57) Schumann, H.; Glanz, M.; Hemling, H.; Ekkehard Hahn, F. *Z. Anorg. Allg. Chem.* **1995**, *621*, 341−345.
(58) Leute, M. PhD Thesis, Universität Ulm, 2007.
(59) MacDonald, M. R.; Ziller, J. W.; Evans, W. J. *J. Am. Chem. Soc.* **2011**, *133*, 15914−15917.
(60) Evans, W. J.; Keyer, R. A.; Ziller, J. W. *J. Organomet. Chem.* **1990**, *394*, 87−97.

DOI: 10.1021/acs.macromol.5b01937
Macromolecules 2016, 49, 1582−1589

Supporting Information:

Ligand Induced Steric Crowding in Rare Earth Metal-Mediated Group Transfer Polymerization of Vinyl-phosphonates: Does Enthalpy Matter?

Benedikt S. Soller,[†] Qian Sun,[†] Stephan Salzinger,[‡] Christian Jandl,[⊥] Alexander Pöthig,[⊥] and Bernhard Rieger*[,†]

† WACKER-Chair of Macromolecular Chemistry, Technische Universität München, Lichtenbergstraße 4, 85748 Garching bei München, Germany

‡ BASF SE, Advanced Materials & Systems Research, GME/D - B001, 67056 Ludwigshafen am Rhein, Germany

⊥ Chair of Inorganic Chemistry, Catalysis Research Center, Technische Universität München, Ernst-Otto-Fischer-Straße 1, 85748 Garching bei München, Germany

Material and Methods

All reactions were carried out under argon atmosphere using standard Schlenk or glovebox techniques. All glassware was heat dried under vacuum prior to use. Unless otherwise stated, all chemicals were purchased from Sigma-Aldrich or Alpha Aesar and used as received. Toluene, THF and pentane were dried using an MBraun SPS-800 solvent purification system. Hexane was dried over 3 Å molecular sieve. Mesitylene was dried over activated aluminum oxide and stored under argon atmosphere over 4 Å molecular sieve. DEVP was prepared according to literature procedures.[1] Monomers were dried over calcium hydride for several weeks and distilled prior to use. NMR spectra were recorded on a Bruker AVIII-300 or AV-500C spectrometer. ^{1}H, ^{13}C and ^{29}Si NMR spectroscopic chemical shifts δ are reported in ppm relative to tetramethylsilane. δ(^{1}H) is calibrated to the residual proton signal, δ(^{13}C) to the carbon signal and δ(^{29}Si) to the deuterium signal of the solvent. ^{31}P NMR spectroscopic chemical shifts are reported in ppm relative to and calibrated to 85% aqueous H_3PO_4. Deuterated solvents were obtained from Sigma Aldrich and dried over 3Å molecular sieve. Elemental analyses were measured at the Laboratory for Microanalytics at the Institute of Inorganic Chemistry at the Technische Universität München.

Activity Measurements

For activity measurements, the stated amount of catalyst (15-50 μmol) is dissolved in 20 mL of toluene and the reaction mixture is thermostated to the desired temperature. Then, the stated amount of DEVP (3.5-13 mmol) is added. During the course of the measurement, the temperature is monitored with a digital thermometer and aliquots (0.5 mL) are taken and quenched by addition to deuterated methanol (0.2 mL). After the stated reaction time, the reaction is quenched by addition of MeOD (0.5 mL). The reaction is carried out in an MBraun Glovebox under argon atmosphere to take aliquots every 6-10 seconds at the beginning of the measurement. For each aliquot, the conversion is determined by ^{31}P NMR spectroscopy, the molecular weight of the formed polymer by GPC-MALS analysis.

Molecular Weight Determination

GPC was carried out on a Varian LC-920 equipped with two PL Polargel columns. As eluent a mixture of 50% THF, 50% water, and 9 g L^{-1} tetrabutylammonium bromide (TBAB) was used. Absolute molecular weights have been determined online by multiangle light scattering (MALS) analysis using a Wyatt Dawn Heleos II in combination with a Wyatt Optilab rEX as concentration source.

Crystallographic Data

General:

Data were collected on an X-ray single crystal diffractometer equipped with a CCD detector (APEX II, κ–CCD), a rotating anode FR591 and a Montel mirror optic by using the SMART software package.[2] The measurements were performed on single crystals coated with perfluorinated ether. The crystals were fixed on the top of a glass fiber and transferred to the diffractometer. Crystals were frozen under a stream of cold nitrogen. A matrix scan was used to determine the initial lattice parameters. Reflections were merged and corrected for Lorenz and polarization effects, scan speed, and background using SAINT.[3] Absorption corrections, including odd and even ordered spherical harmonics were performed using SADABS.[3] Space group assignments were based upon systematic absences, *E* statistics, and successful refinement of the structures. Structures were solved by direct methods with the aid of successive difference Fourier maps,[4] and were refined against all data using the APEX 2 software[2] in conjunction with SHELXL-97 or SHELXL-2014[5] and SHELXLE[6]. Methyl hydrogen atoms were refined as part of rigid rotating groups, with a C–H distance of 0.98 Å and $U_{iso(H)} = 1.5 \cdot U_{eq(C)}$. Other H atoms were placed in calculated positions and refined using a riding model, with methylene and aromatic C–H distances of 0.99 and 0.95 Å, respectively, and $U_{iso(H)} = 1.2 \cdot U_{eq(C)}$. If not mentioned otherwise, non-hydrogen atoms were refined with anisotropic displacement parameters. Full-matrix least-squares refinements were carried out by minimizing $\Sigma w(F_o^2-F_c^2)^2$ with SHELXL-97[5] weighting scheme. Neutral atom scattering factors for all atoms and anomalous dispersion corrections for the non-hydrogen atoms were taken from *International Tables for Crystallography*.[7] Images of the crystal structures were generated with PLATON.[8]

$(C_5H_4TMS)_3Sm$ (CCDC 1421923)

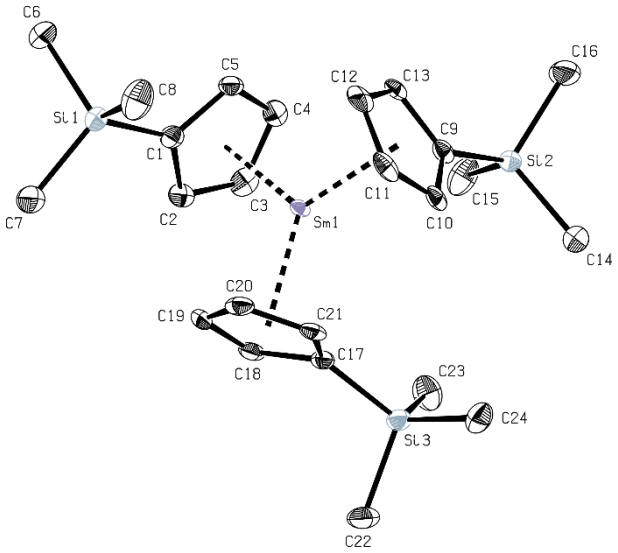

Figure S1. ORTEP drawing of $(C_5H_4TMS)_3Sm$ with 50% ellipsoids. All H atoms have been omitted for clarity.

diffractometer operator C. Jandl
scanspeed 10 s per frame
dx 60 mm
2959 frames measured in 8 data sets
phi-scans with delta_phi = 0.5
omega-scans with delta_omega = 0.5

Crystal data

M_r = 562.18	D_x = 1.404 Mg m^{-3}
Orthorhombic, *Pbca*	Melting point: unknown
Hall symbol: -P 2ac 2ab	Mo *Kα* radiation, λ = 0.71073 Å
a = 8.2756 (4) Å	Cell parameters from 9740 reflections
b = 22.2510 (12) Å	θ = 2.7–28.2°
c = 28.8955 (15) Å	μ = 2.35 mm^{-1}
V = 5320.8 (5) Å^3	*T* = 123 K
Z = 8	Fragment, orange
F(000) = 2296	0.34 × 0.26 × 0.15 mm

Data collection

Radiation source: rotating anode FR591	4521 reflections with i > 2σ(i)
MONTEL optic monochromator	R_{int} = 0.066
Detector resolution: 16 pixels mm^{-1}	θ_{max} = 26.4°, θ_{min} = 1.8°
phi– and ω–rotation scans	h = −10 8
Absorption correction: multi-scan *SADABS*, Bruker, 2008b	k = −27 27
T_{min} = 0.492, T_{max} = 0.746	l = −36 35
73150 measured reflections	

Refinement

Refinement on F^2	Secondary atom site location: difference Fourier map
Least-squares matrix: full	Hydrogen site location: inferred from neighbouring sites
$R[F^2 > 2\sigma(F^2)]$ = 0.025	H-atom parameters constrained
$wR(F^2)$ = 0.056	W = $1/[\Sigma^2(FO^2) + (0.0141P)^2 + 5.6531P]$ WHERE $P = (FO^2 + 2FC^2)/3$
S = 1.11	$(\Delta/\sigma)_{max}$ = 0.002
5439 reflections	$\Delta\rho_{max}$ = 1.59 e $Å^{-3}$
262 parameters	$\Delta\rho_{min}$ = −0.84 e $Å^{-3}$
0 restraints	Extinction correction: none
0 constraints	Extinction coefficient: -
Primary atom site location: structure-invariant direct methods	

Refinement on F^2 for ALL reflections except those flagged by the user for potential systematic errors. Weighted R-factors wR and all goodnesses of fit S are based on F^2, conventional R-factors R are based on F, with F set to zero for negative F^2. The observed criterion of F^2 > 2sigma(F^2) is used only for calculating -R-factor-obs etc. and is not relevant to the choice of reflections for refinement. R-factors based on F^2 are statistically about twice as large as those based on F, and R-factors based on ALL data will be even larger.

(C$_5$Me$_4$H)$_3$Y (CCDC 1421924)

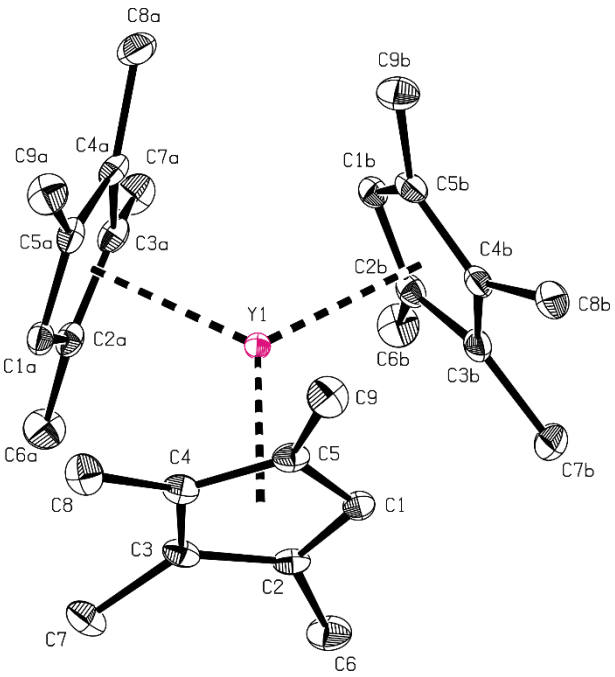

Figure S2. ORTEP drawing of $(C_5Me_4H)_3Y$ with 50% ellipsoids. All H atoms have been omitted for clarity.

Diffractometer operator C. Jandl
scanspeed 5 s per frame
dx 35 mm
6745 frames measured in 20 data sets
phi-scans with delta_phi = 0.5
omega-scans with delta_omega = 0.5

Crystal data

M_r = 452.49	Melting point: unknown
Trigonal, *R*	Mo *K*α radiation, λ = 0.71073 Å
Hall symbol: -R 3	Cell parameters from 9707 reflections
a = 15.5307 (5) Å	θ = 2.6–25.3°
c = 16.5820 (5) Å	μ = 2.54 mm^{-1}
V = 3463.8 (3) Å^3	*T* = 123 K
Z = 6	Fragment, yellow
F(000) = 1440	0.31 × 0.28 × 0.27 mm

Data collection

Radiation source: rotating anode FR591	1386 reflections with i > 2σ(i)
Montel mirror optics monochromator	R_{int} = 0.066
Detector resolution: 16 pixels mm^{-1}	θ_{max} = 25.4°, θ_{min} = 2.0°
phi– and ω–rotation scans	h = −18 18
Absorption correction: multi-scan *SADABS*, Bruker, 2008b	k = −18 18
T_{min} = 0.617, T_{max} = 0.730	l = −19 19
52479 measured reflections	

Refinement

Refinement on F^2	Secondary atom site location: difference Fourier map
Least-squares matrix: full	Hydrogen site location: inferred from neighbouring sites
$R[F^2 > 2\sigma(F^2)]$ = 0.022	H-atom parameters constrained
$wR(F^2)$ = 0.063	W = 1/[$\Sigma^2(FO^2)$ + (0.0369P)^2 + 4.2713P] WHERE P = (FO^2 + 2FC^2)/3
S = 1.14	$(\Delta/\sigma)_{max}$ < 0.001
1424 reflections	$\Delta\rho_{max}$ = 0.33 e Å^{-3}
90 parameters	$\Delta\rho_{min}$ = −0.36 e Å^{-3}
0 restraints	Extinction correction: none
0 constraints	Extinction coefficient: -
Primary atom site location: structure-invariant direct methods	

Refinement on F^2 for ALL reflections except those flagged by the user for potential systematic errors. Weighted R-factors wR and all goodnesses of fit S are based on F^2, conventional R-factors R are based on F, with F set to zero for negative F^2. The observed criterion of F^2 > 2sigma(F^2) is used only for calculating -R-factor-obs etc. and is not relevant to the choice of reflections for refinement. R-factors based on F^2 are statistically about twice as large as those based on F, and R-factors based on ALL data will be even larger.

Comparision of PDEVP Microstructure obtained from substituted Cp_3Ln Initiators

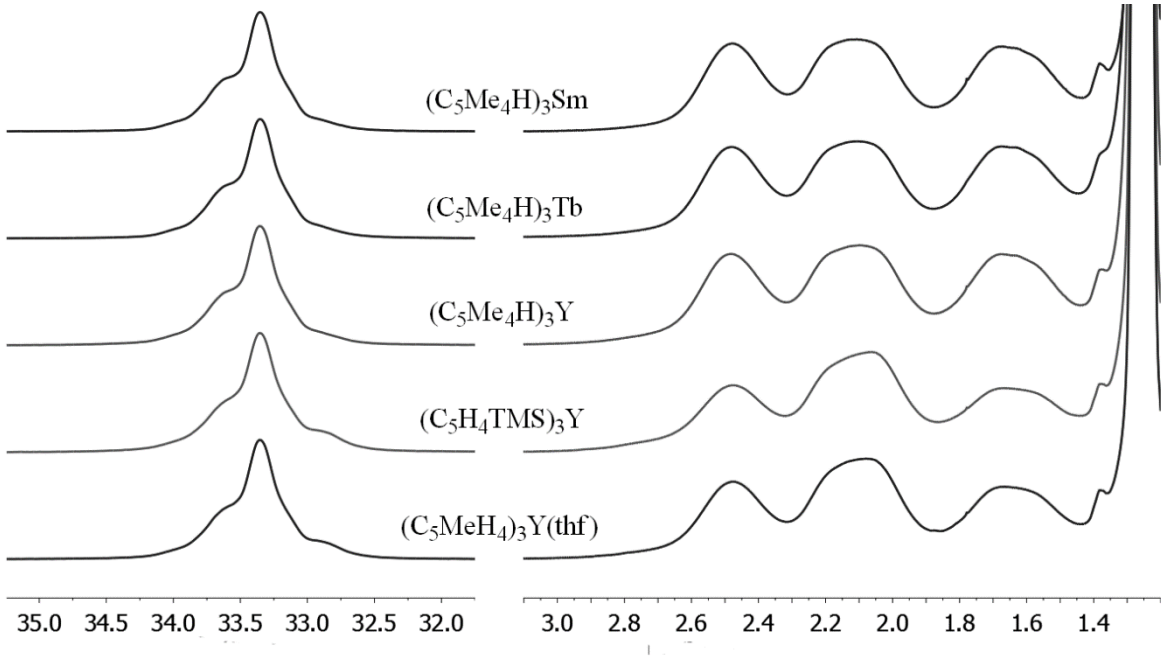

Figure S3. ^{31}P NMR spectra (in D_2O, left) and backbone ^{1}H NMR spectra (in D_2O, right) of PDEVP produced with different rare earth metal centers and different ligand structures.

Temperature Dependent Kinetic Studies

Table S1. Temperature-dependent kinetics for $(C_5H_4Me)_3Y(thf)$-catalyzed DEVP polymerization (1.09 mmol L^{-1} $(C_5H_4Me)_3Y(thf)$, 0.651 mol L^{-1} DEVP, toluene)

T [°C]	TOF [h^{-1}]	I^*_t [%]	TOF/I^*_t [h^{-1}]	Conversion at maximum rate	Rate [mol L^{-1} s^{-1}]	1/T [K^{-1}]	ln(k'/T)
12	13000	22.0	59000	24.4	2.01E-03	3.51E-03	-2.82
18	11000	22.4	48000	20.0	3.24E-03	3.44E-03	-2.44
21	14000	28.2	48000	30.7	4.60E-03	3.40E-03	-2.18
26	23000	33.1	71000	30.8	7.04E-03	3.34E-03	-1.93
30	28000	34.9	81000	35.8	8.50E-03	3.30E-03	-1.74
37	45000	40.4	110000	39.8	1.35E-02	3.22E-03	-1.38
43	48000	34.1	140000	34.7	1.44E-02	3.16E-03	-1.25

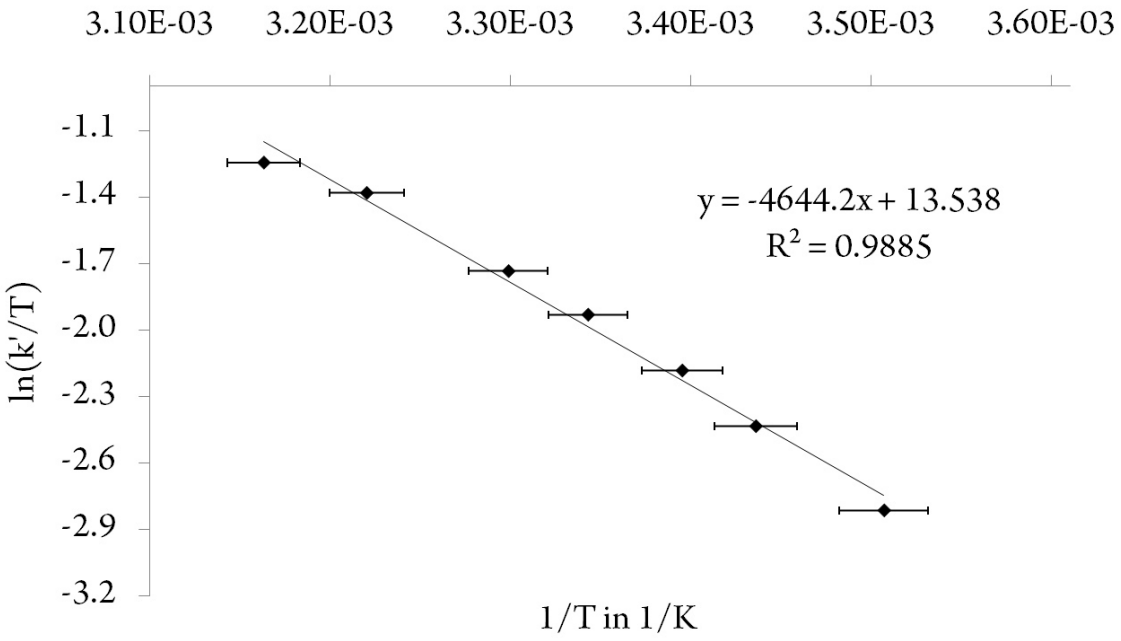

Figure S4: Result for the Eyring-plot of $(C_5H_4Me)_3Y(thf)$-initiated DEVP (10 vol %) polymerization in toluene (12 – 43 °C, $\Delta H^{\ddagger}$ = 38.6 kJ mol^{-1}, $\Delta S^{\ddagger}$ = -84.9 J $(mol\ K)^{-1}$).

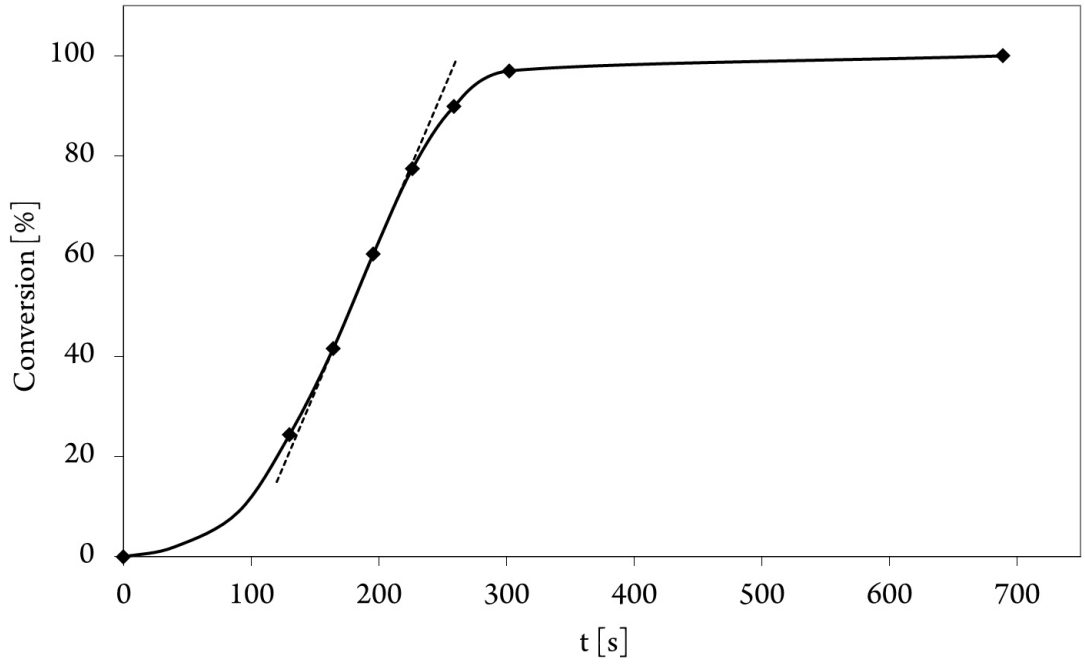

Figure S5: Conversion-reaction time plot for the polymerization of DEVP using $(C_5H_4Me)_3Y(thf)$ (21.7 µmol, 10 vol % DEVP in 20 ml toluene, 12 °C).

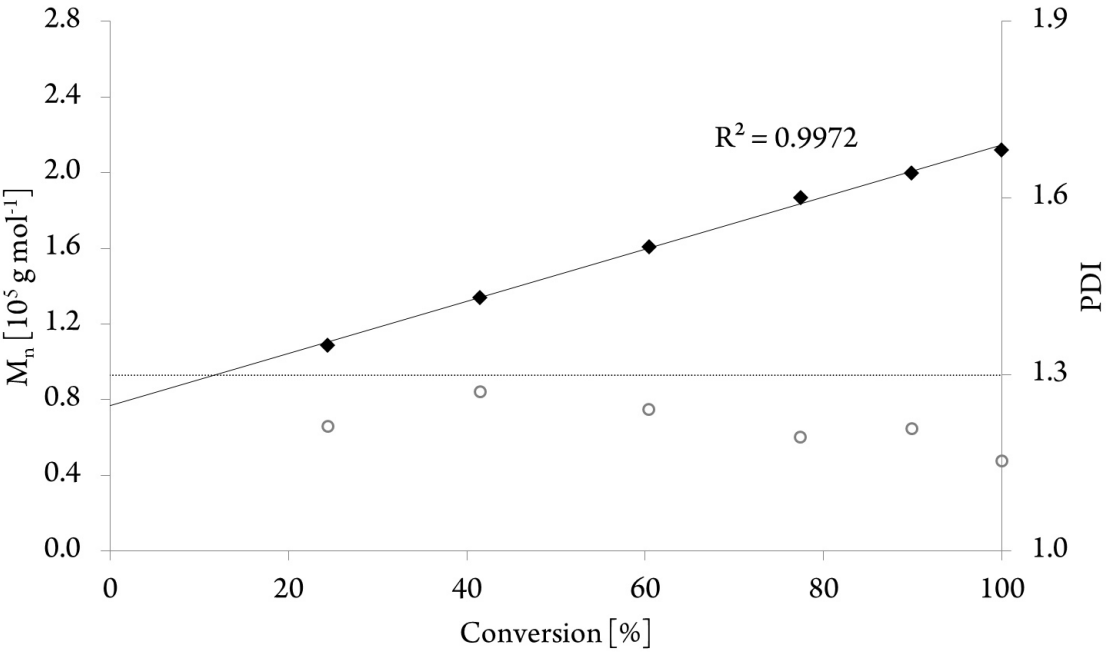

Figure S6: Number average molecular mass conversion plot for the polymerization of DEVP using $(C_5H_4Me)_3Y(thf)$ (21.7 µmol, 10 vol % DEVP in 20 ml toluene, 12 °C).

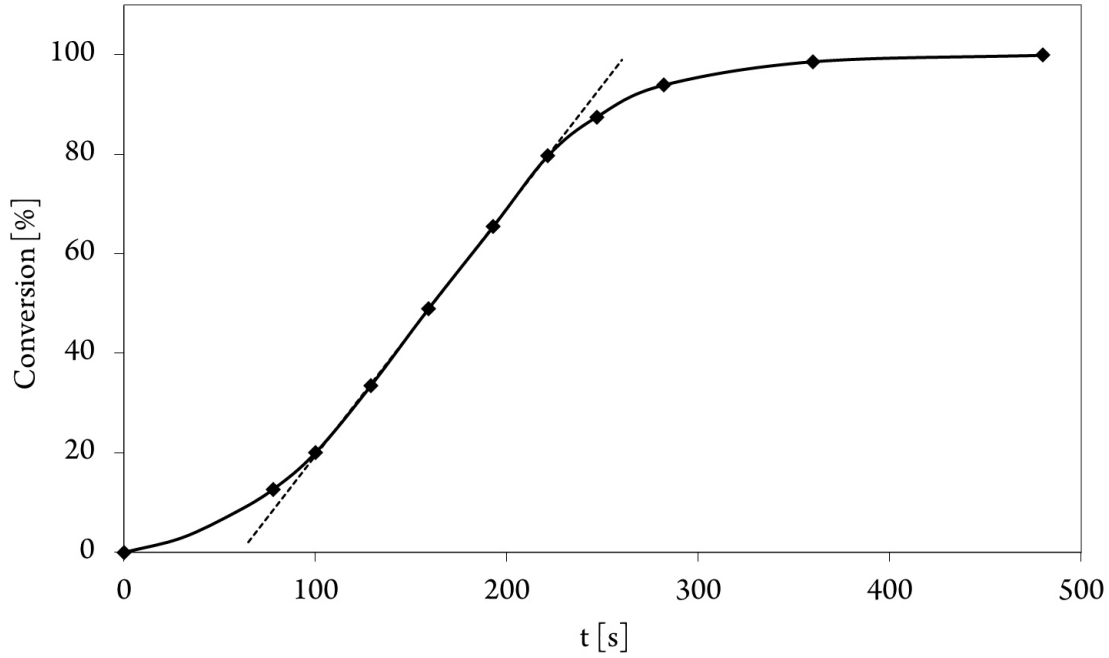

Figure S7: Conversion-reaction time plot for the polymerization of DEVP using $(C_5H_4Me)_3Y(thf)$ (21.7 µmol, 10 vol % DEVP in 20 ml toluene, 18 °C).

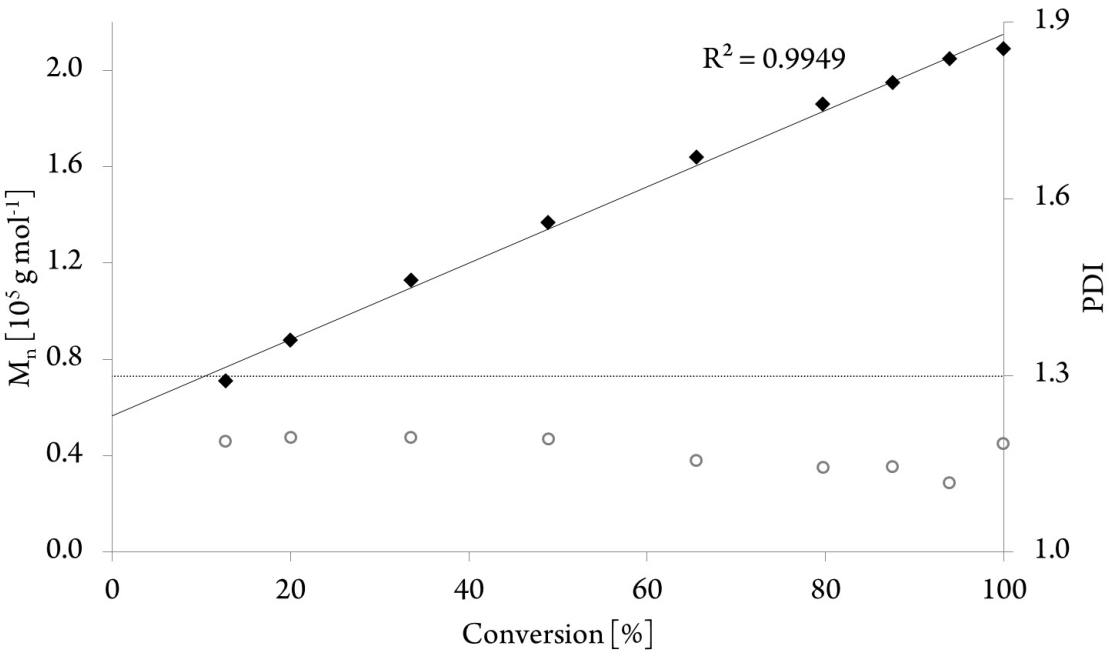

Figure S8: Number average molecular mass conversion plot for the polymerization of DEVP using $(C_5H_4Me)_3Y(thf)$ (21.7 µmol, 10 vol % DEVP in 20 ml toluene, 18 °C).

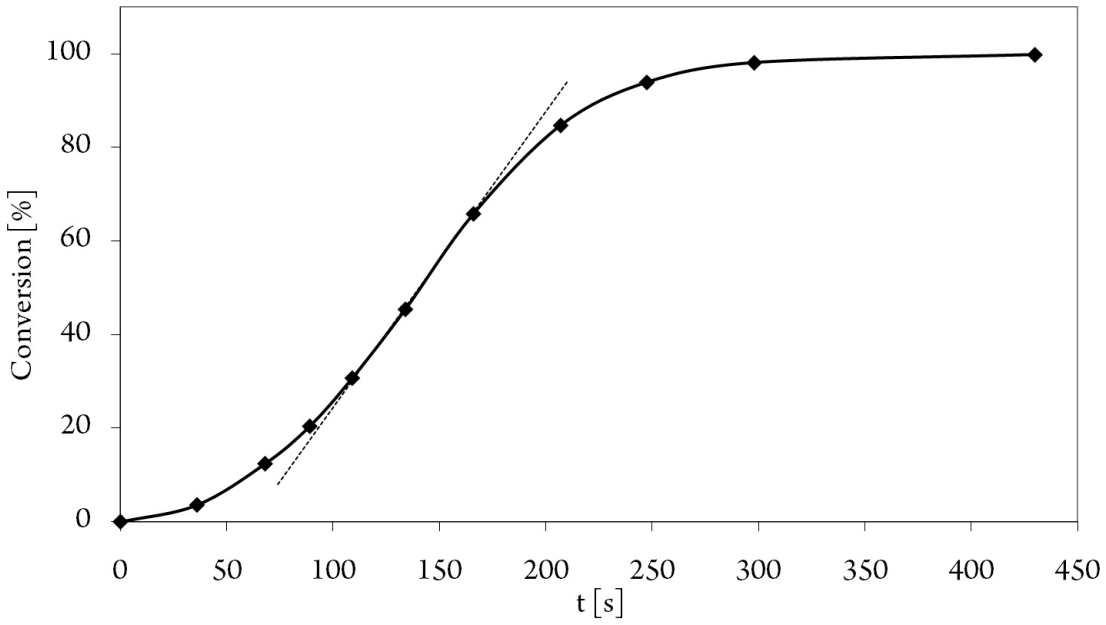

Figure S9: Conversion-reaction time plot for the polymerization of DEVP using $(C_5H_4Me)_3Y(thf)$ (21.7 µmol, 10 vol % DEVP in 20 ml toluene, 21 °C).

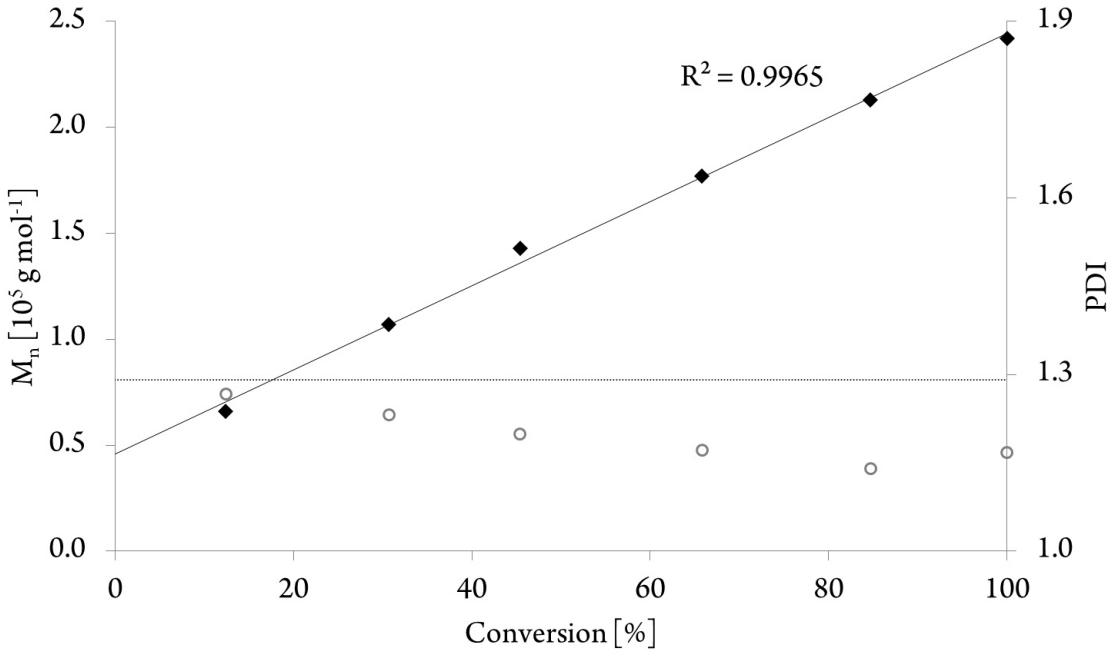

Figure S10: Number average molecular mass conversion plot for the polymerization of DEVP using $(C_5H_4Me)_3Y(thf)$ (21.7 µmol, 10 vol % DEVP in 20 ml toluene, 21 °C).

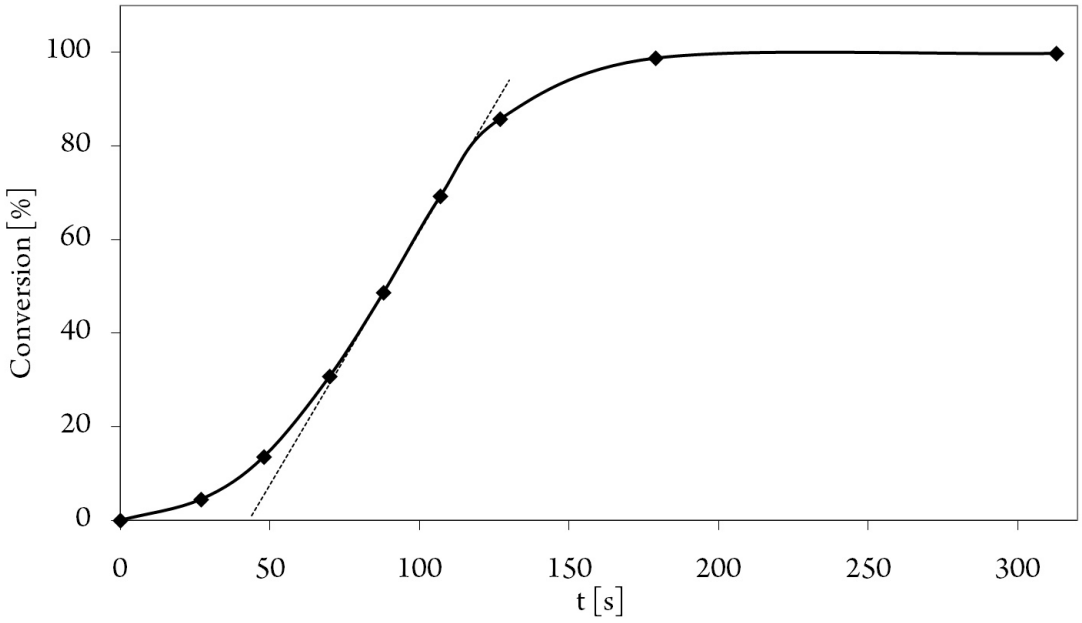

Figure S11: Conversion-reaction time plot for the polymerization of DEVP using $(C_5H_4Me)_3Y(thf)$ (21.7 µmol, 10 vol % DEVP in 20 ml toluene, 26 °C).

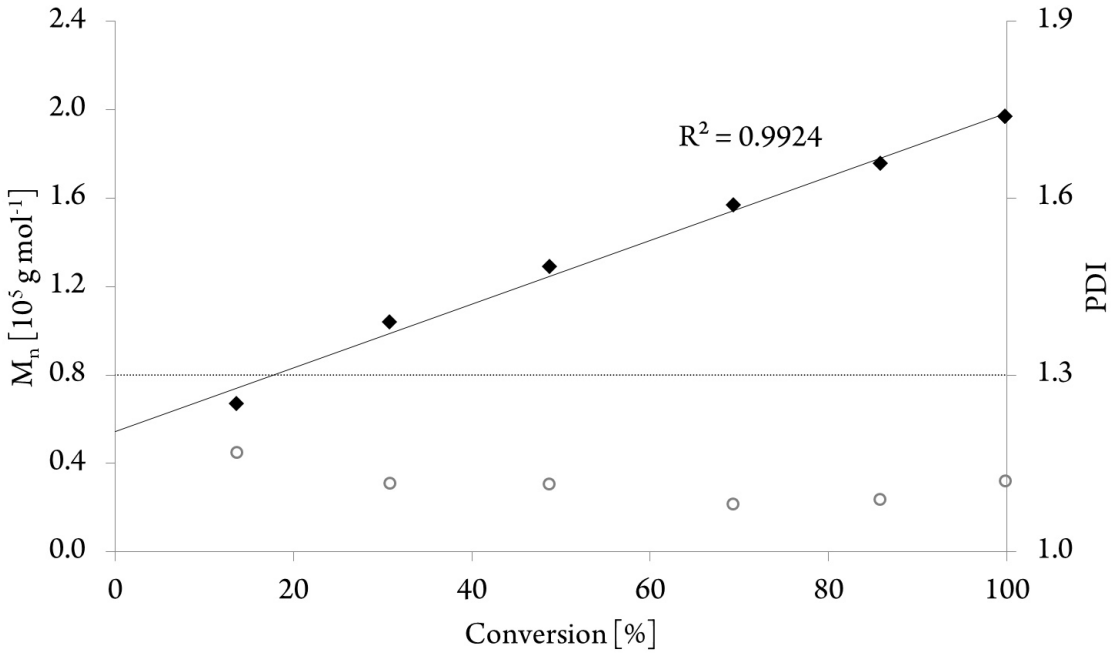

Figure S12: Number average molecular mass conversion plot for the polymerization of DEVP using $(C_5H_4Me)_3Y(thf)$ (21.7 µmol, 10 vol % DEVP in 20 ml toluene, 26 °C).

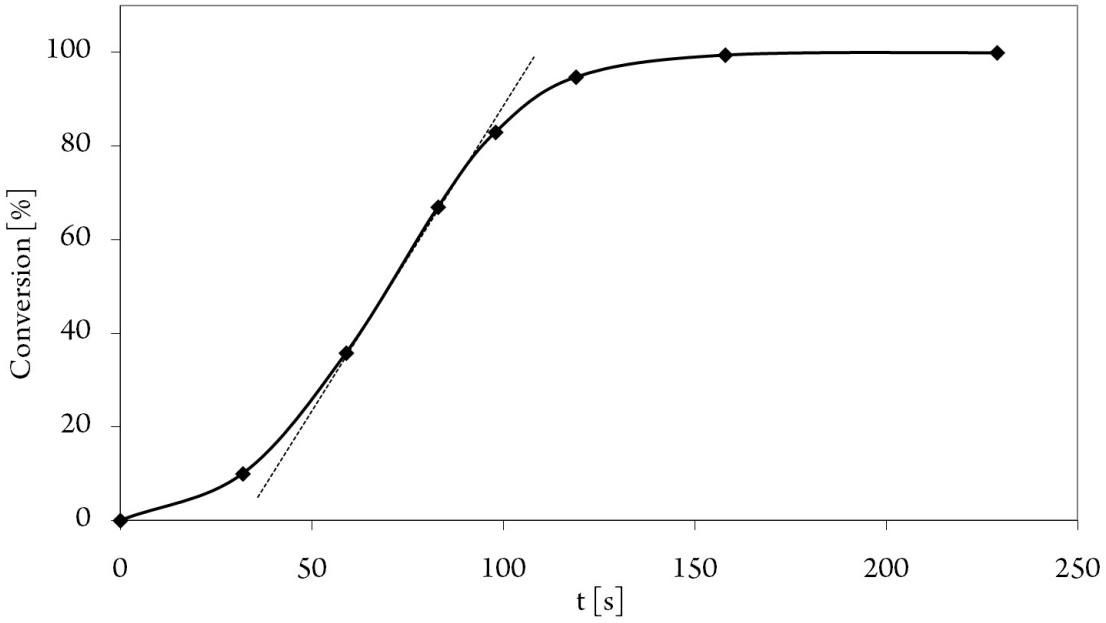

Figure S13: Conversion-reaction time plot for the polymerization of DEVP using $(C_5H_4Me)_3Y(thf)$ (21.7 µmol, 10 vol % DEVP in 20 ml toluene, 30 °C).

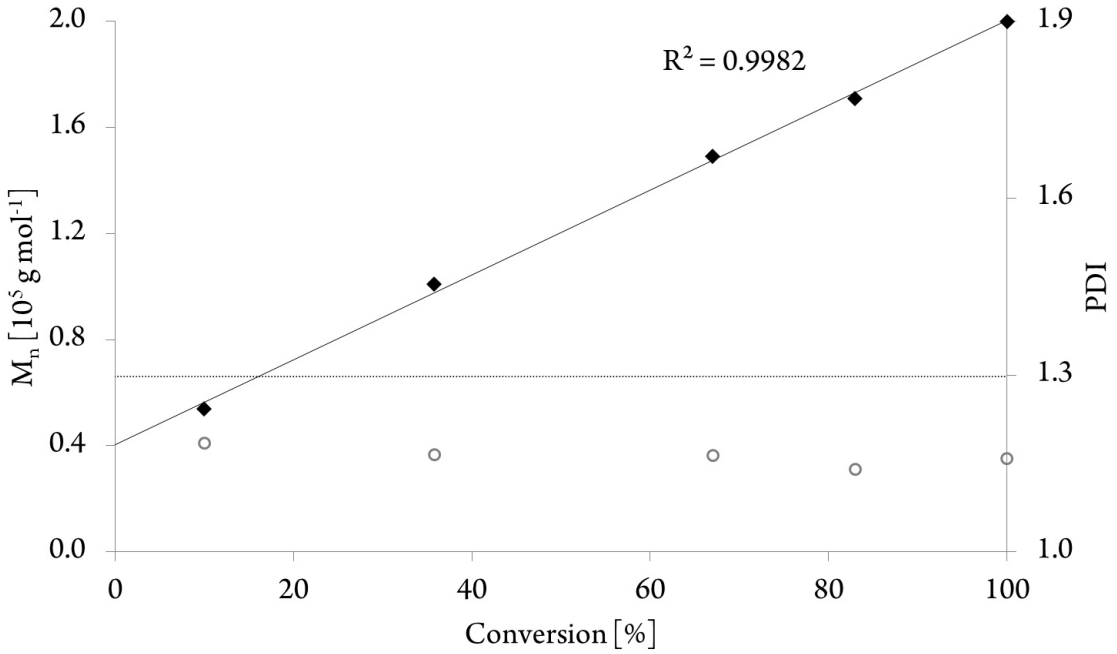

Figure S14: Number average molecular mass conversion plot for the polymerization of DEVP using $(C_5H_4Me)_3Y(thf)$ (21.7 µmol, 10 vol % DEVP in 20 ml toluene, 30 °C).

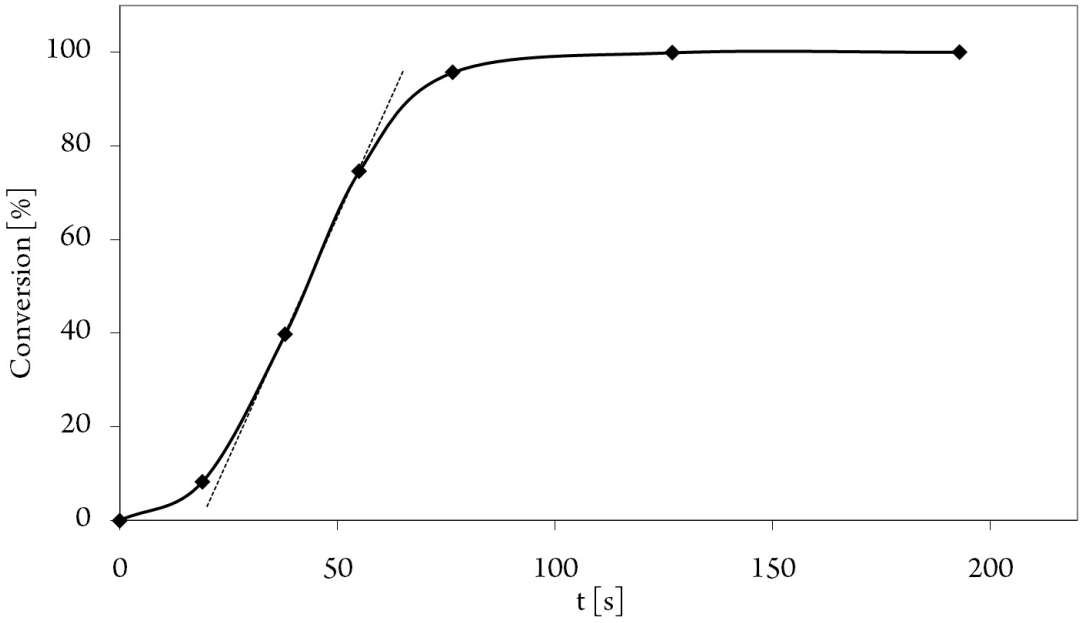

Figure S15: Conversion-reaction time plot for the polymerization of DEVP using $(C_5H_4Me)_3Y(thf)$ (21.7 µmol, 10 vol % DEVP in 20 ml toluene, 37 °C).

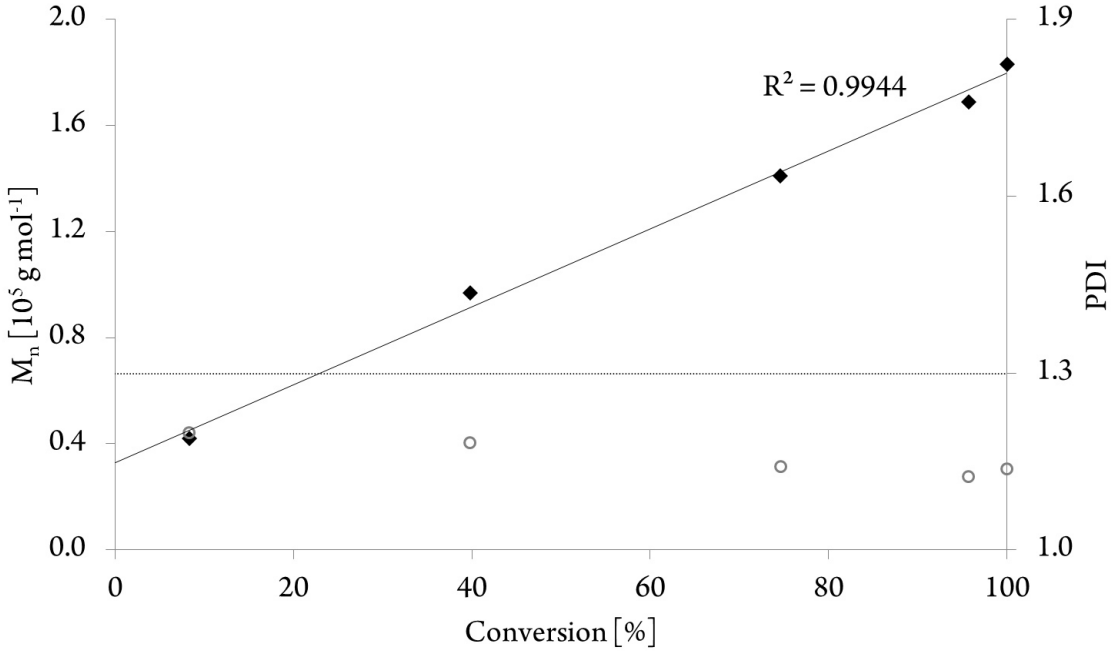

Figure S16: Number average molecular mass conversion plot for the polymerization of DEVP using $(C_5H_4Me)_3Y(thf)$ (21.7 µmol, 10 vol % DEVP in 20 ml toluene, 37 °C).

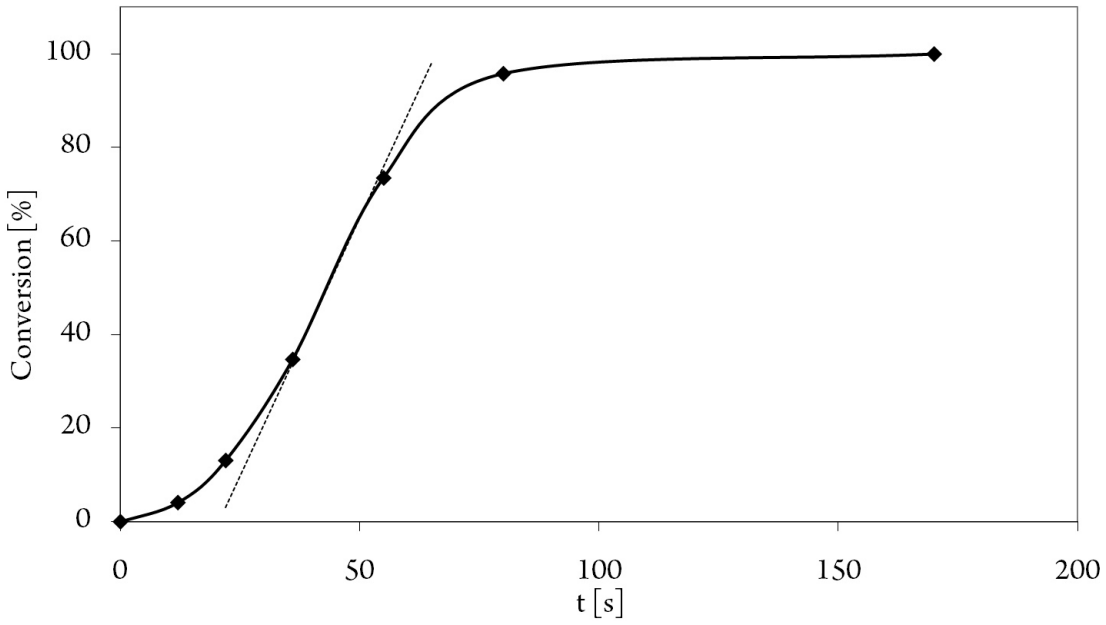

Figure S17: Conversion-reaction time plot for the polymerization of DEVP using $(C_5H_4Me)_3Y(thf)$ (21.7 µmol, 10 vol % DEVP in 20 ml toluene, 43 °C).

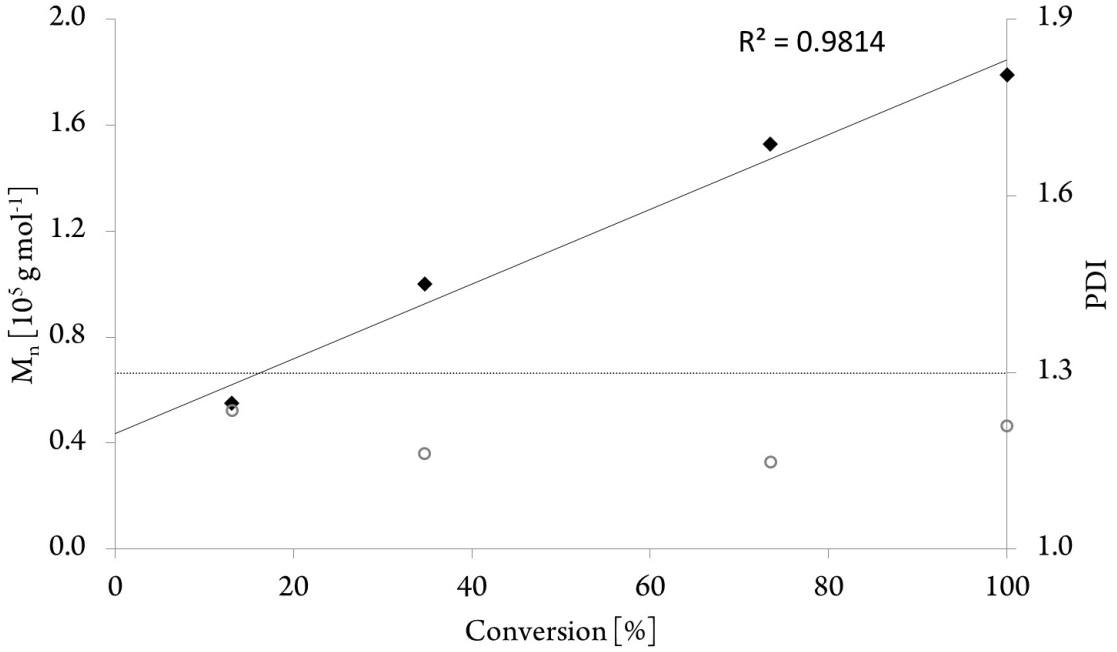

Figure S18: Number average molecular mass conversion plot for the polymerization of DEVP using $(C_5H_4Me)_3Y(thf)$ (21.7 µmol, 10 vol % DEVP in 20 ml toluene, 43 °C).

Table S2. Temperature-dependent kinetics for $(C_5H_4TMS)_3Y$-catalyzed DEVP polymerization (1.09 mmol L^{-1} $(C_5H_4TMS)_3Y$, 0.651 mol L^{-1} DEVP, toluene)

T [°C]	TOF [h^{-1}]	I^*_t [%]	TOF/I^*_t [h^{-1}]	Conversion at maximum rate	Rate [mol L^{-1} s^{-1}]	1/T [K^{-1}]	ln(k'/T)
14	6000	75	8500	4.5	1.92E-03	3.48E-03	-4.33
20	8700	72	12000	10.0	2.52E-03	3.42E-03	-3.98
23	8200	62	13500	5.0	2.91E-03	3.37E-03	-3.74
30	14000	61	23000	6.2	4.23E-03	3.30E-03	-3.38
36	18500	68	27000	8.3	5.56E-03	3.23E-03	-3.20
44	29500	68	43000	13.2	8.88E-03	3.15E-03	-2.71
56	47000	67	71000	14.9	1.36E-02	3.04E-03	-2.28

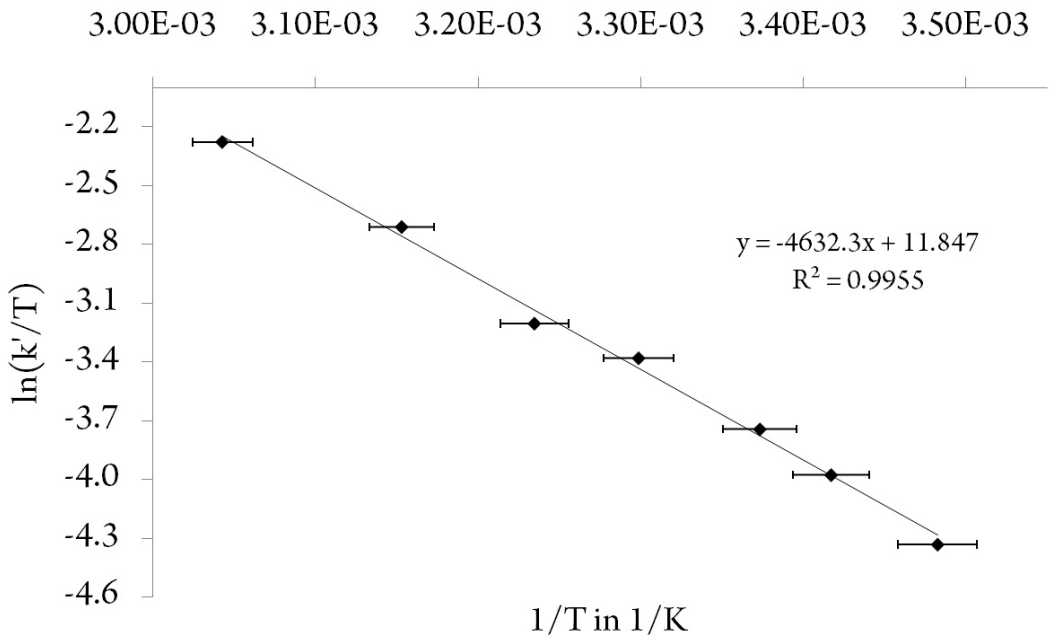

Figure S19: Result for the Eyring-plot of $(C_5H_4TMS)_3Y$-initiated DEVP (10 vol %) polymerization in toluene (14 – 56 °C, $\Delta H^{\ddagger}$ = 38.5 kJ mol^{-1}, $\Delta S^{\ddagger}$ = -99.0 J $(mol\ K)^{-1}$).

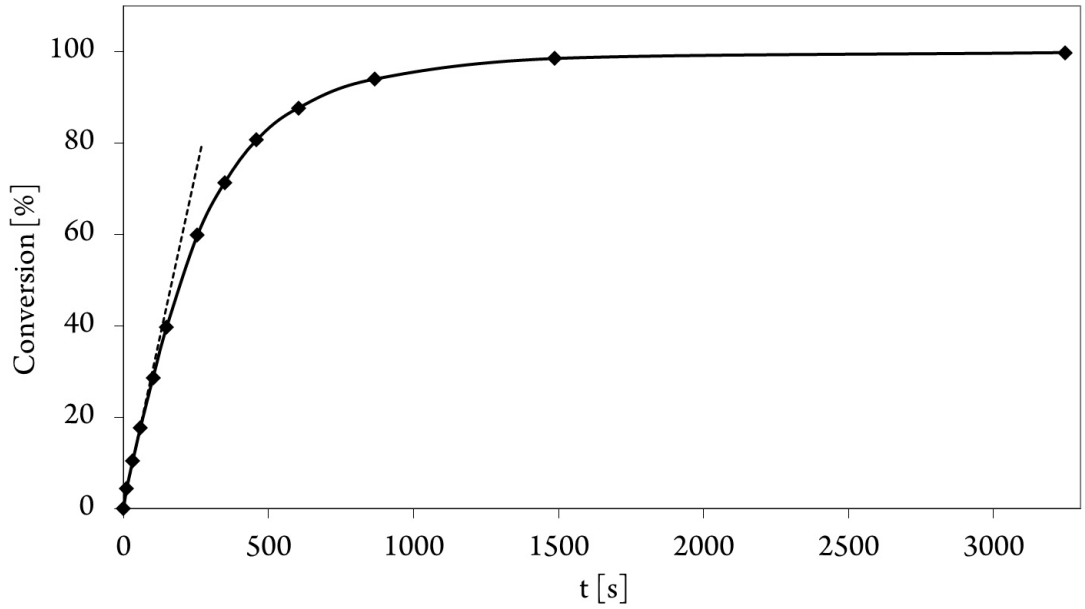

Figure S20: Conversion-reaction time plot for the polymerization of DEVP using $(C_5H_4TMS)_3Y$ (21.7 µmol, 10 vol % DEVP in 20 ml toluene, 14 °C).

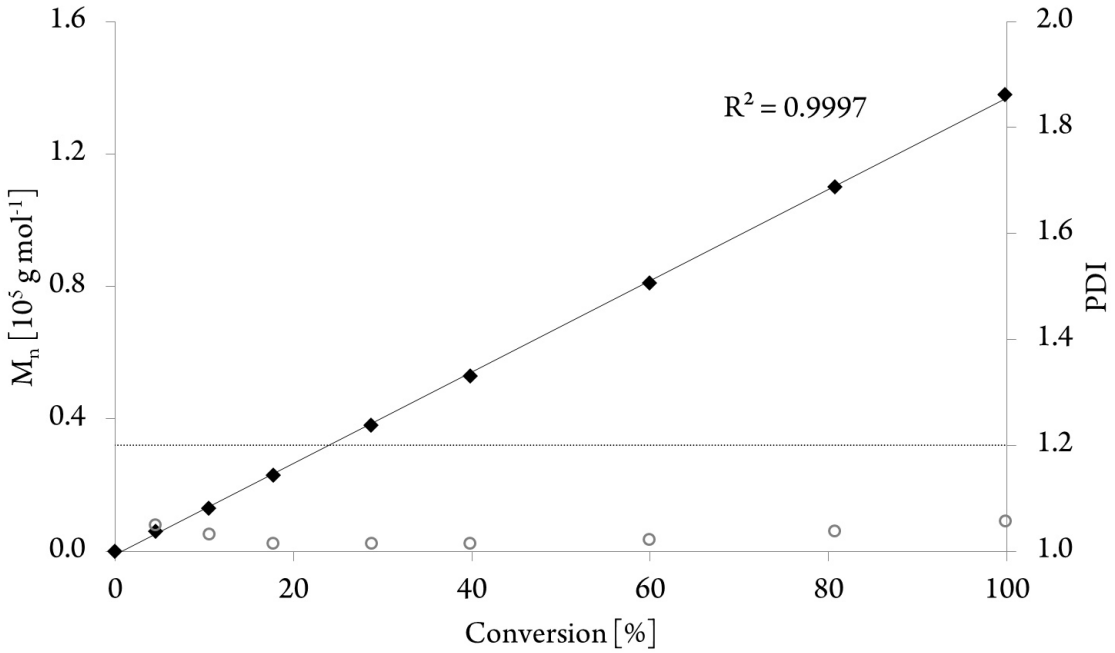

Figure S21: Number average molecular mass conversion plot for the polymerization of DEVP using $(C_5H_4TMS)_3Y$ (21.7 µmol, 10 vol % DEVP in 20 ml toluene, 14 °C).

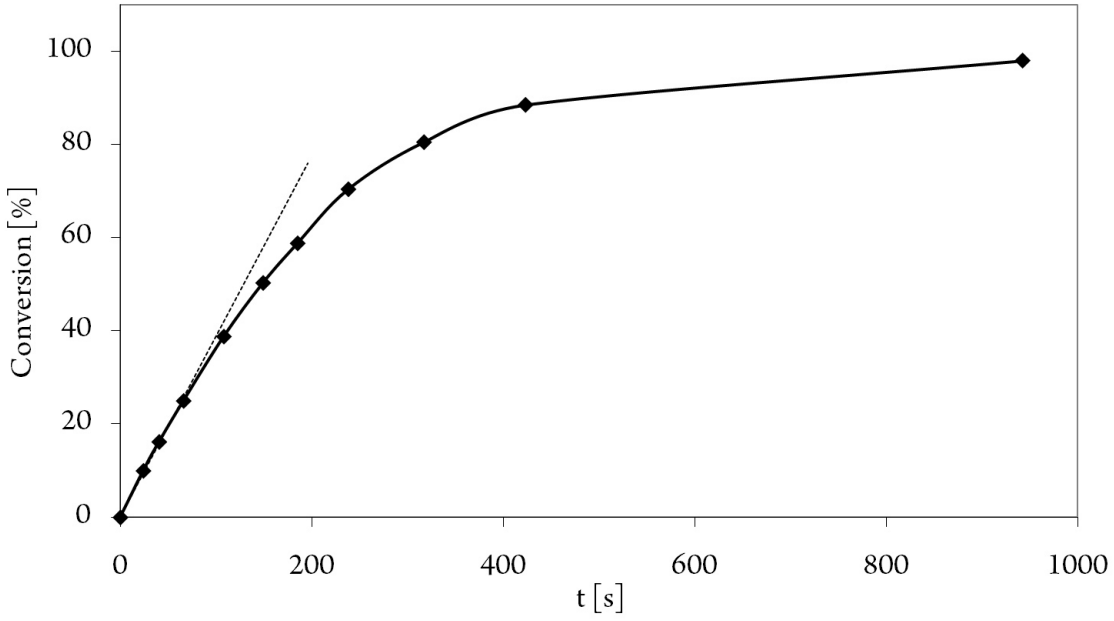

Figure S22: Conversion-reaction time plot for the polymerization of DEVP using $(C_5H_4TMS)_3Y$ (21.7 µmol, 10 vol % DEVP in 20 ml toluene, 20 °C).

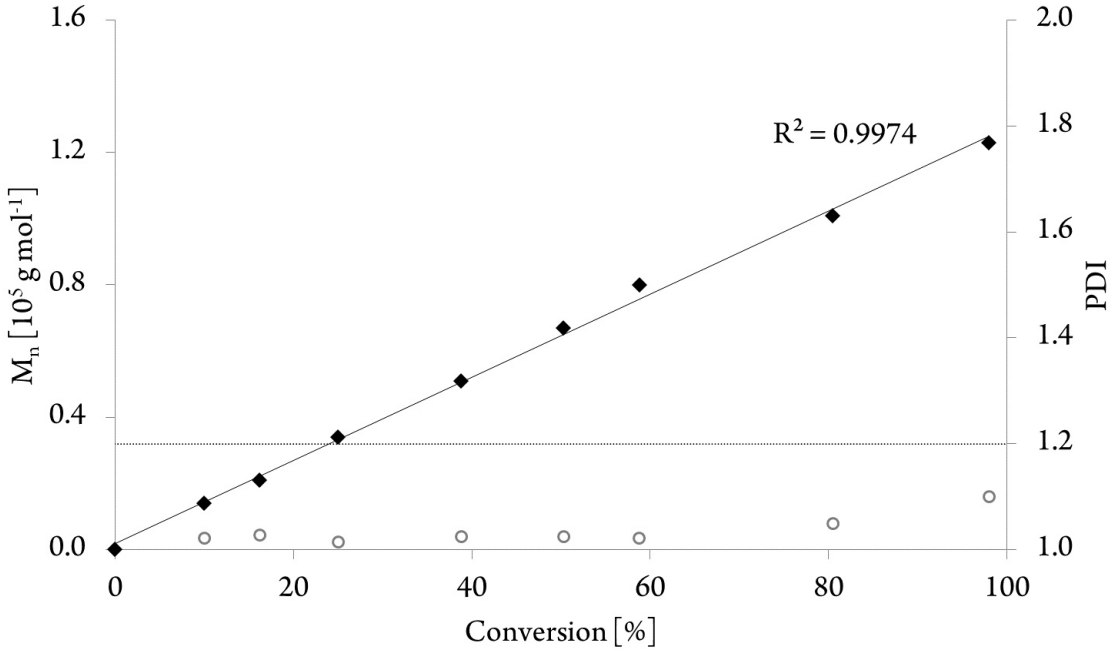

Figure S23: Number average molecular mass conversion plot for the polymerization of DEVP using $(C_5H_4TMS)_3Y$ (21.7 µmol, 10 vol % DEVP in 20 ml toluene, 20 °C).

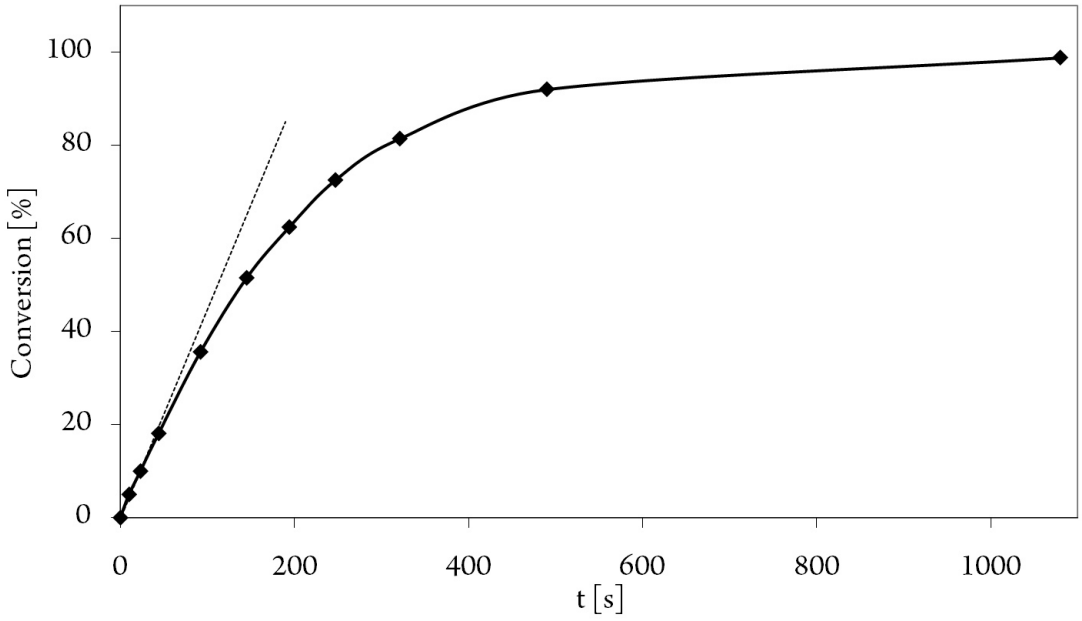

Figure S24: Conversion-reaction time plot for the polymerization of DEVP using $(C_5H_4TMS)_3Y$ (21.7 µmol, 10 vol % DEVP in 20 ml toluene, 23 °C).

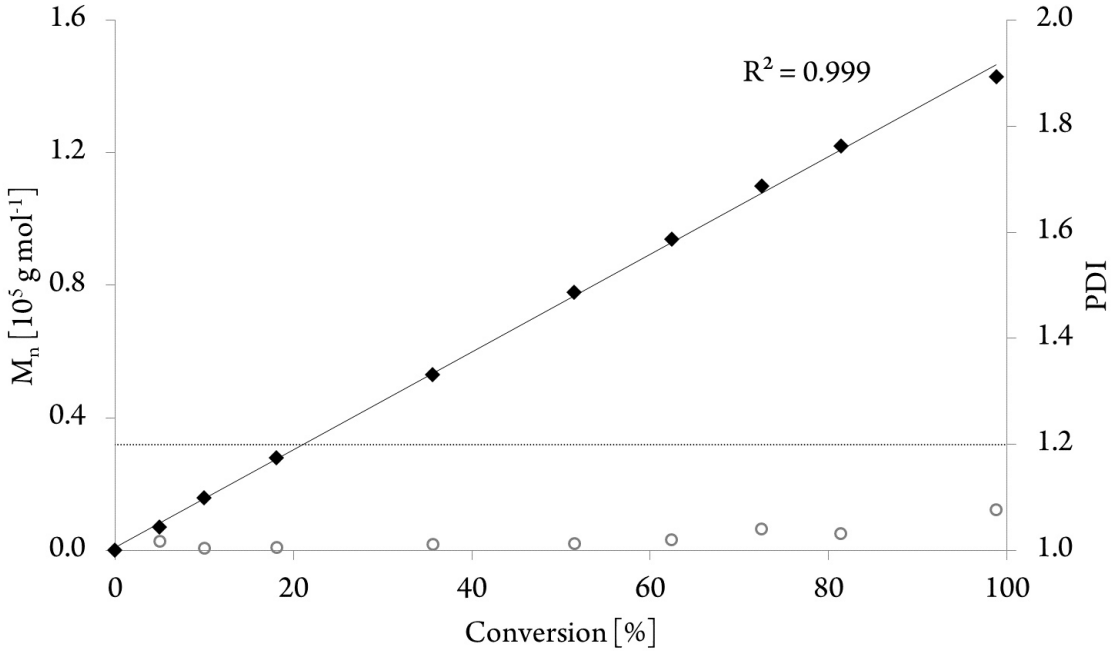

Figure S25: Number average molecular mass conversion plot for the polymerization of DEVP using $(C_5H_4TMS)_3Y$ (21.7 µmol, 10 vol % DEVP in 20 ml toluene, 23 °C).

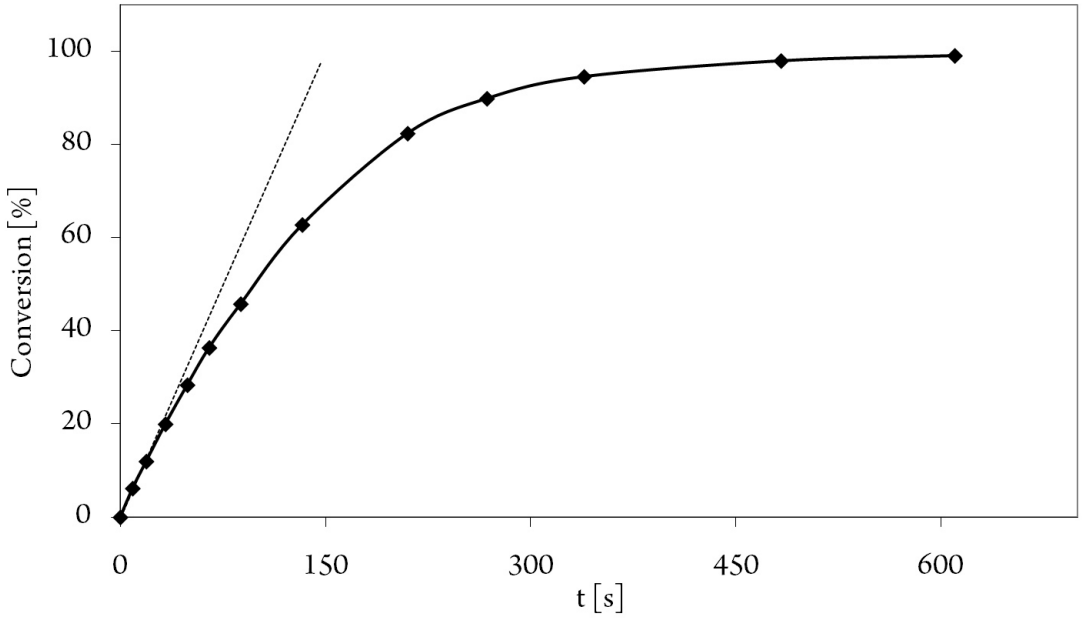

Figure S26: Conversion-reaction time plot for the polymerization of DEVP using $(C_5H_4TMS)_3Y$ (21.7 µmol, 10 vol % DEVP in 20 ml toluene, 30 °C).

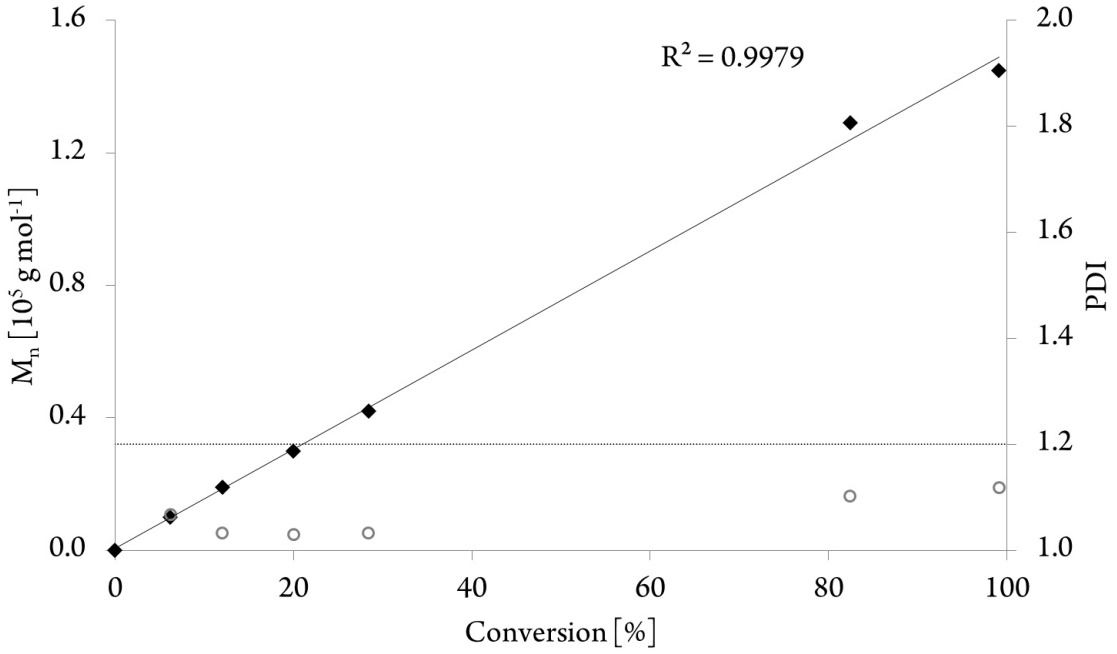

Figure S27: Number average molecular mass conversion plot for the polymerization of DEVP using $(C_5H_4TMS)_3Y$ (21.7 µmol, 10 vol % DEVP in 20 ml toluene, 30 °C).

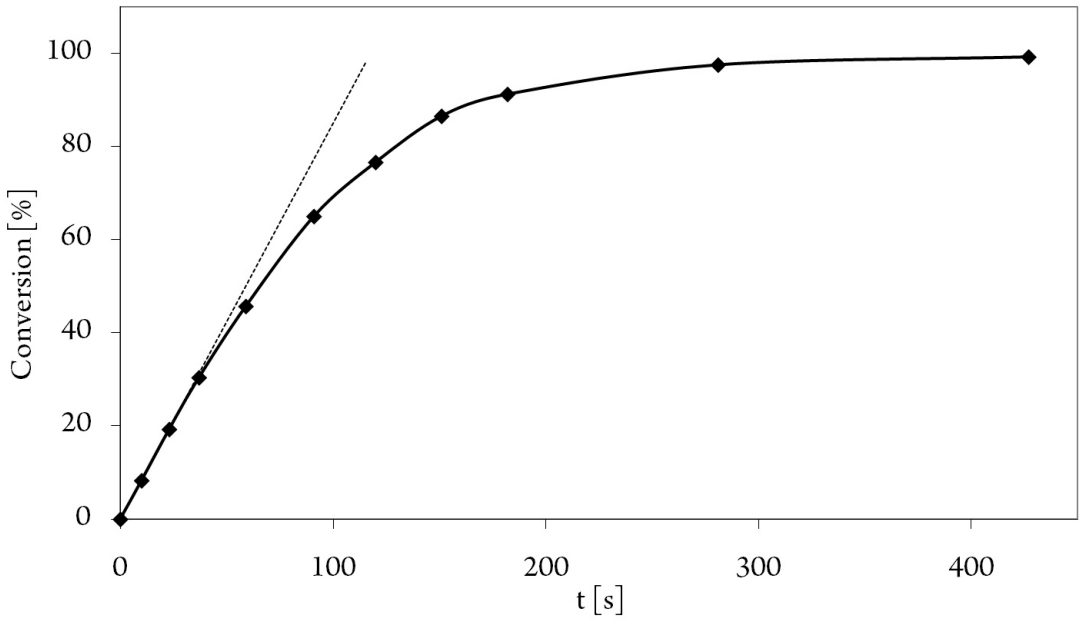

Figure S28: Conversion-reaction time plot for the polymerization of DEVP using $(C_5H_4TMS)_3Y$ (21.7 µmol, 10 vol % DEVP in 20 ml toluene, 36 °C).

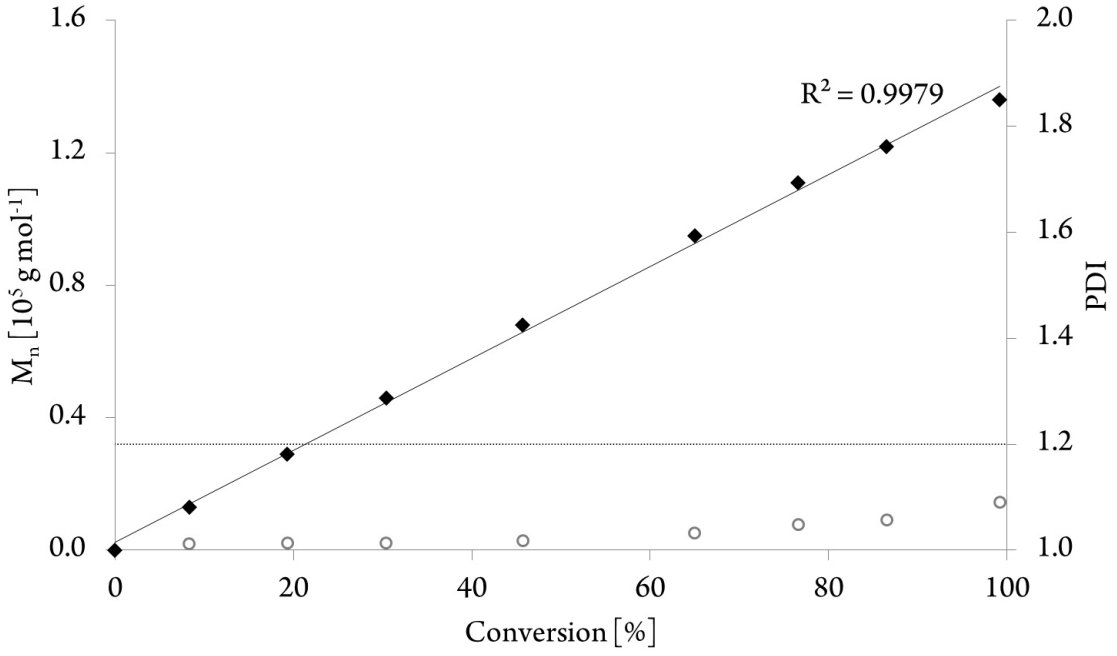

Figure S29: Number average molecular mass conversion plot for the polymerization of DEVP using $(C_5H_4TMS)_3Y$ (21.7 µmol, 10 vol % DEVP in 20 ml toluene, 36 °C).

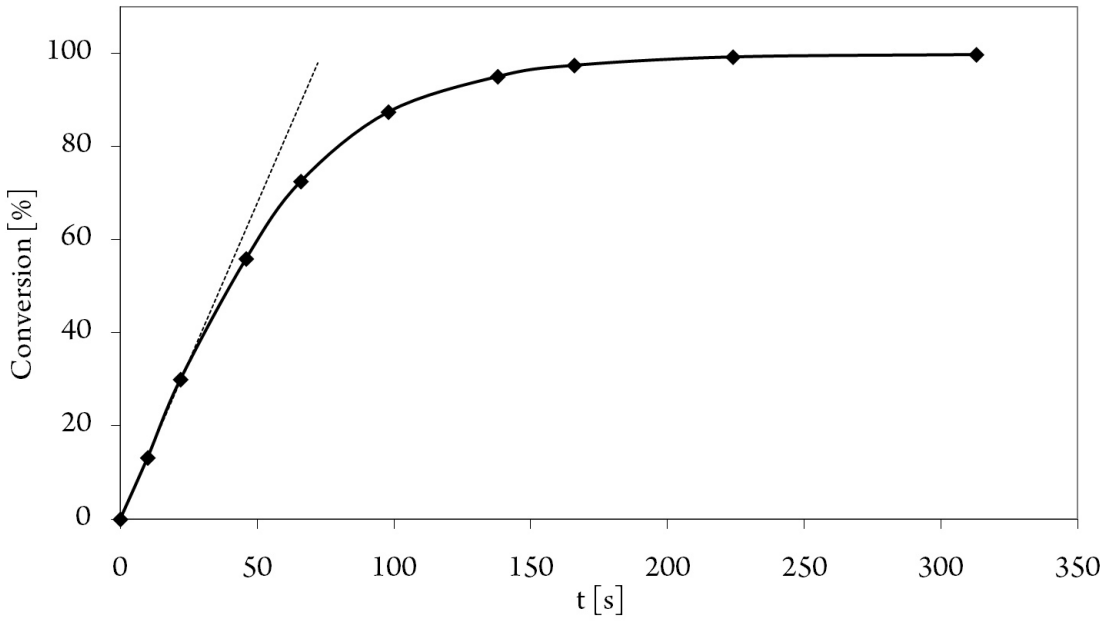

Figure S30: Conversion-reaction time plot for the polymerization of DEVP using $(C_5H_4TMS)_3Y$ (21.7 µmol, 10 vol % DEVP in 20 ml toluene, 44 °C).

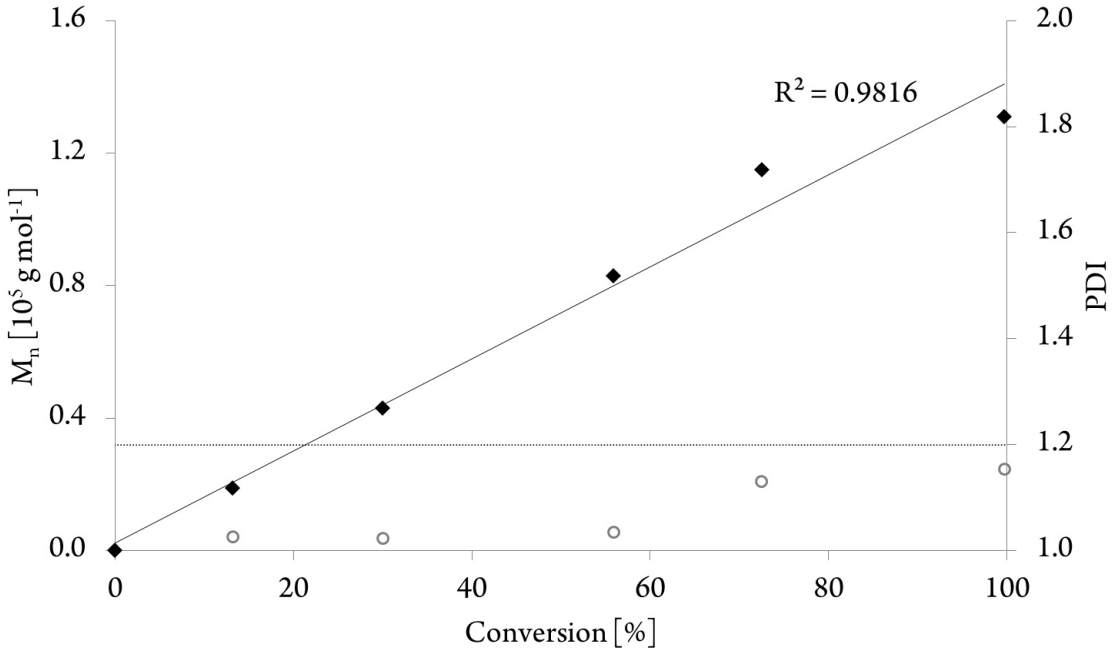

Figure S31: Number average molecular mass conversion plot for the polymerization of DEVP using $(C_5H_4TMS)_3Y$ (21.7 µmol, 10 vol % DEVP in 20 ml toluene, 44 °C).

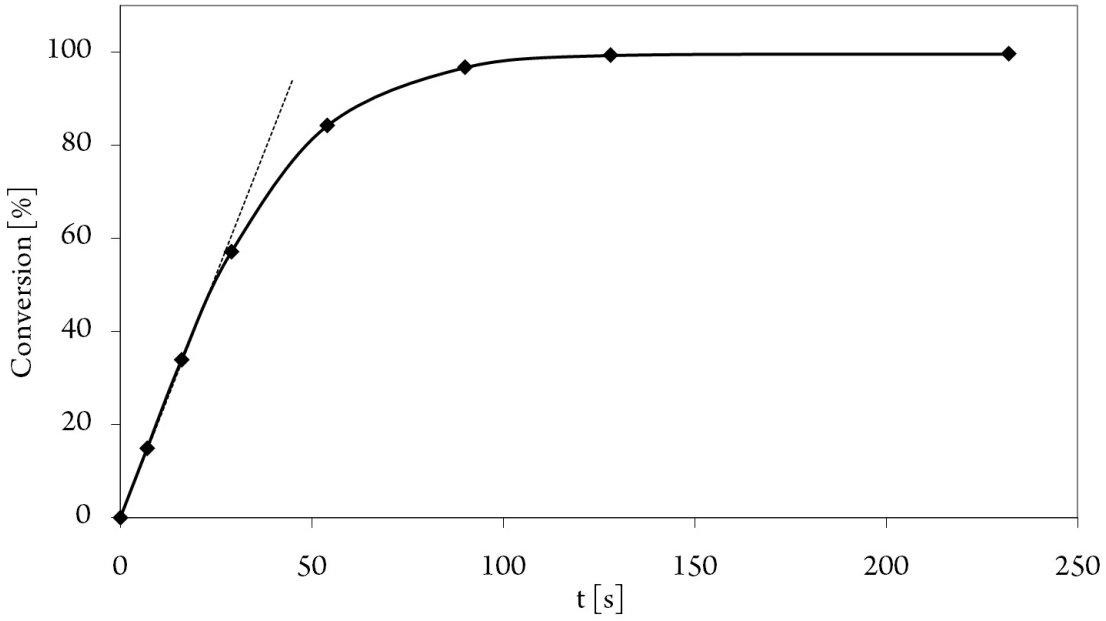

Figure S32: Conversion-reaction time plot for the polymerization of DEVP using $(C_5H_4TMS)_3Y$ (21.7 µmol, 10 vol % DEVP in 20 ml toluene, 56 °C).

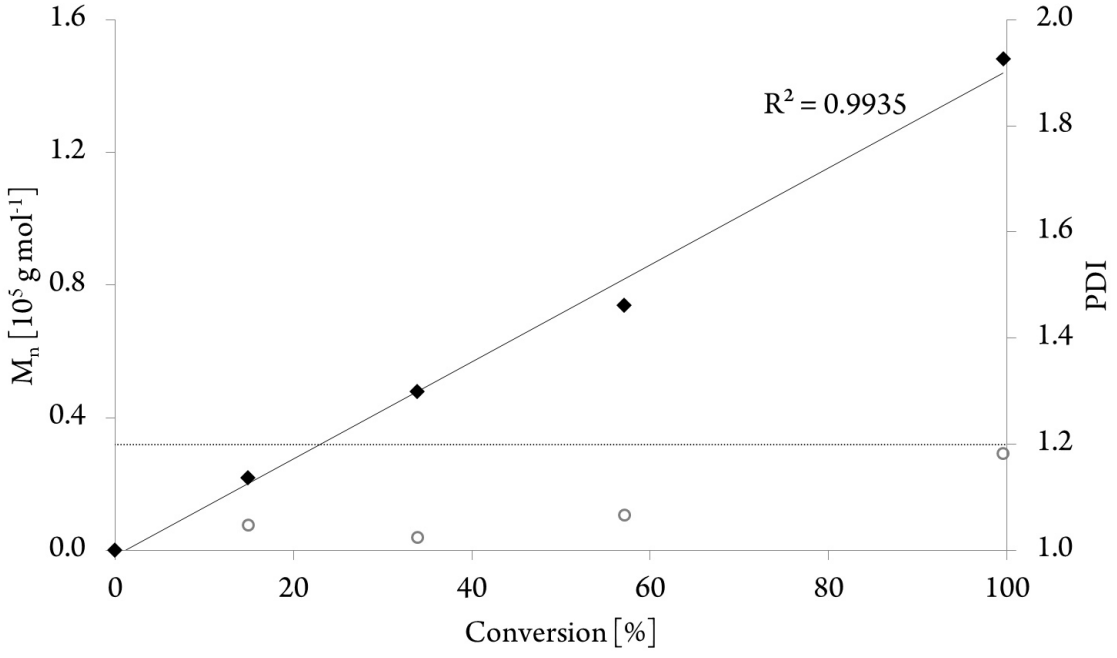

Figure S33: Number average molecular mass conversion plot for the polymerization of DEVP using $(C_5H_4TMS)_3Y$ (21.7 µmol, 10 vol % DEVP in 20 ml toluene, 56 °C).

Table S3. Temperature-dependent kinetics for $(C_5Me_4H)_3Y$-catalyzed DEVP polymerization (1.09 mmol L^{-1} $(C_5Me_4H)_3Y$, 0.651 mol L^{-1} DEVP, toluene)

T [°C]	TOF [h^{-1}]	I^*_t [%]	TOF/I^*_t [h^{-1}]	Conversion at maximum rate	Rate [mol L^{-1} s^{-1}]	1/T [K^{-1}]	ln(k'/T)
16	3500	37.8	9300	10.0	1.06E-03	3.45E-03	-4.19
19	5700	49.8	11400	13.5	1.69E-03	3.42E-03	-3.97
25	9600	51.8	18500	12.1	2.90E-03	3.35E-03	-3.50
30	13200	52.3	25200	15.4	3.97E-03	3.30E-03	-3.18
35	16900	39.4	42800	7.2	5.08E-03	3.24E-03	-2.76
40	23800	53.2	44800	14.7	7.18E-03	3.20E-03	-2.64
45	31100	44.3	70200	7.2	9.38E-03	3.14E-03	-2.29

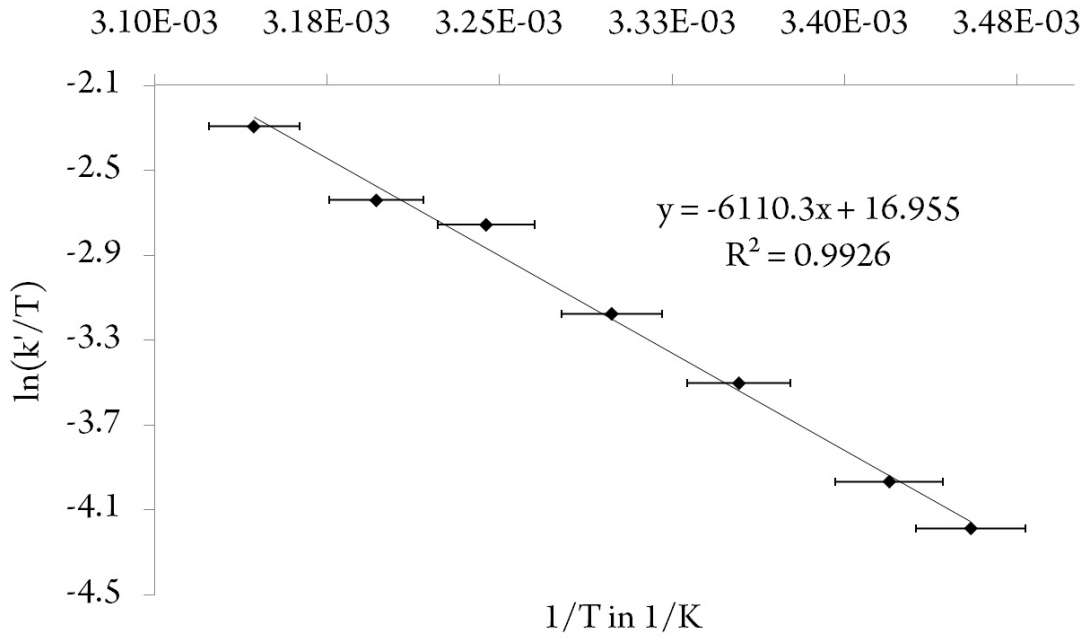

Figure S34: Result for the Eyring-plot of $(C_5H_4Me)_3Y$-initiated DEVP (10 vol %) polymerization in toluene (16 – 45 °C, $\Delta H^{\ddagger}$ = 50.8 kJ mol^{-1}, $\Delta S^{\ddagger}$ = -56.5 J $(mol\ K)^{-1}$).

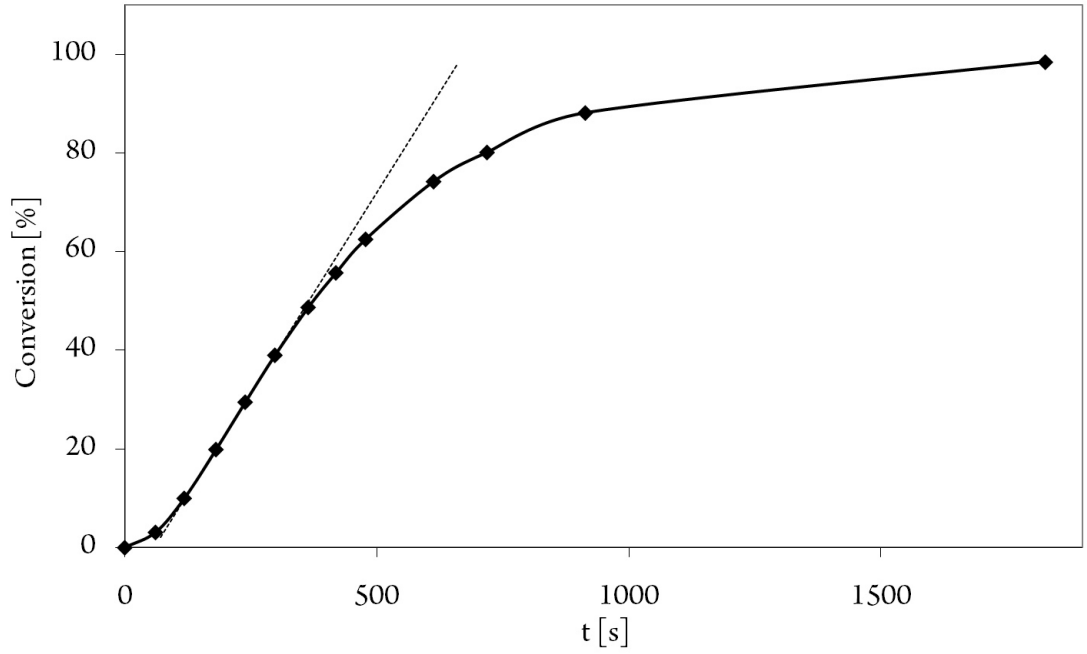

Figure S35: Conversion-reaction time plot for the polymerization of DEVP using $(C_5Me_4H)_3Y$ (21.7 µmol, 10 vol % DEVP in 20 ml toluene, 16 °C).

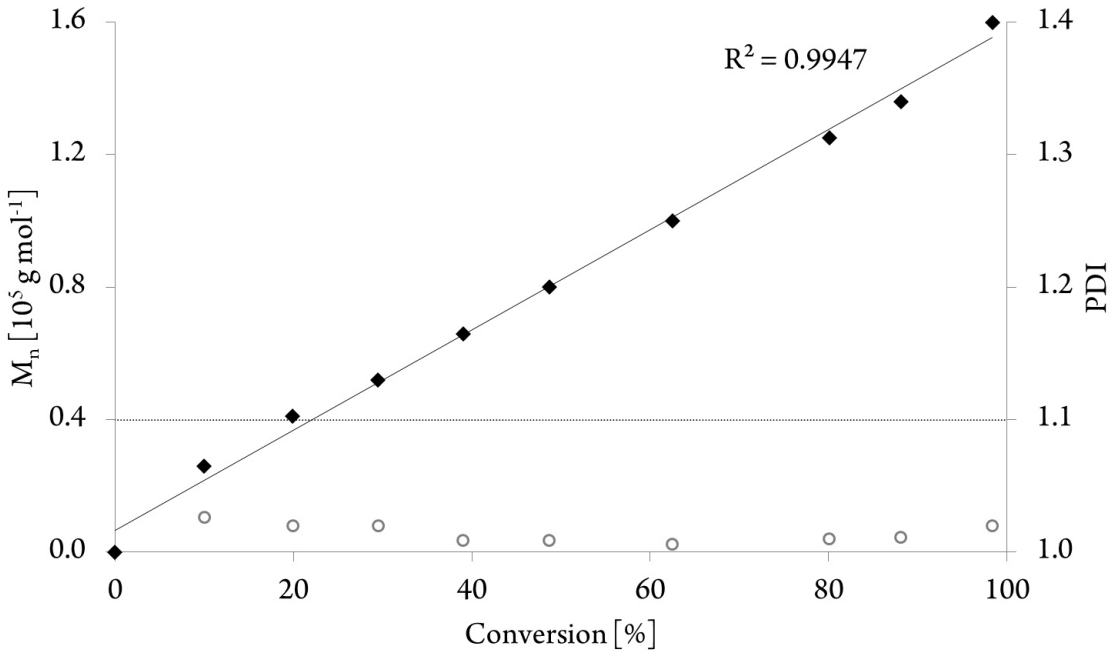

Figure S36: Number average molecular mass conversion plot for the polymerization of DEVP using $(C_5Me_4H)_3Y$ (21.7 µmol, 10 vol % DEVP in 20 ml toluene, 16 °C).

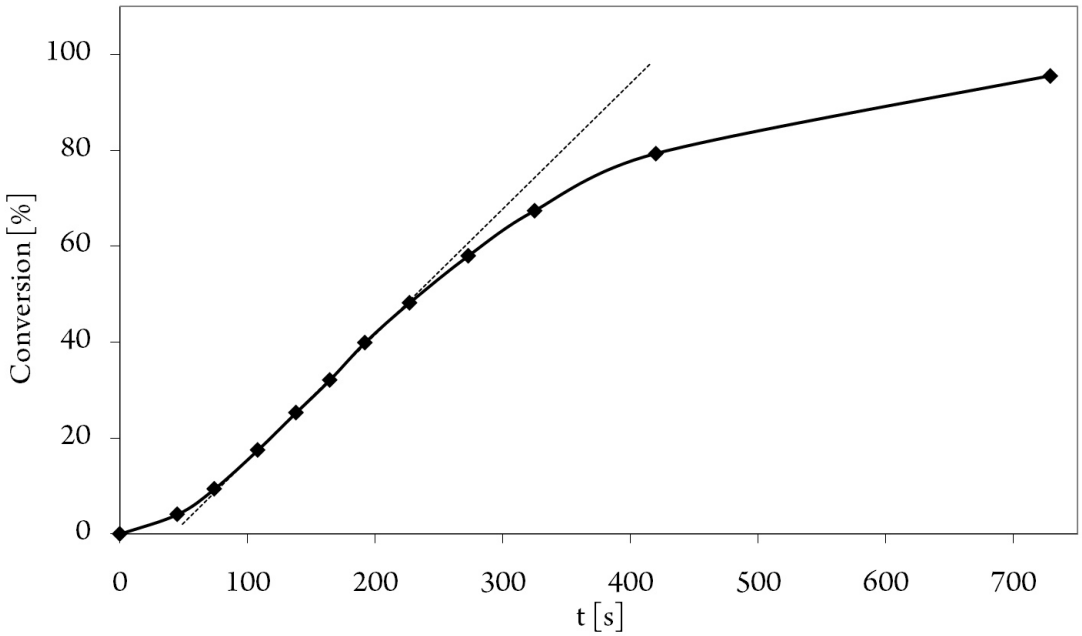

Figure S37: Conversion-reaction time plot for the polymerization of DEVP using $(C_5Me_4H)_3Y$ (21.7 µmol, 10 vol % DEVP in 20 ml toluene, 19 °C).

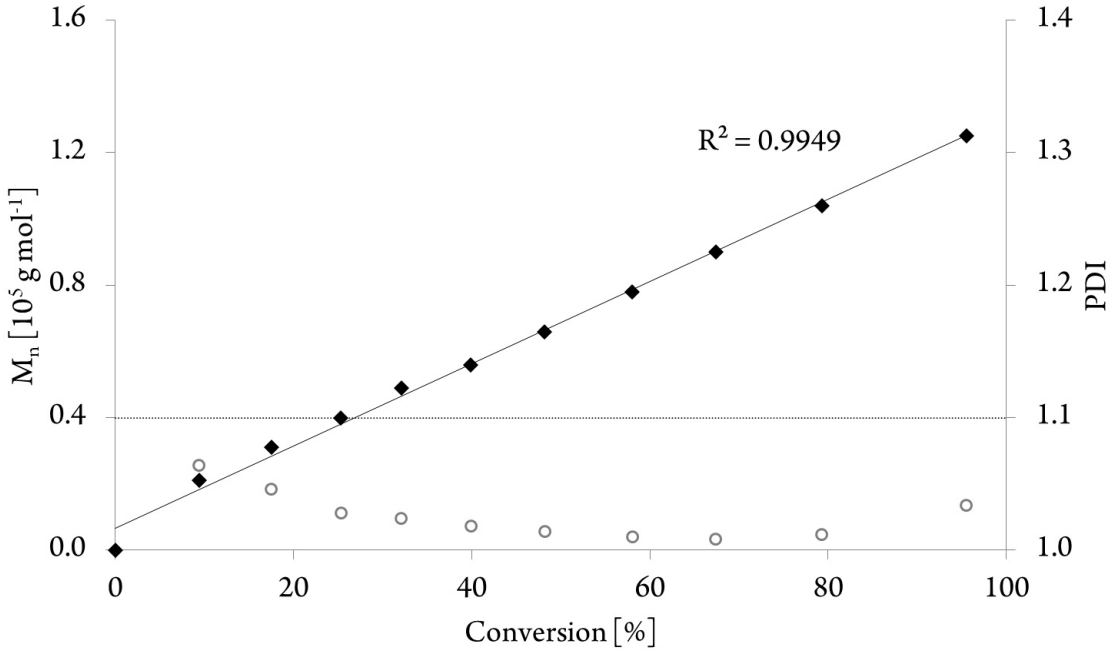

Figure S38: Number average molecular mass conversion plot for the polymerization of DEVP using $(C_5Me_4H)_3Y$ (21.7 µmol, 10 vol % DEVP in 20 ml toluene, 19 °C).

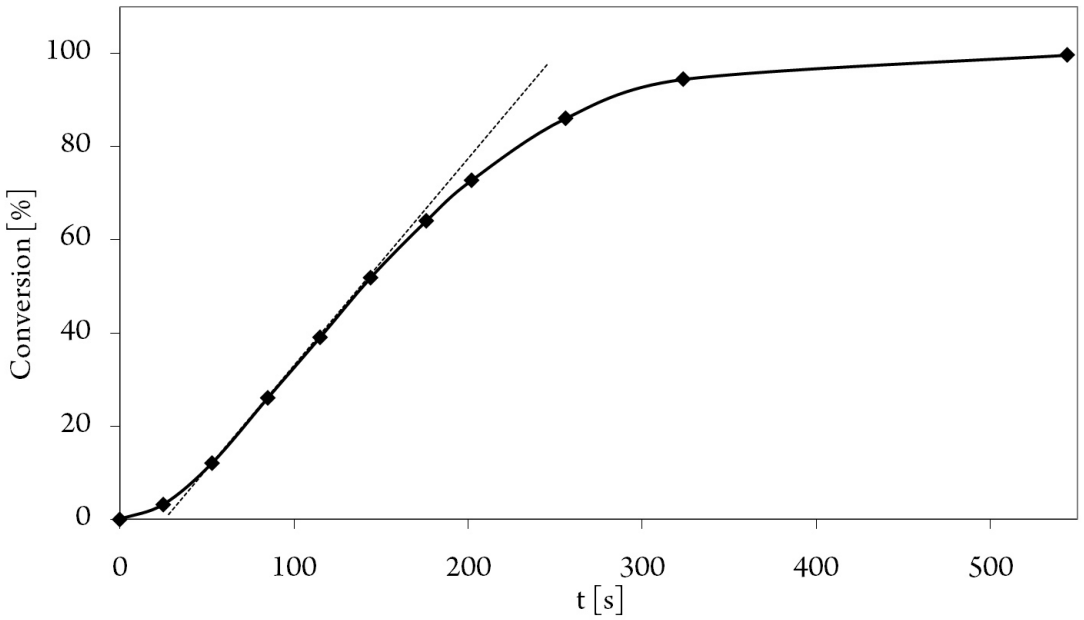

Figure S39: Conversion-reaction time plot for the polymerization of DEVP using $(C_5Me_4H)_3Y$ (21.7 µmol, 10 vol % DEVP in 20 ml toluene, 25 °C).

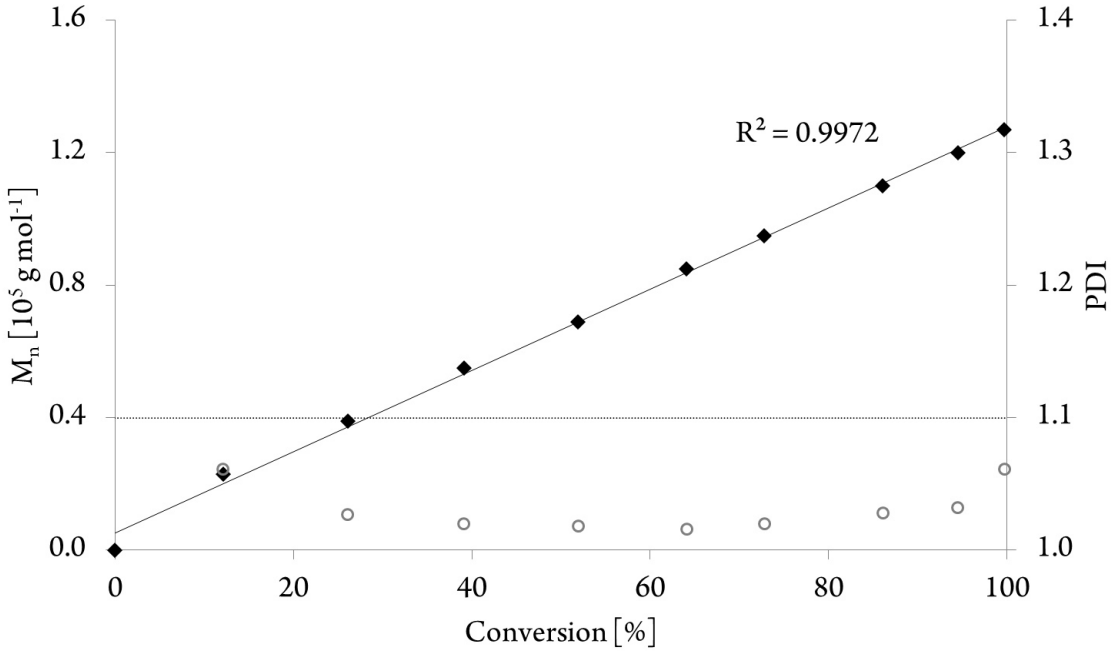

Figure S40: Number average molecular mass conversion plot for the polymerization of DEVP using $(C_5Me_4H)_3Y$ (21.7 µmol, 10 vol % DEVP in 20 ml toluene, 25 °C).

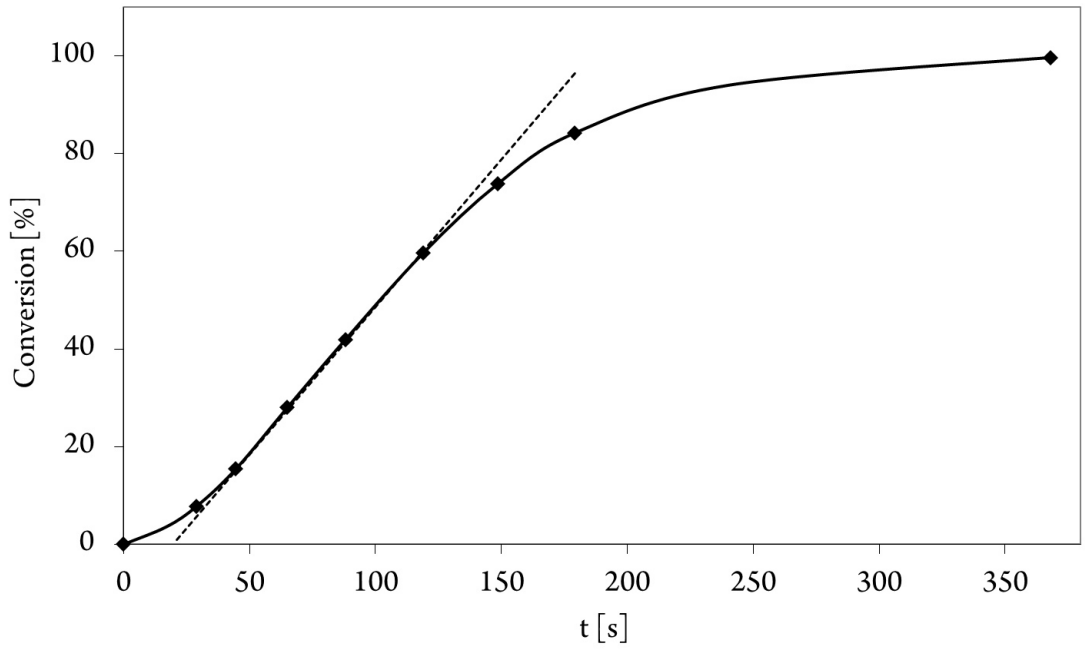

Figure S41: Conversion-reaction time plot for the polymerization of DEVP using $(C_5Me_4H)_3Y$ (21.7 µmol, 10 vol % DEVP in 20 ml toluene, 30 °C).

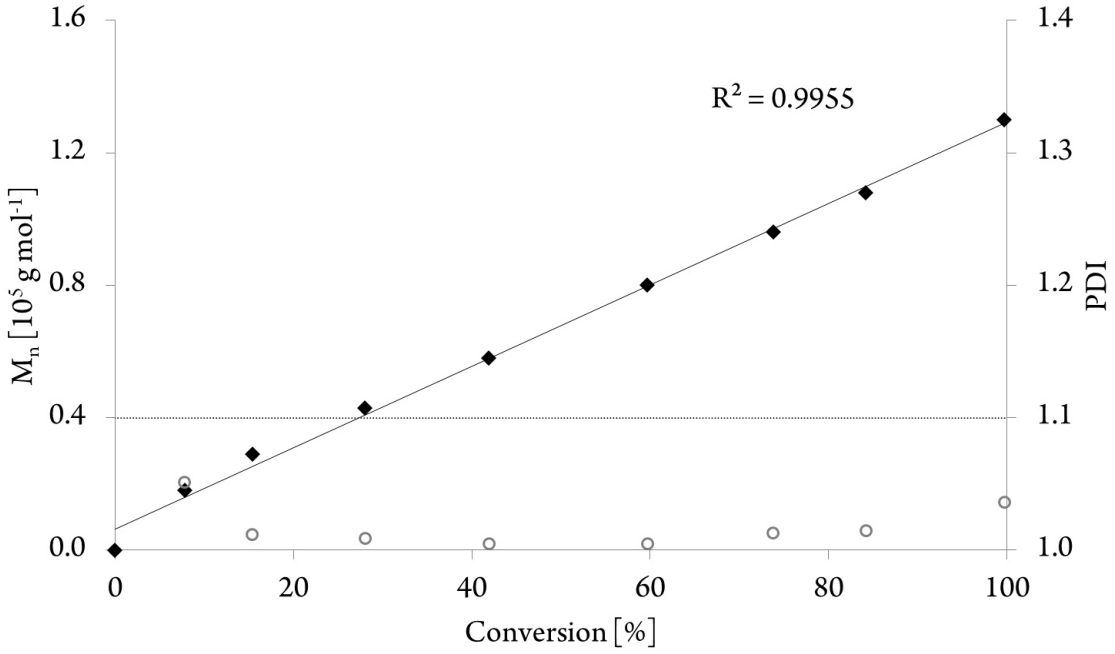

Figure S42: Number average molecular mass conversion plot for the polymerization of DEVP using $(C_5Me_4H)_3Y$ (21.7 µmol, 10 vol % DEVP in 20 ml toluene, 30 °C).

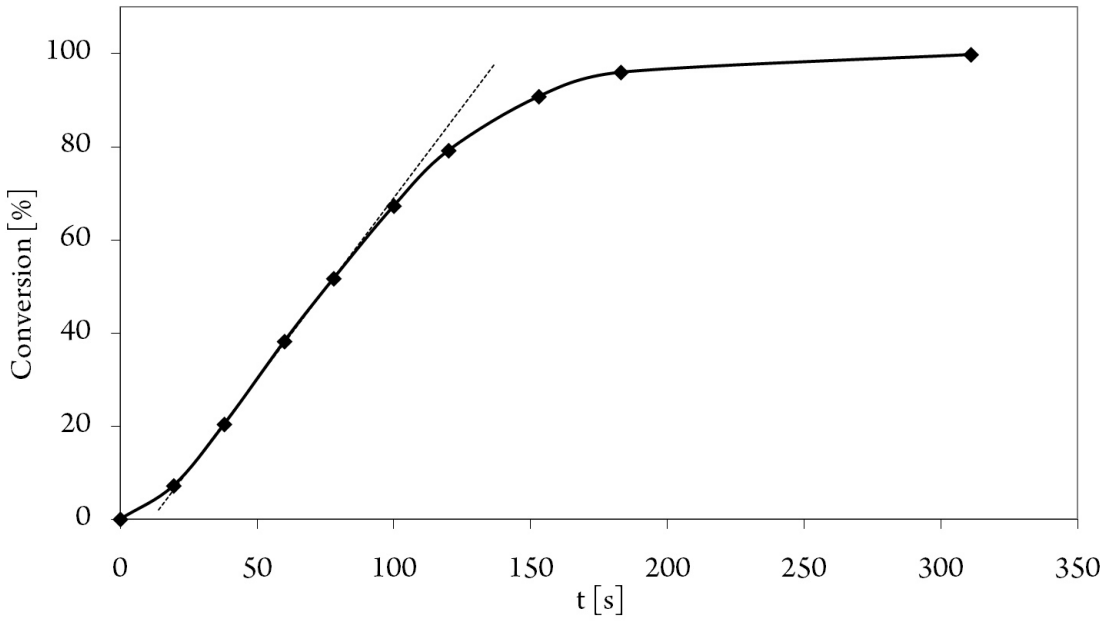

Figure S43: Conversion-reaction time plot for the polymerization of DEVP using $(C_5Me_4H)_3Y$ (21.7 µmol, 10 vol % DEVP in 20 ml toluene, 35 °C).

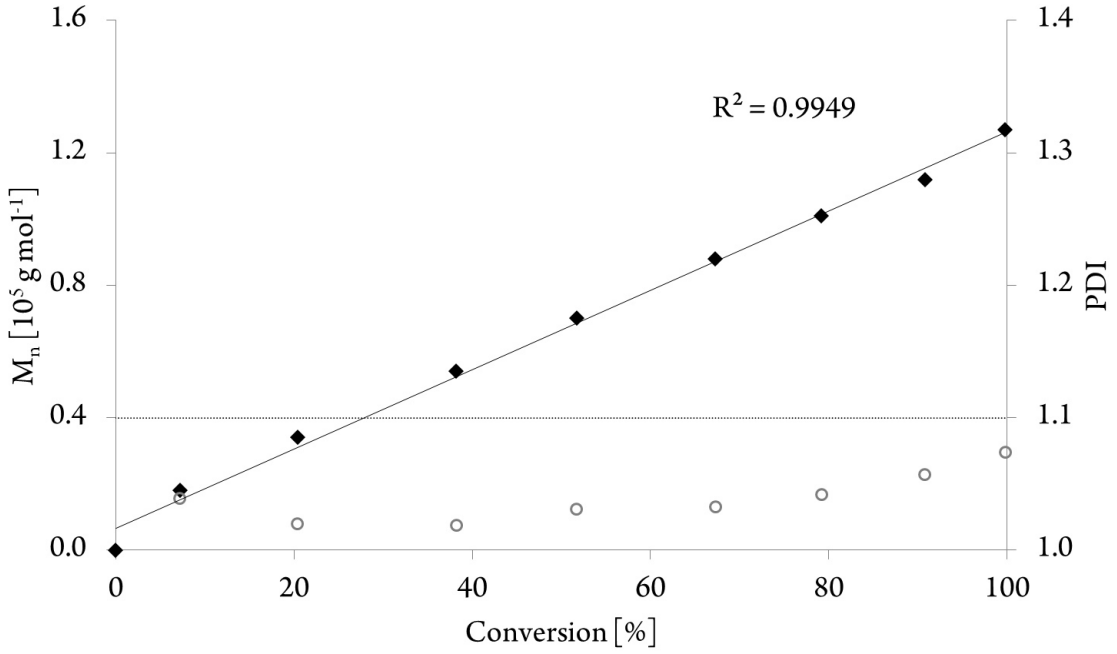

Figure S44: Number average molecular mass conversion plot for the polymerization of DEVP using $(C_5Me_4H)_3Y$ (21.7 µmol, 10 vol % DEVP in 20 ml toluene, 35 °C).

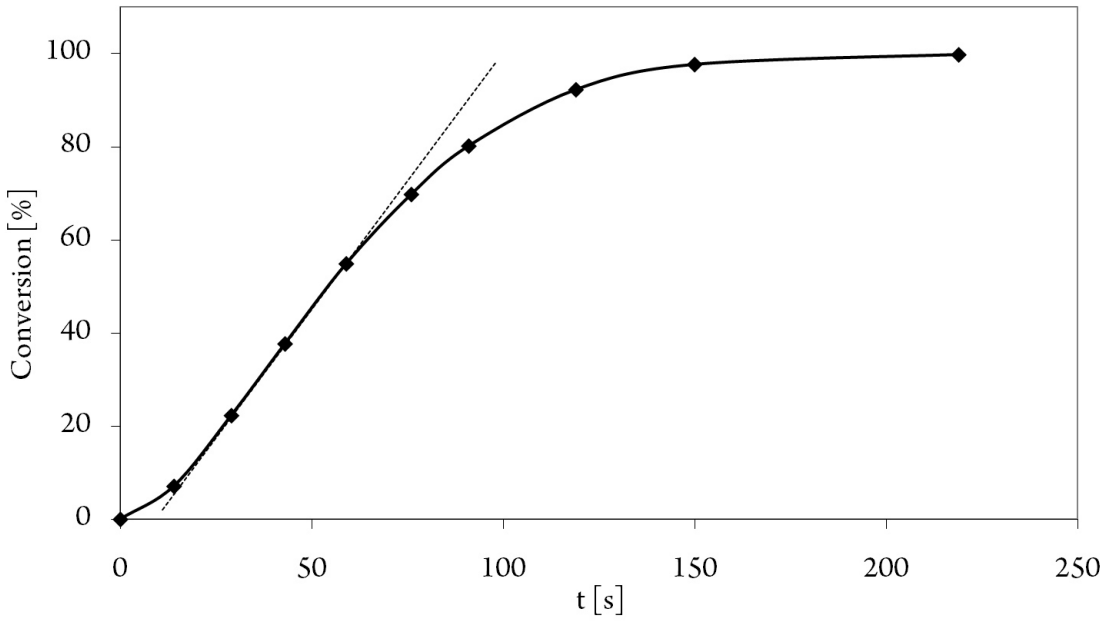

Figure S45: Conversion-reaction time plot for the polymerization of DEVP using $(C_5Me_4H)_3Y$ (21.7 µmol, 10 vol % DEVP in 20 ml toluene, 40 °C).

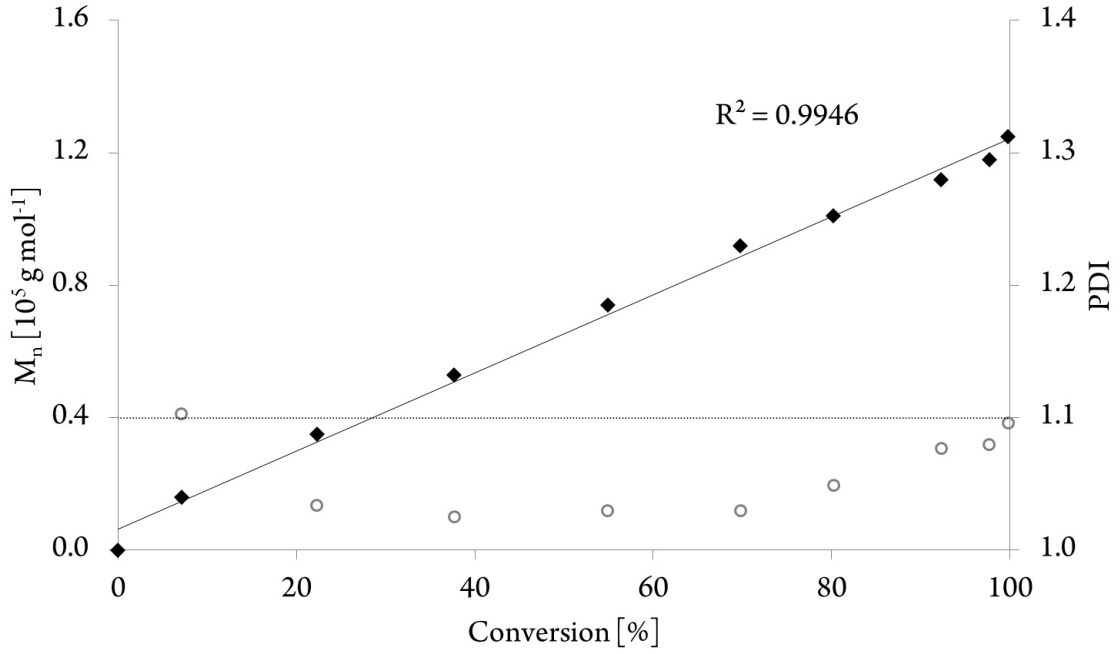

Figure S46: Number average molecular mass conversion plot for the polymerization of DEVP using $(C_5Me_4H)_3Y$ (21.7 µmol, 10 vol % DEVP in 20 ml toluene, 40 °C).

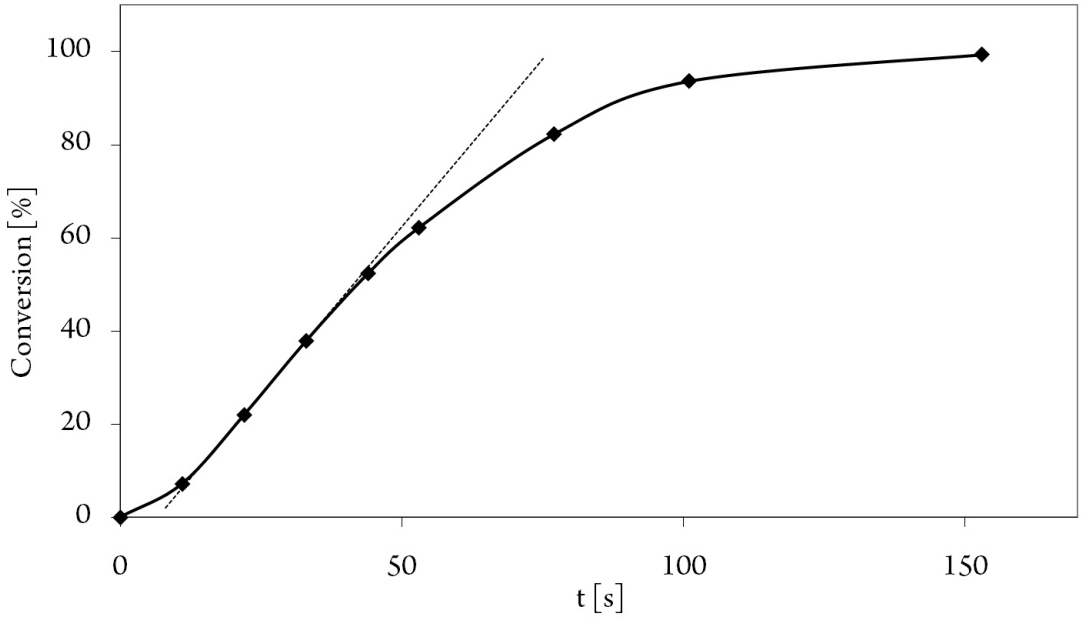

Figure S47: Conversion-reaction time plot for the polymerization of DEVP using $(C_5Me_4H)_3Y$ (21.7 µmol, 10 vol % DEVP in 20 ml toluene, 45 °C).

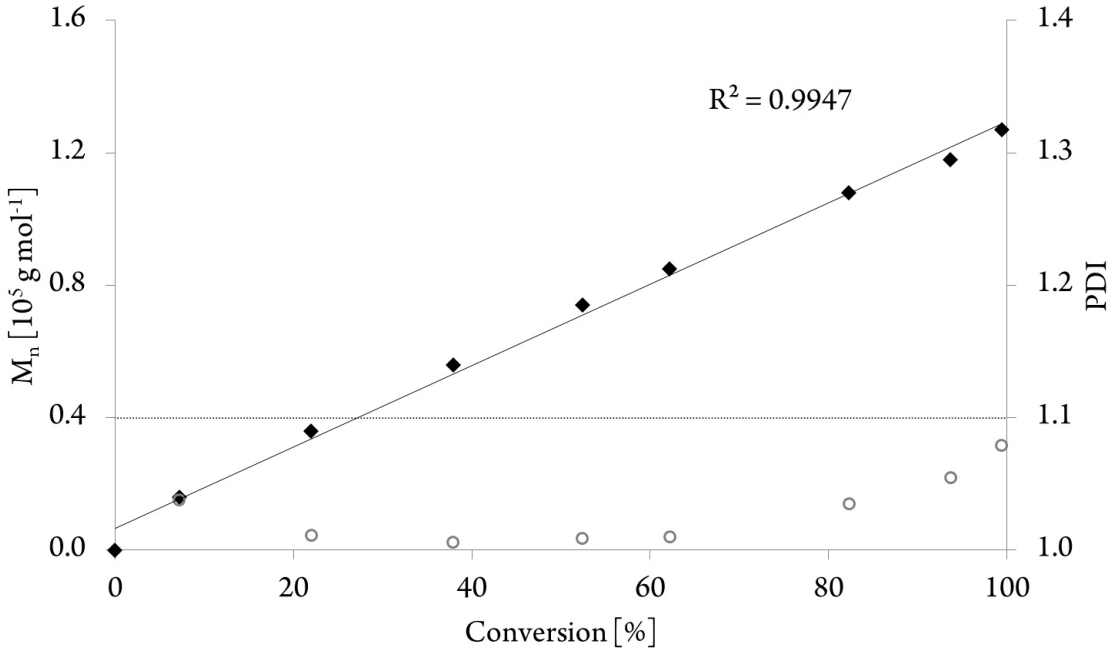

Figure S48: Number average molecular mass conversion plot for the polymerization of DEVP using $(C_5Me_4H)_3Y$ (21.7 µmol, 10 vol % DEVP in 20 ml toluene, 45 °C).

Table S4. Temperature-dependent kinetics for $(C_5Me_4H)_3Tb$-catalyzed DEVP polymerization (1.09 mmol L^{-1} $(C_5Me_4H)_3Tb$, 0.326 mol L^{-1} DEVP, toluene)

T [°C]	TOF [h^{-1}]	I^*_t [%]	TOF/I^*_t [h^{-1}]	Conversion at maximum rate	Rate [mol L^{-1} s^{-1}]	1/T [K^{-1}]	ln(k'/T)
27	3900	42.4	9200	13.8	5.85E-04	3.33E-03	-4.20
33	5200	39.0	13300	11.9	7.83E-04	3.27E-03	-3.86
38	8700	45.0	19300	15.1	1.32E-03	3.21E-03	-3.47
43	11000	40.0	27500	9.2	1.65E-03	3.17E-03	-3.20
47	14800	39.5	37500	11.8	2.22E-03	3.12E-03	-2.88
56	21600	31.2	69200	5.9	3.26E-03	3.04E-03	-2.35
61	38800	52.9	73300	14.4	5.85E-03	2.99E-03	-2.22

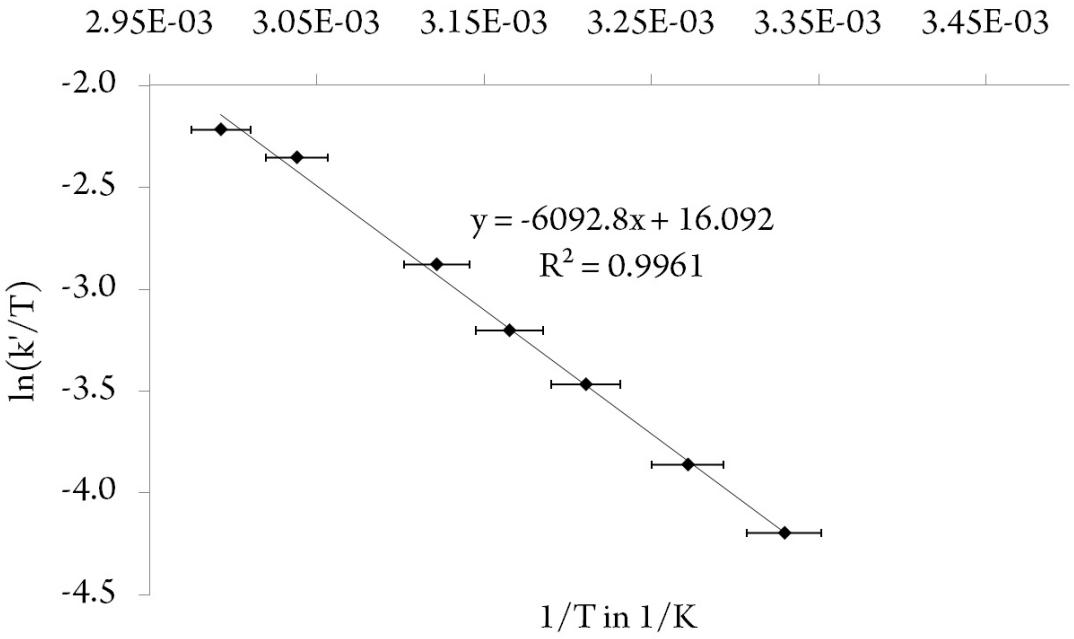

Figure S49: Result for the Eyring-plot of $(C_5Me_4H)_3Tb$-initiated DEVP (10 vol %) polymerization in toluene (27 – 61 °C, $\Delta H^{\ddagger}$ = 50.6 kJ mol^{-1}, $\Delta S^{\ddagger}$ = -63.7 J $(mol\ K)^{-1}$).

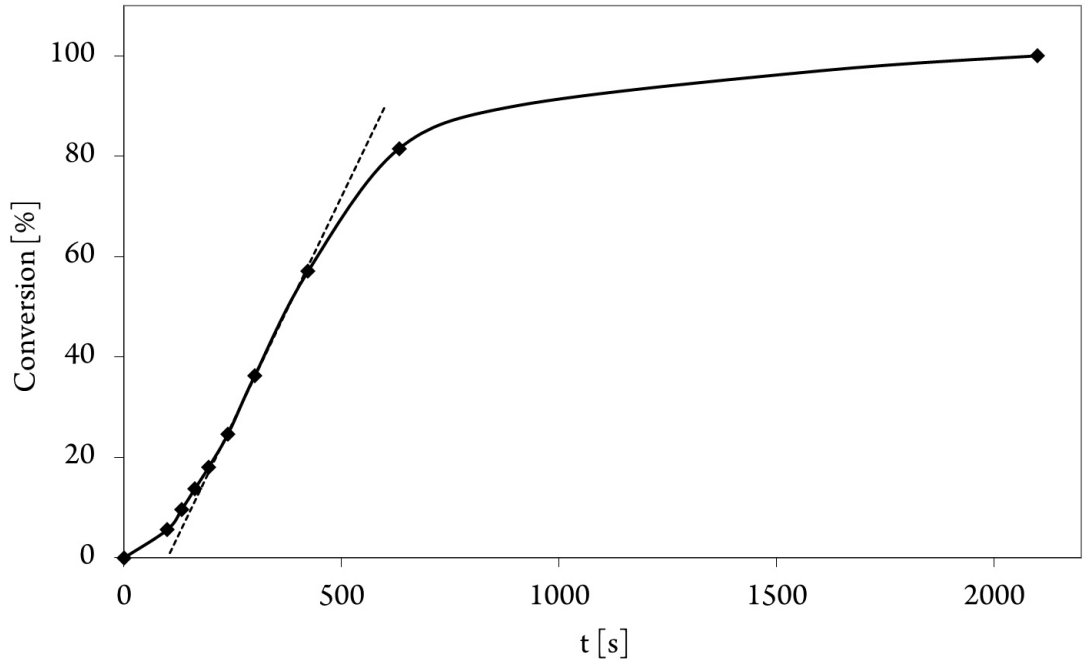

Figure S50: Conversion-reaction time plot for the polymerization of DEVP using $(C_5Me_4H)_3Tb$ (21.7 µmol, 5 vol % DEVP in 20 ml toluene, 27 °C).

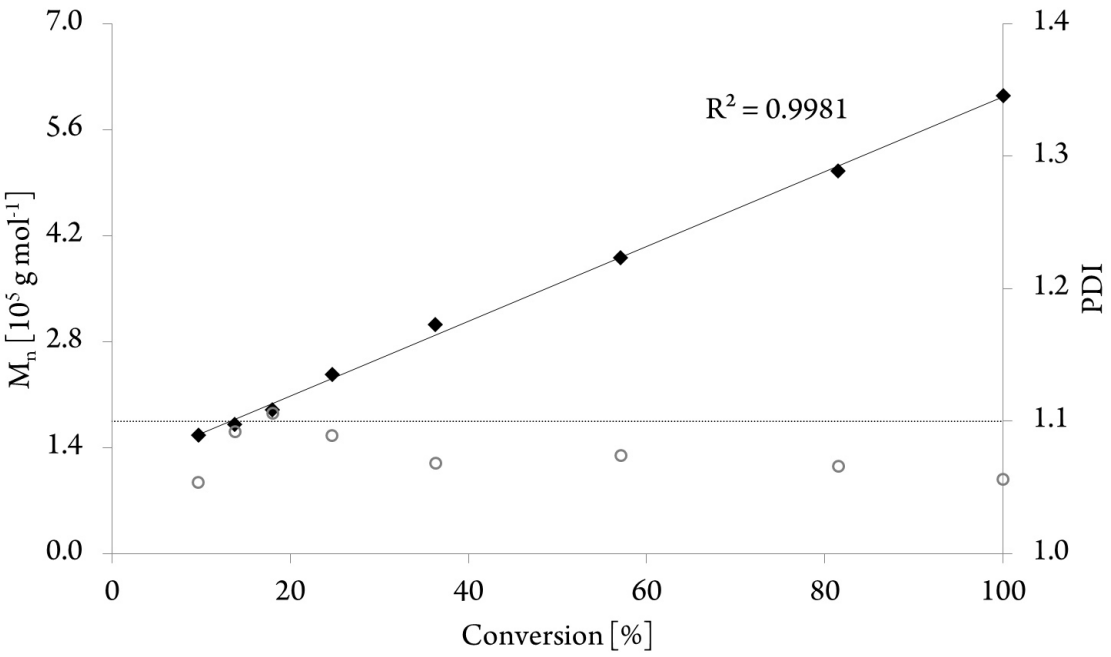

Figure S51: Number average molecular mass conversion plot for the polymerization of DEVP using $(C_5Me_4H)_3Tb$ (21.7 µmol, 5 vol % DEVP in 20 ml toluene, 27 °C).

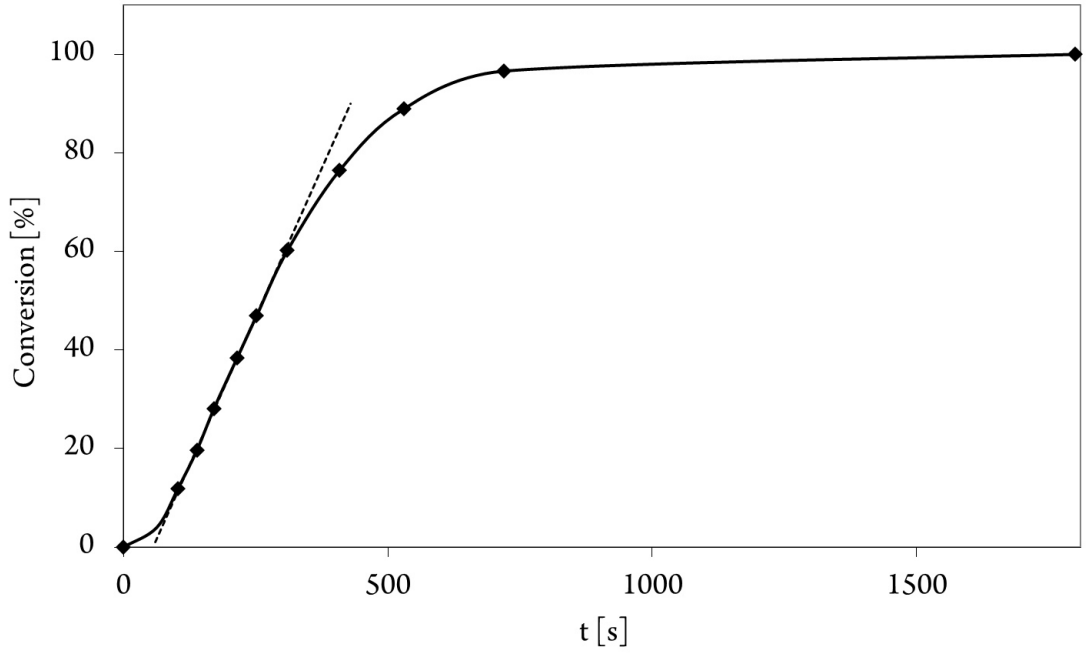

Figure S52: Conversion-reaction time plot for the polymerization of DEVP using $(C_5Me_4H)_3Tb$ (21.7 µmol, 5 vol % DEVP in 20 ml toluene, 33 °C).

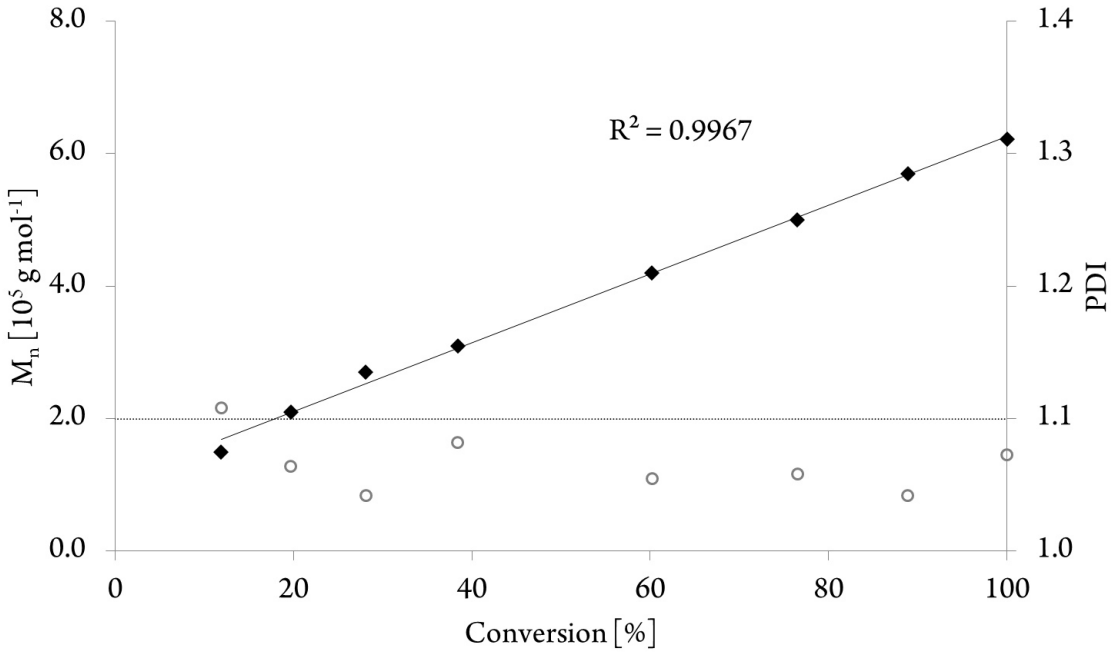

Figure S53: Number average molecular mass conversion plot for the polymerization of DEVP using $(C_5Me_4H)_3Tb$ (21.7 µmol, 5 vol % DEVP in 20 ml toluene, 33 °C).

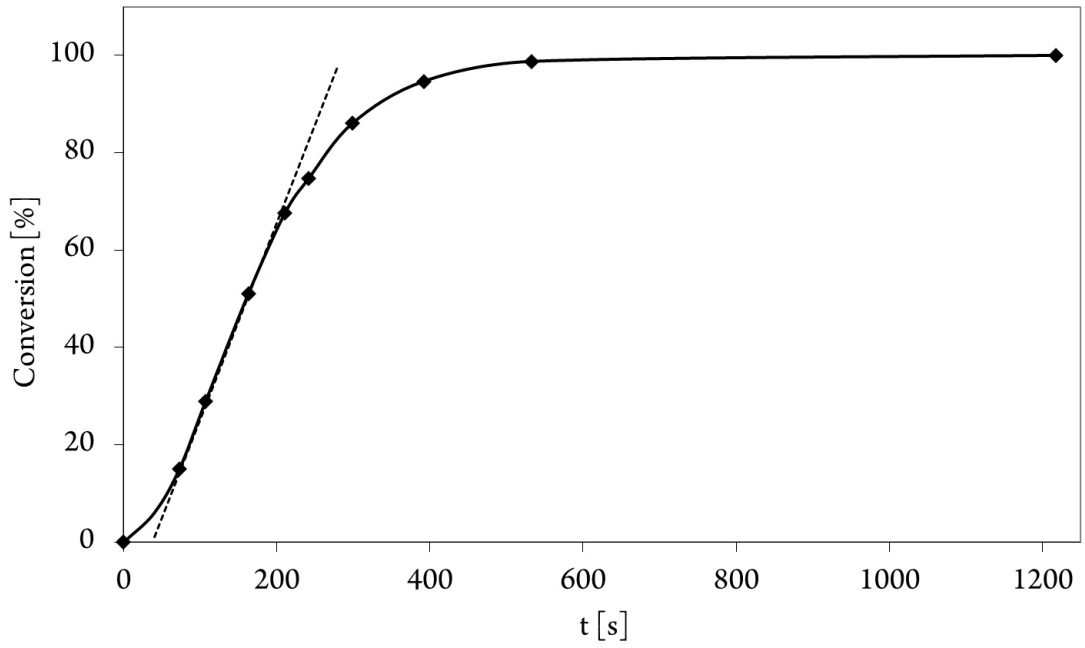

Figure S54: Conversion-reaction time plot for the polymerization of DEVP using $(C_5Me_4H)_3Tb$ (21.7 µmol, 5 vol % DEVP in 20 ml toluene, 38 °C).

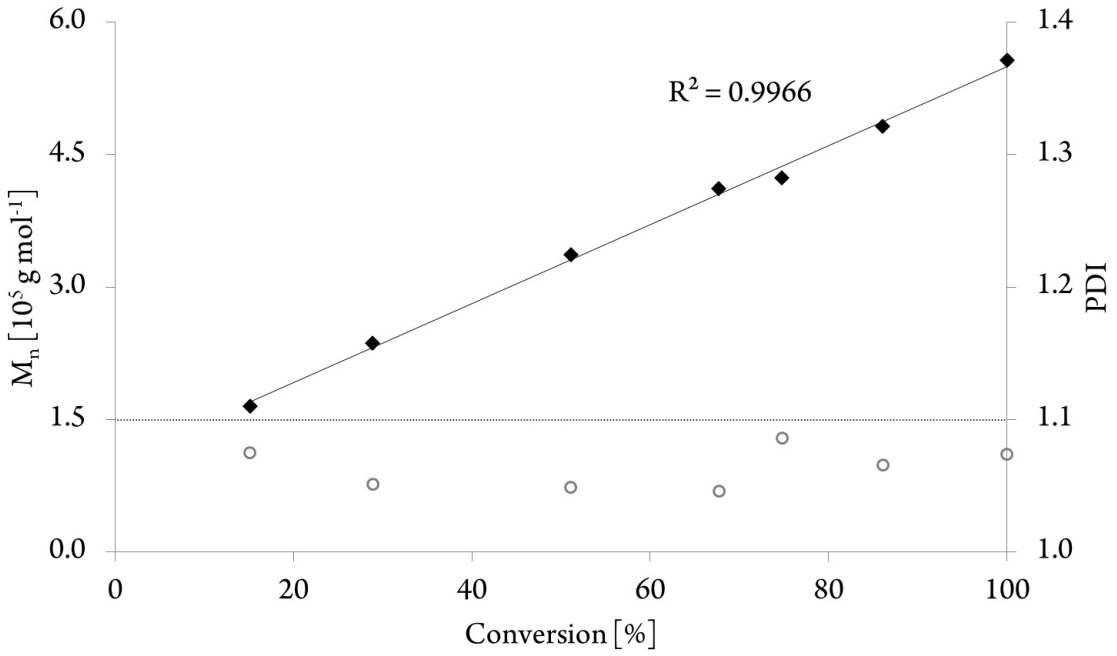

Figure S55: Number average molecular mass conversion plot for the polymerization of DEVP using $(C_5Me_4H)_3Tb$ (21.7 µmol, 5 vol % DEVP in 20 ml toluene, 38 °C).

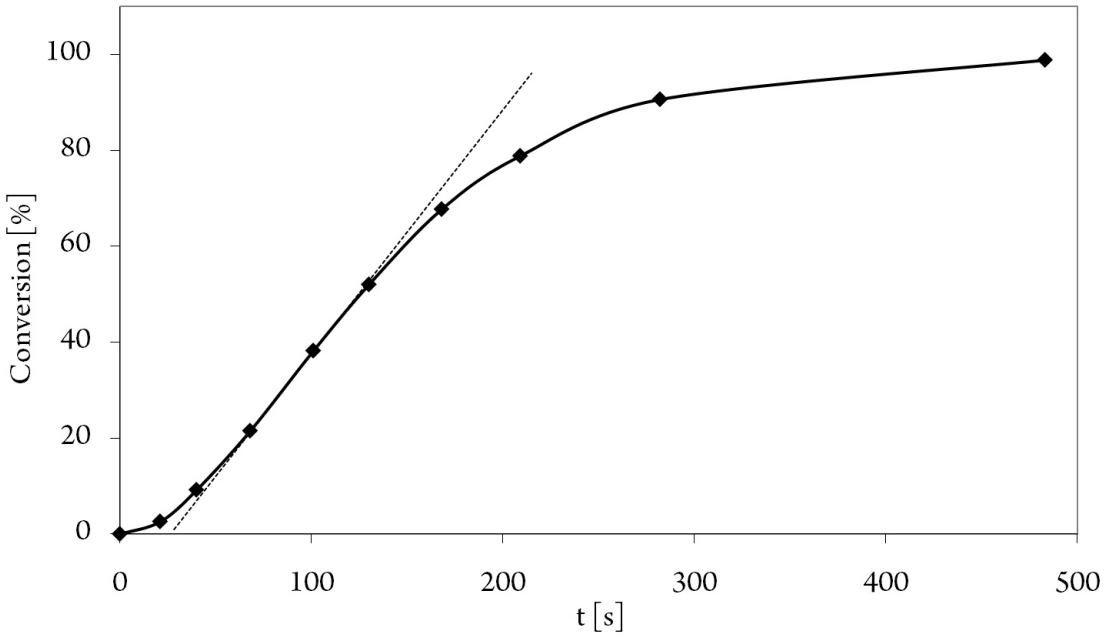

Figure S56: Conversion-reaction time plot for the polymerization of DEVP using $(C_5Me_4H)_3Tb$ (21.7 µmol, 5 vol % DEVP in 20 ml toluene, 43 °C).

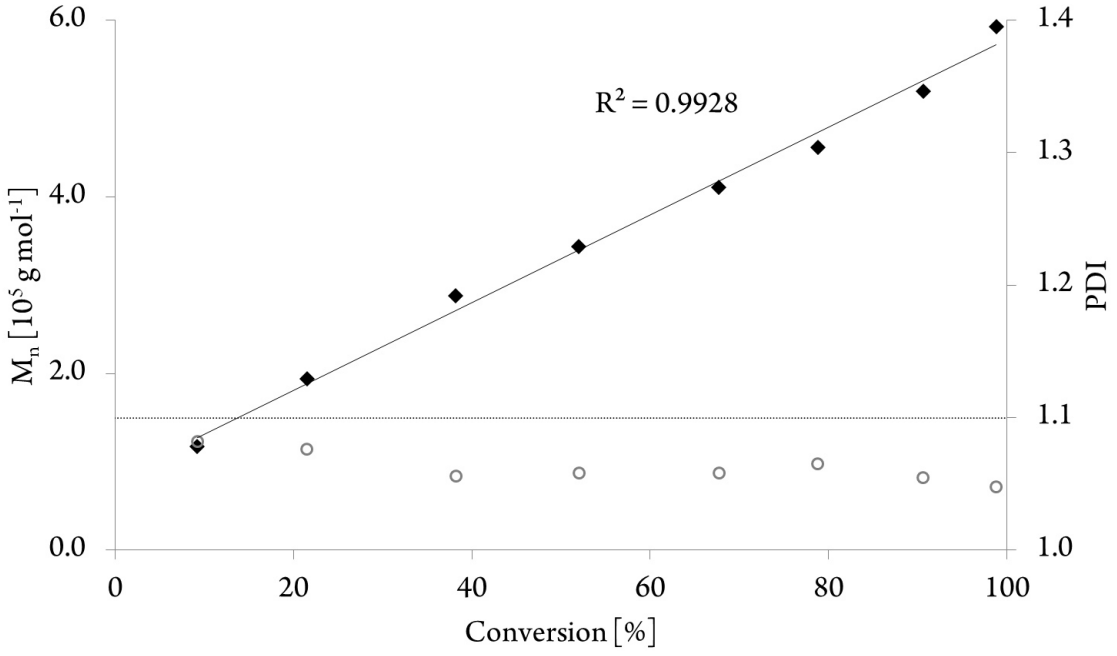

Figure S57: Number average molecular mass conversion plot for the polymerization of DEVP using $(C_5Me_4H)_3Tb$ (21.7 µmol, 5 vol % DEVP in 20 ml toluene, 43 °C).

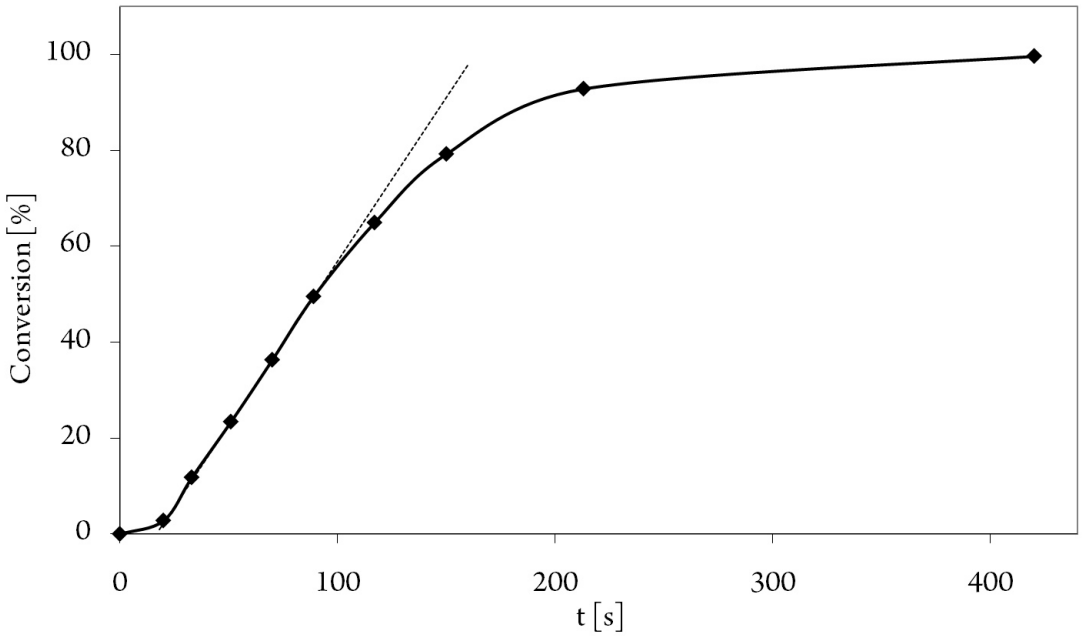

Figure S58: Conversion-reaction time plot for the polymerization of DEVP using $(C_5Me_4H)_3Tb$ (21.7 µmol, 5 vol % DEVP in 20 ml toluene, 47 °C).

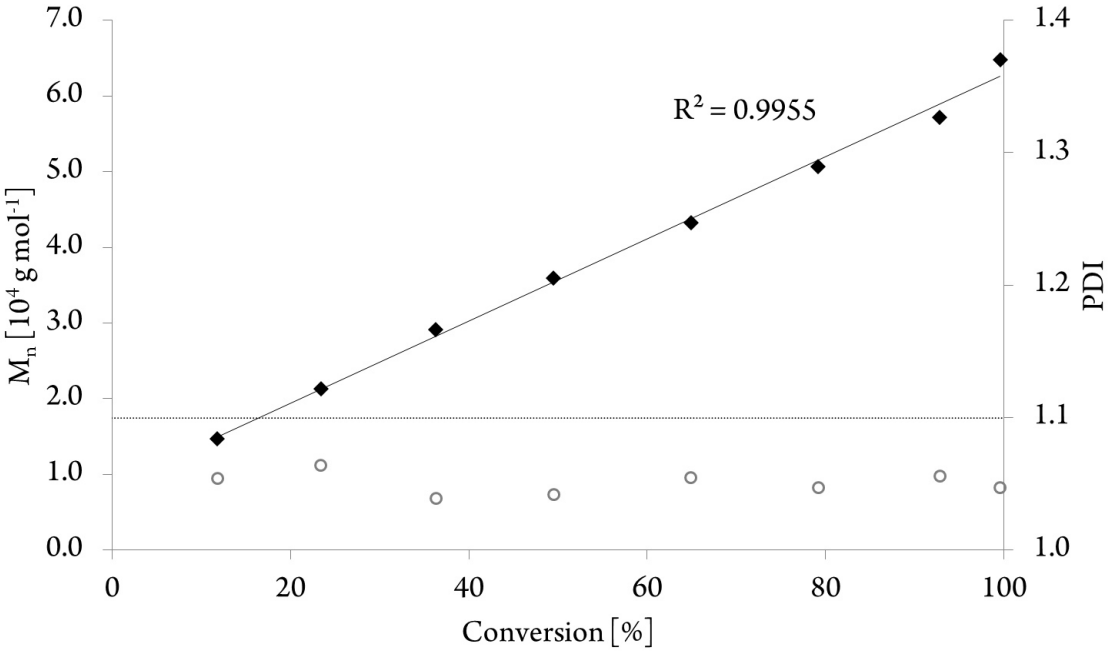

Figure S59: Number average molecular mass conversion plot for the polymerization of DEVP using $(C_5Me_4H)_3Tb$ (21.7 µmol, 5 vol % DEVP in 20 ml toluene, 47 °C).

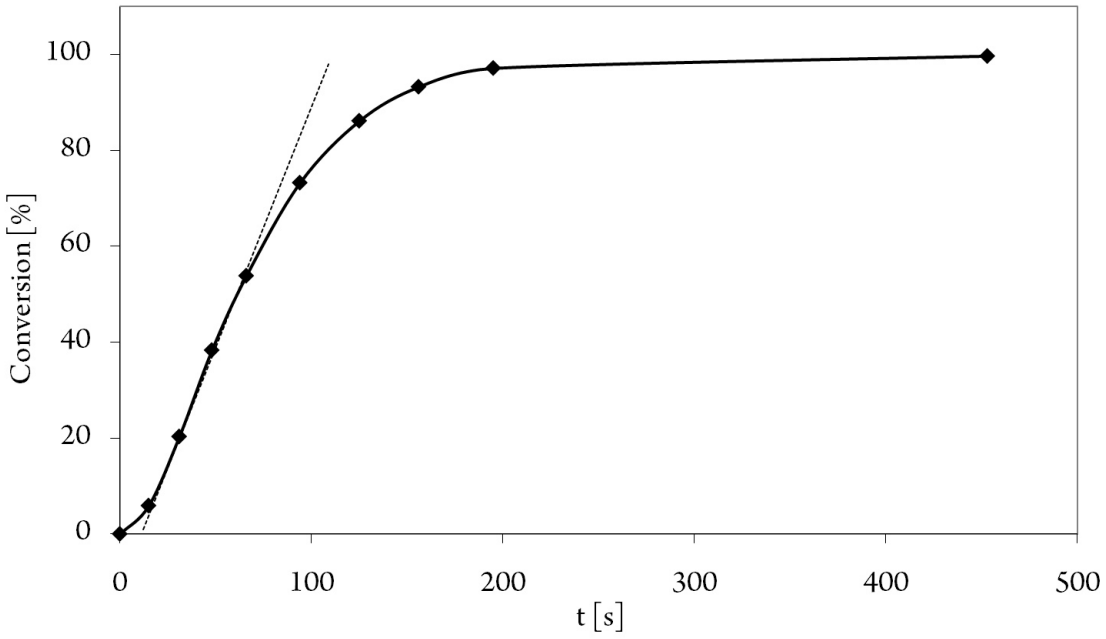

Figure S60: Conversion-reaction time plot for the polymerization of DEVP using $(C_5Me_4H)_3Tb$ (21.7 µmol, 5 vol % DEVP in 20 ml toluene, 56 °C).

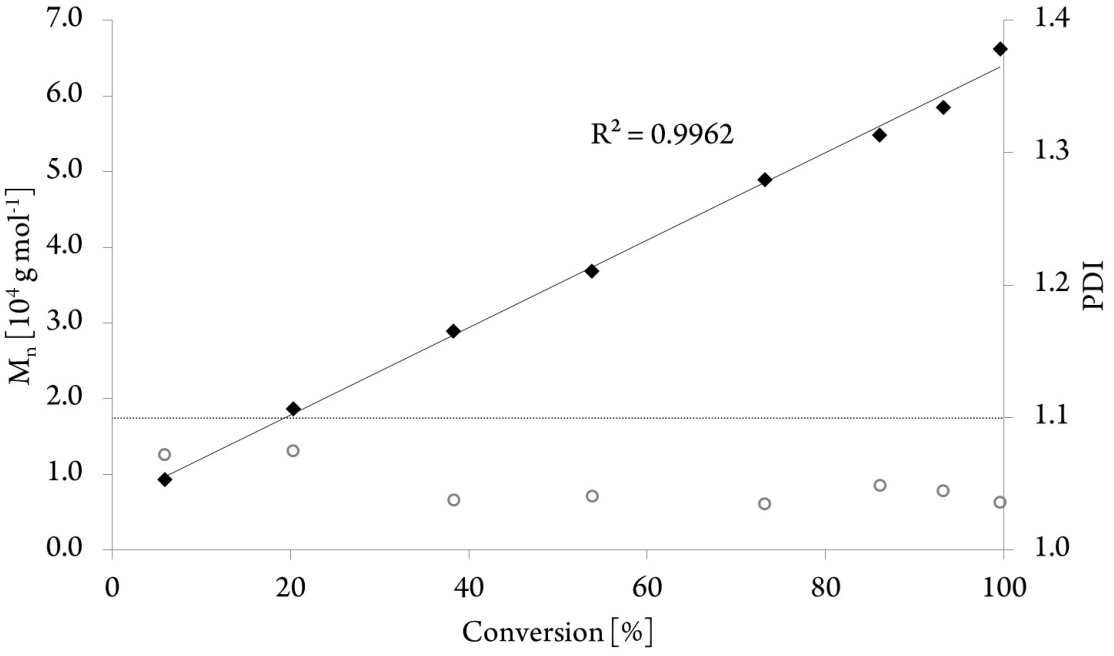

Figure S61: Number average molecular mass conversion plot for the polymerization of DEVP using $(C_5Me_4H)_3Tb$ (21.7 µmol, 5 vol % DEVP in 20 ml toluene, 56 °C).

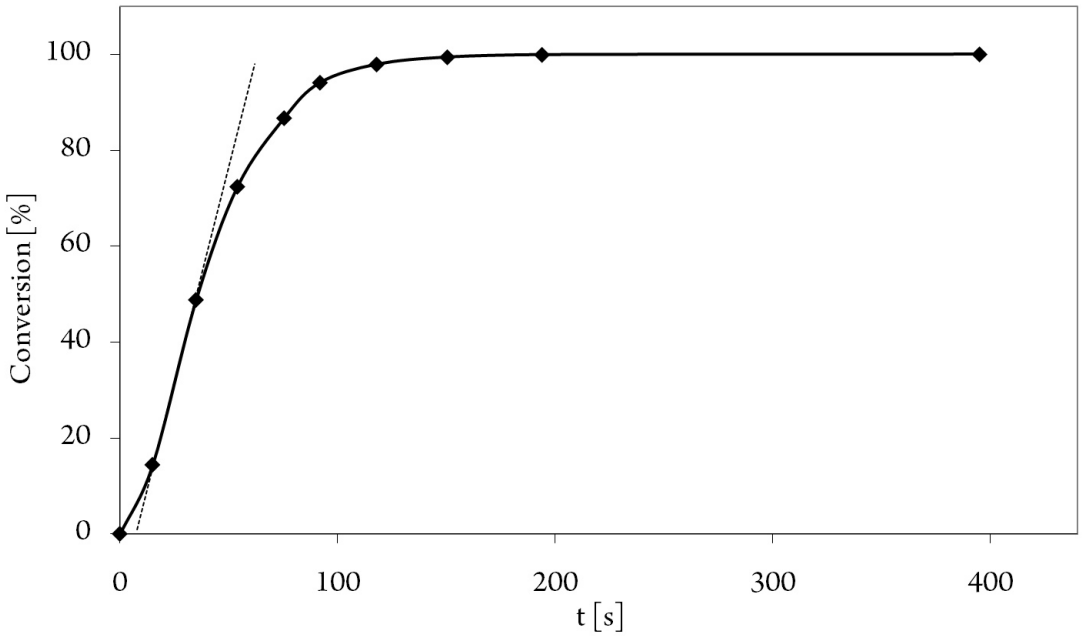

Figure S62: Conversion-reaction time plot for the polymerization of DEVP using $(C_5Me_4H)_3Tb$ (21.7 µmol, 5 vol % DEVP in 20 ml toluene, 61 °C).

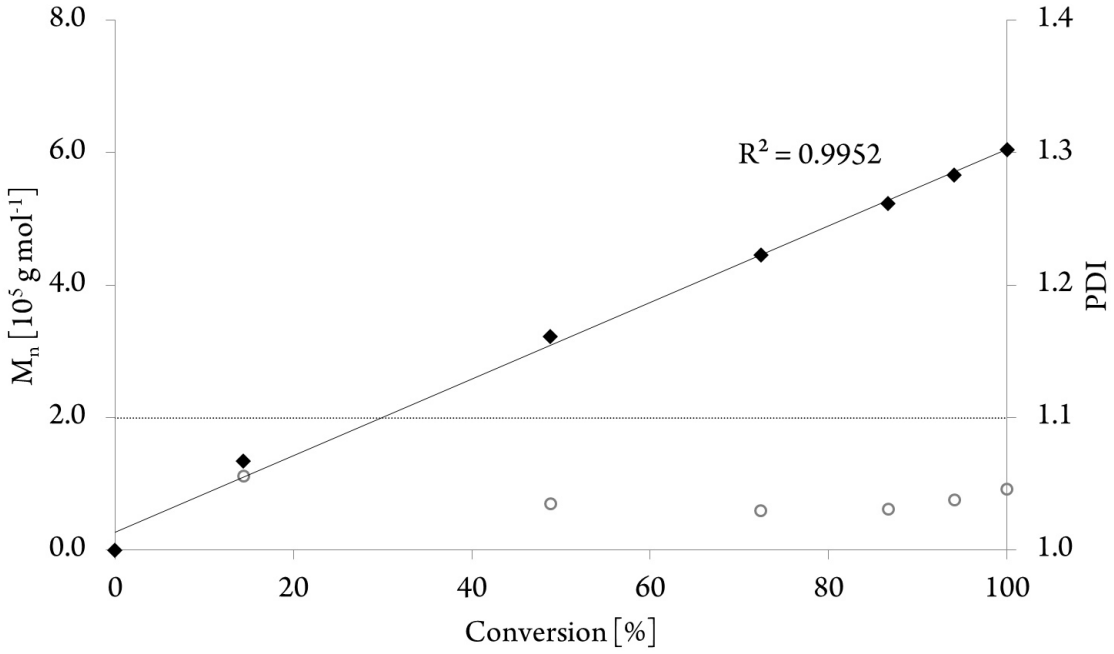

Figure S63: Number average molecular mass conversion plot for the polymerization of DEVP using $(C_5Me_4H)_3Tb$ (21.7 µmol, 5 vol % DEVP in 20 ml toluene, 61 °C).

Table S5. Temperature-dependent kinetics for $(C_5Me_4H)_3Sm$-catalyzed DEVP polymerization (1.09 mmol L^{-1} $(C_5Me_4H)_3Sm$, 0.651 mol L^{-1} DEVP, toluene)

T [°C]	TOF [h^{-1}]	I^*_t [%]	TOF/I^*_t [h^{-1}]	Conversion at maximum rate	Rate [mol L^{-1} s^{-1}]	1/T [K^{-1}]	ln(k'/T)
30	910	25.5	3570	23.3	2.74E-04	3.30E-03	-5.03
36	1200	21.3	5630	11.9	3.52E-04	3.23E-03	-4.76
42	1650	25.4	6500	17.8	4.98E-04	3.18E-03	-4.54
46	2000	20.0	10000	16.4	6.08E-04	3.13E-03	-4.13
51	3100	22.5	13800	8.9	9.46E-04	3.08E-03	-3.91
58	5300	20.5	25850	7.3	1.62E-03	3.02E-03	-3.32

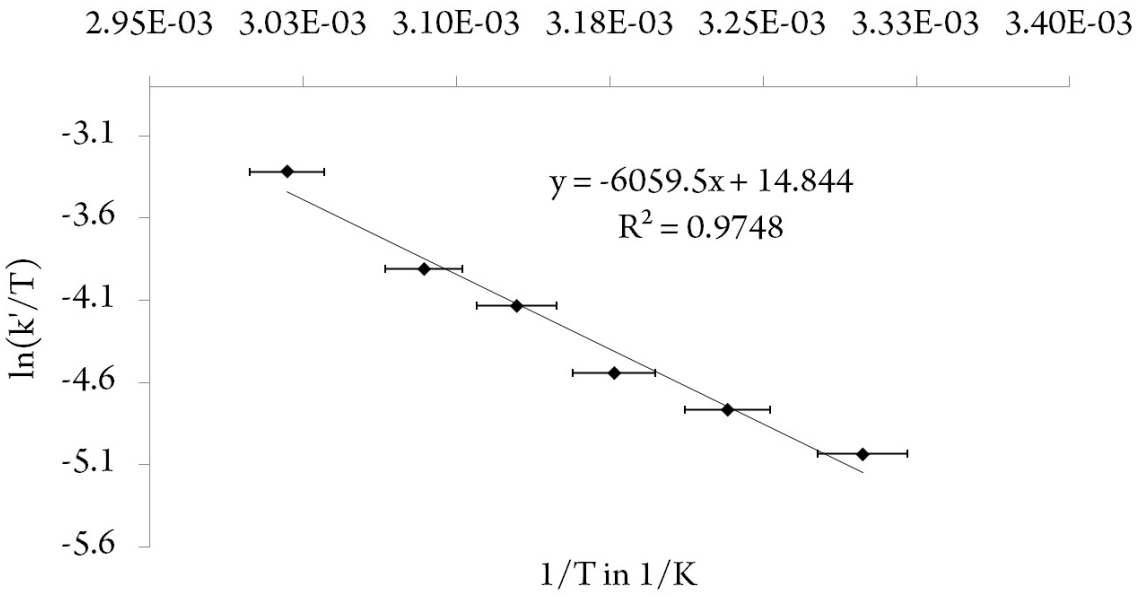

Figure S64: Result for the Eyring-plot of $(C_5Me_4H)_3Sm$-initiated DEVP (10 vol %) polymerization in toluene (30 – 58 °C, $\Delta H^{\ddagger}$ = 50.4 kJ mol^{-1}, $\Delta S^{\ddagger}$ = -74.1 J $(mol\ K)^{-1}$).

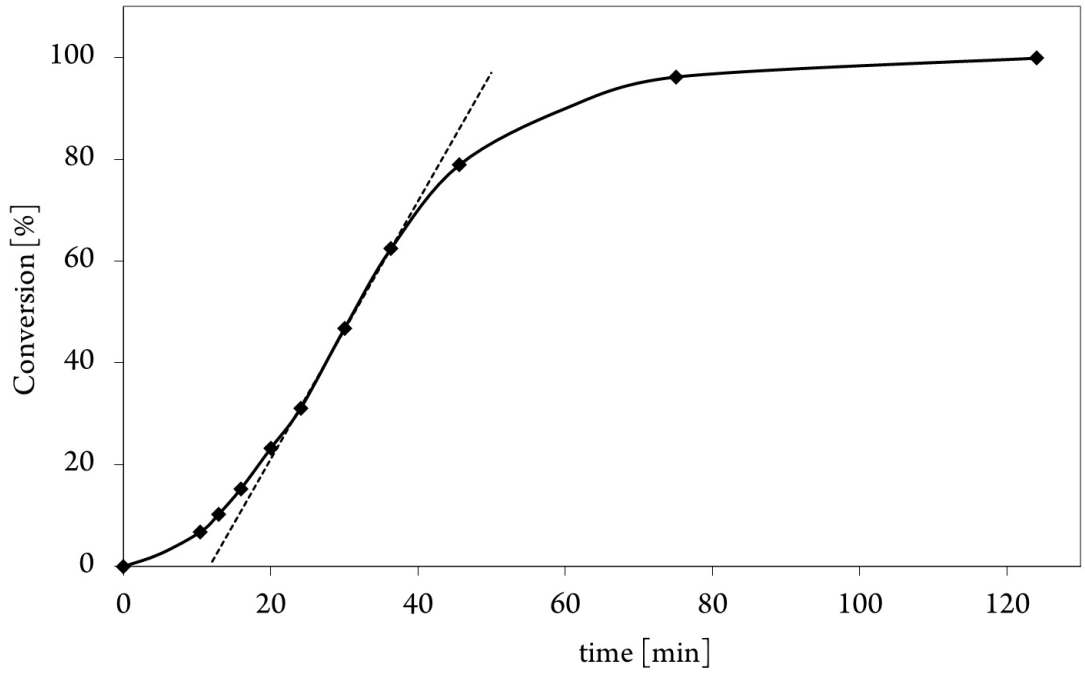

Figure S65: Conversion-reaction time plot for the polymerization of DEVP using $(C_5Me_4H)_3Sm$ (21.7 µmol, 10 vol % DEVP in 20 ml toluene, 30 °C).

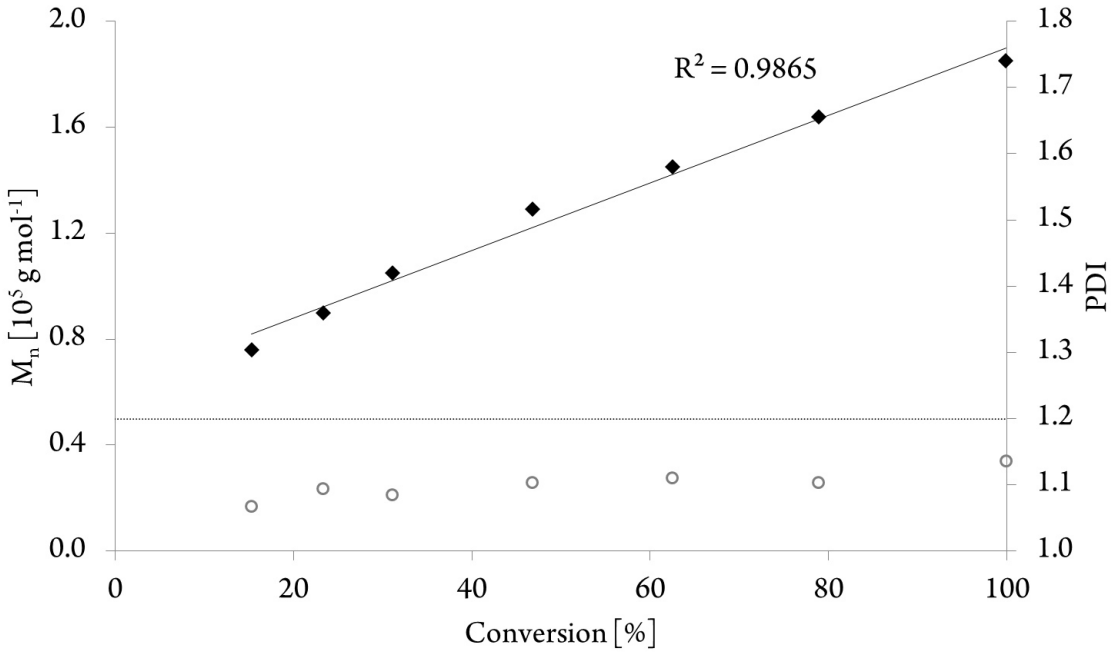

Figure S66: Number average molecular mass conversion plot for the polymerization of DEVP using $(C_5Me_4H)_3Sm$ (21.7 µmol, 10 vol % DEVP in 20 ml toluene, 30 °C).

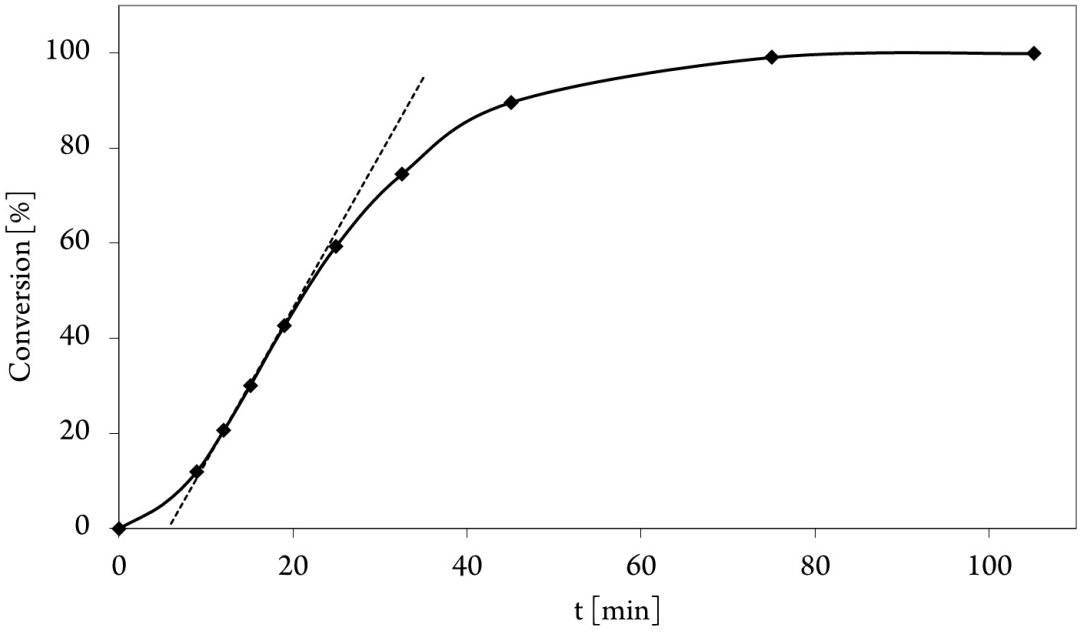

Figure S67: Conversion-reaction time plot for the polymerization of DEVP using $(C_5Me_4H)_3Sm$ (21.7 µmol, 10 vol % DEVP in 20 ml toluene, 36 °C).

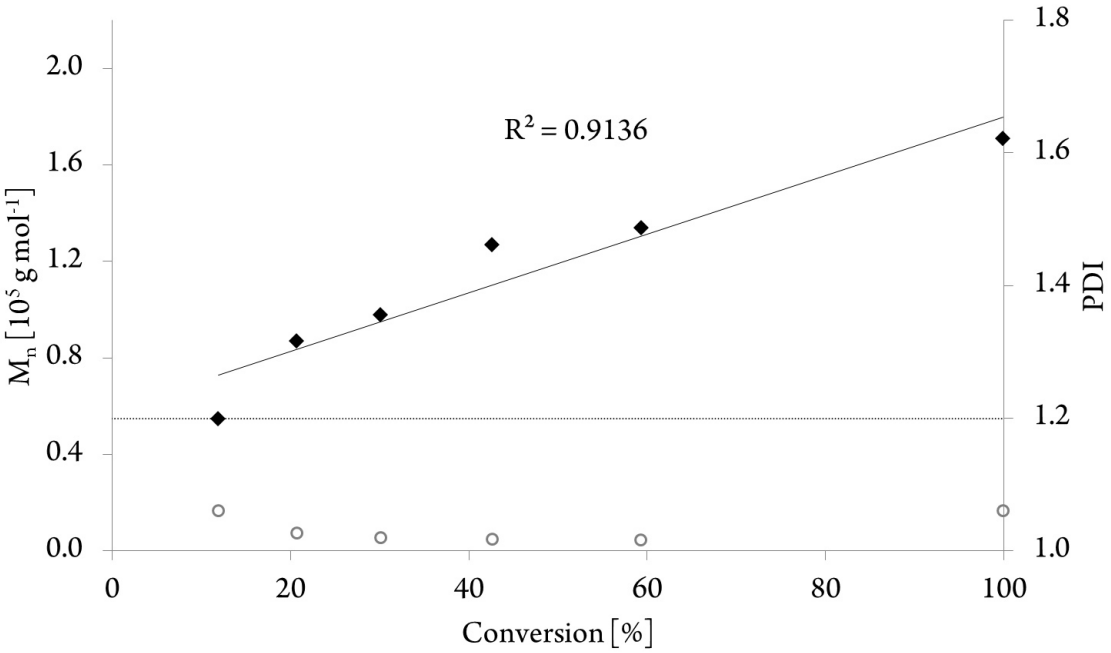

Figure S68: Number average molecular mass conversion plot for the polymerization of DEVP using $(C_5Me_4H)_3Sm$ (21.7 µmol, 10 vol % DEVP in 20 ml toluene, 36 °C).

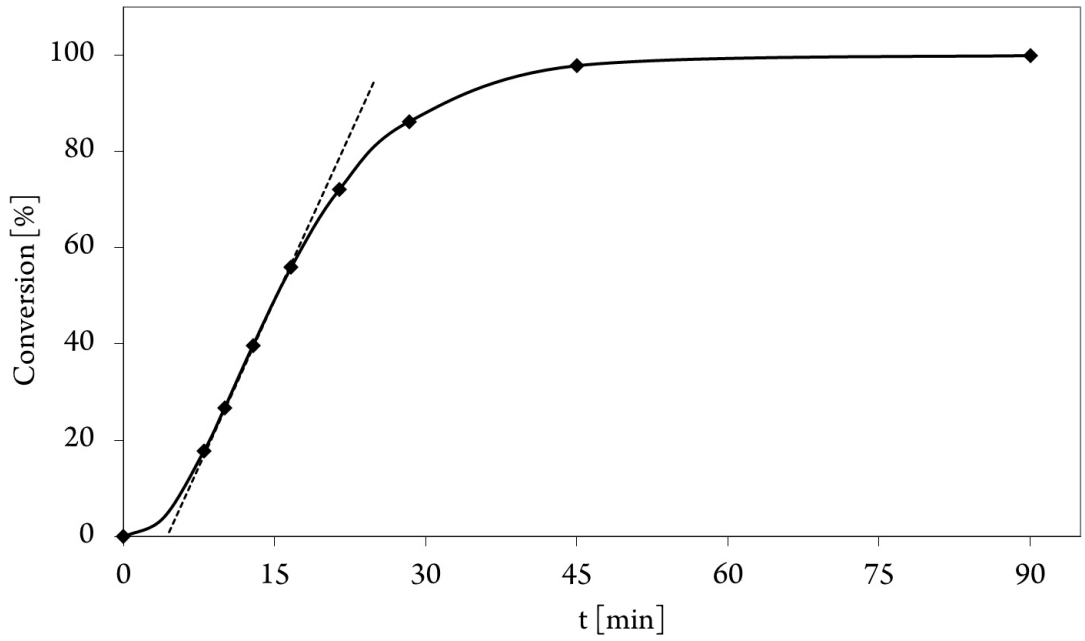

Figure S69: Conversion-reaction time plot for the polymerization of DEVP using $(C_5Me_4H)_3Sm$ (21.7 µmol, 10 vol % DEVP in 20 ml toluene, 42 °C).

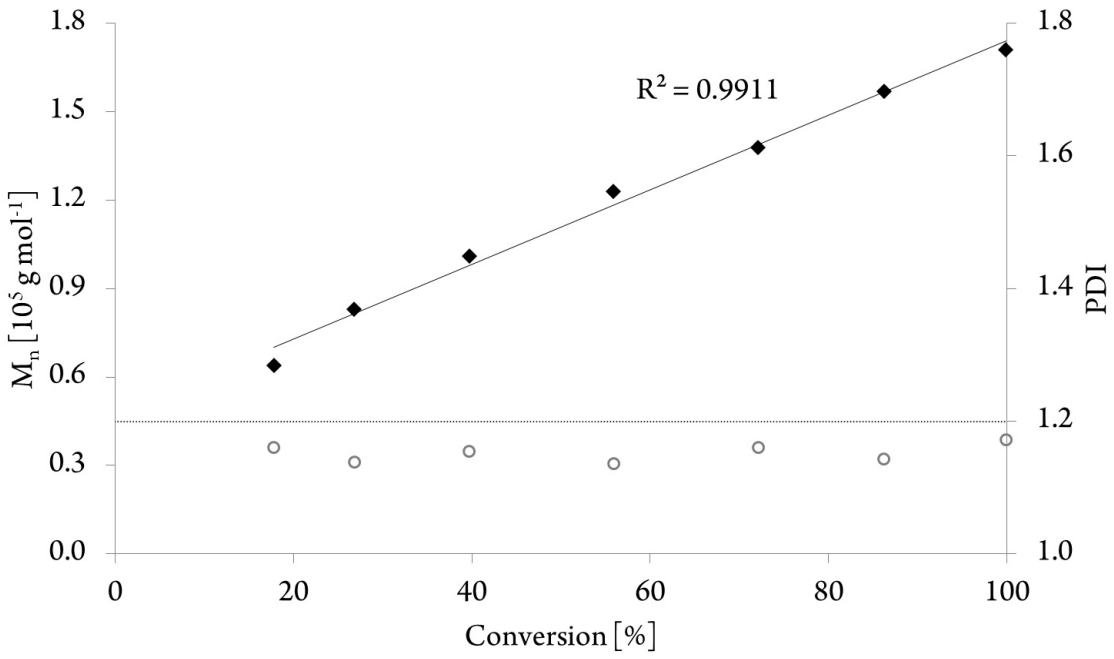

Figure S70: Number average molecular mass conversion plot for the polymerization of DEVP using $(C_5Me_4H)_3Sm$ (21.7 µmol, 10 vol % DEVP in 20 ml toluene, 42 °C).

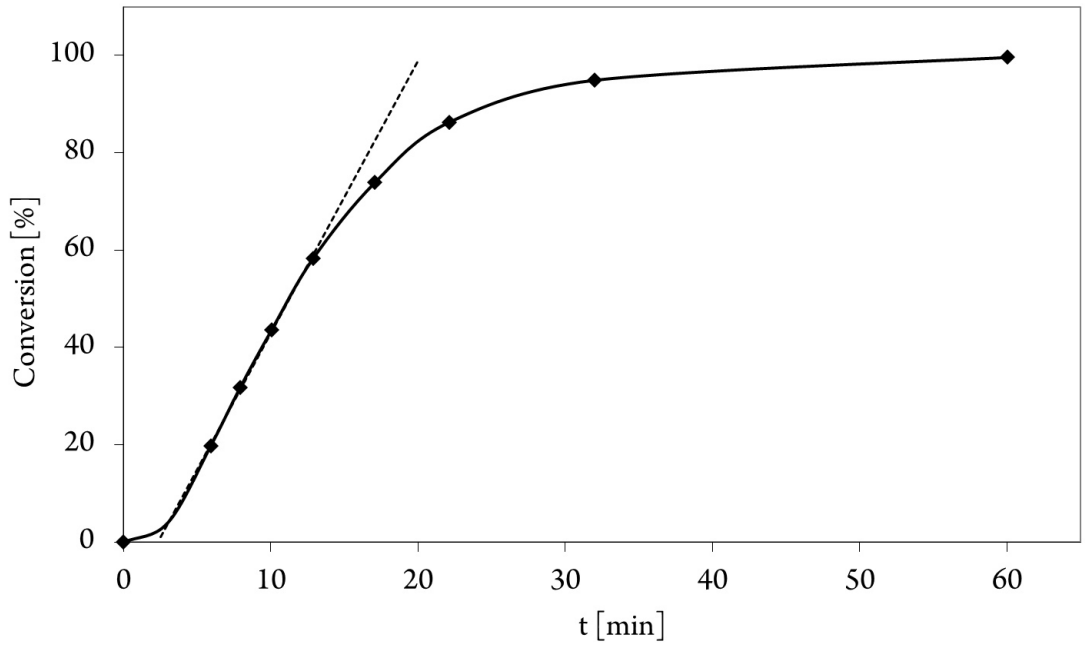

Figure S71: Conversion-reaction time plot for the polymerization of DEVP using $(C_5Me_4H)_3Sm$ (21.7 µmol, 10 vol % DEVP in 20 ml toluene, 46 °C).

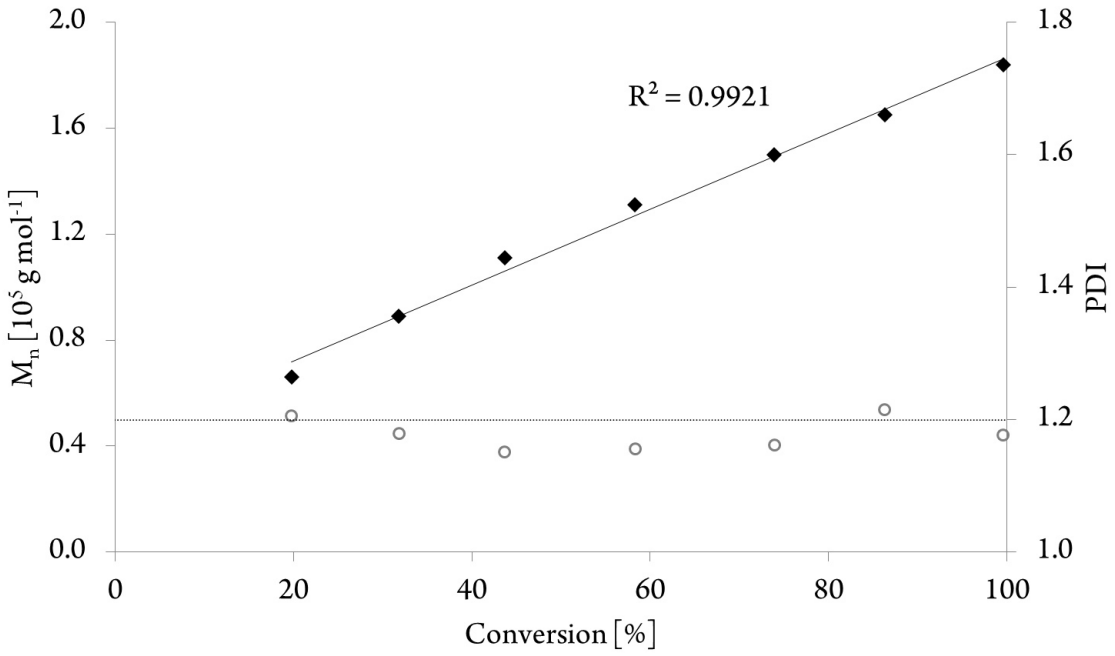

Figure S72: Number average molecular mass conversion plot for the polymerization of DEVP using $(C_5Me_4H)_3Sm$ (21.7 µmol, 10 vol % DEVP in 20 ml toluene, 46 °C).

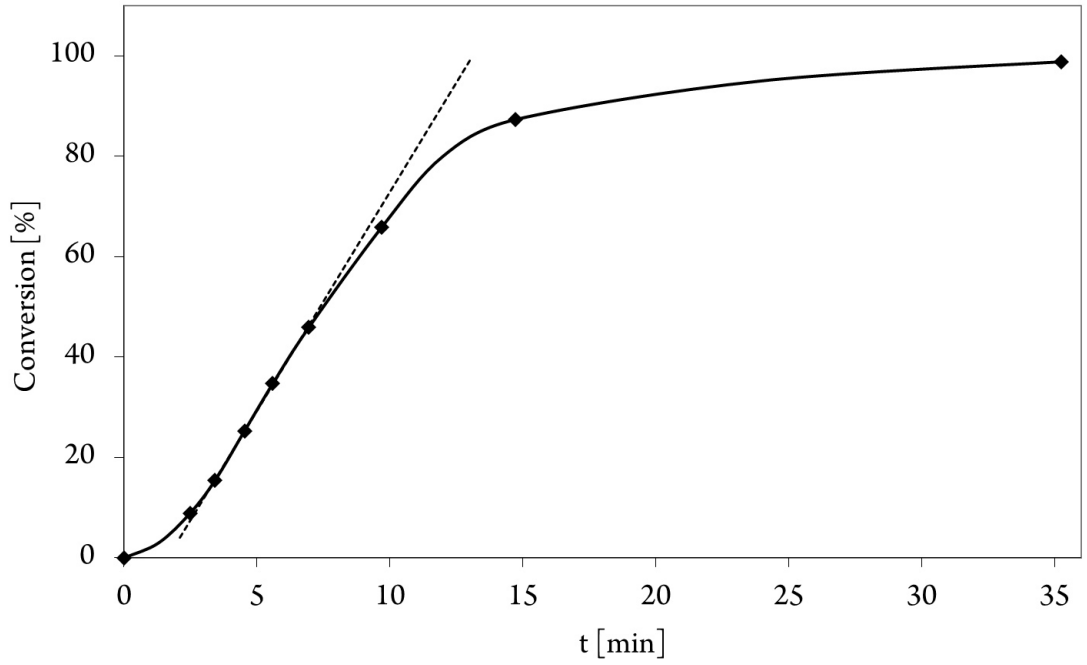

Figure S73: Conversion-reaction time plot for the polymerization of DEVP using $(C_5Me_4H)_3Sm$ (21.7 µmol, 10 vol % DEVP in 20 ml toluene, 51 °C).

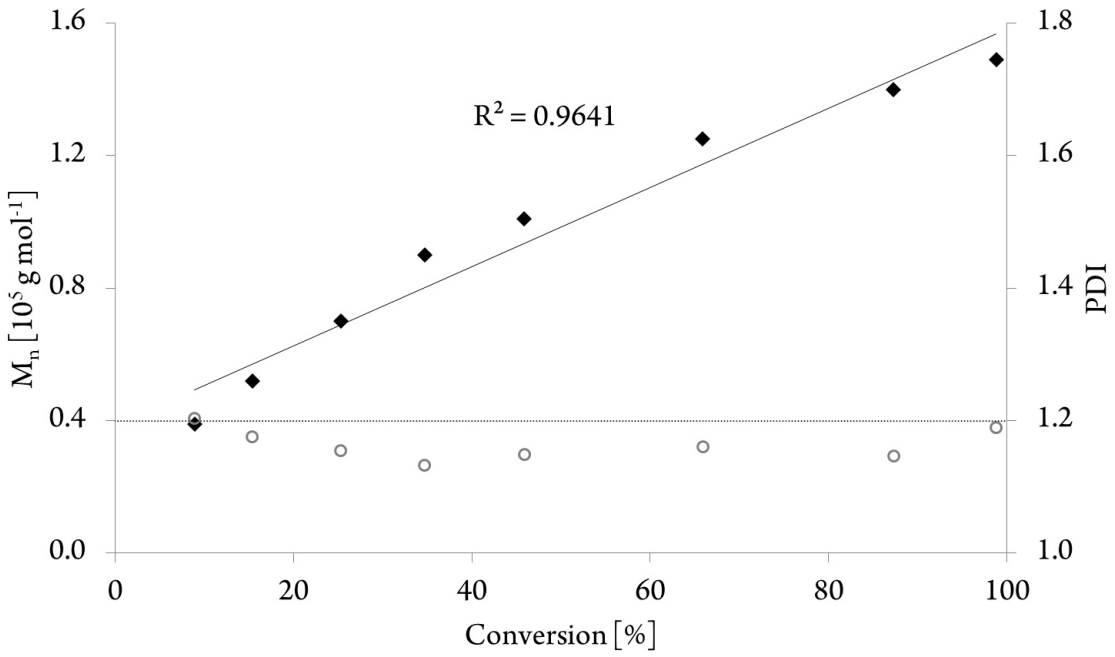

Figure S74: Number average molecular mass conversion plot for the polymerization of DEVP using $(C_5Me_4H)_3Sm$ (21.7 µmol, 10 vol % DEVP in 20 ml toluene, 51 °C).

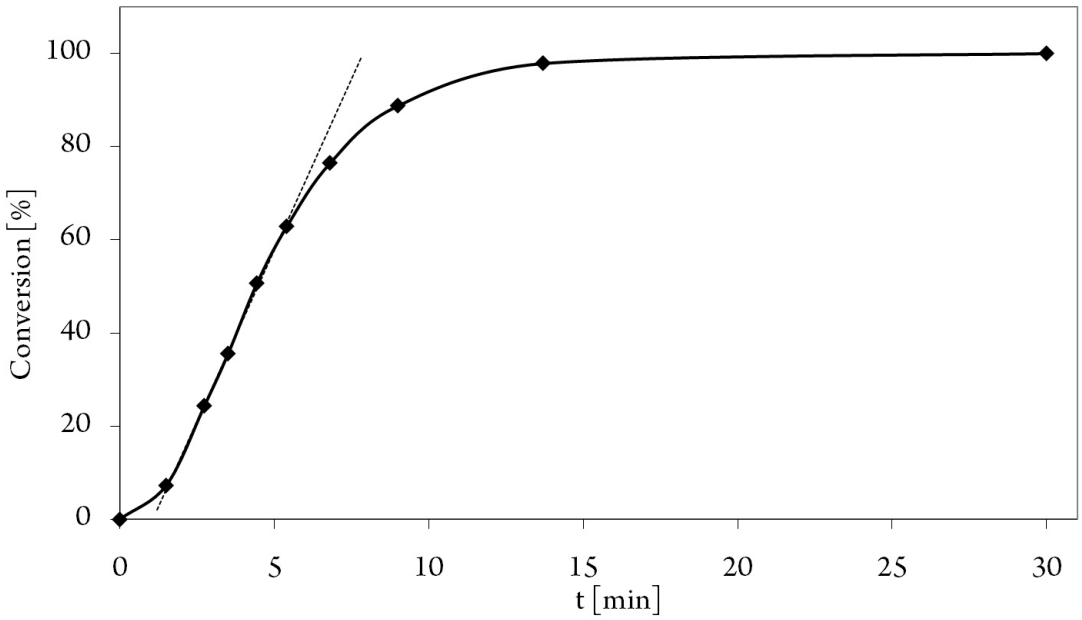

Figure S75: Conversion-reaction time plot for the polymerization of DEVP using $(C_5Me_4H)_3Sm$ (21.7 µmol, 10 vol % DEVP in 20 ml toluene, 58 °C).

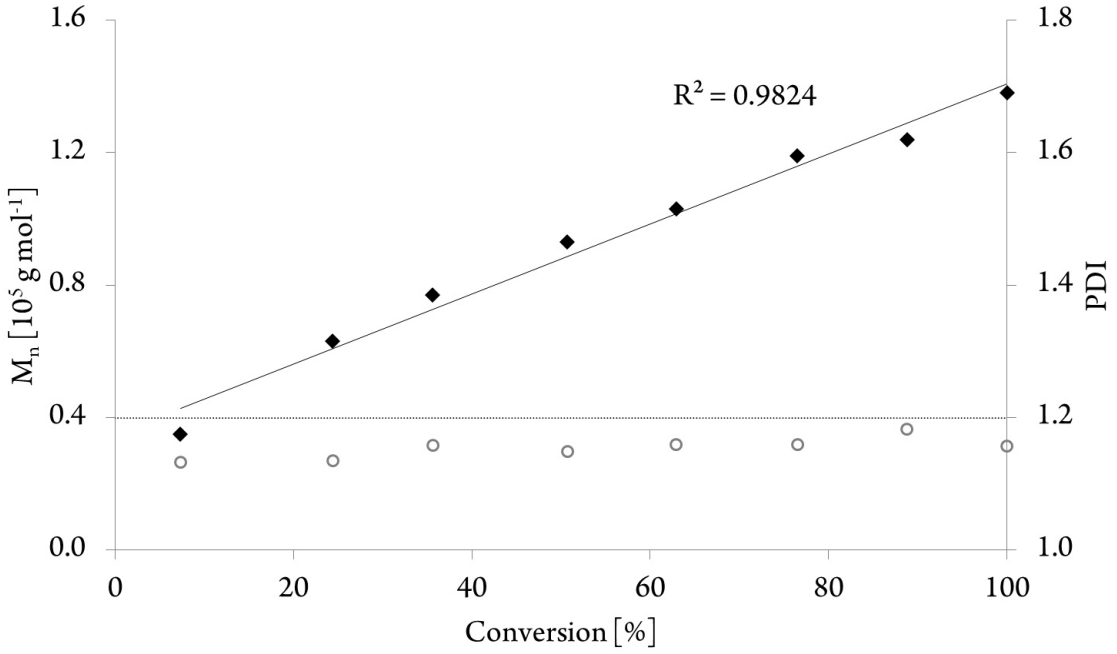

Figure S76: Number average molecular mass conversion plot for the polymerization of DEVP using $(C_5Me_4H)_3Sm$ (21.7 µmol, 10 vol % DEVP in 20 ml toluene, 58 °C).

Influence of the Monomer Water Content on the Normalization Method

The water content of the used monomer plays a crucial role for vinylphosphonate REM-GTP and directly affects the obtained molecular mass distribution, initiation period, polymer molecular weights, or activities. Therefore a normalization of the obtained experimental values is needed to compare the TOF/I^*_t results. In Table S6, the comparison of activity measurements for $(C_5H_4TMS)_3Y$ and $(C_5Me_4H)_3Y$ is shown for DEVP with two different amounts for water, resulting in matching TOF/I^*_t values.

Table S6. DEVP polymerization results for different water content in the monomer

Catalysts	Water content[a] [ppm]	Polymerization time [min]	Conversion[b] [%]	Initiation period[c] [s]	TOF [h^{-1}]	I^*_t[d] [%]	TOF/I^*_t [h^{-1}]	M_n[d] [kDa]	PDI[d]
$(C_5H_4TMS)_3Y$	45	13	95	-[e]	7600	37	20500	196[f]	1.23[f]
$(C_5H_4TMS)_3Y$	15	9	>99	-[e]	14000	61	21000	145	1.12
$(C_5Me_4H)_3Y$	45	7	45	45	3200	16	19700	139[f]	1.35[f]
$(C_5Me_4H)_3Y$	15	6	>99	15	13000	66	19000	115	1.05

a) Determined by Karl Fischer titration. b) Determined by ^{31}P NMR spectroscopic measurements. c) Initiation period, reaction time until 3% conversion is reached. d) Determined by GPC-MALS, $I^* = M_{th}/M_n$, $M_{th} = eq._{(Monomer)} \times M_{Mon} \times$ conversion (I^*_t at the maximum rate, I^* at the end of the reaction). e) No initiation period observed. f) Determined for incomplete conversion.

Activity Measurement for DIVP

Initial studies with DIVP resulted in a significant decrease in activity while using substituted tris(cyclopentadienyl) RE catalysts (Figure S77). Therefore, activity measurements were not possible for DIVP and in this work exclusively DEVP was used.

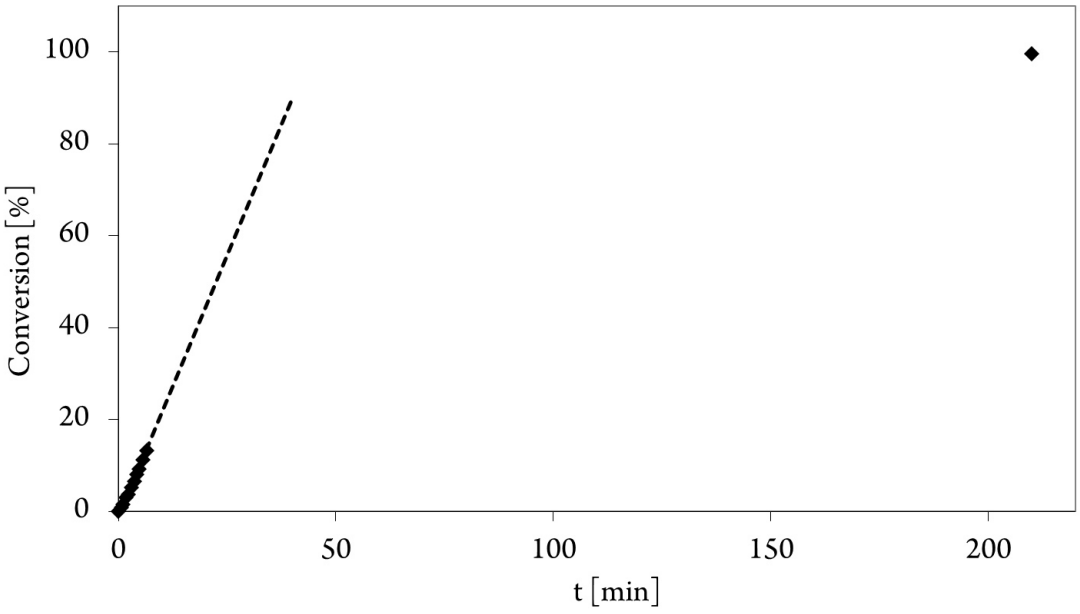

Figure S77: Conversion-reaction time plot for the polymerization of DIVP using $(C_5Me_4H)_3Y$ (21.7 µmol, 7.5 vol % DIVP in 20 ml toluene, 20 °C).

References

[1] Leute, M. *PhD Thesis*, Universität Ulm, **2007**.

[2] *APEX* suite of crystallographic software. *APEX* 2 Version 2013.4. Bruker AXS Inc., Madison, Wisconsin, USA (2013).

[3] *SAINT*, Version 8.27b and *SADABS* Version 2012/1. Bruker AXS Inc., Madison, Wisconsin, USA (2012).

[4] Sheldrick, G. M. "**SHELXS-97**", Program for Crystal Structure Solution, Göttingen, (1997).

[5] Sheldrick, G. M. "**SHELXL-97**", University of Göttingen, Göttingen, Germany, (1998). *or* Sheldrick, G. M. "**SHELXL-2014**", University of Göttingen, Göttingen, Germany, (2014).

[6] Huebschle, C. B., Sheldrick, G. M. & Dittrich, B. "**SHELXLE**", *J. Appl. Cryst.* **2011**, *44*, 1281- 1284.

[7] International Tables for Crystallography, Vol. C, Tables 6.1.1.4 (pp. 500-502), 4.2.6.8 (pp. 219-222), and 4.2.4.2 (pp. 193-199), Wilson, A. J. C., Ed., Kluwer Academic Publishers, Dordrecht, The Netherlands, 1992.

[8] Spek, A. L. "**PLATON**", A Multipurpose Crystallographic Tool, Utrecht University, Utrecht, The Netherlands, (2011).

4.5 Stereospecific Rare Earth Metal-Mediated Group Transfer Polymerization of Vinylphosphonates via Yttrium Constrained Geometry Complexes

Status: Draft

Journal: Journal of the American Chemical Society

Publisher: American Chemical Society

Article Type: Article

DOI:

Authors: Benedikt S. Soller, Philipp Pahl, Stephan Salzinger, Alexander Pöthig, Wolfgang Eisenreich, and Bernhard Rieger

4.5.1 Abstract

Within this chapter, the feasibility of RE CGCs for the stereoregular REM-GTP of vinylphosphonates is presented in a draft manuscript. Before this manuscript is suitable for publication, a signal assignment needs to be established, carefully performed, and throughout applied to the obtained PDEVP samples.

Stereospecific Rare Earth Metal-Mediated Group Transfer Polymerization of Vinylphosphonates via Yttrium Constrained Geometry Complexes

Benedikt S. Soller,[†] Philipp Pahl,[†] Wolfgang Eisenreich,[§] Stephan Salzinger,[‡] Alexander Pöthig,[⊥] and Bernhard Rieger[†,*]

[†] WACKER-Chair of Macromolecular Chemistry, Technische Universität München, Lichtenbergstraße 4, 85748 Garching bei München, Germany

[§] Chair of Biochemistry, Technische Universität München, Lichtenbergstraße 4, 85748 Garching bei München, Germany

[‡] BASF SE, Advanced Materials & Systems Research, GME/D - B001, 67056 Ludwigshafen am Rhein, Germany

[⊥] Chair of Inorganic Chemistry, Catalysis Research Center, Technische Universität München, Ernst-Otto-Fischer-Straße 1, 85748 Garching bei München, Germany

Coordinative-anionic Polymerization, Constrained Geometry Complex, Stereoregular Polymerization, Group Transfer Polymerization, Poly(vinylphosphonate)s, Rare Earth Metals, σ-Bond Metathesis, C–H Bond Activation

Supporting Information Placeholder

ABSTRACT: Reported herein is the first controlled stereospecific rare earth metal-mediated group transfer polymerization of vinylphosphonates using yttrium constrained geometry complexes. These constrained geometry complexes are obtained via simple alkane elimination reaction of $Y(CH_2TMS)_3(thf)_2$ and $(C_5Me_4H)XNHtBu$ ligands. Initiating ligands such as $-CH_2TMS$, activated heteroaromatic ligands ($CH_2(C_5H_2Me_2N)$), and activated internal alkynes are used to study and optimize the initiation reaction. The activated heteroaromatic and internal alkyne ligands are obtained via σ-bond metathesis reaction and represent a class of conjugated ligands avoiding the hindered initiation reaction of basic $-CH_2TMS$ ligands for α-C–H acidic vinylphosphonates. Furthermore, the influence of the ligand substitution on the propagation reaction is studied for X = $-SiMe_2-$ and $-CH_2CH_2-$ bridging units. The linker was found to have a significant impact on the obtained molecular weight of poly(diethyl vinylphosphonate) and for the ethyl-bridged CGCs low initiator efficiencies I^* and for the more rigid dimethylsiyl bridge high initiator efficiencies I^* (up to 86%) and narrow PDIs (< 1.1) were obtained. The produced poly(vinylphosphonate)s show high isotacticities and the first signal assignment and quantification of pentads in ^{31}P-NMR is conducted based on two-dimensional HMBC measurements. The signal assignment is based on HSQC, HMBC, and other two-dimensional NMR measurements.

Introduction

Owing to the ubiquitous use of polymeric materials in our modern consumer based societies, a detailed understanding of the relationship between synthesis and properties of the final polymer is of fundamental relevance.[1-2] In biological systems, the functions and properties of proteins and enzymes are directed by the primary structure and the corresponding three dimensional macromolecular structures. The infinite unique physical properties of man-made materials are addressed by the polymer microstructure. Whether a polymer is an amorphous, glassy, or rubbery material with the ability to deform under stress without rupture or a crystalline solid possessing high dimensional stability depends on its microstructure, *i.e.*, a detailed regular architecture of its substituents along the main chain. The physical properties of widely used plastics, such as polyolefins, largely depend on the local structure of monomer linkage. Group 4 metallocenes had an indisputable role for a deeper perception on the stereospecific polymerization of propylene.[3] Furthermore, isoelectronic rare earth element (RE) metallocenes, are known for the living polymerization of ethylene or polar monomers and were previously found to be highly active for the polymerization of vinylphosphonates.[4] Other classic polymerization methods, such as radical or anionic polymerizations only result in low conversions and no high molecular mass poly(vinylphosphonate)s are obtained.[5-7]

RE metal-mediated group transfer polymerization (REM-GTP, also termed coordinative anionic polymerization in literature) was originally discovered in 1992 by Yasuda et al. for the stereoregular polymerization of methyl methacrylate (MMA).[8] The polymerization of MMA, vinylphosphonates, and other conjugated nitrogen-containing monomers was summarized in review articles.[9-

[10] Phosphorus-containing polymers belong to an interesting type of materials as phosphorus groups can provide various material properties. Phosphorus-based materials are attributed to show high biocompatibilities,[11-13] find applications in dental adhesives or bone concrete,[14-16] materials for energy applications,[17-23] and halogen-free flame retardants.[24-26]

Vinylphosphonates are distinguished monomers for such applications as they belong to one of the simplest and longest known phosphorus-containing monomers.[10] Flame-retardant coating and additives of poly(dialkyl vinylphosphonate)s (PDAVP) and poly(ditolyl vinylphosphonate) have been tested for their use as halogen-free flame retardants for polycarbonate.[27] Poly(diethyl vinylphosphonate) (PDEVP) shows amphiphilic behavior and is soluble in organic solvents and water. Therefore, upon heating, aqueous PDEVP solutions have a lower critical solution temperature (LCST) close to the physiological range[28] and by selected choices of the copolymerization of DEVP with other vinylphosphonates, random PDEVP copolymers show a highly tunable LCST over the entire temperature range of water from 5 to 92 °C.[29]

A first study on ligand induced steric crowding with the aim to study the influence of the substituents on the microstructure was recently published for several RE metallocenes, however, resulted in the formation of atactic poly(vinylphosphonate)s.[30] A main finding from temperature dependent activity measurements and the determination of thermodynamic parameters $\Delta H^{\ddagger}$ and $\Delta S^{\ddagger}$ had been the high flexibility of the used bulky substituents to minimize steric overcrowding at the metal center and in return no stereoregularity was induced by such substituted ligand systems.[30] To date, only few reports in literature exits on the stereoregularity of poly(vinylphosphonate)s.[10] Rabe et al. reported the synthesis of PDEVPs with molecular masses between 65 and 84 kDa using readily available $Ln(bdsa)_3(thf)_2$ (Ln = La, Nd, Sm) precursor complexes, resulting in extremely broad PDIs, [*mm*] contents up to 79%, and conversions below 80%.[31] However, the [*mm*] content could not be quantified using isolated peaks due to overlapping or poorly resolved signals.[31]

A detailed study and the precise synthesis of stereoregular poly(vinylphosphonate)s is missing in literature. With respect to the results of ligand induced steric crowding (*vide supra*), we chose to study sterically crowded and rigid (*i.e.*, bridged) RE constrained geometry complexes (CGC) to minimize the flexibility during the propagation reaction, further limiting the degree of freedom, and to facilitate a suitable conformation of the transition state to induce a stereoregular polymerization for vinylphosphonates.

Results and Discussion

Since the original introduction by the Bercaw group, bridged amino-cyclopentadienyl and on this motif based amino-metallocene ligands (*i.e.* indenyl, fluorenyl) have evolved to be widely used for RE and group 4 metal polymerization catalysts.[32-33] Based on these brigded amido-cyclopentadienyl ligands, Dow Chemical and Exxon Chemical independently developed so called "constrained geometry" group 4 complexes (CGC), being one of the most versatile and industrially important single site olefin polymerization catalysts.[34-41] CGCs differ from bridged metallocene complexes in their steric demand, with the amide ligand being more accessible and in their electronic configuration (see Figure 1).

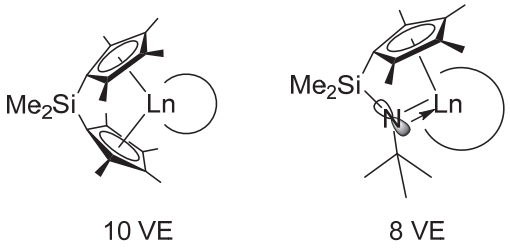

Figure 1. Comparison of the steric and electronic factors for bridged RE metallocenes (left) and RE CGCs (right) (VE = valence electrons from the ligand).

In literature, bridged metallocene RE complexes are often prepared from salt metathesis reaction in a straight forward synthesis.[42-43] However, salt metathesis for RE metals can result in laborious purification steps due to the formation of ate-complexes or insoluble oligomeric organometallic products.[33,44-45] In an alternative approach, RE CGCs can be synthesized via simple alkane elimination of tetramethylsilane from the reaction of $Y(CH_2TMS)_3(thf)_2$ and the corresponding ligand in a one-step reaction.[46] To study the effect of RE CGCs for the REM-GTP of vinylphosphonates several RE complexes were synthesized following the modified procedure of alkane elimination (see Chart 1).[46]

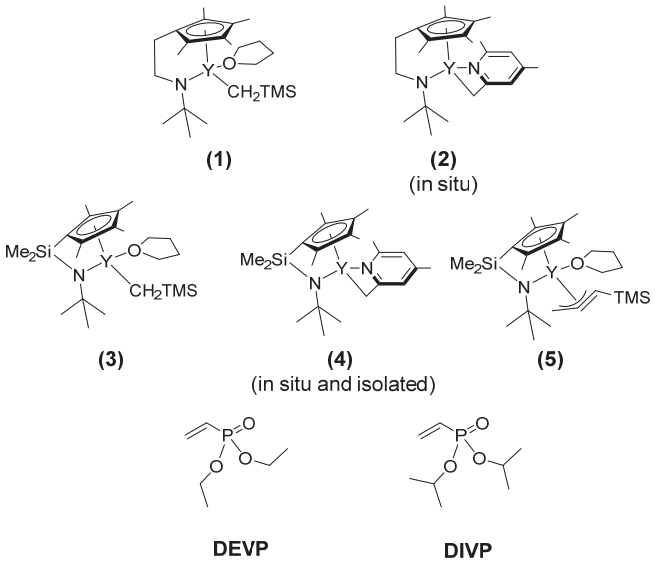

Chart 1. Overview on Catalysts and monomers used in this study

In this work two different bridging units ($-SiMe_2-$ and $-CH_2CH_2-$) were synthesized and starting from the RE–CH_2TMS complexes, the initiating ligand was exchanged with *sym*-collidine and 1-trimethylsilyl-1-propyne. The C–H bond activation of these substrates proceeds via σ-bond metathesis and was studied by Teuben et al. and previously applied by Mashima et al. for the end group functionalization of 2-vinylpyridine oligomers.[47-49]

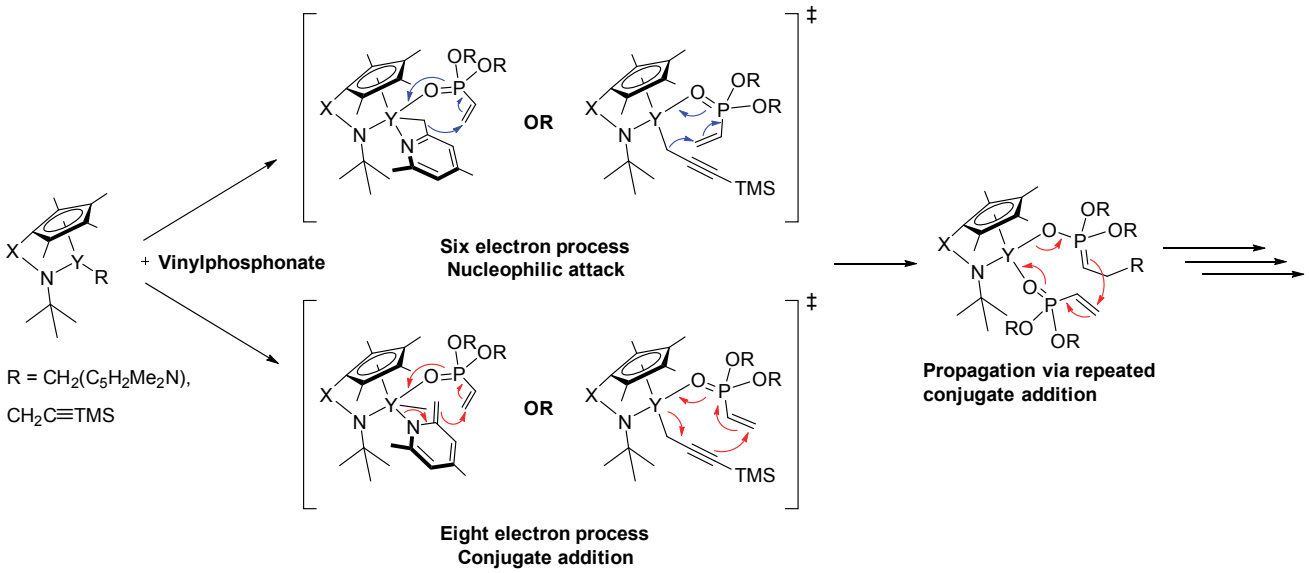

Figure 2. Proposed initiation reaction via nucleophilic transfer (six electron process, blue) or conjugate addition (eight electron process, red) and propagation via a repeated conjugate addition of the polymer chain to the coordinated monomer at the metal center.

We primarily chose to study initiating ligands derived from *sym*-collidine and 1-trimethylsilyl-1-propyne to avoid the initiation problems of $-CH_2TMS$ ligands (long initiation delay, low initiator efficiencies I^*) with α-C–H acidic vinylphosphonates.[50] Previously, with this regard, only *sym*-collidine was used for vinylphosphonate REM-GTP by our group for simple $(C_5H_5)_2LnCH_2TMS(thf)$ (Ln = Y, Lu) complexes.[51] In this study, we extend this approach to internal alkynes to study if also this ligand class results in an improved initiation reaction compared to $-CH_2TMS$. The enhanced initiation is attributed to a mechanistic match between initiation and propagation, both following an eight-electron process (see Figure 2).[51]

A dimeric crystal structure was obtained for complex **(4)** (see Figure 3). From the bond distance of the coordinated methylene group, a shortened and partial double bond character can be seen for the C16–C17 bond (1.467(3) Å) compared to the nonactivated C21–C23 methyl group (1.495(7) Å) supporting the conjugated addition pathway for the initiation reaction via an eight electron process for these activated ligands (see Figure 2). The crystallographic results are compared with other values from literature in Table 1.

Table 1. Bond Distances for Yttrium Ortho Methyl Pyridine Complexes

	Ref. [51]	Ref. [52]	This Work
$H_2C–C_{Ar}$ Bond Distrance [Å]	1.456(5)	1.416(7)	1.467(3)
$H_3C–C_{Ar}$ Bond Distrance [Å]		1.478 – 1.504	

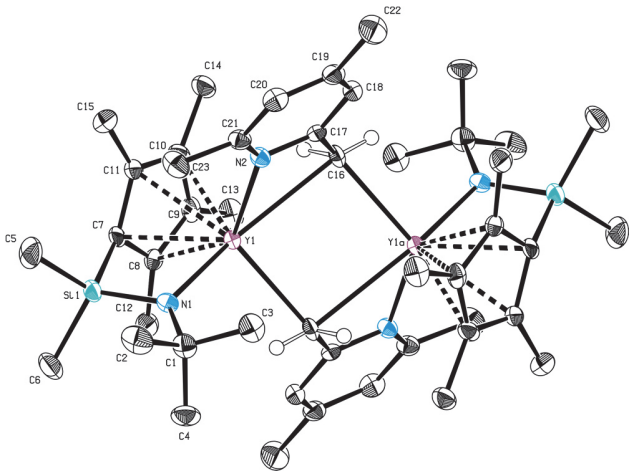

Figure 3. ORTEP drawing of complex **(4)** with 50% ellipsoids. All H atoms have been omitted for clarity. Selected bond distances (Å) and angles (deg): C16–C17, 1.467(3); C21–C23, 1.496(3); Y1–C16, 2.574(2); Y1–C1–C2, 85.56(13); N1–C2–C1, 116.21(19).

The polymerization results for all catalysts over a wide range of temperatures is summarized in Table 2. Previously, alkyl initiators were reported to have broad PDIs for the living REM-GTP of vinylphosphonates in the range of 1.3 – 1.5.[50] In this study, the applied RE–CH_2TMS complexes show an improved initiation reaction resulting in overall lower PDIs and higher initiator efficiencies I^* for these RE alkyl complexes. Additionally, the overall positive impact of the applied constrained geometry ligand sphere on the initiation reaction is further supported by the activated (4,6-dimethylpyridin-2-yl)methyl and 3-(trimethylsilyl)prop-2-ynyl ligands. For both activated initiating ligands a decrease of the PDI and strong increase of the initiator efficiency (I^* > 77%) is seen. At lower temperatures, less complexes are active for the

Table 2. Polymerization Results for the Polymerization of DEVP

Catalyst	Reaction time [min]	Polymerization temperature [°C]	Conversion[a] [%]	M_n[b] [kDa]	PDI[b]	I^*[b] [%]	[*mmmm*][a] [%]
(**Y-1**) (CH_2TMS)	1.0	30	> 99	449	1.26	11	n.d.
(**Y-2**) ($CH_2(C_5H_2Me_2N)$	1.0	30	> 99	255	1.38	19	n.d.
(**Y-3**) (CH_2TMS)	1.0	30	> 99	153	1.19	32	n.d.
(**Y-4**) ($CH_2(C_5H_2Me_2N)$	1.0	30	> 99	80	1.03	62	n.d.
(**Y-5**) ($CH_2(C{\equiv}CTMS)$	1.0	30	> 99	66	1.01	75	n.d.
(**Y-1**) (CH_2TMS)	2.5	10	> 99	450	1.29	11	n.d.
(**Y-3**) (CH_2TMS)	2.5	10	> 99	155	1.26	32	n.d.
(**Y-4**) ($CH_2(C_5H_2Me_2N)$	2.5	10	> 99	59	1.04	83	n.d.
(**Y-5**) ($CH_2(C{\equiv}CTMS)$	2.5	10	> 99	57	1.09	86	n.d.
(**Y-3**) (CH_2TMS)	5.0	−10	> 99	214	1.20	23	n.d.
(**Y-4**) ($CH_2(C_5H_2Me_2N)$	5.0	−10	> 99	57	1.04	86	n.d.
(**Y-5**) ($CH_2(C{\equiv}CTMS)$	5.0	−10	> 99	60	1.13	82	n.d.
(**Y-3**) (CH_2TMS)	10	−30	> 99	333	1.24	15	n.d.
(**Y-4**) ($CH_2(C_5H_2Me_2N)$	10	−30	> 99	77	1.06	64	n.d.
(**Y-5**) ($CH_2(C{\equiv}CTMS)$	10	−30	> 99	73	1.18	67	n.d.
(**Y-1**) (CH_2TMS)	45	−78	> 99	833	1.05	6	n.d.
(**Y-2**) ($CH_2(C_5H_2Me_2N)$	45	−78	> 99	957	1.06	5	n.d.
(**Y-3**) (CH_2TMS)	20	−78	> 95	1102	1.07	4	n.d.
(**Y-4**) ($CH_2(C_5H_2Me_2N)$	20	−78	> 99	151	1.13	33	n.d.
(**Y-5**) ($CH_2(C{\equiv}CTMS)$	20	−78	> 99	188	1.29	26	n.d.

a) Determined by ^{31}P NMR spectroscopic measurements. b) Determined by GPC-MALS, $I^* = M_{th}/M_n$, M_{th} = eq.$_{(Monomer)} \times M_{Mon} \times$ conversion (I^* = at the end of the reaction).

polymerization of vinylphosphonates and higher molecular mass polymers are obtained. This effect is stronger for the applied RE–CH_2TMS complexes, however, can also be seen for complexes **(4)** and **(5)** (I^* = 62 – 75% at 30 °C; 26 – 33% at −78 °C).

We were furthermore interested in the impact of ligand modifications for RE CGCs on the propagation reaction of vinylphosphonate REM-GTP. Therefore, we decided to synthesize complexes with two different bridging units (*vide supra*). In the case of propylene migratory insertion, it has been shown that catalysts based on silyl bridges are superior to their ethylene-bridged analogues in both activity and stereospecificity.[53-56] Interestingly, for the repeated conjugate addition of MMA, the opposite trend was observed with ethylene-bis(indenyl) based zirconium catalysts, producing PMMA with higher isotacticities, but in some cases suffering from low initiator efficiencies.[57-58] Furthermore, it has been shown that silyl-bridged-*ansa*-zirconocenes (*rac*-$Me_2Si(Ind)ZrMe_2$) have lower stereoselectivities and propagation rates than the corresponding *rac*-$CH_2CH_2(Ind)ZrMe_2$ compounds.[59]

First polymerization experiments with the ethylene bridged complexes **(1)** and **(2)** resulted in highly viscous toluene solutions and quantitative conversions were observed via ^{31}P-NMR. Due to the high viscosities, polymerizations were conducted in 5% monomer solutions. After workup of the polymer samples unexpectedly high molecular masses with broadened PDIs were detected via GPC-MALS. Therefore, the used ethylene bridged complexes 1 and 2 were found to be not feasible to further investigate the impact of CGCs for vinylphosphonate REM-GTP.

Therefore, we investigated the silyl bridged analog RE CGC structures. In literature, one-membered silicon bridges are discussed as preferable over the two-membered ethylene bridge as they provide higher rigidity and favorable electronic characteristics to the metallocene for migratory insertion (see Figure 4).[54-55] Also for the REM-GTP of vinylphosphonates we observed a strong positive impact of the silyl bridge and PDEVPs with high initiator efficiencies I^* and lower PDIs were obtained (see Table 2).

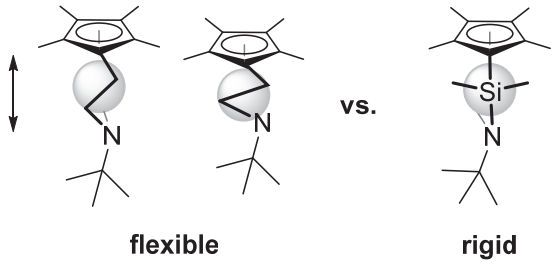

Figure 4. Higher flexibility for ethylene bridges in comparison to the corresponding silyl bridge.

Therefore, in the case of RE CGC vinylphosphonate REM-GTP, silyl bridged complexes seem favored due to their higher rigidity

preventing an unwanted flexibility with the sterically demanding vinylphosphonate monomers.[55] This is in contrast to the isoelectronic cationic zirconocene polymerization of (meth)acrylates and (meth)acrylamides where ethylene bridges are mostly used as they provide a good access to the metal center for the sterically demanding eight-membered propagation reaction.[9,57] The influence of the bridging unit has been summarized for migratory insertion in review articles.[60-61]

The activities and normalized TOFs are shown for the polymerization of DEVP at 30 °C in Table 3. Due to the overall high viscosities diluted 5 vol% monomer solutions were used to ensure sufficient stirring until high conversions. The obtained values can therefore not directly be compared with previous literature results (for 10 vol% solutions).

Table 3. Results of the Activity Measurements

Catalyst	Init. period	Conv. [%]	I^* [%]	TOF [h^{-1}]	TOF/I^* [h^{-1}]
(**1**)	-	> 99	11	> 125 000	> 265 000
(**2**, in situ)	-	> 99	19	> 125 000	> 265 000
(**3**)	-	> 99	32	> 125 000	> 265 000
(**4**)	-	> 99	62	> 125 000	202 000
(**4**, in situ)	-	> 99	78	> 125 000	160 000
(**5**)	-	> 99	75	> 125 000	167 000

We attribute the high observed activities of the applied RE CGCs to a good accessibility of the RE metal center for sterically demanding vinylphosphonates via the amido site and a simultaneously high steric demand of the ligand system at the substituted cyclopentadienyl moiety. Previously, increased steric demand was found to increase activity until steric overcrowding results in lower activities due to entropic reasons.[30] The applied methyl–Cp substituents should further result in a lower entropic barrier $\Delta S^{\ddagger}$ increasing the activity.[30] Temperature dependent activity measurements to determine reaction enthalpies an entropies with less active RE CGCs are a target for future studies.

The measured activities for complex (**1**) or (**2**) are lower than for the corresponding complexes with a silyl bridging unit. However, this stems from low initiator efficiencies; the normalized TOF/I^* values are in similar ranges (see Table 3). In contrast to results for other polar monomers,[9] the herein presented constrained geometry complexes are more active, efficient and controlled for the polymerization of DEVP; also compared to other substituted tris(cyclopentadienyl) RE initiators.[30] Previously, the polymerization velocity of MMA or acrylates was found to decrease for RE CGCs or *ansa*-lanthanocene catalysts.[62-65] Higher activities are observed for the polymerization of DEVP using RE CGCs. However, the herein used complexes were found to be limited for the polymerization of the sterically more demanding monomer diisopropyl vinylphosphonate (DIVP) and no quantitative polymer formation was observed (conv. = up to 82% at 10 °C; up to 32% at −30 °C see SI).

^{1}H NMR and ^{31}P NMR studies of the obtained PDEVP samples in D_2O showed a significant change of the different signal sets compared to previous produced (atactic) polymers (see Figure 5).

The previously observed minor shoulder signal on the right becomes one of the main signals if RE CGCs are used for the polymerization. However, the literature on the microstructure of poly(vinylphosphonate)s is scare and mostly limited by poor resolution or overlapping signals in NMR measurements.[10,31,66] Therefore, a reevaluation and new signal assignment of the microstructure for poly(vinylphosphonate)s was needed within this work.

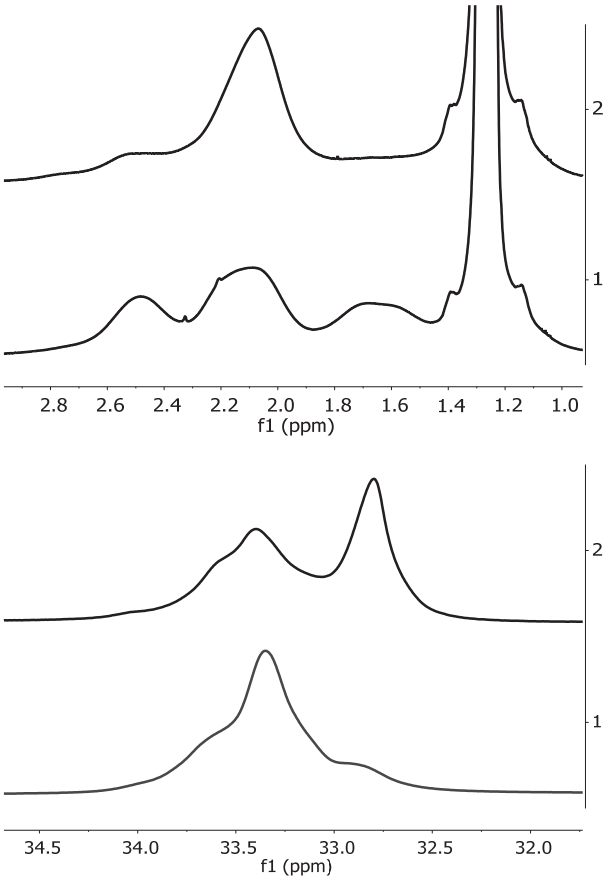

Figure 5. a) ^{1}H NMR of the backbone PDEVP signals and b) ^{31}P-NMR of isotactic (top) and atactic (bottom) PDEVP in D_2O.

The methine (^{1}H) and ^{31}P signals can only split into triads, pentads, or higher (2n) sequence signal sets. For the corresponding methylene signals only diads, tetrads, and higher (2n+1) sequences can be observed (see Figure 6).

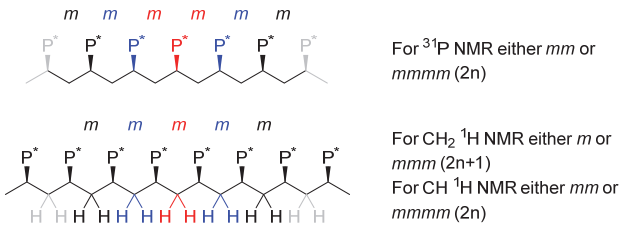

Figure 6. Microstructure of poly(vinylphosphonate)s and resulting signal sets for different positions.

The signal assignment was attempted with long term two-dimensional NMR measurements, however, so far only reliable HSQC spectra were obtained (see Figure 7). The more important

^{31}P signal assignment is so far hampered by low resolutions (see Figure 8). A stronger magnetic field and a NMR spectrometer with the ability to excite ^{31}P nuclei in combination with a good ^{1}H detection can be used in the future to obtain better spectra.

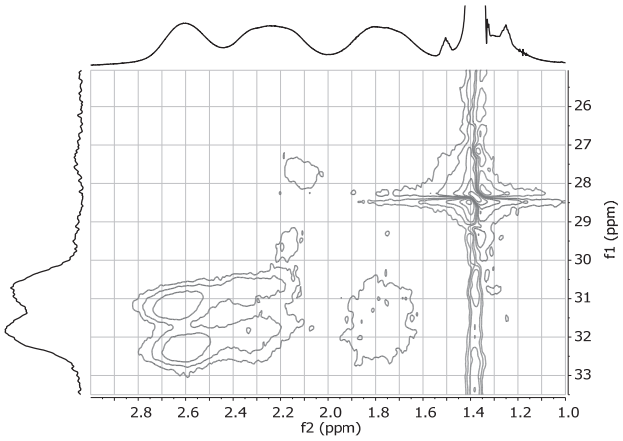

Figure 7. ^{1}H^{13}C HSQC of atactic PDEVP in D_2O.

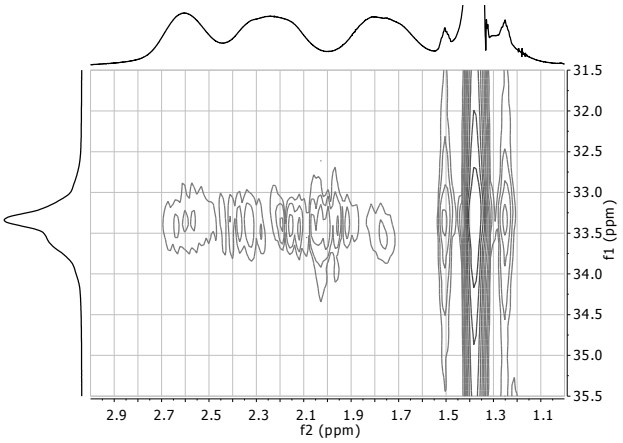

Figure 8. ^{1}H^{31}P HMBC of atactic PDEVP in D_2O.

To reliably quantify the assigned [*mmmm*] signals, a peak deconvolution of the signals in ^{31}P NMR is an effective way to obtain single values. The results of the peak deconvolution are also shown in Table 2 and one example for the peak deconvolution of atactic PDEVP in D_2O is shown in Figure 9.

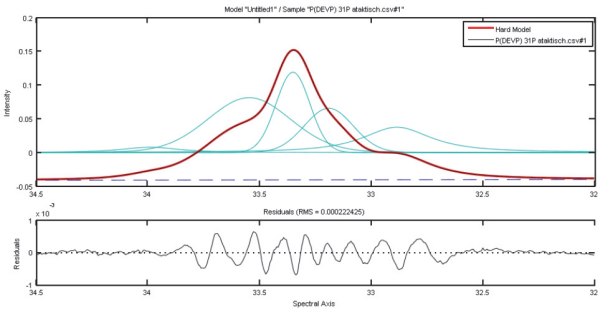

Figure 9. Algorithm based peak deconvolution for atactic PDEVP in D_2O. Five signal sets are obtained (top). Signal residue after peak deconvolution (bottom).

Conclusion

REM-GTP combines the advantages of both living-anionic and coordinative polymerizations with a high control over the molecular weight, low PDIs, formation of block copolymers, or the introduction of chain end functionalities. The RE metal center stabilizes the growing chain end and suppresses side reaction, activates the coordinated monomer, and stereospecific polymerizations were reported.

In this study, the first stereoregular and precise synthesis of highly isotactic poly(vinylphosphonate)s is presented. Furtheremore, a method to determine the tacticity of poly(vinylphosphonate)s via ^{31}P-NMR is shown. We present a signal attribution for PDEVP based on two dimensional HSQC and HMBC NMR measurements and a quantification of the overlapping ^{31}P signals using peak deconvolution methods is made.

The herein applied RE CGCs are sterically crowded and show an accessible metal center resulting in high activities and a confined propagation reaction yielding stereoregular poly-(vinylphosphonate)s. Modifications of the bridging unit were performed in this work and rigid silyl bridges were found to show superior properties compared to the more flexible ethylene bridges. Further ligand modifications and their impact on the polymerization behavior of vinylphosphonates for bridged complexes are currently on the way.[56,67]

Before this manuscript is suitable for publication, a signal assignment needs to be carefully performed and throughout applied to the obtained PDEVP samples. Peak deconvolution methods need to be used for the quantification of the signals. The impact of the bridging unit on the stereoregularity needs to be evaluated for PDEVP and the signal assignment needs to be extended for PDIVP. The results for PDIVP, including GPC measurements, yields, and quantification of the corresponding triads or pentads should be included in the manuscript or SI. Furthermore, the impact of the tacticity of the obtained poly(vinylphosphonate) samples on the material properties (T_g, T_m, LCST) should be included in this reports and needs to be evaluated using DSC and cloud point measurements.

Experimental Section

General

All reactions were carried out under argon atmosphere using standard Schlenk or glovebox techniques. All glassware was heat dried under vacuum prior to use. Unless otherwise stated, all chemicals were purchased from Sigma-Aldrich, Acros Organics, or ABCR and used as received. Toluene, THF, and pentane were dried using an MBraun SPS-800 solvent purification system. Hexane was dried over 4 Å molecular sieve. The ligands, $(C_5Me_4H)CH_2CH_2NH$*t*Bu and $(C_5Me_4H)SiMe_2NH$*t*Bu were synthesized according to literature procedures.[68-69] $Y(CH_2TMS)_3(thf)_2$ was obtained according to literature procedures.[70] $(C_5Me_4)SiMe_2N$*t*BuY$CH_2TMS(thf)$ was obtained according to literature procedures.[46,69] The monomers DEVP and DIVP were prepared according to literature procedures, died over CaH_2 for several weeks and distilled prior to use.[71] NMR spectra were recorded on a Bruker AVIII-300 or AV-500C spectrometer. ^{1}H, ^{13}C and ^{29}Si NMR spectroscopic chemical shifts δ are reported in ppm relative to tetramethylsilane. δ(^{1}H) is calibrated to the residual

F

proton signal, δ(^{13}C) to the carbon signal and δ(^{29}Si) to the deuterium signal of the solvent. ^{31}P NMR spectroscopic chemical shifts are reported in ppm relative to and calibrated to 85% aqueous H_3PO_4. Deuterated solvents were obtained from Sigma Aldrich and dried over 3 Å molecular sieve. Elemental analyses were measured at the Laboratory for Microanalytics at the Institute of Inorganic Chemistry at the Technische Universität München. Note: Elemental analyses of RE CGCs have to be performed quickly as a decomposition reaction with preheated and dried tin or aluminum containers takes place even under inert gas atmosphere (as observed as a constant weight loss inside a glove box and a ~1% lower carbon content/10 min.)

Activity measurements

For activity measurements, the stated amount of catalyst (21.7 μmol) is dissolved in 20 ml of toluene and the reaction mixture is thermostated to the desired temperature. Then, the stated amount of DEVP (6.5 mmol) is added. During the course of the measurement, the temperature is monitored with a digital thermometer and aliquots (0.5 ml) are taken and quenched by addition to deuterated methanol (0.2 ml). After the stated reaction time, the reaction is quenched by addition of MeOD (0.5 ml). The reaction is carried out in an MBraun Glovebox under argon atmosphere to take aliquots every 6-10 seconds at the beginning of the measurement. For each aliquot, the conversion is determined by ^{31}P NMR spectroscopy, the molecular weight of the formed polymer by GPC-MALS analysis.

Molecular Weight Determination

GPC was carried out on a Varian LC-920 equipped with two PL Polargel columns. As eluent a mixture of 50% THF, 50% water, and 9 g L^{-1} tetrabutylammonium bromide (TBAB) was used. Absolute molecular weights have been determined online by multiangle light scattering (MALS) analysis using a Wyatt Dawn Heleos II in combination with a Wyatt Optilab rEX as concentration source.

Complex Synthesis

$LiCH_2TMS$ was synthesized following an adapted literature procedure.[69] Lithium granulate (1.72 g, 249 mmol, 3.3 eq.) and chloromethyltrimethylsilane (9.25 g, 75 mmol, 1 eq.) are suspended in hexane (100 mL) and the mixture is heated at 35 °C for 24 h. Lithium was exempt of lithiumchloride several times using an ultrasonic bath. The supernatant solution was isolated using a filter cannula. The residue is extracted three times with hexane (15 ml) and the solvent is removed in vacuo, yielding a white pyrophoric solid (6.25 g, 66 mmol, 88%). ^{1}H NMR (300 MHz, C_6D_6) δ = 0.16 (s, 9H), -2.08 (s, 2H). ^{13}C NMR (75 MHz, C_6D_6) δ = 3.6, -4.7. Anal. Calcd for $C_4H_{11}LiSi$: C, 51.03; H, 11.78. Found: C, 51.14; H, 12.00.

$YCl_3(thf)_{3.5}$ A glass thimble is charged inside a glovebox to 2/3 with yttrium(III) chloride and is placed in a Soxhlet extractor. All glass joints of the reaction setup are diligently sealed using Teflon grease. The Soxhlet extractor is attached to a Schlenk flask with 150 ml THF, a reflux condenser, and a pressure valve using a Schlenk line outside the glovebox. The oil bath is heated at 110 °C and THF is heated to reflux for 36 h under vigorous stirring. After cooling the Schlenk flask to room temperature and detaching it from the reaction setup, THF is removed in vacuo. The product is obtained as a white powder and the amount of coordinating THF is determined by elemental analysis. The yield is nearly quantitative if pure yttrium (III)chloride is used as a starting material. Anal. Calcd for $YCl_3(thf)_{3.5}$: C, 37.56; H, 6.30. Found: C, 37.45; H, 6.33.

$YCH_2TMS_3(thf)_2$ was synthesized following an adapted literature procedure.[69] $YCl_3(thf)_{3.5}$ (1.79 g, 4 mmol, 1 eq.) is suspended in pentane (25 ml). A solution of trimethylsilylmethyl lithium (1.13 g, 12 mmol, 3 eq.) in pentane (35 ml) is added dropwise at 0 °C and the reaction solution is stirred at 0 °C for 2 h. The supernatant solution is isolated using a filter cannula and the residue is extracted with pentane (2x 10 ml). The solvent is removed in vacuo and the product is obtained as a white solid (1.78 g, 3.6 mmol, 90%). ^{1}H NMR (300 MHz, C_6D_6) δ = 4.01–3.87 (m, 8 H), 1.36–1.21 (m, 8 H), 0.31 (s, 27 H), -0.67 (d, 6 H). ^{13}C NMR (75 MHz, C_6D_6) δ = 69.8, 33.8, 25.2, 4.5.

$(C_5Me_4)CH_2CH_2NtBuYCH_2TMS(thf)$ (1) In an argon-filled glovebox, $Y(CH_2TMS)_3(thf)_2$ (988 mg, 1.89 mmol, 1 eq.) is dissolved in pentane (18 ml) and the mixture is cooled to 0 °C outside a glovebox. A solution of $(C_5Me_4H)CH_2CH_2NHtBu$ (418 mg, 1.89 mmol, 1 eq.) in pentane (7 ml) is added dropwise and the reaction solution is stirred for 2 h at 0 °C. Volatile compounds are removed in vacuo, resulting in a yellow solid. The crude product is washed with cold pentane and dried in vacuo. The product is purified by recrystallization from pentane and is obtained is a slightly yellow crystalline solid (787 mg, 1.68 mmol, 89%). ^{1}H NMR (300 MHz, C_6D_6) δ = 3.89–3.81 (t, 2H), 3.60–3.20 (m, 4H), 3.02 (t, 2H), 2.25–1.96 (m, 12H), 1.34 (s, 9H), 1.08–0.97 (m, 4H), 0.36 (s, 9H), -0.97 (d, 2H). ^{13}C NMR (75 MHz, C_6D_6) δ = 126.4, 126.2, 126.0, 68.5, 53.7, 52.4, 28.2, 25.8, 23.2, 22.7, 9.1, 3.0, -2.0. ^{29}Si NMR (99 MHz, C_6D_6) δ = -2.86. Anal. Calcd for $C_{23}H_{44}NOSiY$: C 59.08, H 9.48, N 3.00. Found: C 58.70, H 9.43, N 3.17.

$(C_5Me_4)CH_2CH_2NtBuY(CH_2(C_5H_2Me_2N))$ (2) In an argon-filled glovebox, $(C_5Me_4)CH_2CH_2NtBuYCH_2TMS(thf)$ (170 mg, 0.36 mmol, 1 eq.) is suspended in pentane (7.5 ml) and sym-collidine (43.5 mg, 0.36 mmol, 1 eq.) is added dropwise. The reaction solution is stirred at room temperature for 30 minutes and volatile compounds are removed in vacuo. The product is obtained as a yellow solid (139 mg, 0.32 mmol, 90%). ^{1}H NMR (300 MHz, C_6D_6) δ = 6.41 (s, 1 H), 6.35 (s, 1 H), 3.58 (m, 2 H), 3.08 (m, 2 H), 2.51 (s, 3 H), 2.44 (s, 2 H), 2.36 (s, 3 H), 2.25 (s, 3 H), 2.04 (s, 3 H), 1.96 (s, 3 H), 1.78 (s, 3 H), 0.97 (s, 9 H).

$(C_5Me_4)Me_2SiNtBuYCH_2TMS(thf)$ (3) was synthesized according to an adapted literature procedure.[46,69] In an argon-filled glovebox, $Y(CH_2TMS)_3(thf)_2$ (4.4 g, 8.9 mmol, 1 eq.) is dissolved in pentane (90 ml) and cooled to 0 °C. A pentane solution (35 ml) of $(C_5Me_4H)SiMe_2NHtBu$ (2.24 g, 8.9 mmol, 1 eq.) is added dropwise and the mixture is stirred under cooling for 2 h. The mixture is filtered and volatile compounds are removed in vacuo. 3.7 g of the yellow crude product (84%) are obtained and further purified by recrystallization from pentane. The product is obtained as a white powder. ^{1}H NMR (300 MHz, C_6D_6) δ = 3.38–3.15 (m, 4H), 2.21 (s, 12H), 1.39 (s, 9H), 1.03–0.96 (m, 4H), 0.77 (s, 6H), 0.31 (s, 9H), -0.90 (d, J = 3.2 Hz, 2H). ^{13}C NMR (75 MHz, C_6D_6) δ = 4.7, 8.4, 11.5, 14.0, 24.7, 26.2, 36.0, 54.0, 70.7, 106.6, 122.3, 126.4. ^{29}Si NMR (99 MHz, C_6D_6) δ = -2.73, -25.06. Anal. Calcd for $C_{23}H_{46}NOSi_2Y$: C, 55.51; H, 9.32; N, 2.81. Found: C, 55.77; H, 9.50; N, 2.85.

$(C_5Me_4)Me_2SiNtBuY(CH_2(C_5H_2Me_2N))$ (4) In an argon-filled glovebox, $(C_5Me_4)SiMe_2NtBuYCH_2TMS(thf)$ (2.2 g, 4.4 mmol, 1 eq.) is dissolved in pentane (100 ml) and sym-collidine

(0.54 g, 4.4 mmol, 1 eq.) in 20 ml pentane is added dropwise to the stirred solution. The mixture is stirred at room temperature for 30 min and volatile compounds are removed in vacuo. The yellow residue (1.85 g, 4.0 mmol, 91%) is washed once with cold pentane and the crude product is recrystallized from toluene. The product is obtained as yellow crystals (1.63 g, 3.6 mmol, 80%). ^{1}H NMR (500 MHz, C_6D_6) δ = 6.40 (s, 1H), 5.86 (s, 1H), 2.58 (s, 3H), 2.38 (s, 3H), 2.20 (s, 3H), 2.09 (s, 3H), 1.93 (s, 3H), 1.78 (s, 3H), 1.01 (s, 9H), 0.85 (s, 3H), 0.78 (s, 3H). ^{13}C NMR (126 MHz, C_6D_6) δ = 172.0, 155.0, 150.1, 127.5, 126.9, 123.1, 122.3, 119.3, 116.2, 107.1, 54.8, 41.3 (d), 33.9, 26.1, 20.8, 16.1, 14.6, 11.9, 11.5, 8.8, 7.9. ^{29}Si NMR (99 MHz, C_6D_6) δ = -25.36. Anal. Calcd for $C_{23}H_{37}N_2SiY$: C, 60.24; H, 8.13; N, 6.11. Found: C, 59.66; H, 8.24; N, 5.92.

$(C_5Me_4)Me_2SiN$*t*$BuY(CH_2(C{\equiv}CTMS))$ (5) In an argon-filled glovebox, $(C_5Me_4)SiMe_2N$*t*$BuYCH_2TMS(thf)$ (1.42 g, 2.9 mmol, 1 eq.) is dissolved in toluene (50 ml) and 1-trimethylsilylprop-1-yne (0.38 g, 3.4 mmol, 1.2 eq.) is added to the mixture. The solution is heated at 60 °C for 1 h and volatile compounds are removed in vacuo. The product is purified by recrystallization from pentane and obtained as a slightly yellow solid (950 mg, 1.82 mmol, 64%). ^{1}H NMR (500 MHz, C6D6) δ = 3.63–3.39 (m, 4H), 2.56–1.95 (m, 14H), 1.35 (s, 9H), 1.16–1.07 (m, 4H), 0.92–0.75 (m, 6H), 0.32 (s, 9H). ^{13}C NMR (126 MHz, C6D6) δ = 166.6 (s), 127.0 (s), 125.5 (s), 123.9 (s), 120.5 (s), 107.2 (s), 105.8 (d), 72.9 (s), 54.0 (s), 38.3 (d), 35.5 (s), 25.2 (d), 15.3 (s), 14.1 (s), 11.3 (s), 8.9 (s), 8.6 (s), 2.2 (s). ^{29}Si NMR (99 MHz, C6D6) δ = -12.65, -25.97. Anal. Calcd for $C_{25}H_{46}NOSi_2Y$: C, 57.55; H, 8.89; N, 2.68. Found: C, 57.45; H, 9.14; N, 2.77.

ASSOCIATED CONTENT

Supporting Information

Detailed procedures for activity measurements, polymerizations results, ^{31}P NMR peak deconvolution, and detailed information for single crystal X-ray structure determination. This material is available free of charge *via* the Internet at http://pubs.acs.org.

AUTHOR INFORMATION

Corresponding Author

* rieger@tum.de

Author Contributions

B.S.S. and S.S. conceived the idea. B.S.S. designed the experiments. P.P. and W.E. performed the NMR measurements. B.S.S. and P.P. performed the experiments. B.S.S. and P.P. wrote the manuscript and participated in data analyses and discussions. A.P. measured and resolved the crystal structure data. B.R. directed the project. All authors have given approval to the final version of the manuscript.

Notes

The authors declare no competing financial interest.

ACKNOWLEDGMENT

The authors thank Peter T. Altenbuchner and Alexander Kronast for valuable discussions. Felix Geitner and Dmitri Starkov are thanked for their preparative work synthesizing some of the complexes. Martin Machat is thanked for his help conducting high temperature NMR measurements. Stephan Salzinger is grateful for a generous scholarship from the Fonds der Chemischen Industrie.

REFERENCES

(1) Koltzenburg, S.; Maskos, M.; Nuyken, O.; Mülhaupt, R. *Polymere: Synthese, Eigenschaften und Anwendungen*; Springer, **2013**.
(2) Odian, G. *Principles of Polymerization*; Wiley, **2004**.
(3) Brintzinger, H. H.; Fischer, D.; Mülhaupt, R.; Rieger, B.; Waymouth, R. M. *Angew. Chem. Int. Ed. Engl.* **1995**, *34*, 1143-1170.
(4) Seemann, U. B.; Dengler, J. E.; Rieger, B. *Angew. Chem.* **2010**, *122*, 3567-3569.
(5) Deng, N.; Ni, X.; Shen, Z. *Designed Monomers and Polymers* **2015**, *18*, 470-478.
(6) Kawauchi, T.; Ohara, M.; Udo, M.; Kawauchi, M.; Takeichi, T. *J. Polym. Sci., Part A: Polym. Chem.* **2010**, *48*, 1677-1682.
(7) Salzinger, S.; Rieger, B. *Macromol. Rapid Commun.* **2012**, *33*, 1327-1345.
(8) Yasuda, H.; Yamamoto, H.; Yokota, K.; Miyake, S.; Nakamura, A. *J. Am. Chem. Soc.* **1992**, *114*, 4908-4910.
(9) Chen, E. Y. X. *Chem. Rev.* **2009**, *109*, 5157-5214.
(10) Soller, B. S.; Salzinger, S.; Rieger, B. *Chem. Rev.* **2016**, *116*, 1993–2022.
(11) Abueva, C. D. G.; Lee, B.-T. *Int. J. Biol. Macromol.* **2014**, *64*, 294-301.
(12) Tan, J.; Gemeinhart, R. A.; Ma, M.; Mark Saltzman, W. *Biomaterials* **2005**, *26*, 3663-3671.
(13) Monge, S.; Canniccioni, B.; Graillot, A.; Robin, J.-J. *Biomacromolecules* **2011**, *12*, 1973-1982.
(14) Ellis, J.; Anstice, M.; Wilson, A. D. *Clinical Materials* **1991**, *7*, 341-346.
(15) Ellis, J.; Wilson, A. D. *Dent. Mater.* **1992**, *8*, 79-84.
(16) Moszner, N.; Salz, U.; Zimmermann, J. *Dent. Mater.* **2005**, *21*, 895-910.
(17) Magnusson, C. D.; Liu, D.; Chen, E. Y. X.; Kelland, M. A. *Energy & Fuels* **2015**, *29*, 2336-2341.
(18) Bock, T.; Möhwald, H.; Mülhaupt, R. *Macromol. Chem. Phys.* **2007**, *208*, 1324-1340.
(19) Allcock, H. R.; Hofmann, M. A.; Ambler, C. M.; Lvov, S. N.; Zhou, X. Y.; Chalkova, E.; Weston, J. *Journal of Membrane Science* **2002**, *201*, 47-54.
(20) Berber, M. R.; Fujigaya, T.; Sasaki, K.; Nakashima, N. *Sci. Rep.* **2013**, *3*.
(21) Berber, M. R.; Fujigaya, T.; Nakashima, N. *ChemCatChem* **2014**, *6*, 567-571.
(22) Lee, S.-I.; Yoon, K.-H.; Song, M.; Peng, H.; Page, K. A.; Soles, C. L.; Yoon, D. Y. *Chem. Mater.* **2012**, *24*, 115-122.
(23) Dimitrov, I.; Takamuku, S.; Jankova, K.; Jannasch, P.; Hvilsted, S. *Journal of Membrane Science* **2014**, *450*, 362-368.
(24) Banks, M.; Ebdon, J. R.; Johnson, M. *Polymer* **1994**, *35*, 3470-3473.
(25) Price, D.; Pyrah, K.; Hull, T. R.; Milnes, G. J.; Ebdon, J. R.; Hunt, B. J.; Joseph, P.; Konkel, C. S. *Polym. Degrad. Stab.* **2001**, *74*, 441-447.
(26) Price, D.; Pyrah, K.; Hull, T. R.; Milnes, G. J.; Ebdon, J. R.; Hunt, B. J.; Joseph, P. *Polym. Degrad. Stab.* **2002**, *77*, 227-233.
(27) Lanzinger, D.; Salzinger, S.; Soller, B. S.; Rieger, B. *Industrial & Engineering Chemistry Research* **2015**, *54*, 1703-1712.
(28) Salzinger, S.; Seemann, U. B.; Plikhta, A.; Rieger, B. *Macromolecules* **2011**, *44*, 5920-5927.
(29) Zhang, N.; Salzinger, S.; Rieger, B. *Macromolecules* **2012**, *45*, 9751-9758.
(30) Soller, B. S.; Sun, Q.; Salzinger, S.; Jandl, C.; Pöthig, A.; Rieger, B. *Macromolecules* **2016**, *49*, 1582-1589.
(31) Rabe, G. W.; Komber, H.; Häussler, L.; Kreger, K.; Lattermann, G. *Macromolecules* **2010**, *43*, 1178-1181.

(32) Shapiro, P. J.; Bunel, E.; Schaefer, W. P.; Bercaw, J. E. *Organometallics* **1990**, *9*, 867-869.
(33) Zimmermann, M.; Anwander, R. *Chem. Rev.* **2010**, *110*, 6194-6259.
(34) McKnight, A. L.; Waymouth, R. M. *Chem. Rev.* **1998**, *98*, 2587-2598.
(35) McKnight, A. L.; Masood, M. A.; Waymouth, R. M.; Straus, D. A. *Organometallics* **1997**, *16*, 2879-2885.
(36) Okuda, J. *Dalton Transactions* **2003**, 2367-2378.
(37) Canich, J. A. M.; US 5026798 A, **1991**.
(38) Canich, J. A. M.; Licciardi, G. F.; US 5057475 A, **1991**.
(39) Canich, J. A. M.; EP 0420436 A1, **1991**.
(40) Stevens, J. C.; Timmers, F. J.; Wilson, D. R.; Schmidt, G. F.; Nickias, P. N.; Rosen, R. K.; Knight, G. W.; Lai, S. Y.; EP 0416815 A2, **1991**.
(41) Stevens, J. C.; Neithamer, D. R.; EP 0418044 A2, **1991**.
(42) Fontaine, F.-G.; Tilley, T. D. *Organometallics* **2005**, *24*, 4340-4342.
(43) Kirillov, E.; Lehmann, C. W.; Razavi, A.; Carpentier, J.-F. *Organometallics* **2004**, *23*, 2768-2777.
(44) Tilley, T. D.; Andersen, R. A. *Inorg. Chem.* **1981**, *20*, 3267-3270.
(45) Evans, W. J.; Seibel, C. A.; Ziller, J. W. *J. Am. Chem. Soc.* **1998**, *120*, 6745-6752.
(46) Hultzsch, K. C.; Spaniol, T. P.; Okuda, J. *Angew. Chem. Int. Ed.* **1999**, *38*, 227-230.
(47) Duchateau, R.; Brussee, E. A. C.; Meetsma, A.; Teuben, J. H. *Organometallics* **1997**, *16*, 5506-5516.
(48) Quiroga Norambuena, V. F.; Heeres, A.; Heeres, H. J.; Meetsma, A.; Teuben, J. H.; Hessen, B. *Organometallics* **2008**, *27*, 5672-5683.
(49) Kaneko, H.; Nagae, H.; Tsurugi, H.; Mashima, K. *J. Am. Chem. Soc.* **2011**, *133*, 19626-19629.
(50) Salzinger, S.; Soller, B. S.; Plikhta, A.; Seemann, U. B.; Herdtweck, E.; Rieger, B. *J. Am. Chem. Soc.* **2013**, *135*, 13030-13040.
(51) Soller, B. S.; Salzinger, S.; Jandl, C.; Pöthig, A.; Rieger, B. *Organometallics* **2015**, *34*, 2703-2706.
(52) Guan, B.-T.; Wang, B.; Nishiura, M.; Hou, Z. *Angew. Chem. Int. Ed.* **2013**, *52*, 4418-4421.
(53) Kaminsky, W.; Külper, K.; Brintzinger, H. H.; Wild, F. R. W. P. *Angew. Chem. Int. Ed.* **1985**, *24*, 507-508.
(54) Herrmann, W. A.; Rohrmann, J.; Herdtweck, E.; Spaleck, W.; Winter, A. *Angew. Chem. Int. Ed. Engl.* **1989**, *28*, 1511-1512.
(55) Spaleck, W.; Kueber, F.; Winter, A.; Rohrmann, J.; Bachmann, B.; Antberg, M.; Dolle, V.; Paulus, E. F. *Organometallics* **1994**, *13*, 954-963.
(56) Stehling, U.; Diebold, J.; Kirsten, R.; Roell, W.; Brintzinger, H. H.; Juengling, S.; Muelhaupt, R.; Langhauser, F. *Organometallics* **1994**, *13*, 964-970.
(57) Vidal, F.; Gowda, R. R.; Chen, E. Y. X. *J. Am. Chem. Soc.* **2015**, *137*, 9469-9480.
(58) Bolig, A. D.; Chen, E. Y. X. *J. Am. Chem. Soc.* **2002**, *124*, 5612-5613.
(59) Deng, H.; Shiono, T.; Soga, K. *Macromolecules* **1995**, *28*, 3067-3073.
(60) Wang, B. *Coord. Chem. Rev.* **2006**, *250*, 242-258.
(61) Shapiro, P. J. *Coord. Chem. Rev.* **2002**, *231*, 67-81.
(62) Kirillov, E.; Toupet, L.; Lehmann, C. W.; Razavi, A.; Carpentier, J.-F. *Organometallics* **2003**, *22*, 4467-4479.
(63) Yao, Y.; Zhang, Y.; Zhang, Z.; Shen, Q.; Yu, K. *Organometallics* **2003**, *22*, 2876-2882.
(64) Fabri, F.; Muterle, R. B.; Oliveira, W. d.; Schuchardt, U. *Polymer* **2006**, *47*, 4544-4548.
(65) Jian, Z.; Zhao, W.; Liu, X.; Chen, X.; Tang, T.; Cui, D. *Dalton Transactions* **2010**, *39*, 6871-6876.
(66) Komber, H.; Steinert, V.; Voit, B. *Macromolecules* **2008**, *41*, 2119-2125.
(67) Schöbel, A.; Herdtweck, E.; Parkinson, M.; Rieger, B. *Chemistry – A European Journal* **2012**, *18*, 4174-4178.
(68) van Leusen, D.; Beetstra, D. J.; Hessen, B.; Teuben, J. H. *Organometallics* **2000**, *19*, 4084-4089.
(69) Hultzsch, K. C. *PhD Thesis*, Universität Mainz, **1999**.
(70) Hultzsch, K. C.; Voth, P.; Beckerle, K.; Spaniol, T. P.; Okuda, J. *Organometallics* **1999**, *19*, 228-243.
(71) Leute, M. *PhD Thesis*, Universität Ulm, **2007**.

4.6 Poly(vinylphosphonate)s as Macromolecular Flame Retardants for Polycarbonate

Status: Published online: January 23, 2015

Journal: Industrial & Engineering Chemistry Research

Volume 54, issue 6, pages 1703–1712

Publisher: American Chemical Society

Article Type: Article

DOI: 10.1021/ie504084q

Authors: Dominik Lanzinger, Stephan Salzinger, Benedikt S. Soller, and Bernhard Rieger

4.6.1 Abstract

Phosphorus-containing compounds are known for their flame retardant properties and are used in industrial applications. In this chapter, the flame retardant properties of poly(vinylphosphonate)s are presented for polycarbonate as a possible alternative to persistent and bioaccumulating halogen-based flame retardant additives. Simple dip coating of polycarbonate specimen into poly(dialkyl vinylphosphonate) solutions results in the formation of transparent coatings with several μm thickness and a correlation between coating thickness and flame retardant properties was found presumably due to the formation of free poly(vinylphosphonic acid) during combustion. Poly(diisopropyl vinylphosphonate) coatings were found to represent highly effective flame retardants for polycarbonate. Extrusion of poly(dialkyl vinylphosphonate)s with polycarbonate is not possible due to decomposition of the poly(vinylphosphonate) at elevated temperatures or in the case of hygroscopic PDEVP the evaporation of water in the blend was observed. Therefore, blends with aromatic poly(vinylphosphonate ester) side chains were prepared as poly(ditolyl vinylphosphonate) shows no ester side chain decomposition and main chain decomposition takes place at temperatures above 350 °C. The flame retardant behavior of poly(vinyl phosphonate)s is attributed to acting as a radical scavenger in the gas phase or in the condensed phase by char formation.

Benedikt S. Soller synthesized PDTVP and supported the first author Dominik Lanzinger in performing TGA analyses and interpreting the experimental results.

I&EC research
Industrial & Engineering Chemistry Research

Article

pubs.acs.org/IECR

Poly(vinylphosphonate)s as Macromolecular Flame Retardants for Polycarbonate

Dominik Lanzinger, Stephan Salzinger, Benedikt S. Soller, and Bernhard Rieger*

WACKER-Lehrstuhl für Makromolekulare Chemie, Technische Universität München, Lichtenbergstraße 4, 85748 Garching bei München, Germany

Supporting Information

ABSTRACT: A series of poly(dialkyl vinylphosphonate)s (PDAVPs) have recently been reported to be available via rare earth metal-mediated group transfer polymerization (REM-GTP). We extend the existing portfolio of polyvinylphosphonates (PVPs) by presenting poly(ditolyl vinylphosphonate) (PDTVP) as the first example of a poly(diaryl vinylphosphonate) (PDArVP). Thermogravimetric analyses revealed that, for PDTVP, in contrast to the selected PDAVPs, side group cleavage does not occur. Instead, thermal decomposition takes place in a one-step mechanism at high temperatures above 350 °C. A series of PDAVPs and PDTVP were tested for their performance as flame-retardant additives (FRA) as well as flame-retardant coatings (FRC) for polycarbonate (PC). We thereby found that PDTVP is a promising FRA, because of its high thermal stability and its compatibility with polycarbonate. Poly(diisopropyl vinylphosphonate) (PDIVP) shows excellent performance as an FRC, because it forms a stable, blistered crust of poly(vinylphosphonic acid) (PVPA) upon flame treatment.

INTRODUCTION

The global demand of polycarbonate (PC) in 2011 was estimated to be ~3.5 million metric tons and is expected to rise to 4.5 million metric tons by the end of 2016, with 20% of the PC produced being used in electrical and electronic applications (E&E).[1] Especially for these E&E applications, flame-retardant polycarbonate compositions are essential. For this purpose, usually, PC is blended with one or various flame-retardant additives (FRAs) in order to obtain flame-retardant resins.[2,3] The most common FRAs used in polymer resins are halogen-based, e.g., epoxy oligomers made from tetrabromobisphenol A (TBBPA), low-molecular-weight polycarbonates from TBBPA, or polybrominated trimethylphenylindanes.[2,4] Although bromine-based FRAs (BrFRAs) are very compatible with PC and yield blends with good mechanical properties, they must be used in relatively high ratios (6−15 wt %) in order to achieve UL94 V-0 rating.[3] Moreover, BrFRAs are critical from an environmental point of view, because some of them have been shown to be persistent and bioaccumulating[5] and the combustion of BrFRA containing polymer resins leads to the formation of highly toxic dibenzo-*p*-dioxins and dibenzofurans.[6]

Another potent class of flame retardants for PC are alkylsulfonates and arlysulfonates, which can provide V-0 ratings at loadings <0.1 wt % but suffer from the disadvantage of causing hazing.[3,7] Siloxane FRAs, especially silsesquioxane spheres, cause drastic changes in the mechanical properties of the PC resin already at loadings of 5 wt %.[8]

Similar to halogen-based FRAs, phosphorus-based FRAs are capable of acting not only in the condensed phase by enhancing charring, intumescence, or inorganic glass formation, but also in the gas phase, by flame inhibition due to PO radicals that react with more-reactive radicals in the flame zone.[9−12] Because of their good compatibility with PC, especially aromatic phosphates are very compelling FRAs for PC.[13−15] Although triphenylphosphate (TPP) is a cost-effective FRA, it causes problems when compounded with PC, i.e., because of its volatility and sensitivity toward hydrolysis.[16] Better alternatives are less-volatile phosphates, such as resorcinol bis(diphenyl phosphate) and Bisphenol A bis(diphenyl phosphate).[13,16,17] However, phosphonates show superior performance, because they are more stable toward hydrolysis and less volatile than phosphates. Sterically hindered diaryl arylphosphonates such as dimesityl phenylphosphonate (DMPP) were recently reported to be effective FRAs in PC at low loadings of 3−5 wt %.[18] However, a big disadvantage of most low-molecular-weight phosphorus-based FRAs is their negative effect on the glass-transition temperature, as well as on the melt viscosity of the corresponding PC/FRA blends.[9,19] Oligomeric and polymeric FRAs could be shown to have less impact on these crucial material properties.[20,21] Various poly(phosphonate)s with phosphorus-containing main chains (PMCPPs) are known in the literature and have been suggested as flame-retardant materials.[22] Poly(phosphonate)s based on diphenyl methylphosphonate and Bisphenol A or similar phenols have been recently commercialized.[22] Homopolymers, co-polymers, and branched polymers of this class are used as FRAs (e.g., for PC) or as nonburning specialty polymers.[21−28] In contrast to PMCPPs, poly(vinylphosphonate)s (PVPs) contain phosphonate moieties in their side chains and, therefore, possess a more-robust carbon-based backbone, which is insensitive toward hydrolysis and may provide PC/FRA compositions with even better properties than PC/PMCPP systems.

Nevertheless, despite the intriguing potential applications, the development of PVP homopolymers is mainly limited by the absence of efficient synthetic strategies, for instance, radical

Received: October 21, 2014
Revised: December 30, 2014
Accepted: January 23, 2015
Published: January 23, 2015

DOI: 10.1021/ie504084q
Ind. Eng. Chem. Res. 2015, 54, 1703−1712

and ionic approaches mostly resulted in low yields and degrees of polymerization.[29−31] Recently, our group and other researchers found that poly(dialkyl vinylphosphonate)s (PDAVPs) with high and defined molar mass as well as low polydispersity can be synthesized by rare earth metal-mediated group transfer polymerization (REM-GTP), not only in bulk or solution,[2,19,32,33] but also on silicon substrates.[34,35] Because of their poor accessibility, PDAVP homopolymers have not yet been studied as FRAs. In contrast to these homopolymers, co-polymers of vinylphosphonates (VPs) and styrene, methyl methacrylate, acrylonitrile, and acrylamide are readily available using radical polymerization. The flame-retarding effect of the incorporated VP co-monomer to these co-polymers was hereby found to be comparatively weak.[36]

Fire protection may not only be achieved by incorporating one or several FRAs into the polymer matrix, but also by coating of the polymer surface.[37] Although coating is a common method to enhance fire resistance of steel or wood, only few flame-retardant coatings (FRCs) for polymers are known.[38] Plasma-induced graft polymerization is a complex strategy to achieve surface modification and was successfully used to introduce fire resistance to diverse polymers.[37] Jimenez et al. recently presented examples of intumescent coatings for polyurethanes, polypropylene, and PC.[39] Next to adhesion problems, these coatings suffer from poor transparency and high coating thickness of ∼200 μm. Wenz et al. found that the flame resistance of PC may also be introduced by metal coatings.[40] Poly(vinylphosphonate)s are transparent, nonflammable polymers that could serve as easy-to-apply coatings for polymeric matrices.

In this manuscript, we present poly(ditolyl vinylphosphonate) (PDTVP) as the first example of a poly(diaryl vinylphosphonate) (PDArVP). The thermal decomposition of PDTVP was investigated and is compared to the literature known poly(dialkyl vinylphosphonate)s (PDAVPs) PDEVP, PDPVP, and PDIVP with ethyl, *n*-propyl, and *iso*-propyl groups, respectively.[41] The mentioned poly(vinylphosphonate)s (PVPs) were tested for their potential as flame-retardant additives (FRAs) or coatings (FRCs) for PC and compared to dimesityl phenylphosphonate (DMPP) as a benchmark low-molecular-weight flame retardant. In contrast to the aliphatic PDAVPs, aromatic PDTVP was found to be compatible with PC, yielding transparent blends. Based on thermogravimetric analyses (TGA), conclusions on the flame-retarding mechanism of PDTVP are drawn. PDTVP/PC blends with PDTVP contents of up to 20 wt % were produced, and UL 94 V testing, as well as stress strain measurements, were performed. Since PDIVP was found to be a very effective FRC, because of its intumescence, UL 94 V testing was performed using various coating thicknesses and different sample body thicknesses.

RESULTS AND DISCUSSION

Rare Earth Metal-Mediated Group Transfer Polymerization (REM-GTP) of Diaryl Vinylphosphonates. We have previously presented the rare earth metal-mediated homopolymerization and copolymerization of different dialkyl vinylphosphonates (alkyl = methyl, ethyl, *n*-propyl, isopropyl).[9,31,33,34,41] A new class of vinylphosphonates is obtained by replacing alkyl groups by aromatic substituents, such as *p*-tolyl (see Scheme 1). These poly(diaryl vinylphosphonate)s (PDArVP) are of high interest, because of their high thermal stability, as well as their high solubility in aromatic polymers, such as PC. Diaryl vinylphosphonates (DArVP) are readily accessible in one step from β-chloroethylphosphonic dichloride.

Scheme 1. REM-GTP of Vinyl Phosphonates

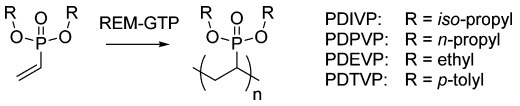

However, we found that REM-GTP of DTVP proceeds slowly and not quantitatively. Previous studies with vinylphosphonates revealed that late lanthanides (i.e., smaller cation radii) lead to faster polymerization rates and especially late tris(cyclopentadienyl) complexes show high conversions and initiator efficiencies. However, for DArVP, conversions with tris(cyclopentadienyl) Ln catalysts (e.g., Cp_3Lu) were found to be ∼40%. Therefore, we used the yttrium-based $[Cp_2YStBu]_2$ complex for the polymerization of DTVP and a conversion of 58% (as observed via ^{31}P NMR spectroscopy) was achieved.

The observed decrease in monomer reactivity for DTVP, compared to sterically less-demanding vinylphosphonates, is in good agreement with previous mechanistic studies, which conclude the rate-determining step of DAVP polymerization to be an associative displacement (S_N2-type substitution) of the growing polymer chain by a monomer (see Scheme 2).[42] The stronger steric shielding of the active site by the more rigid aromatic side groups, in comparison to flexible alkyl side chains, gives a good explanation for the slower polymerization reaction, in the case of DTVP.

Although the conversion is not quantitative, the polymerization reaction seems to proceed in a living fashion with one catalyst molecule producing only one polymer chain. At full conversion a M_n of 32 kDa would be expected. Taking into account, that only 58% of the monomer has been consumed, the expected M_n is 17 kDa (32 kDa × 0.58 = 18 kDa). The observed molecular weight (M_n) is 16 kDa at a low PDI of 1.4.

Thermal Decomposition of PVPs. The thermal stabilities of PDEVP, and PDIVP have been investigated previously by TGA in nitrogen atmosphere.[2] In the case of PDEVP and PDIVP, the first elimination step proceeds mainly via side group cleavage by elimination of ethylene (300 °C) and propylene (250 °C), respectively, leading to the formation of poly(vinylphosphonic acid) (PVPA). During the second decomposition step at a temperature range of 420−510 °C, backbone fragmentation occurs.[2] TGA experiments show that the first decomposition step for PDPVP occurs at 290 °C, being comparable to the thermal stability of PDEVP. It is assumed that scission of the C−O bond of the dialkyl phosphonate proceeds via a transition state with reduced electron density at the α-carbon of the alkyl chain. Hence, the higher thermal stability of PDEVP and PDPVP, compared to PDIVP, can be explained by the lower stability of primary (ethyl or 1-propyl) in comparison to secondary (2-propyl) alkyl cations.[14] As shown in Figure 1a, the thermal decomposition of PDTVP takes place at higher temperature (380 °C). Since side group cleavage is not possible for PDTVP, decomposition occurs at higher temperature and is assumed to proceed via main chain fragmentation.

TGA was also performed under a synthetic air atmosphere (Figure 1b), showing similar results, with respect to side group scission in the case of PDIVP and PDPVP. In the presence of oxygen, for PDEVP, the first decomposition step starts at lower temperature leading to a higher weight loss corresponding to the elimination of diethyl ether and the formation of P−O−P

DOI: 10.1021/ie504084q
Ind. Eng. Chem. Res. 2015, 54, 1703−1712

Scheme 2. Elemental Steps of Rare Earth-Mediated GTP of Vinylphosphonates with an S_N2-Type Associative Displacement of the Polymer Phosphonate Ester by a Vinylphosphonate Monomer as the Rate-Determining Step[a]

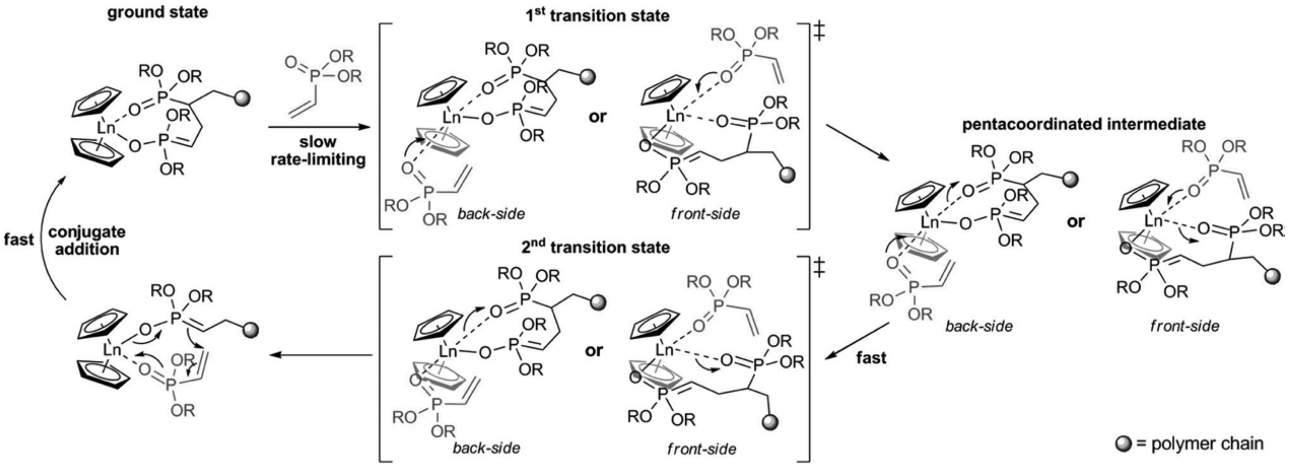

[a]Reprinted with permission from ref 9. Copyright 2013, American Chemical Society, Washington, DC.

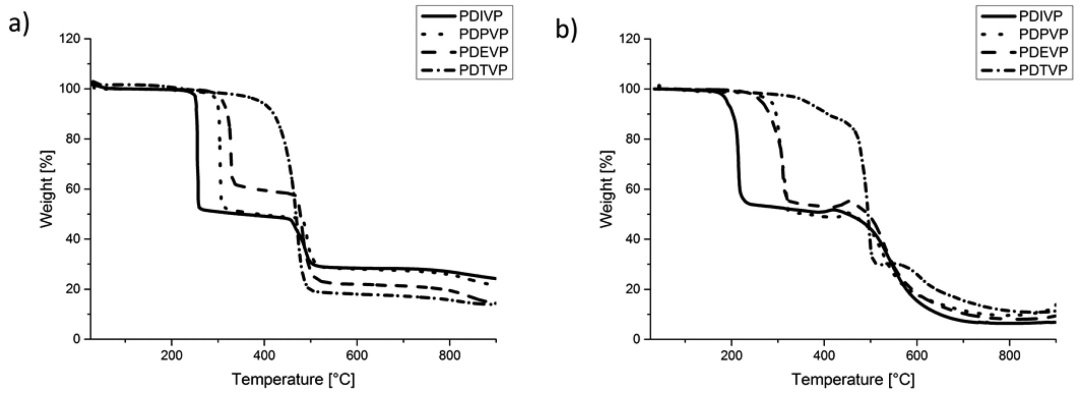

Figure 1. TGA thermograms of PDIVP, PDPVP, PDEVP, and PDTVP (a) under a nitrogen atmosphere and (b) under a synthetic air atmosphere.

bridges, while the polymer backbone seems to remain intact. For all PDAVPs, in the case of TGA under air, a weight gain was observed before the second decomposition step starts. We assume that oxidation leads to an increase in weight before backbone fragmentation yields volatile compounds. The amount of residual char after heating to 900 °C was significantly lower for all PVPs when TGA was performed under air.

PVPs as Flame-Retardant Additives (FRAs) for PC. In order to compare our results to literature-known systems, we chose dimesityl phenylphosphonate (DMPP) as a benchmark phosphonate FRA and prepared PC/DMPP blends with different FRA contents.[13] Compared to results presented in the literature, we found the flame-retarding effect of DMPP to be much weaker. The addition of 1 wt % DMPP to PC even leads to a longer average total flaming combustion time (TFCT). The sample bodies get extinguished by dripping of the burning part of the sample body, which precludes a V-0 or V-1 rating in the UL 94 V test. The longer TFCT is most likely caused by the flame-retarding effect of DMPP, leading to a slower combustion with less energy being released. Sample bodies with higher DMPP contents (5, 10, and 20 wt %) show a decrease in the TFCT values with increasing DMPP contents, whereby dripping occurs for all blends.

The observed facilitated dripping can be explained by a decrease in the glass-transition temperature (T_g) with increasing DMPP contents (Figure 2), which was confirmed by dynamic scanning calorimetry (DSC). Furthermore, a decrease in the melt viscosity might also play a significant role.

Tensile tests with DMPP/PC blends with 0, 1, and 20 wt % FRA content were performed, showing lower values for yield strain and strain at break, as well as increasing yield strengths (see Figure 3).

PDIVP. Next to a sufficient flame-retarding effect, FRAs for PC must meet two key requirements: (1) sufficient thermal stability for the high processing temperatures (230−315 °C), and (2) sufficient compatibility with PC. As shown previously, PDIVP already starts to decompose at 250 °C under a nitrogen atmosphere. Attempts to produce PDIVP/PC blends at 240 °C resulted in complete decomposition of PDIVP to PVPA, which was verified via ^{1}H NMR spectroscopy of the produced blend. The obtained PVPA/PC blends are slightly yellowish and opaque. No flammability or mechanical tests were performed with these blends.

PDPVP. Although PDPVP decomposes at higher temperatures than PDIVP, again, decomposition to PVPA was observed during processing. Therefore, no further experiments were performed with PDPVP/PC blends.

DOI: 10.1021/ie504084q
Ind. Eng. Chem. Res. 2015, 54, 1703−1712

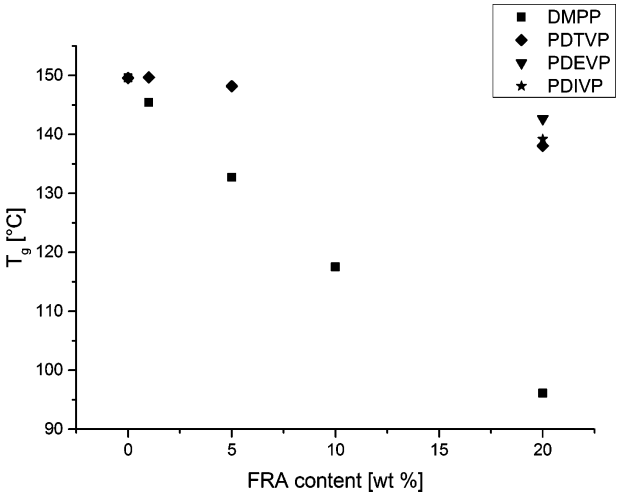

Figure 2. Glass-transition temperature (T_g) values of PC/FRA blends, as determined by DSC.

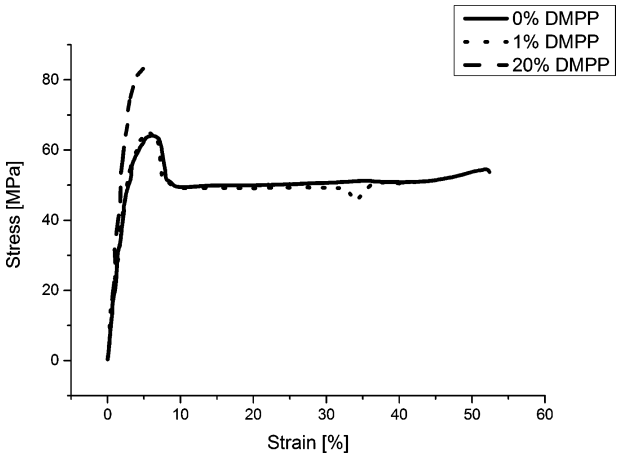

Figure 3. Stress–strain curves for PC/DMPP blends.

PDEVP. Thermally more stable PDEVP does not decompose under equal conditions. However, during compression molding of the opaque white blend, gas bubbles formed inside the sample, because of the evaporation of water. The hygroscopic PDEVP leads to a relatively high water uptake of the blend, which could not be avoided since the compression molding was performed under an air atmosphere. Because of this fact, no homogeneous specimen for mechanical analysis could be obtained. Flammability tests showed that a high PDEVP content of 20 wt % leads to facilitated dripping. Therefore, PDEVP is not suitable as a FRA for PC under these conditions. Differential scanning calorimetry (DSC) measurements revealed that the T_g value of PDEVP/PC blends (142.0 °C for a 20 wt % PDEVP/PC blend) is only slightly lower than the T_g of pure PC (149.6 °C). Therefore, a lower T_g value does not seem to be the reason for the facilitated dripping. Instead, we assume that either inhomogeneity of the specimen due to gas bubbles or a change in melt viscosity is responsible.

PDTVP. Because of its higher thermal stability, PDTVP does not decompose upon blending with PC, which could be verified by ^{1}H NMR analysis. The obtained PDTVP/PC blends are transparent. Since the T_g value of PDTVP is higher than the processing temperature, this transparency indicates good solubility of PDTVP in molten PC. Furthermore, no phase separation seems to take place during the cooling of the blend, because this would lead to hazing. Raman spectroscopy showed a homogeneous distribution of PDTVP in PC. According to this good compatibility, PDTVP and possibly also further PDArVPs are promising candidates as FRAs for PC. Similar to DMPP/PC blends, PDTVP/PC blends with low PDTVP contents of 1, 5, and 10 wt % show dripping of burning polymer, whereas blends that contain 20 wt % PDTVP do not drip at all. Upon the addition of low amounts of PDTVP, the TFCT is increased, relative to that of pure PC. In analogy to DMPP, the addition of more FRA leads to lower TFCT values (7–19 s) for 20 wt % PDTVP/PC blends resulting in a V-1 rating (see Figure 4).

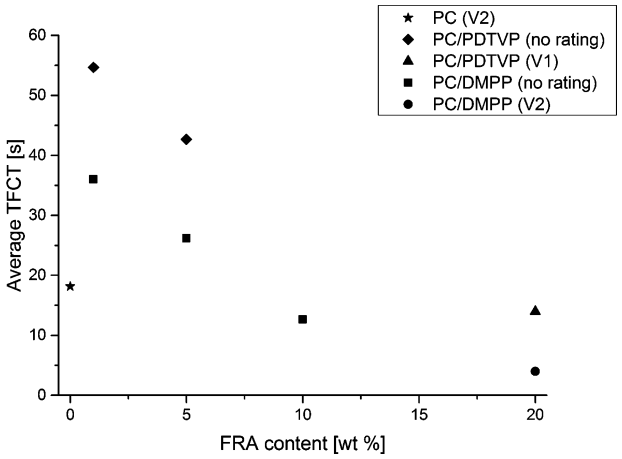

Figure 4. UL 94 V test results (TFCT and rating) of PC/PDTVP and PC/DMPP blends.

DSC measurements reveal that the T_g value is only slightly affected by the PDTVP content (Figure 2). The fact that PDTVP, in contrast to DMPP and other low-molecular-weight phosphorus-based FRAs, does not influence the T_g value of the FRA/PC blend and leads to nondripping compositions demonstrates the great potential of PDArVPs as FRAs.[43]

Figure 5 shows that high PDTVP contents lead to brittle blends, which do not show necking and break under lower stress than pure PC samples, although the yield strength of 50.8 MPa is still relatively high.

TGA of PC and PC/FRA Blends under an Air Atmosphere. In contrast to literature reports,[44] TGA experiments only showed very little charring for pure PC (2%). The decomposition mechanism of PC under air was investigated by Jang et al.[44] and was found to mainly take place via chain scission of the isopropylidene linkage. The addition of DMPP, the benchmark low-molecular-weight FRA did not enhance charring. In contrast, for blends of PC with PDIVP and PDEVP, respectively, slightly increased amounts of residual char were found (3 and 4 wt %, respectively). In case of the PC/PDTVP blend, which reached a V-1 rating in the UL 94 V test, the amount of residual char after heating to 900 °C was relatively high (9 wt %). It is known from the literature that phosphorus-based flame retardants can act in the gas phase, as well as in the condensed phase.[10,22] In the gas phase, the flame retardancy mechanism is mainly contributed to the formation of PO* radicals, which are more stable—and, therefore, less reactive—than hydrogen or hydroxyl radicals and can act as a

DOI: 10.1021/ie504084q
Ind. Eng. Chem. Res. 2015, 54, 1703–1712

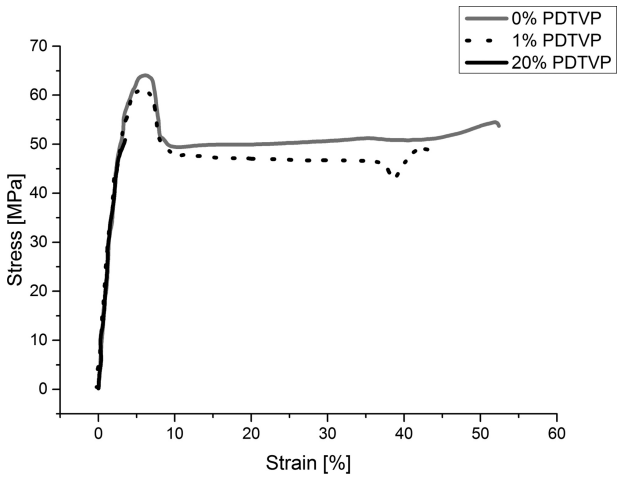

Figure 5. Stress−strain curves for PC/PDTVP blends.

radical scavenger by recombination with other radicals.[10] The flame-retarding effect in the condensed phase is mainly contributed to the tendency of phosphorus compounds to react with decomposition products of oxygen containing polymers to form phosphoric acid. Condensation of phosphoric acid leads to the formation of pyrophosphoric acid and metaphosphoric acid and, thus, the release of water vapor, which dilutes the gas phase in the combustion zone. Even more important is the fact that phosphoric acid, as well as pyrophosphoric acid can catalyze the dehydratation of alcohols and thus lead to the formation of double bonds and aromatization. Phosphates and carbonized residues form char, which acts as a protective layer for the polymer.[22]

TGA data from Figure 6 shows, that DMPP already starts to volatilize at 225 °C. After complete volatilization of DMPP, the

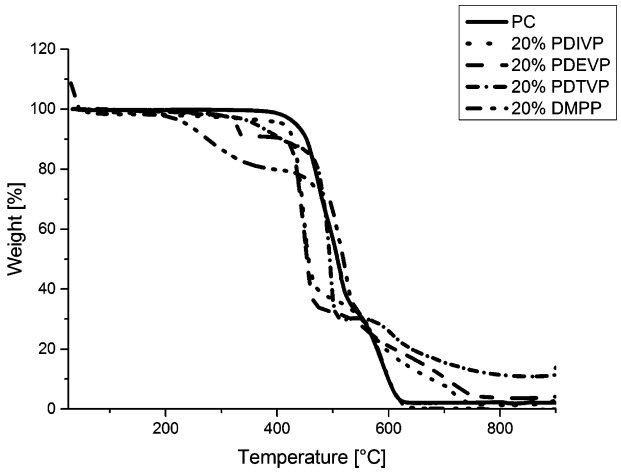

Figure 6. TGA thermograms of PC and 20 wt % blends of PDIVP, PDEVP, PDTVP, and DMPP in PC under a synthetic air atmosphere.

remaining PC behaves analogous to pure PC. Therefore, DMPP is very unlikely to be effective in the condensed phase, but might well act in the gas phase. As mentioned above, for the PC/PDIVP blend, the first decomposition step of PDIVP has already taken place during the preparation of the blend leading to poly(vinylphosphonic acid) (PVPA). Surprisingly, volatilization of PC in this PC/PVPA blend starts at lower temperatures, which might be due to the acidity of PVPA. For PC/PDEVP, the first decomposition step of PDEVP to PVPA takes place at 325 °C. The rate of the thermal decomposition of the PC/PDTVP blend is significantly slower at temperatures above 550 °C, compared to pure PC, and no degradation is observed above 730 °C. A relatively large amount (9 wt %) of char is formed, which reveals that PDTVP is highly active in the condensed phase. Because of its polymeric structure and low volatility, PDTVP is assumed to be less active in the gas phase.

PVPs as Flame-Retardant Coatings (FRCs) for Polycarbonate (PC). Since the PVPs used are transparent, solid, and very soluble in various solvents, they appear to be predestined as FRCs for PC products. DMPP was used as a reference monomeric FRC in order to reveal advantages of polymeric FRCs. Coating was performed by simple dip coating of PC samples with FR solutions of defined concentrations using different solvents.

DMPP was applied to PC specimens 0.9 mm in size with a coating thicknesses of 5−75 μm. No significant change in combustion behavior was observed, compared to uncoated PC. DMPP coatings from dichloromethane (0.1 g (DMPP)/mL (CH_2Cl_2)) and methanol (0.1 g (DMPP)/mL (MeOH)) both were transparent up to coating thicknesses of 75 or 33 μm, respectively. Exceeding this maximum coating thickness leads to the formation of white powder, instead of smooth layers.

PDEVP. Preliminary experiments proved that coatings of 115 and 243 μm lead to a significant reduction of the total flaming combustion time (TFCT), to 13.1 and 1.6 s, respectively, with no dripping during combustion. Coatings from water and MeOH are colorless and transparent. PDEVP, as a FRC, has not been studied in more detail, because the solubility of PDEVP in water is a major disadvantage. The extinguishing water may dissolve the coating and rinse it off the PC surface, which then would be unprotected and could be easily ignited. Nevertheless, embedding PDEVP into a varnish formulation that protects it from being rinsed off the substrate might result in highly efficient FRCs.

PDPVP. Coating experiments with PDPVP were not performed since PDPVP did not seem to be suitable for this application, because of its unusual mechanical properties. In contrast to PDIVP and PDTVP, PDPVP is not a solid, brittle polymer; instead, it feels soft and sticky when stored in air.

PDIVP. PDIVP was coated from MeOH solutions of different concentrations. Although coatings from low-concentration solutions (0.01 g (PDIVP)/mL (MeOH) and (0.05 g (PDIVP)/mL (MeOH)) were opaque, solutions from higher-concentration solutions (0.1 g (PDIVP)/mL (MeOH)) were transparent. SEM micrographs of these coatings (Figure 7) show that, depending on the concentration of the coating solution, the morphology of the coating differs from inhomogeneously distributed PDIVP on the PC surface to

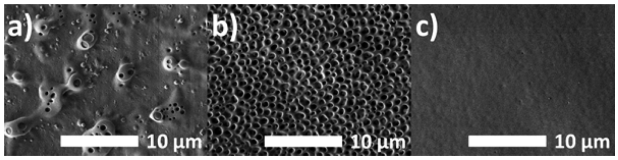

Figure 7. SEM micrographs of PDIVP coatings from MeOH solutions with concentrations of (a) 0.01, (b) 0.05, and (c) 0.1 g (PDIVP)/mL (MeOH).

DOI: 10.1021/ie504084q
Ind. Eng. Chem. Res. 2015, 54, 1703−1712

spongelike PDIVP architectures or almost perfectly smooth PDIVP layers.

We could further show that coatings with turbid, spongelike structures can be converted to smooth, transparent coatings by dipping the samples in pentane at room temperature (see Figure 8).

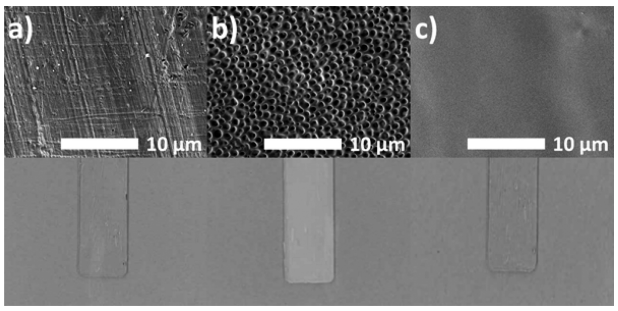

Figure 8. (Top) SEM micrographs and (bottom) optical photographs of (a) an uncoated sample, (b) a sample coated with 0.05 mL (PDIVP)/mL (MeOH)), and (c) a sample coated and post-treated with pentane.

The coating thickness could be altered by performing several coating steps using a 0.1 g/mL solution of PDIVP in MeOH. As shown by Figure 9, the coating thickness per coating step thereby is reproducibly ~6 μm.

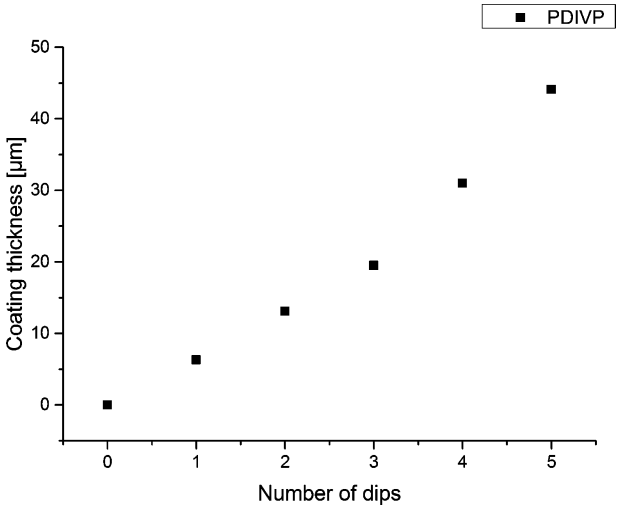

Figure 9. Thickness of the PDIVP coating, depending on the number of dips.

PDIVP coatings were shown to have an outstanding effect on the flammability of PC specimens 0.9 mm in size (see Figure 10). The TFCT of the samples decreased with increasing coating thickness and dripping is effectively suppressed at coating thicknesses of only 13 μm. UL 94 rating V-1 was reached for coating thicknesses of at least 30 μm and V-0 rating was reached for coating thicknesses of at least 60 μm.

Flammability testing of PDIVP-coated PC samples with a thickness of 3 mm gave different results. Although coating thicknesses of up to 50 μm were tested, none of the tested samples could be rated according to UL-94 V because the TFCT exceeded 30 s per specimen. Combustion of the samples

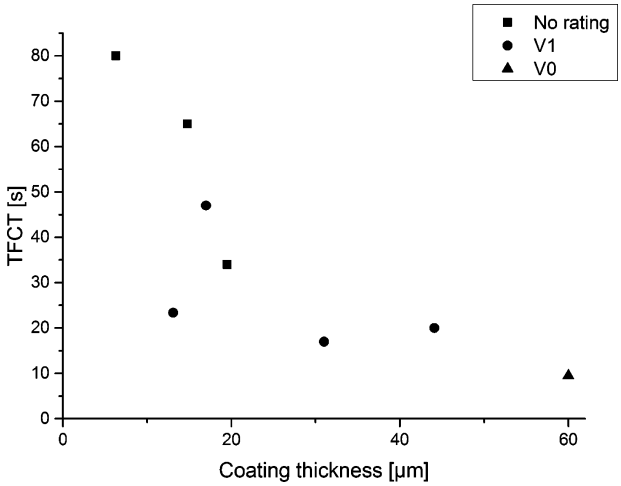

Figure 10. UL 94 V test results (TFCT and rating) of PDIVP-coated PC sample bodies 0.9 mm in size.

is slowed by the coating, but the weight of molten PC leads to failure of the protective layer. Unprotected, viscous PC immediately ignites when getting into contact with the flames. Since most of the surface remains protected by char crust, dripping is delayed drastically but not prevented. PDIVP, in contrast to PDEVP and PDPVP, is not water-soluble and, thus, the PDIVP coating does not age upon contact with moisture and is not rinsed off by extinguishing water.

PDTVP. PDTVP can be coated from diethyl ether solution (0.1 g PDTVP per mL Et_2O) to form transparent, colorless layers. Flammability tests showed that there is no significant effect of the coating, even with coating thicknesses of up to 60 μm.

Different Flame-Retarding Effect of PDEVP and PDIVP, Compared to PDTVP FRCs. In contrast to PDTVP, PDEVP and PDIVP could be shown to be very effective FRCs for PC. In order to elucidate the cause of the flame-retarding effect of PDEVP and PDIVP, UL-94 specimens were examined after testing and the removal of carbon black (see Figure 11).

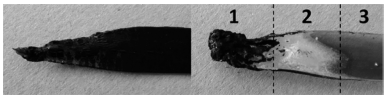

Figure 11. UL-94 V PC specimen coated with PDTVP (23 μm) (left) and PDIVP (31 μm) (right). The ignition sites face toward the left side.

As known from TGA results and flammability tests, PDEVP and PDIVP are intumescent and form stable, blistered crusts of poly(vinylphosphonic acid) (PVPA) at high temperatures. For flame-treated PDEVP- and PDIVP-coated sample bodies, three different zones can be identified. At the site of flame impingement (zone 1), a black crust formed and the sample body is considerably deformed. In zone 2, the coating was converted to a blistered crust. The upper part of the specimens (zone 3) is not affected by the treatment. We assume that, in zone 1, a char crust is formed that mainly consists of PVPA and its decomposition products, as well as carbonized polymer. This char crust acts as a protective barrier, separating the PC from oxygen as well as protecting it from flame impingement. In zone 2, which was exposed to less heat during the flame

DOI: 10.1021/ie504084q
Ind. Eng. Chem. Res. 2015, 54, 1703−1712

treatment, a stable, blistered layer of PVPA (zone 2) is formed, serving as a highly effective protective barrier for the subjacent PC. In zone 3, the coating, as well as the PC, remain unchanged.

For specimens coated with PDTVP, dripping occurred during UL 94 V testing. This dripping explains necking on the bottom side of the sample bodies. Upon flame treatment, the PDTVP-coated sample bodies show deformation due to softening of the PC and, thus, rupture of the protective PDTVP coating. Unprotected PC combusts and, thus, more energy is released, leading to more deformation and, as a result, dripping of PC. No intumescence was observed for PDTVP, which can be rationalized by the fact that decomposition of PDTVP proceeds via backbone fragmentation instead of the formation of low-molecular-weight volatiles and a blistered crust of PVPA. Even high concentrations of PDTVP on the surface of the sample bodies do not lead to sufficient flame retardancy. This indicates that PTDVP is somewhat effective in the gas phase but mainly acts in the condensed phase, as described above.

To summarize, intumescence, in combination with the formation of a stable blistered PVPA crust, which was observed for PDEVP and PDIVP, seems to be the key requirement for effective flame retardancy of PVP coatings.

CONCLUSION

We could show that not only PDAVPs, but also PDArVPs are available by REM-GTP, although the yields are significantly lower for PDArVPs. TGA was performed for PDPVP and PDTVP indicating that PDPVP decomposes in a two-step mechanism similar to PDEVP and PDIVP, while PDTVP decomposes at higher temperature in a one-step mechanism, resulting in backbone fragmentation.

PDEVP, PDIVP, PDPVP, and PDTVP were tested for their suitability as FRAs for PC. Because of their lack of thermal stability, PDIVP and PDPVP decompose during the compounding procedure and therefore form opaque blends of PVPA and PC. Thermally more stable PDEVP does not decompose under the same conditions but PDEVP/PC blends are opaque, indicating that PDEVP is incompatible with PC. Furthermore, because of the hygroscopicity of PDEVP, gas bubbles form during compression molding, leading to inhomogeneous sample bodies. In contrast to these aliphatic PDAVPs, PDTVP, as a representative for an aromatic PDArVPs, forms transparent blends with PC. PDTVP is compatible with PC; it does not decompose during the processing and no phase separation from PC occurs. PDTVP/PC blends were compared to DMPP/PC blends, with DMPP representing a low-molecular-weight reference FRA. In contrast to DMPP, the addition of PDTVP does not cause a strong decrease in the T_g value of PC. DMPP/PC blends show facilitated dripping of burning polymer during UL 94 V testing, which leads to relatively short TFCTs and a V2 rating. For PDTVP/PC blends with high PDTVP contents, no dripping occurred during the UL 94 V test, resulting in a V-1 rating. The fact that PDTVP does not reduce the T_g value dramatically and dripping can be suppressed by addition of sufficient amounts of PDTVP shows its advantage over low-molecular-weight phosphorus-based FRAs such as DMPP. TGA of PC/FRA blends which was carried out under synthetic air showed that PDTVP enhances charring of PC and, thus, in contrast to DMPP, is active in the condensed phase. Mechanical testing revealed that the addition of PDTVP to PC leads to brittleness of the blends, leading to lower yield strengths.

Furthermore, we could demonstrate that PDAVPs can be effective FRCs if they decompose via a two-step mechanism, whereby, in the first decomposition step, the alkyl residues are eliminated as the corresponding alkenes and PVPA is formed. Because of the formation of a continuous, blistered layer of PVPA by exposure to heat, these coatings can be regarded as intumescent. PDTVP, which is an example of a PDArVP, in contrast, decomposes via scission of the polymer main chain and, therefore, does not develop a foamed protective layer.

In the case of PDIVP, we could show that the morphology of the coating is dependent on the solvent and the concentration of the coating solution. Reproducible coating thicknesses could be achieved by dip coating from a 1 g/mL solution in MeOH. The dependency of the TFCT and the UL 94 V rating on the coating thickness was investigated in detail for PC specimens 0.9 mm in size.

For specimens 3 mm in size, PDIVP coatings lead to a slowdown of the combustion, resulting in longer TFCTs, but fail to avoid dripping in UL 94 V tests. The weight of the molten PC in the sample bodies leads to failure of the protective layer.

Dripping of burning polymer is one major issue for monomeric FRAs (such as DMPP), as well as, to a lesser extent, polymeric FRAs (such as PDTVP). Even the highly effective FRCs made from PDIVP suffer from this problem when applied to thicker PC samples. This issue could be addressed by the combined use of antidripping agents, such as polytetrafluoroethylene (PTFE), together with such flame retardants.[45]

EXPERIMENTAL SECTION

General. All reactions were carried out under an argon atmosphere, using standard Schlenk or glovebox techniques. All glassware was heat dried under vacuum prior to use. Unless otherwise stated, all chemicals were purchased from Sigma–Aldrich, Acros Organics, or ABCR and used as received. Toluene and tetrahydrofuran (THF) were dried using an MBraun SPS-800 solvent purification system. The catalysts used—Cp_2YStBu, PDEVP, PDPVP, PDIVP, and β-chloroethylphosphonic acid dichloride—were prepared according to literature procedures.[9,33,46,47] Monomers were dried over calcium hydride and distilled prior to polymerization. A 3-mm-thick Makrolon GP clear 099 sheet and Makrolon 2808 pellets were supplied by Bayer Material Science.

NMR spectra were recorded on a Bruker AVIII-300 or AV-500CRYO spectrometer. ^{1}H NMR and ^{13}C NMR spectroscopic chemical shifts (δ, in ppm) are reported, relative to tetramethylsilane. $\delta(^1H)$ is calibrated to the residual proton signal, while $\delta(^{13}C)$ is calibrated to the carbon signal of the deuterated solvent. ^{31}P NMR spectroscopic chemical shifts are reported (in ppm) relative to and calibrated to 85% H_3PO_4. Deuterated solvents were obtained from Deutero or Eurisotop and were used as received. Elemental analyses were measured at the Laboratory for Microanalytics at the Institute of Inorganic Chemistry at the Technische Universität München. TGA was performed on a TAInstruments Model TGA-Q5000 under a nitrogen atmosphere or under synthetic air with a heating rates of 10 K min^{-1}. GPC was performed on a Varian Model LC-920 system that was equipped with two analytical PL Polargel M columns. As the eluent, a mixture of 50% THF, 50% water, and 9 g L^{-1} tetrabutylammonium bromide (TBAB) was used in the case of PDEVP; for the analysis of PDPVP, PDIVP, and PDTVP, the eluent was THF with 6 g L^{-1} TBAB. Absolute

DOI: 10.1021/ie504084q
Ind. Eng. Chem. Res. 2015, 54, 1703–1712

molecular weights have been determined online, via multiangle light-scattering (MALS) analysis, using a Wyatt Dawn Heleos II system, in combination with a Wyatt Optilab rEX system as a concentration source. High-resolution scanning electron microscopy (HR-SEM) was performed on a JEOL Model JSM-7500F instrument at the Institute of Silicon Chemistry, TU München, using an accelerating voltage of 1 kV for secondary electron observation.

Synthesis of Dimesityl-Phenylphosphonate (DMPP). A quantity of 103.9 g (0.763 mol, 2 equiv) 2,4,6-trimethylphenol and 74.38 g (0.382 mol, 1 equiv) phenylphosphonic dichloride are suspended in 750 mL of pyridine. The reaction mixture is refluxed for 24 h at 140 °C. After cooling, pyridine is removed under reduced pressure to yield a brownish solid. After the addition of 1 L of distilled water, the suspension is stirred for 1 h. Filtration yields a brownish powder. The crude product was washed with MeOH to yield 105.33 g (0.267 mol, 70%) of DMPP as a white powder.

^{1}H NMR Analysis. ^{1}H NMR (CD_2Cl_2, 298 K, 500 MHz): δ = 8.05−7.98 (m, 2H), 7.66−7.60 (m, 1H), 7.56−7.50 (m, 2H), 6.79 (s, 4H), 2.22 (s, 6H), 2.07 (s, 12H).

^{13}C NMR Analysis. ^{13}C NMR (CD_2Cl_2, 298 K, 126 MHz): δ = OAr: 146.03 (ipso, d, $^{2}J_{PC}$ = 9.8 Hz), 134.53 (para, d, $^{5}J_{PC}$ = 2.0 Hz), 130.16 (ortho, d, $^{3}J_{PC}$ = 3.2 Hz), 129.51 (meta, d, $^{4}J_{PC}$ = 1.9 Hz), 20.81 (para-CH_3, s), 17.66 (ortho-CH_3, s), Ar: 132.85 (para, d, $^{4}J_{PC}$ = 3.1 Hz), 132.12 (ortho, d, $^{2}J_{PC}$ = 9.8 Hz), 128.93 (ipso, d, $^{1}J_{PC}$ = 193.8 Hz), 128.50 (meta, d, $^{3}J_{PC}$ = 15.5 Hz).

^{31}P NMR Analysis. ^{31}P NMR (CD_2Cl_2, 298 K, 203 MHz): δ = 10.38 (s).

Analysis of $C_{24}H_{27}O_3P$. Calcd for $C_{24}H_{27}O_3P$: C, 73.08; H, 6.90; P, 7.85. Found: C, 73.06; H, 6.96; P, 7.79.

Synthesis of Di-*p*-tolyl vinylphosphonate (DTVP). A quantity of 288 g (2.66 mol, 2.2 equiv) of 4-methylphenol were slowly added to a mixture of 219 g (1.21 mol, 1 equiv) β-chloroethylphosphonic acid dichloride and 404 g (3.99 mol, 3.3 equiv) triethylamine in 500 mL of toluene at 0 °C. The reaction mixture is warmed to room temperature, stirred overnight, and filtered. The eluate is concentrated *in vacuo*, the residue is dissolved in dichloromethane (DCM), and extracted three times with 5 wt % aqueous NaOH. The combined organic phases are dried over Na_2SO_4, filtered, and concentrated *in vacuo*. The raw product is purified by distillation, yielding 231 g of DTVP (0.84 mol, 69%) as a yellow liquid.

^{1}H NMR Analysis. ^{1}H NMR (CD_2Cl_2, 298 K, 500 MHz): δ = 7.19−7.06 (m, 8H, CH_{Ar}), 6.55−6.17 (m, 3H, CH═CH_2), 2.33 (s, 6H, CH_3).

^{13}C NMR Analysis. ^{13}C NMR (CD_2Cl_2, 298 K, 126 MHz): δ = OAr: 148.5 (ipso, d, $^{2}J_{PC}$ = 7.6 Hz), 135.5 (para, d, $^{5}J_{PC}$ = 1.5 Hz), 130.7 (ortho, s), 120.8 (meta, d, $^{3}J_{PC}$ = 4.3 Hz), 20.98 (CH_3, s), Vinyl: 138.6 (CH_2, d, $^{2}J_{PC}$ = 2.5 Hz), 125.4 (CH, d, $^{1}J_{PC}$ = 185.5 Hz).

^{31}P NMR Analysis. ^{31}P NMR (CD_2Cl_2, 298 K, 203 MHz): δ = 10.4 (s).

Analysis of $C_{16}H_{17}O_3P$. Calcd for $C_{16}H_{17}O_3P$: C, 66.66; H, 5.94; P, 10.74. Found: C, 66.26; H, 5.96; P, 10.64.

Synthesis of Poly(ditolyl vinylphosphonate) (PDTVP). A quantity of 0.5 mmol (1 equiv) of catalyst (Cp_2YStBu or Cp_3Lu) is suspended in 40 mL of toluene. Under vigorous stirring, a solution of 16 g DTVP (50.6 mmol, 100 equiv) in 25 mL of toluene is added at room temperature and the clear solution is stirred overnight. The polymer is purified by precipitation from the reaction solution with excess pentane. The obtained polymer was dissolved in toluene and precipitated with pentane three more times, to remove the remaining monomer and oligomers. Residual solvents were removed under vacuum at 70 °C overnight. The total yield was 6 g (38%).

^{31}P NMR Analysis. ^{31}P NMR (CD_2Cl_2, 298 K, 203 MHz): δ = 25.7 (s).

Analysis of $(C_{16}H_{17}O_3P)_n$. Anal. Calcd for $(C_{16}H_{17}O_3P)_n$: C, 66.66; H, 5.94; P, 10.74. Found: C, 64.95; H, 5.83; P, 10.39.

Other Properties. Molecular weight: 16 kDa, PDI = 1.4.

FRA/PC-Blend Preparation. Makrolon 2808 pellets were milled using a Retsch Model ZM 200 centrifugal mill under liquid nitrogen cooling. The PC powder was dried overnight at 60 °C under vacuum and stored under an argon atmosphere. FRA/PC blends were produced by premixing powders of the corresponding FRA with PC powder and compounding this mixture in a Daca Instruments microcompounder at 240 °C and 60 rpm for 20 min. The obtained polymer strand was cut into pellets ∼1 mm in size.

Raman Spectroscopy of a 20 wt % PDTVP/PC Blend. A Senterra Raman spectrometer (Bruker Optics, Ettlingen, Germany) equipped with a 785-nm laser was used for the analysis of a 20 wt % PDTVP/PC blend. A laser power of 10 mW was chosen. A baseline correction was accomplished with the OPUS 7.2 software for spectra measured by Raman spectroscopy using the concave rubber band method. The spectra were normalized with maximum normalization, for comparison purposes. The spot diameter was ca. 5 μm. Raman spectra were measured at 300 different locations of the sample body (20 × 15 matrix with a distance of 5 μm between the spot centers). Within a range of ±6%, the ratio of the signals of the Raman scattering at 808.5 cm^{-1} (PDTVP) and 889.5 cm^{-1} (PC) was constant over the complete matrix.

UL 94-V Sample Body Preparation. UL 94-V sample bodies with dimensions of 0.9 mm × 13 mm × 125 mm or 3.0 mm × 13 mm × 125 mm were prepared by compression molding, using a self-constructed mold and a Servitec Polystat 200 T table top press. The polymer was filled into the mold and heated to 240 °C for 20 min before the mold is compressed.

Pure PC UL-94-V sample bodies of 3.0 mm × 13 mm × 125 mm were cut from a 3-mm-thick Makrolon GP clear 099 sheet for coating experiments.

Flammability Testing. Flammability was tested using a UL 94-V testing procedure as described in DIN EN 60695-11-10. Sample bodies as described above were exposed to the methane gas flame for 10 s. The flaming combustion time after the ignition period was measured. The flame treatment was repeated for another 10 s and the flaming combustion time was measured again. Since there was no significant glowing after the extinguishing of the samples, the glowing combustion time was not measured. A piece of cotton wool was placed 30 cm below the lower edge of the sample bodies, to determine whether or not dripping polymer ignites this cotton wool.

The original UL 94-V test requires two sets of five sample bodies. In this study, we decided to reduce the number of sample bodies to three in the case of the FRA/PC blends and to one in the case of FRC-coated PC samples. As a result, criteria for the different ratings have been adapted.

For a V-0 rating, the TFCT of each specimen must not exceed 10 s. In addition, neither flaming nor glowing combustion must reach the specimen holding clamp and no burning particles are allowed to drip onto the cotton wool and ignite it.

DOI: 10.1021/ie504084q
Ind. Eng. Chem. Res. 2015, 54, 1703−1712

In order to reach a V-1 rating, the flaming combustion time after each ignition must not exceed 30 s and the average TFCT must not exceed 50 s. Furthermore, neither flaming nor glowing combustion must reach the specimen holding clamp and no burning particles are allowed to drip onto the cotton wool and ignite it. V-2 rating criteria are equal to those of V-1 rating, except that ignition of the cotton wool by dripping burning particles is allowed. In case the FCT after one ignition exceeds 30 s, or the TFCT exceeds 50 s, no rating (according to UL 94 V) is possible.

Tensile Test Sample Body Preparation. Tensile testing sample bodies were prepared in a manner analogous to the UL 94-V sample bodies 0.9 mm in size, by using a mold with dimesnions of 0.9 mm × 30 mm × 52 mm. From the obtained polymer plate, sample bodies (40 mm in length) that had been subjected to ISO 527 tensile testing were stamped using a punching machine.

Measurement of Mechanical Properties. Yield strength and yield strain were determined according to ISO 527 tensile testing, using a Zwick Model BZ1-MM14450.ZW01 material testing machine.

Dip-Coating Procedure. PC sample bodies were dipped into FRC solutions of the given concentration for ∼1 s. Excess solution was removed immediately by shaking.

■ ASSOCIATED CONTENT

Supporting Information

NMR spectra of DMPP, DPVP, PDTVP, and PC/FRA blends. This material is available free of charge via the Internet at http://pubs.acs.org/.

■ AUTHOR INFORMATION

Corresponding Author

*Tel.: +49-89-289-13570. Fax: +49-89-289-13562. E-mail: rieger@tum.de.

Notes

The authors declare no competing financial interest.

■ ACKNOWLEDGMENTS

The authors thank LEDtronics for providing a picture of LED tube light bulbs (T4 Size, E12 Candelabra Base) for use as the TOC graphic.

■ REFERENCES

(1) *IHS Chemical 2012 World Polycarbonate and ABS Analysis*; 2012.
(2) Levchik, S. V.; Weil, E. D. Flame Retardants in Commercial Use or in Advanced Development in Polycarbonates and Polycarbonate Blends. *J. Fire Sci.* **2006**, *24*, 137.
(3) Levchik, S. V.; Weil, E. D. Overview of recent developments in the flame retardancy of polycarbonates. *Polym. Int.* **2005**, *54*, 981.
(4) Alaee, M.; Arias, P.; Sjödin, A.; Bergman, A. An overview of commercially used brominated flame retardants, their applications, their use patterns in different countries/regions and possible modes of release. *Environ. Int.* **2003**, *29*, 683.
(5) de Wit, C. A. An overview of brominated flame retardants in the environment. *Chemosphere* **2002**, *46*, 583.
(6) Wichmann, H.; Dettmer, F. T.; Bahadir, M. Thermal formation of PBDD/F from tetrabromobisphenol A—A comparison of polymer linked TBBP A with its additive incorporation in thermoplastics. *Chemosphere* **2002**, *47*, 349.
(7) Ishikawa, T.; Maki, I.; Koshizuka, T.; Ohkawa, T.; Takeda, K. Effect of Perfluoroalkane Sulfonic Acid on the Flame Retardancy of Polycarbonate. *J. Macromol. Sci., Part A: Pure Appl. Chem.* **2004**, *41*, 523.
(8) Wang, J.; Xin, Z. Flame retardancy, thermal, rheological, and mechanical properties of polycarbonate/polysilsesquioxane system. *J. Appl. Polym. Sci.* **2010**, *115*, 330.
(9) Salzinger, S.; Soller, B. S.; Plikhta, A.; Seemann, U. B.; Herdtweck, E.; Rieger, B. Mechanistic Studies on Initiation and Propagation of Rare Earth Metal-Mediated Group Transfer Polymerization of Vinylphosphonates. *J. Am. Chem. Soc.* **2013**, *135*, 13030.
(10) Schartel, B. Phosphorus-based Flame Retardancy Mechanisms—Old Hat or a Starting Point for Future Development? *Materials* **2010**, *3*, 4710.
(11) Price, D.; Pyrah, K.; Hull, T. R.; Milnes, G. J.; Ebdon, J. R.; Hunt, B. J.; Joseph, P. Flame retardance of poly(methyl methacrylate) modified with phosphorus-containing compounds. *Polym. Degrad. Stab.* **2002**, *77*, 227.
(12) Price, D.; Pyrah, K.; Hull, T. R.; Milnes, G. J.; Ebdon, J. R.; Hunt, B. J.; Joseph, P.; Konkel, C. S. Flame retarding poly(methyl methacrylate) with phosphorus-containing compounds: comparison of an additive with a reactive approach. *Polym. Degrad. Stab.* **2001**, *74*, 441.
(13) Levchik, S. V.; Weil, E. D. A Review of Recent Progress in Phosphorus-based Flame Retardants. *J. Fire Sci.* **2006**, *24*, 345.
(14) Lu, S.-Y.; Hamerton, I. Recent developments in the chemistry of halogen-free flame retardant polymers. *Prog. Polym. Sci.* **2002**, *27*, 1661.
(15) Green, J. A Review of Phosphorus-Containing Flame Retardants. *J. Fire Sci.* **1992**, *10*, 470.
(16) Pawlowski, K. H.; Schartel, B. Flame retardancy mechanisms of triphenyl phosphate, resorcinol bis(diphenyl phosphate) and bisphenol A bis(diphenyl phosphate) in polycarbonate/acrylonitrile−butadiene−styrene blends. *Polym. Int.* **2007**, *56*, 1404.
(17) Perret, B.; Pawlowski, K.; Schartel, B. Fire retardancy mechanisms of arylphosphates in polycarbonate (PC) and PC/acrylonitrile-butadiene-styrene. *J. Therm. Anal. Calorim.* **2009**, *97*, 949.
(18) Joo, B. J.; Lee, M. S.; Lee, B. K. Sterically Hindered Phenolic Phosphonates and Polycarbonate Resin Composition Using the Same U.S. Patent US2009149587 A1, June 11, 2009.
(19) Seemann, U. B.; Dengler, J. E.; Rieger, B. High-Molecular-Weight Poly(vinylphosphonate)s by Single-Component Living Polymerization Initiated by Rare-Earth-Metal Complexes. *Angew. Chem., Int. Ed.* **2010**, *49*, 3489.
(20) Wang, C. S.; Shieh, J. Y. Synthesis and flame retardancy of phosphorus containing polycarbonate. *J. Polym. Res.* **1999**, *6*, 149.
(21) Freitag, D.; Go, P.; Stahl, G. Compositions comprising polyphosphonates and additives that exhibit an advantageous combination of properties, and methods related thereto. U.S. Patent US2007/203269 A1, Aug. 30, 2007.
(22) Chen, L.; Wang, Y.-Z. Aryl Polyphosphonates: Useful Halogen-Free Flame Retardants for Polymers. *Materials* **2010**, *3*, 4746.
(23) Wanzke, W.; Hoerold, S.; Lebel, M.-A.; Freitag, D. Flame retardant combinations for polyesters and flame retarded polyester moulding compositions therefrom. U.S. Patent US 2011/0263745 A1, Oct. 27, 2011.
(24) Freitag, D. Method for the production of block copolycarbonate/phosphonates and composition therefrom. U.S. Patent US 2011/0039987 A1, Feb. 17, 2011.
(25) Stahl, G.; Lebel, M.-A.; Freitag, D. Flame retardant engeneering polymer compositions. U.S. Patent US 2009/0043013 A1, Feb. 12, 2009.
(26) Freitag, D. Poly(block-phosphonato-ester) and poly(block-phosphonato-carbonate) and methods of making same. U.S. Patent US 2007/0129511 A1, June 7, 2007.
(27) Freitag, D.; Go, P. Insoluble and branched polyphosphonates and methods related thereto. U.S. Patent US 2009/0032770 A1, Feb. 5, 2009.
(28) Schmidt, M.; Freitag, D.; Bottenbruch, L.; Reinking, K. Aromatische polyphosphonate: Thermoplastische Polymere von extremer Brandwidrigkeit. *Angew. Makromol. Chem.* **1985**, *132*, 1.

DOI: 10.1021/ie504084q
Ind. Eng. Chem. Res. 2015, 54, 1703−1712

(29) Bingöl, B.; Meyer, W. H.; Wagner, M.; Wegner, G. Synthesis, Microstructure, and Acidity of Poly(vinylphosphonic acid). *Macromol. Rapid Commun.* **2006**, *27*, 1719.
(30) Bingöl, B.; Hart-Smith, G.; Barner-Kowollik, C.; Wegner, G. Characterization of Oligo(vinyl phosphonate)s by High-Resolution Electrospray Ionization Mass Spectrometry: Implications for the Mechanism of Polymerization. *Macromolecules* **2008**, *41*, 1634.
(31) Salzinger, S.; Rieger, B. Rare Earth Metal-Mediated Group Transfer Polymerization of Vinylphosphonates. *Macromol. Rapid Commun.* **2012**, *33*, 1327.
(32) Rabe, G. W.; Komber, H.; Häussler, L.; Kreger, K.; Lattermann, G. Polymerization of Diethyl Vinylphosphonate Mediated by Rare-Earth Tris(amide) Compounds. *Macromolecules* **2010**, *43*, 1178.
(33) Zhang, N.; Salzinger, S.; Rieger, B. Poly(vinylphosphonate)s with Widely Tunable LCST: A Promising Alternative to Conventional Thermoresponsive Polymers. *Macromolecules* **2012**, *45*, 9751.
(34) Zhang, N.; Salzinger, S.; Deubel, F.; Jordan, R.; Rieger, B. Surface-Initiated Group Transfer Polymerization Mediated by Rare Earth Metal Catalysts. *J. Am. Chem. Soc.* **2012**, *134*, 7333.
(35) Soller, B. S.; Zhang, N.; Rieger, B. Catalytic Precision Polymerization: Rare Earth Metal-Mediated Synthesis of Homopolymers, Block Copolymers, and Polymer Brushes. *Macromol. Chem. Phys.* **2014**, *215*, 1946.
(36) Banks, M.; Ebdon, J. R.; Johnson, M. The flame-retardant effect of diethyl vinyl phosphonate in copolymers with styrene, methyl methacrylate, acrylonitrile and acrylamide. *Polymer* **1994**, *35*, 3470.
(37) Bourbigot, S.; Duquesne, S. Fire retardant polymers: Recent developments and opportunities. *J. Mater. Chem.* **2007**, *17*, 2283.
(38) Messori, M.; Toselli, M.; Pilati, F.; Fabbri, E.; Fabbri, P.; Busoli, S.; Pasquali, L.; Nannarone, S. Flame retarding poly(methyl methacrylate) with nanostructured organic−inorganic hybrids coatings. *Polymer* **2003**, *44*, 4463.
(39) Jimenez, M.; Duquesne, S.; Bourbigot, S. Fire protection of polypropylene and polycarbonate by intumescent coatings. *Polym. Adv. Technol.* **2012**, *23*, 130.
(40) Wenz, E.; Eckel, T.; Schartel, B.; Beck, U.; Hertwig, A.; Weise, M.; Strümpfel, J.; Reinhold, E. Flame-resistant coated molded polycabonate articles. Int. Patent WO 2006/131229 A2, Dec. 14, 2006.
(41) Salzinger, S.; Seemann, U. B.; Plikhta, A.; Rieger, B. Poly(vinylphosphonate)s Synthesized by Trivalent Cyclopentadienyl Lanthanide-Induced Group Transfer Polymerization. *Macromolecules* **2011**, *44*, 5920.
(42) Quinn, L. *A Guide to Organophosphorous Chemistry*; John Wiley & Sons: New York, 2000.
(43) Wawrzyn, E. *Novel routes in flame retardancy of bisphenol A polycarbonate/impact modifi er/aryl phosphate blends*. Ph.D. Thesis, Freie Universität Berlin, Berlin, Jan. 2013.
(44) Jang, B. N.; Wilkie, C. A. The thermal degradation of bisphenol A polycarbonate in air. *Thermochim. Acta* **2005**, *426*, 73.
(45) Briers, J.; Dillon, M. P.; Linert, J. G.; Nuyttens, R. R., Polymer melt additive composition and use thereof. U.S. Patent US 2005/0250908 A1, Nov. 10, 2005.
(46) Yang, J.; Liang, Y.; Salzinger, S.; Zhang, N.; Dong, D.; Rieger, B. Poly(vinylphosphonate)s functionalized polymer microspheres via rare earth metal-mediated group transfer polymerization. *J. Polym. Sci., Part A: Polym. Chem.* **2014**, *52*, 2919.
(47) Leute, M. Macromolecules with Phosphorous Functionalities. Ph.D. Thesis, Universität Ulm, Ulm, Germany, Oct. 2007.

DOI: 10.1021/ie504084q
Ind. Eng. Chem. Res. 2015, 54, 1703−1712

Supporting Information for:

Poly(vinylphosphonate)s as Macromolecular Flame Retardants for Polycarbonate

*Dominik Lanzinger, Stephan Salzinger, Benedikt S. Soller, Bernhard Rieger**

WACKER-Lehrstuhl für Makromolekulare Chemie , Technische Universität München, Lichtenbergstraße 4, 85747 Garching
E-mail: rieger@tum.de

Contents **Page**

I. NMR spectra of DTVP

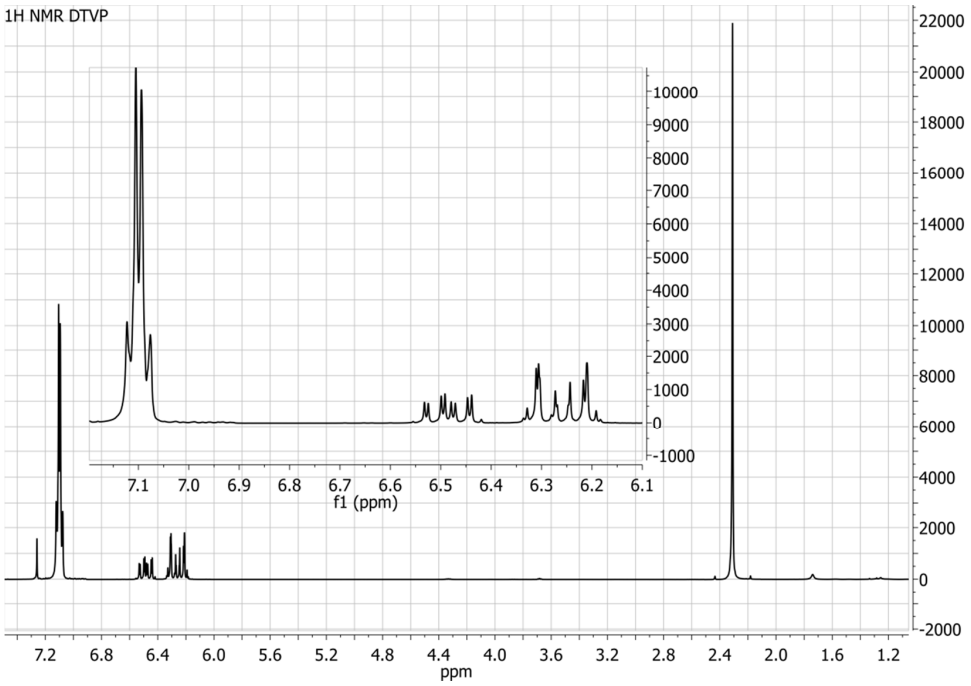

Scheme S 1: ^{1}H NMR spectrum of DTVP ($CDCl_3$, 298 K, 500 MHz)

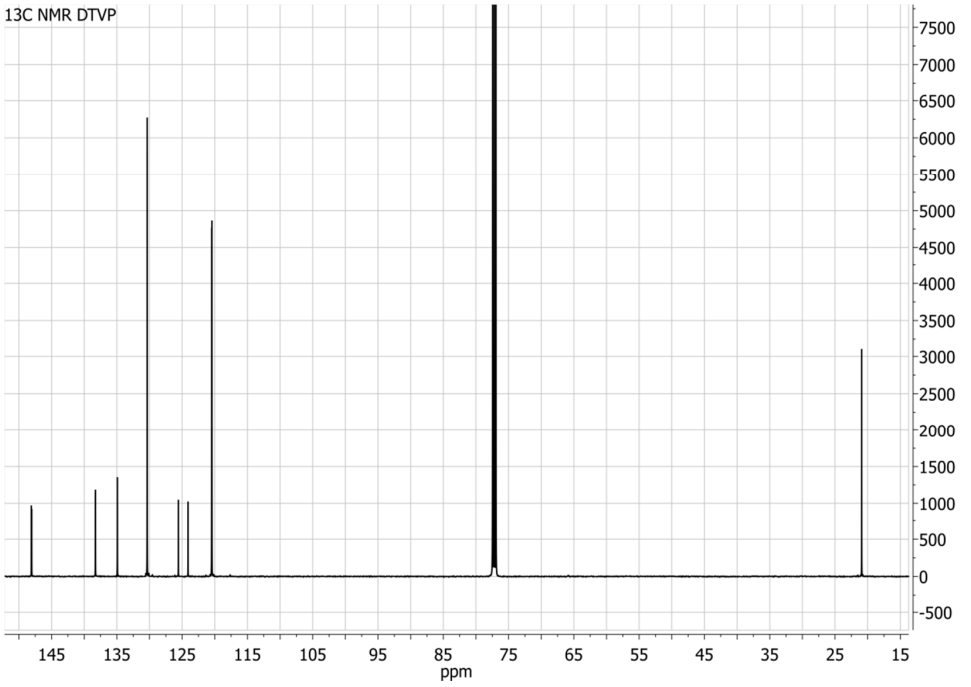

Scheme S 2: ^{13}C NMR spectrum of DTVP ($CDCl_3$, 298 K, 126 MHz)

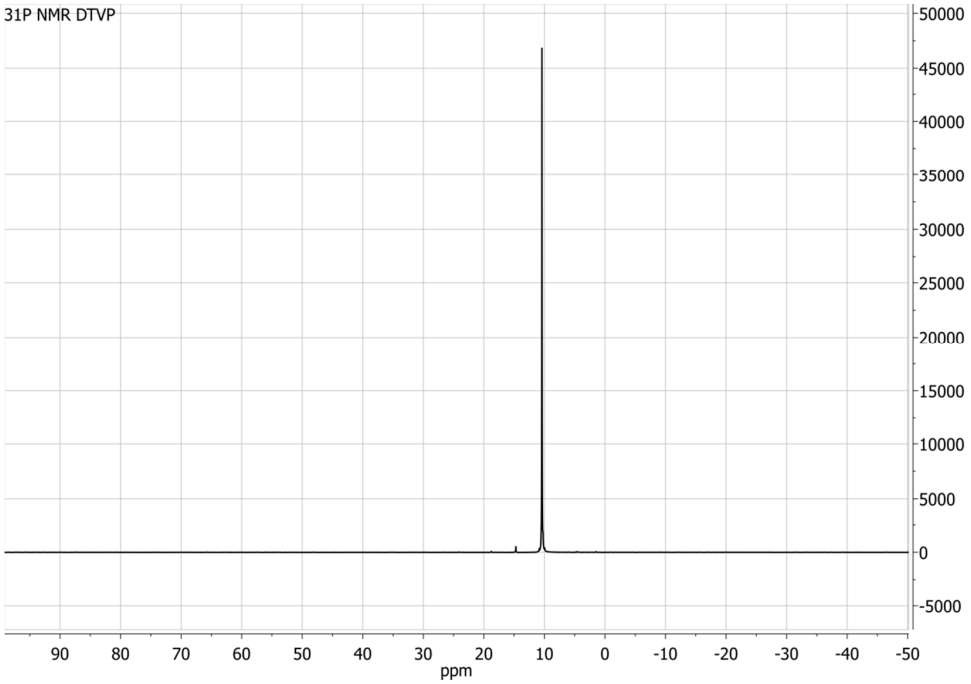

Scheme S 3: ^{31}P NMR spectrum of DTVP ($CDCl_3$, 298 K, 203 MHz)

II. NMR spectra of PDTVP

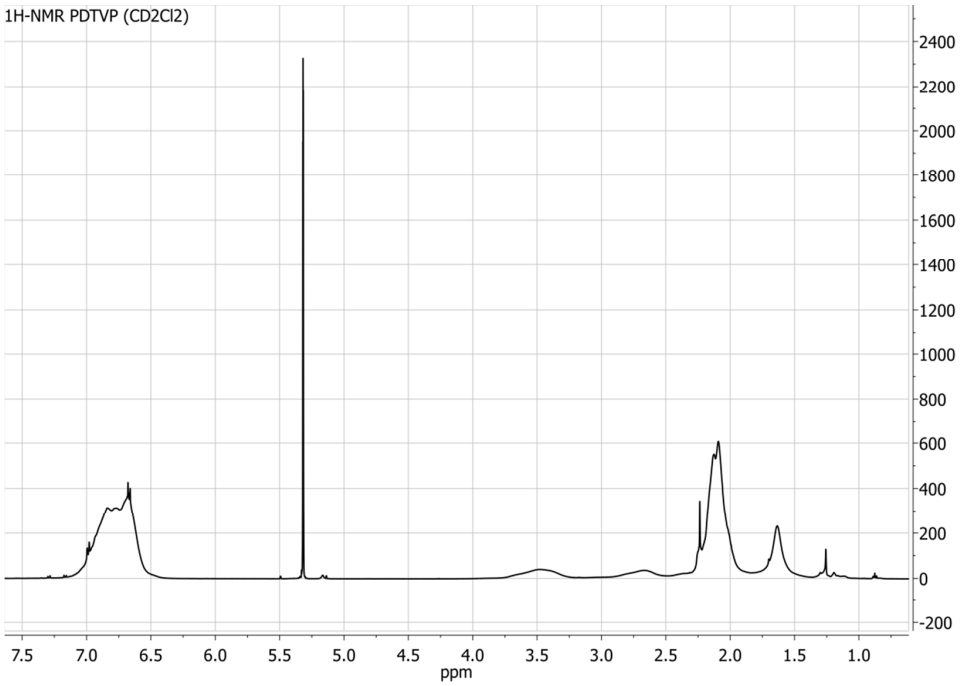

Scheme S 4: ^{1}H NMR spectrum of PDTVP (CD_2Cl_2, 298 K, 500 MHz)

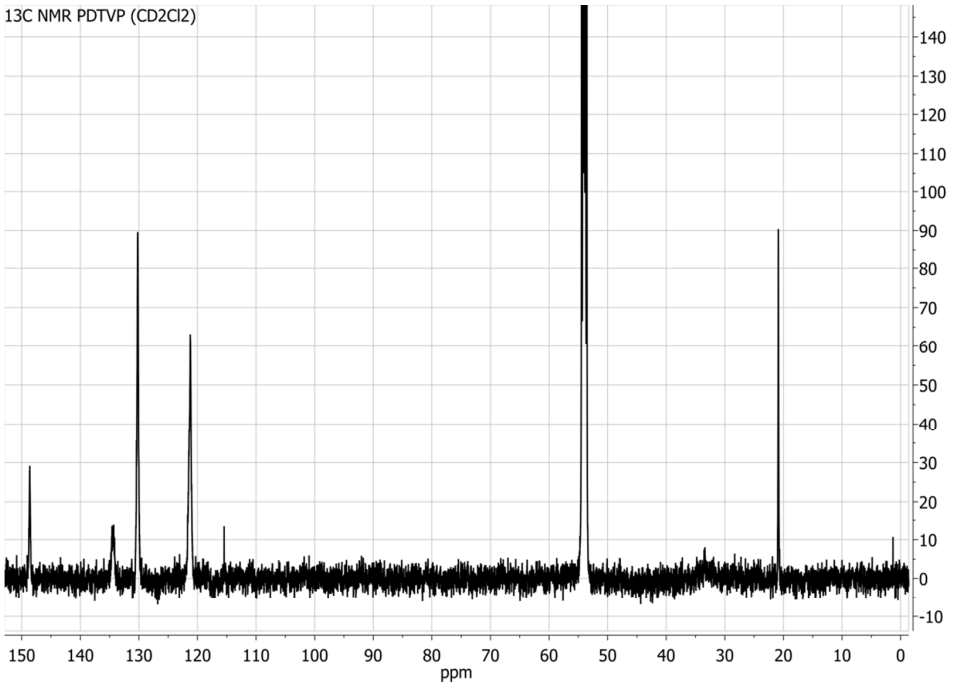

Scheme S 5: ^{13}C NMR spectrum of PDTVP (CD_2Cl_2, 298 K, 126 MHz)

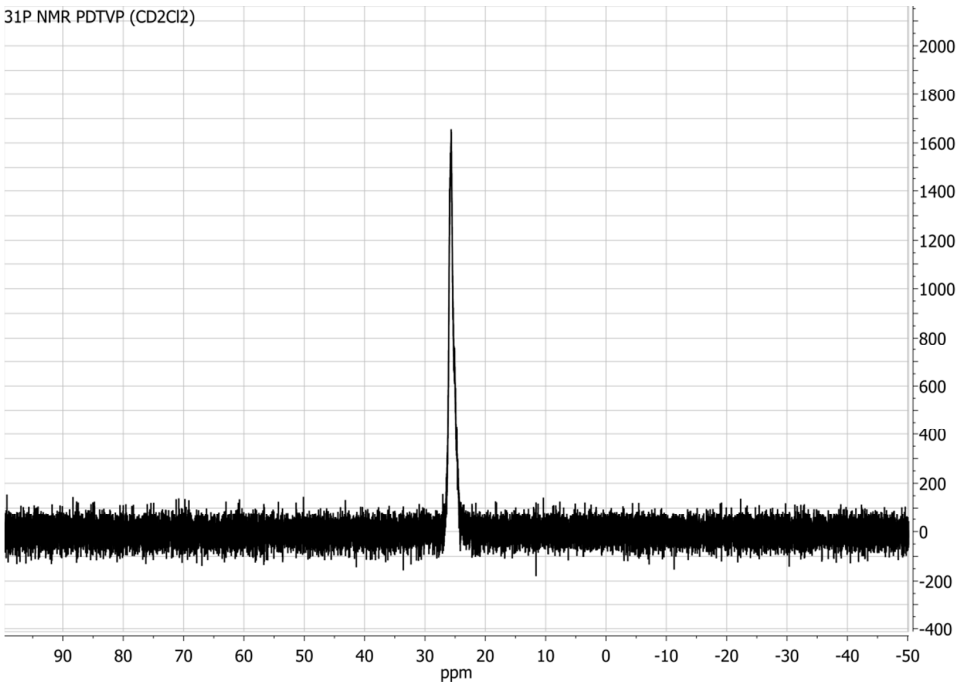

Scheme S 6: ^{31}P NMR spectrum of PDTVP (CD_2Cl_2, 298 K, 203 MHz)

III. NMR spectra of DMPP

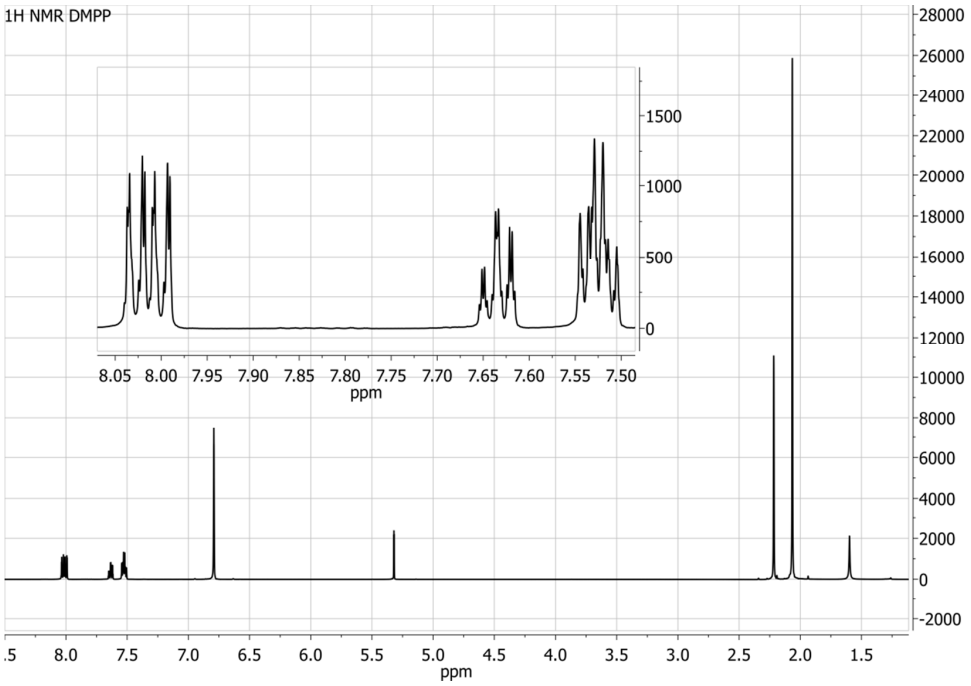

Scheme S 7: ^{1}H NMR spectrum of DMPP (CD_2Cl_2, 298 K, 500 MHz)

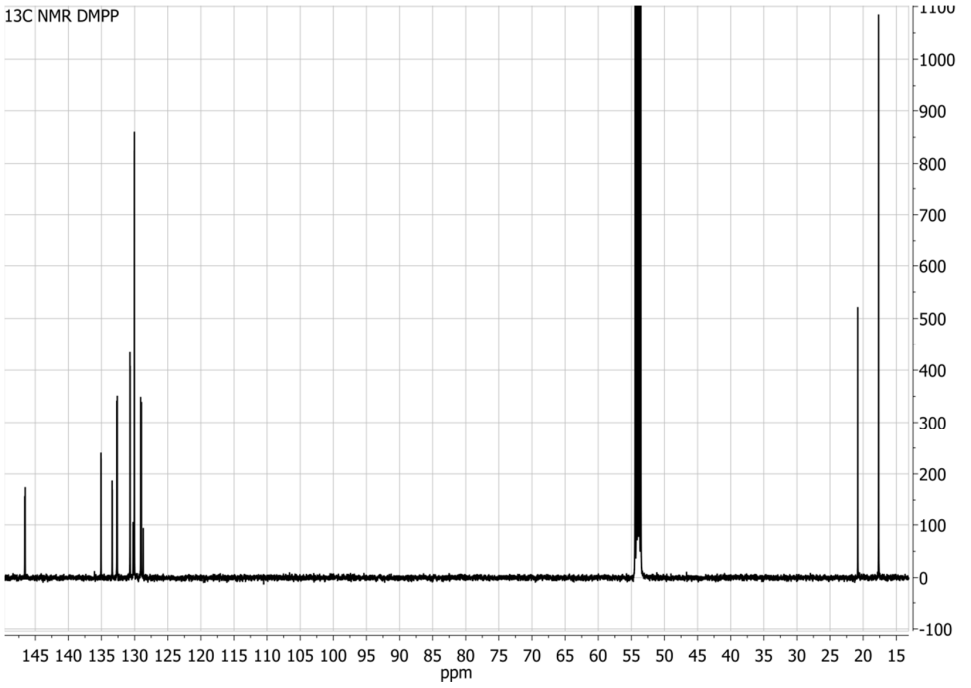

Scheme S 8: ^{13}C NMR spectrum of DMPP (CD_2Cl_2, 298 K, 126 MHz)

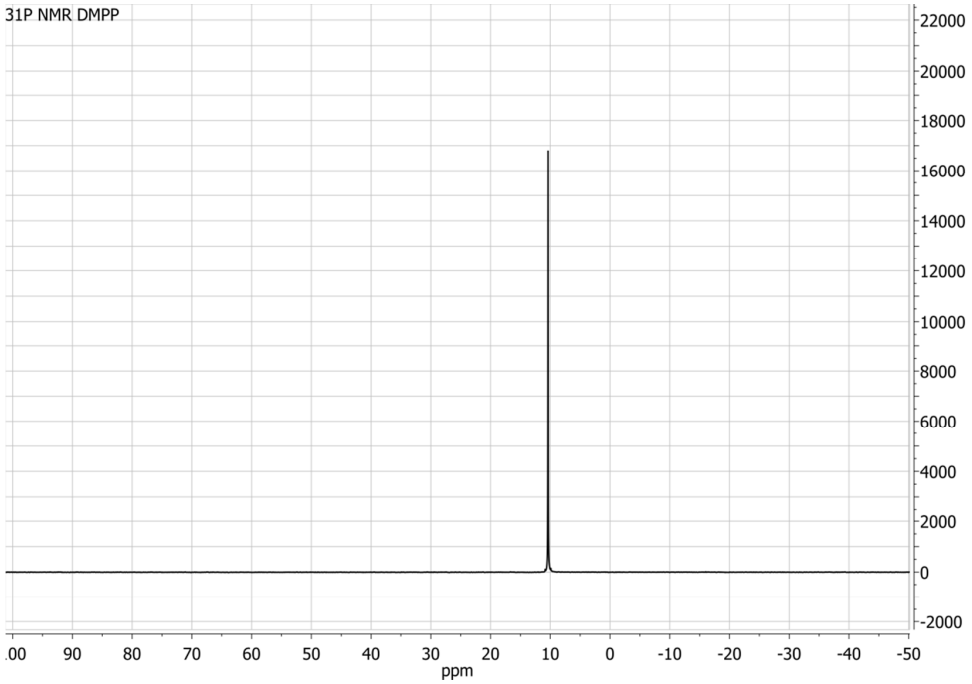

Scheme S 9: ^{31}P NMR spectrum of DMPP (CD_2Cl_2, 298 K, 203 MHz)

IV. NMR Spectra of a PC/PVPA blend

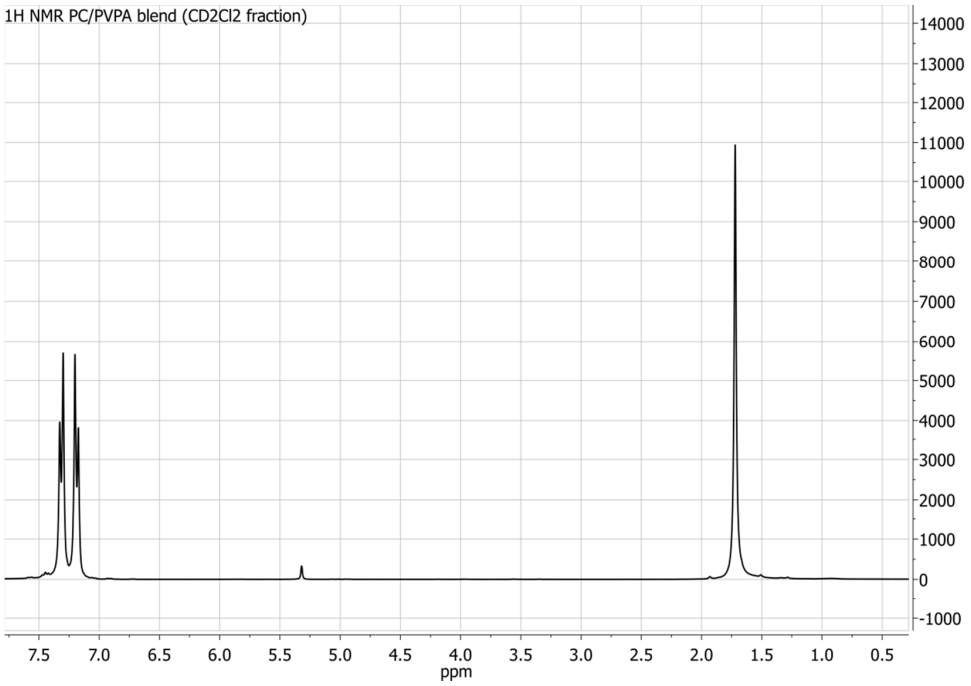

Scheme S 10: ^{1}H NMR spectrum of the CD_2Cl_2 soluble fraction (containing only PC) of a PC/PVPA blend obtained by compounding a PC/PDIVP or PC/PDPVP blend with 20 wt% of the corresponding FRA (CD_2Cl_2, 298 K, 500 MHz)

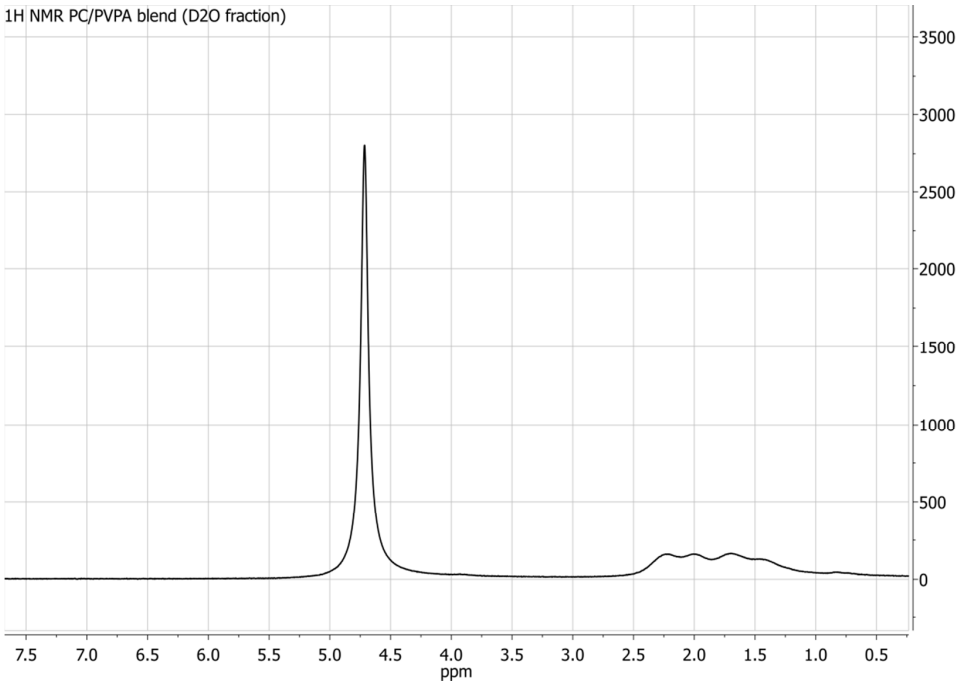

Scheme S 11: ^{1}H NMR spectrum of the D_2O soluble fraction (containing only PVPA) of a PC/PVPA blend obtained by compounding a PC/PDIVP or PC/PDPVP blend with 20 wt% of the corresponding FRA (D_2O, 298 K, 500 MHz)

No remaining PDIVP or PDPVP could be detected in the CD_2Cl_2 soluble fractions indicating complete decomposition by side group cleavage. The ^{1}H NMR spectrum of the D_2O soluble fraction exclusively shows PVPA signals in accordance to literature.[1]

V. NMR spectra of a PC/DMPP blend

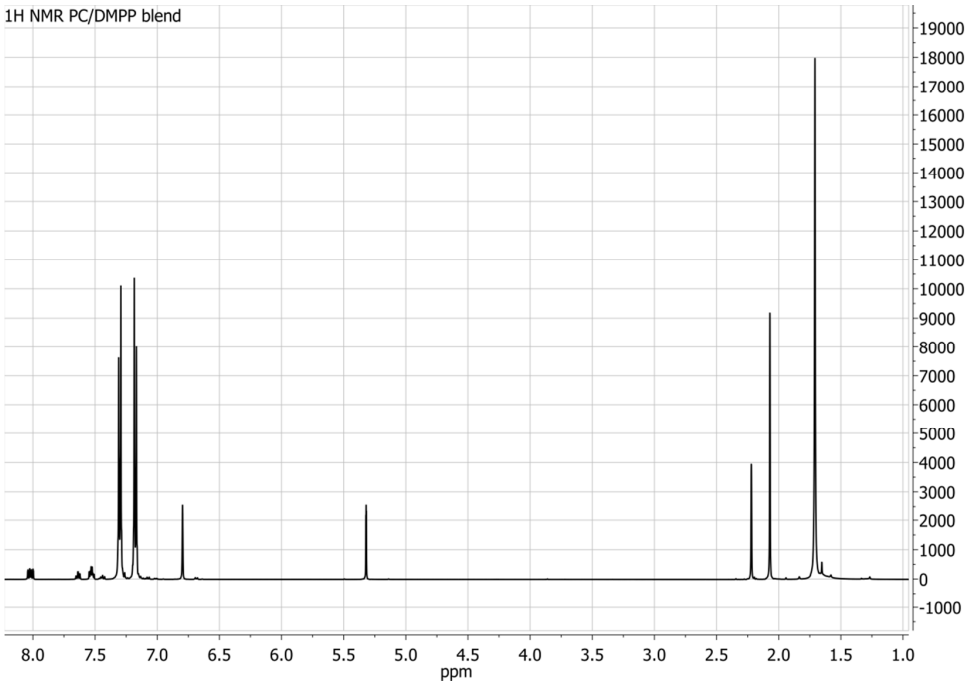

Scheme S 12: ^{1}H NMR spectrum of a PC/DMPP blend with 20 wt% DMPP (CD_2Cl_2, 298 K, 500 MHz)

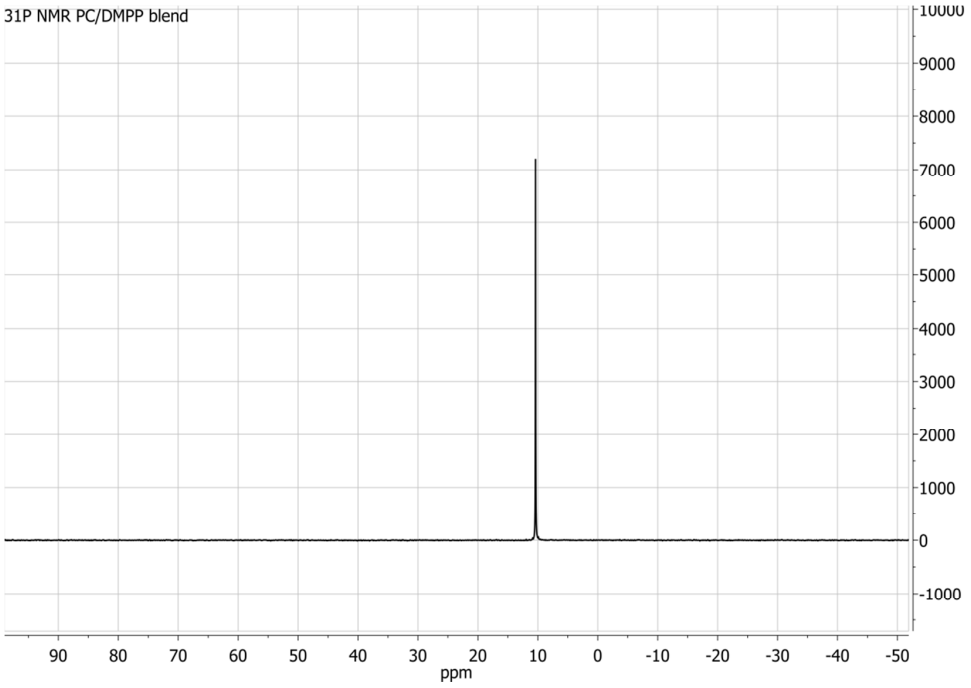

Scheme S 13: ^{31}P NMR spectrum of a PC/DMPP blend with 20 wt% DMPP (CD_2Cl_2, 298 K, 203 MHz)

VI. NMR spectra of a PC/PDEVP blend

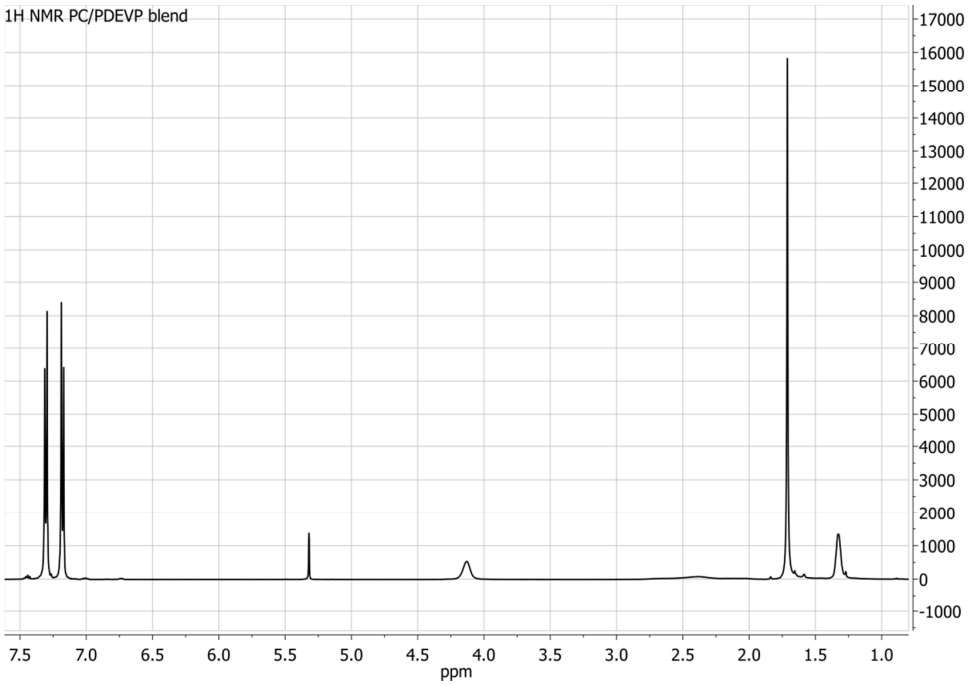

Scheme S 14: ^{1}H NMR spectrum of a PC/PDEVP blend with 20 wt% PDEVP (CD_2Cl_2, 298 K, 500 MHz)

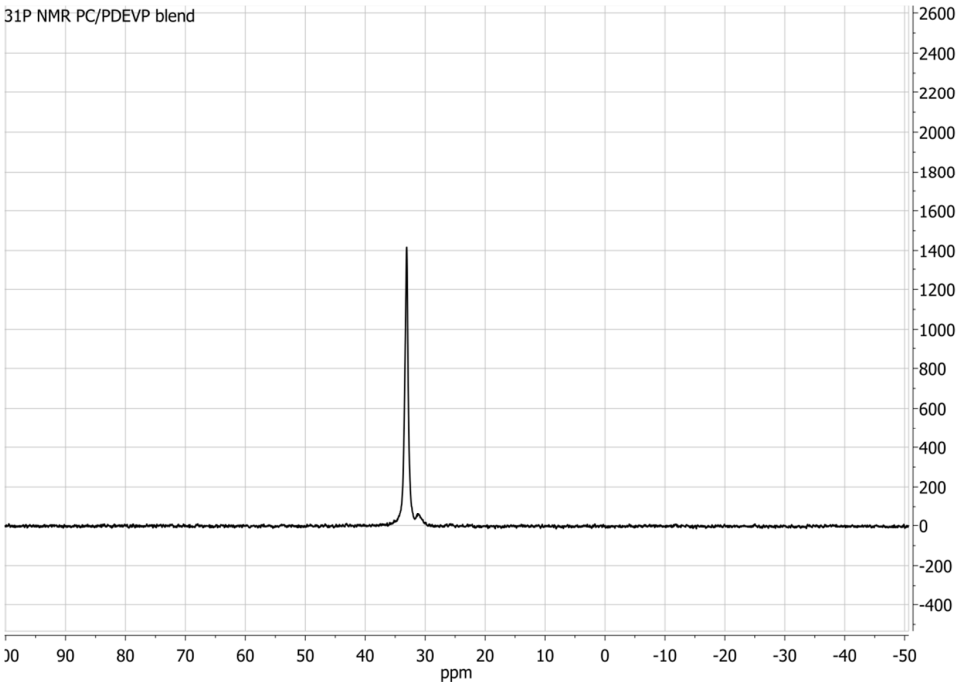

Scheme S 15: ^{31}P NMR spectrum of a PC/PDEVP blend with 20 wt% PDEVP (CD_2Cl_2, 298 K, 203 MHz)

VII. NMR spectra of a PC/PDTVP blend

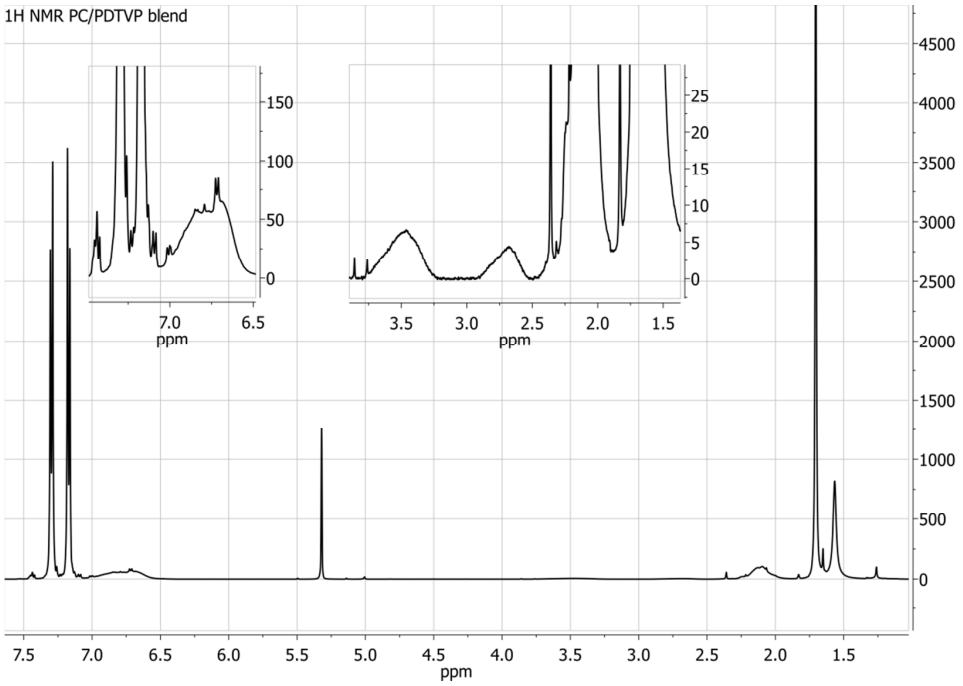

Scheme S 16: ^{1}H NMR spectrum of a PC/PDTVP blend with 20 wt% PDTVP (CD_2Cl_2, 298 K, 500 MHz)

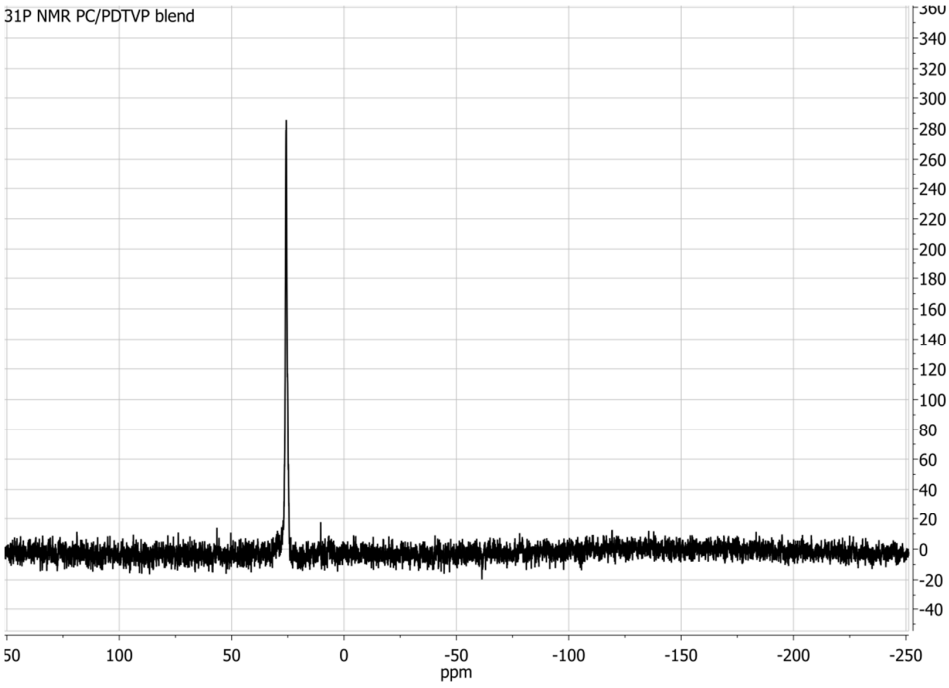

Scheme S 17: ^{31}P NMR spectrum of a PC/PDTVP blend with 20 wt% PDTVP (CD_2Cl_2, 298 K, 203 MHz)

VIII. Raman spectra of PC, PDTVP and a 20 wt% PC-PDTVP blend

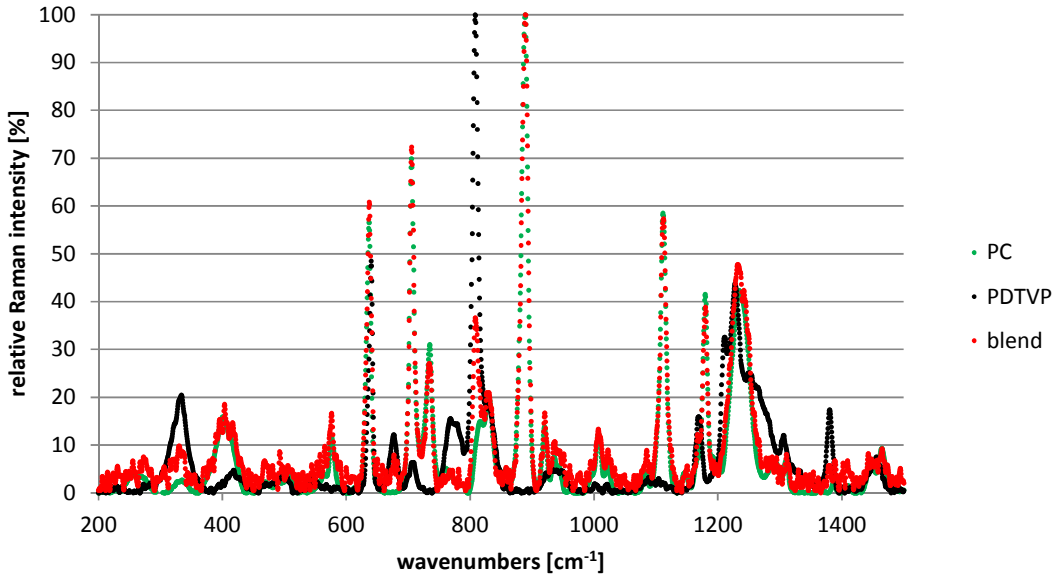

4.7 Rare Earth Metal-Mediated Group-Transfer Polymerization: From Defined Polymer Microstructures to High-Precision Nano-Scaled Objects

Status: Published online: June 4, 2013

Journal: Journal of the American Chemical Society

Volume 135, issue 24, pages 8810–8813

Publisher: American Chemical Society

Article Type: Communication

DOI: 10.1021/ja4036175

Authors: Ning Zhang, Stephan Salzinger, Benedikt S. Soller, and Bernhard Rieger

4.7.1 Abstract

This chapter reports on the first efficient synthesis of poly(2-isopropenyl-2-oxazoline) (PIPOx) and high molecular mass poly(2-vinylpyridine) (P2VP) with narrow polydispersity via RE metal-mediated group transfer polymerization as one of the first examples for REM-GTP to proceed via a nitrogen N–Ln coordination. Previous REM-GTP copolymerization studies have shown that the addition sequence of the comonomers is crucial for monomers with different coordination strengths to the metal center, *i.e.*, monomers can only be polymerized in order of increasing coordination strength and/or sufficient nucleophilicity, *i.e.*, monomers can only be polymerized in order of decreasing pKa values. In order to examine the relative coordination strength of the newly employed *N*-coordinating monomers IPOx and 2VP, statistical copolymerizations were conducted, establishing a monomer reactivity order for REM-GTP as DEVP > MMA > IPOx > 2VP. Consecutive polymerization of different monomers is hereby only possible in order of increasing coordination strength, sufficient nucleophilicity, and restricted to comonomers with similar polarity. In combination with LCROP, PIPOx was converted to molecular brushes and nano-scaled objects with defined backbone and poly(2-oxazoline) side chains using a grafting-from method.

The first author Ning Zhang was supported by second authors Benedikt S. Soller and Stephan Salzinger in synthesizing copolymer structures, establishing a monomer reactivity order, and interpreting the experimental results.

JACS
JOURNAL OF THE AMERICAN CHEMICAL SOCIETY

Communication

pubs.acs.org/JACS

Rare Earth Metal-Mediated Group-Transfer Polymerization: From Defined Polymer Microstructures to High-Precision Nano-Scaled Objects

Ning Zhang,*[,†] Stephan Salzinger,[‡] Benedikt S. Soller,[‡] and Bernhard Rieger*[,‡]

[†]Changchun Institute of Applied Chemistry, Chinese Academy of Sciences, Changchun 130022, China

[‡]WACKER-Lehrstuhl für Makromolekulare Chemie, Technische Universität München, 85747 Garching bei München, Germany

Supporting Information

ABSTRACT: Poly(2-isopropenyl-2-oxazoline) (PIPOx) and poly(2-vinylpyridine) (P2VP) have been efficiently synthesized using bis(cyclopentadienyl)methylytterbium (Cp_2YbMe) as catalyst. The polymerizations of 2-isopropenyl-2-oxazoline (IPOx) and 2-vinylpyridine (2VP) follow a living group-transfer polymerization (GTP) mechanism, allowing a precise molecular-weight control of both polymers with very narrow molecular-weight distribution. The GTP of IPOx and 2VP occurs via N coordination at the rare earth metal center, which has rarely been reported previously. The relative coordination strength of different monomers at the ytterbium center is determined by copolymerization investigations to be in the order of DEVP > MMA > IPOx > 2VP. In combination with living cationic ring-opening polymerization, PIPOx is converted to molecular brushes with defined backbone and poly(2-oxazoline) side chains using the *grafting-from* method.

Since the first report on rare earth metal-mediated group-transfer polymerization (REM-GTP) by Yasuda et al. in 1992,[1] researchers have devoted their efforts to optimizing reaction conditions and initiator efficiency and extending its utilization for various monomers, e.g., (meth)acrylates and (meth)acrylamides.[2−4] In view of the mechanism, this type of polymerization is recognized as coordinative anionic, and due to its similarity to silyl ketene acetal-initiated GTP, it is also referred to as transition metal-mediated GTP.[4−12] Because of its highly living character, REM-GTP leads to strictly linear polymers with very narrow molecular-weight distribution (Đ < 1.1), exhibits a linear increase of the average molar mass upon monomer conversion, and allows the synthesis of block copolymers as well as the introduction of chain end functionalities.[2−4,11] Coordination of the growing chain end at the catalyst suppresses side reactions and allows stereospecific polymerization as well as activity optimization by varying both the metal center and the catalyst ligand sphere.[4,11] Accordingly, REM-GTP combines the advantages of living ionic and coordinative polymerizations and thus allows a precise adjustment of the polymer architecture and microstructure.

Recently, our group and other researchers showed that REM-GTP is not restricted to common (meth)acrylates but is also applicable to several other monomer classes of interest, e.g., vinylphosphonates and vinylpyridines.[6−8,11,13,14] Moreover, we reported on the development of a surface-initiated group-transfer polymerization (SI-GTP) mediated by rare earth metal catalysts, allowing the perfect decoration of substrates with polymer brushes of specific functionality.[15] Inspired by these recent advances and the high precision offered by REM-GTP, we have made it a major focus of our research to extend the applicability of this method to further monomer classes and to evaluate the utilization of REM-GTP for the production of tailor-made functional polymer-based architectures. In this context, this Communication describes the efficient polymerization of 2-isopropenyl-2-oxazoline (IPOx) and 2-vinylpyridine (2VP) through REM-GTP, occurring via N coordination of the monomer at the rare earth metal center. Copolymerization experiments are conducted to compare the coordination strength of the different monomers to the rare earth metal. Moreover, REM-GTP is combined with living cationic ring-opening polymerization (LCROP), giving the first access to poly(2-oxazoline) molecular brushes with narrow side chain and backbone chain length distribution.

IPOx is a versatile dual-functional monomer comprising an oxazoline and a vinyl moiety. On one hand, it can undergo LCROP of the heterocyclic motif, resulting in defined poly(2-oxazoline)s for a variety of applications in biomedicine.[16−24] On the other hand, radical/anionic polymerization of the vinylidene functionality of IPOx leads to poly(2-isopropenyl-2-oxazoline) (PIPOx) with a broad molecular-weight distribution,[16,25] even though anionic and reversible addition−fragmentation polymerization finitely improves the distribution character.[26,27] Living anionic polymerization, owing to the strict operating conditions and solvent effects,[28] is not a preferred method for the polymerization of IPOx. Moreover, due to a strong complexation of pendant 2-oxazoline units by copper, attempts to polymerize IPOx by atom-transfer radical polymerization (ATRP) were not successful.[25] There seems to be no truly successful method by which PIPOx with controlled molecular weight and narrow Đ (Đ < 1.1) is accessible. Also for 2VP, another functional monomer comprising a C═C—C═N functionality, there is a continuing demand to seek superior methods for efficient and convenient polymerization. Inspired by the electronic and structural similarity between IPOx/2VP and (meth)acrylates or vinylphosphonates, as well as initial investigations on rare earth metal-

Received: April 11, 2013
Published: June 4, 2013

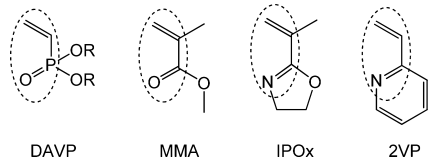

Figure 1. Molecular structures of dialkyl vinylphosphonates (DAVP), methyl methacrylate (MMA), 2-isopropenyl-2-oxazoline (IPOx), and 2-vinylpyridine (2VP).

mediated 2VP polymerization,[13] we examined the polymerizability of IPOx/2VP employing rare earth metal complexes as catalysts (Figure 1).

Initially, the polymerization of IPOx was conducted at room temperature in the presence of Cp_2YbCl and Cp_3Yb. In contrast to using MMA and vinylphosphonates,[4,11,29] no polymerization was observed using Cp_2YbCl as initiator. This was attributed to the rather weak coordination strength (*vide infra*) of IPOx at the metal center, inhibiting cleavage of the dimeric complex $[Cp_2YbCl]_2$. This hypothesis could be confirmed by X-ray structure analysis of single crystals obtained from a mixture of IPOx and Cp_2YbCl in toluene, which were found to be the $[Cp_2YbCl]_2$ starting material. Using Cp_3Yb as catalyst, low yields of polymer could be isolated after several hours of polymerization at room temperature. The poor efficiency of Cp_3Yb for IPOx in contrast to its high reactivity for DEVP polymerization under identical reaction conditions is attributed to the lower steric crowding of the intermediate Cp_3Yb(IPOx) in comparison to Cp_3Yb(DEVP), leading to an inefficient initiation of IPOx REM-GTP by Cp_3Yb.[7]

Using Cp_2YbMe as initiator, polymerization of IPOx proceeded smoothly at room temperature, exhibiting high reaction velocity; i.e., monomer conversion reached 95% within 2 h at room temperature, as monitored by *in situ* ^{1}H NMR (Figure 2). According to MMA, the methyl group was found to be an efficient initiator for IPOx polymerization (Table 1).[4] This

Table 1. Summary of Different Polymerization of IPOx (Monomer:Initiator = 200:1)

initiator	T (°C)	TOF[a,b] (h^{-1})	PDI[c]	M_n[c] (kDa)	I^*[d] (%)	reaction time (h)/ conversion[b] (%)
Cp_3Yb	25	—	—	—	—	10/trace
Cp_2YbMe	25	380	1.04	21	95	1.5/92
BuLi	25	3100	1.5	40	53	0.2/95
BuLi	−78	18	1.2	2.5	—	2/18
AIBN	60	—	2.0	18	—	8/59

[a]The turnover frequency (TOF) was defined as the maximum slope of the conversion vs reaction time plot. [b]Determined by ^{1}H NMR. [c]Determined by GPC-MALS. [d]$I^* = M_{th}/M_n$, $M_{th} = 200M_{Mon} \times$ conversion + $M_{end\ group}$.

is attributed to the absence of an acidic α-CH, as Cp_2YbMe was found to yield a rather inefficient initiation by deprotonation for vinylphosphonate REM-GTP.[29] The obtained PIPOx was characterized by ^{1}H NMR (Figure 2). After REM-GTP, the IPOx vinylene proton signals (5.76 and 5.39 ppm) disappear completely, and new peaks at 1.76−2.13 ppm originating from protons of formed methylene groups arise. The 2-oxazoline ring was well preserved after polymerization, as can be seen from ^{1}H NMR, with chemical shifts of the oxazoline ring protons slightly shifted from 3.92 and 4.26 ppm to 3.76 and 4.16 ppm, respectively. ^{1}H and ^{13}C NMR spectroscopic analysis (Figure

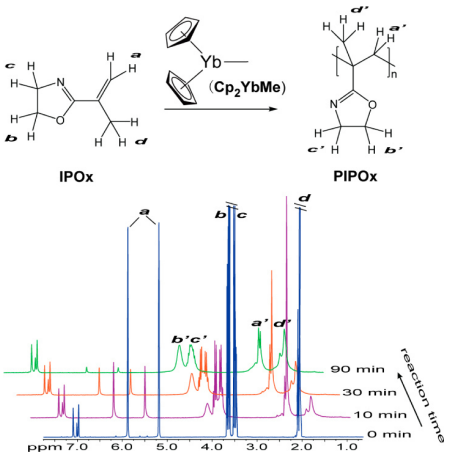

Figure 2. Reaction scheme for GTP of IPOx and polymerization kinetics as detected by *in situ* ^{1}H NMR and assignment of corresponding signals.

S2) indicates the produced PIPOx to be atactic ([mr] = 35%), which can be attributed to the rather small steric demand of the Cp ligands, which is insufficient to induce a stereospecific polymerization.

To elucidate the underlying initiation process, oligomers were produced by using an IPOx:Cp_2YbMe ratio of 5:1 in toluene and subsequently analyzed by electrospray ionization mass spectrometry (ESI-MS). For all peaks, the molar mass of the corresponding oligomers was found to be $n \times M_{IPOx} + 17$ or $n \times M_{IPOx} + 39$ g/mol (see Figure 4b and Table S1). The remaining 17 or 39 g/mol corresponds to a methyl group, which initiated chain growth, a H^+ (or Na^+), and a proton from the termination reaction during methanolic workup. Therefore, transfer of a coordinated ligand (CH_3) to a monomer in the initial step is evident. According to MMA, REM-GTP of IPOx is believed to proceed via an eight-membered ring chelate as shown in Figure 3a, with chain growth occurring by conjugate addition of a coordinated monomer to the covalently bound chain end.[4,11] Attempts to isolate IPOx adducts or the eight-membered intermediate by mixing IPOx and Cp_2YbMe in 1:1 and 2:1

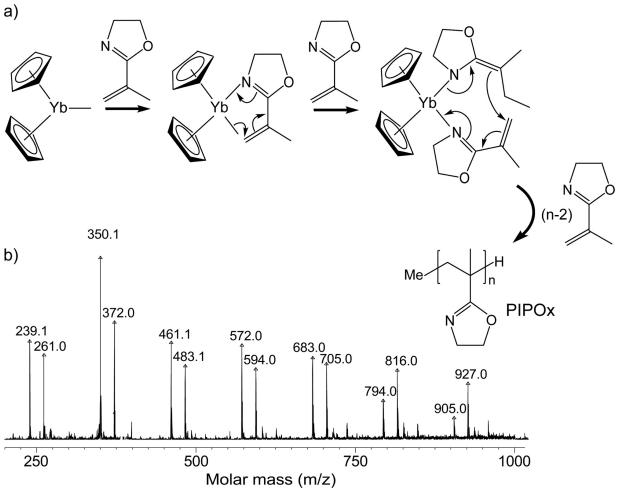

Figure 3. (a) Schematic illustration of REM-GTP of IPOx concerning initiation and propagation. (b) Structure of 2-isopropenyl-2-oxazoline oligomer and its ESI-MS spectrum.

dx.doi.org/10.1021/ja4036175 | *J. Am. Chem. Soc.* 2013, 135, 8810−8813

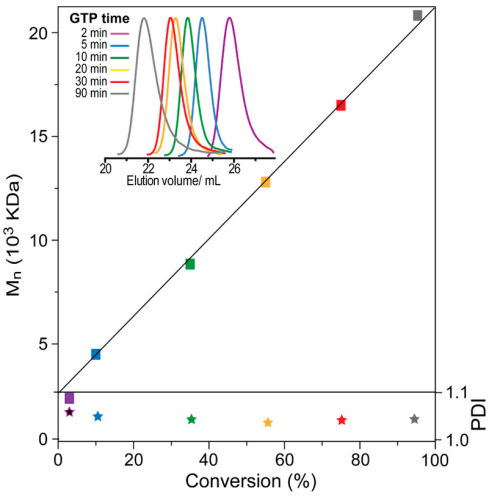

Figure 4. Linear growth of the absolute molecular weight (M_n) determined by multi-angle laser light scattering as a function of IPOx conversion (determined by ^{1}H NMR). Inset: GPC traces as detected by retention volume.

molar ratios at room temperature and −35 °C were unsuccessful, consistently yielding oligomeric PIPOx. However, according to previous literature on rare earth metal oxazoline complexes[30,31] and rare earth metal-mediated 2VP polymerization,[13] we presume the coordination of the eight-membered intermediate as well as the monomer to proceed via the N atom of the oxazoline moiety, thus providing one of the first examples of REM-GTP to proceed via N coordination at the metal center.

To further examine the character of the established REM-GTP of IPOx, aliquots were taken at regular time intervals during the polymerization and analyzed by gel permeation chromatography multi-angle light scattering (GPC-MALS) to estimate the absolute number-averaged molar mass (M_n) and the polydispersity index (PDI) of PIPOx. A plot of the M_n (from 2.05×10^3 to 2.10×10^4 g/mol) vs monomer (IPOx) conversion (from 2.1% to 95%, respectively) reveals a linear relationship between these two parameters (Figure 4), whereas the PDI remains extremely narrow (PDI < 1.07) for polymers obtained at all conversions. The linear growth of molecular weight against monomer conversion is ascribed to the highly living character of REM-GTP and the observed high initiator efficiency (I^* = 95%).

In order to demonstrate the superiority of REM-GTP in comparison to other polymerization techniques, the polymerization of IPOx initiated by azobisisobutyronitrile (AIBN) and *n*-butyllithium (BuLi) at different temperatures was investigated. As expected, free radical polymerization of IPOx performed at 60 °C afforded PIPOx with broad polydispersity (PDI = 2.0, conversion = 59%). Living anionic polymerization of IPOx at −78 °C for 2 h yielded a polymer with improved molar mass distribution (PDI = 1.2) but slow polymer chain growth rate (M_n = 2.5 kDa after 2 h polymerization, conversion = 18%). Anionic polymerization of IPOx at room temperature largely increased the polymerization velocity, however, at the cost of side reactions and loss of control. As a result, the PDI of the obtained polymer increased significantly (PDI = 1.5). The polymerization results for different methods and the used reaction conditions are summarized in Table 1.

In order to verify the versatility of REM-GTP for other monomers, which coordinate to the metal center via an N atom, we subjected another structural similar monomer, i.e. 2VP, to the REM-GTP reaction conditions. To our delight, the GTP of 2VP occurred and afforded poly(2-vinylpyridine) (P2VP, 43 kDa) in 24 h at room temperature. We found the activity and the initiator efficiency of 2VP REM-GTP to be much lower (TOF = 44 h^{-1}, I^* = 45%) (Figure S4) than those for IPOx (TOF = 380 h^{-1}, I^* = 95%) (Figure S1), which may be attributed to the electron delocalization and thus the weak N−Yb coordination. Nevertheless, the PDI of obtained P2VP was narrow (PDI = 1.1) at all monomer conversions (Figure S6). Hence, we attribute the low initiator efficiency to an initial catalyst deactivation by impurities. It was recently shown by Mashima et al. that end-functionalized P2VP could be efficiently obtained by yttrium complex-catalyzed polymerization.[13] Albeit our simple ytterbium complex exhibits relatively lower activity in the polymerization of 2VP, the catalyst led to high molar mass P2VP. Therefore, further investigation on the optimization of the catalyst is necessary. It is worth mentioning that ESI-MS investigation of oligomeric P2VP indicates the initiation to occur via a methyl transfer (Figure S5), even though an α-CH is present in 2VP. According to the small steric demand of the Cp ligands, as expected, produced P2VP is atactic as indicated from ^{1}H and ^{13}C NMR analysis (Figure S3).

In REM-GTP copolymerizations, the addition sequence of the comonomers is critical for monomers with different coordination strength to the metal center; i.e., monomers can only be polymerized in order of increasing coordination strength.[6,11,32] In order to examine the relative coordination strength of the newly employed N-coordinating monomers IPOx and 2VP, statistical copolymerizations using DEVP, MMA, IPOx, and 2VP were conducted. Consistently, only the corresponding homopolymers of the stronger coordinating comonomer were obtained, as observed via NMR spectroscopy, revealing a monomer coordination strength to the ytterbium center in an order of DEVP > MMA > IPOx > 2VP. Accordingly, sequential copolymerization yielded diblock copolymers in sequences of PMMA-*b*-PDEVP, PIPOx-*b*-PMMA, and PIPOx-*b*-PDEVP, as well as P2VP-*b*-PIPOx and P2VP-*b*-PDEVP, while diblock copolymerization in the reverse sequence only afforded homopolymers of PDEVP, PMMA, and PIPOx, respectively (Table S1). However, diblock copolymer synthesis was found to be hindered by a proposed encapsulation of the catalyst during polymerization of the rather hydrophilic IPOx and 2VP. This hypothesis is underlined by precipitation of formed high-molecular-weight PIPOx and P2VP from toluene solution and by ineffective initiation of a second, more hydrophobic comonomer (e.g., MMA) by the PIPOx or P2VP macroinitiator. Moreover, if the degree of polymerization of the first, hydrophilic block is kept low (below 20), an improvement of the PIPOx macroinitiator efficiency could be observed. Chain termination is not a major limitation, as the formation of block copolymers for the more hydrophilic DEVP as second comonomer was feasible (Table S1). Analysis of the molecular weight of the obtained copolymers was complicated due to aggregation, even at the low applied concentration in the GPC-MALS setup (and was verified via analysis of samples with different concentration). A more detailed study on REM-GTP copolymerizations is currently underway.

Some of us have reported previously on the synthesis of molecular brushes with poly(2-oxazoline) side chains and a PIPOx backbone via a *grafting-from* method using LCROP.[25] Since the backbone was prepared by free radical and anionic polymerization, the resulting molecular brushes were of broad molecular mass distribution. Herein, we use REM-GTP-prepared PIPOx as the backbone polymer. After reaction with

dx.doi.org/10.1021/ja4036175 | *J. Am. Chem. Soc.* 2013, 135, 8810−8813

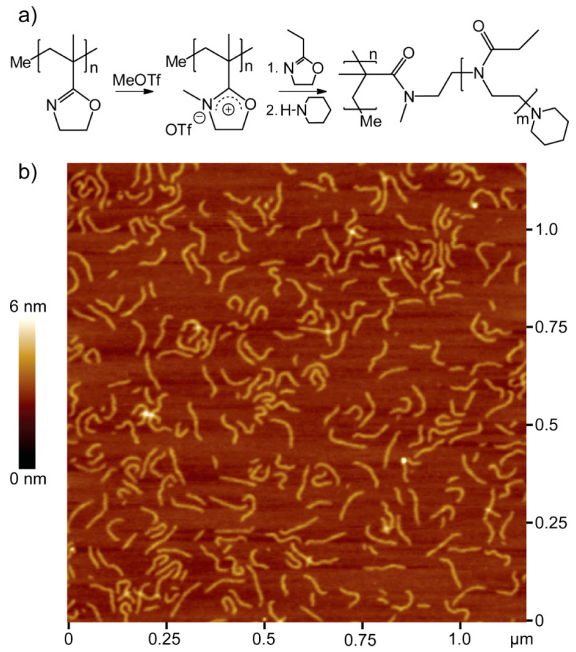

Figure 5. AFM scan of the molecular brush P(IPOx-*g*-EtOx). The polymer was deposited by dip-coating from a dilute chloroform solution onto freshly cleaved mica substrates.

methyl triflate, a polyoxazolinium salt is formed as a macroinitiator. Then, molecular brush side chains are formed by LCROP of 2-ethyl-2-oxazoline (EtOx) (Figure 5a). As verified by AFM measurements, all the molecular brushes adopt a stretched conformation due to the repulsion of poly(2-oxazoline) side chains (Figure 5b). Moreover, the contour length distribution is remarkably narrow, which corroborates the narrow molecular mass distribution of the PIPOx backbone. The combination of REM-GTP and LCROP is to our knowledge the first example for the synthesis of well-defined poly(2-oxazoline) molecular brushes with narrow side and backbone chain length distribution.

In conclusion, we have demonstrated an efficient method to prepare poly(2-isopropenyl-2-oxazoline) and poly(2-vinylpyridine) with high molecular weight and very narrow molecular-weight distribution via rare earth metal-mediated GTP. The present study is one of the first examples for REM-GTP to proceed via N−rare earth metal coordination. According to the highly living character of REM-GTP, the molecular weight of PIPOx and P2VP increased linearly with monomer conversion. We established a monomer reactivity order for REM-GTP as DEVP > MMA > IPOx > 2VP, which can be ascribed to the coordination strength of the respective monomers at the rare earth metal center. Consecutive polymerization of different monomers is hereby only possible in order of increasing coordination strength, and restricted to comonomers with similar polarity. Moreover, well-defined molecular brushes could be synthesized via the first combination of REM-GTP of IPOx and successive *grafting-from* LCROP of 2-oxazolines.

■ ASSOCIATED CONTENT

Supporting Information

Detailed procedures and NMR spectra. This material is available free of charge via the Internet at http://pubs.acs.org.

■ AUTHOR INFORMATION

Corresponding Author

ning.zhang@ciac.jl.cn; rieger@tum.de

Notes

The authors declare no competing financial interest.

■ ACKNOWLEDGMENTS

N.Z. acknowledges start-up funding from Changchun Institute of Applied Chemistry, Chinese Academy of Sciences, and the National Natural Science Foundation of China. S.S. is grateful for a generous scholarship from the Fonds der Chemischen Industrie.

■ REFERENCES

(1) Yasuda, H.; Yamamoto, H.; Yokota, K.; Miyake, S.; Nakamura, A. *J. Am. Chem. Soc.* **1992**, *114*, 4908.
(2) Yasuda, H.; Ihara, E. *Adv. Polym. Sci.* **1997**, *133*, 53.
(3) Yasuda, H. *Prog. Polym. Sci.* **2000**, *25*, 573.
(4) Chen, E. Y. X. *Chem. Rev.* **2009**, *109*, 5157.
(5) Webster, O. W. *Adv. Polym. Sci.* **2004**, *167*, 1.
(6) Seemann, U. B.; Dengler, J. E.; Rieger, B. *Angew. Chem., Int. Ed.* **2010**, *49*, 3489.
(7) Salzinger, S.; Seemann, U. B.; Plikhta, A.; Rieger, B. *Macromolecules* **2011**, *44*, 5920.
(8) Zhang, N.; Salzinger, S.; Rieger, B. *Macromolecules* **2012**, *45*, 9751.
(9) Yasuda, H.; Tamai, H. *Prog. Polym. Sci.* **1993**, *18*, 1097.
(10) Boffa, L. S.; Novak, B. M. *Chem. Rev.* **2000**, *100*, 1479.
(11) Salzinger, S.; Rieger, B. *Macromol. Rapid Commun.* **2012**, *33*, 1327.
(12) Yasuda, H. *J. Polym. Sci., Part A: Polym. Chem.* **2001**, *39*, 1955.
(13) Kaneko, H.; Nagae, H.; Tsurugi, H.; Mashima, K. *J. Am. Chem. Soc.* **2011**, *133*, 19626.
(14) Rabe, G. W.; Komber, H.; Haeussler, L.; Kreger, K.; Lattermann, G. *Macromolecules* **2010**, *43*, 1178.
(15) Zhang, N.; Salzinger, S.; Deubel, F.; Jordan, R.; Rieger, B. *J. Am. Chem. Soc.* **2012**, *134*, 7333.
(16) Tomalia, D. A.; Thill, B. P.; Fazio, M. J. *Polym. J.* **1980**, *12*, 661.
(17) Hoogenboom, R. *Angew. Chem., Int. Ed.* **2009**, *48*, 7978.
(18) Schlaad, H.; Diehl, C.; Gress, A.; Meyer, M.; Demirel, A. L.; Nur, Y.; Bertin, A. *Macromol. Rapid Commun.* **2010**, *31*, 511.
(19) Luxenhofer, R.; Schulz, A.; Roques, C.; Li, S.; Bronich, T. K.; Batrakova, E. V.; Jordan, R.; Kabanov, A. V. *Biomaterials* **2010**, *31*, 4972.
(20) Adams, N.; Schubert, U. S. *Adv. Drug Delivery Rev.* **2007**, *59*, 1504.
(21) Viegas, T. X.; Bentley, M. D.; Harris, J. M.; Fang, Z.; Yoon, K.; Dizman, B.; Weimer, R.; Mero, A.; Pasut, G.; Veronese, F. M. *Bioconjugate Chem.* **2011**, *22*, 976.
(22) Knop, K.; Hoogenboom, R.; Fischer, D.; Schubert, U. S. *Angew. Chem., Int. Ed.* **2010**, *49*, 6288.
(23) Luxenhofer, R.; Sahay, G.; Schulz, A.; Alakhova, D.; Bronich, T. K.; Jordan, R.; Kabanov, A. V. *J. Controlled Release* **2011**, *153*, 73.
(24) Barz, M.; Luxenhofer, R.; Zentel, R.; Vicent, M. J. *Polym. Chem.* **2011**, *2*, 1900.
(25) Zhang, N.; Huber, S.; Schulz, A.; Luxenhofer, R.; Jordan, R. *Macromolecules* **2009**, *42*, 2215.
(26) Kagiya, T.; Matsuda, T.; Zushi, K. *J. Macromol. Sci., Chem.* **1972**, *A6*, 1349.
(27) Weber, C.; Neuwirth, T.; Kempe, K.; Ozkahraman, B.; Tamahkar, E.; Mert, H.; Becer, C. R.; Schubert, U. S. *Macromolecules* **2012**, *45*, 20.
(28) Odian, G. *Principles of Polymerization*, 4th ed.; John Wiley & Sons, Inc.: New York, 2004.
(29) Salzinger, S.; Soller, B. S.; Plikhta, A.; Seemann, U. B.; Herdtweck, E.; Rieger, B. *J. Am. Chem. Soc.*, submitted.
(30) Ward, B. D.; Bellemin-Laponnaz, S.; Gade, L. H. *Angew. Chem., Int. Ed.* **2005**, *44*, 1668.
(31) Lukešová, L.; Ward, B. D.; Bellemin-Laponnaz, S.; Wadepohl, H.; Gade, L. H. *Organometallics* **2007**, *26*, 4652.
(32) Mariott, W. R.; Chen, E. Y. X. *Macromolecules* **2005**, *38*, 6822.

Supporting Information

Rare Earth Metal-Mediated Group Transfer Polymerization: From Defined Polymer Microstructures to High Precision Nano-Scaled Objects

Ning Zhang,* Stephan Salzinger, Benedikt S. Soller, and Bernhard Rieger*

Changchun Institute of Applied Chemistry, Chinese Academy of Sciences, Changchun, 130022, China

WACKER-Lehrstuhl für Makromolekulare Chemie, Technische Universität München, Lichtenbergstrasse 4, 85747 Garching bei München, Germany

Materials and methods

Chemicals were purchased from Sigma-Aldrich or Acros Organics and used without further treatment if not otherwise stated. All reactions were carried out under argon atmosphere using standard Schlenk techniques or an *MBraun* glovebox. All glassware was heat-dried under vacuum prior to use. Toluene was dried applying an *MBraun* SPS-800 and used as received. Tetrahydrofurane (THF) was distilled over potassium prior to use. Cp_2YbMe, diethyl vinylphosphonate were prepared according to literature. [1,2,3,4] Monomers were dried over calcium hydride and distilled prior to polymerization.

NMR spectra were recorded on a *Bruker* ARX-300 spectrometer. ^1H NMR spectroscopic chemical shifts δ are reported in ppm relative to tetramethylsilane and calibrated to the residual proton signal of the deuterated solvent. Deuterated solvents were obtained from Deutero Deutschland GmbH and used as received. ESI MS analytical measurements were performed with methanol solutions on a Varian 500-MS spectrometer, using 70 keV in the positive ionization mode. Atomic force microscopy (AFM) scans were obtained with a Nanoscope IIIa scanning probe microscope from Veeco Instruments (Mannheim, Germany). The microscope was operated in tapping mode using Si cantilevers with a resonance frequency of 270 kHz, a driving amplitude of 1.52 V at a scan rate of 0.6 Hz.

Oligomerization

5 eq of the monomer were added to 1 eq of catalyst in toluene. The resulting mixture was stirred for 2 hours at room temperature and quenched by addition of MeOH or acidified (37w% HCl_{aq}) MeOH. Volatiles were removed under reduced pressure and the residue was extracted with MeOH. For end group analysis, ESI MS measurements of the methanolic extract were performed.

Homo- and statistical copolymerizations

Polymerizations were performed in 30 mL of toluene, using a catalyst concentration of 0.33 mg mL^{-1} (10 mg of catalyst). After dissolving the catalyst in the solvent at room temperature, the calculated amount of the monomer (mixture) was added. The reaction was stirred for the stated reaction time and then quenched with MeOH (0.5

mL). The polymer was precipitated by addition of the reaction mixture to hexane (150 mL) and decanted from solution. Residual solvents were removed by drying the polymer under vacuum at 70 °C overnight.

Sequential copolymerization

After dissolving the calculated amount of catalyst in toluene at room temperature, the first monomer was added (monomer concentration 10vol% in toluene). The reaction mixture was stirred for 2 hours (4 hours in case of 2VP) and divided into aliquots. One aliquot was quenched by addition of 0.5 mL MeOH, to each of the other aliquots, the calculated amount of a second monomer was added, the reaction mixtures stirred for another 2 hours at room temperature and quenched by addition of 0.5 mL MeOH. The polymers were precipitated by addition of the reaction mixtures to hexane (150 mL) and decanted from solution. Residual solvents were removed by drying the polymers under vacuum at 70 °C overnight.

Molecular weight determination

GPC was carried out on a Varian LC-920 equipped with two PL Polargel columns. As eluent a mixture of 50% THF, 50% water, and 9 g L^{-1} tetrabutylammonium bromide (TBAB) was used in the case of PDEVP, PIPOx, P2VP, P(IPOx-b-DEVP) and P(2VP-b-DEVP); for PMMA, P(MMA-b-DEVP) and P(IPOx-b-MMA) analysis, the eluent was THF with 6 g L^{-1} TBAB. Absolute molecular weights have been determined online by multiangle light scattering (MALS) analysis using a Wyatt Dawn Heleos II in combination with a Wyatt Optilab rEX as concentration source.

Kinetics by *in-situ* ^{1}H NMR spectroscopy

In-situ NMR measurements were conducted in a sealable NMR tube in toluene-d8 or C_6D_6. After mixing a solution of 1 mg Cp_2YbMe, 3 mL deuterated solvent and the calculated amount of monomer, 0.6 mL of the reaction solution was immediately transferred to an NMR tube. The NMR spectroscopic measurements were conducted at room temperature.

Kinetics by aliquots method

After dissolving 10 mg of Cp_2YbMe in 30mL toluene or toluene-d8 at room temperature, the calculated amount of monomer was added in one injection. Aliquots were taken from the reaction solution at regular time intervals and quenched by addition to (deuterated) MeOH. For each aliquot, the conversion is determined by gravimetry or ^{1}H NMR spectroscopy, the molecular weight of the formed polymer by GPC-MALS analysis.

Reactivity, ^{1}H NMR, ^{13}C NMR, ESI MS and GPC spectra

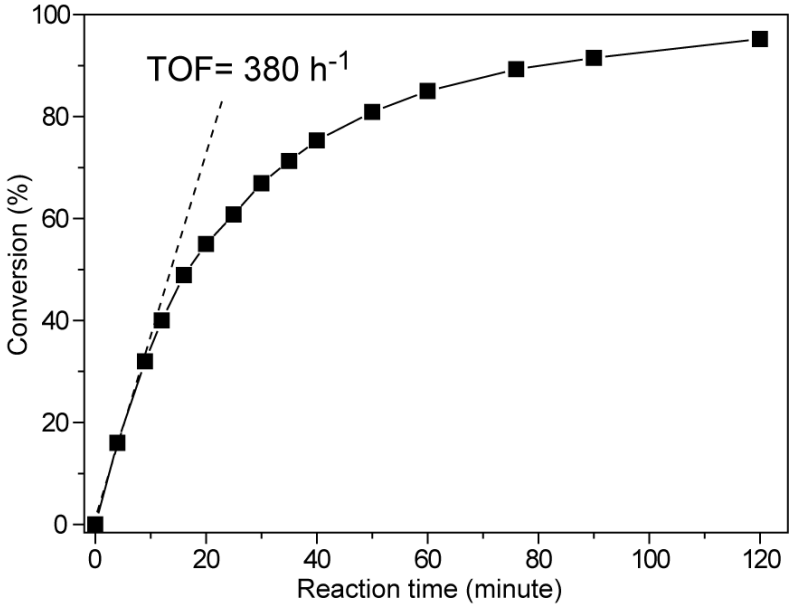

Figure S1. Determination of the catalytic activity of Cp_2YbMe for the polymerization of IPOx (TOF = 380 h^{-1}) by *in situ* ^{1}H NMR spectroscopy (initial [IPOx]:[catalyst] = 200:1; [catalyst] = 0.33mg mL^{-1}).

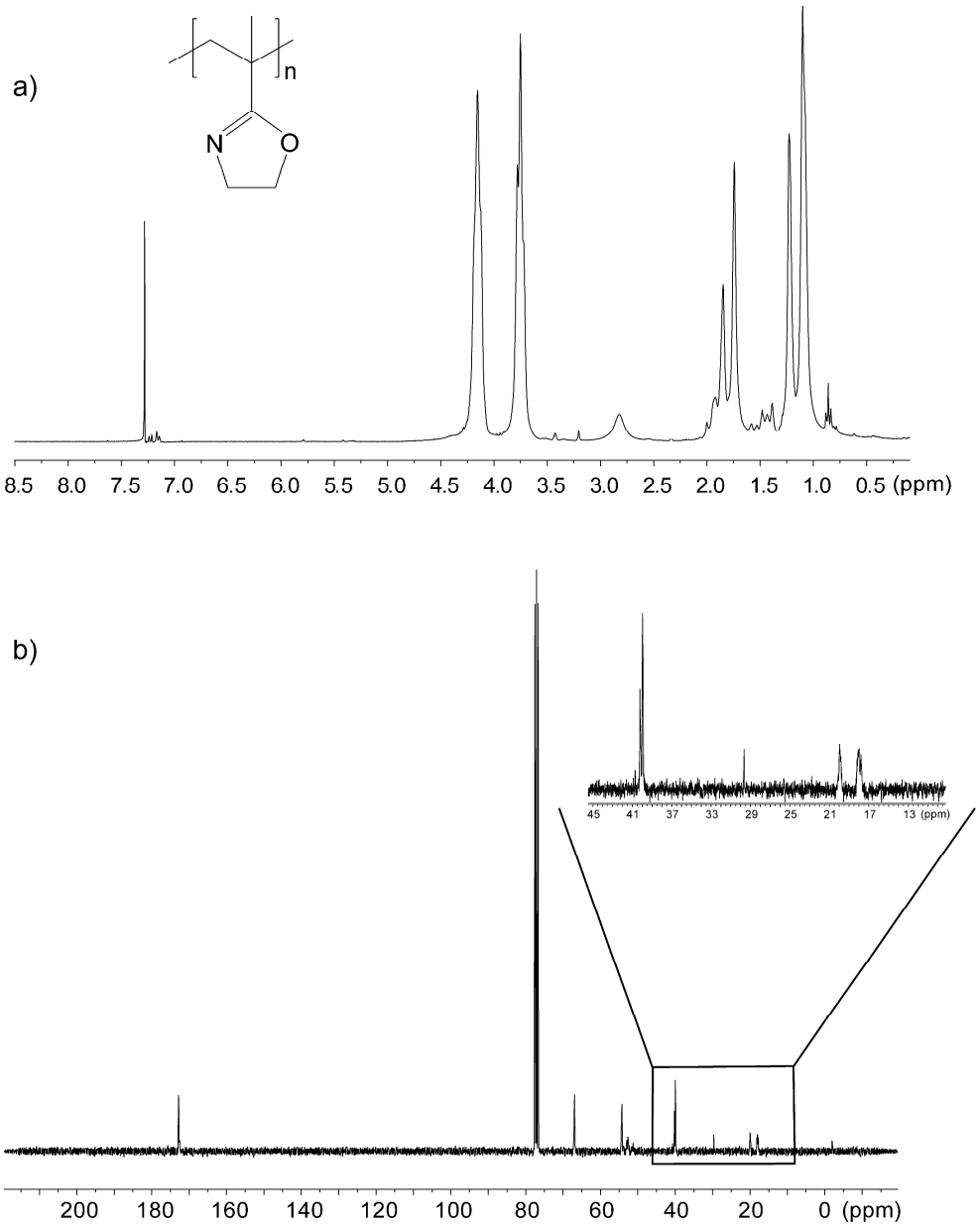

Figure S2. ^{1}H a) and ^{13}C b) NMR spectra of PIPOx.

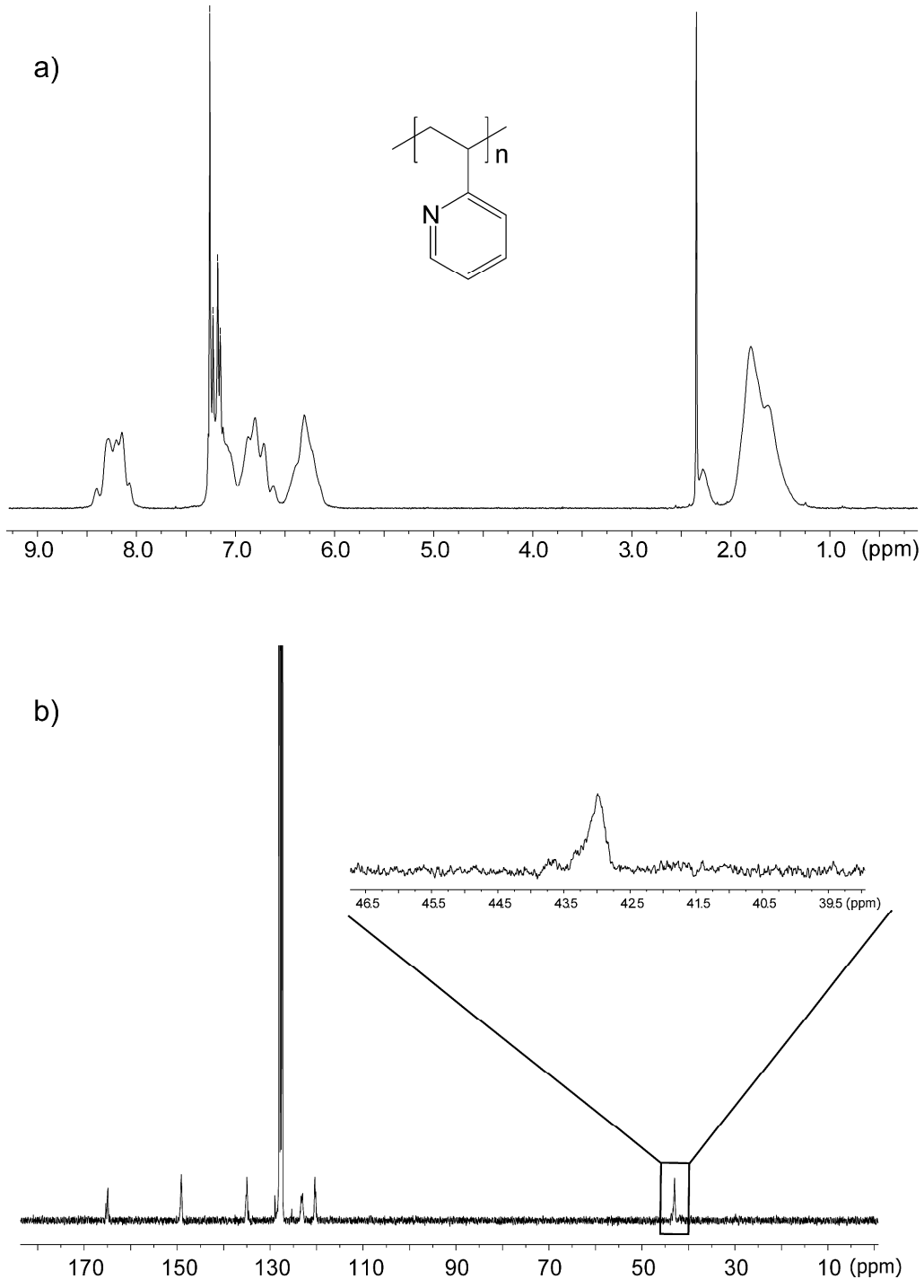

Figure S3. ^{1}H a) and ^{13}C b) NMR spectra of P2VP.

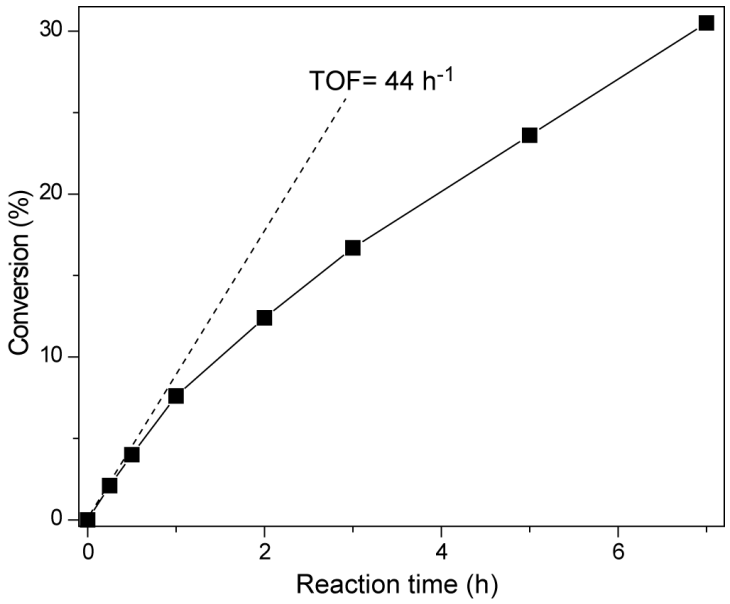

Figure S4. Determination of the catalytic activity of Cp_2YbMe for the polymerization of 2VP (TOF = 44 h^{-1}) by *in situ* ^1H NMR spectroscopy (initial [2VP]:[catalyst] = 500:1; [catalyst] = 0.33mg mL^{-1}).

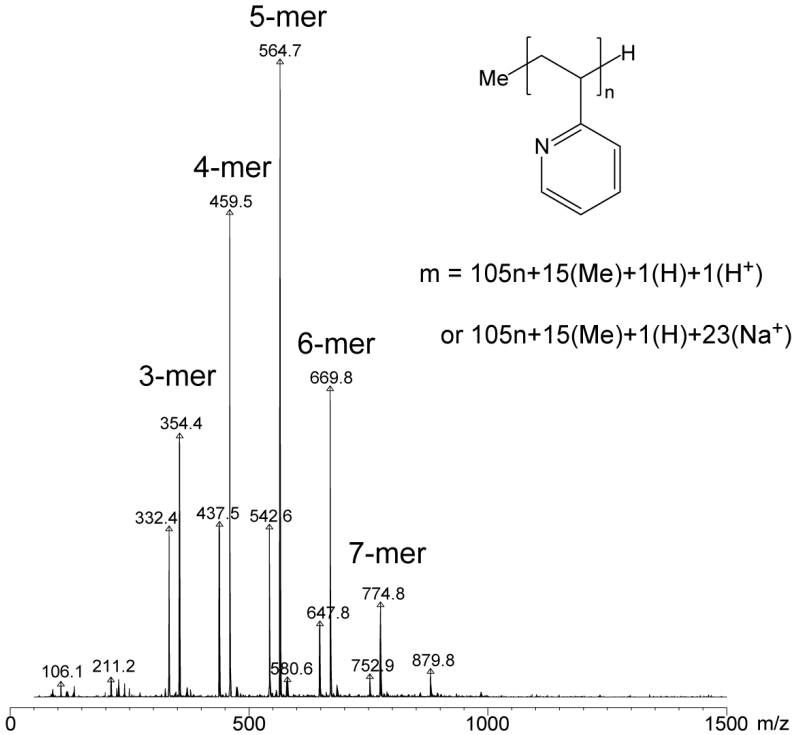

Figure S5. Structure of poly(2-vinylpyridine) (P2VP) oligomer and its ESI MS spectrum.

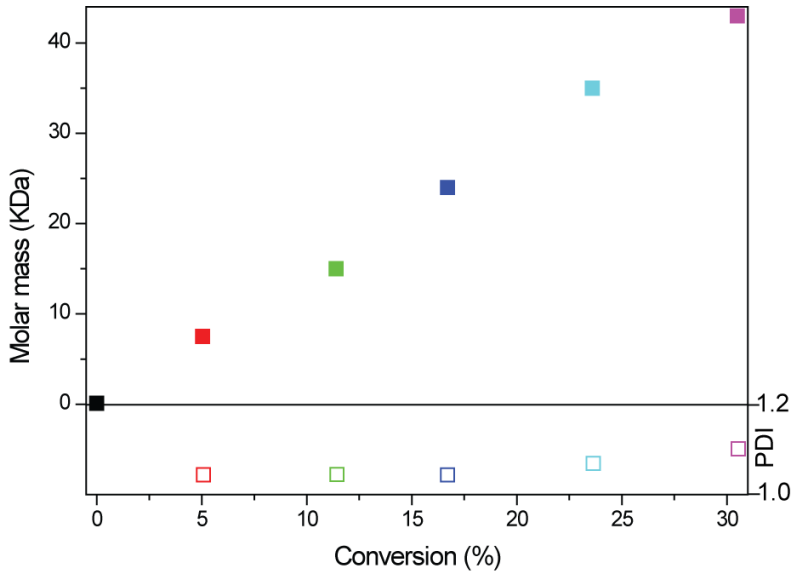

Figure S6. Linear growth of the absolute molecular weight (M_n) and polydispersity of P2VP determined by multi-angle laser light scattering as a function of 2VP conversion.

Table S1. Homo- and block copolymers of 2VP, IPOx, MMA and DEVP synthesized by Cp_2YbMe-initiated REM-GTP.

	M_n[a](kDa)	PDI[a]	I^*[b](%)	Comonomer ratio A/B[c]	Yield[d] (%)
$P2VP_{100}$	14	1.01	75	—	96
$P(2VP_{100}$-b-$IPOx_{100})$	29 (14)	1.01 (1.01)	74 (82)	1:1.18	98
$P(2VP_{100}$-b-$MMA_{100})$	14	1.01	—	1:0	46
$P(2VP_{100}$-b-$DEVP_{100})$	31	1.04	87	1:1.07	96
$P(2VP_{20}$-b-$MMA_{80})$	—	—	—	1:0	—
$PIPOx_{100}$	9.1	1.03	120	—	89
$P(IPOx_{100}$-b-$MMA_{100})$	9.2	1.02	—	1:0	44
$P(IPOx_{100}$-b-$DEVP_{100})$	1100 (10)	1.40 (1.03)	3 (~1)	1:0.69	62
$P(IPOx_{20}$-b-$MMA_{80})$	aggregation		—	1:1.69	50
$P(IPOx_{20}$-b-$DEVP_{50})$	390 (2.6)	1.70 (1.12)	3 (2)	1:2.71	62
$PMMA_{100}$	12	1.10	83	—	98
$P(MMA_{100}$-b-$DEVP_{100})$	22	1.20	120	1.15:1	94

[a]Determined by GPC-MALS, [b]$I^* = M_{th}/M_n$, number in brackets give the I^* of the macroinitator for polymerization of block B (in case of bimodal distributions), [c]determined by ^1H NMR, [d]determined by weighing of the components.

References

(1) Seemann, U. B.; Dengler, J. E.; Rieger, B. *Angew. Chem. Int. Ed.* **2010**, *49*, 3489-3491.
(2) Evans, W. J.; Dominguez, R.; Hanusa, T. P. *Organometallics* **1986**, *5*, 263-270.
(3) Ely, N. M.; Tsutsui, M. *Inorg. Chem.* **1975**, *14*, 2680-2687.
(4) Leute, M. PhD Thesis, Universitity of Ulm, **2007**.

4.8 Versatile 2-Methoxyethylaminobis(phenolate)yttrium Catalysts: Catalytic Precision Polymerization of Polar Monomers via Rare Earth Metal-Mediated Group Transfer Polymerization

Status: Published online: November 10, 2014

Journal: Macromolecules

Volume 47, issue 22, pages 7742–7749

Publisher: American Chemical Society

Article Type: Article

DOI: 10.1021/ma501754u

Authors: Peter T. Altenbuchner, Benedikt S. Soller, Stefan Kissling, Thomas Bachmann, Alexander Kronast, Sergei I. Vagin, and Bernhard Rieger

4.8.1 Abstract

The REM-GTP with nonmetallocene catalyst systems is evaluated for various Michael-type monomers and conducted together with the ring-opening polymerization of β-butyrolactone. 2-Methoxyethylamino-bis(phenolate)-yttrium trimethylsilylmethyl complexes with varying steric demand in the ortho-positions of the aromatic system were synthesized and showed moderate to high activities in the REM-GTP of 2-vinylpyridine, 2-isopropenyl-2-oxazoline, diethyl vinylphosphonate, diisopropyl vinylphosphonate and *N,N*-dimethylacrylamide as well as in the ring-opening polymerization of β-butyrolactone. Mechanistic studies found the reaction order in catalyst and monomer to be one for the REM-GTP of 2-vinylpyridine. Hence, the catalyst systems follow a living monometallic group-transfer polymerization mechanism. Temperature dependent reaction kinetics were conducted and allowed thermodynamic conclusions about the influence of the bulky substituents around the metal center for the polymerization of 2-vinylpyridine. The controlled polymerization of *N,N*-dimethylacrylamide can be increased by using active 2-vinylpyridine RE macroinitiators and block copolymerizations with precise molecular-weight control and very narrow molecular weight distributions were found to be possible.

The first author Peter T. Altenbuchner was supported by second author Benedikt S. Soller in GPC-MALS measurements, activity measurements, copolymer synthesis, and interpreting the experimental results.

Macromolecules

Article

pubs.acs.org/Macromolecules

Versatile 2-Methoxyethylaminobis(phenolate)yttrium Catalysts: Catalytic Precision Polymerization of Polar Monomers via Rare Earth Metal-Mediated Group Transfer Polymerization

Peter T. Altenbuchner, Benedikt S. Soller, Stefan Kissling, Thomas Bachmann, Alexander Kronast, Sergei I. Vagin, and Bernhard Rieger*

WACKER-Lehrstuhl für Makromolekulare Chemie, Technische Universität München, Lichtenbergstraße 4, 85748 Garching bei München, Germany

Supporting Information

ABSTRACT: The present study is one of the first examples for rare earth metal-mediated group transfer polymerization (REM-GTP) with non-metallocene catalyst systems. 2-Methoxyethylaminobis(phenolate)yttrium trimethylsilylmethyl complexes were synthesized and showed moderate to high activities in the rare earth metal-mediated group transfer polymerizations of 2-vinylpyridine, 2-isopropenyl-2-oxazoline, diethyl vinylphosphonate, diisopropyl vinylphosphonate, and *N,N*-dimethylacrylamide as well as in the ring-opening polymerization of β-butyrolactone. Reaction orders in catalyst and monomer were determined for the REM-GTP of 2-vinylpyridine. The mechanistic studies revealed that the catalyst systems follow a living monometallic group transfer polymerization mechanism allowing a precise molecular-weight control of the homopolymers and the block copolymers with very narrow molecular weight distributions. Temperature-dependent reaction kinetics were conducted and allowed conclusions about the influence of the bulky substituents around the metal center on the polymerization activity. Additional polymerization experiments concerning the combination of REM-GTP and ROP to obtain block copolymers were performed.

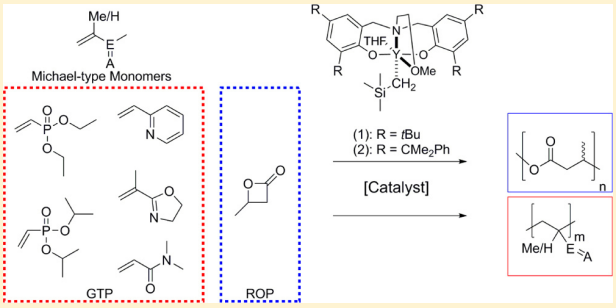

INTRODUCTION

The metal-mediated group transfer polymerization (GTP) was first employed in 1992 by two independent groups. Yasuda et al. used samarocene $[Cp^*_2SmH]_2$ catalysts for the polymerization of methyl methacrylate (MMA) whereas Collins and Ward employed a two-component group 4 metallocene system.[1] Since then, great effort has been put into the development of new and more efficient catalysts as well as into the expansion of the accessible monomers through GTP. Apart from MMA, dialkyl vinyl phosphonates (DAVP), 2-isopropenyl-2-oxazoline (IPOx), *N,N*-dimethylacrylamide (DMAA), and 2-vinylpyridine (2VP) were successfully homo- and copolymerized.[2] So far, only a few examples for non-metallocene rare earth metal catalysts for the polymerization of Michael-type monomers can be found in the literature, and the predominant catalyst systems are still of the general structure $[Cp^R_2LnX]$.[2d,3] The general ability of non-metallocene yttrium complexes as initiators for the GTP of MMA was previously studied via DFT calculations.[4] The results indicated that alcoholate initiators are not able to polymerize MMA due to an endothermic limitation of the initiation but DFT signified toward amido initiators as valid options for the GTP of MMA.[4] In a recent effort the mechanistic proceedings during the REM-GTP were elucidated and shown to have a monometallic propagation mechanism via an eight-membered-ring intermediate.[5] Contrary to the monometallic propagation of lanthanide catalysts, a monometallic as well as a bimetallic pathway is thought possible for group 4 metal catalysts.[2d,6] In the bimetallic mechanism one catalyst molecule bears the growing chain end, while the other activates the monomer. P2VP is an underrepresented polymer in the literature, and only scarce examples for controlled polymerization are available although interesting material properties for membranes and drug delivering carriers are reported for P2VP copolymers.[7] The polymerization of 2VP to poly(2-vinylpyridine) can be achieved via anionic polymerization or REM-GTP.[2a,3a,8] Compared to the simple anionic polymerization, REM-GTP has several advantages, e.g., strictly linear polymer growth, very narrow molecular weight distributions ($D < 1.1$), and increased operation temperature of the polymerization. The living character makes REM-GTP particularly suitable for block copolymerizations.[2a,7e] The currently available metallocene catalyst systems lack the activities necessary to further explore the potential applications of homo- and copolymer structures of

Received: August 26, 2014
Revised: October 15, 2014
Published: November 10, 2014

Scheme 1. Synthesis of 2-Methoxyethylaminobis(phenolate)yttrium Trimethylsilylmethyl Complexes [(L)M($CH_2Si(CH_3)_3$)(thf)]

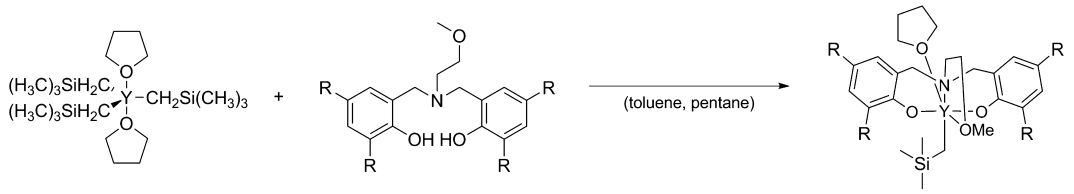

P2VP. The metallocene system Cp_2YbMe yielded turnover frequencies (TOF) of 44 h^{-1} for the REM-GTP of 2VP and molecular weights up to 14 kg/mol.[2a] Other literature reports of the REM-GTP of 2VP did not focus on the polymerization itself rather produced oligomeric P2VP and investigated the possibilities for the end-group functionalization through C−H bond activation.[3a]

However, to this date no highly active catalyst for the controlled polymerization of 2VP has been described in the literature. Mechanistic studies on initiation, propagation, and rate-determining step (RDS) of the 2VP polymerization have so far not been conducted.

Therefore, in this work the authors report the synthesis of highly versatile and highly active 2-methoxyethylaminobisphenolate yttrium catalysts for the homopolymerization and block copolymerization of Michael-type monomers such as 2VP, DEVP, DIVP, IPOx, and DMAA. The newly developed system was furthermore employed in mechanistic studies. The steric influence around the reactive metal center was evaluated using kinetic *in situ* ATR-IR measurements. The determination of the reaction order in catalyst and monomer combined with temperature-dependent reaction kinetics (Eyring plot) further elucidates the processes during the polymerization. The results presented in this article add valuable insight into the general picture of the REM-GTP mechanism and introduce a highly active catalyst system for the precise polymerization of functional monomers for the synthesis of high performance, high precision materials.

DISCUSSION

The REM-GTP of 2VP was investigated with 2-methoxyethylaminobis(phenolate)yttrium trimethylsilylmethyl complexes [$(ONOO)^{R}M(CH_2Si(CH_3)_3)(thf)$] which differ in the nature of the *o*-phenolate substituents (R) (Scheme 1). The catalysts are accessible through a straightforward synthesis from readily available compounds in good yields. The respective ligand is reacted with 1 equiv of [$Y(CH_2Si(CH_3)_3)_3(thf)_2$] in a mixture of pentane and toluene at ambient temperature to generate the catalyst.

The homopolymerizations of 2VP, DEVP, DIVP, IPOx, and DMAA with catalysts **1** and **2** proceed rapidly under mild conditions. The respective ligands were chosen to address the question of steric influence on the REM-GTP. According to the small steric demand of Cp ligands, only atactic P2VP has so far been produced with those systems. Mashima et al. however obtained isotactic oligomeric P2VP with yttrium ene−diamido complexes.[3a] As we synthesized 2-methoxyethylaminobis(phenolate)yttrium trimethylsilylmethyl complexes with increased steric demand around the yttrium center, we expected to restrict the accessibility and thereby influence the activities of the catalysts and possibly also the tacticities of the resulting polymers. First, the initiation mechanism was elucidated by end-group analysis of oligomeric P2VP generated by reacting $(ONOO)^{tBu}Y(CH_2Si(CH_3)_3)(thf)$ with 10 equiv of 2VP and monitoring the reaction via NMR. Time-resolved ^1H NMR spectra show a shift of the respective $CH_2Si(CH_3)_3$ methyl groups (Figure S18). The subsequent ESI-MS analysis found signals corresponding to $n \times M_{Mon} + M_I$ with either H^+ or Na^+ as charge carrier ($M_I = CH_2Si(CH_3)_3$).

The initiating $CH_2Si(CH_3)_3$ groups were clearly visible in the ESI-MS; therefore, a transfer of the coordinated ligand during the initiation through a six-membered intermediate is evident (Figure 1). Our studies showed no activity of 2-methoxyethylaminobis(phenolate)yttrium bisdimethylsilylamide complexes for the REM-GTP of Michael-type monomers. The alkyl initiators of catalysts **1** and **2** however initiate the polymerization of *β*-butyrolactone (BL), DEVP, DIVP, 2VP, IPOx, and DMAA at room temperature. Catalyst **1** showed the highest activities for the polymerization of DMAA with quantitative conversion of 200 equiv of monomer in 15 min at 0 °C. The activity of catalyst **1** decreased in the order of DMAA > IPOx > 2VP > DEVP > DIVP (Tables 1 and 2). The polymerization of DMAA at room temperature proceeded in an uncontrolled fashion producing PDMAA with broad PDI within less than 1 min. At 0 °C it was possible to control the polymerization and achieve quantitative yields of atactic PDMAA within 15 min with slightly broadened PDI (1.69) due to the high activity.

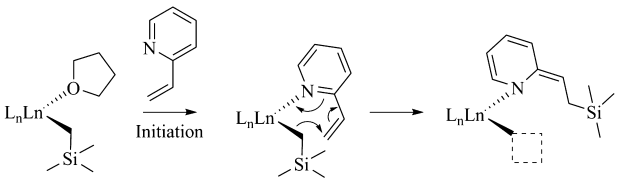

Figure 1. Six-membered initiation mechanism for 2VP and $L_nLn(CH_2Si(CH_3)_3)$.

The polymerization of 2VP proceeds in a living fashion, as discernible by the narrow polydispersities ($1.01 \leq x \leq 1.07$) and the good match between experimentally determined and the theoretically expected M_n values (Figure 3). To further examine the character of the polymerization with our 2-methoxyethylaminobis(phenolate)yttrium trimethylsilylmethyl complexes aliquots were taken at regular time intervals during the polymerization. These aliquots were analyzed by gel permeation chromatography multiangle light scattering (GPC-MALS) to obtain the absolute molecular mass (M_n) against the monomer (2VP) conversion as can be seen in Figure 3. The plots reveal a linear relationship between M_n and

Table 1. REM-GTP and ROP Polymerization Results of Catalyst 1[a]

entry	[M]/[Cat]	[M]	solvent	time [h]	conv [%]	$M_{n,calc}$ ($\times 10^4$)[b] [g/mol]	$M_{n,exp}$ ($\times 10^4$) [g/mol]	M_w/M_n	I^*[c]	P_r[d]	TOF [h^{-1}]
1	200	2VP	toluene	2	99	2.2	2.2	1.01	0.99		1100
2	200	DEVP	toluene	3.3	99	3.3	9.0	1.10	0.36		480
3	200	DIVP	toluene	5	25	1.0	3.4	1.09	0.28		42
4	200	IPOx	toluene	0.17	99	2.2	2.4	1.12	0.93		1500
5	600	2VP	toluene	4	99	6.6	11.0	1.02	0.60		420
6[e]	200	DMAA	CH_2Cl_2	0.25	99	2.0	6.2	1.69	0.32		
7[f]	600	BL	CH_2Cl_2	1	89	4.6	8.6[g]	1.50[g]	0.54	0.81	6000

[a]Reactions performed with [M] = 27 mmol at 25 °C in 20 mL of solvent, conversions determined by gravimetry, and $M_{n,expd}$ determined by GPC-MALS. [b]$M_{n,calc}$ from $M_{n,calc} = M \times (([M]/[Cat]) \times \text{conversion})$. [c]$I^* = M_{n,calc}/M_{exp}$. [d]$P_r$ is the probability of racemic linkages between monomer units and is determined by ^{13}C NMR spectroscopy. [e]Reaction conducted at −78 °C. [f]Reaction performed with [*rac*-BL] = 8.57 mmol at 25 °C in 5 mL of CH_2Cl_2 and conversion determined by ^1H NMR spectroscopy. [g]$M_{n,exp}$ and M_w/M_n values determined by GPC in $CHCl_3$ vs polystyrene standards.

Table 2. REM-GTP and ROP Polymerization Results of Catalyst 2[a]

entry	[M]/[Cat]	[M]	solvent	time [h]	conv [%]	$M_{n,calc}$ ($\times 10^3$)[b] [g/mol]	$M_{n,exp}$ ($\times 10^3$) [g/mol]	M_w/M_n	I^*[c]	P_r[d]	TOF [h^{-1}]
1	200	2VP	toluene	1.5	99	2.1	2.9	1.03	0.72		430
2	600	2VP	toluene	3	82	5.2	11.2	1.04	0.46		230
3[e]	600	BL	CH_2Cl_2	1	99	5.2	14.2[f]	1.60[f]	0.36	0.88	15800

[a]Reactions performed with [M] = 27 mmol at 25 °C in 20 mL of solvent, conversions determined by gravimetry, and $M_{n,expd}$ determined by GPC-MALS. [b]$M_{n,calc}$ from $M_{n,calc} = M \times (([M]/[Cat]) \times \text{conversion})$. [c]$I^* = M_{n,calc}/M_{exp}$. [d]$P_r$ is the probability of racemic linkages between monomer units and is determined by ^{13}C NMR spectroscopy. [e]Reaction performed with [*rac*-BL] = 8.57 mmol at 25 °C in 5 mL of CH_2Cl_2 and conversion determined by ^1H NMR spectroscopy. [f]$M_{n,expd}$ and M_w/M_n values determined by GPC in $CHCl_3$ vs polystyrene standards.

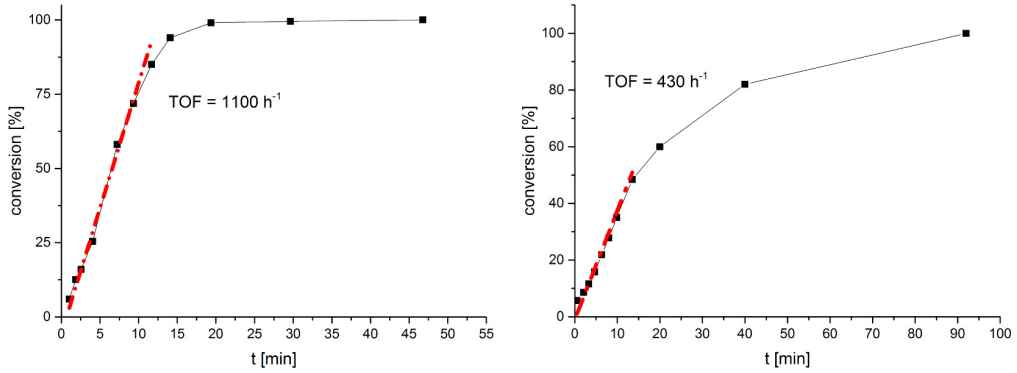

Figure 2. (left) Determination of catalytic activity of $(ONOO)^{tBu}Y(CH_2Si(CH_3)_3)(thf)$ (catalyst 135 μmol, 2VP 27 mmol, toluene 20 mL, T = 25 °C). (right) Determination of catalytic activity of $(ONOO)^{CMe2Ph}Y(CH_2Si(CH_3)_3)(thf)$ (catalyst 135 μmol, 2VP 27 mmol, toluene 20 mL, T = 25 °C).

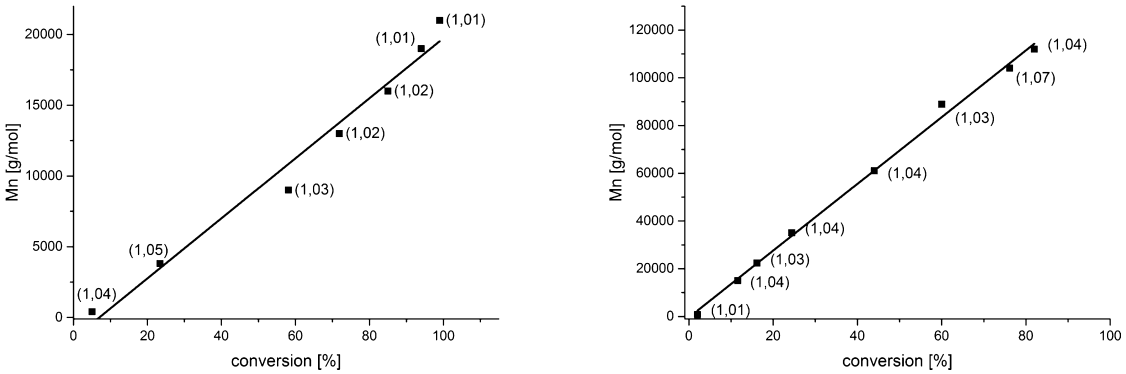

Figure 3. Linear growth of the absolute molecular weight (M_n) determined by GPC-MALS as a function of monomer conversion (determined gravimetically), with respective PDI values shown in parentheses: (left) catalyst **1**, 135 μmol, 2VP 27 mmol, toluene 20 mL, 25 °C; (right) catalyst **2**, 43 μmol, 2VP 27 mmol, toluene 20 mL.

conversion while retaining a very narrow PDI throughout the polymerization (PDI < 1.05).

Catalyst **1** yields atactic polymer in the case of P2VP, PDEVP, PDIVP, and PDMAA at ambient conditions. Catalyst

dx.doi.org/10.1021/ma501754u | *Macromolecules* 2014, 47, 7742−7749

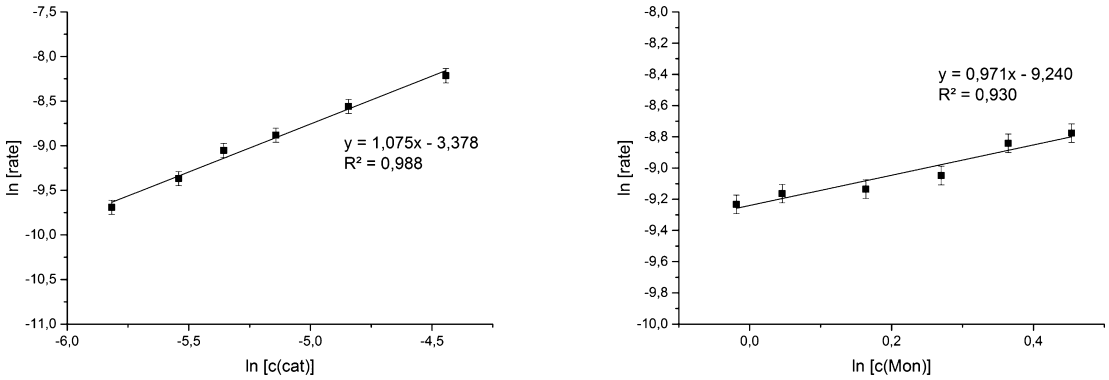

Figure 4. (left) Determination of catalyst order (ONOO)^{tBu}Y(CH$_2$Si(CH$_3$)$_3$)(thf) (catalyst 22−85 μmol, 2VP 8.6 mmol, toluene 5.5 mL). (right) Determination of monomer order (ONOO)^{tBu}Y(CH$_2$Si(CH$_3$)$_3$)(thf) (catalyst 42 μmol, 2VP 7−11.5 mmol, toluene 5.5 mL).

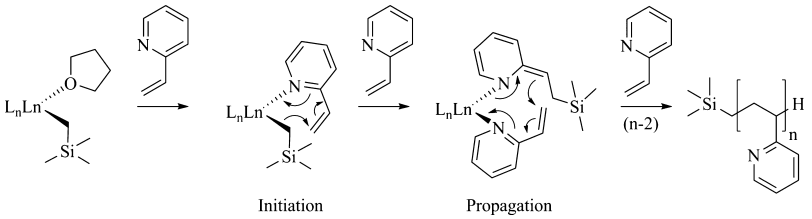

Figure 5. Schematic illustration concerning the initiation and propagation of REM-GTP of 2VP.

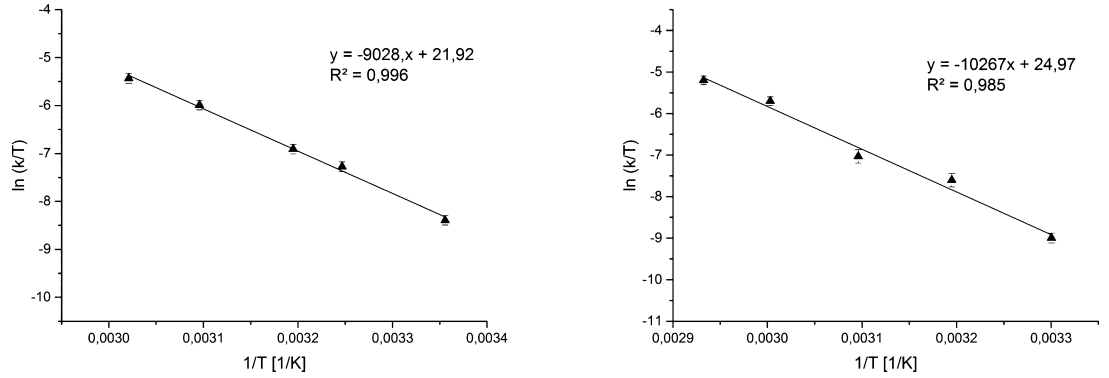

Figure 6. (left) Eyring plot for (ONOO)^{tBu}Y(CH$_2$Si(CH$_3$)$_3$)(thf) the polymerization of 2VP (catalyst 42 μmol, 2VP 8.6 mmol, toluene 5.5 mL, temperature 298−331 K). (right) Eyring plot for (ONOO)^{CMe2Ph}Y(CH$_2$Si(CH$_3$)$_3$)(thf) the polymerization of 2VP (catalyst 42 μmol, 2VP 8.6 mmol, toluene 5.5 mL, temperature 303−333 K).

2 was not active for the polymerization of DEVP, DIVP, and also produced atactic P2VP. Temperature variations between −20 and 60 °C did not change the tacticities of the resulting polymer. The generally occurring color change of the polymerization solution of 2VP probably due to the coordination to the catalyst was not observed at −78 °C. Also, prolonged stirring at this temperature did not produce polymer. We attribute this to the inability of 2VP to coordinate to the catalyst, replacing the coordinated THF molecule. Consequently, no initiation and polymerization could be observed until the temperature was elevated to −20 °C. The effect of the steric influence of catalysts **1** and **2** on the activity in the 2VP GTP was investigated through gravimetric kinetic measurements. For 2-methoxyethylaminobis(phenolate)yttrium trimethylsilylmethyl complexes the activity for GTP decreases with increased steric demand. The activity for the 2VP GTP dropped from 1100 h^{-1} with catalyst **1** to 430 h^{-1} with catalyst **2**. Catalyst **2** showed no activity for the polymerization of DEVP and DIVP.

To ensure that the activity differences are not only differences in initiator efficiency (I^*), aliquots were taken from the reaction and I^* was determined through GPC analysis. For catalyst **1** the I^* was found to be 99%, whereas for catalyst **2** I^* was only 72% at 25 °C. The measured I^* made the direct comparison of both catalysts possible and showed that the activity difference is due to the steric destabilization of the intermediate eight-membered transition state during the polymerization which increases the activation barrier for the S_N2-type associative dissplacement of the polymer by a 2VP monomer. Previous studies showed that the S_N2-type associative dissplacement is the rate-determining step (RDS) for the metallocene REM-GTP of phosphorus-containing vinyl polymers.[5a]

Kinetics. Generally, a monometallic as well as a bimetallic mechanism is thought possible for the GTP depending on the

dx.doi.org/10.1021/ma501754u | *Macromolecules* 2014, 47, 7742−7749

Table 3. Activation Enthalpy $\Delta H^{\ddagger}$ and Entropy $\Delta S^{\ddagger}$ and the Dependence on the Steric Demand of the Ligand Structure

	$(ONOO)^{tBu}Y(CH_2Si(CH_3)_3)(thf)$	$(ONOO)^{CH2Ph}Y(CH_2Si(CH_3)_3)(thf)$
$\Delta H^{\ddagger}$ (±2) (kJ/mol)	75.1	85.4
$-\Delta S^{\ddagger}$ (±3) (J/(K mol))	15.3	10.1

employed catalyst system. Therefore, kinetic *in situ* ATR-IR measurements were conducted for the REM-GTP of 2VP with catalysts **1** and **2**. The formal rate law for catalyzed polymerizations reads

$$r = k \times [\mathrm{Cat}]^m \times [\mathrm{Mon}]^n \quad (1)$$

Thus, for the determination of the reaction orders, first, the initial monomer concentration is kept constant to determine the order in catalyst (m). For different catalyst concentrations of otherwise identical reaction conditions, the plot of $\ln(r)$ against $\ln([\mathrm{Cat}])$ yields a reaction order of $m = 1$ (Figure 4, left). Furthermore, the order in monomer was determined according to eq 2.

$$r = k \times [\mathrm{Mon}]^n \quad (2)$$

For different monomer concentrations at otherwise identical conditions the reaction rate was measured. Plotting $\ln(r)$ against $\ln([\mathrm{Mon}])$ gave the order in monomer $n = 1$ (Figure 4, right). These results show that the REM-GTP of 2VP with 2-methoxyethylaminobis(phenolate)yttrium catalysts follows a monometallic Yasuda-type polymerization mechanism (Figure 5) as was also found for metallocene systems with phosphorus-containing monomers.[5a]

Through these results no exact explanation for the steric influence of the ligand on the catalytic activity can be given. Hence, temperature-dependent kinetic measurements were undertaken to determine the activation enthalpies $\Delta H^{\ddagger}$ and entropies $\Delta S^{\ddagger}$ according to the Eyring equation

$$\ln\frac{k}{T} = -\frac{\Delta H^{\ddagger}}{RT}\frac{1}{T} + \ln\frac{k_B}{h} + \frac{\Delta S^{\ddagger}}{R} \quad (3)$$

with the rate constant k, the temperature T, the ideal gas constant R, the Boltzmann constant k_B, and the Planck constant h. Plotting $\ln(k/T)$ against $1/T$ gives the activation enthalpy and entropy of the rate-determining step. The measurements were performed with catalyst $(ONOO)^{tBu}Y(CH_2Si(CH_3)_3)$-(thf) and $(ONOO)^{CMe2Ph}Y(CH_2Si(CH_3)_3)(thf)$ under identical conditions in an ATR-IR autoclave.

Eyring plot studies for the polymerization of polar monomers are rare in the literature.[9] The activities in previous studies were found to be mainly determined by entropic effects. REM-GTP Eyring plot measurements with different lanthanides (Y, Tb, Tm, and Lu) were performed with DEVP and DIVP.[5a] A decreased entropic contribution was observed with a decreased metal radius (i.e., faster propagation rates), and an increased entropic influence was found for sterically more demanding monomers (i.e., slower propagation rates). The 2-methoxyethylaminobis(phenolate)yttrium trimethylsilylmethyl complexes used for the Eyring plot measurements with 2VP show a different trend compared the lanthanocene catalysts. An increased steric demand in *ortho*-position of these complexes leads to an increase in both the $\Delta H^{\ddagger}$ and the $-T\Delta S^{\ddagger}$. Bulkier ligands around the metal center destabilize the propagation ground state by restraining the eight-membered transition state. The increased steric crowding furthermore interferes with the associative displacement of the polymer by a 2VP monomer.

These destabilizing effects are of enthalpic and of entropic nature. The enthalpic $\Delta H^{\ddagger}$ contribution to the RDS is increased from 75.1 kJ/mol for catalyst **1** to 85.4 kJ/mol for catalyst **2**. The entropic $-\Delta S^{\ddagger}$ contribution has a minor influence but nevertheless is also raised from 15.3 J/(K mol) for catalyst **1** to 10.1 J/ (K mol) for the more sterically crowded catalyst **2**.

ROP of β-Butyrolactone. The activities of both 2-methoxyethylaminobis(phenolate)yttrium catalysts were tested for the ring-opening polymerization (ROP) of BL. In general, initiators for the polymerization of lactones are alcoholates and amides, whereas alkyl initiators are not commonly used for the ROP with lanthanide catalysts. As expected, narrow polydispersities for PHB were achieved (<1.6), and the measured molecular weights are in good agreement with the theoretically calculated values (Tables 1 and 2). Both polymerization types, the REM-GTP[5a,10] as well as the ROP,[11] have a monometallic initiation and propagation mechanism with first-order kinetics in catalyst and monomer. In the literature similar 2-methoxyethylaminobis(phenolate)yttrium catalysts were previously used for the ring-opening polymerization (ROP) of β-butyrolactone.[12] Catalysts **1** and **2** show good activities (TOF = 6000 and 15 800 h^{-1}) toward the ROP and produced syndiotactic PHB (P_r = 0.81−0.88). The order in activity for catalysts **1** and **2** for the ROP is reversed compared to the GTP. The bulky catalyst **2** is more active for ROP whereas the less crowded complex **1** shows higher activities for GTP. For a good ROP and GTP catalyst a balance has to be found for the steric crowding introduced through the ligand. Bulkier ligands increase the activity for the ROP as dimer formation is suppressed, and the carbonyl-alkoxy chelate during the ROP is not hindered. Catalyst **2** exhibits an activity almost 3 times higher than catalyst **1** for the ring-opening polymerization of BL. GTP, however, proceeds faster with catalyst **1** as the eight-membered transition state for the propagation of polar monomers is sterically more demanding and destabilized by catalyst **2**. Catalyst **1** (1100 h^{-1}) is more than twice as fast as catalyst **2** (430 h^{-1}) for the polymerization of 2VP.

Block Copolymerization. In the literature numerous examples can be found for the copolymerization of lactones[13] and the copolymerization of Michael-type monomers.[2a,d] Only a few examples can be found for the combination of GTP and ROP, and they are limited to the copoylmerization of (meth)acrylate and ε-caprolactone and δ-valerolactone.[14] The use of anionic initiators has been reported for trials to produce polyester and polyhydrocarbon copolymers, but only homopolymer formation with very broad molecular weight distributions could be observed.[15] Also modified PHB has been investigated to afford macromolecular initiators which produce polymeric material with narrow dispersities.[16] There, PHB modifications prior to the polymerization are necessary which enable the radical copolymerization of PHB and acrylates. As our compounds **1** and **2** were suitable catalysts for the GTP and ROP we were interested if these different polymerization methods can be combined and utilized to produce block copolymers.

dx.doi.org/10.1021/ma501754u | *Macromolecules* 2014, 47, 7742−7749

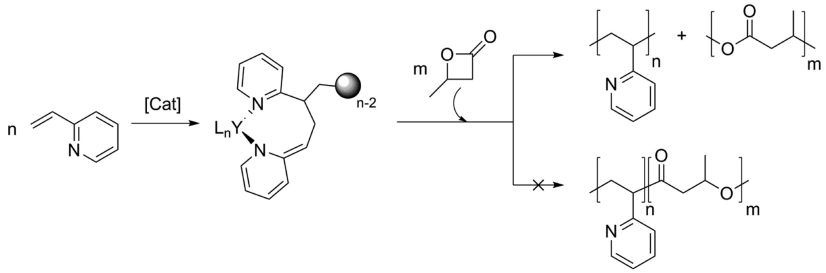

Figure 7. Experimental steps toward the attempted block copolymerization of 2VP and BL (catalyst **1** 34 μmol, [Cat]:[2VP]:[BL] = 1:100:100, 25 °C, 5 mL of CH_2Cl_2).

Table 4. Copolymerization Experiments with Catalyst 1

		$M_{n,expd}$[a] ($\times 10^4$) [g/mol]	$M_{n,calcd}$ ($\times 10^4$) [g/mol]	PDI[b]	comonomer ratio A/B[c]	yield[d] [%]	I^*[e]
1	$P2VP_{100}$-*b*-$PDEVP_{100}$	3.0	2.7	1.05	1:1.1	96	0.90
2	$P2VP_{100}$-*b*-$PIPOx_{100}$	2.6 (1.3)	2.2	1.03 (1.01)	1:1.2	97	0.85
3	$P2VP_{100}$-*b*-$PDMAA_{100}$[f]	3.3 (1.6)	2.0	1.24 (1.04)	1:1.6	97	0.63

[a]Reactions performed with [M] = 4.3, [Cat] = 43 μmol at 25 °C in 5 mL of CH_2Cl_2; numbers in parentheses give the respective data for the aliquot sample taken in the case of bimodal distributions. [b]Determined by GPC-MALS. [c]Determined by ^{1}H NMR. [d]Determined by weighing of the components. [e]$I^* = M_{n,calc}/M_{n,exp}$; numbers in parentheses give the I^* of the macroinitiator for polymerization of block B (in the case of bimodal distributions). [f]Reaction performed at 0 °C.

In comparison to other Michael-type monomers, 2VP coordinates the weakest to the metal center (DEVP > MMA > IPOx > 2VP).[2a] For REM-GTP the addition sequence of the monomers is crucial for monomers with different coordination strength. In our study we picked up on the concept and tried to use the low coordination strength of P2VP to the metal center to obtain block copolymer structures by sequential addition (Figure 7). Low-temperature polymerization experiments showed that at −78 °C 2VP is not polymerized. For a successful block copolymerization, BL needs to be able to replace the coordinated eight-membered intermediate of the REM-GTP while the P2VP chain end needs to have enough nucleophilicity to ring-open the coordinated lactone. Therefore, we chose 2VP as monomer to obtain P2VP and use the pending polymer chain on the yttrium catalyst as macroinitiator for the subsequent ROP of BL. The very high initiator efficiencies of catalyst **1** should suppress homopolymer formation of PHB and facilitate the subsequent isolation of the block copolymer. The polymerization of block A (P2VP) is conducted in dichloromethane to ensure complete conversion without precipitation of P2VP. An aliquot is taken for later GPC-MALS analysis, and subsequently, BL is added and stirred for an additional 2 h after which an aliquot NMR is once again taken to ensure full conversion of BL. The separation of the block-AB-copolymer is attempted by precipitation with hexane and washing cycles with methanol and thf, but only homopolymers were isolated (Figure 7).

Possible reasons for the inability to produce block copolymers might stem from the inadequate nucelophilicity of macroinitiator at the catalyst or chain scission of P2VP-*b*-PHB. Furthermore, the formation of PHB homopolymer could be explained by traces of unreacted catalyst molecules. The general activity of the pending P2VP chain toward block copolymerization was successfully tested with Michael-type monomers (*vide infra*, Table 4) and yielded block copolymers to ensure the livingness of the P2VP chain. Ensuing, the reaction conditions were systematically varied. Excess of BL was added as well as catalyst concentration, monomer loading of monomer A, solvent, and temperature screened. Aside from 2VP, other Michael-type monomers such as DEVP and IPOx were employed in copolymerization experiments with BL and did not show any block copolymer formation either. Under all tested conditions homopolymer could be isolated, but no block copolymer formation was observed.

The initiation of the ROP of BL was still puzzling as the initiator efficiency of catalyst **1** under the reaction conditions was 99%. Of course, trace quantities of catalyst which catalyze the ROP of BL might be a possible explanation for the generation of PHB homopolymer. Therefore, GPC measurements of the isolated PHB homopolymers were performed. They showed average M_n (PDI ∼ 1.5) and I^* of around 20−30%. The PHB homopolymer signals do not exhibit any initiating group. From NMR measurements crotonic end groups can be excluded as they show characteristic shifts and are visible already at very low concentrations (see Figures S6 and S7). Therefore, the hypothesis of trace amounts of catalyst initiating the BL polymerization can be discarded. The experimental results point toward a deprotonation of BL and a subsequent anionic ROP or chain scission. Further mechanistic studies have to be performed to reveal the mechanism in detail.

The general ability of our catalyst system was tested in block copolymerization experiments with Michael-type monomers. REM-GTP block copolymerization was conducted with 2VP as block A and DEVP, IPOx, and DMAA as block B. As with the previous copolymerization attempts with BL also here samples were taken after 2 h for later GPC-MALS analysis. Monomodal distribution was found for P2VP-*b*-PDEVP (Table 4, entry 1). In the GPC of the other copolymers (P2VP-*b*-PIPOx; P2VP-*b*-PDMAA) remaining P2VP block was observed which could be unambiguously assigned through the comparison with GPCs of the aliquot samples. The remaining P2VP is probably the result of quenching processes though trace amounts of water in the monomer B. The separation of the P2VP-*b*-PDMAA block copolymers was achieved through washing cycles with toluene and water.

The PDIs of the obtained block copolymers were narrow (PDI = 1.03−1.24), and the calculated M_n fit well to the

dx.doi.org/10.1021/ma501754u | *Macromolecules* 2014, 47, 7742−7749

experimentally determined values. More defined polymer structures were obtained during block copolymerization of 2VP and DMAA due to the employed P2VP macroinitiator. The PDI of PDMAA was 1.69, whereas for the $P2VP_{100}$-*b*-$PDMAA_{100}$ block copolymer a PDI of 1.24 could be achieved. The significant decrease of the polydispersity can be attributed to a different initiation mechanism of the macroinitiator P2VP compared to alkyl initiators. Similar results were achieved for the polymerization of DMAA with zirconocenes using enolates as initiating ligands.[2b,10] For α-acid monomers like DMAA, initiation can proceed via either deprotonation of the α-CH or nucleophilic transfer, both being six-electron processes. The P2VP macroinitiator is supposed to coordinate to the metal via an enamide and can initiate via an eight-membered ring, matching the propagation step during the polymerization and therefore initiate uniformly.

CONCLUSION

2-Methoxyethylaminobis(phenolate)yttrium trimethylsilylmethyl complexes $[(ONOO)^{R}Y(CH_2Si(CH_3)_3)(thf)]$ were synthesized and showed moderate to high activities in the rare earth metal-mediated group transfer polymerization of 2-vinylpyridine, diethyl vinylphosphonate, diisopropyl vinylphosphonate, *N*,*N*-dimethylacrylamide, and 2-isopropenyl-2-oxazoline as well as in the ring-opening polymerization of β-butyrolactone. The present study is one of the first examples for REM-GTP with non-metallocene catalyst systems covering a large variety of polar monomers. Catalyst **1** exhibits the highest TOF for the REM-GTP of 2-vinylpyridine reported in the literature. The reaction orders in catalyst and monomer were determined, and temperature-dependent reaction kinetics (Eyring plot) were conducted for the polymerization of 2-vinylpyridine. The mechanistic studies through kinetic *in situ* ATR-IR measurements of the 2VP polymerization revealed that 2-methoxyethylaminobis(phenolate) catalyst systems follow a living monometallic group transfer polymerization mechanism allowing a precise molecular weight control of the homopolymers and the block copolymers with very narrow molecular weight distributions. Generally the steric demand of the *ortho*-position in the ligand structure had a pronounced influence on the catalytic activity. For the REM-GTP less sterically demanding catalysts exhibited higher activities contrary to the activities in the ROP where higher steric crowding gave increased activities. This can be attributed to the difference in steric demand of the different propagation mechanisms. The combination of REM-GTP and ROP to form block copolymers was investigated. Efforts to utilize the versatility of the catalyst system to produce block copolymer structures for a mechanistic crossover of GTP and ROP proved unsuccessful probably due to inadequate nucleophilicity of the Michael-type monomers used as macroinitiator. However, REM-GTP block copolymerization of 2VP with DEVP, IPOx, and DMAA with high activities were possible with 2-methoxyethylaminobis(phenolate)yttrium trimethylsilylmethyl complexes.

EXPERIMENTAL SECTION

General. All reactions were carried under an argon atmosphere using standard Schlenk or glovebox techniques. All glassware was heat-dried under vacuum prior to use. Unless otherwise stated, all chemicals were purchased from Sigma-Aldrich, Acros Organics, or ABCR and used as received. Toluene, thf, and pentane were dried using an MBraun SPS-800 solvent purification system. Hexane was dried over 3 Å molecular sieves. The precursor complex $Ln(CH_2Si(CH_3)_3)_3(thf)_2$ is prepared according to literature procedure.[17,18] The monomers, 2-vinylpyridine, diethyl vinylphosphonate, diisopropyl vinylphosphonate, 2-isopropenyl-2-oxazoline, *N*,*N*-dimethylacrylamide, and β-butyrolactone were dried over calcium hydride and distilled prior to use.

NMR spectra were recorded on a Bruker AVIII-300 spectrometer. ^1H and ^{13}C NMR spectroscopic chemical shifts δ are reported in ppm relative to the residual proton signal. δ (^1H) is calibrated to the residual proton signal and δ (^{13}C) to the carbon signal of the solvent. Deuterated solvents were obtained from Sigma-Aldrich and dried over 3 Å molecular sieves. Elemental analysis were measured at the Laboratory for Microanalysis at the Institute of Inorganic Chemistry at the Technische Universität München. ESI-MS analytical measurements were performed with methanol and isopropanol solutions on a Varian 500-MS spectrometer. GPC was carried out on a Varian LC-920 equipped with two PL Polargel columns. As eluent a mixture of THF and 6 g L^{-1} tetrabutylammonium bromide (TBAB) was used. Absolute molecular weights have been determined online by multiangle light scattering (MALS) analysis using a Wyatt Dawn Heleos II in combination with a Wyatt Optilab rEX as concentration source. GPC for poly(hydroxybutyrate) was carried out on a Polymer Laboratories GPC50 Plus chromatograph. As eluent, chloroform with 1.5 g L^{-1} tetrabutylammonium tetrafluoroborate was used. Polystyrene standards were used for calibration. *In situ* IR measurements were carried out using a Mettler−Toledo system under an argon atmosphere.

Kinetics by the Aliquots Method. After dissolving 0.14 mmol of $(ONOO)^{tBu}Y(CH_2Si(CH_3)_3)(thf)$ in 20 mL of toluene at room temperature, the corresponding amount of monomer (27 mmol) was added in one injection. Aliquots were taken from the reaction solution at regular time intervals and quenched by addition of MeOH. For each aliquot, the conversion is determined by gravimetry, and the molecular weight of the polymer is measured by GPC-MALS analysis.

Catalyst Synthesis. *General Procedure for the Synthesis of (L)Y(CH$_2$Si(CH$_3$)$_3$)(thf).* One equivalent of proligand $H_2(ONOO)^{X}$ in toluene is added to a stirred solution of $Ln(CH_2Si(CH_3)_3)_3(thf)_2$ in pentane. The resulting solution is stirred overnight at room temperature. The solvent is removed *in vacuo*, and the resulting solid is washed with pentane.

*$(ONOO)^{tBu}Y(CH_2Si(CH_3)_3)(thf)$ (**1**).* ^1H NMR (298 K, 300 MHz, C_6D_6): δ = 7.61 (m, 2H), 7.09 (m, 2H), 3.97−3.86 (m, 4H), 3.79 (m, 2H), 2.90 (m, 2H), 2.78 (s, 3H), 2.43 (m, 2H), 2.26−2.15 (m, 2H), 2.11 (s, 3H), 1.81 (s, 18H), 1.46 (s, 18H), 1.23−1.09 (m, 4H), 0.51 (s, 4H), −0.38 (m, 2H). ^{13}C NMR (298 K, 75 MHz, C_6D_6): δ = 161.67, 161.64, 136.73, 129.33, 125.65, 124.47, 124.16, 74.08, 71.88, 64.89, 61.36, 49.31, 35.65, 34.29, 32.31, 30.36, 25.58, 25.07, 4.91. EA: calculated: C 64.97, H 9.31, N 1.85; found: C 65.02, H 9.44, N 1.85.

*$(ONOO)^{CMe2Ph}Y(CH_2Si(CH_3)_3)(thf)$ (**2**).* ^1H NMR (298 K, 300 MHz, C_6D_6): δ = 7.63 (m, 2H), 7.51−7.37 (m, 8H), 7.28−7.14 (m, 8H), 7.17−7.04 (m, 2H), 7.00−6.88 (m, 2H), 6.78 (m, 2H), 3.30 (d, ^2J = 12.4 Hz, 2H), 2.96 (m, 4H), 2.72 (s, 3H), 2.48 (m, 2H), 2.38 (m, 2H), 2.07 (s, 6H), 1.95 (m, 2H), 1.78 (s, 24H), 1.05 (s, 2H), 0.47 (s, 9H), −0.82 (m, 2H). ^{13}C NMR (298 K, 75 MHz, C_6D_6): δ = 161.16, 153.15, 152.45, 136.11, 136.02, 128.29, 127.92, 127.31, 126.55, 125.85, 125.79, 124.52, 124.45, 73.76, 70.89, 63.99, 60.97, 48.93, 42.74, 32.44, 31.79, 31.66, 28.51, 25.07, 5.22. EA: calculated: C 72.81, H 7.81, N 1.39; found: C 73.10, H 7.77, N 1.57.

ASSOCIATED CONTENT

Supporting Information

Oligomer analysis and GPC data, conversion vs reaction time diagrams for DEVP, DIVP, and PIPOx, LCST behavior of P2VP, additional ^1H NMR spectra of the catalysts, DSC and TGA data. This material is available free of charge via the Internet at http://pubs.acs.org.

AUTHOR INFORMATION

Corresponding Author

*E-mail rieger@tum.de; Tel +49-89-289-13570; Fax +49-89-289-13562 (B.R.).

Notes

The authors declare no competing financial interest.

ACKNOWLEDGMENTS

The authors thank BASF SE for financial support.

ABBREVIATIONS

BL, β-butyrolactone; REM-GTP, rare earth metal-mediated group transfer polymerization; MMA , methyl methacrylate; DAVP, dialkyl vinyl phosphonates; IPOx, 2-isopropenyl-2-oxazoline; DMAA, *N*,*N*-dimethylacrylamide; 2VP, 2-vinylpyridine; RDS, rate-determining step.

REFERENCES

(1) (a) Yasuda, H.; Yamamoto, H.; Yokota, K.; Miyake, S.; Nakamura, A. *J. Am. Chem. Soc.* **1992**, *114*, 4908. (b) Collins, S.; Ward, D. G. *J. Am. Chem. Soc.* **1992**, *114*, 5460.

(2) (a) Zhang, N.; Salzinger, S.; Soller, B. S.; Rieger, B. *J. Am. Chem. Soc.* **2013**, *135*, 8810. (b) Mariott, W. R.; Chen, E. Y. X. *Macromolecules* **2005**, *38*, 6822. (c) Chen, E. Y. X. *Dalton Trans.* **2009**, 8784. (d) Chen, E. Y. X. *Chem. Rev.* **2009**, *109*, 5157. (e) Salzinger, S.; Rieger, B. *Macromol. Rapid Commun.* **2012**, *33*, 1327. (f) Rabe, G. W.; Komber, H.; Haussler, L.; Kreger, K.; Lattermann, G. *Macromolecules* **2010**, *43*, 1178. (g) Salzinger, S.; Seemann, U. B.; Plikhta, A.; Rieger, B. *Macromolecules* **2011**, *44*, 5920. (h) He, J.; Zhang, Y.; Chen, E. Y. X. *Synlett* **2014**, *25*, 1534.

(3) (a) Kaneko, H.; Nagae, H.; Tsurugi, H.; Mashima, K. *J. Am. Chem. Soc.* **2011**, *133*, 19626. (b) Hu, Y.; Wang, X.; Chen, Y.; Caporaso, L.; Cavallo, L.; Chen, E. Y. X. *Organometallics* **2013**, *32*, 1459.

(4) Fang, J.; Tschan, M. J. L.; Brule, E.; Robert, C.; Thomas, C. M.; Maron, L. *Dalton Trans.* **2013**, *42*, 9226.

(5) (a) Salzinger, S.; Soller, B. S.; Plikhta, A.; Seemann, U. B.; Herdtweck, E.; Rieger, B. *J. Am. Chem. Soc.* **2013**, *135*, 13030. (b) Zhang, Y.; Ning, Y.; Caporaso, L.; Cavallo, L.; Chen, E. Y. X. *J. Am. Chem. Soc.* **2010**, *132*, 2695.

(6) (a) Collins, S.; Ward, D. G.; Suddaby, K. H. *Macromolecules* **1994**, *27*, 7222. (b) Li, Y.; Ward, D. G.; Reddy, S. S.; Collins, S. *Macromolecules* **1997**, *30*, 1875.

(7) (a) Hayward, R. C.; Chmelka, B. F.; Kramer, E. J. *Adv. Mater.* **2005**, *17*, 2591. (b) Sun, W.; Wang, Z.; Yao, X.; Guo, L.; Chen, X.; Wang, Y. *J. Membr. Sci.* **2014**, *466*, 229. (c) Popescu, M.-T.; Korogiannaki, M.; Marikou, K.; Tsitsilianis, C. *Polymer* **2014**, *55*, 2943. (d) Klinger, D.; Wang, C. X.; Connal, L. A.; Audus, D. J.; Jang, S. G.; Kraemer, S.; Killops, K. L.; Fredrickson, G. H.; Kramer, E. J.; Hawker, C. J. *Angew. Chem., Int. Ed.* **2014**, *53*, 7018. (e) Soller, B. S.; Zhang, N.; Rieger, B. *Macromol. Chem. Phys.* **2014**, *215*, 1946−1962.

(8) (a) Tsitsilianis, C.; Voulgaris, D. *Macromol. Chem. Phys.* **1997**, *198*, 997. (b) Hückstädt, H.; Göpfert, A.; Abetz, V. *Macromol. Chem. Phys.* **2000**, *201*, 296. (c) Gohy, J.-F.; Antoun, S.; Jerome, R. *Macromolecules* **2001**, *34*, 7435. (d) Natalello, A.; Tonhauser, C.; Berger-Nicoletti, E.; Frey, H. *Macromolecules* **2011**, *44*, 9887. (e) Atanase, L. I.; Riess, G. *J. Colloid Interface Sci.* **2013**, *395*, 190. (f) Tanaka, S.; Goseki, R.; Ishizone, T.; Hirao, A. *Macromolecules* **2014**, *47*, 2333.

(9) Frauenrath, H.; Keul, H.; Hoecker, H. *Macromolecules* **2001**, *34*, 14.

(10) Miyake, G.; Caporaso, L.; Cavallo, L.; Chen, E. Y. X. *Macromolecules* **2009**, *42*, 1462.

(11) (a) Ding, K.; Miranda, M. O.; Moscato-Goodpaster, B.; Ajellal, N.; Breyfogle, L. E.; Hermes, E. D.; Schaller, C. P.; Roe, S. E.; Cramer, C. J.; Hillmyer, M. A.; Tolman, W. B. *Macromolecules* **2012**, *45*, 5387. (b) Pepels, M. P. F.; Bouyahyi, M.; Heise, A.; Duchateau, R. *Macromolecules* **2013**, *46*, 4324. (c) Wang, L.; Bochmann, M.; Cannon, R. D.; Carpentier, J.-F.; Roisnel, T.; Sarazin, Y. *Eur. J. Inorg. Chem.* **2013**, *2013*, 5896.

(12) Amgoune, A.; Thomas, C. M.; Ilinca, S.; Roisnel, T.; Carpentier, J.-F. *Angew. Chem., Int. Ed.* **2006**, *45*, 2782.

(13) (a) Jaffredo, C. G.; Carpentier, J.-F.; Guillaume, S. M. *Macromolecules* **2013**, *46*, 6765. (b) Bouyahyi, M.; Duchateau, R. *Macromolecules* **2014**, *47*, 517−524. (c) Jaffredo, C. G.; Chapurina, Y.; Guillaume, S. M.; Carpentier, J.-F. *Angew. Chem., Int. Ed.* **2014**, in press. (d) Hong, M.; Chen, E. Y. X. *Macromolecules* **2014**, *47*, 3614. (e) Du, G.; Wei, Y.; Zhang, W.; Dong, Y.; Lin, Z.; He, H.; Zhang, S.; Li, X. *Dalton Trans.* **2013**, *42*, 1278.

(14) (a) Kostakis, K.; Mourmouris, S.; Karanikolopoulos, G.; Pitsikalis, M.; Hadjichristidis, N. *J. Polym. Sci., Part A: Polym. Chem.* **2007**, *45*, 3524. (b) Ihara, E.; Morimoto, M.; Yasuda, H. *Macromolecules* **1995**, *28*, 7886. (c) Yasuda, H.; Ihara, E. *Macromol. Chem. Phys.* **1995**, *196*, 2417.

(15) Solaro, R.; Cantoni, G.; Chiellini, E. *Eur. Polym. J.* **1997**, *33*, 205.

(16) (a) Arslan, H.; Menteş, A.; Hazer, B. *J. Appl. Polym. Sci.* **2004**, *94*, 1789. (b) Arslan, H.; Hazer, B.; Kowalczuk, M. *J. Appl. Polym. Sci.* **2002**, *85*, 965. (c) Arslan, H.; Yeşilyurt, N.; Hazer, B. *J. Appl. Polym. Sci.* **2007**, *106*, 1742. (d) Nguyen, S.; Marchessault, R. H. *Macromolecules* **2004**, *38*, 290. (e) Zhang, X.; Yang, H.; Liu, Q.; Zheng, Y.; Xie, H.; Wang, Z.; Cheng, R. *J. Polym. Sci., Part A: Polym. Chem.* **2005**, *43*, 4857.

(17) Hultzsch, K. C.; Voth, P.; Beckerle, K.; Spaniol, T. P.; Okuda, J. *Organometallics* **2000**, *19*, 228.

(18) (a) Tshuva, E. Y.; Groysman, S.; Goldberg, I.; Kol, M.; Goldschmidt, Z. *Organometallics* **2002**, *21*, 662−670. (b) Amgoune, A.; Thomas, C. M.; Roisnel, T.; Carpentier, J.-F. *Chem.−Eur. J.* **2005**, *12*, 169−179.

Versatile 2-Methoxyethylaminobis(phenolate)yttrium Catalysts: Catalytic Precision Polymerization of Polar Monomers via Rare Earth Metal-Mediated Group Transfer Polymerization

Peter T. Altenbuchner[†], Benedikt S. Soller[†], Stefan Kissling[†], Thomas Bachmann[†], Alexander Kronast[†], Sergei I. Vagin[†], Bernhard Rieger[†*]

[†]WACKER-Lehrstuhl für Makromolekulare Chemie, Technische Universität München, Lichtenbergstraße 4, 85748 Garching bei München, Germany

Table of Contents

1. General Information

Acitivity Measurements and Kinetic Analysis in the *in situ* ATR-IR:
For activity measurements, the stated amount of catalyst (42 – 135 µmol) is dissolved in 5 mL of dichloromethane, and the reaction mixture is transferred into the *in situ* IR autoklave and thermostatted to the desired temperature. Then, the stated amount of monomer (4.3-27 mmol) is added. During the course of the experiment the temperature is kept at the desired temperature (±1 K). In case of block copolymerization experiments, an aliquot sample is taken after complete conversion of the first monomer A for GPC-MALS analysis. Monomer B (4.3 mmol) is added subsequently and the reaction mixture is stirred until full conversion. After the stated reaction time, the reaction is quenched by addition of wet chloroform (0.5 mL) and an aliquot is taken to determine the conversion. The polymer is precipitated in excess hexane, filtered off and freeze dried from destilled H_2O.

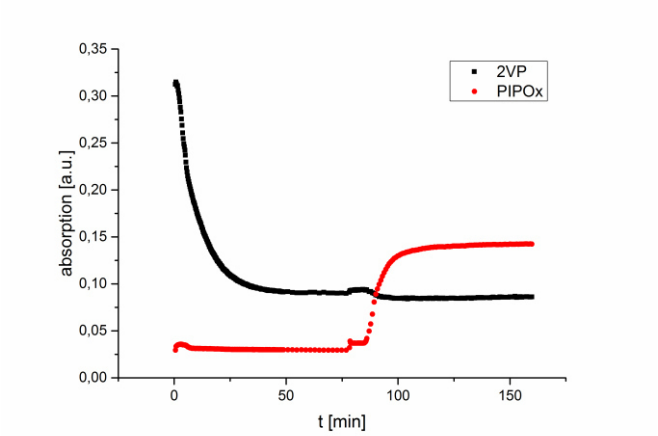

Figure S 1 ATR-IR block copolymerization experiment with block A P2VP (802 cm^{-1}) and block B PIPOx (1607 cm^{-1}).

The block copolymerization of 2VP and PIPOx was monitored in the ATR-IR (Figure S 1) through which the decrease of 2VP to complete conversion and the increase of PIPOx could be observed. The polymerization of IPOx was initiated immediately after the addition and preceded to full conversion within 30 minutes.

Sequential copolymerization

After dissolving the calculated amount of catalyst in dichlormethane at room temperature, the first monomer was added. The reaction mixture was stirred for 2 hours. One aliquot was taken and quenched by the addition of 0.5 mL MeOH while the calculated amount of a second monomer was added to the reaction solution and stirred for another 2 hours at room temperature (in case of DMAA: at – 78 °C) and quenched by addition of 0.5 mL MeOH. The polymers were precipitated by addition of the reaction mixtures to hexane (150 mL) and decanted from solution. Residual solvents were removed by drying the polymers under vacuum at 60 °C overnight.

Molecular weight determination

GPC was carried out on a Varian LC-920 equipped with two PL Polargel columns. As eluent a mixture of 50% THF, 50% water, and 9 g L-1 tetrabutylammonium bromide (TBAB) was used in the case of PDEVP, PIPOx, P2VP, P(2VP-b-PDEVP), P(2VP-b-PIPOx), P(2VP-b-PDMAA) and P(2VP-b-DEVP); for PDIVP analysis, the eluent was THF with 6 g L-1 TBAB. Absolute molecular weights have been determined online by multiangle light scattering (MALS) analysis using a Wyatt Dawn Heleos II in combination with a Wyatt Optilab rEX as concentration source.

GPC for Polyhydroxybutyrate samples was carried on a Polymer Laboratories GPC50 Plus chromatograph. As eluent, chloroform with 1.5 g L-1 tetrabutylammonium tetrafluoroborate was used. Polystyrene standards were used for calibration.

Kinetics by aliquots method

In the Glovebox the calculated amount of catalyst was dissolved in 20mL toluene at room temperature and the calculated amount of monomer was added in one injection. Aliquots were taken from the reaction solution at regular time intervals and quenched by addition to MeOH. For each aliquot, the conversion is determined by gravimetry or ^{1}H NMR spectroscopy and the molecular weight of the formed polymer by GPC-MALS analysis.

2. Analytical Data

2.1 Nuclear Magnetic Resonance Spectroscopy (NMR)

a.)

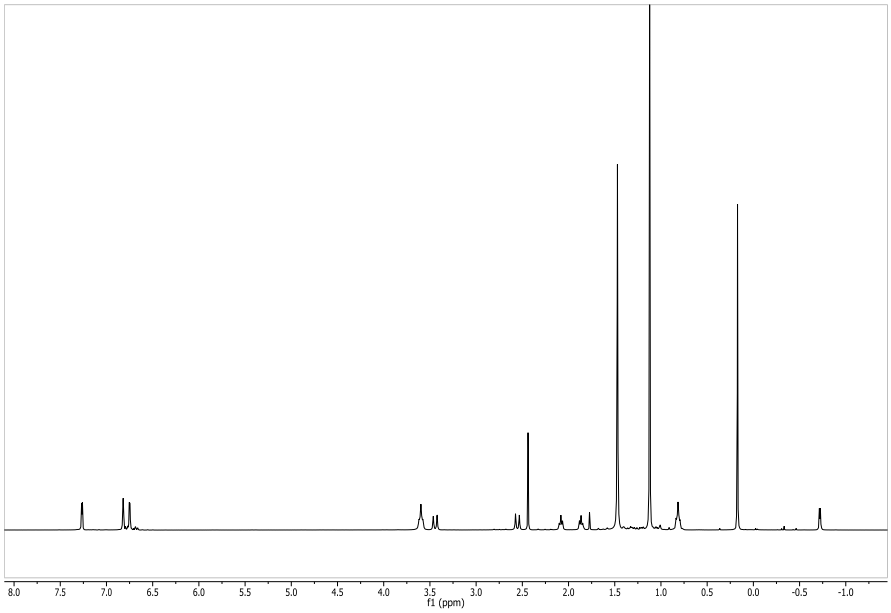

b.)

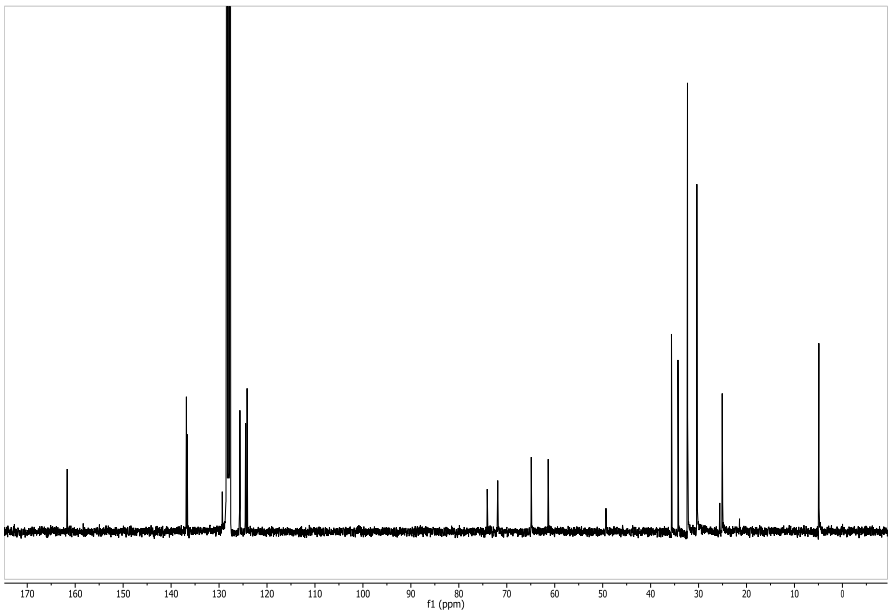

Figure S 2 a.) ^{1}H NMR spectrum b.) ^{13}C NMR spectrum of catalyst (ONOO)$^{t\mathrm{Bu}}$Y($CH_2Si(CH_3)_3$)(thf) in C_6D_6.

a.)

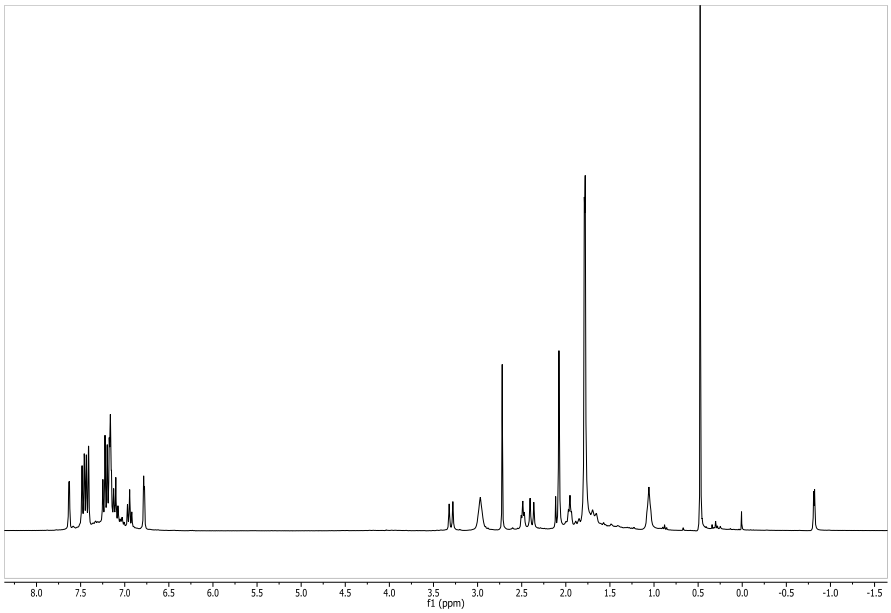

b.)

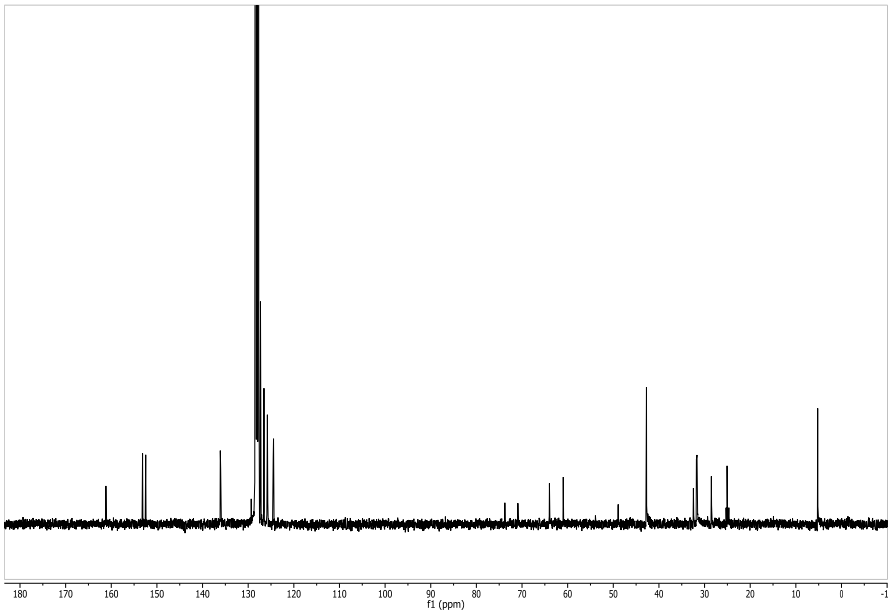

Figure S 3 a.) ^{1}H NMR spectrum b.) ^{13}C NMR spectrum of catalyst (ONOO)^{CMe2Ph}Y($CH_2Si(CH_3)_3$)(thf) in C_6D_6.

a.)

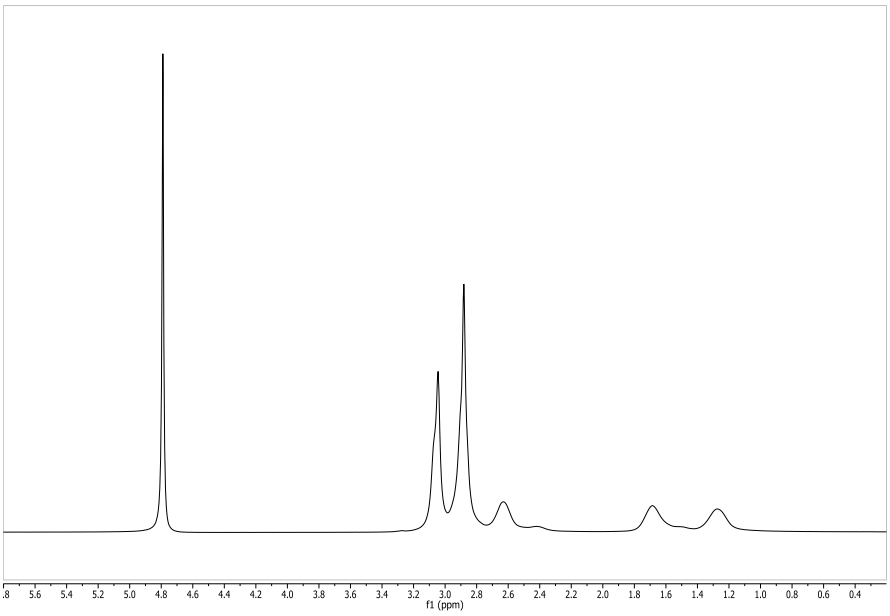

b.)

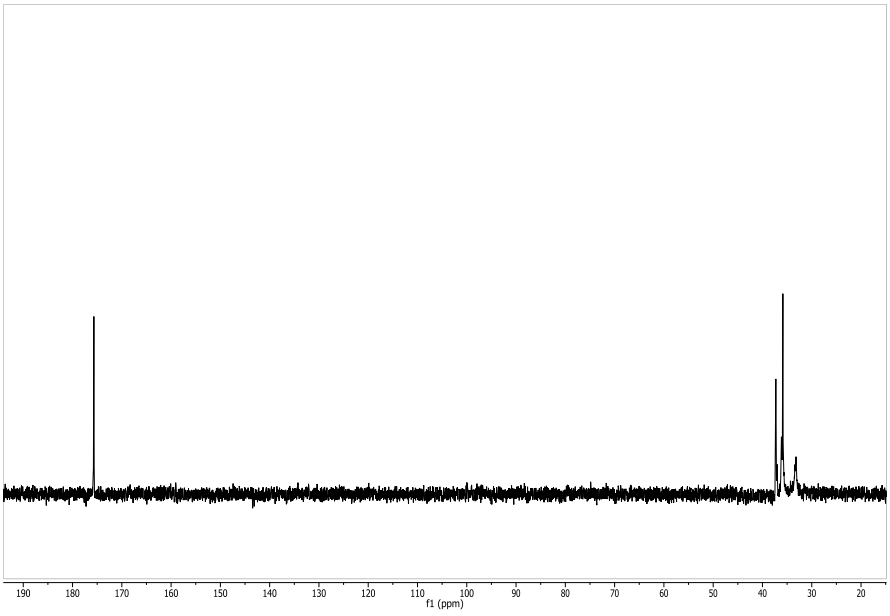

Figure S 4 ^{1}H a.) and ^{13}C b.) NMR spectra of PDMAA in D_2O.

a.)

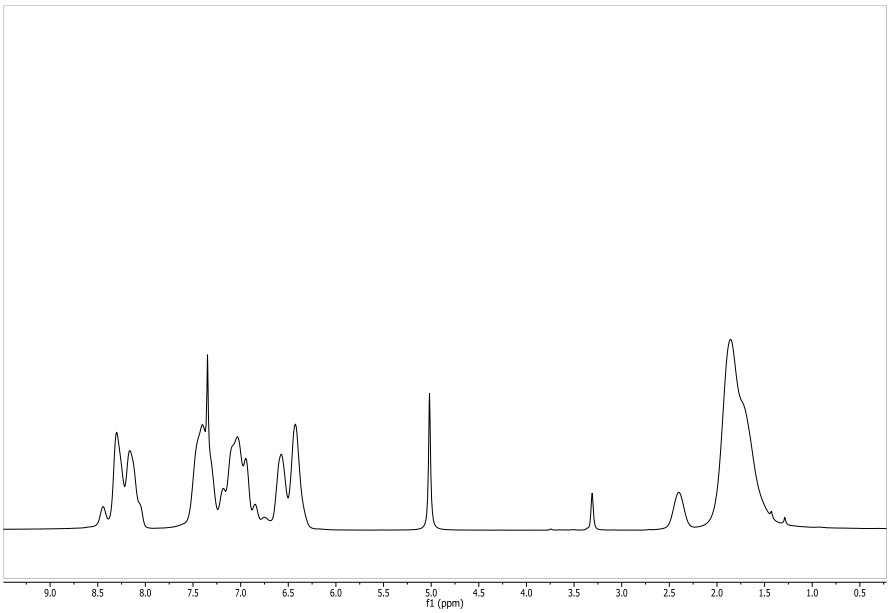

b.)

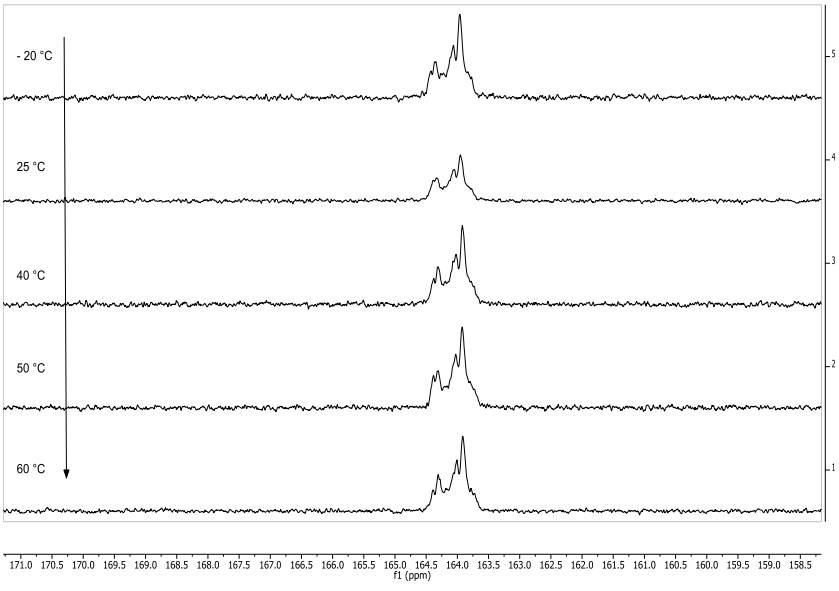

Figure S 5 a.) ^{1}H NMR P2VP b.) Polymer samples synthesized at different temperatures. Aromatic quaternary ^{13}C NMR resonances of P2VP in $CDCl_3$ measured at 25 °C.[1]

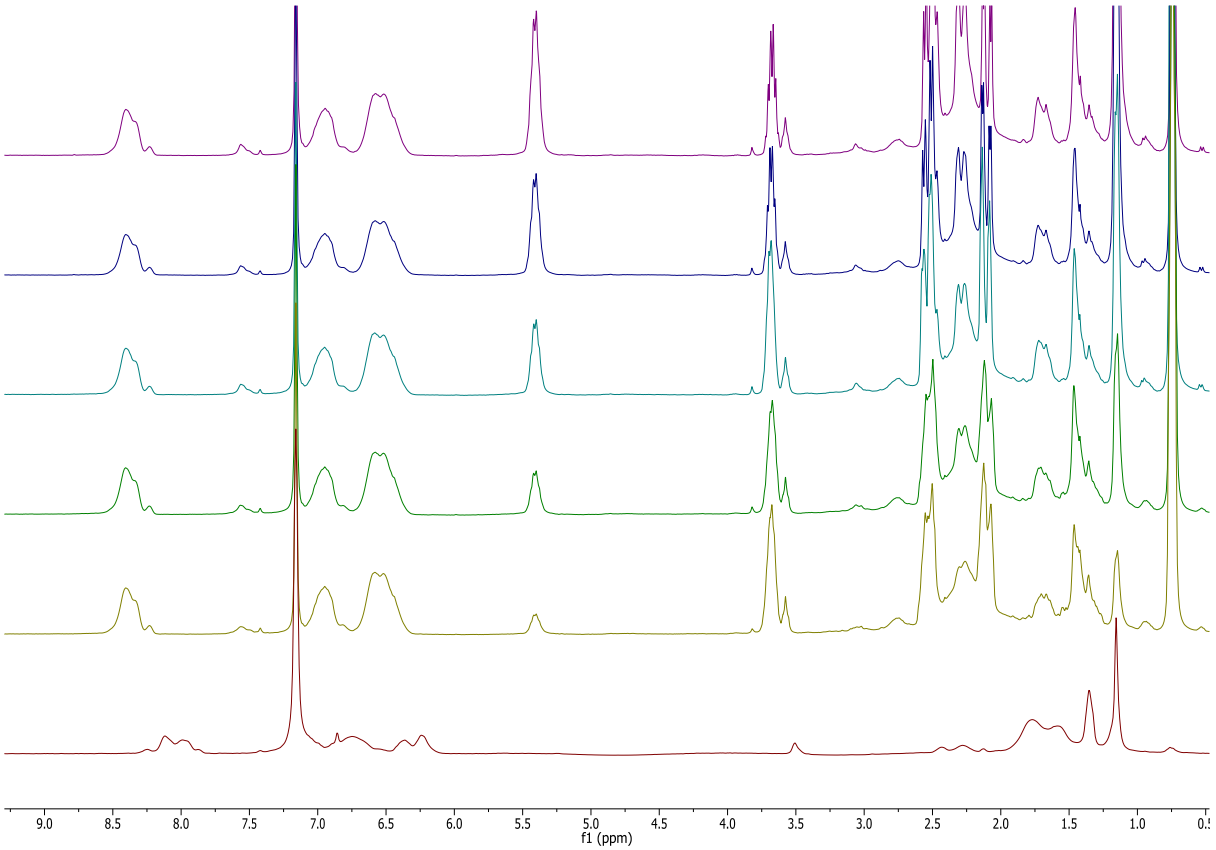

Figure S 6 ^{1}H NMR experiment with (ONOO)^{tBu}Y($CH_2Si(CH_3)_3$)(thf) (catalyst 13 µmol, 2VP 0.14 mmol, BL 0.14 mmol, C_6D_6 0.5 mL, T = 25 °C): Polymerization of monomer A (P2VP) and subsequent polymerization of monomer B (BL).

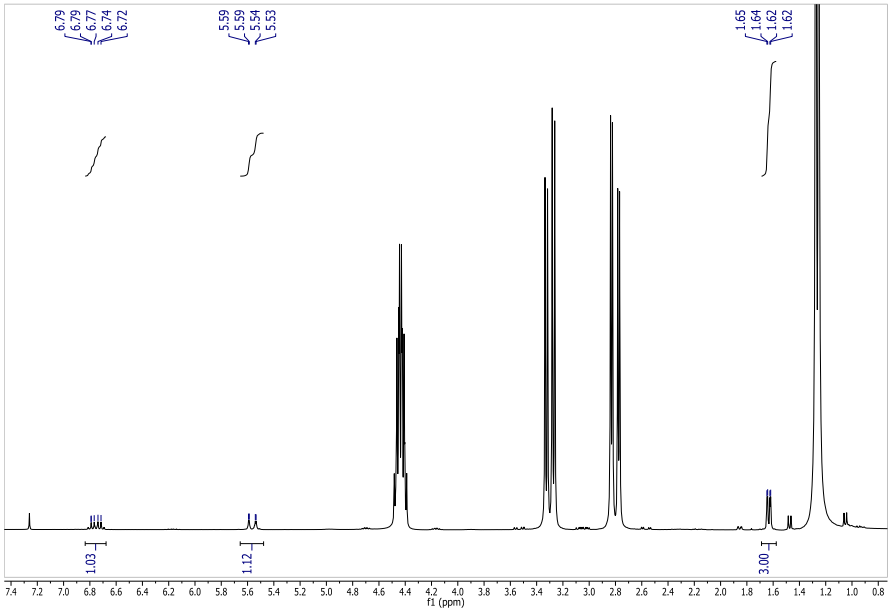

Figure S 7 ^{1}H NMR of BL with traces of crotonic acid in $CDCl_3$.

2.2 Kinetic Data

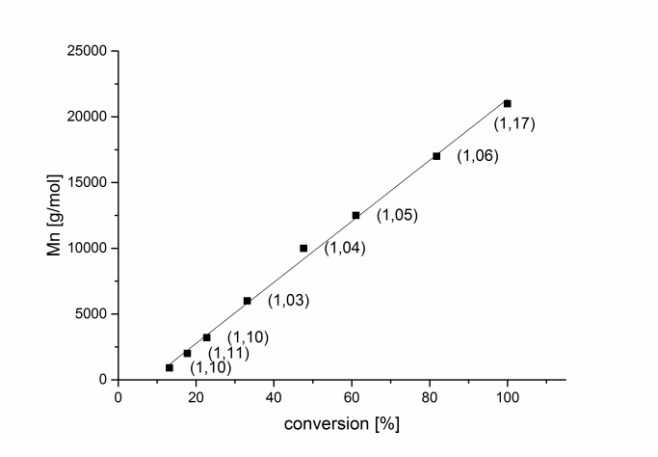

Figure S 8 Growth of the absolute molecular weight (M_n) determined by GPC-MALS as a function of monomer conversion (determined gravimetically), respective PDI values shown in brackets: catalyst 1, 135 µmol, IPOx 27 mmol, toluene 20 mL, 25 °C.

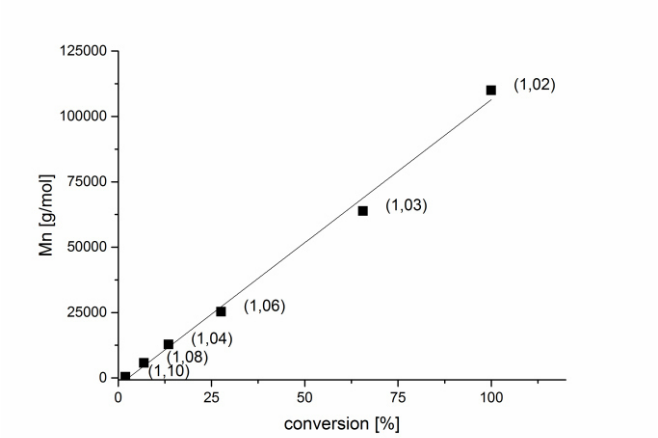

Figure S 9 Growth of the absolute molecular weight (M_n) determined by GPC-MALS as a function of monomer conversion (determined gravimetically), respective PDI values shown in brackets: catalyst 1, 43 µmol, 2VP 27 mmol, toluene 20 mL, 25 °C.

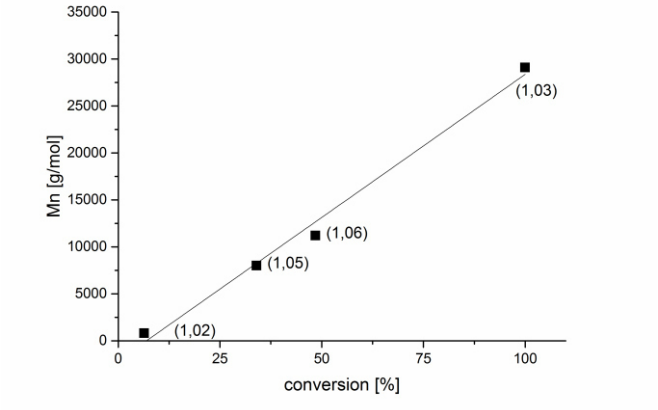

Figure S 10 Growth of the absolute molecular weight (M_n) determined by GPC-MALS as a function of monomer conversion (determined gravimetically), respective PDI values shown in brackets: catalyst 2, 43 µmol, 2VP 135 mmol, toluene 20 mL, 25 °C.

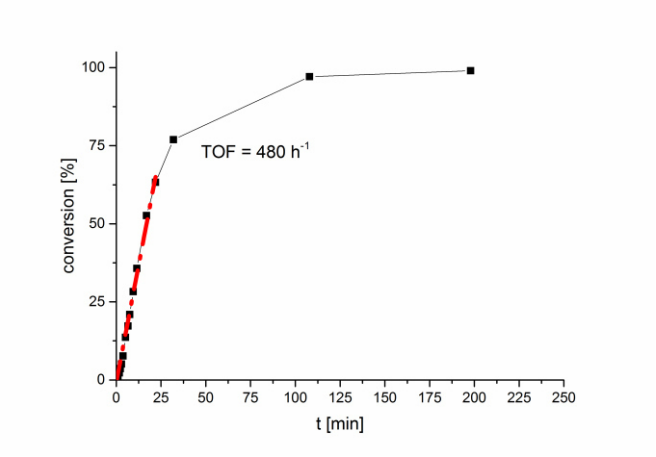

Figure S 11 Determination of catalytic activity of (ONOO)^{tBu}Y($CH_2Si(CH_3)_3$)(thf) (catalyst 135 µmol, DEVP 27 mmol, toluene 20 mL, T = 25 °C).

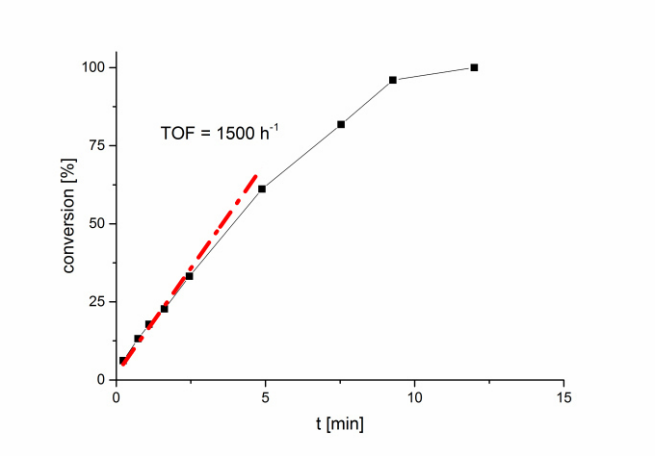

Figure S 12 Determination of catalytic activity of (ONOO)^{tBu}Y($CH_2Si(CH_3)_3$)(thf) (catalyst 135 µmol, IPOx 27 mmol, toluene 20 mL, T = 25 °C).

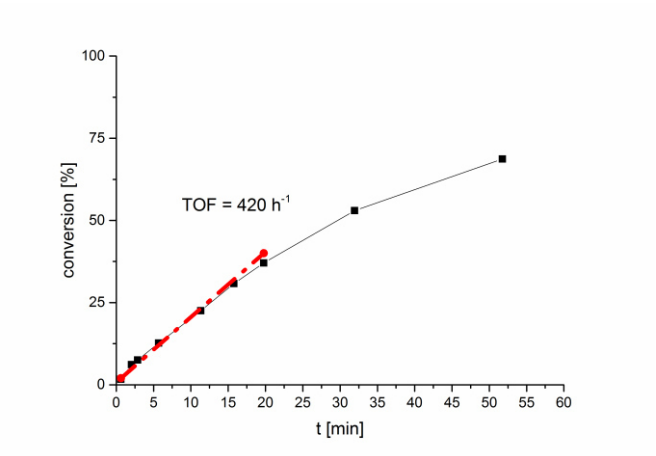

Figure S 13 Determination of catalytic activity of (ONOO)^{tBu}Y($CH_2Si(CH_3)_3$)(thf) (catalyst 43 µmol, 2VP 27 mmol, toluene 20 mL, T = 25 °C).

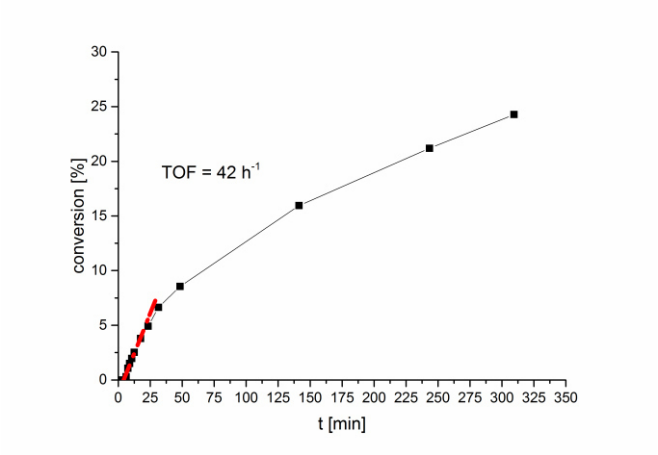

Figure S 14 Determination of catalytic activity of (ONOO)^{tBu}Y(CH$_2$Si(CH$_3$)$_3$)(thf) (catalyst 135 µmol, DIVP 27 mmol, toluene 20 mL, T = 25 °C).

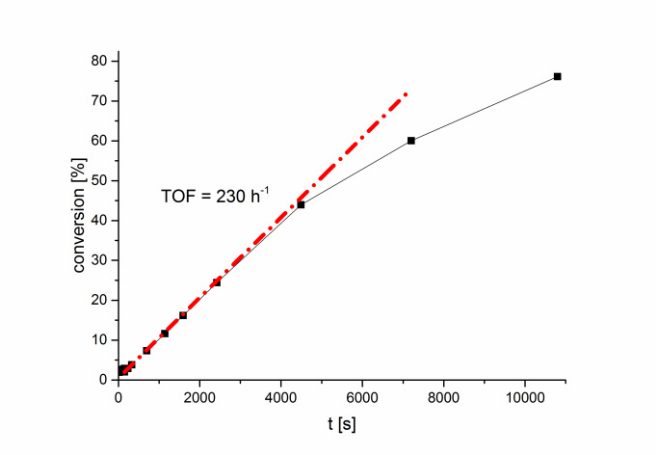

Figure S 15 Determination of catalytic activity of (ONOO)^{CMe2Ph}Y(CH$_2$Si(CH$_3$)$_3$)(thf) (catalyst 43 µmol, 2VP 27 mmol, toluene 20 mL, T = 25 °C).

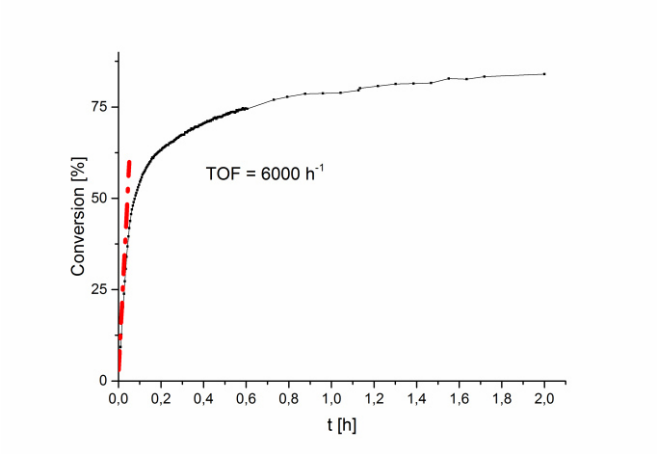

Figure S 16 Determination of catalytic activity of (ONOO)^{tBu}Y(CH$_2$Si(CH$_3$)$_3$)(thf) (catalyst 14.3 µmol, BL 9 mmol, dichloromethane 5 mL, T = 25 °C).

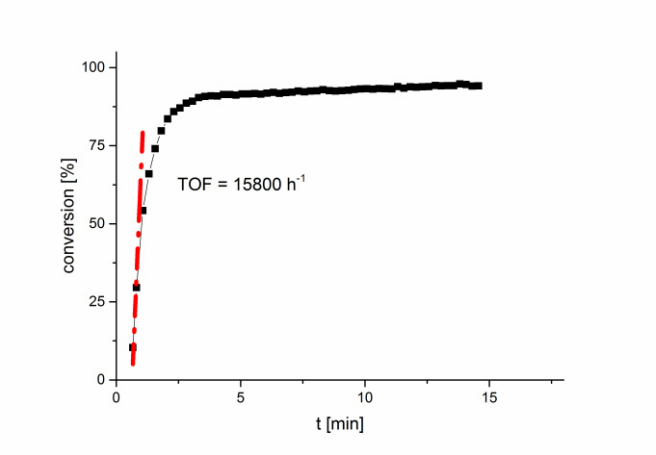

Figure S 17 Determination of catalytic activity of (ONOO)^{CMe2Ph}Y($CH_2Si(CH_3)_3$)(thf) (catalyst 14.3 µmol, BL 9 mmol, dichloromethane 5 mL, T = 25 °C).

2.3 Endgroup Analysis

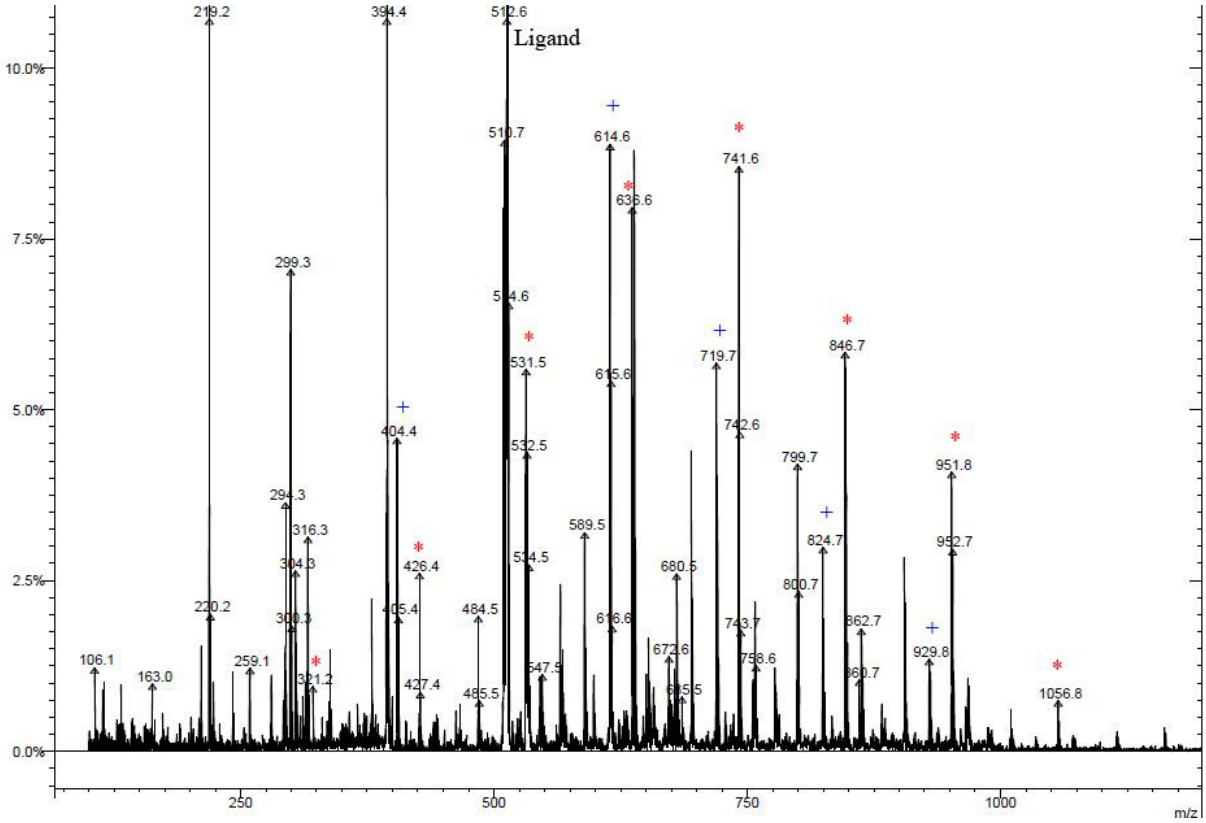

Figure S 18 Endgroup analysis ESI-MS measured in *i*PrOH; Catalyst 1 (40 µmol of catalyst, 0.4 mmol 2VP, 0.5 mL C_6D_6, 20 °C): (*) [(n x M) + (CH_2TMS) + (Na)]$^+$ (+) [(n x M) + (CH_2TMS) + H]$^+$.

2.4 LCST (Lower critical solution temperature)

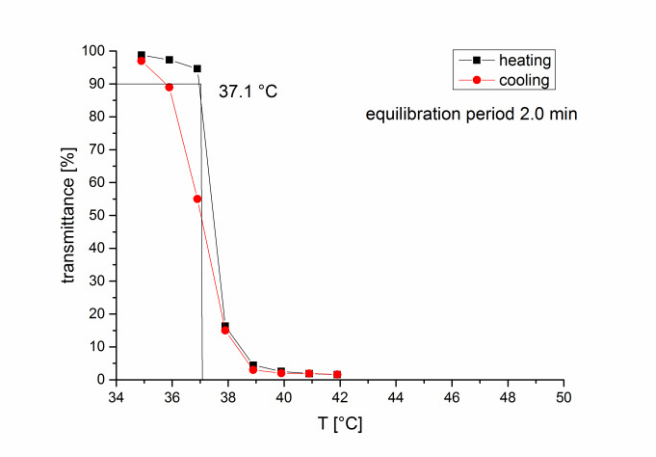

Figure S 19 Determination of the cloud point (lower critical solution temperature, LCST) of P2VP homopolymer. The cloud point was determined at 10 % decrease of transmittance for a 5.0 wt % dest. H_2O:THF =1:1, $M_n = 2.2x10^4$ g/mol, PDI = 1.01.

2.5 Eyring-Plot Data

Table S 1 Eyring plot for (ONOO)^{tBu}Y($CH_2Si(CH_3)_3$)(thf) initiated 2VP (catalyst 42 µmol, 2VP 8.6 mmol, toluene 5.5 mL, temperature 298 – 331 K).

T [K]	$v_{initial}$ [mol/L]	c(Mon) [mol/L]	n(Mon) [mol]	k (L/mols)	ln(k/T)	1/T
313	0,00215641	1,177845	0,008560015	0,31321527	-6,907067763	0,00319489
298	0,00043782	1,177845	0,008560015	0,06359269	-8,452350272	0,0033557
298	0,00046452	1,177845	0,008560015	0,06747082	-8,393153525	0,0033557
323	0,00557182	1,177845	0,008560015	0,80929836	-5,989239946	0,00309598
308	0,0014717	1,177845	0,008560015	0,21376218	-7,272990962	0,00324675
331	0,00997805	1,177845	0,008560015	1,44929656	-5,431040069	0,00302115

Table S 2 Eyring plot for (ONOO)^{CMe2Ph}Y($CH_2Si(CH_3)_3$)(thf) initiated 2VP (catalyst 42 µmol, 2VP 8.6 mmol, toluene 5.5 mL, temperature 303 – 333 K.

T [K]	$v_{initial}$ [mmol/mL]	c(Mon) [mol/L]	n(Mon) [mol]	k (L/mols)	ln(k/T)	1/T
333	0,00774761	1,177845	0,008560015	1,11611147	-5,698291743	0,003003
313	0,00108568	1,177845	0,008560015	0,15640177	-7,601530334	0,00319489
323	0,00198724	1,177845	0,008560015	0,28627943	-7,028439244	0,00309598
303	0,00026055	1,177845	0,008560015	0,03753452	-8,996226965	0,00330033
341	0,01309903	1,177845	0,008560015	1,88703067	-5,196877958	0,00293255

2.6 Thermogravimetric analysis (TGA) and Differential scanning calorimetry (DSC)

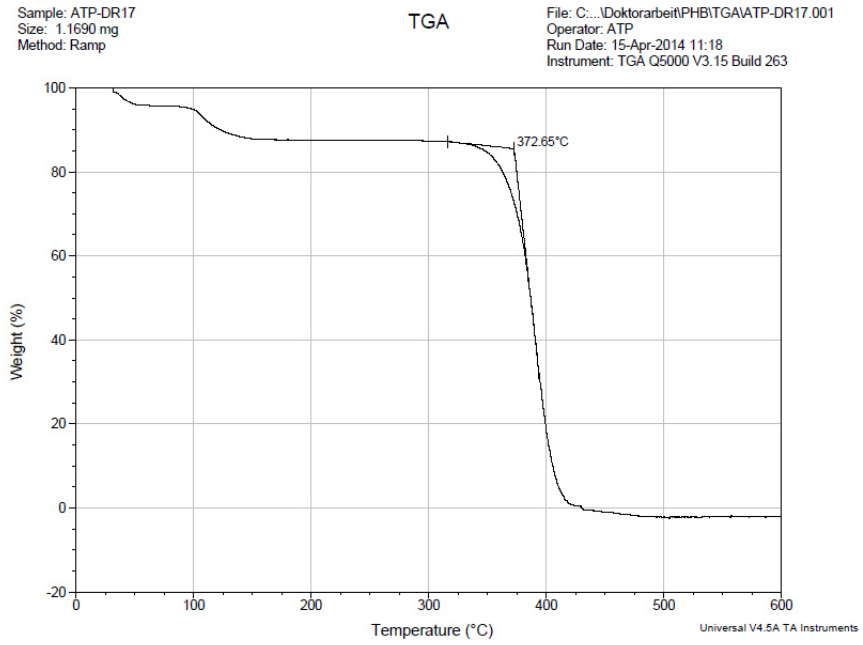

Figure S 20 TGA thermogram for P2VP reported in table 2, entry 2

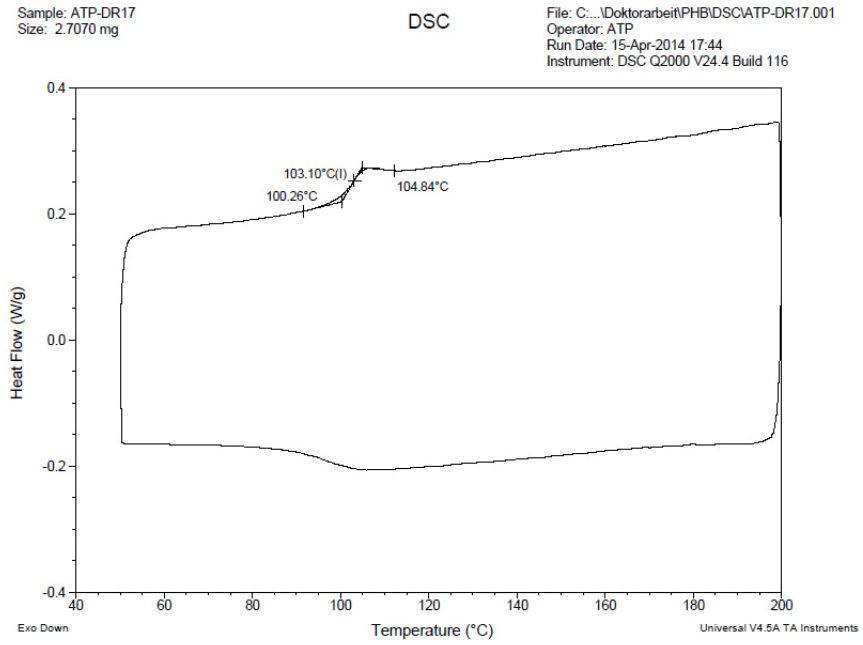

Figure S 21 DSC thermogram for P2VP reported in table 2, entry 2.

2.7 Gel-permeation chromatography (GPC) Data

2.7.1 Homopolymerization

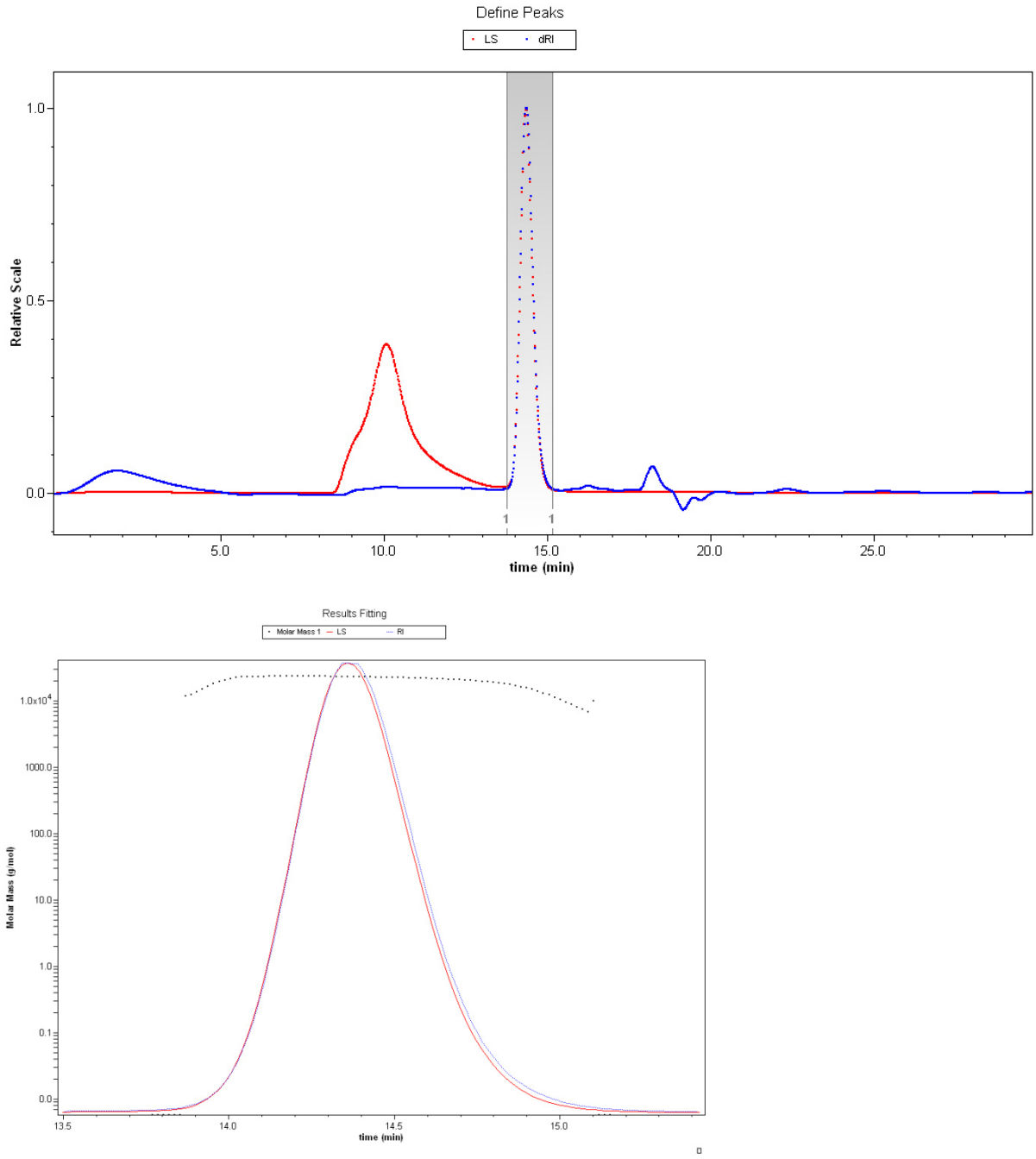

Figure S 22 REM-GTP (2VP), table 1, entry 1, conversion 99%.

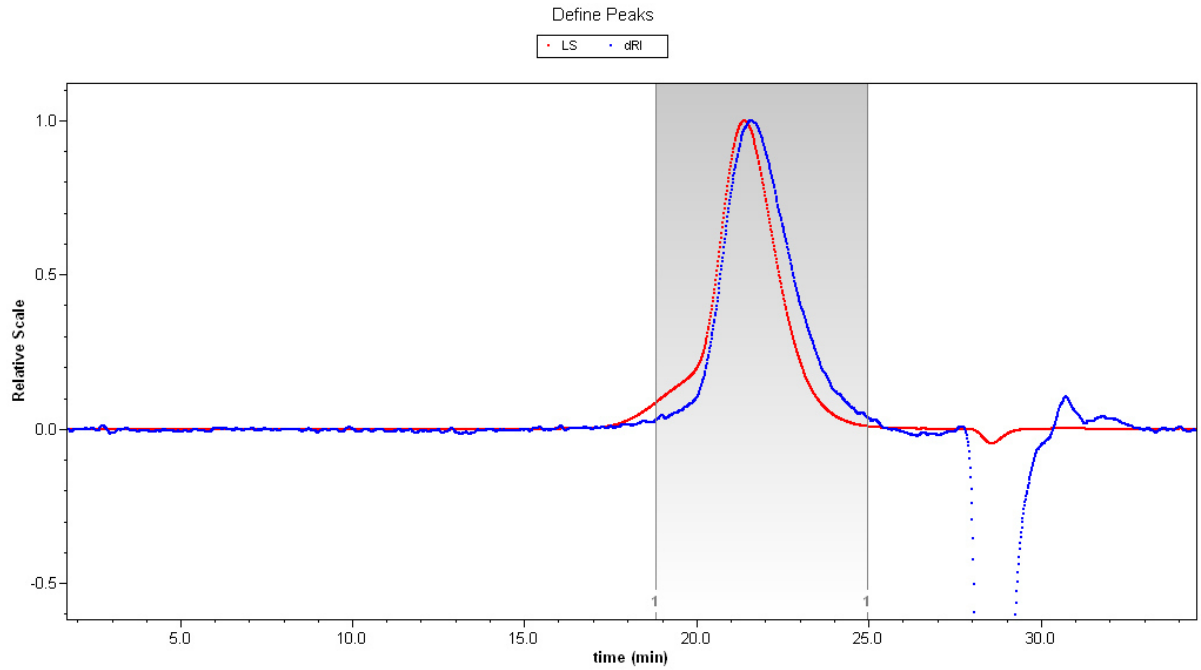

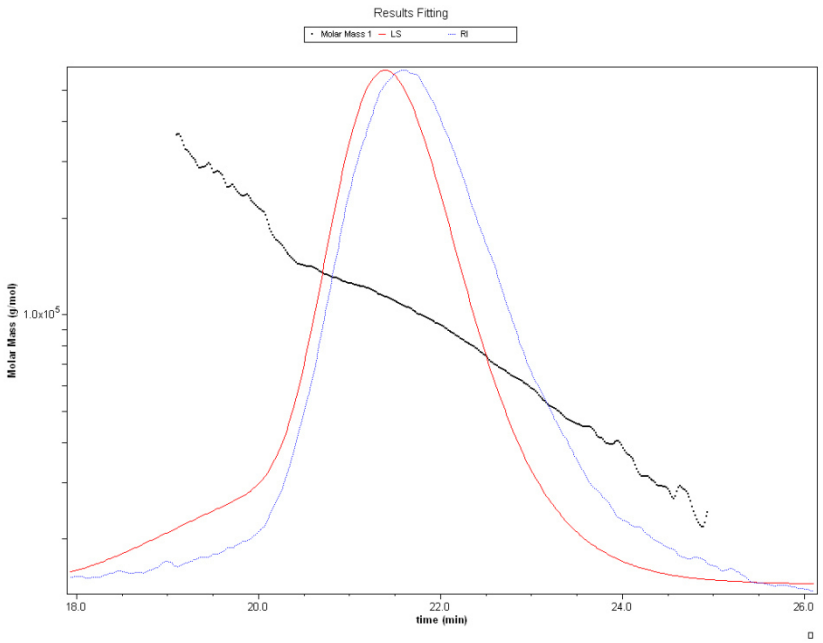

Figure S 23 REM-GTP (DEVP), table 1, entry 2, conversion 99%.

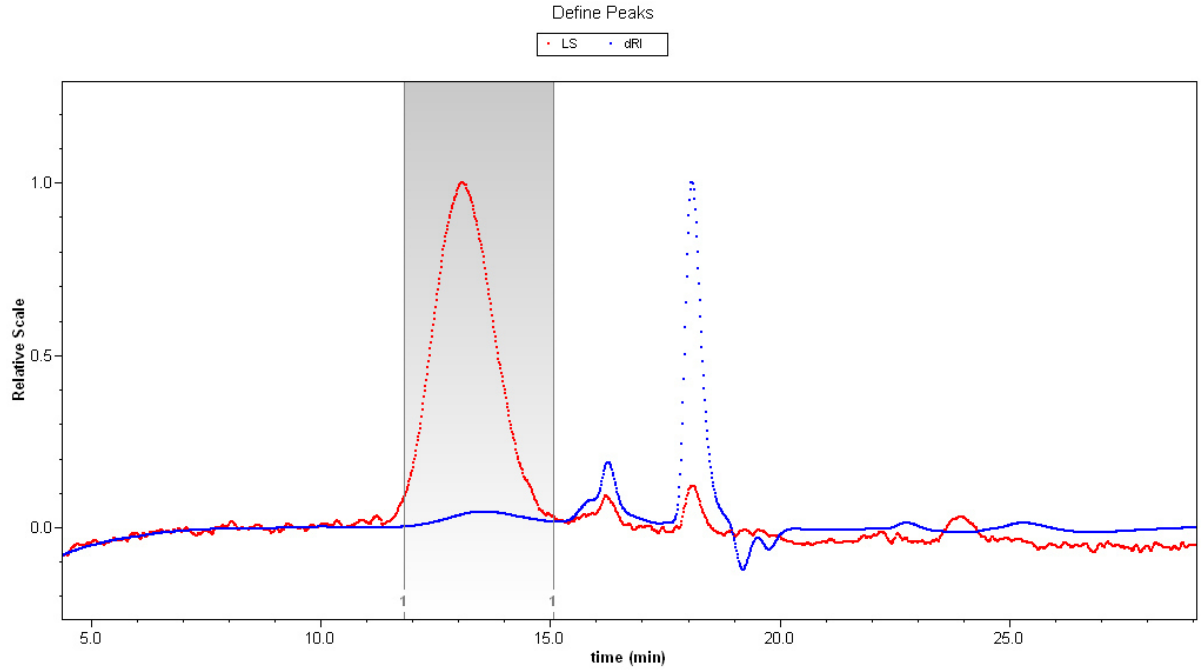

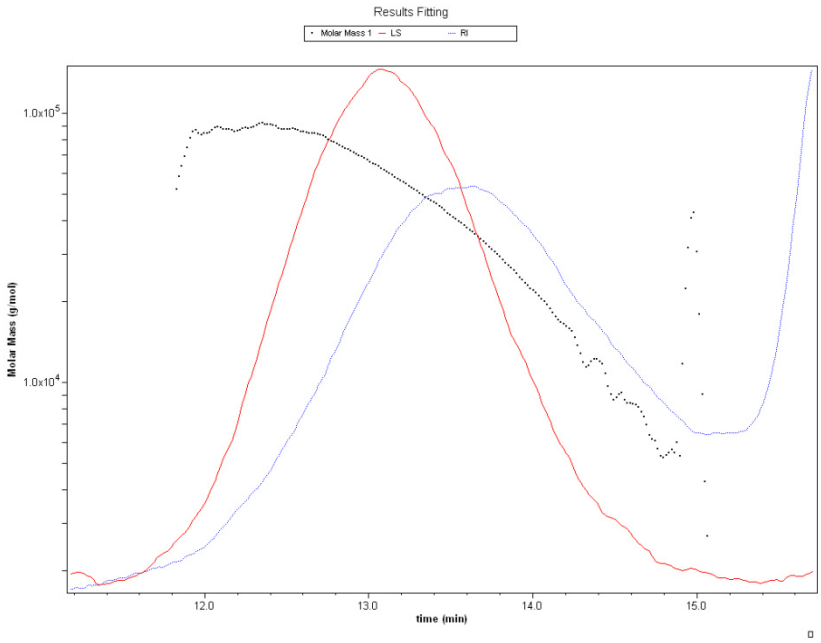

Figure S 24 REM-GTP (DIVP), table 1, entry 3, conversion 25%.

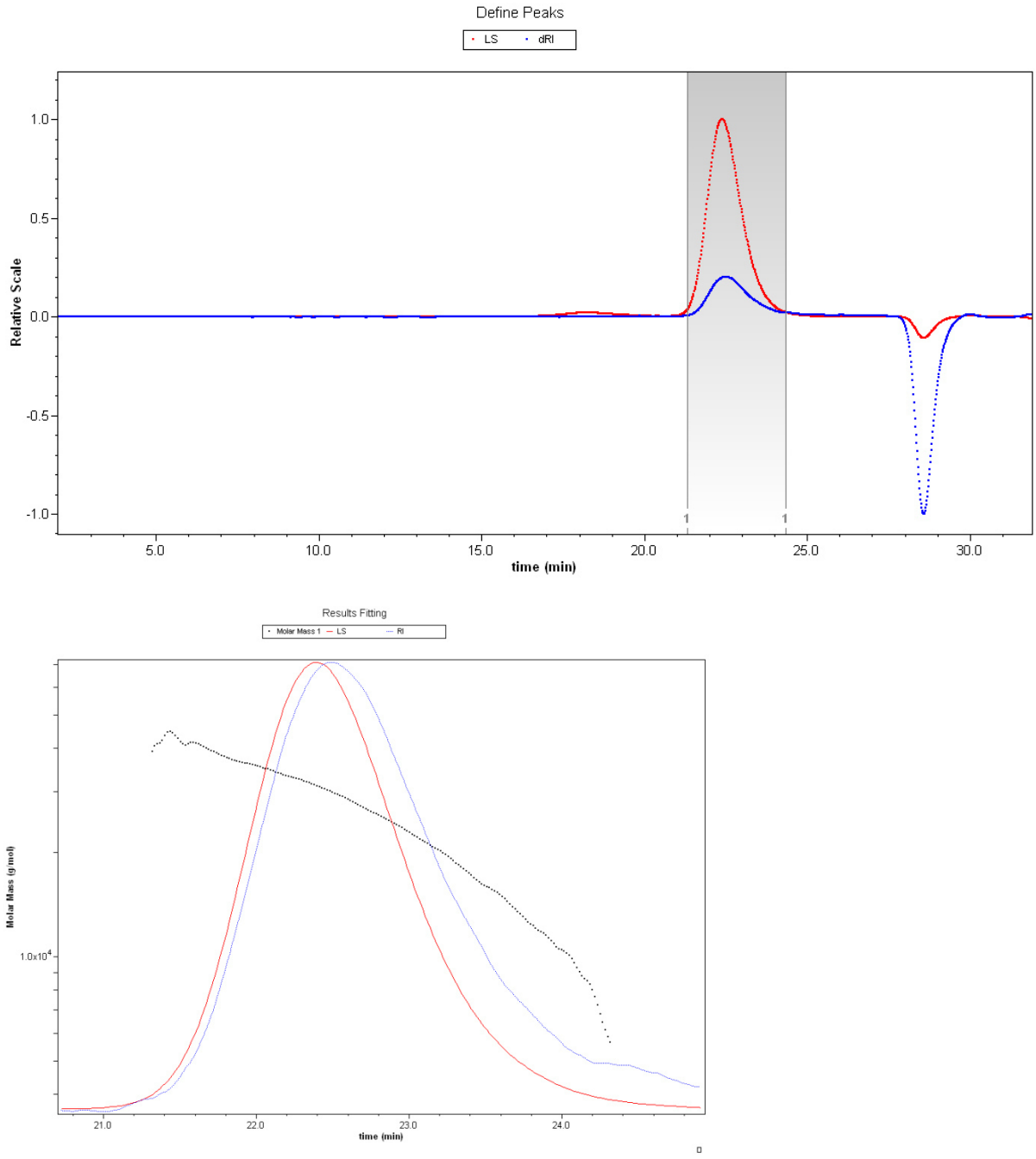

Figure S 25 REM-GTP (IPOx), table 1, entry 4, conversion 99%.

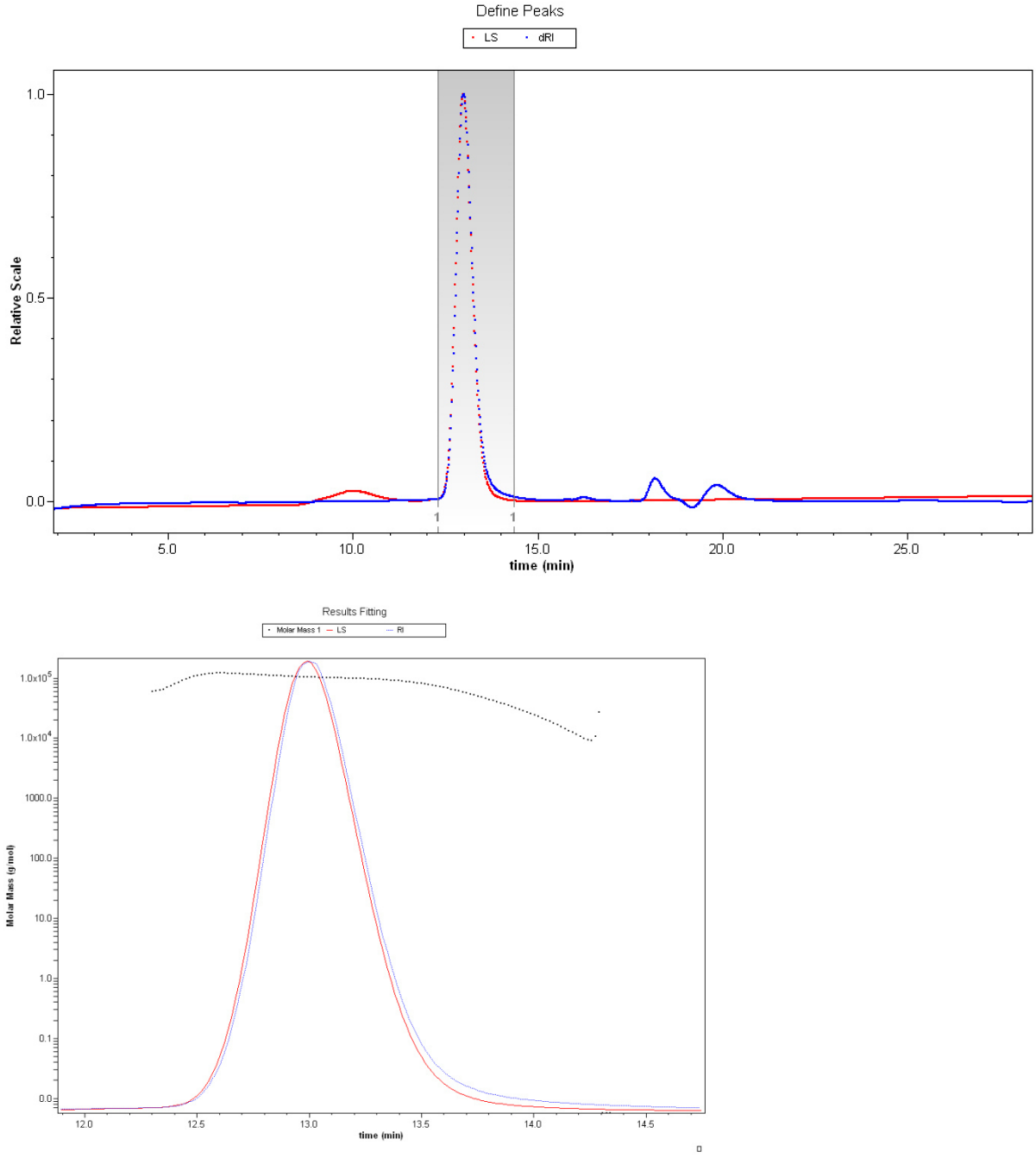

Figure S 26 REM-GTP (2VP), table 1, entry 5, conversion 99%.

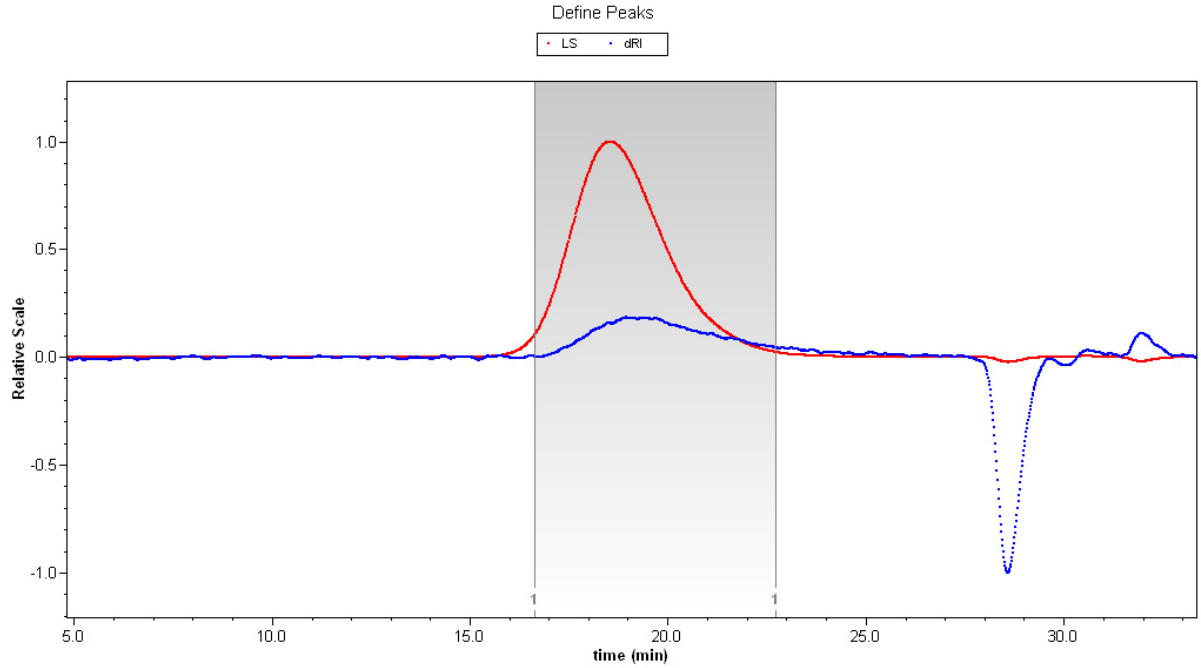

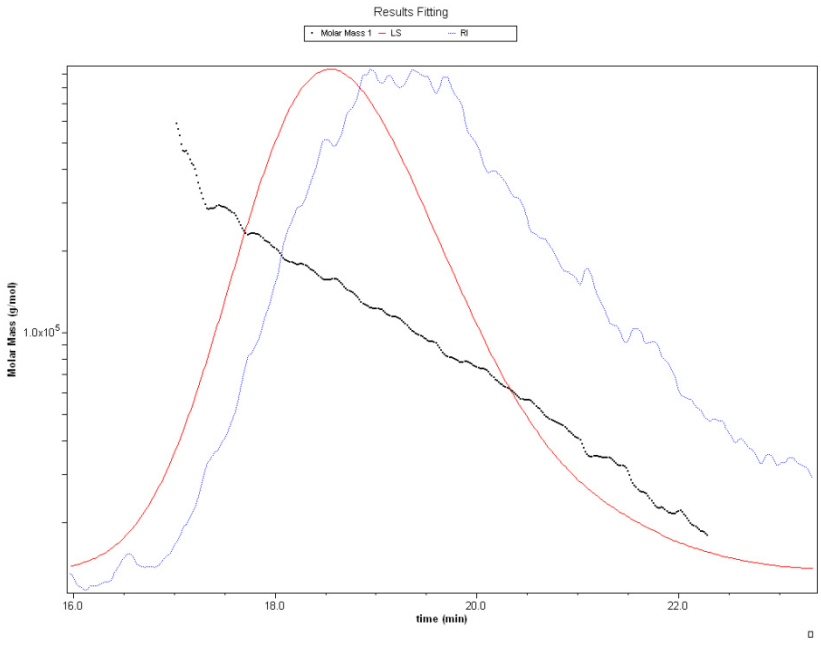

Figure S 27 REM-GTP (DMAA), table 1, entry 6, conversion 99%.

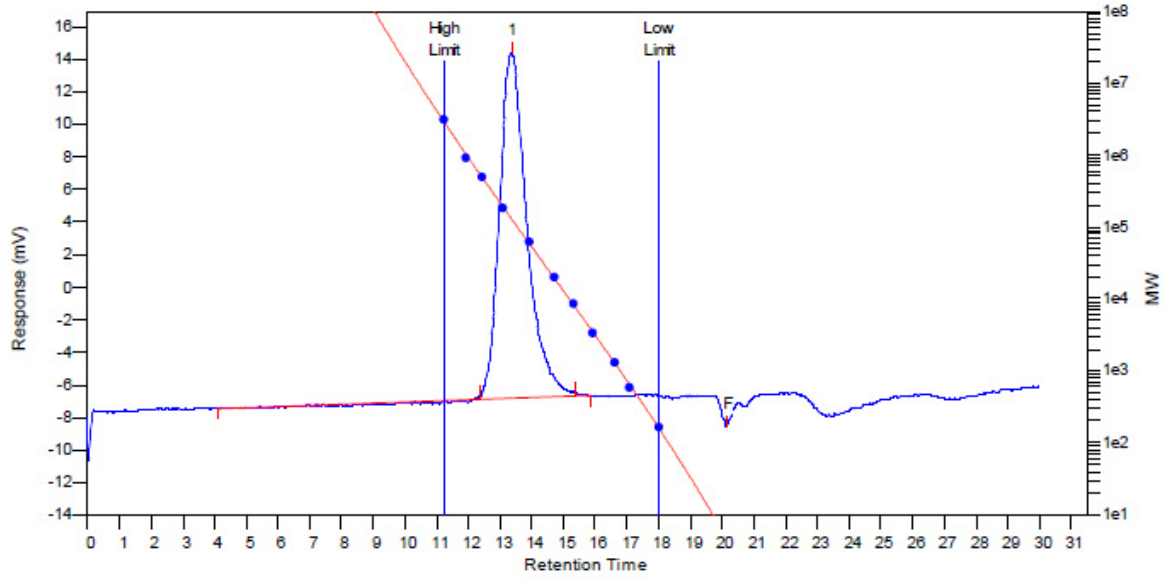

MW Averages

Peak No	Mp	Mn	Mw	Mz	Mz+1	Mv	PD
1	129276	85510	130306	173311	216079	124085	1.52387
2	0	0	0	0	0	0	0

Figure S 28 ROP (BL), table 1, entry 7, conversion 89%.

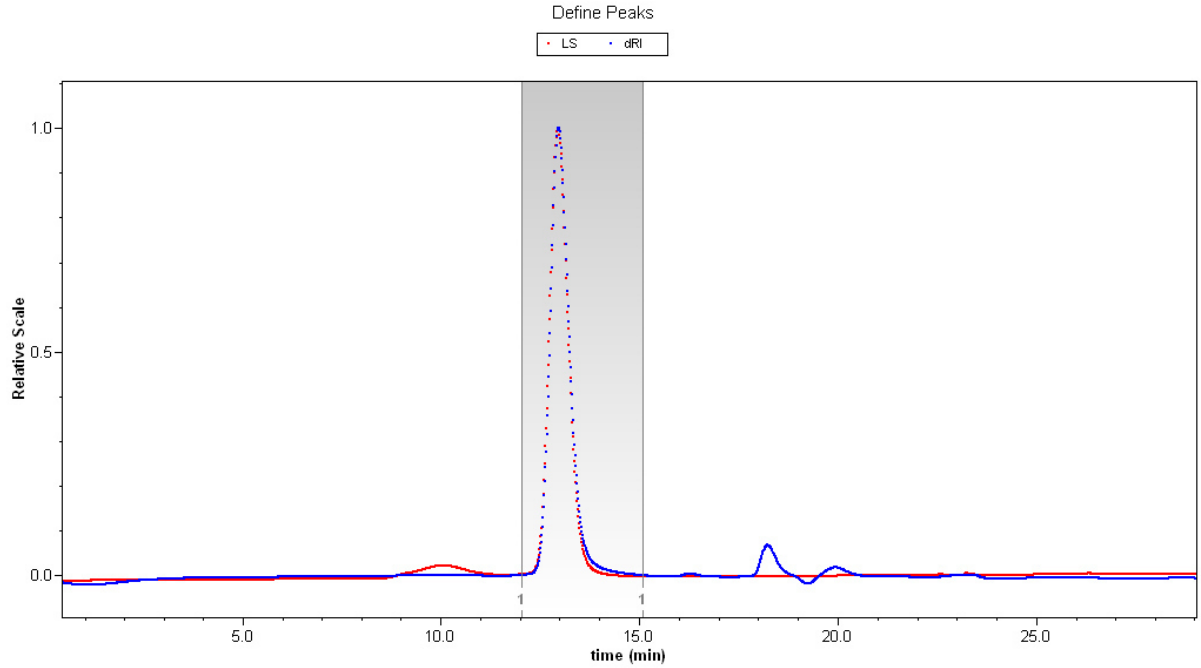

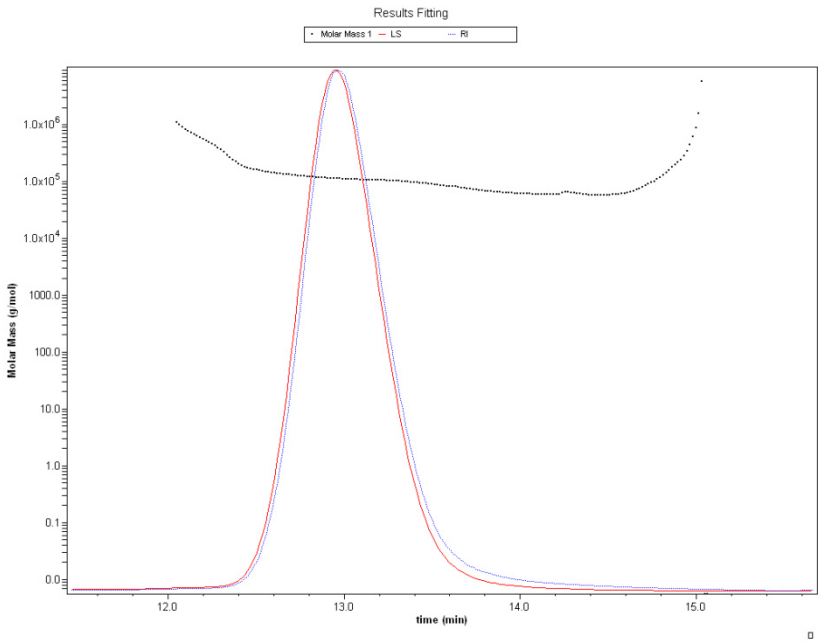

Figure S 29 REM-GTP (2VP), table 2, entry 1, conversion 99%.

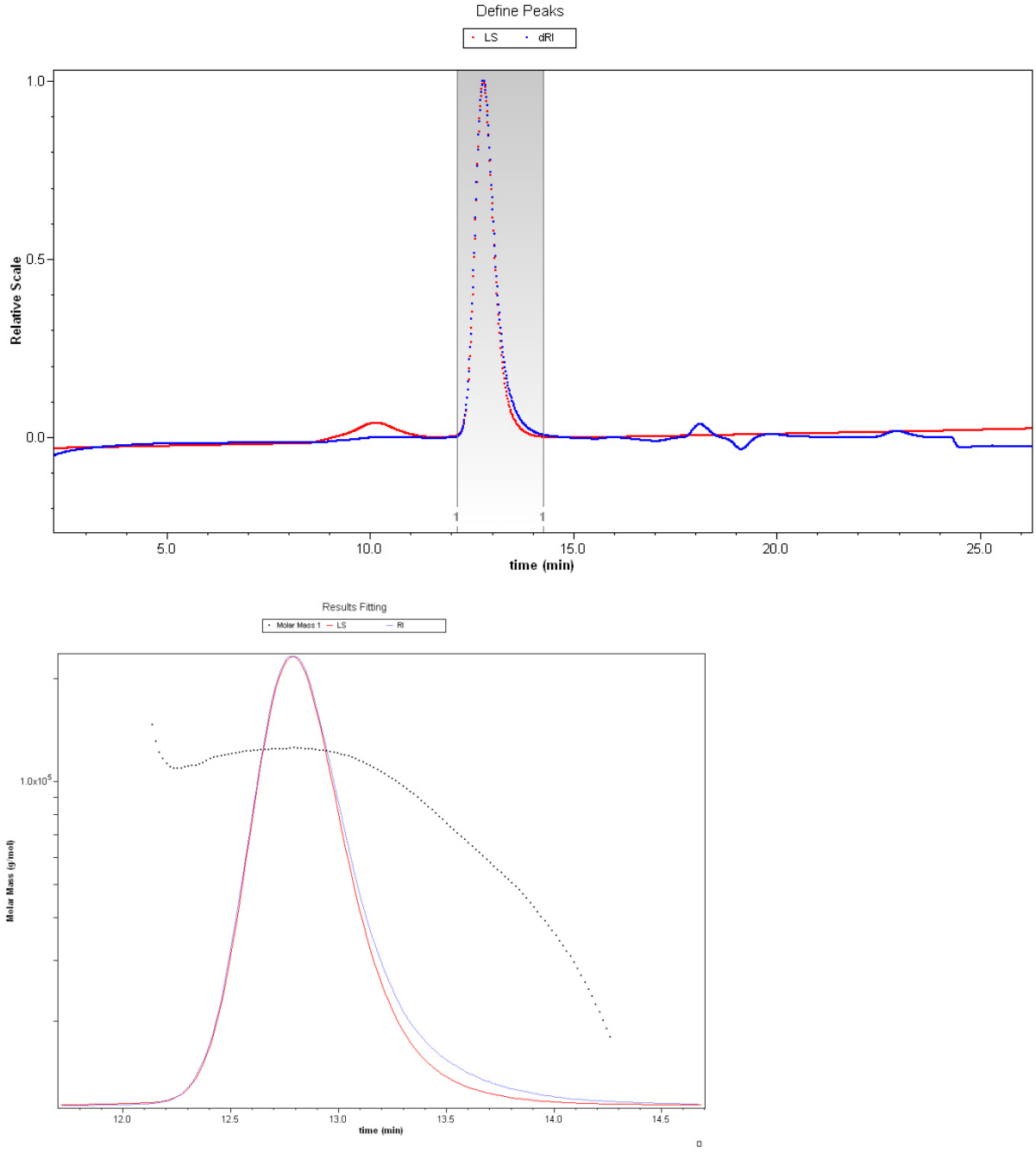

Figure S 30 REM-GTP (2VP), table 2, entry 2, conversion 82%.

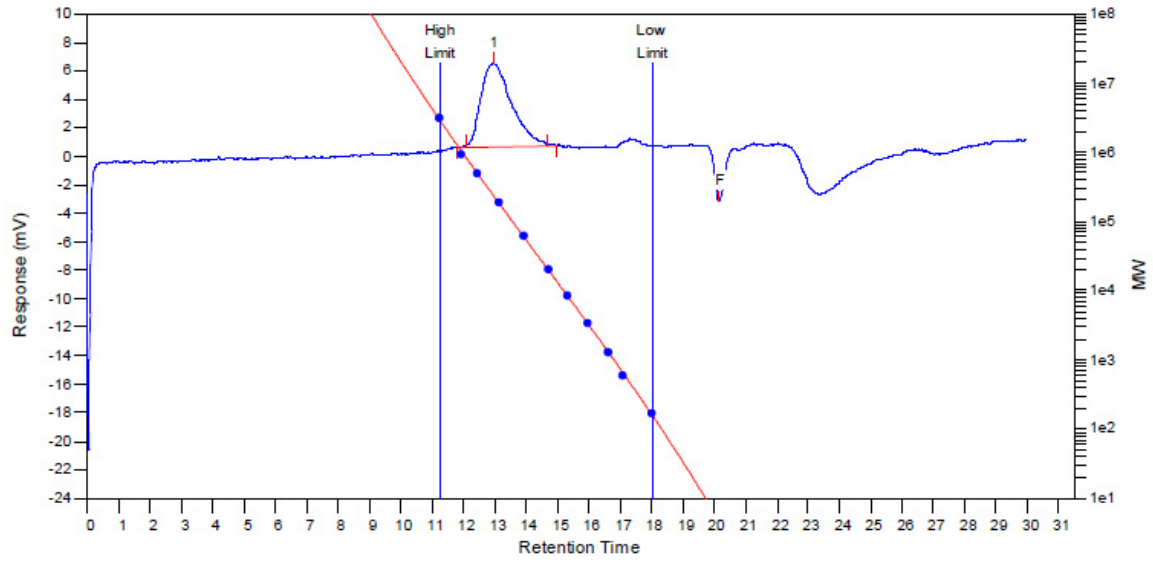

MW Averages

Peak No	Mp	Mn	Mw	Mz	Mz+1	Mv	PD
1	232020	141585	222664	303406	374741	210730	1.57265
2	0	0	0	0	0	0	0

Figure S 31 ROP (BL), table 2, entry 3, conversion 99%.

2.7.2 Block copolymerization

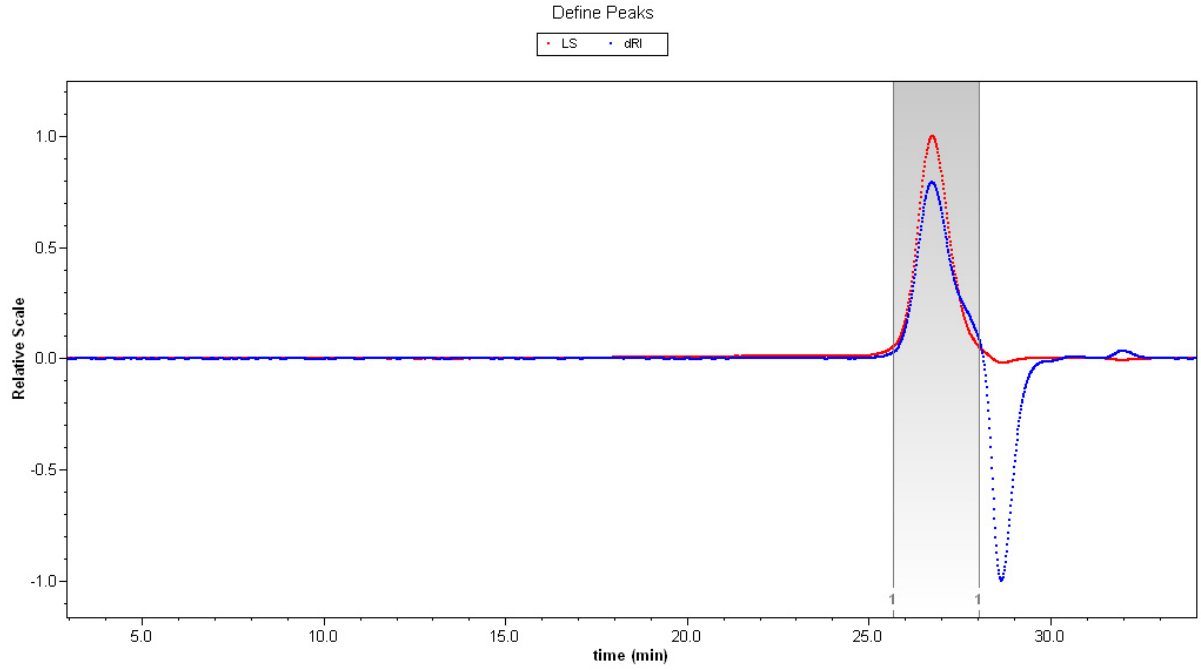

Figure S 32 REM-GTP (P2VP-b-PDEVP), table 4, entry 1.

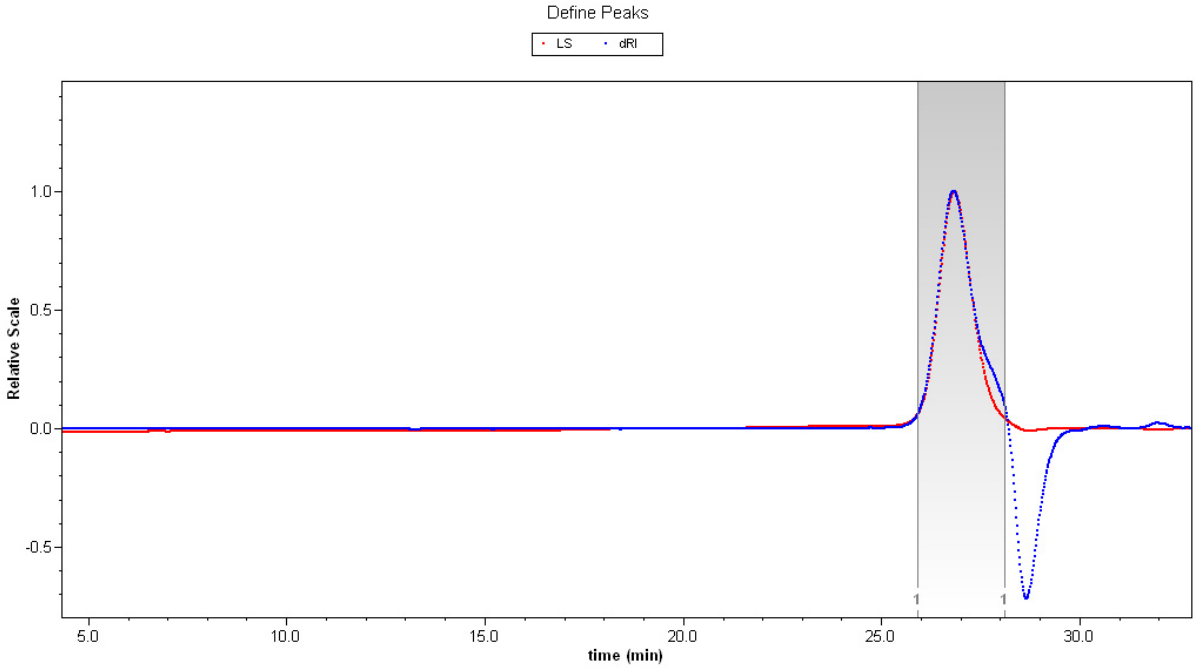

Figure S 33 REM-GTP (P2VP), table 4, entry 2 (aliquot sample).

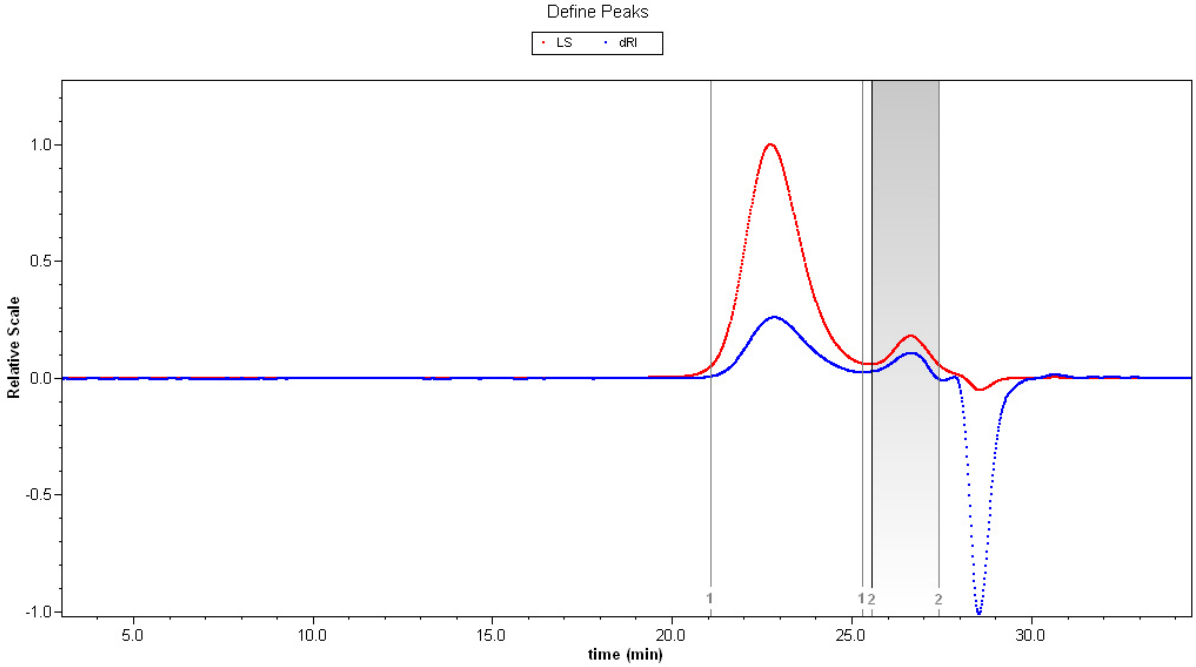

Figure S 34 REM-GTP (P2VP-b-PIPOx), table 4, entry 2.

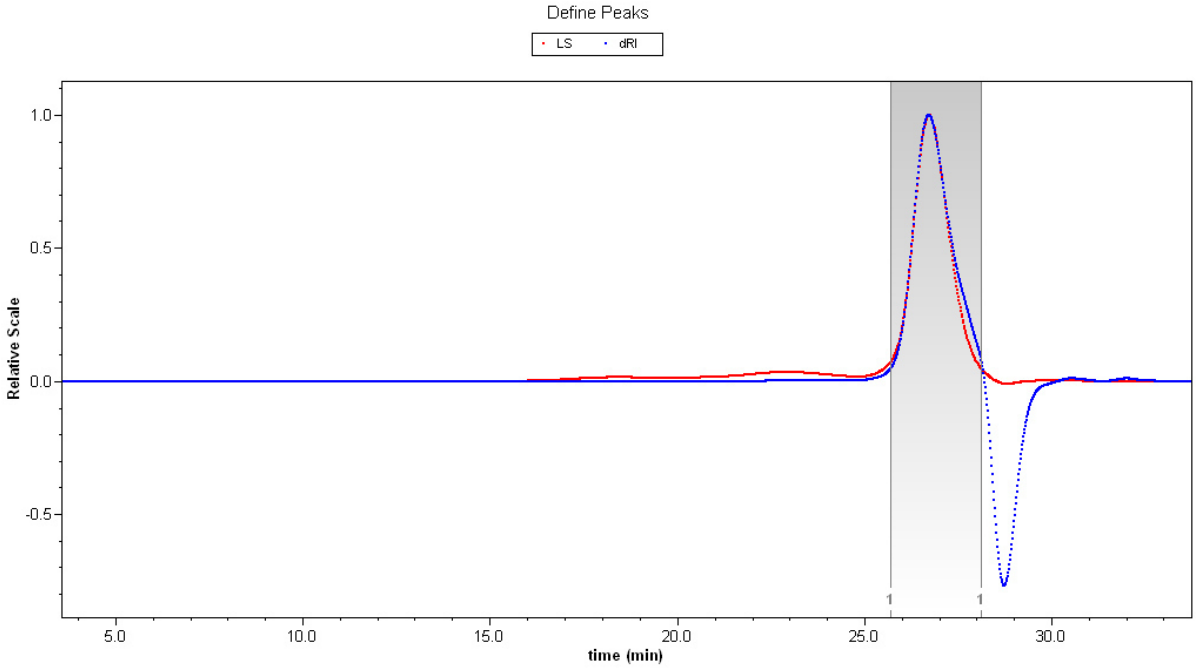

Figure S 35 REM-GTP (P2VP), table 4, entry 3 (aliquot sample).

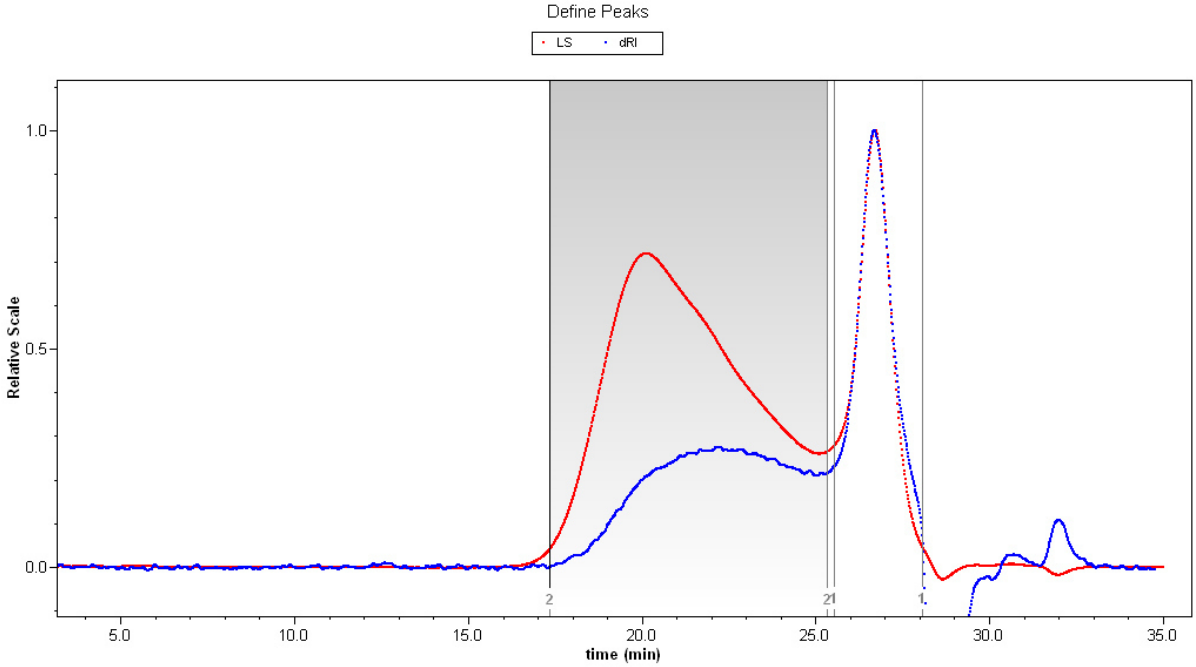

Figure S 36 REM-GTP (P2VP-b-PDMAA), table 4, entry 3.

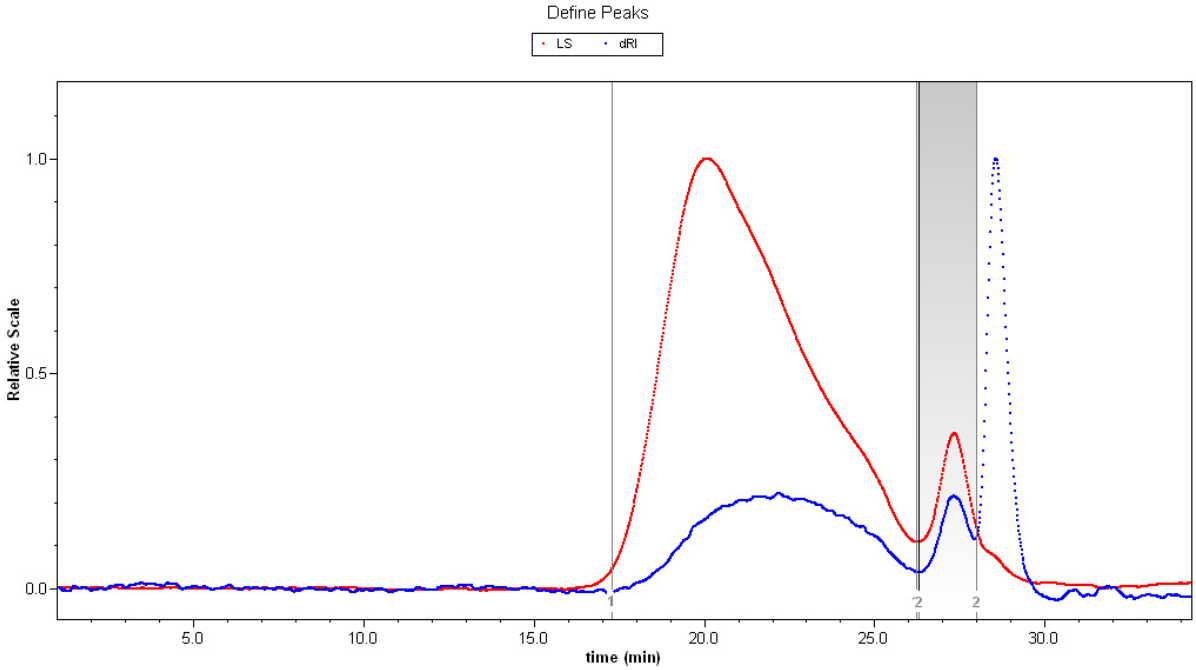

Figure S 37 REM-GTP (P2VP-b-PDMAA), table 4, entry 3: 2 hours washing with toluene.

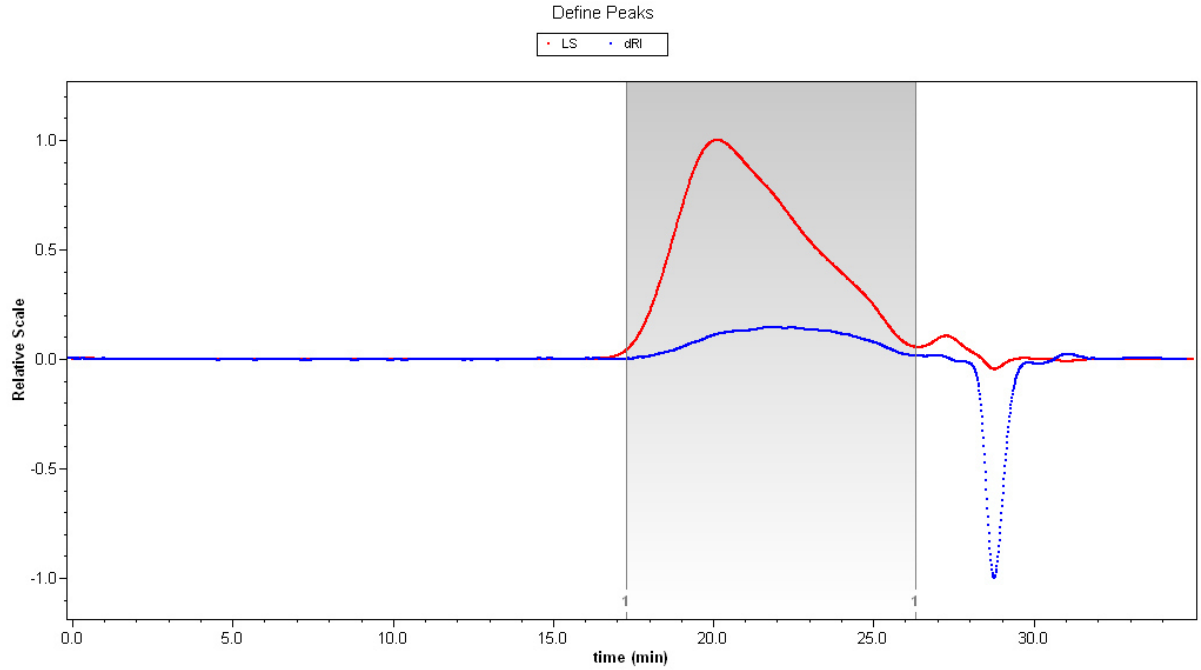

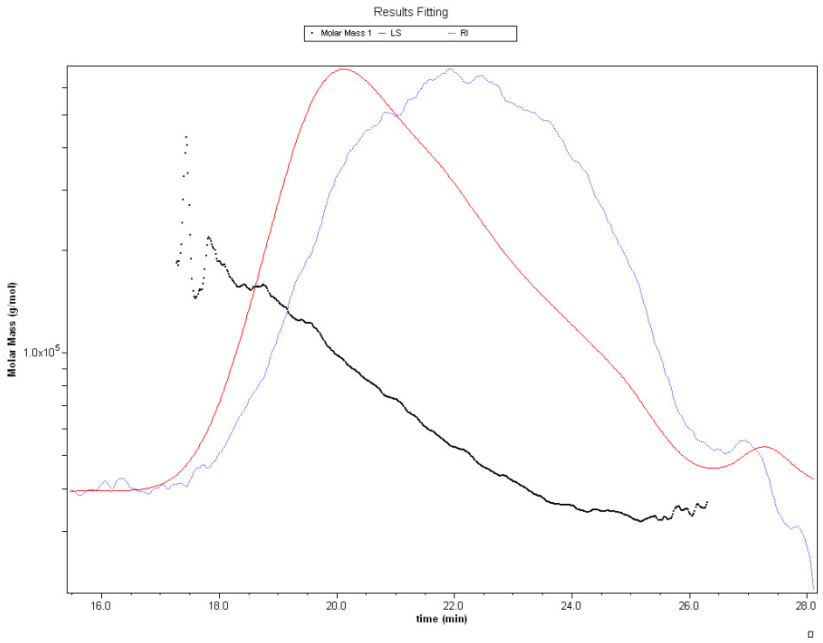

Figure S 38 REM-GTP (P2VP-b-PDMAA), table 4, entry 3: 48 hours washing with toluene.

1. Dimov, D. K.; Hogen-Esch, T. E. *Macromolecules* **1995,** 28, (22), 7394-400.

4.9 Catalytic Precision Polymerization: Rare Earth Metal-Mediated Synthesis of Homopolymers, Block Copolymers, and Polymer Brushes

Status: Published online: August 22, 2014

Journal: Macromolecular Chemistry and Physics

Volume 215, issue 20, pages 1946–1962

Publisher: Wiley

Article Type: Review

DOI: 10.1002/macp.201400271

Authors: Benedikt S. Soller, Ning Zhang, and Bernhard Rieger

4.9.1 Abstract

This review summarizes selected literature references on the precise synthesis of homopolymers, block copolymers, and polymer brushes using RE complexes and especially focusses on the work of Yasuda for the synthesis of block copolymers and Teuben and Marks for the end-group functionalization of polyolefins. The work of Rieger et al. is presented in detail for the synthesis of polymer brushes and the mechanistic insights on vinylphosphonate REM-GTP.

The first author Benedikt S. Soller was supervised by the corresponding authors Prof. Ning Zhang and Prof. Bernhard Rieger and supported in writing the manuscript.

Title: Catalytic Precision Polymerization: Rare Earth Metal-Mediated Synthesis of Homopolymers, Block Copolymers, and Polymer Brushes

Author: Benedikt S. Soller,Ning Zhang,Bernhard Rieger

Publication: Macromolecular Chemistry and Physics

Publisher: John Wiley and Sons

Date: Aug 22, 2014

Order Completed

Thank you for your order.

This Agreement between Benedikt Soller ("You") and John Wiley and Sons ("John Wiley and Sons") consists of your license details and the terms and conditions provided by John Wiley and Sons and Copyright Clearance Center.

Your confirmation email will contain your order number for future reference.

Get the printable license.

License Number	3873141042880
License date	May 20, 2016
Licensed Content Publisher	John Wiley and Sons
Licensed Content Publication	Macromolecular Chemistry and Physics
Licensed Content Title	Catalytic Precision Polymerization: Rare Earth Metal-Mediated Synthesis of Homopolymers, Block Copolymers, and Polymer Brushes
Licensed Content Author	Benedikt S. Soller,Ning Zhang,Bernhard Rieger
Licensed Content Date	Aug 22, 2014
Licensed Content Pages	17
Type of use	Dissertation/Thesis
Requestor type	Author of this Wiley article
Format	Print and electronic
Portion	Full article
Will you be translating?	No
Title of your thesis / dissertation	Rare Earth Metal-Mediated Group Transfer Polymerization of Vinylphosphonates: Initiation, Propagation, and Stereoregularity
Expected completion date	Jul 2016
Expected size (number of pages)	450
Requestor Location	Benedikt Soller Licherbergstr. 4 Munich, Germany 81667 Attn: Benedikt Soller
Billing Type	Invoice
Billing address	Benedikt Soller Licherbergstr. 4 Munich, Germany 81667 Attn: Benedikt Soller
Total	0.00 USD

Catalytic Precision Polymerization: Rare Earth Metal-Mediated Synthesis of Homopolymers, Block Copolymers, and Polymer Brushes

Benedikt S. Soller, Ning Zhang,* Bernhard Rieger*

Recent studies have shown that rare earth metal-mediated group transfer polymerization (REM-GTP) can be applied to a variety of polar monomers, besides the classic (meth)-acrylates or (meth)acrylamides, giving access to new polymeric materials. This article highlights progress in this new field and gives a current overview of the initiation and propagation of vinylphosphonates, the extension to Michael-type nitrogen-coordinating monomers, and application to block copolymers, statistical copolymers, and 2D and 3D structures. Based on molecular understanding and high-precision synthesis, REM-GTP represents a versatile method for the preparation of new materials.

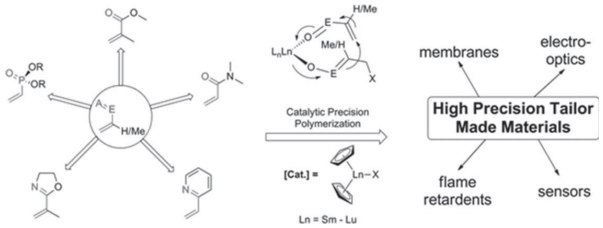

1. Introduction

From the synthesis of macromolecules via their transformation in tools to the production of final components, the information content is increasing significantly for each step. The overall worldwide polymer output is growing by 3% a year and 80% of fabrication are made from commodity plastics.[1] Therefore, most polymers in use derive from just a few commodity monomers with limited diversity due to commercial reasons. Accordingly, our modern consumer-based societies are hard to imagine without synthetic materials. Materials of the future face challenging applications in health care, mobility, or the energy sector and to meet this demand, a high precision synthesis of the macromolecule is mandatory. However, for large-volume polymerizations, the production process needs to be highly efficient, environmental friendly, and scalable. Catalytic reaction sequences completely fulfill these requirements in an ideal manner. With regard to these trends and requirements, this review focuses on a variety of high precision polymers, well-defined materials, their properties, new monomers, and the corresponding polymerization techniques.

B. S. Soller, Prof. B. Rieger
WACKER-Lehrstuhl für Makromolekulare Chemie, Technische Universität München, Lichtenbergstraße 4, 85747, Garching bei München, Germany
E-mail: rieger@tum.de
Dr. N. Zhang
Changchun Institute of Applied Chemistry, Chinese Academy of Sciences, Changchun 130022, China
E-mail: ning.zhang@ciac.ac.cn

2. Scope of This Review

Diverse polymer structures can be summarized under the term precision polymers and in general well-defined materials are attributed as precision materials. The methods of possible modifications are as broad as the range of available methods and material properties are often addressed by functional groups derived from heteroatoms in the polymer. The number of possible functionalities is vast and in combination with macromolecular principles, a wide range of high precision tailor-made materials are accessible. Therefore, in this review, the authors want to give a summary of the latest developments in the field of rare earth metal-mediated group transfer polymerization (REM-GTP) of polar monomers and interesting properties derived from innovative high precision materials. An overview of possible structures is given in Figure 1. Within this review, the authors focus on the synthesis and properties of homopolymers, end-functionalized polymers, block, random,

Macromol. Chem. Phys. **2014**, *215*, 1946–1962

DOI: 10.1002/macp.201400271

alternating copolymers, and furthermore graft and surface graft polymers via catalytic (i.e., REM-GTP) methods.

Other techniques, like living radical polymerization or post-polymerization modifications also afford interesting materials.[2] However, the use of multistep reactions, characterization, and purification of modified polymers can be complex operations and are beyond the scope of this review. Rare earth metal catalysts have distinguished features in the polymerization of polar and unpolar monomers, show unique polymerization properties and were thus used for the efficient synthesis of a variety of high precision materials in the last two decades. This review presents latest trends in the field of REM-GTP. The extensively investigated chemistry of cationic and isoelectronic group IV complexes is highlighted where needed. Other metal-assisted or non-catalytic polymerization methods (i.e., radical polymerization) are not covered within this review (vide supra).

3. Methyl Methacrylate Polymerization Via Nonbridged Lanthanocenes

A giant leap in the polymerization of polar monomers was achieved via the combination of the known silyl ketene acetal group transfer polymerization (SKA-GTP)[3] with lanthanide and cationic group IV metallocene complexes. Simultaneously in 1992, the groups of Yasuda and Collins reported the living polymerization of methyl methacrylate (MMA) via organometallic complexes.[4] Using the neutral samarocene $[(C_5Me_5)_2SmH]_2$, Yasuda et al.[4a] produced high-molecular-weight poly(methyl methacrylate) (PMMA) ($\bar{M}_n > 50$ kDa) with narrow polydispersities (PDI = 1.02–1.05) and a high syndiotacticity of up to 95%. The mechanism of initiation via nucleophilic transfer of a hydrido ligand and an eight-membered transition state was proven by the crystal structure of the MMA adduct $(C_5Me_5)_2Sm(MMA)_2H$. In the first step, the hydrido-bridged dimer has to be opened by coordination of one monomer molecule. The initiation follows a 1,4-addition of the hydrido ligand to MMA and an enolate is formed (Figure 2). The thus formed active species can further add to coordinating monomer through a repeated conjugated addition via the eight-membered transition state.

Similar to this approach, the polymerization of MMA via a cationic zirconocene was reported by Collins and Ward in 1992. Initiation follows a transfer of the initiating methyl ligand to the chain end. The mechanism was identified by ^{13}C-labeled initiators and methyl-end groups in the final PMMA polymer, respectively.[4b] Cationic group IV compounds do require a cocatalyst

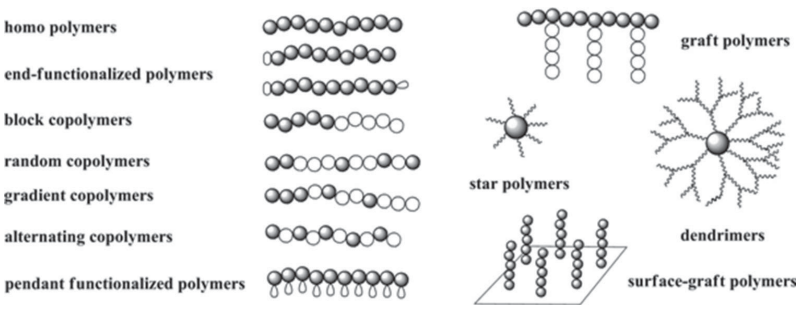

Figure 1. Overview of different types of precision materials.

Benedikt Soller studied chemistry at the Technische Universität München and received his M.Sc. in 2013. In 2009, he carried out research on emulsion polymerization at BASF SE in Ludwigshafen. During his master's studies, he spent two months at King Abdullah University of Science and Technology in Saudi Arabia as part of a research stay and six months at Ateneo de Manila University in the Philippines as exchange student. In his master's thesis in the group of Prof. Bernhard Rieger, he focused on novel initiators for REM-GTP. His Ph.D. is concerned with heteroatom functionalized vinylic monomers and synthesis of novel group three complexes.

Ning Zhang received his M.Sc. in Chemistry in 2006 from Jilin University (China). He subsequently obtained his Ph.D. in 2010 from Technische Universität München (TUM) in Germany under the supervision of Prof. Rainer Jordan. After a postdoctoral research position with Prof. Bernhard Rieger at TUM, Ning joined the Changchun Institute of Applied Chemistry, Chinese Academy of Sciences in 2012. His current research interest includes synthetic polymer chemistry, stimuli-responsive materials, and surface modification via controlled polymerization.

Bernhard Rieger studied chemistry at the Ludwig-Maximilians-Universität München (LMU) and received his Ph.D. in 1988. After research at the University of Massachussetts at Amherst and in the plastics laboratory of BASF SE, he received his Habilitation in 1995 at the University of Tübingen. In 1996, he became Professor at the Department Materials and Catalysis at the University of Ulm. Since 2006, he has been Professor at TUM at the WACKER-Chair of Macromolecular Chemistry and director of the Institute of Silicon Chemistry. He has received a teaching award from the Federal State of Baden-Württemberg and the Philip-Morris Award.

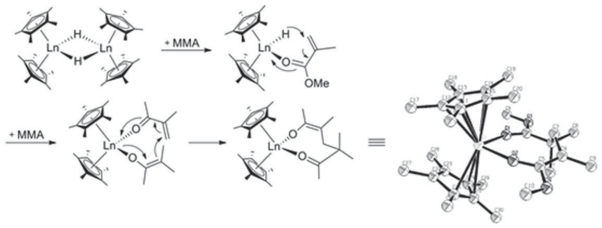

Figure 2. Initiation and propagation steps in MMA polymerization by $[Cp_2^*LnH]_2$ (Ln = Sm). Redrawn from ref.[4a]

for activation and therefore effects of counterions or ion-pairing on the stereochemistry and polymerization activity can be observed. Furthermore, group IV GTP can either follow a monometallic or bimetallic mechanism (Figure 3).[5] Both pathways were originally considered and endorsed by theoretical calculations.[6]

The initiation of neutral lanthanides proceeds either via a nucleophilic attack of a ligand, deprotonation of an acidic monomer, or by redox initiation in the case of divalent lanthanide complexes. The mechanism of unpolar and polar monomer initiation for a divalent samarocene is shown in Figure 4.[7] A radical initiation was proposed by Boffa and Novak[8] and experiments were conducted for ethylene and MMA.[8]

A similar monometallic mechanism of initiation and propagation for isoelectronic neutral lanthanides and cationic group IV complexes is discussed in literature.[5] Both the rare earth metal-mediated- and the group IV GTP are living type polymerizations, combining the advantages of living ionic and coordination polymerizations and both proceed via a repeated conjugated addition of the active enolate species to the monomer.

Therefore, REM-GTP is a versatile method for the synthesis of precision polymers, designed functional and hybrid materials. A detailed discussion of the prior name giving SKA-driven GTP and its mechanism is given in a review.[9] Recent interesting developments of SKA-GTP and the use of Lewis base organocatalysts are summarized in a review.[10]

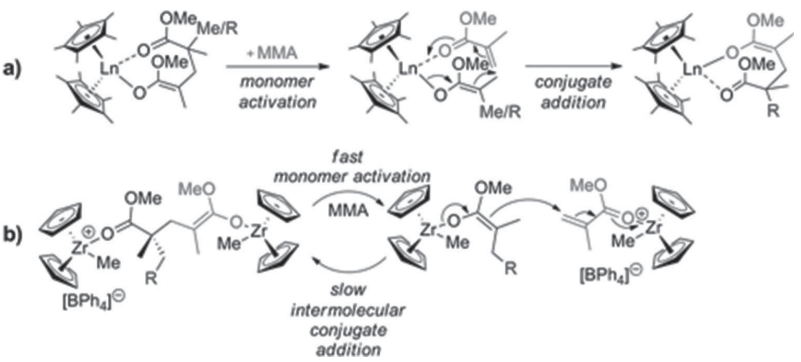

Figure 3. a) Monometallic lanthanide and b) bimetallic group IV propagation step for GTP of MMA (R = polymer chain).

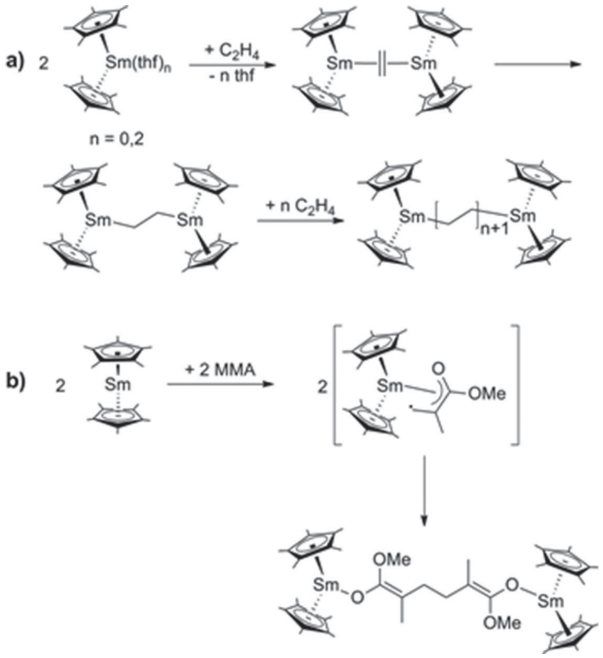

Figure 4. Proposed single-electron transfer initiation mechanism of a Sm(III) bisinitiator from divalent decamethylsamarocene.

Intensive research on REM-GTP has been carried out over the past two decades, optimizing reaction conditions, initiator efficiency, and control over the stereoregularity, on the use of different metals, as well as on their implementation to a variety of monomers, for example, different (meth)-acrylates or (meth)acrylamides (see Figure 5).[5,11]

4. Poly(vinylphosphonate)s

4.1. Mechanism of REM-GTP

Poly(vinylphosphonate)s with high molecular masses are not satisfactorily accessible via classical polymerization methods such as radical polymerization or ionic polymerization.[12] A review article covering the early chemistry of poly(vinylphosphonate)s including radical and classical anionic approaches was published in 2012.[13] In addition, attempts to polymerize vinylphosonates via frustrated Lewis pairs are reported with low activities in literature (TOF = 6–10 h^{-1}).[14]

Driven by the structural similarity of vinylphosphonates and MMA, our group started research in the field of REM-GTP for the polymerization of dialkyl vinylphosphonates (DAVP). In

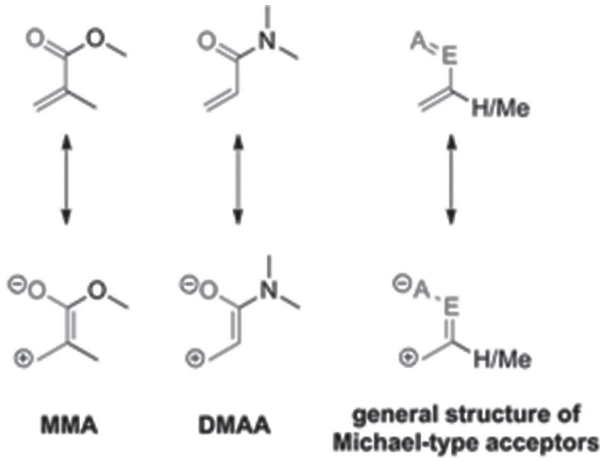

Figure 5. General structure of typical Michael-type acceptors suitable for REM-GTP.

2010, we reported the first example of high-molecular-weight poly(diethyl vinylphosphonate) (PDEVP) with molecular weights up to $\bar{M}_w = 10^6$ g mol^{-1} and first block copolymer structures of MMA and DEVP via trivalent ytterbocenes.[15] The complexes Cp_2YbX were used in this study with σ-donor chloro and methyl ligands (X = Cl, Me). The polymerization proceeds rapidly and follows a living GTP mechanism, demonstrated by kinetic studies and copolymerization experiments.[15] However, the mechanism of initiation follows a complex reaction pathway depending on the nature of the initiating ligand X (see Figure 6).[16]

For a deeper understanding of both, the initiation and propagation of DAVP REM-GTP mechanistic studies were conducted.[16] In contrast to the polymerization of MMA and analogous to acrylonitrile,[17] strongly basic alkyl ligands are poor initiators for α-acidic vinylphosphonates. The initiation of vinylphosphonates for methyl or CH_2TMS ligands does not follow a 1,4-addition. It results in a deprotonation of DAVP at the α-position and an allenylic phosphonate intermediate is formed. The polymerization of vinylphosphonates via alkyl initiators shows long initiation delays, supposedly due to the slow formation and low reactivity of a deprotonated vinylphosphonate species.[16] The molecular mass of the final polymer is significantly higher than expected from the original monomer to catalyst ratio. Therefore, alkyl initiators are unsuitable for REM-GTP of α-acidic DAVP.[15,16]

Alkoxides are efficient and well-known initiators for the group III ring-opening polymerization (ROP) of lactones like ε-caprolactone or β-butyrolactone.[18] However, for the GTP of polar monomers alkoxides do not follow a 1,4-addition to the monomer and no polymer is formed when MMA is used.[16,19] This can be explained by the extreme oxophilic nature of rare earth metals and DFT calculations for bis(penoxyamine) yttrium catalysts strengthen the observation that the endothermic formation of an MMA isopropyloxide adduct is unlikely.[19] Nevertheless, the second insertion of a hypothetical adduct was calculated to proceed via the conjugate addition as reported by Yasuda et al.[4a,19] Therefore, it can be concluded that the propagation of MMA is hindered by an insufficient alkoxy initiator. Interestingly, the polymerization of DEVP is possible with $[Cp_2LnO\mathit{i}Pr]_2$ complexes via ligand exchange of the $Cp_2LnO\mathit{i}Pr$(DEVP) adduct- forming $CpLn(O\mathit{i}Pr)_2$(DEVP) and Cp_3Ln(DEVP) with Cp_3Ln(DEVP) being the active species (see Figure 7).[16]

High activities and acceptable initiator efficiencies for the polymerization of DEVP were obtained by the use of $[Cp_2LnS\mathit{t}Bu]_2$ thiolato complexes. Thiolates are not basic enough to deprotonate vinylphosphonates and the Ln–sulfur bond is reasonably weak to ensure a high driving

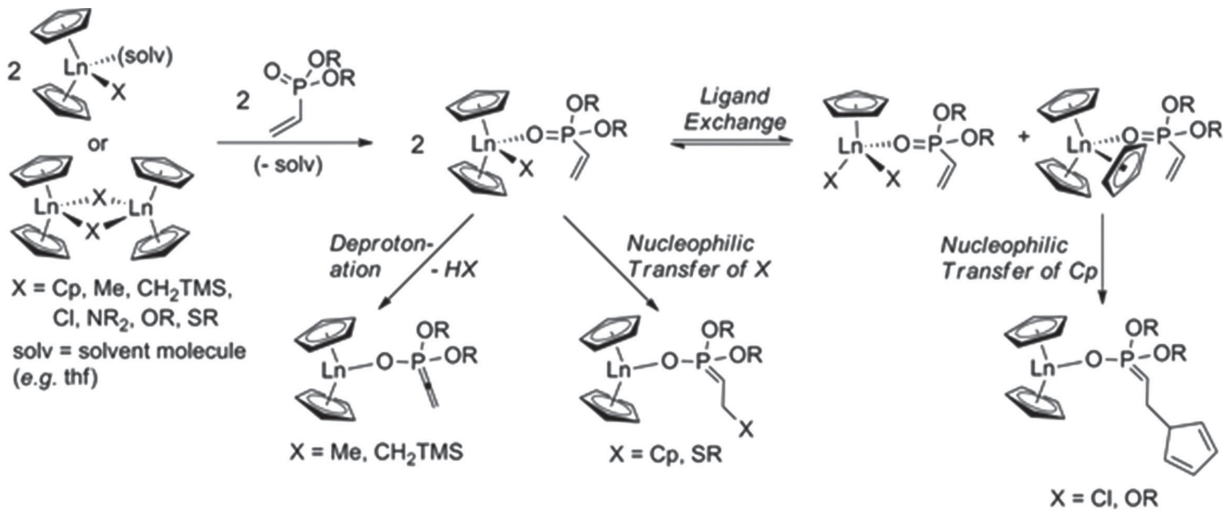

Figure 6. Initiation of dialkyl vinylphosphonate GTP using unbridged trivalent rare earth metallocenes (Cp_2LnX).

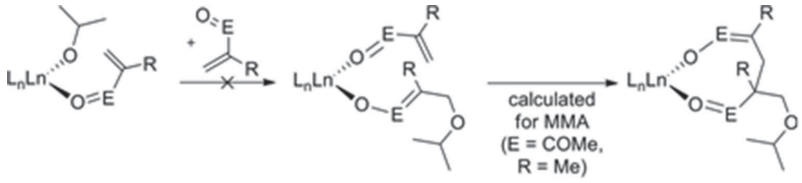

Figure 7. Calculated initiation and propagation of MMA via yttrium bisphenoxide complexes.

force for the formation of a reactive [(DEVP)S*t*Bu]$^-$ adduct. The first step involves a 1,4-addition of the ligand to the monomer at which the initiation delay is short within a few seconds (compared to a few minutes in the case of deprotonation or ligand exchange).

A drawback for $[Cp_2LnStBu]_2$ complexes is the dimeric structure causing an initiation delay for monomers like DEVP and being unreactive for weaker coordinating monomers that do not open the dimeric structure in the first step (see hydride dimer in Figure 2). Furthermore, $[Cp_2YStBu]_2$ exhibits a shorter initiation delay compared to the sterically more crowded $[Cp_2LuStBu]_2$. Lutetium has a smaller ionic radius and thus the coordination of the monomer to the metal is hampered. Therefore, the lutetium dimer is more stable and opening by coordination of a monomer is energetically disfavored. For complexes with bulky substituents at the ligand, a formation of the dimer can be hindered. This can avoid the limiting step of opening a dimeric structure for weak coordinating monomers (see Figure 8).

The mechanism of initiation for Cp_2LnCl complexes does not follow a nucleophilic transfer of a chloro ligand to the monomer either. For the case of Cp_2YbCl, a strong temperature dependency of the degree of polymerization and propagation rate was found for DEVP.[15] At temperatures below 0 °C, no activation of Cp_2YbCl could be observed, indicating the energy barrier of activation is too high for the initiating mechanism. The active species of Cp_2LnCl compounds is again formed originally from the ligand exchange reaction of the vinylphosphonate adduct Cp_2LnX(DAVP), resulting in $CpLnX_2$(DAVP) and Cp_3Ln(DAVP). The tris(cyclopentadienyl) Cp_3Ln(DAVP) adduct is the active species and initiates the GTP of DAVP via a nucleophilic transfer of one cyclopentadienyl ligand. The mechanism of a ligand exchange reaction was proven for Cp_2YCl by using diethyl ethyl phosphonate (DEEP).[16] The phosphonate DEEP is not a Michael-type acceptor and cannot be polymerized via a conjugated system. Therefore, DEEP induces a ligand exchange that can be followed by ^{1}H-NMR spectroscopy. Furthermore, by overlaying a saturated benzene solution of $CpYCl_2$(DEEP) and Cp_3Y(DEEP) with pentane, single crystals suitable for x-ray spectroscopy could be obtained and characterized as Cp_3Y(DEEP) (Figure 9).

So far, a variety of Cp_2LnX complexes for the GTP of vinylphosphonates have been synthesized and tested for their activities and initiation mechanism. Depending on the nature of the initiating ligand, the activities of Cp_2LnX complexes differ significantly for the same active species in the propagation step (Table 1). Therefore, new initiators for neutral lanthanides have to be investigated. Ideal initiators should have high initiator efficiencies, sufficient activities, form a stable end group that can be modified for further applications. Additionally, they should initiate the polymerization via an eight-membered ring to match the propagation ground state of REM-GTP.

The propagation and activity of DAVP polymerization can be easily followed by time-resolved analysis of monomer conversion by ^{31}P-NMR and molecular masses of the formed polymers allow the determination of the initiator efficiency throughout the whole reaction. Such

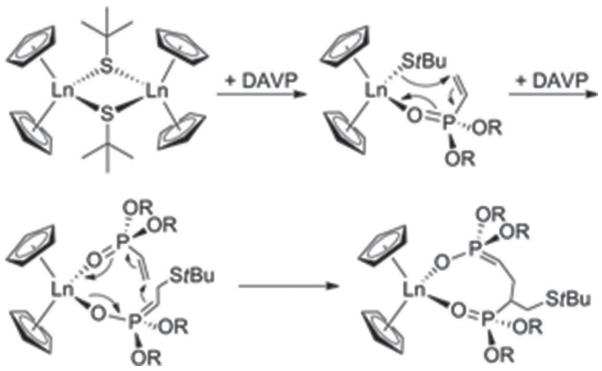

Figure 8. Initiation and propagation of DAVP polymerization via thiolato initiators.

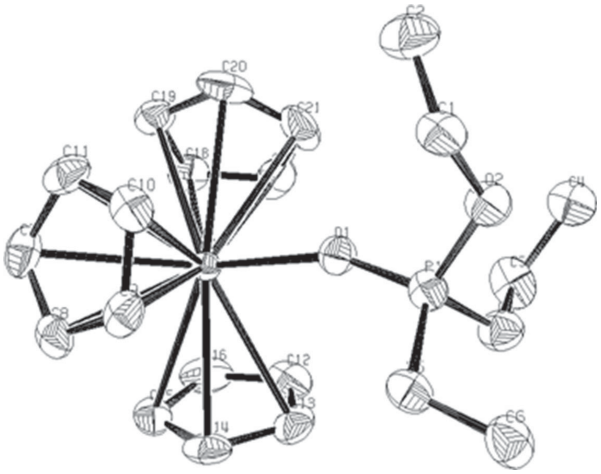

Figure 9. Crystal structure of the adduct Cp_3Y(DEEP) from the ligand exchange reaction of Cp_2YCl and DEEP (hydrogen atoms are omitted for clarity). Redrawn from ref.[16]

Table 1. Polymerization results for Cp_2LnX catalysts with different initiators.

Catalyst	Reaction time	Conversion[a] [%]	Init. period[b]	$\bar{M}_n$[c] [kDa]	I^*[c] [%]	TOF[a]/I^* [h^{-1}]	End group[d]	Extent of ligand exchange[e]
$[Cp_2YCl]_2$	6 h	70	100 min	740	9.3	3700	Cp	15%
$Cp_2Y(bdsa)(thf)$	3 h	95	15 min	1040	9.0	7200	Cp, bdsa (olefinic)[f]	3%
$[Cp_2Y(OiPr)]_2$	30 h	26	2.5 h	1070	2.4	2000	Cp	<0.5% (10%)[g]
$Cp_2Y(OAr)(thf)$	30 h	–	–	–	–	–	–	<0.5%
$[Cp_2Y(StBu)]_2$	3 min	100	5 s	150	65	69 000	StBu (olefinic)[f]	4%
$Cp_2Y(CH_2TMS)(thf)$	40 min	88	5 min	510	17	10 000	olefinic	5%
$[Cp_2LuCl]_2$	1.5 h	93	7 min	780	11.7	20 500	Cp	3%
$Cp_2Lu(bdsa)(thf)$	3 h	96	20 min	1350	7.0	21000	Cp, bdsa (olefinic)[f]	1%
$[Cp_2Lu(OiPr)]_2$	30 h	52	9 h	1270	4.0	600	Cp	<0.5% (<1%)[g]
$Cp_2Lu(OAr)(thf)$	30 h	<1	–	–	–	–	–	<0.5%
$[Cp_2Lu(StBu)]_2$	1.5 min	100	15 s	210	47	220 000	StBu (olefinic)[f]	2%
$Cp_2Lu(CH_2TMS)(thf)$	30 min	92	5 min	1130	8.0	39 000	olefinic	1%

[a]Determined by ^{31}P-NMR spectroscopic measurement; [b]Initiation period, reaction time until 3% conversion is reached; [c]Determined by GPC-MALS, $I^* = M_{th}/\bar{M}_n$, $M_{th} = 600 \times M_{Mon} \times$ conversion; [d]Determined by ESI MS; [e]Conversion of Cp_2LnX for addition of 5 eq. of DEEP, determined from ^1H-NMR spectroscopic signals of Cp_2LnX(DEEP) and Cp_3Ln(DEEP); [f]Olefinic chain ends formed by end-group elimination; [g]Number in brackets: extent of dimer opening for addition of 5 eq. of DEEP, determined from ^1H-NMR spectroscopic signals of $Cp_2Ln(OiPr)$(DEEP) and DEEP.

a normalization method is needed for polymerizations with fast propagation and comparatively slow initiation (Figure 10). By using this method, both the catalyst and monomer order of rare earth metal-mediated vinylphosphonate GTP were determined to be one (Figure 11).[16]

Therefore, REM-GTP of vinylphosphonates follows a Yasuda-type monometallic propagation mechanism, with an S_N2-type associative displacement of the polymer phosphonate ester by a monomer and the formation of a pentacoordinate intermediate as the rate-determining step (see Figure 12).

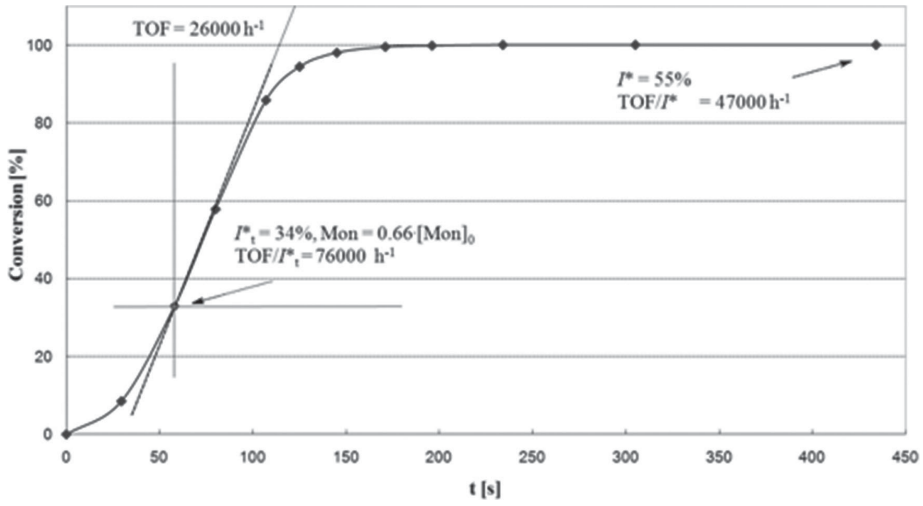

Figure 10. Example for an initiation delay of a DAVP polymerization and the influence of the initator efficiency *I*.

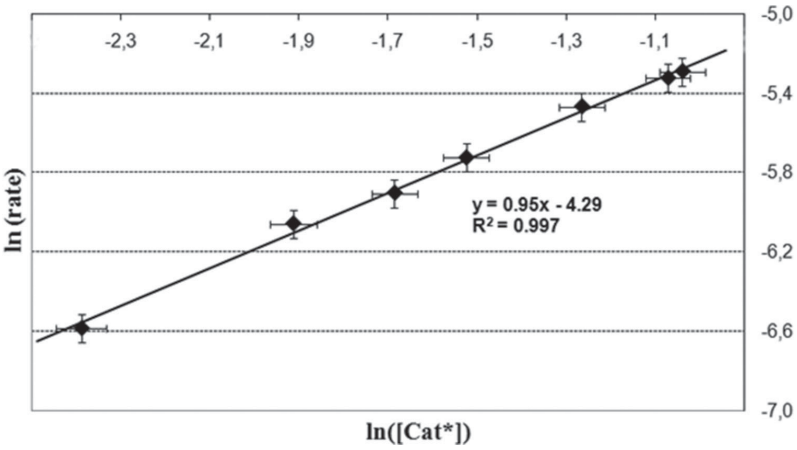

Figure 11. Determination of catalyst order (Cp_3Tm, 5 vol% DEVP in toluene, 30 °C).

The reaction speed was found to accelerate with decreasing ionic radii for REM-GTP of DAVP. Contrary to previous findings of Yasuda et al.[4a] that larger lanthanides polymerize MMA faster than the late rare earths yttrium or lutetium. The reaction speed for MMA increases from lutetium to samarium (Sm > Y > Lu).[4a] To address the metal-dependent change in activity, time-dependent kinetic measurements of DAVP were performed to quantify activation enthalpies $\Delta H^{\ddagger}$ and entropies $\Delta S^{\ddagger}$. Interestingly, it was shown that the increase in activity with decreasing metal size is not caused by a change of the reaction enthalpy $\Delta H^{\ddagger}$ (i.e., ring strain or the Ln—(O—P) bond strength). The propagation rate of vinylphosphonate GTP is mainly determined by the activation entropy, that is, the change of rotational and vibrational restrictions within the eight-membered metallacycle in the rate-determining step as a function of the steric demand of the metallacycle side chains and the steric crowding at the metal center. Therefore, the lesser rotational and vibrational degrees of freedom in sterically crowded (i.e., smaller) lanthanides destabilize the propagation ground state and increase the activity. This questions the general principle that the metal center should be widely accessible for GTP due to the demanding eight-membered transition state.

The thermodynamic measurements underline the importance of tuning the metal–ligand interaction for enhanced selectivities. This can either be done by changing the metal center or by modifying the substituents of the ligand to vary the steric demand at the complex and the amount of rotational and vibrational freedom of the ground state. Since both the order of catalyst and monomer are one, the metal center stabilizes the growing chain end and decreases side reactions such as chain transfer or termination. The activation of the monomer at the active site allows a well-controlled polymerization even at elevated temperatures. For these reasons, REM-GTP provides much higher activities in comparison to other living polymerizations and simultaneously yields precision polymers with narrow polydispersities, end-group functionalities, block copolymer structures, or defined grafted polymers.

5. Nitrogen-Coordinating Monomers

For years, REM-GTP research focused on (meth) acrylates, (meth)acrylamides or the newer class of

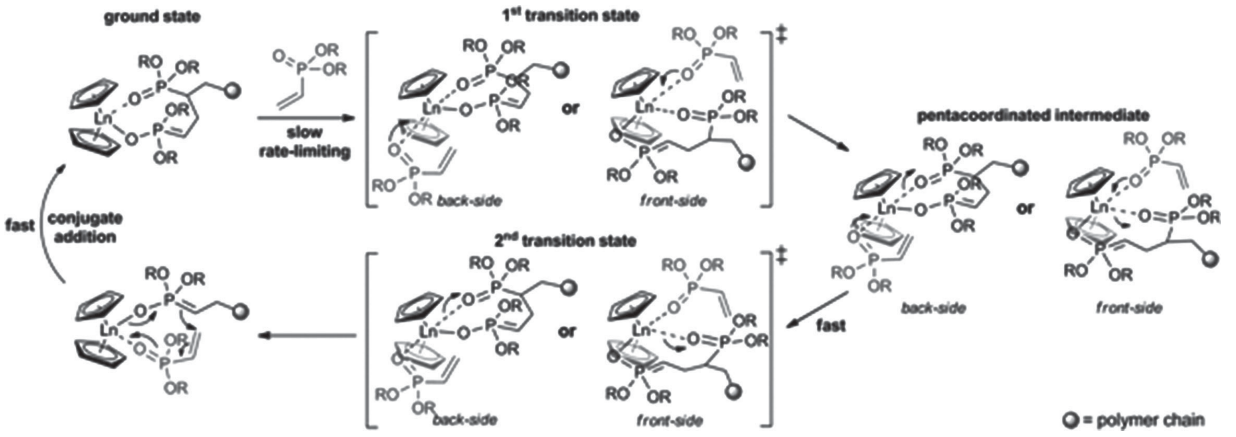

Figure 12. Elemental steps of rare earth metal-mediated GTP of vinylphosphonates. Reproduced with permission.[16] Copyright 2013, American Chemical Society.

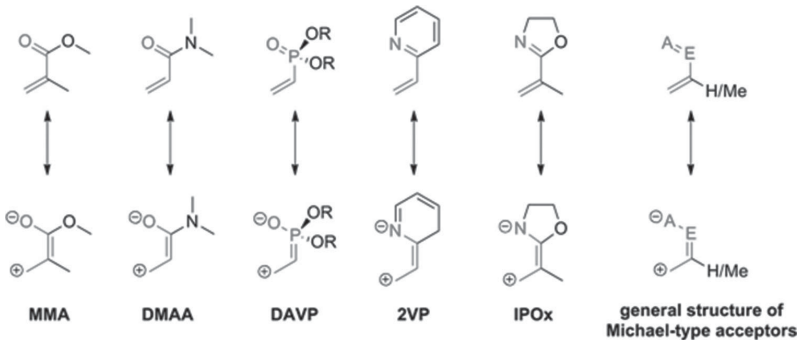

Figure 13. General structure of O- and N-coordinating Michael-type acceptors suitable for REM-GTP.

vinylphosphonates. Such monomers coordinate to the metal center via an oxygen moiety. In this chapter, we want to discuss new developments in the field of REM-GTP made possible by the extension of the monomer classes, to nitrogen-coordinating substrates, mainly 2-isopropenyl-2-oxazoline (IPOx) and 2-vinylpyridine (2VP) (see Figure 13).

5.1. Poly(2-isopropenyl-2-oxazoline) and Poly(2-vinylpyridine)

Conventional radical or anionic polymerization of the vinylidene moiety of IPOx affords poly(2-isopropenyl-2-oxazoline) (PIPOx) with a broad-molecular-weight distribution, though anionic and reversible addition–fragmentation chain transfer polymerization can improve the distribution character to a certain extent.[20] For instance, living anionic polymerization is not a preferred method for the polymerization of IPOx due to the strict operating condition and solvent effect required.[21] Moreover, polymerization of IPOx by atom transfer radical polymerization (ATRP) is not feasible due to a strong complexation of pendant 2-oxazoline units by copper.

Inspired by the high precision offered by REM-GTP, it has been a major focus of our research to extend the applicability of this method to further monomer classes. Moreover, the structural similarity among IPOx, vinylphosphonates, and MMA provides the possibility that IPOx can be polymerized via REM-GTP. In 2013, we reported the first example of high-molecular-weight PIPOx with PDI below 1.1 catalyzed by Cp_2YbMe.[22] The polymerization proceeds rapidly at room temperature and following a living GTP mechanism, and monomer conversion reaches 95% within 2 h as monitored by in situ ^{1}H-NMR (Figure 14). ESI-MS experiments of oligomers produced by using an IPOx to Cp_2YbMe ratio of 5 to 1 in toluene indicate a transfer of a coordinated ligand (CH_3) to a monomer in the initial step (Figure 15).

A plot of the $\bar{M}_n$ as a function of monomer (IPOx) conversion (from 2% to 95%, respectively) demonstrates a linear relationship between these two parameters (Figure 16). It is worth mentioning that the PDI remains extremely narrow (PDI < 1.07) for polymers obtained at all conversions. The linear growth of molecular weight versus monomer conversion is attributed to the highly living character of REM-GTP and the determined high initiator efficiency ($I^* = 95\%$).

The REM-GTP is superior to other conventional polymerization techniques, e.g., radical polymerization initiated by AIBN and anionic polymerization initiated by BuLi. Free radical polymerization of IPOx performed at 60 °C affords PIPOx with broad polydispersity (PDI = 2.0) (conversion = 59%). Living anionic polymerization of IPOx at −78 °C for 2 h yields a polymer with improved molar mass distribution (PDI = 1.2), but slow polymer chain growth rate ($\bar{M}_n$ = 2.5 kDa after 2 h polymerization, conversion = 18%). Anionic polymerization of IPOx at room temperature significantly increased the polymerization velocity, whereas at the cost of side reactions and loss of control. As a result, the PDI of the obtained polymer increased obviously (PDI = 1.5). The polymerization results for different methods and the used reaction conditions are summarized in Table 2.

The REM-GTP is also applicable to other monomer exhibiting similar structural feature, for example, 2VP

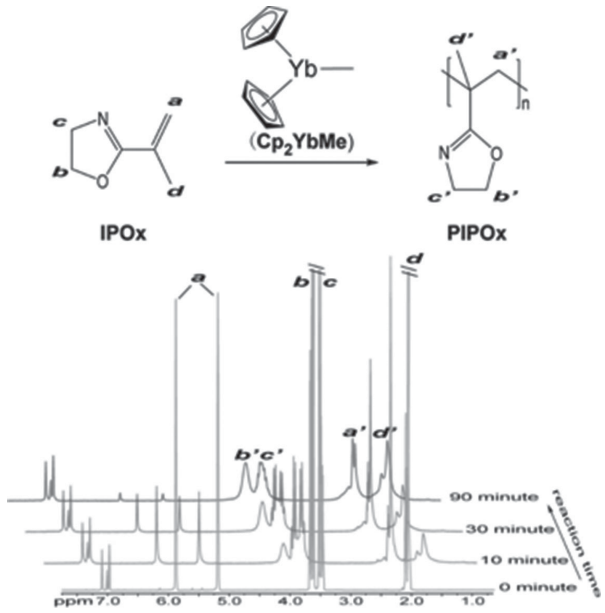

Figure 14. Reaction scheme for REM-GTP of IPOx and polymerization kinetics as detected by in situ ^{1}H-NMR and assignment of corresponding signals. Reproduced with permission.[22] Copyright 2013, American Chemical Society.

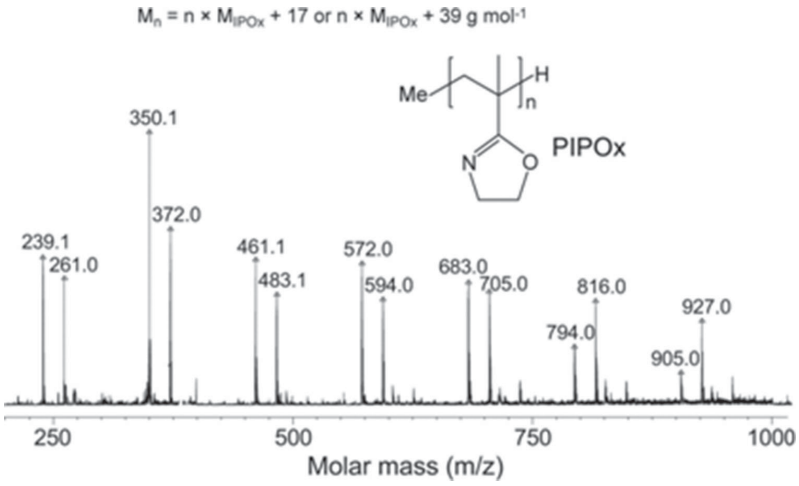

Figure 15. Structure of 2-isopropenyl-2-oxazoline oligomer and its ESI-MS spectrum. Reproduced with permission.[22] Copyright 2013, American Chemical Society.

using Cp_2YbMe as a catalyst, yielding high-molecular-weight poly(2-vinylpyridine) (P2VP). However, the activity and the initiator efficiency of 2VP REM-GTP is much lower (TOF = 44 h^{-1}, I^* = 45%) than those for IPOx (TOF = 380 h^{-1}, I^* = 95%) (Figure 17), which probably due to the electron delocalization and thus the weak *N*-Yb coordination. It should be noted that the PDI of obtained P2VP is narrow (PDI = 1.1) at all monomer conversions (Figure 18). The REM-GTP of IPOx and 2VP provides the first example of REM-GTP occurs via *N*-coordination at the rare earth metal center.

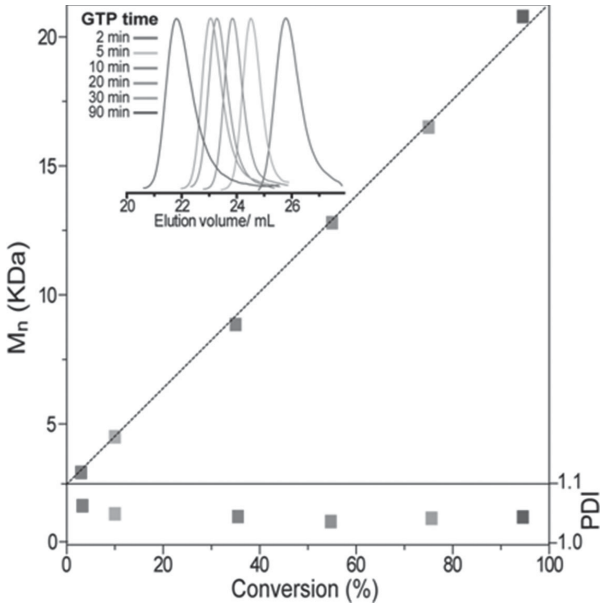

Figure 16. Linear growth of the absolute molecular weight (M_n) determined by multiangle laser light scattering as a function of IPOx conversion (determined by ^{1}H-NMR). Inset: GPC traces as detected by retention volume. Reproduced with permission.[22] Copyright 2013 American Chemical Society.

6. Copolymer Structures

6.1. Block Copolymers

Rare earth metal-catalyzed coordination polymerization, REM-GTP and REM-ROP are living type polymerizations. Therefore, block copolymer structures are possible by using different olefins (polyinsertion), polar monomers (GTP), and cyclic lactones (ROP). Furthermore, rare earth metals can also catalyze the formation of block copolymers from monomers with different propagation steps, i.e., structures of polyolefins and polar monomers or polar monomers and cyclic esters.[23] By using the mechanistic crossover of organo–rare earth metal compounds, these different polymerization methods can be combined for a living high precision synthesis of functional, tailor-made materials. In contrast to polymer blends or random copolymers, of which material properties can be intermediate to the original homopolymers, block copolymers often show improved behavior due to microphase separation of the different segments, formation of discrete domains, and generation of otherwise unattainable morphologies. However, the synthesis of block copolymers can be an ambitious task facing poor solubility, difficult characterization, micelle formation, and poisoning of the usually oxophilic metal centers by polar monomers. One of the first examples for a complex being able to polymerize olefins and lactones is the sterically crowded $(C_5Me_5)_3Sm$.[23c,d] The production of poly(ethylene) from $(C_5Me_5)_3Sm$ is remarkable and attributed to a reactive η^1 single bond of one C_5Me_5 ligand to the metal (Figure 19).[23c] Considerable progress in the field of sterically crowded lanthanides with interesting behavior has been made in the past years.[24]

A consecutive GTP of different monomers for the formation of block copolymers is only possible in order of similar or increasing coordination strength. A reverse sequence, first, a strong coordination monomer, or the simultaneous addition of monomers with different coordination strength usually leads to the formation of only one homopolymer.

The living polymerization of different alkyl acrylates (methyl acrylate, ethyl acrylate, butyl acrylate) was investigated by using $(Cp^*)_2LnMe(thf)$ (Ln = Sm, Y), yielding: poly(methyl acrylate) $\bar{M}_n = 48 \times 10^3$ g mol^{-1}, PDI = 1.04, poly(ethyl acrylate) $\bar{M}_n = 55 \times 10^3$ g mol^{-1}, PDI = 1.04, and poly(butyl acrylate) $\bar{M}_n = 70 \times 10^3$ g mol^{-1}, PDI = 1.05.[25]

Table 2. Summary of different polymerization of IPOx (Monomer/initiator = 200/1).

Initiator	T [°C]	TOF[a,b] [h^{-1}]	PDI[c]	$\bar{M}_n$[c] [kDa]	I*[d] [%]	Reaction time/conversion[b] [h]/[%]
Cp_2YbMe	25	380	1.04	21	95%	1.5/92
BuLi	25	3100	1.5	40	53%	0.2/95
BuLi	–78	18	1.2	2.5	–	2/18
AIBN	60	–	2.0	18	–	8/59

[a]The turnover frequency (TOF) vs reaction time plot; [b]Determined by ^{1}H-NMR; [c]Determined by GPC-MALS; [d]$I^* = M_{theo}/\bar{M}_n$, $M_{theo} = 200 \times M_{Mon} \times$ conversion + $M_{endgroup}$.

Furthermore, triblock ABA copolymers of MMA/butyl acrylate/MMA were synthesized to obtain thermoplastic elastomers. The butyl acrylate middle block is soft leading to compression sets up to 58% and an elongation of 163% for block copolymers with the ratio 8:72:20.[25a,c,26] ABC triblockpolymers of MMA/ethyl acrylate/ethyl methacrylate (26:48:26) improved the material properties (compression set = 62%, elongation = 276%).[25c]

Sequential block copolymerization of MMA and dimethyl acrylamide (DMAA) leads to the formation of the well-defined, highly isotactic block copolymer PMMA-*b*-PDMAA. In reverse order, only the homopolymer PDMAA is formed.[27] This is attributed to either the active amide enolate being not active enough to insert into MMA or a weaker coordination of MMA and being unable to replace the amide oxygen at the active site.[27] The combination of chiral ansa-zirconocene ester enolates with Lewis acids results in a highly active ion-pairing polymerization of MMA and DMAA; the living nature of this polymerization system allows for the synthesis of well-defined diblock and triblock copolymers of MMA with longer-chain alkyl methacrylates.[28] Unique *it-b-st* stereomultiblock microstructures of *it*-PMMA-*b*-*st*-PMMA can also be obtained from diastereospecific ion pairs.[29]

ABA copolymers of MMA and different acrylates are accessible from divalent $(C_5Me_5)_2Sm$ or $(C_5Me_5)_2Sm(thf)_2$ via single-electron transfer initiation (Figure 4).[30]

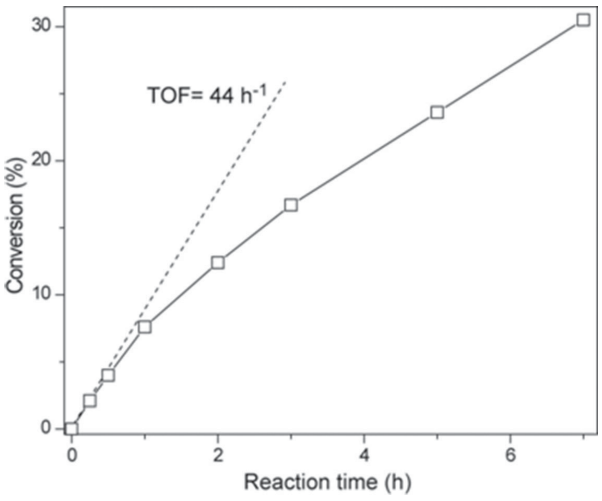

Figure 17. Determination of the catalytic activity of Cp_2YbMe for the polymerization of 2VP (TOF = 44 h^{-1}) by in situ ^{1}H-NMR spectroscopy (initial [2VP]:[catalyst] = 500:1; [catalyst] = 0.33 mg mL^{-1}). Reproduced with permission.[22] Copyright 2013, American Chemical Society.

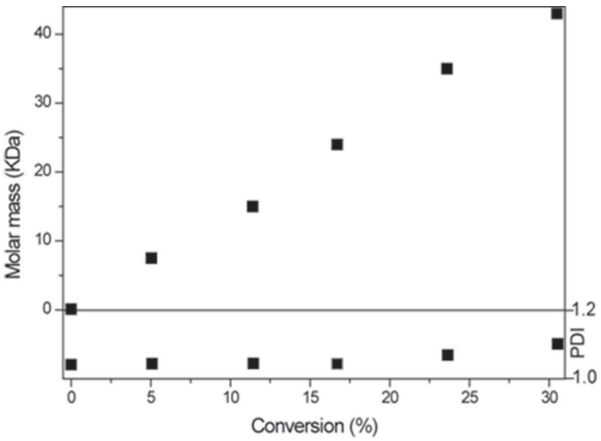

Figure 18. Linear growth of the absolute molecular weight (M_n) and polydispersity of P2VP determined by multiangle laser light scattering as a function of 2VP conversion. Reproduced with permission.[22] Copyright 2013, American Chemical Society.

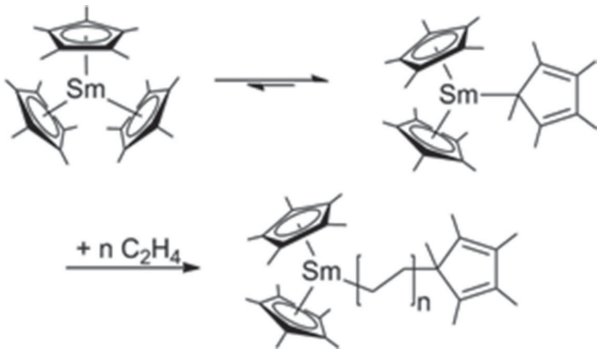

Figure 19. Proposed mechanism for the ethylene polymerization with the sterically crowded $(C_5Me_5)_3Sm$. Redrawn from ref.[23c]

Table 3. Homo- and block copolymers of 2VP, IPOx, MMA, and DEVP synthesized by Cp_2YbMe-initiated REM-GTP.[15,22]

	$\bar{M}_n$ [a] [kDa]	PDI[a]	I^*[b] [%]	Comonomer ratio A/B[c]	Yield[d] [%]
$P2VP_{100}$	14	1.01	75	–	96
$P(2VP_{100}\text{-}b\text{-}IPOx_{100})$	29(14)	1.01(1.01)	74(82)	1:1.18	98
$P(2VP_{100}\text{-}b\text{-}MMA_{100})$	14	1.01	–	1:0	46
$P(2VP_{100}\text{-}b\text{-}DEVP_{100})$	31	1.04	87	1:1.07	96
$P(2VP_{20}\text{-}b\text{-}MMA_{80})$	–	–	–	1:0	–
$PIPOx_{100}$	9.1	1.03	120	–	89
$P(IPOx_{100}\text{-}b\text{-}MMA_{100})$	9.2	1.02	–	1:0	44
$P(IPOx_{100}\text{-}b\text{-}DEVP_{100})$	1100 (10)	1.40 (1.03)	3 (~1)	1:0.69	62
$P(IPOx_{20}\text{-}b\text{-}MMA_{80})$	Aggregation	–	–	1:1.69	50
$P(IPOx_{20}\text{-}b\text{-}DEVP_{50})$	390 (2.6)	1.70 (1.12)	3 (2)	1:2.71	62
$PMMA_{100}$	12	1.10	83	–	98
$P(MMA_{100}\text{-}b\text{-}DEVP_{100})$	22	1.20	120	1.15:1	94

[a]Determined by GPC-MALS; [b]$I^* = M_{theo}/\bar{M}_n$, number in brackets gives the I^* of the macroinitator for polymerization of block B (in the case of bimodal distributions); [c]Determined by ^{1}H-NMR; [d]Determined by weighing of the components.

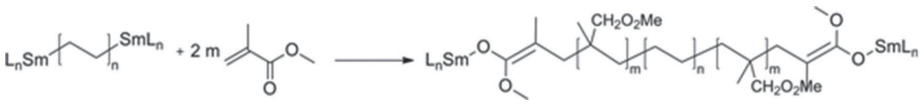

Figure 20. Poly(MMA-*co*-ethylene-*co*-MMA) ABA block copolymers from divalent Samarocenes.

Furthermore, the copolymerization of higher 1-olefins with polar monomers is possible by using bridged yttrium and samarium compounds with bulky substituents.[31] Using the unique properties of divalent samarium catalysts, the ABA block copolymers from ethylene with MMA, ε-caprolactone (CL), and 2,2-dimethyltrimethylene carbonate (DTC) poly(MMA-*co*-ethylene-*co*-MMA), poly(CL-*co*-ethylene-*co*-CL), or poly(DTC-*co*-ethylene-*co*-DTC) were synthesized (Figure 20).[32]

Consecutive polymerization of different monomers is only possible in order of increasing coordination strength and limited to monomers with similar polarities. Statistical copolymerizations of monomers with different coordination strength, i.e., DEVP, MMA, IPOx, and 2VP reveal that only corresponding homopolymers of the stronger coordinating comonomer were obtained indicated by NMR spectroscopy, suggesting a monomer coordination strength to the ytterbium center in an order of DEVP > MMA > IPOx > 2VP.[22] Thereafter, sequential copolymerization gave diblock copolymers in sequences of PMMA-*b*-PDEVP, PIPOx-*b*-PMMA, and PIPOx-*b*-PDEVP, as well as P2VP-*b*-PIPOx and P2VP-*b*-PDEVP, whereas diblock copolymerization in the reverse sequence only gave homopolymers of PDEVP, PMMA, and PIPOx, respectively.[22] Nevertheless, diblock copolymer synthesis was hindered by a possible encapsulation of the catalyst during polymerization of the relatively hydrophilic IPOx and 2VP (Table 3). This hypothesis is confirmed by precipitation of formed high-molecular-weight PIPOx and P2VP from toluene solution and by an insufficient initiation of a second, more hydrophobic comonomer (e.g., MMA) by the PIPOx or P2VP macroinitiator. When the degree of polymerization of the first hydrophilic block is below 20, an improvement of the PIPOx macroinitiator efficiency was observed. It is worth mentioning that the chain termination should not be a major limitation, as the formation of block copolymers for the more hydrophilic DEVP as second comonomer was feasible. Analysis of the molecular weight of the obtained copolymers is complicated due to aggregation, even at the low applied concentration in the GPC-MALS setup (Figure 21).[22]

N-heterocyclic carbene (NHC) lutetium bis((trimethylsilyl)methyl) complexes can promote the formation of

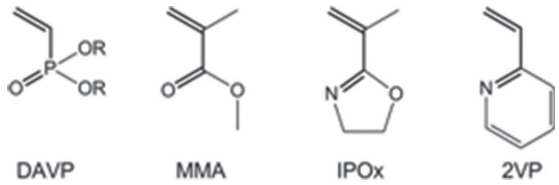

Figure 21. Comparison of oxygen-coordinating vinylphosphonates, methyl methacrylate and nitrogen-coordinating 2-isopropenyl-2-oxazoline, 2-vinylpyridine.

poly(3,4-isoprene)-*b*-polycaprolactone block copolymers with controllable molecular weight (from 4.9×10^4 to 10.2×10^4 g mol^{-1}) and narrow polydispersities.[33] Copolymerization of monomers with different propagation mechanisms (i.e., ethylene, propylene, and MMA) was also achieved for cationic group IV metallocenes, giving PE-*b*-*it*-PMMA, *it*-PP-*b*-*it*-PMMA, or *at*-PP-*b*-*st*-PMMA blockcopolymers.[34]

6.2. Statistical Copolymers

In the case of statistical REM-GTP copolymerization, monomers are required to have the same propagation step and similar reactivity. Therefore, the random copolymerization of olefins with polar monomers represents an unmet challenge for a direct copolymerization via rare earth metals or early transition metals.[5]

For REM-GTP, the coordination strength of different monomers needs to be nearly identical to allow the formation of statistical copolymers, due to the high oxophilicity of rare earth metals. Already slight changes in the polarity or coordination strength of the monomers can promote the formation of block copolymers or homopolymers instead of statistical copolymers. Therefore, in most cases, defined block copolymer structures are reported in literature for REM-GTP (vide supra).

However, statistical copolymers of MMA and BMA (*n*-butyl methacrylate) were synthesized and their copolymerization parameters determined indicating an alternating character. Both, Fineman–Ross ($rMMA_{0.65}$, $rBMA_{0.78}$) and the Kelen–Tüdõs parameters gave monomer reactivity ratios less than unity with the product of the ratios ($rMMA \cdot rBMA$) = 0.45 (Kelen–Tüdõs method), indicating that there is a greater tendency for cross-propagation than for homopolymerization and that the copolymer formed instantaneously has a somewhat alternating character.[35] The random copolymers of methyl acrylate, ethyl acrylate, and *n*-butyl acrylate were described by Yasuda and Ihara.[25a]

Statistical copolymers of DAVP can be synthesized via REM-GTP using easily accessible tris(cyclopentadienyl) ytterbium Cp_3Yb. The copolymerization parameters determined by activity measurements indicate the formation of almost perfectly random copolymers (r_1, $r_2 \approx 1$) (Figure 22).[36] Therefore, the polymerization rate of vinylphosphonate GTP is mainly limited by the steric demand of the growing polymer chain end. Poly(vinylphosphonate)s (e.g., PDEVP) show an amphiphilic behavior and are soluble in water and lighter alcohols. Thus, PDEVP exhibits a lower critical solution temperature (LCST) in water following a coil–globule transition mechanism, with cloud points usually ranging in the physiological range.[37] The cloud point of a polymer solution generally depends on the molar mass, concentration, and polymer architecture (linear, star, block, etc.).[37,38] PDEVP with high and defined molecular mass can easily be prepared from tris(cyclopentadienyl) lanthanide complexes and the thermoresponsive behavior shows a sharp phase transition upon heating due to the narrow molecular weight distribution.[37] The polymerization rate of DAVP via Cp_3Ln catalysts accelerates with decreasing ionic radius of the used metal (i.e., lutetium being the fastest metal; TOF/I* > 265 000 h^{-1}; PDI < 1.2).[37] This effect of steric crowded complexes is attributed to entropic reasons and was confirmed by Eyring plots for several Cp_2LnX systems (vide supra).[16] The free poly(vinylphosphonic acid) can be obtained from PDAVPs via thermal

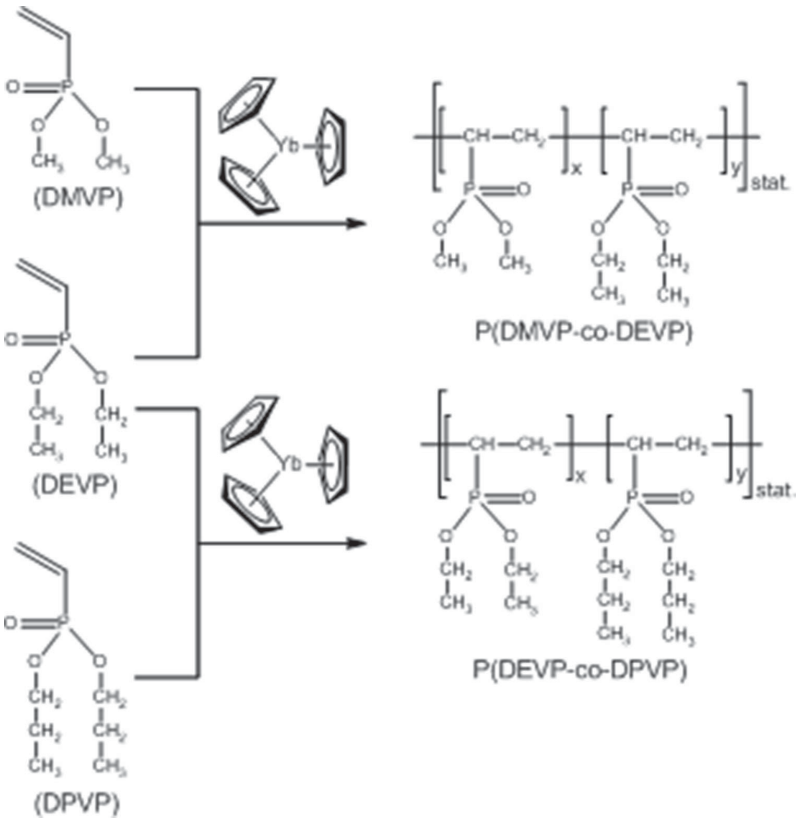

Figure 22. Molecular structure of the dialkyl vinylphosphonates and their conversion to random copoly(dialkyl vinylphosphonate)s via Cp_3Yb-initiated GTP. Reproduced with permission.[36] Copyright 2012, American Chemical Society.

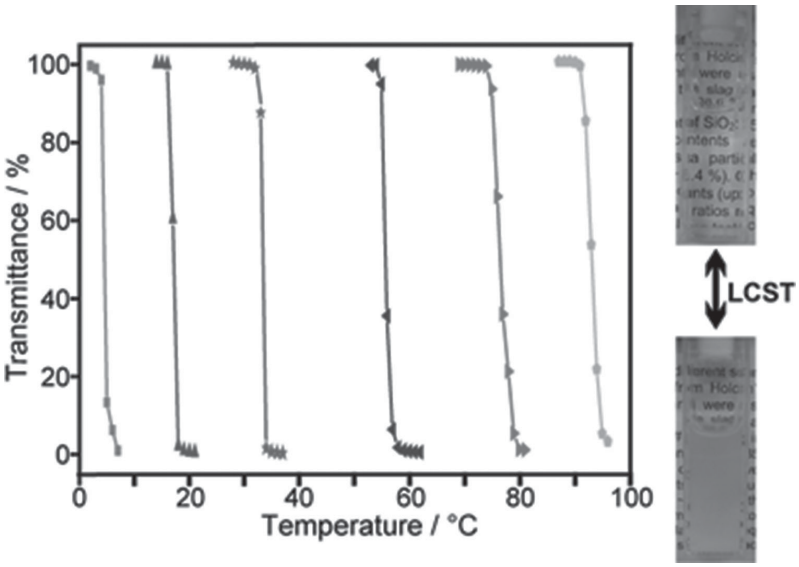

Figure 23. Determination of the cloud points of DEVP–DAVP copolymers with different DEVP content and optical pictures of PDAVP copolymer in aqueous solution below and above the LCST.

treatment (elimination of ethylene from PDEVP or propylene from PDIVP) or transesterification and subsequent hydrolysis under mild conditions.[37]

Copolymers of diethyl vinylphosphonate and dimethyl- or di-*n*-propyl vinylphosphonate synthesized by this method show thermoresponsive properties, i.e., exhibit a tunable LCST following a coil-globule transition mechanism, with cloud points between 5 and 92 °C. Moreover, the LCST can be precisely adjusted by varying the comonomer composition and increases linearly with the content of hydrophilic comonomer. These thermoresponsive poly(vinylphosphonate)s also exhibit a sharp and reversible phase transition, and minor environmental effects such as concentration and additives on their cloud point. In combination with its high biocompatibility, statistical P(DAVP)s are an interesting new precision material showing a narrow and tunable LCST compared to other established thermoresponsive materials (see Figure 23).[36]

7. End-Capped Polymers

End-capped polymers are a very simple, yet vital building block for further modifications of high precision materials. Polymers with defined end groups can be efficiently functionalized by azide–alkine click reactions,[39] thiol ene click reactions,[40] or Diels–Alder cyclizations.[41]

One of the first examples of rare earth metal complexes introducing specific end group functionalities to polyolefins is presented in the work of Teuben and co-workers[42] Thiophene is readily metalated at the alpha position by $[(C_5Me_5)_2LaH]_2$ via σ-bond metathesis and $(C_5Me_5)_2La(SC_4H_3)$ is formed.[42b] Upon addition of ethylene, thiophenyl terminated poly(ethylene) is formed in a catalytic cycle (Figure 24).

Besides thiophene, also silane, phosphine and amine-terminated polyethylenes were synthesized.[43–45] This represents an alternative way to introduce heteroatom functionalities into unpolar materials derived from olefins (see Figure 25).

Mashima and co-workers[46] published an improved method to functionalize polymers from polar monomers with defined end group functionalities. A variety of pyridinyl and internal alkynyl initiators were synthesized for the polymerization of 2VP via

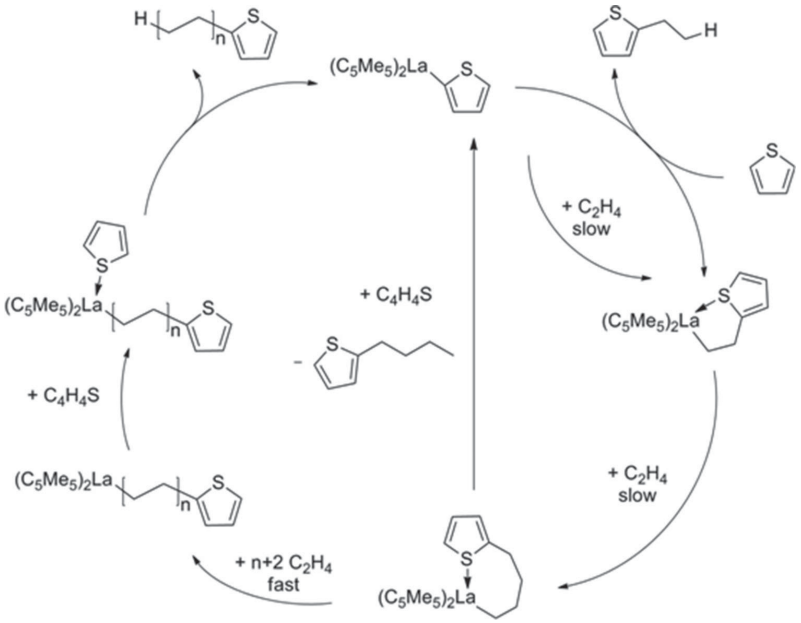

Figure 24. Catalytic cycle for the production of thiophene end capped poly(ethylene). Redrawn from ref.[42b]

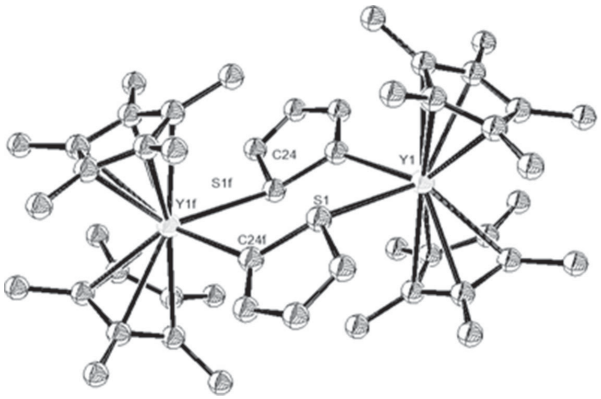

Figure 25. Molecular structure of a thiophenyl-bridged yttrocene (hydrogen atoms are omitted for clarity). Redrawn from ref.[42b]

C—H activation at yttrium ene-diamido complexes. The catalysts can be prepared in situ via σ-bond metathesis, or for the complexes a, b, and c (Figure 26), they were isolated and tested for their application in 2VP polymerization. Thus, P2VP was obtained with various stable pyridine and alkyne end groups that can be further modified or used for other applications and monomers.

The ability of rare earth metal complexes to selectively undergo σ-bond metathesis opens up a wide field for introducing functionalities of polar heteroaromatic groups to unpolar polyolefins. Also post-polymerization modifications of polar monomers with functional end group and other building blocks can be combined to create distinguished features for precision materials (e.g., click chemistry vide supra).[47]

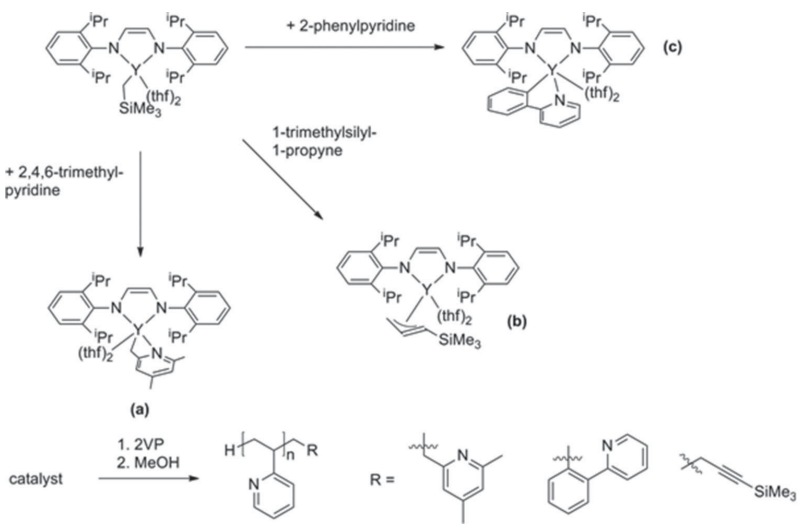

Figure 26. C–H activation of heteroaromatic compounds and internal alkynes. Synthesis of end-capped P2VP. Redrawn from ref.[46]

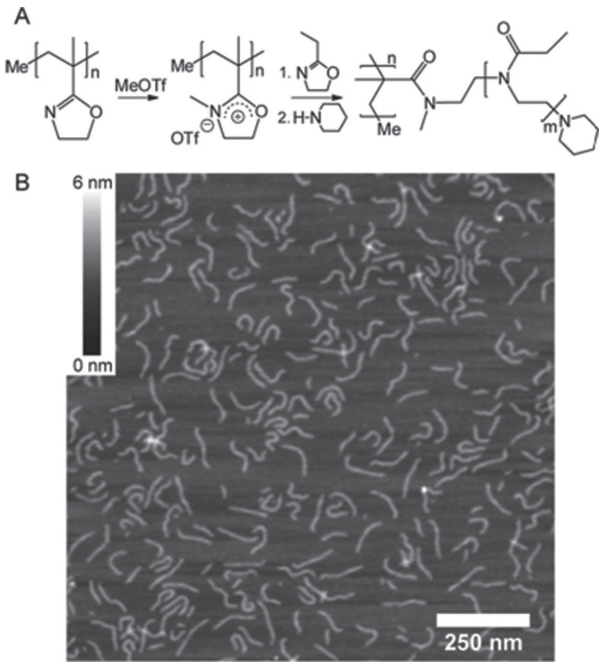

Figure 27. AFM scan of the molecular brush P(IPOx-*g*-EtOx). The polymer was deposited by dip-coating from a dilute chloroform solution onto freshly cleaved mica substrates. Reproduced with permission.[22] Copyright 2013, American Chemical Society.

8. One- and Two-Dimensional Polymer Brushes

REM-GTP combines the advantages of both living ionic and coordinative polymerizations and gives access to various polymers with high molecular weight and low dispersity. Besides solution polymerization, REM-GTP, in combination with other polymerization techniques, allows the preparation of 2D and also 3D polymer brushes. Our group used REM-GTP-prepared PIPOx as the backbone polymer to react with methyl triflate, forming a polyoxazolinium salt as a macroinitiator. Then, molecular brush side chains are formed by living cationic ring-opening polymerization (LCROP) of 2-ethyl-2-oxazoline (EtOx) (Figure 27). As verified by AFM measurements, all the molecular brushes adopt a stretched conformation due to the repulsion of poly(2-oxazoline) side chains (Figure 27). Moreover, the contour length distribution is narrow, which corroborates the narrow molecular mass distribution of the PIPOx backbone, giving access to macromolecular objects with a highly

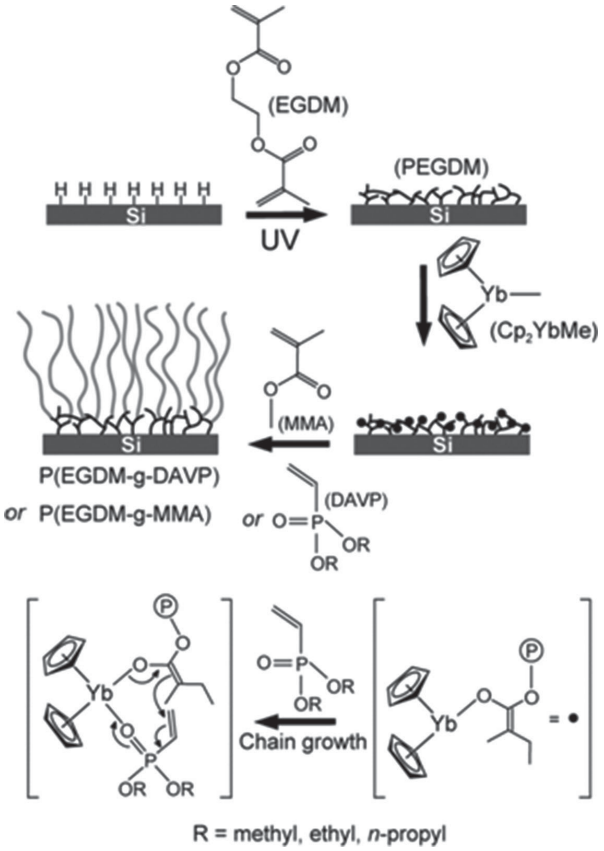

Figure 28. Preparation of precoating layer, ytterbocene catalyst immobilization, and subsequent SI-GTP of MMA or DAVP from a PEGDM film on silicon wafer; below: SI-GTP reaction mechanism for initiation and chain growth. Reproduced with permission.[56] Copyright 2012, American Chemical Society.

uniform distributed architecture on the micrometer scale.

Surface-initiated polymerizations (SIP) are used for all polymerization types to prepare dense polymer brushes on surfaces and particles.[48] To tailor the chemical and physical properties of target substrates, radical polymerization,[49] ionic polymerization,[50] coordination polymerization,[51] ring-opening,[52] or metathesis polymerization[53] and catalytic polycondensation[54] were used in the field of SIP. For instance, surface-initiated atom transfer radical polymerization (SI-ATRP) gained great interest, as it can be performed even at room temperature in an aqueous solution.[55]

We presented the first example of a surface-initiated group transfer polymerization (SI-GTP) mediated by rare earth metal catalysts for 3D polymer brush synthesis (Figure 28).[56] First, a PEGDM network is created by photohydrosilylation/self-initiated photografting and photopolymerization (SIPGP) of ethylene glycol dimethacrylate (EGDM) directly on hydrogen-terminated silicon.

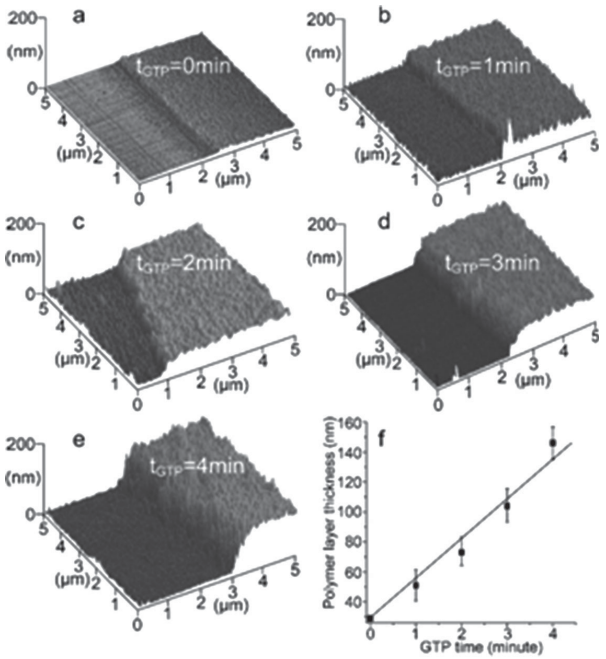

Figure 29. Three-dimensional representation of AFM scans of a PEGDM film on silicon wafer and polymer brushes after SI-GTP of DEVP. a) SIPGP of EGDM for 30 min gives PEGDM film with a thickness of 29 ± 6 nm. b–e) SI-GTP of DEVP on the same substrate after 1, 2, 3 and 4 min results in 51 ± 11, 73 ± 9, 104 ± 11 and 146 ± 12 nm thick polymer brush layer respectively. f) P(EGDM-*g*-DEVP) layer thickness as a function of SI-GTP time. Reproduced with permission.[56] Copyright 2012, American Chemical Society.

The preserved methacrylate functionalities can be reacted with Cp_2YbMe, serving as efficient initiators for the successive SI-GTP of (meth)acrylates or DAVP to form polymer brushes. An extremely rapid and almost constant polymer layer thickness growth rate of 57 and 26.5 nm min^{-1} was found for MMA and DEVP, respectively (Figure 29). The method is applicable to functional monomers, which cannot be polymerized by other surface-initiated polymerizations and thus broaden the range of accessible functional polymer brushes. Moreover, the preparation of functional thermoresponsive PDEVP brushes is demonstrated as well. Poly(vinylphosphonic acid) is easily accessible under mild conditions by polymer-analogous reactions. The nontoxic and thermoswitchable surfaces are of great interest for diverse biological and medical applications including controlled cell growth and cell release as well as proton conducting films.[56]

9. Conclusion

Within the past few decades, the demand for precision materials with defined properties has been a main

driving force in polymer science. REM-GTP as a living polymerization offers precise control of the polymer molecular mass and the polymer microstructure, and therefore leads to tunable material properties. The advantages of REM-GTP for the polymerization of new materials from polar monomers are remarkable for (meth)acrylates and (meth)acrylamides, where alternatives exist, 2-vinylpyridine or 2-isopropenyl-2-oxazoline, having less feasible polymerization techniques and DAVP being satisfactorily accessible only via REM-GTP.

This allows the high precision synthesis of macromolecular structures, such as random copolymers, block copolymers, as well as end-funtionalized polymers. Such materials will give access to so far unknown physical and mechanical properties as well as new applications for new classes of materials.

Received: May 19, 2014; Revised: June 20, 2014; Published online: August 22, 2014; DOI: 10.1002/macp.201400271

Keywords: coordinative anionic polymerization; group transfer polymerization; polar monomers; rare earth metals

[1] D. W. Hapke, in *Plastics Europe, Plastics – the Facts*, Plastics Europe, **2013**.
[2] a) M. Ouchi, T. Terashima, M. Sawamoto, *Chem. Rev.* **2009**, *109*, 4963; b) K. Satoh, M. Kamigaito, *Chem. Rev.* **2009**, *109*, 5120.
[3] O. W. Webster, W. R. Hertler, D. Y. Sogah, W. B. Farnham, T. V. RajanBabu, *J. Am. Chem. Soc.* **1983**, *105*, 5706.
[4] a) H. Yasuda, H. Yamamoto, K. Yokota, S. Miyake, A. Nakamura, *J. Am. Chem. Soc.* **1992**, *114*, 4908; b) S. Collins, D. G. Ward, *J. Am. Chem. Soc.* **1992**, *114*, 5460.
[5] E. Y. X. Chen, *Chem. Rev.* **2009**, *109*, 5157.
[6] a) Y. Li, D. G. Ward, S. S. Reddy, S. Collins, *Macromolecules* **1997**, *30*, 1875; b) R. Sustmann, W. Sicking, F. Bandermann, M. Ferenz, *Macromolecules* **1999**, *32*, 4204; c) F. Bandermann, M. Ferenz, R. Sustmann, W. Sicking, *Macromol. Symp.* **2001**, *174*, 247.
[7] W. J. Evans, D. M. DeCoster, J. Greaves, *Macromolecules* **1995**, *28*, 7929.
[8] L. S. Boffa, B. M. Novak, *Macromolecules* **1994**, *27*, 6993.
[9] O. Webster, *New Synthetic Methods, Advances in Polymer Science, Vol 167*, Springer, Berlin/Heidelberg, Germany **2004**, p. 1.
[10] a) K. Fuchise, Y. Chen, T. Satoh, T. Kakuchi, *Polym. Chem.* **2013**, *4*, 4278; b) M. Rikkou-Kalourkoti, O. W. Webster, C. S. Patrickios, *Encyclopedia of Polymer Science and Technology, Vol. 6*, Wiley, Hoboken, NJ, USA **2014,** pp. 527.
[11] L. S. Boffa, B. M. Novak, *Chem. Rev.* **2000**, *100*, 1479.
[12] T. Kawauchi, M. Ohara, M. Udo, M. Kawauchi, T. Takeichi, *J. Polym. Sci., Part A: Polym. Chem.* **2010**, *48*, 1677.
[13] S. Salzinger, B. Rieger, *Macromol. Rapid Commun.* **2012**, *33*, 1327.
[14] Y. Zhang, G. M. Miyake, M. G. John, L. Falivene, L. Caporaso, L. Cavallo, E. Y. X. Chen, *Dalton Trans.* **2012**, *41*, 9119.
[15] U. B. Seemann, J. E. Dengler, B. Rieger, *Angew. Chem.* **2010**, *122*, 3567.
[16] S. Salzinger, B. S. Soller, A. Plikhta, U. B. Seemann, E. Herdtweck, B. Rieger, *J. Am. Chem. Soc.* **2013**, *135*, 13030.
[17] a) K. C. Hultzsch, T. P. Spaniol, J. Okuda, *Angew. Chem. Int. Ed.* **1999**, *38*, 227; b) K. C. Hultzsch, *Ph.D. Thesis*, Universität Mainz, Mainz, Germany **1999**.
[18] a) A. Amgoune, C. M. Thomas, S. Ilinca, T. Roisnel, J.-F. Carpentier, *Angew. Chem. Int. Ed.* **2006**, *45*, 2782; b) A. Amgoune, C. M. Thomas, T. Roisnel, J.-F. Carpentier, *Chem. – A Eur. J.* **2006**, *12*, 169; c) M. Bouyahyi, N. Ajellal, E. Kirillov, C. M. Thomas, J.-F. Carpentier, *Chem. Eur. J.* **2011**, *17*, 1872.
[19] J. Fang, M. J. L. Tschan, E. Brule, C. Robert, C. M. Thomas, L. Maron, *Dalton Trans.* **2013**, *42*, 9226.
[20] a) D. A. Tomalia, B. P. Thill, M. J. Fazio, *Polym. J.* **1980**, *12*, 661; b) N. Zhang, S. Huber, A. Schulz, R. Luxenhofer, R. Jordan, *Macromolecules* **2009**, *42*, 2215; c) T. Kagiya, T. Matsuda, K. Zushi, *J. Macromol. Sci., Part A: Chem.* **1972**, *6*, 1349; d) C. Weber, T. Neuwirth, K. Kempe, B. Ozkahraman, E. Tamahkar, H. Mert, C. R. Becer, U. S. Schubert, *Macromolecules* **2012**, *45*, 20.
[21] G. Odian, *Principles of Polymerization,* Wiley, Hoboken, NJ, USA **2004**.
[22] N. Zhang, S. Salzinger, B. S. Soller, B. Rieger, *J. Am. Chem. Soc.* **2013**, *135*, 8810.
[23] a) H. Yasuda, M. Furo, H. Yamamoto, A. Nakamura, S. Miyake, N. Kibino, *Macromolecules* **1992**, *25*, 5115; b) W. J. Evans, K. J. Forrestal, J. T. Leman, J. W. Ziller, *Organometallics* **1996**, *15*, 527; c) W. J. Evans, K. J. Forrestal, J. W. Ziller, *Angew. Chem. Int. Ed. Engl.* **1997**, *36*, 774; d) W. J. Evans, K. J. Forrestal, J. W. Ziller, *J. Am. Chem. Soc.* **1998**, *120*, 9273.
[24] a) W. J. Evans, B. L. Davis, T. M. Champagne, J. W. Ziller, *Proc. Natl. Acad. Sci.* **2006**, *103*, 12678; b) M. R. MacDonald, J. W. Ziller, W. J. Evans, *J. Am. Chem. Soc.* **2011**, *133*, 15914; c) M. R. MacDonald, J. E. Bates, M. E. Fieser, J. W. Ziller, F. Furche, W. J. Evans, *J. Am. Chem. Soc.* **2012**, *134*, 8420; d) M. R. MacDonald, J. E. Bates, J. W. Ziller, F. Furche, W. J. Evans, *J. Am. Chem. Soc.* **2013**, *135*, 9857; e) J. K. Peterson, M. R. MacDonald, J. W. Ziller, W. J. Evans, *Organometallics* **2013**, *32*, 2625; f) W. J. Evans, *Inorg. Chem.* **2007**, *46*, 3435.
[25] a) H. Yasuda, E. Ihara, *Macromol. Chem. Phys.* **1995**, *196*, 2417; b) H. Yasuda, E. Ihara, in *Metal Complex Catalysts Supercritical Fluid Polymerization Supramolecular Architecture, Advances in Polymer Science, Vol. 133*, (Eds: D. A. Canelas, J. M. DeSimone, A. Harada, E. Ihara, K. Mashima, A. Nakamura, Y. Nakayama, H. Yasuda), Springer, Berlin/Heidelberg, Germany **1997**, pp. 53; c) H. Yasuda, *J. Polym. Sci., Part A: Polym. Chem.* **2001**, *39*, 1955.
[26] E. Ihara, M. Morimoto, H. Yasuda, *Macromolecules* **1995**, *28*, 7886.
[27] W. R. Mariott, E. Y. X. Chen, *Macromolecules* **2005**, *38*, 6822.
[28] Y. Ning, H. Zhu, E. Y. X. Chen, *J. Organomet. Chem.* **2007**, *692*, 4535.
[29] E. Y. X. Chen, M. J. Cooney, *J. Am. Chem. Soc.* **2003**, *125*, 7150.
[30] L. S. Boffa, B. M. Novak, *Tetrahedron* **1997**, *53*, 15367.
[31] G. Desurmont, T. Tokimitsu, H. Yasuda, *Macromolecules* **2000**, *33*, 7679.
[32] G. Desurmont, M. Tanaka, Y. Li, H. Yasuda, T. Tokimitsu, S. Tone, A. Yanagase, *J. Polym. Sci., Part A: Polym. Chem.* **2000**, *38*, 4095.
[33] C. Yao, D. Liu, P. Li, C. Wu, S. Li, B. Liu, D. Cui, *Organometallics* **2014**, *33*, 684.

Macromolecular
Chemistry and Physics

www.mcp-journal.de

[34] a) H. Frauenrath, S. Balk, H. Keul, H. Höcker, *Macromol. Rapid Commun.* **2001**, *22*, 1147; b) J. Jin, E. Y. X. Chen, *Macromol. Chem. Phys.* **2002**, *203*, 2329.
[35] A. Rodriguez-Delgado, E. Y. X. Chen, *Macromolecules* **2005**, *38*, 2587.
[36] N. Zhang, S. Salzinger, B. Rieger, *Macromolecules* **2012**, *45*, 9751.
[37] S. Salzinger, U. B. Seemann, A. Plikhta, B. Rieger, *Macromolecules* **2011**, *44*, 5920.
[38] a) F. A. Plamper, M. Ruppel, A. Schmalz, O. Borisov, M. Ballauff, A. H. E. Müller, *Macromolecules* **2007**, *40*, 8361; b) W. Li, A. Zhang, K. Feldman, P. Walde, A. D. Schlüter, *Macromolecules* **2008**, *41*, 3659; c) J. Roeser, B. Heinrich, C. Bourgogne, M. Rawiso, S. Michel, V. Hubscher-Bruder, F. Arnaud-Neu, S. Méry, *Macromolecules* **2013**, *46*, 7075; d) N. Zhang, R. Luxenhofer, R. Jordan, *Macromol. Chem. Phys.* **2012**, *213*, 1963; e) S. Furyk, Y. Zhang, D. Ortiz-Acosta, P. S. Cremer, D. E. Bergbreiter, *J. Polym. Sci., Part A: Polym. Chem.* **2006**, *44*, 1492.
[39] J. A. Opsteen, J. C. M. van Hest, *Chem. Commun.* **2005**, 57.
[40] A. B. Lowe, *Polym. Chem.* **2010**, *1*, 17.
[41] a) H. Durmaz, F. Karatas, U. Tunca, G. Hizal, *J. Polym. Sci., Part A: Polym. Chem.* **2006**, *44*, 499; b) H. Durmaz, B. Colakoglu, U. Tunca, G. Hizal, *J. Polym. Sci., Part A: Polym. Chem.* **2006**, *44*, 1667; c) H. Durmaz, A. Dag, O. Altintas, T. Erdogan, G. Hizal, U. Tunca, *Macromolecules* **2006**, *40*, 191.
[42] a) B.-J. Deelman, M. Booij, A. Meetsma, J. H. Teuben, H. Kooijman, A. L. Spek, *Organometallics* **1995**, *14*, 2306; b) S. N. Ringelberg, A. Meetsma, B. Hessen, J. H. Teuben, *J. Am. Chem. Soc.* **1999**, *121*, 6082.
[43] K. Koo, P.-F. Fu, T. J. Marks, *Macromolecules* **1999**, *32*, 981.
[44] a) A. M. Kawaoka, T. J. Marks, *J. Am. Chem. Soc.* **2004**, *126*, 12764; b) A. M. Kawaoka, T. J. Marks, *J. Am. Chem. Soc.* **2005**, *127*, 6311.
[45] a) S. B. Amin, T. J. Marks, *J. Am. Chem. Soc.* **2007**, *129*, 10102; b) S. B. Amin, S. Seo, T. J. Marks, *Organometallics* **2008**, *27*, 2411.
[46] H. Kaneko, H. Nagae, H. Tsurugi, K. Mashima, *J. Am. Chem. Soc.* **2011**, *133*, 19626.
[47] H. Tsurugi, K. Yamamoto, H. Nagae, H. Kaneko, K. Mashima, *Dalton Trans.* **2014**, *43*, 2331.
[48] S. Edmondson, V. L. Osborne, W. T. S. Huck, *Chem. Soc. Rev.* **2004**, *33*, 14.
[49] a) R. Barbey, L. Lavanant, D. Paripovic, N. Schüwer, C. Sugnaux, S. Tugulu, H.-A. Klok, *Chem. Rev.* **2009**, *109*, 5437; b) K. Matyjaszewski, P. J. Miller, N. Shukla, B. Immaraporn, A. Gelman, B. B. Luokala, T. M. Siclovan, G. Kickelbick, T. Vallant, H. Hoffmann, T. Pakula, *Macromolecules* **1999**, *32*, 8716; c) K. Ohno, Y. Ma, Y. Huang, C. Mori, Y. Yahata, Y. Tsujii, T. Maschmeyer, J. Moraes, S. Perrier, *Macromolecules* **2011**, *44*, 8944; d) Z. Bao, M. L. Bruening, G. L. Baker, *J. Am. Chem. Soc.* **2006**, *128*, 9056.
[50] a) Q. Zhou, S. Wang, X. Fan, R. Advincula, J. Mays, *Langmuir* **2002**, *18*, 3324; b) R. Advincula, in *Surface-Initiated Polymerization I, Advances in Polymer Science*, *Vol. 197*, (Ed: R. Jordan), Springer, Berlin/Heidelberg, Germany **2006**, pp. 107; c) R. Jordan, A. Ulman, *J. Am. Chem. Soc.* **1998**, *120*, 243; d) R. Jordan, A. Ulman, J. F. Kang, M. H. Rafailovich, J. Sokolov, *J. Am. Chem. Soc.* **1999**, *121*, 1016.
[51] a) D. Priftis, N. Petzetakis, G. Sakellariou, M. Pitsikalis, D. Baskaran, J. W. Mays, N. Hadjichristidis, *Macromolecules* **2009**, *42*, 3340; b) J. Zheng, Y. Wang, L. Ye, Y. Lin, T. Tang, J. Zhang, *Macromol. Rapid Commun.* **2014**, *35*, 1198.
[52] a) K. Yoon, Y. Kim, I. Choi, *J. Polym. Res.* **2005**, *11*, 265; b) P. Viville, R. Lazzaroni, E. Pollet, M. Alexandre, P. Dubois, *J. Am. Chem. Soc.* **2004**, *126*, 9007.
[53] a) Q. Ye, X. Wang, S. Li, F. Zhou, *Macromolecules* **2010**, *43*, 5554; b) C. J. Faulkner, R. E. Fischer, G. K. Jennings, *Macromolecules* **2010**, *43*, 1203; c) G. Jiang, R. Ponnapati, R. Pernites, M. J. Felipe, R. Advincula, *Macromolecules* **2010**, *43*, 10262; d) M. Weck, J. J. Jackiw, R. R. Rossi, P. S. Weiss, R. H. Grubbs, *J. Am. Chem. Soc.* **1999**, *121*, 4088.
[54] a) N. Marshall, S. K. Sontag, J. Locklin, *Chem. Commun.* **2011**, *47*, 5681; b) N. Marshall, S. K. Sontag, J. Locklin, *Macromolecules* **2010**, *43*, 2137; c) T. Beryozkina, K. Boyko, N. Khanduyeva, V. Senkovskyy, M. Horecha, U. Oertel, F. Simon, M. Stamm, A. Kiriy, *Angew. Chem. Int. Ed.* **2009**, *48*, 2695.
[55] J. Pyun, T. Kowalewski, K. Matyjaszewski, *Macromol. Rapid Commun.* **2003**, *24*, 1043.
[56] N. Zhang, S. Salzinger, F. Deubel, R. Jordan, B. Rieger, *J. Am. Chem. Soc.* **2012**, *134*, 7333.

5 Conclusion and Outlook

REM-GTP combines the advantages of both living-anionic and coordinative polymerizations. After extensive research on (meth)acrylate and (meth)acrylamide polymerizations has been made in the 1990s and 2000s, this field of research is receiving increased attention in the past years for the polymerization of novel polar monomers. These monomers do not have to be new regarding its synthesis, first report, or application via other polymerization techniques; however, have not been polymerized prior by RE catalysts and their polymerization using metal complexes often results in distinct advantages such as low PDI, good control over the degree of polymerization, high activities, stereoregular polymerizations, formation of block copolymers, or the introduction of chain end functionalities (see Table 4).

Table 4. Comparison of Living-anionic and Coordinative Polymerizations

Living-type polymerization	Coordinative polymerization
Easy control over molecular weight	Stabilization of the growing chain end
Low polydispersity	Suppression of side reactions
Formation of block copolymers	Activation of the coordinated monomer
Introduction of chain end functionalities	Stereospecific polymerization

The field of polymerization catalysis of commercially available monomers has crucially advanced research in the field of RE metalorganic chemistry. After the original discoveries of Yasuda et al. and Chen et al. research activities slowed down in the past years for the polymerization of (meth)acrylates and (meth)acrylamides. The introduction of new monomers such as vinylphosphonates has given this field new impulses and after advantages in this field with simple RE complexes were conducted it was a major scope of this thesis to establish new synthetic methods for the synthesis of RE metallocenes and to apply different ligand systems for the REM-GTP of vinylphosphonates. The usage of ligand-induced steric crowding with different substituents at the cyclopentadienyl core was expected to lead to first insights for a stereoregular polymerization of vinylphosphonates. Furthermore, the limitation of vinylphosphonate REM-GTP by an inefficient initiation by traditionally used strongly basic carbanion initiators (*e.g.*, methyl, $-CH_2TMS$ ligands) was a scientific problem to be solved and alternative efficient and synthetically accessible initiating ligands needed to be identified.

This work presents an updated review covering the latest publications until 2015 on the REM-GTP of polar monomers and the extension from vinylphosphonates to *N*-coordinating monomers in Chapter 4.1. In Chapter 4.2, the first in-depth mechanistic study on initiation and propagation of vinylphosphonate REM-GTP is presented and the dependence of the activities as a function of the metal ionic radius is explained by thermodynamic considerations.

The REM-GTP of vinylphosphonates was shown to follow a monometallic Yasuda-type polymerization mechanism, with an S_N2-type associative displacement of the polymer phosphonate ester by a monomer as the rate-determining step. Surprisingly, the activation entropy $\Delta S^{\ddagger}$ of the rate determining step is strongly affected by the metal radius and the monomer size, whereas these parameters show only minor influence on the activation enthalpy $\Delta H^{\ddagger}$ for the applied unsubstituted RE metallocenes. Accordingly, the propagation rate of REM-GTP is mainly determined by the change of rotational and vibrational restrictions within the eight-membered metallacycle in the rate-determining step. This result stands in large contrast to previous measurements on (meth)acrylate REM-GTP and explains the reverse correlation between activity and the radius of the metal center. Furthermore, a major mechanistic improvement of vinylphosphonate REM-GTP has been the application of *sym*-collidine hydrocarbyl initiators obtained by C–H bond activation. The C–H bond activation proceeds via σ-bond metathesis and was found to depend heavily on the size of the used metal center for yttrium and lutetium (see Chapter 4.3). The high initiator efficiencies and lack of an initiation period were attributed to the proposed mechanistic match between initiation and propagation, where both follow an eight membered-ring transition state. This assumption is supported by crystallographic findings that the activated and initiating methylene group of *sym*-collidine has a partial double bond character.

Chapter 4.4 presents the first study on ligand induced steric crowding for substituted tris(cyclopentadienyl) RE complexes for the polymerization of vinylphosphonates. Temperature-dependent kinetic analyses are performed for several methyl-, trimethylsilyl-, and tetramethylcyclopentadienyl-substituted tris(cyclopentadienyl) complexes to determine the activation enthalpies $\Delta H^{\ddagger}$ and entropies $\Delta S^{\ddagger}$ according to the Eyring equation. The bond distances of the pentacoordinate intermediate were found to be prolonged for $(C_5Me_4H)_3Ln$ complexes (Ln = Sm, Tb, Y) and a change in the reaction enthalpy $\Delta H^{\ddagger}$ is observed compared to un- and monosubstituted compounds. Furthermore, the microstructure of all obtained poly(vinylphosphonate) samples has to be considered atactic despite various used metal centers or ligand systems. The setback of atactic poly(vinylphosphonate)s was found to be in contrast to previous reports of Yasuda et al. for syndiotactic PMMA and our original expectations.

Therefore, we further developed and refined our procedure of ligand induced steric crowding leading to the identification and application of constrained geometry complexes as possible candidates for the REM-GTP of vinylphosphonates. For a stereoregular polymerization of vinylphosphonates, rigid (*i.e.*, bridged) and partly sterically crowded ligand systems had to be evaluated in a next step. CGCs consist of a bridged amide and cyclopentadienyl binding motive and often a sterically crowded (C_5Me_4R) coordination sphere is used with an accessible amide such as $RNtBu^-$ (R = bridge). In Chapter 4.5, a manuscript draft for the stereoregular REM-GTP of vinylphosphonates using such RE CGCs is shown in

a stadium prior to submission for a journal. Additional measurements to verify the signal attribution in ^{31}P NMR to quantify the amount of [*mm*] triads or [*mmmm*] pentads are needed before publication.

Furthermore, the material properties of several aliphatic and aromatic poly(vinylphosphonate)s and their application as macromolecular flame retardants for polycarbonate were performed and are shown in Chapter 4.6. Coatings of aliphatic poly(vinylphosphonate)s were prepared by simple dip coating and PC blends with aromatic poly(vinylphosphonate)s (PDTVP) were obtained by compounding at 240 °C and 60 rpm for 20 minutes. PDTVP is a promising flame retardant additive, because of its high thermal stability and its compatibility with polycarbonate. PDIVP shows excellent performance as a flame retardant coating, because it forms a stable, blistered crust of poly(vinylphosphonic acid) upon flame treatment. The conversion of PDTVP was found to be significantly lower even for extended reaction times (< 40%, overnight) and should be further investigated in a mechanistic study.

The first report on the facile and efficient REM-GTP of the versatile dual-functional monomer 2-isopropenyl-2-oxazoline (IPOx) is presented in Chapter 4.7. The reaction of $(C_5H_5)_2YbMe$ with IPOx, yields high molecular weight PIPOx with an unprecedented low polydispersity (PDI < 1.05). This method was also found to be applicable to 2-vinylpyridine (2VP), giving access to P2VP of defined molar mass and narrow molecular weight distribution. REM-GTP of IPOx and 2VP occurs via *N*-coordination at the RE metal center, which has rarely been reported previously. Copolymerization studies were further conducted in this work and a reactivity order was established for the REM-GTP of polar monomers being: DEVP ~ DMAA >> MA > MMA >> IPOx >> 2VP. This behavior is attributed to the coordination strength of the respective monomers at the RE metal center and/or the nucleophilicity of the growing polymer chain end. Consecutive polymerizations of different monomers are therefore only possible in order of increasing coordination strength/sufficient nucleophilicity, and restricted to comonomers with a similar polarity.

New ligand systems for the REM-GTP of polar monomers were introduced in Chapter 4.8. 2-Methoxyethylaminobis(phenolate)-yttrium catalysts with varying steric demand were synthesized and showed moderate to high activities in the polymerization experiments (DMAA > 2VP ~ IPOX > DEVP > DIVP). The general low activities for vinylphosphonates limit these systems and steric crowding was found to be disadvantageous resulting in lower activities. Mechanistic investigations with 2VP revealed that 2-methoxyethylamino-bis(phenolate)-yttrium catalysts follow a monometallic GTP mechanism allowing the production of blockcopolymers. This initial study on bis(phenolate) yttrium complexes started significant research activities in this area leading to reports on stereoregular 2VP polymerizations and the application of well-known P2VP-*b*-PDEVP block copolymers for drug delivery systems due to

micellization in aqueous solutions and their versatile properties (amphiphilic behavior, pH-switchable, tunable LCST).

A second review on the precise synthesis of homopolymers, block copolymers, statistical copolymers, surface modifications, and polymer brushes featuring selected examples of the work of Yasuda, Evans, Teuben, Chen, and our group is presented in Chapter 4.9.

The three main findings of this thesis advancing the field of vinylphosphonate REM-GTP are:

I. Hydrocarbyl initiators from C–H bond activation are highly active, efficient initiators for vinylphosphonates and the stable C–C end-group allows further application of this method for surface decorations.
II. Ligand induced steric crowding of substituted unbridged tris(cyclopentadienyl) RE metallocenes does not induce any change on the microstructure of vinylphosphonates. The metal–monomer and metal–poly(phosphonate ester) bond distances were found to be prolonged for the pentacoordinated intermediate.
III. RE CGCs were found to give access to highly isotactic poly(vinylphosphonate)s. A missing signal attribution for the microstructure of vinylphosphonates limits the validity of the obtained samples so far for publication.

REM-GTP is a fascinating topic in macromolecular polymerization catalysis and one of the few topics in RE element and group IV polymerization chemistry that develops steadily. In future studies, the following experimental research should be conducted to understand and learn more about this chemistry.

In the last years, SI-GTP was successfully transferred from surfaces and microscopic spheres to nano particles. The applied photografting and photopolymerization lead to agglomeration and inconsistent analytic data for materials on the sub-micron scale. Therefore, free-standing nanoparticles should be studied having lutidine or internal alkyne functionalities on their surface and such compounds can be linked with RE catalysts by C–H bond activation giving access to the wide range of accessible monomers for the decoration of such particles. First, highly promising studies were conducted for the synthesis of free-standing poly(vinylphosphonate) covered SiNPs via SI-GTP (see Figure 19).[306]

Sample	Diameter [nm]	%PD [%]
SiNC-alkyne	3.0	34.3
SiNC-*g*PDIVP	64.2	38.5

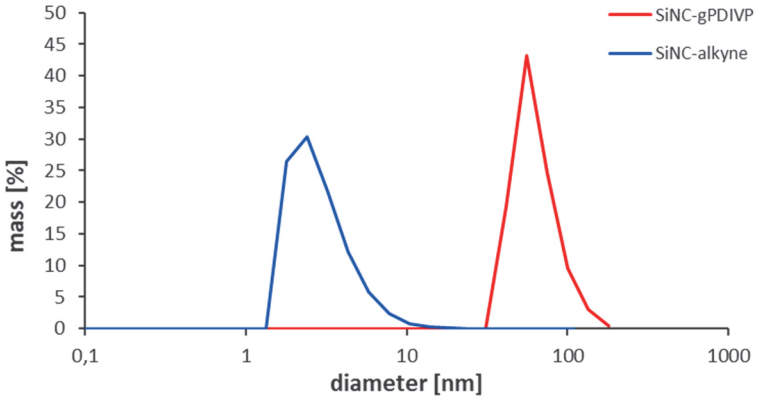

Figure 19. SI-GTP of DIVP from free standing SiNC.[306]

To date, steric crowding via the metal center leads to increased activities with decreased cation size and lutetium was found to be amongst the ideal RE metal centers. The smaller cation center scandium can have different behavior compared to the other RE elements and shows no influence of relativistic effects (*vide supra*). However, the effect of scandium should be studied and no work has been performed so far on the REM-GTP of vinylphosphonates using Sc. In first experiments simple Sc compounds such as $(C_5H_5)_3Sc$ can be used and based on these results ligand induced steric crowding can be investigated for synthetically accessible Sc complexes.

First preliminary polymerization studies with yttrium CGCs showed high stereoregularities for PDEVP. In further studies, also other ligands can be used for the synthesis of a wider variety of CGCs and the impact of ligand modifications can be studied in detail (see Chart 5).

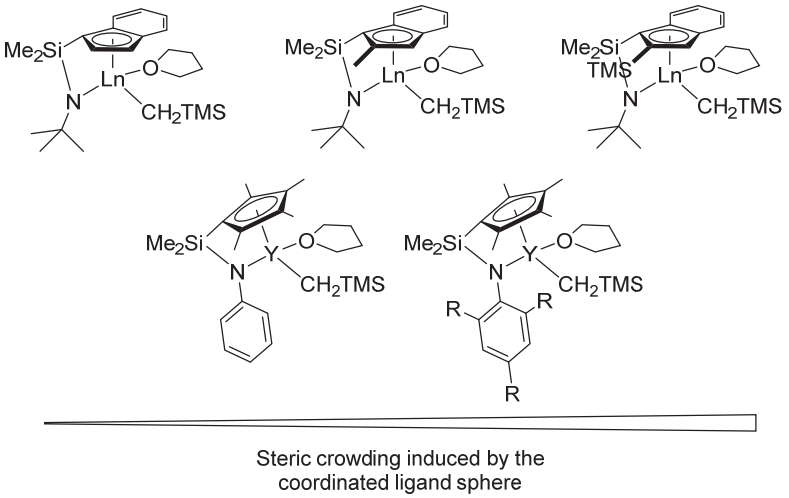

Chart 5. Overview of possible different RE CGCs to be evaluated for vinylphosphonate REM-GTP.

The experimental results of vinylphosphonate REM-GTP should be assisted in the future by theoretical calculations. For example, the postulated 1,4-addition of ($CH_2(C_5NMe_2H_2)$ initiators vs. a deprotonation is supported by the partial double bond character of the activated methylene group (see Chapter 4.3), however, a computational proof will advance this class of novel initiators in comparison to the well-established zirconocene enolate compounds. The differences in activity for $(C_5H_5)_2YCH_2TMS(thf)$ and $(C_5H_5)_2LuCH_2TMS(thf)$ for the C–H bond activation of *sym*-collidine can be investigated by theoretical investigations.

Furthermore, the resulting atactic and isotactic PDAVP microstructure can be computed for several metallocene complexes with different metal centers or ligand spheres. In particular, a theoretical explanation for the syndiotactic PMMA microstructure (mediated by a $(C_5H_4TMS)_2SmR$ unit) and vice versa atactic PDEVP microstructure (mediated by a $(C_5H_4TMS)_2LnR$ unit (R = Sm, Y)) will create a significant amount of knowledge for chemists working in related fields (see Chapter 4.4).[307-308] Also the transition state of vinylphosphonate REM-GTP and its proposed eight-membered ring can be investigated by theoretical calculations and compared to the (proposed and observed) inpolymerizability of α-methyl substituted vinylphosphonates.[61] DFT calculations can also help to better understand the polymerizability of DEVP in contrast to the inpolymerizability of DEMVP (see Chapter 1.3) and can be extended to other monomer classes (2VP *vs.* 2-vinylthiophene/2-vinylfuran).

In summary, in this thesis a novel approach for the previously existing initiation problems for the REM-GTP of vinylphosphonates is presented by the use of hydrocarbyl initiators obtained via σ-bond metathesis. The high activities and initiator efficiencies without any observable initiation period are attributed to a mechanistic match of initiation and propagation, both proceeding via an eight membered transition state. Furthermore, the first research on ligand induced steric crowding was conducted within this thesis and the effects of the performed modifications on molecular mass, propagation rate, initiation

delay, and molecular mass distribution were monitored via activity measurements using a normalization method for living polymerizations, and the correlation between steric crowding and activity were presented. The insights from this study was helpful to target and apply RE CGCs as possible candidates for a stereoregular polymerization of vinylphosphonates. A comparison of previously applied RE complexes and catalysts that were developed during this work are briefly shown in Chart 6.

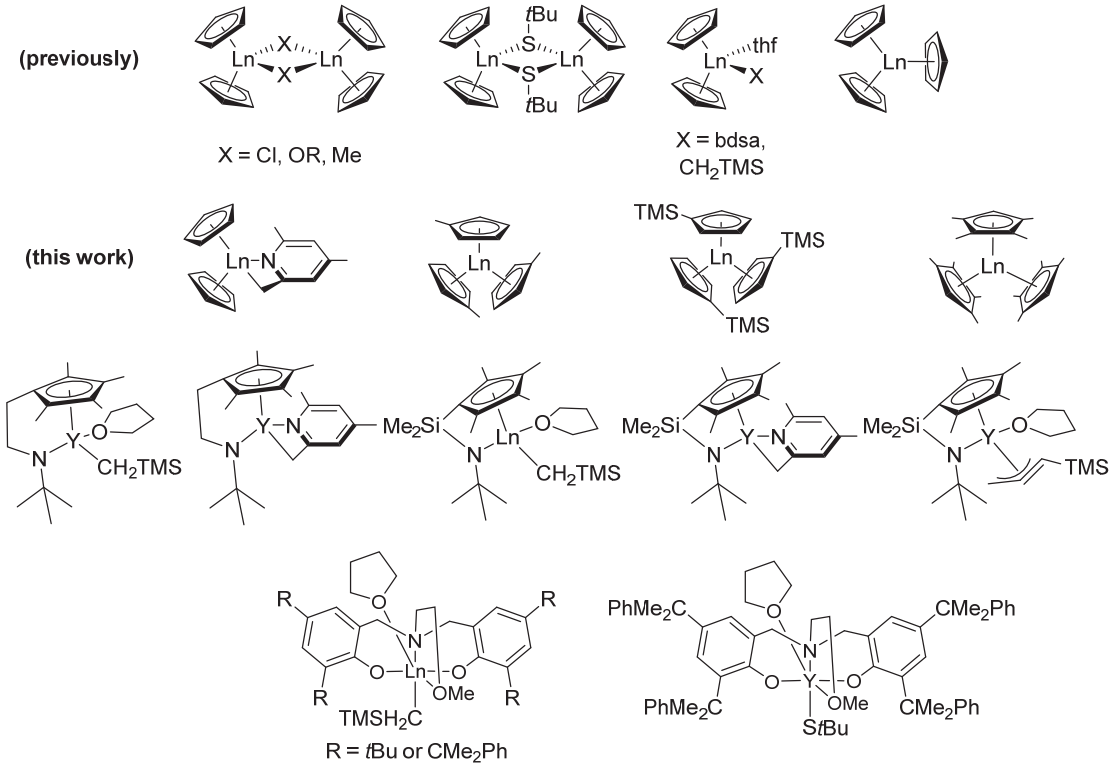

Chart 6. Overview on previous used complexes of our group and application of new ligand systems and initiators within this work.

6 Experimental Part

6.1 General Considerations

All reactions with oxygen or moisture sensitive compounds were carried out under argon atmosphere (Argon 4.8, 99.998%, Westfalen AG, Münster) using standard Schlenk or glovebox techniques (LABmaster 130, company M. Braun). All glassware was heat dried under vacuum prior to use. Unless otherwise stated, all chemicals were purchased from Sigma-Aldrich, Acros Organics, or ABCR and used as received.

6.1.1 Solvents

Absolute solvents were used unless otherwise stated and stored over activated 4 Å molecular sieve. Toluene, THF, dichloromethane, and pentane were dried using an MBraun SPS-800 solvent purification system. Hexane was dried over activated 4 Å molecular sieve.

6.1.2 Analytic Methods

NMR spectra were recorded on a Bruker AVIII-300 or AV-500C spectrometer. ^{1}H, ^{13}C, and ^{29}Si NMR spectroscopic chemical shifts δ are reported in ppm relative to tetramethylsilane. $\delta(^{1}H)$ is calibrated to the residual proton signal, $\delta(^{13}C)$ to the carbon signal, and $\delta(^{29}Si)$ to the deuterium signal of the solvent. ^{31}P NMR spectroscopic chemical shifts are reported in ppm relative to and calibrated to 85% aqueous H_3PO_4. Deuterated solvents were obtained from Sigma Aldrich and dried over 3 Å molecular sieve. Following abbreviations are used for signal multiplets: s = singlet, d = doublet, t = triplet, q = quartet, sext. = sextet, m = multiplet.

Solvent NMR shifts are taken from the publication of Fulmer et al..[309]

Deuterated solvent: $CDCl_3$ (^{1}H NMR δ = 7.26 ppm; ^{13}C NMR δ = 77.2 ppm),

C_6D_6 (^{1}H NMR δ = 7.16 ppm; ^{13}C NMR δ = 128.1 ppm),

THF-d_8 (^{1}H NMR δ = 1.72, 3.58 ppm; ^{13}C NMR δ = 25.3, 67.2 ppm),

D_2O (^{1}H NMR δ = 4.79 ppm).

6.1 General Considerations

ESI MS analytical measurements were performed with methanol solutions on a Varian 500-MS spectrometer in positive ionization mode. Elemental analyses were measured at the Laboratory for Microanalytics at the Institute of Inorganic Chemistry at the Technische Universität München. IR spectra were recorded under argon atmosphere on a Bruker Vertex 70 spectrometer with a Bruker Platinum ATR setup and the integrated MCT detector. RE metal complex samples were applied as THF solutions or Et_2O suspension and measured after complete evaporation of the solvent under argon.

6.1.3 Molecular Weight Determination (GPC-MALS)

GPC was carried out on a Varian LC-920 equipped with two PL Polargel columns. As eluent a mixture of 50% THF, 50% water, and 9 g L^{-1} tetrabutylammonium bromide (TBAB) or THF and 6 g L^{-1} TBAB were used. Absolute molecular weights have been determined online by multiangle light scattering (MALS) analysis using a Wyatt Dawn Heleos II in combination with a Wyatt Optilab rEX as concentration source.

6.1.4 General Procedure for the Activity Measurements of Polar Monomers

For activity measurements, the stated amount of catalyst (21.7 μmol) is dissolved in 20 ml of toluene and the reaction mixture is thermostated to the desired temperature. Then, the stated amount of DAVP (13 mmol) is added. During the course of the measurement, the temperature is monitored with a digital thermometer and aliquots (0.5 ml) are taken and quenched by addition to deuterated methanol (0.2 ml). After the stated reaction time, the reaction is quenched by addition of MeOD (0.5 ml). The reaction is carried out in an MBraun Glovebox under argon atmosphere to take aliquots every 6 – 10 seconds at the beginning of the measurement. For each aliquot, the conversion is determined by ^{31}P NMR spectroscopy, the molecular weight of the formed polymer is determined by GPC-MALS analysis. The polymerization is stopped after complete monomer conversion by the addition of 1 ml MeOD and the polymer is precipitated by the addition of the toluene solution to pentane. After solvent evaporation, the polymer is obtained by freeze drying.

The conversion time diagram for non-phosphorus-containing monomers can be followed via ^{1}H NMR in C_6D_6 using less MeOD or from a stem solution using a gravimetric method.

6.1.5 General Procedure for Oligomerization Experiments

5 Eq. of the respective monomer are added to 1 eq. of catalyst (22–38 μmol) in toluene (2 ml). The resulting mixture is stirred for 2 hours at room temperature and quenched by addition of MeOH. Volatiles were removed under reduced pressure and the residue is extracted with MeOH. For end group analysis, ESI-MS measurements of the methanolic extract are performed.

6.1.6 Freeze Drying of Polymer Samples

Polymer solutions were first precipitated after stopping the polymerization in a suitable solvent (*e.g.*, pentane) and decanted off. The polymer samples were either dissolved in water or benzene and volatile compounds were removed by freeze drying using a VaCo 5-II machine of Zirbus technology GmbH (Bad Grund). A pressure of 2 mbar was used to sublimate the solvent and volatile compounds were collected at a condensation temperature of –90 °C.

6.2 Monomer Syntheses

6.2.1 Synthesis of Nitroethylene

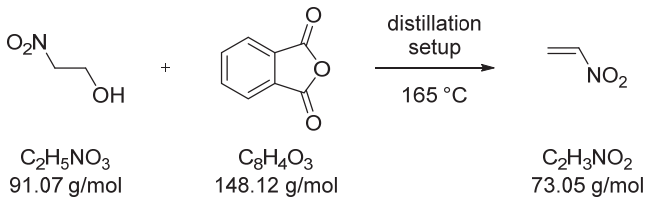

Procedure

Nitroethylene was synthesized following an adapted literature procedure.[310] 2-Nitroethanol (5.0 g, 54.9 mmol, 1.0 eq.) and phthalic anhydride (10.5 g, 70.9 mmol, 1.3 eq.) are mixed under argon atmosphere and heated to 120 °C at 65 mbar. The melt is afterwards distilled at 165 °C and 65 mbar and the product is collected at −78 °C. Spectroscopic data are in agreement with literature results.[311]

^{1}H NMR (300 MHz, $CDCl_3$) δ = 7.13 (d, 1H), 6.64 (d, 1H), 5.91 (s, 1H).

^{13}C NMR (75 MHz, $CDCl_3$) δ = 146.6, 123.0.

Yield 3.1 g, 42.2 mmol, 77%

6.2.2 Synthesis of Diethyl 2-Bromoethylphosphonate

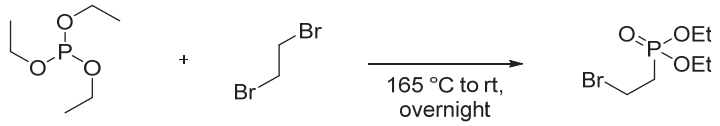

$C_6H_{15}O_3P$ 166.16 g/mol | $C_2H_4Br_2$ 187.86 g/mol | $C_6H_{14}BrO_3P$ 245.05 g/mol

Procedure

250 ml Triethyl phosphite (243 g, 1.46 mol, 1 eq.) and 500 ml 1,2-dibromoethane (1090 g, 5.84 mol, 4 eq.) are mixed in a 1 L flask with Vigreux column and distillation bridge. The mixture is heated at 165 °C until the distillation of ethyl bromide is completed. After heating the solution for additional 4 h, the reaction is cooled to room temperature and stirred overnight. Low boiling compounds are removed by rotary evaporation at 30 mbar and 60 °C. The product diethyl 2-bromoethylphosphonate is obtained as a colorless liquid after vacuum distillation (b.p. 73 °C, 0.06 mbar).

^{1}H NMR (300 MHz, $CDCl_3$) δ = 3.85–3.94 (m, 2H), 3.27–3.35 (q, 2 H), 2.11–2.21 (m, 2 H), 1.11 (t, 6H).

^{31}P NMR (203 MHz, $CDCl_3$) δ = 25.4.

Yield 229 g, 0.935 mol, 64%

6.2.3 Synthesis of Diethyl Vinylphosphonate

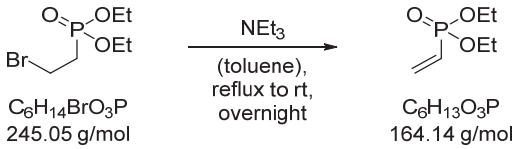

$C_6H_{14}BrO_3P$
245.05 g/mol

$C_6H_{13}O_3P$
164.14 g/mol

Procedure

Diethyl 2-bromoethylphosphonate is heated to reflux for 6 h with a 10% excess of triethylamine (concentration = 1 mol/l in toluene), cooled to room temperature and stirred overnight. Triethylammonium bromide is filtered off and washed with toluene and the solvent is removed in vacuo. The product is obtained as a colorless liquid after vacuum distillation (b.p. 39 °C, 0.1 mbar).

Diethylethyl vinylphosphonate is formed as a byproduct and should be limited to less than 0.3% (determined by ^{31}P NMR, ppm = 33.6 ppm) via distillation in the first Michaelis-Arbuzov reaction to secure reliable polymerization results.

^{1}H NMR (300 MHz, $CDCl_3$) δ = 5.78–6.10 (m, 3 H), 3.81–3.89 (m, 4 H), 1.09 (t, 6H).

^{13}C NMR (75 MHz, $CDCl_3$) δ = 133.9, 126.9 (d), 124.3 (d), 60.4, 15.1.

^{31}P NMR (203 MHz, $CDCl_3$) δ = 17.9.

Yield 87%

6.2.4 Synthesis of Diisopropyl 2-Bromoethylphosphonate

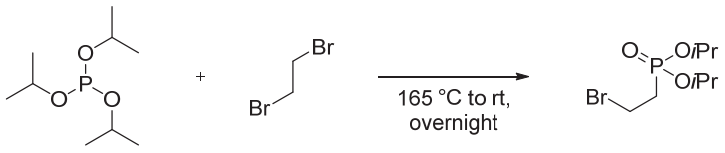

$C_9H_{21}O_3P$
208.24 g/mol

$C_2H_4Br_2$
187.86 g/mol

$C_8H_{18}BrO_3P$
273.11 g/mol

Procedure

250 ml Triisopropyl phosphite (211 g, 1.0 mol, 1 eq.) and 350 ml 1,2-dibromoethane (760 g, 4.0 mol, 4 eq.) are mixed in a 1 L flask with Vigreux column and distillation bridge. The mixture is heated at 145 °C until the distillation of 2-propylbromide is completed. After heating the solution for additional 4 h the reaction is cooled to room temperature and stirred overnight. Low boiling compounds are removed by rotary evaporation at 30 mbar and 60 °C. The product diisopropyl 2-bromoethylphosphonate is obtained as a colorless liquid after vacuum distillation (b.p. 70 °C, 0.15 mbar).

^{1}H NMR (300 MHz, $CDCl_3$) δ = 4.60 (sext, 2H), 3.40 (q, 2H), 2.16–2.34 (m, 2H), 1.25 (d, 12H).

^{31}P NMR (203 MHz, $CDCl_3$) δ = 23.3.

Yield 191 g, 700 mmol, 70%

6.2.5 Synthesis of Diisopropyl Vinylphosphonate

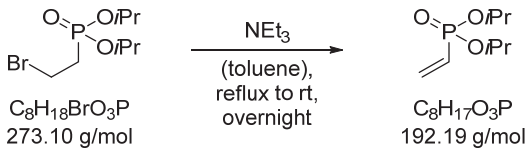

$C_8H_{18}BrO_3P$
273.10 g/mol

$C_8H_{17}O_3P$
192.19 g/mol

Procedure

Diisopropyl 2-bromoethylphosphonate is heated to reflux for 6 h with a 10% excess of triethylamine (concentration = 1 mol/l in toluene), cooled to room temperature and stirred overnight. Triethylammonium bromide is filtered off and washed with toluene and the solvent is removed in vacuo. The product is obtained as a colorless liquid after vacuum distillation (b.p. 39 °C, 0.1 mbar).

^{1}H NMR (300 MHz, $CDCl_3$) δ = 5.78–6.33 (m, 3 H), 4.44–4.69 (m, 2H), 1.20 (d, 12H).

^{13}C NMR (75 MHz, $CDCl_3$) δ = 134.2 (s), 127.5 (d), 70.3 (s), 23.9 (s).

^{31}P NMR (203 MHz, $CDCl_3$) δ = 15.7.

Yield 91%

6.3 Synthesis of Ligands

6.3.1 Synthesis of Trimethylsilylcyclopentadiene

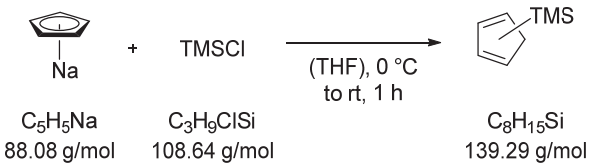

Procedure

Trimethylcyclopentadiene is synthesized following adapted literature procedures.[307,312] $Na(C_5H_5)$ (18 g, 205 mmol, 1 eq.) is dissolved in 75 ml THF and cooled to 0 °C. The solution is vigorously stirred and 29 ml TMSCl (24.6 g, 226 mmol, 1.1 eq.) are added quickly. The solution is warmed to room temperature overnight and the reaction is stopped by the addition of saturated $NaHCO_3$ solution. The aqueous phase is washed three times with hexane and the combined organic phases are dried over Na_2SO_4. The solvents are removed in vacuo and the product is obtained as a colorless liquid after vacuum distillation (b.p. 45 °C, 31 mbar).

^{1}H NMR (300 MHz, $CDCl_3$) δ = 6.64–6.41 (m, 4H), 3.39 (s, 1H), -0.03 (s, 9H).

^{13}C NMR (75 MHz, $CDCl_3$) δ = 133.3, 130.0, 52.1, -2.1.

Yield 25 g, 192 mmol, 94%

6.3.2 Synthesis of Bis(trimethylsilyl)cyclopentadiene

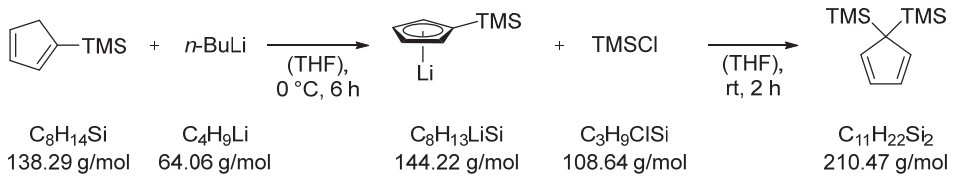

$C_8H_{14}Si$	C_4H_9Li	$C_8H_{13}LiSi$	C_3H_9ClSi	$C_{11}H_{22}Si_2$
138.29 g/mol	64.06 g/mol	144.22 g/mol	108.64 g/mol	210.47 g/mol

Procedure

C_5H_5TMS is dried over 4 Å molecular sieve under argon atmosphere. C_5H_5TMS (6.66 g, 48.2 mmol, 1 eq.) is dissolved in 40 ml THF and cooled to 0 °C. *n*-BuLi (19.3 ml, 48.2 mmol, 1 eq.) is added dropwise to the solution and stirred for 6 h at 0 °C. TMSCl (5.76 g, 53 mmol, 1.1 eq.) is added quickly and the solution is allowed to warm to room temperature. The reaction is stopped after 2 h by the addition of saturated $NaHCO_3$ and the combined phases are washed three times with hexane. The solvents are removed in vacuo and the crude product is purified by vacuum distillation (b.p. 54 °C, 7 mbar).

^{1}H NMR (300 MHz, $CDCl_3$) δ = 6.72 (m, 2H), 6.52 (m, 2H), -0.03 (s, 18H).

^{13}C NMR (75 MHz, $CDCl_3$) δ = 136.0, 130.4, -0.8.

Yield 5.9 g, 0.28 mmol, 58%

6.3.3 Synthesis of 2,3,5,6-Tetrahydro-2,3,5,6-tetramethyl-γ-pyrone

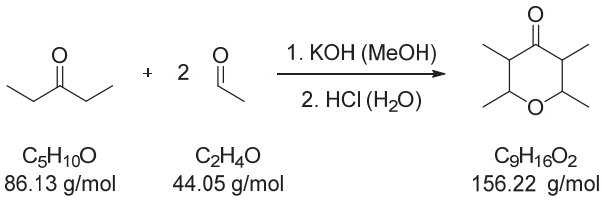

Procedure

2,3,5,6-Tetrahydro-2,3,5,6-tetramethyl-γ-pyrone is synthesized following an adapted literature procedure.[313] KOH (50 g, 0.89 mol) are dissolved in 300 ml methanol and cooled to 0 °C. 250 ml 3-Pentanone (204 g, 2.36 mol, 1 eq.) are added to the solution and 530 ml acetaldehyde (418 g, 9.44 mol, 4 eq.) are added dropwise over 6 h while the temperature of the solution is kept at 0 °C. The solution is stirred at this temperature overnight and 80 ml conc. HCl are added dropwise to stop the reaction. 150 ml 1 M HCl are added and phase separation is reached after Et_2O (300 ml) is added. The aqueous phase is washed three times with Et_2O and volatile compounds are removed in vacuo. The crude product is purified by vacuum distillation using a sufficient (> 20 cm) Vigreux column and 2,3,5,6-Tetrahydro-2,3,5,6-tetramethyl-γ-pyrone is obtained as a yellow liquid (b.p. 74 – 83 °C, 23 mbar). The product is stored in a fridge to prevent decomposition.

^{1}H NMR (300 MHz, $CDCl_3$) δ = 3.33 (dq, 2H), 2.27 (m, 2H), 1.32 (d, 6H), 0.96 (d, 6H).

Yield: 221 g, 1.42 mmol, 60%

6.3.4 Synthesis of 2,3,4,5-Tetramethylcylopent-2-enone

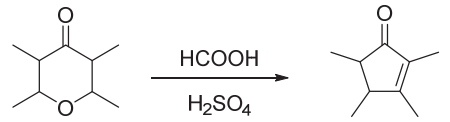

$C_9H_{16}O_2$
156.22 g/mol

$C_9H_{14}O$
138.21 g/mol

Procedure

2,3,4,5-Tetramethylcylopent-2-enone is synthesized following an adapted literature procedure.[313] 650 ml Formic acid (793 g, 17.6 mol, 17.6 eq.) are cooled to 0 °C and 225 ml H_2SO_4 (122 g, 1.25 mol, 1.25 eq.) are slowly added (exothermic reaction). The solution is allowed to warm to room temperature and 2,3,5,6-Tetrahydro-2,3,5,6-tetramethyl-γ-pyrone (158 g, 1 mol, 1 eq.) is added dropwise. After the addition is complete, the reaction mixture is heated at 50 °C for 24 h. The reaction is stopped by pouring the solution onto 100 g ice and the aqueous phase is washed three times with Et_2O. The volume of the combined organic phases is reduced in vacuo and washed with 10% aqueous NaOH solution until the aqueous layer has a basic pH value. The combined organic phases are washed twice with sat. NaCl solution and dried over Na_2SO_4. The crude product mixture is then purified by fractional distillation through sufficient Vigreux column (> 20 cm). The product is obtained as a yellow liquid (b.p. 85 – 89 °C, 20 mbar).

^{1}H NMR (300 MHz, $CDCl_3$) δ = 2.24 (m, 1H), 1.97 (m, 3H), 1.88 (m, 1H), 1.67 (m, 3H), 1.16 (m, 6H).

Yield 99 g, 716 mmol, 71%

6.3.5 Synthesis of 1,2,3,4-Tetramethylcyclopentadiene

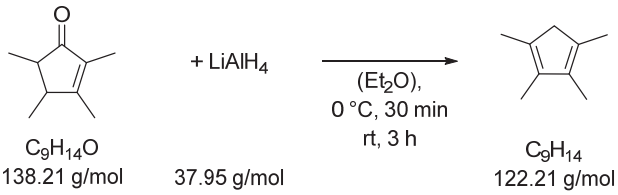

Procedure

2,3,4,5-Tetramethylcylopent-2-enone (19.1 g, 138 mmol, 1 eq.) is dissolved in Et_2O and cooled to 0 °C. $LiAlH_4$ (6.56 g, 173 mmol, 1.25 eq.) is added in portions (exothermic) and the suspension is stirred under cooling for 30 min. The suspension is allowed to warm to room temperature and after 3 h the reaction setup is cooled to 0 °C and 50 ml MeOH and 50 ml 6 N HCl are added subsequently. The aqueous phase is washed three times with ether and the combined organic phases are reduced in volume and dried over Na_2SO_4. *p*-Toluenesulfonic acid is added to the ether solution and the reaction is heated to reflux for 3 h. The reaction is mixture is washed twice with sat. $NaHCO_3$ solution, dried over Na_2SO_4 and volatile compounds are removed in vacuo. The crude product mixture is then purified by fractional distillation and the product is obtained as a colorless liquid (b.p. 53 °C, 21 mbar).

^{1}H NMR (300 MHz, $CDCl_3$) δ = 2.76–2.66 (m, 2H), 1.89 (s, 6H), 1.82–1.74 (m, 6H).

Yield 10.6 g, 87 mmol, 63%

6.3.6 Synthesis of 6,6-Dimethylfulvene

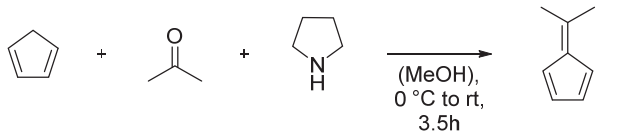

C_5H_6	C_3H_6O	C_4H_9N	C_8H_{10}
66.10 g/mol	58.08 g/mol	71.12 g/mol	106.17 g/mol

Procedure

Freshly cracked C_5H_6 is dried over 4 Å molecular sieve. C_5H_6 (66.1 g, 1 mol, 1.25 eq.) is cooled to 0 °C in 120 ml dry MeOH. Dry acetone (46.5 g, 0.8 mol, 1 eq.) and pyrrolidine (56.9 g, 0.8 mol, 1 eq.) are mixed together under argon atmosphere and the combined solutions are added to C_5H_6 by cannulation. After complete addition the solution is allowed to warm to room temperature and stirred for 2 – 2.5 h. Glacial acetic acid (49 ml) are added and the dark red solution is stirred for one hour at room temperature. The reaction is stopped by the addition of ice and the aqueous phase is washed three times with Et_2O. The combined organic phases are washed with water and dried over $MgSO_4$. The solvent is removed in vacuo and the crude product is obtained as a yellow liquid. The product has to be stored in a fridge and decomposes quickly above 80 °C.

^{1}H NMR (300 MHz, $CDCl_3$) δ = 6.56–6.46 (m, 4H), 2.21 (s, 6H).

Yield 71.5 g, 0.67 mol, 67%

6.3.7 Synthesis of *N*-*t*Butylethanimine

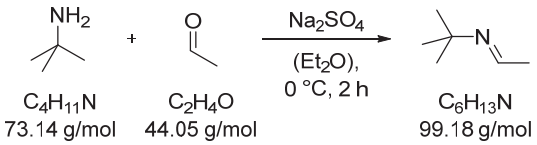

Procedure

Acetaldehyde (43.7 g, 992 mmol, 1.1 eq.) is added to a suspension of Na_2SO_4 in 400 ml Et_2O and cooled to 0 °C. *tert*-Butylamine (66 g, 902 mmol, 1 eq.) is added dropwise to the mixture and the reaction is stirred for 2 h. The majority of acetaldehyde and roughly 3/4 of the volume of Et_2O are removed in vacuo and Na_2SO_4 is filtered off. The product is stored over molecular sieve in the fridge as a 24% solution.

^{1}H NMR (300 MHz, $CDCl_3$) δ = 7.68 (q, 1H), 1.95 (d, 3H), 1.16 (s, 9H).

Yield 67%

6.3.8 Synthesis of $(C_5Me_4H)CH_2CH_2NHtBu$

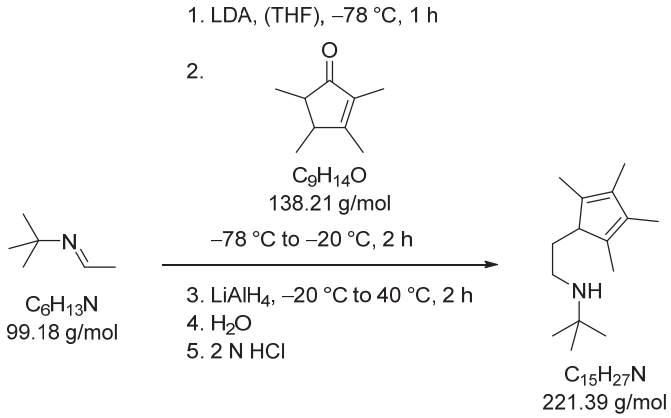

Procedure

$(C_5Me_4H)CH_2CH_2NHtBu$ was synthesized following an adapted literature procedure.[314] LDA (18.5 g, 173 mmol, 1 eq.) is dissolved in 250 ml THF and cooled to −78 °C. *N*-*t*Butylethanimine (17.2 g, 173 mmol, 1 eq.) is added dropwise and the reaction is stirred for 30 min. 2,3,4,5-Tetramethylcylopent-2-enone (23.9 g, 173 mmol, 1 eq.) is added dropwise to the solution and the mixture was stirred for another 30 minutes at −78 °C. The temperature was allowed to warm to −40 °C over 1 h and then $LiAlH_4$ (8.2 g, 216 mmol, 1.25 eq.) is added to the stirred mixture and the temperature was gradually raised to 40 °C. After 2 h the suspension was cooled to 0 °C and the reaction was stopped by the addition of water. The mixture was dried over Na_2SO_4, filtered, and washed with Et_2O. The filtrate was concentrated in vacuo and stirred for 1 h at room temperature with 175 ml 2 N HCl. The organic phase is separated and the aqueous phase is first washed with Et_2O and then a solution of 17.5 g NaOH in 90 ml water is added, followed by the extraction with Et_2O. The combined organic phases are dried over Na_2SO_4 and volatile compound are removed in vacuo. The crude product mixture is then purified by fractional distillation and the product is obtained as a yellow liquid (b.p. 56 °C, 0.02 mbar).

^{1}H NMR (300 MHz, $CDCl_3$) δ = 2.74–1.97 (m, 9H), 1.90–1.75 (m, 9H), 1.20–1.00 (m, 12H).

Yield 6.8 g, 30.7 mmol, 18%

6.3.9 Synthesis of $(C_5Me_4H)SiMe_2Cl$

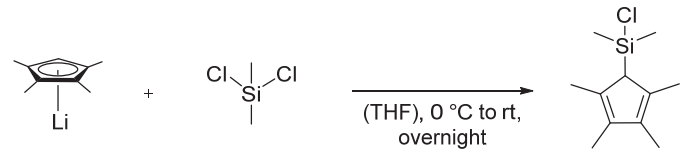

$C_9H_{13}Li$
128.14 g/mol

$C_2H_6Cl_2Si$
129.06 g/mol

$C_{11}H_{19}ClSi$
214.81 g/mol

Procedure

$(C_5Me_4H)SiMe_2Cl$ was synthesized according to a modified literature procedure.[315] A solution of 9.3 ml Dichlorodimethylsilane (9.9 g, 77 mmol, 3.4 eq.) in THF (50 ml) is cooled to 0 °C. $Li(C_5Me_4H)$ (2.9 g, 23 mmol, 1 eq.) is added in portions to the solution and the mixture is allowed to warm to room temperature overnight. Volatile compounds are carefully removed under reduced pressure while keeping the mixture at 0 °C and the remaining mixture is extracted with pentane and filtered. The filtrate is carefully dried in vacuo and the product is obtained as a red oil.

^{1}H NMR (300 MHz, C_6D_6) δ = 2.89 (s, 1H), 1.92 (s, 6H), 1.71 (s, 6H), 0.14 (s, 6H).

Yield 4.4 g, 20 mmol, 90%

6.3.10 Synthesis of $(C_5Me_4H)SiMe_2NHtBu$

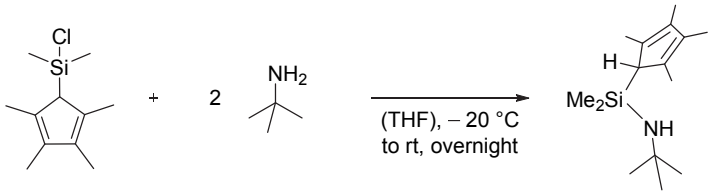

$C_{11}H_{19}ClSi$ 214.81 g/mol | $C_4H_{11}N$ 73.14 g/mol | $C_{15}H_{29}NSi$ 251.49 g/mol

Procedure

$(C_5Me_4H)SiMe_2NHtBu$ was synthesized according to a modified literature procedure.[315] $(C_5Me_4H)SiMe_2Cl$ (4.4 g, 20 mmol, 1 eq.) is dissolved in THF (50 ml) and cooled to −20 °C. $tBuNH_2$ (3.6 g, 49 mmol, 2.4 eq.) is added in portions and the mixture is stirred for 15 min under cooling. The mixture is allowed to warm to room temperature overnight and a yellow suspension is formed. Volatile compounds are removed in vacuo and the mixture is suspended in pentane (50 ml), filtered, and dried under reduced pressure. The crude product mixture is then purified by fractional distillation and the product is obtained as a yellow liquid (b.p. 55 °C, 0.03 mbar).

^{1}H NMR (300 MHz, C_6D_6) δ = 2.78 (s, 1H), 2.03 (s, 6H), 1.86 (s, 6H), 1.10 (s, 9H), 0.12 (s, 6H).

^{13}C NMR (126 MHz, C_6D_6) δ = 135.4, 133.3, 57.0, 49.4, 33.9, 15.1, 11.5, 1.4.

Yield 3.9 g, 15.5 mmol, 76%

6.3.11 Synthesis of C_5Me_5H

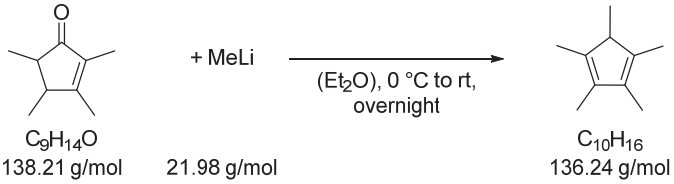

Procedure

MeLi (28.9 g, 256 mmol, 1.2 eq.) is cooled to 0 °C in 160 ml Et_2O and 2,3,4,5-Tetramethylcylopent-2-enone (29.5 g, 213 mmol, 1 eq.) is added dropwise to the solution. The solution is allowed to warm to room temperature overnight. The reaction is stopped by the addition of 8.5 ml MeOH and 40 ml of water and the organic phase is washed with sat. NH_4Cl, sat. 6 N HCl, and water. The combined aqueous phases are extracted with Et_2O, the combined organic phases are dried over Na_2SO_4, and volatile compound are removed in vacuo. The crude product mixture is then purified by fractional distillation and the product is obtained as a yellow liquid (b.p. 63 °C, 20 mbar).

^{1}H NMR (300 MHz, $CDCl_3$) δ = 2.50 (m, 1H), 1.80 (d, 6H), 1.01 (d, 3H).

Yield 27.8 g, 204 mmol, 96% (crude product)

6.4 Synthesis of Lithiumalkyls

6.4.1 Synthesis of $LiCH_2TMS$

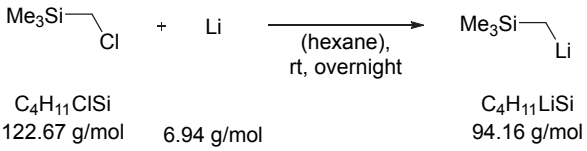

Procedure

Lithium granulate (1.72 g, 249 mmol, 3.3 eq.) and chloromethyltrimethylsilane (9.25 g, 75 mmol, 1 eq.) are suspended in hexane (100 ml) and the mixture is heated at 35 °C for 24 h. Lithium was exempt of LiCl several times using an ultrasonic bath. The supernatant solution was isolated using a filter cannula. The residue is extracted with hexane (20 ml) and the solvent is removed in vacuo, yielding a white pyrophoric solid. The product can be further purified if needed by sublimation (10^{-3} mbar, 100 °C).

^{1}H NMR (300 MHz, C_6D_6) δ = 0.16 (s, 9H), -2.08 (s, 2H).

^{13}C NMR (75 MHz, C_6D_6) δ = 3.6 (s), -4.7 (s).

EA calculated: C, 51.03; H, 11.78;

found: C, 51.14; H, 12.00.

Yield 6.25 g, 66 mmol, 88%

6.5 Synthesis of Substituted Cyclopentadienyl Alkali Metal Salts

6.5.1 Synthesis of $K(C_5H_4Me)$ from Elemental Potassium

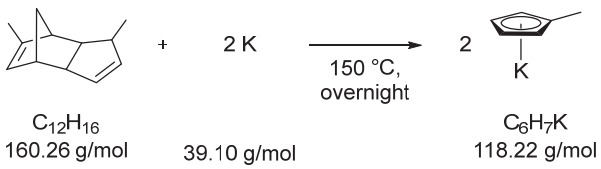

Procedure

Commercial methylcyclopentadiene dimer contains up to 10% cyclopentadiene. If not purified, this will lead to major purity problems for derived organometallic compounds, particularly for those containing several C_5H_4Me ligands. Therefore, the crude methylcyclopentadiene dimer was purified by repeated cracking and distillation using a 40 cm Vigreux column. The first ~10% of the distillate is discarded and ~70% of the remainder is collected. The methylcyclopentadiene is redistilled using the same experimental setup until a product purity of >99% is obtained.

Purified methylcyclopentadiene dimer (60 ml) is placed in a 250 ml Schlenk flask with a metal reflux condenser and potassium (3.31 g, 84.6 mmol) is added at room temperature and the experimental setup is heated at 150 °C overnight. The produced hydrogen gas is released via an overpressure valve on top of the reflux condenser. The mixture is filtered using a Schlenk frit and washed two times with 50 ml of pentane. The product is obtained as a white pyrophoric solid.

^{1}H NMR (300 MHz, THF-d_8) δ = 5.28 (m, 4H), 2.08 (s, 3H).

^{13}C (75 MHz, THF-d_8) δ = 111.5 (s), 102.2 (s), 101.1 (s), 12.9 (s).

Yield 7 g, 59.2 mmol, 70%

Purity 99% $K(C_5H_4Me)$ (determined by NMR)

6.5.2 Synthesis of $K(C_5H_4Me)$ via Deprotonation

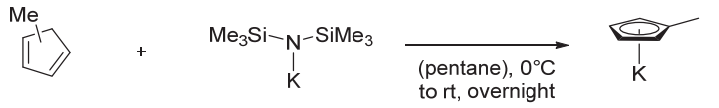

C_6H_8
80.13 g/mol

$C_6H_{18}KNSi_2$
199.49 g/mol

C_6H_7K
118.22 g/mol

Procedure

Methylcyclopentadiene (5.75 g, 71.8 mmol, 1 eq.) is dissolved in 250 ml pentane and cooled to 0 °C. A toluene solution of potassium bis(trimethylsilyl)amide (15 g, 75.3 mmol, 1.05 eq.) is added dropwise and the suspension is allowed to warm to room temperature overnight. The white suspension is filtered and the residue is washed with 50 ml pentane, 50 ml of a pentane THF mixture, and 10 ml THF. The remaining solvents are removed under vacuum and $K(C_5H_4Me)$ is obtained as a white pyrophoric powder.

^1H NMR (300 MHz, THF-d_8) δ = 5.28 (m, 4H), 2.08 (s, 3H).

^{13}C (75 MHz, THF-d_8) δ = 111.5 (s), 102.2 (s), 101.1 (s), 12.9 (s).

Yield (8.80 g, 67.6 mmol, 94%).

Purity >99% $K(C_5H_4Me)$ (determined by NMR)

6.5.3 Synthesis of Li(C$_5$H$_4$TMS)

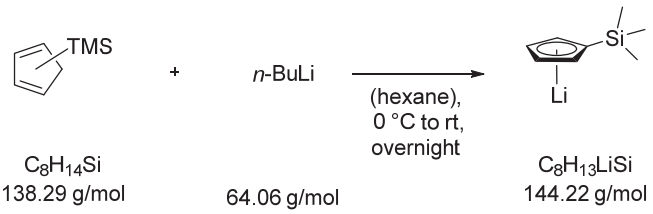

Procedure

Li(C$_5$H$_4$TMS) was synthesized following an adapted literature procedure.[307] A solution of C$_5$H$_5$TMS (10.2 g, 73.5 mmol, 1 eq.) in pentane (70 ml) is cooled to 0 °C and 33 ml of a 2.5 M *n*-BuLi hexane solution (5.1 g, 80.3 mmol, 1.1 eq.) are added dropwise. The mixture is allowed to warm to room temperature overnight. The suspension is filtered and washed three times with pentane. Volatile compounds are removed in vacuo and the product is obtained as a white pyrophoric powder.

^{1}H NMR (300 MHz, THF-d$_8$) δ = 5.92 (t, ^3J = 3.2, 1.7 Hz, 2H), 5.85 (t, ^3J = 3.2, 1.7 Hz, 2H), 0.10 (s, 9H).

^{13}C NMR (75 MHz, THF-d$_8$) δ = 111.5 (s), 106.6 (s), 103.4 (s), 1.5 (s).

Yield 10.2 g, 70.7 mmol, 96%

6.5.4 Synthesis of K(C$_5$H$_4$TMS)

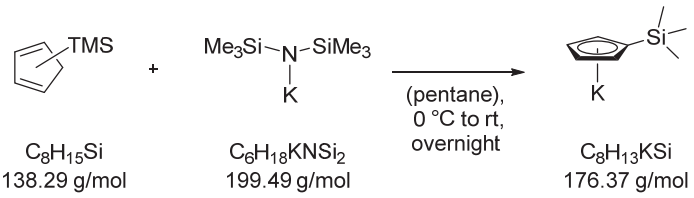

$C_8H_{15}Si$	$C_6H_{18}KNSi_2$		$C_8H_{13}KSi$
138.29 g/mol	199.49 g/mol		176.37 g/mol

Procedure

K(C$_5$H$_4$TMS) was synthesized following an adapted literature procedure.[167] C$_5$H$_5$TMS (3.5 g, 25 mmol, 1 eq.) is dissolved in pentane (125 ml) and cooled to 0 °C. A solution of potassium bis(trimethylsilyl)amide (5.5 g, 27.5 mmol, 1.1 eq.) in toluene (38 ml) is added dropwise and the mixture is allowed to warm to room temperature overnight. The white suspension is filtered and the residue is washed three times with pentane (50 ml). Volatile compounds are removed under vacuum and K(C$_5$Me$_4$H) is obtained as a white pyrophoric powder.

^{1}H NMR (300 MHz, THF-d$_8$) δ = 5.78 (t, 2H), 5.67 (t, 2H), 0.07 (s, 9H).

^{13}C NMR (75 MHz, THF-d$_8$) δ = 112.8 (s), 111.1 (s), 108.4 (s), 1.6 (s).

Yield 4.0 g, 23 mmol, 92%

6.5.5 Synthesis of $K(C_5Me_4H)$

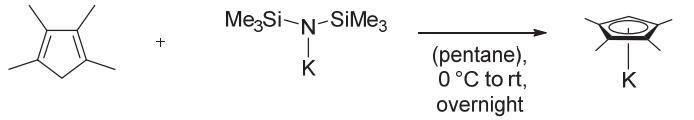

C_9H_{14}	$C_6H_{18}KNSi_2$	$C_9H_{13}K$
122.21 g/mol	199.49 g/mol	160.30 g/mol

Procedure

Tetramethylcyclopentadiene (4.75 g, 38.9 mmol, 1 eq.) is dissolved in pentane (70 ml) and cooled to 0 °C. A solution of potassium bis(trimethylsilyl)amide (7.90 g, 39.6 mmol) in toluene (55 ml) is added dropwise and the mixture is allowed to warm to room temperature overnight. The white suspension is filtered and the residue is washed three times with 40 ml pentane. The remaining solvents are removed under vacuum and $K(C_5Me_4H)$ is obtained as a white pyrophoric powder (5.80 g, 36.1 mmol, 93%).

^{1}H NMR	(300 MHz, THF-d_8) δ = 4.88 (s, 1H), 1.90 (s, 6H), 1.84 (s, 6H).
^{13}C NMR	(75 MHz, THF-d_8) δ = 108.0 (s), 108.8 (s), 102.7 (s), 13.5 (s), 11.3 (s).
EA	calculated: C, 67.43; H, 8.17;
	found: C, 66.72; H, 8.15.
Yield	6.0 g, 37.7 mmol, 97%

6.5.6 Synthesis of Li(C_5Me_4H)

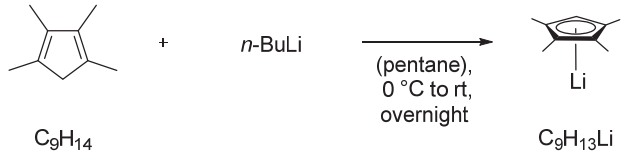

C_9H_{14}		$C_9H_{13}Li$
122.21 g/mol	64.06 g/mol	128.14 g/mol

Procedure

A solution of $C_5Me_4H_2$ (4.2 g, 34.3 mmol, 1 eq.) in pentane (100 ml) is cooled to 0 °C and 14.4 ml of a 2.5 M *n*-BuLi hexane solution (2.3 g, 36.0 mmol, 1.05 eq.) are added dropwise. The mixture is allowed to warm to room temperature overnight. The suspension is filtered and washed three times with pentane (30 ml). Volatile compounds are removed in vacuo and the product is obtained as a white pyrophoric powder.

^{1}H NMR (360 MHz, THF-d_8) δ = 4.96 (s, 1H), 1.88 (s, 6H), 1.83 (s, 6H).

Yield 4.2 g, 33.0 mmol, 96%

6.5.7 Synthesis of Indenyl Lithium

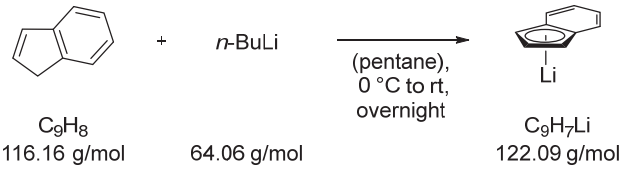

Procedure

9.3 ml Indene (9.2 g, 80 mmol, 1 eq.) are dissolved in pentane (100 ml) and the mixture is cooled to 0 °C. 32 ml of a 2.5 M *n*-BuLi hexane solution (5.1 g, 80 mmol, 1 eq.) are added dropwise and the mixture is allowed to warm to room temperature overnight. The suspension is filtered and washed three times with pentane (30 ml). Volatile compounds are removed in vacuo and the product is obtained as a white pyrophoric powder.

^{1}H NMR (300 MHz, THF-d_8) δ = 7.30 (dd, J = 6.1, 3.1 Hz, 2H), 6.52 (t, J = 3.4 Hz, 1H), 6.43 (dd, J = 6.1, 3.1 Hz, 2H), 5.91 (d, J = 3.4 Hz, 2H).

^{13}C NMR (75 MHz, THF-d_8) δ = 129.7 (s), 119.6 (s), 115.5 (s), 114.0 (s), 91.5 (s).

Yield 8.5 g, 70 mmol, 87%

6.6 Synthesis of substituted Tris(cyclopentadienyl) RE Complexes

6.6.1 Synthesis of $(C_5H_4Me)_3Y(thf)$

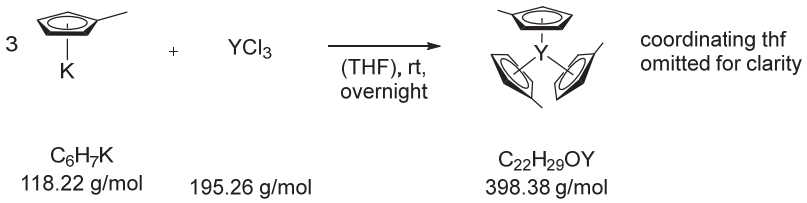

Procedure

$(C_5H_4Me)_3Y(thf)$ was synthesized following an adapted literature procedure. [316] In an argon-filled glovebox, YCl_3 (0.44 g, 2.23 mmol, 1 eq.) is suspended in 30 ml THF and $K(C_5H_4Me)$ (0.83 g, 6.99 mmol, 3.1 eq.) is added stepwise. The colorless mixture is sealed in a 100 ml sidearm Schlenk flask and stirred at room temperature overnight. The solvent is removed under vacuum from the resulting pale yellow mixture and the obtained solids are stirred in 20 ml toluene at 80 °C for 1 h. The mixture is filtered to remove gray-white insoluble material, presumably KCl and excess $K(C_5H_4Me)$. Removal of toluene under vacuum yields $(C_5H_4Me)_3Y(thf)$ as a pale yellow microcrystalline solid (533 mg, 1.34 mmol, 60%).

^{1}H NMR	(300 MHz, THF-d_8) δ = 5.79 (t, ^3J = 2.7 Hz, 6H), 5.63 (t, ^3J = 2.7 Hz, 6H), 3.61 (m, 4H), 2.16 (s, 9H) 1.77 (m, 4H).
^{13}C NMR	(75 MHz, THF-d_8) δ = 117.9 (s), 115.0 (s), 108.2 (s), 68.0 (s), 26.2 (s), 15.2 (s).
EA	calculated: C, 66.33; H, 7.34;
	found: C, 66.02; H 7.30.
Yield	553 mg, 1.34 mmol, 60%

6.6.2 Synthesis of $[(C_5H_4TMS)_2YCl]_2$

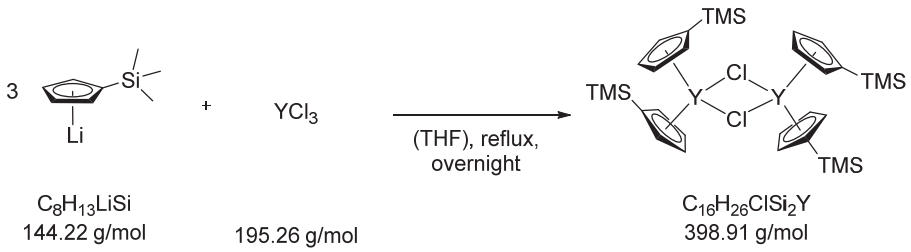

$C_8H_{13}LiSi$
144.22 g/mol

195.26 g/mol

$C_{16}H_{26}ClSi_2Y$
398.91 g/mol

Procedure

YCl_3 (685 mg, 3.51 mmol, 1 eq.) is suspended in 20 ml THF and stirred at 50 °C for 2. After cooling to room temperature, a solution of $Li(C_5H_4TMS)$ (1.76 g, 10.9 mmol, 3.1 eq.) in THF (15 ml) is added dropwise to the suspension. The mixture is heated to reflux overnight. Volatile compounds are removed in vacuo and the product is recrystallized from hexane.

^{1}H NMR (300 MHz, C_6D_6) δ = 6.80 (t, ^3J= 2.3 Hz, 4H), 6.46 (t, ^3J= 2.3 Hz, 4H), 0.31 (s, 18H).

^{13}C NMR (126 MHz, C_6D_6) δ= 123.6 (s), 121.1 (s), 117.0 (s), 0.3 (s).

^{29}Si NMR (99 MHz, C_6D_6) δ = -9.58.

EA calculated: C 48.17; H, 6.57;

found: C 46.36; H, 6.38.

Yield 854 mg, 2.14 mmol, 61%

6.6.3 Synthesis of $(C_5H_4TMS)_3Y$

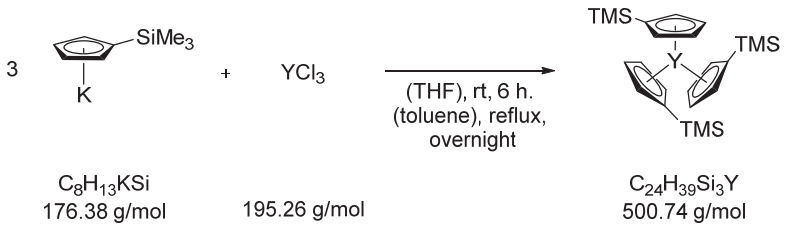

Procedure

$(C_5H_4TMS)_3Y$ was synthesized following an adapted literature procedure.[140] YCl_3 (724 mg, 3.7 mmol, 1 eq.) is suspended in 25 ml THF and heated at 50 °C for 2 h. The mixture is allowed to warm to room temperature and a solution of $K(C_5H_4TMS)$ (2.03 g, 11.5 mmol, 3.1 eq.) in THF (30 ml) is added in portions. The yellow solution is stirred at room temperature for 4 h and THF is removed in vacuo. The mixture is suspended in 44 ml toluene and heated at 100 °C for 12 h. Toluene is removed in vacuo, the mixture is suspended in 40 ml hexane, and stirred at room temperature for 1 h. The mixture is filtered a d washed two times with hexane. The product is recrystallized from pentane and is isolated as a yellow powder.

^{1}H NMR	(300 MHz, C_6D_6) δ = 6.55 (t, ^3J = 2.4 Hz, 6H), 6.22 (t, ^3J = 2.4 Hz, 6H), 0.21 (s, 27H).
^{13}C NMR	(126 MHz, C_6D_6) δ = 124.7 (s), 120.7 (s), 115.4 (s), 0.2 (s).
^{29}Si NMR	(99 MHz, C_6D_6) δ = -10.41.
EA	calculated: C 57.57; H, 7.85;
	found: C 57.22; H, 7.97.
Yield	1.0 g, 2.0 mmol, 89%

6.6.4 Synthesis of $(C_5H_4TMS)_3Sm$

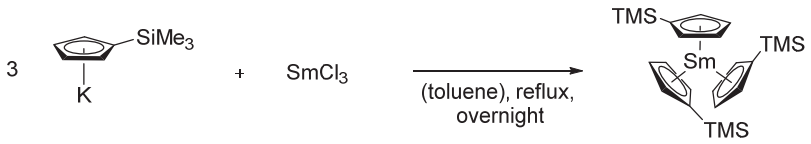

$C_8H_{13}KSi$
176.38 g/mol

256.71 g/mol

$C_{24}H_{39}Si_3Y$
562.19 g/mol

Procedure

$(C_5H_4TMS)_3Sm$ was synthesized following an adapted literature procedure.[317] In an argon-filled glovebox, $SmCl_3$ (128 mg, 0.50 mmol) is suspended in 7 ml toluene and $K(C_5H_4TMS)$ (273 mg, 1.55 mmol) is added stepwise. The colorless mixture is sealed in a 25 ml sidearm Schlenk flask and heated to reflux overnight. The solvent is removed under vacuum from the resulting yellow mixture and the obtained solids are stirred in hexane for 1 h under reflux. The mixture is filtered to remove gray-white insoluble material, presumably KCl and excess $K(C_5H_4TMS)$. Removal of hexane under vacuum yields $(C_5H_4TMS)_3Sm$ as an orange microcrystalline solid. Orange crystals of $(C_5H_4TMS)_3Sm$ suitable for X-ray diffraction were grown from a concentrated pentane solution at -35 °C by slowly evaporating the solvent to dryness.

EA: calculated: C, 51.27; H, 6.99;

found: C, 51.38; H 7.08.

Yield 194 mg, 0.36 mmol, 69%

6.6.5 Synthesis of $(C_5Me_4H)_3Y$

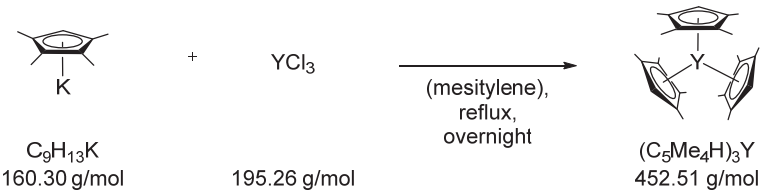

Procedure

In an argon-filled glovebox, YCl_3 (344 mg, 1.76 mmol, 1 eq.) is suspended in 15 ml THF and $K(C_5Me_4H)$ (890 mg, 5.55 mmol, 3.15 eq.) is added stepwise. The colorless mixture is sealed in a 50 ml sidearm Schlenk flask and stirred at room temperature overnight. The solvent is removed under vacuum from the resulting yellow mixture and the obtained solids are stirred in 22 ml of mesitylene at 150 °C for 16 h. The solvent is removed under vacuum and the mixture is filtered to remove gray-white insoluble material, presumably KCl and excess $K(C_5Me_4H)$. Removal of mesitylene under vacuum yields $(C_5Me_4H)_3Y$ as a pale yellow microcrystalline solid. Single crystals of $(C_5Me_4H)_3Y$ suitable for X-ray diffraction were grown from a 0.05 M toluene solution and by cooling to −35 °C in a glovebox freezer.

^{1}H NMR	(300 MHz, C_6D_6) δ = 6.04 (s, 3H), 2.03 (s, 18H), 1.83 (s, 18H).
^{13}C NMR	(75 MHz, C_6D_6) δ = = 124.1 (s), 114.4 (d), 113.8 (d), 26.4 (s), 15.4 (s).
EA	calculated: C, 71.67; H, 8.64;
	found: C, 71.57; H 8.74.
Yield	580 mg, 1.28 mmol, 73%

6.7 Syntheses of Lanthanide Precursor Complexes

6.7.1 Synthesis of $YCl_3(thf)_{3.5}$

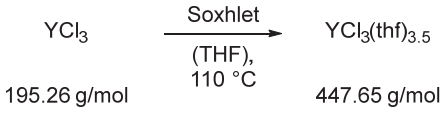

Procedure

A glass thimble is charged inside a glovebox to 2/3 with yttrium(III) chloride (approximately 10 g) and is placed in a 30 ml Soxhlet extractor. All glass joints of the reaction setup are diligently sealed using Teflon grease. The Soxhlet extractor is attached to a Schlenk flask with 150 ml THF, a reflux condenser, and a pressure valve using a Schlenk line outside the glovebox. The oil bath is heated at 110 °C and THF is heated to reflux for 36 h under vigorous stirring. After cooling the Schlenk flask to room temperature and detaching it from the reaction setup, THF is removed in vacuo. The product is obtained as a white powder and the amount of coordinating THF is determined by elemental analysis. The yield is nearly quantitative if pure lanthanide (III)chloride is used as a starting material.

For further reactions with $LiCH_2TMS$, remaining, non-coordinating THF needs to be completely removed, to avoid the formation of ate-complexes.[204] The composition of $YCl_3(thf)_{3.5}$ and a detailed structural discussion of polymeric $YCl_3(thf)_2$ and $[trans\text{-}YCl_2(thf)_5]^+$, $[trans\text{-}YCl_4(thf)_2]^-$ was reported by Sobota et al..[318]

EA calculated: C, 37.56; H, 6.30;

found: C, 37.45; H, 6.33.

Yield quantitative

6.7.2 Synthesis of $Y(CH_2TMS)_3(thf)_2$

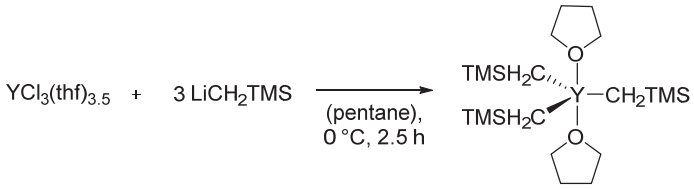

Procedure

$YCl_3(thf)_{3.5}$ (1.79 g, 4 mmol, 1 eq.) is suspended in pentane (25 ml). A solution of trimethylsilylmethyl lithium (1.13 g, 12 mmol, 3 eq.) in pentane (35 ml) is added dropwise at 0 °C and the reaction solution is stirred at 0 °C for 2 h. The supernatant solution is isolated using a filter cannula and the residue is extracted with pentane (2x 10 ml). The solvent is removed in vacuo and the product is obtained as a white solid.

^{1}H NMR (300 MHz, C_6D_6) δ = 4.01–3.87 (m, 8 H), 1.36–1.21 (m, 8 H), 0.31 (s, 27 H), -0.67 (d, 6 H).

^{13}C NMR (75 MHz, C_6D_6) δ = 69.8 (s), 33.8 (s), 25.2 (s), 4.5 (s).

Yield 1.78 g, 3.6 mmol, 90%

6.7.3 Synthesis of $LuCl_3(thf)_3$

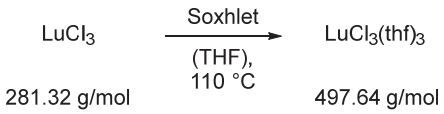

Procedure

A glass thimble is charged inside a glovebox to 2/3 with lutetium(III) chloride (approximately 10 g) and is placed in a 30 ml Soxhlet extractor. All glass joints of the reaction setup are diligently sealed using Teflon grease. The Soxhlet extractor is attached to a Schlenk flask with 150 ml THF, a reflux condenser, and a pressure valve using a Schlenk line outside the glovebox. The oil bath is heated at 110 °C and THF is heated to reflux for 24 h under vigorous stirring. After cooling the Schlenk flask to room temperature and detaching it from the reaction setup, THF is removed in vacuo. The product is obtained as a white powder and the amount of coordinating THF is determined by elemental analysis. The yield is nearly quantitative if pure lanthanide (III)chloride is used as a starting material.

For further reactions with $LiCH_2TMS$, remaining, non-coordinating THF need to be completely removed, to avoid the formation of ate-complexes.[204]

EA calculated: C, 28.96; H, 4.86;

found: C, 28.94; H, 4.94.

Yield quantitative

6.7.4 Synthesis of $Lu(CH_2TMS)_3(thf)_2$

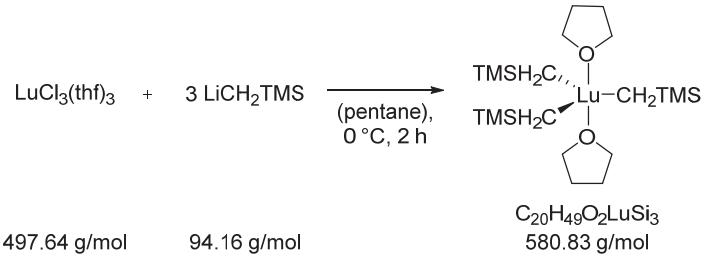

Procedure

$LuCl_3(thf)_3$ (2.23 g, 4.48 mmol, 1 eq.) is suspended in pentane (35 ml). A solution of trimethylsilylmethyl lithium (2.26 g, 13.44 mmol, 3 eq.) in pentane (25 ml) is added dropwise at 0 °C and the reaction solution is stirred at 0 °C for 2 h. The supernatant solution is isolated using a filter cannula and the residue is extracted with pentane (2x 10 ml). The solvent is removed in vacuo and the product is obtained as a white solid.

^{1}H NMR (300 MHz, C_6D_6) δ = 3.99–3.90 (m), 1.38–1.27 (m), 0.26 (s, 27H), -0.93 (s, 6H).

^{13}C NMR (75 MHz, C_6D_6) δ = 71.0 (s), 41.8 (s), 25.1 (s), 4.8 (s).

Yield 2.22 g, 3.82 mmol, 85%

6.7.5 Synthesis of $Sc(CH_2TMS)_3(thf)_2$

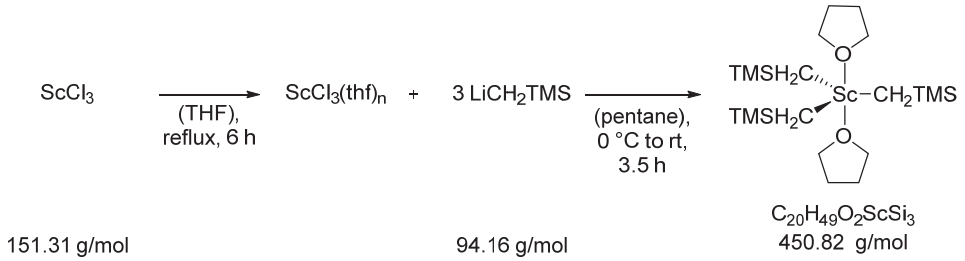

Procedure

$ScCl_3$ (664 mg, 4.39 mmol, 1 eq.) is heated to reflux in THF (9 ml) for 4 h. After removal of the solvent in vacuo, the white powder is suspended in 60 ml pentane and cooled to 0 °C. $LiCH_2TMS$ (1.24 g, 13.2 mmol, 3eq, in 25 ml pentane) is added dropwise and the combined solutions are stirred for 2 h. The solution is allowed to warm to room temperature for 1 h. The white suspension is filtered and the residue is washed two times with 15 ml of pentane.

^{1}H NMR (300 MHz, C_6D_6) δ = 4.10–4.02 (m, 8H), 1.43–1.32 (m, 8H), 0.26 (s, 27H), -0.31 (s, 6H).

^{13}C NMR (75 MHz, C_6D_6) δ = 69.4 (s), 23.2 (s), 2.3 (s), -1.9 (s).

Yield: 1.0 g, 2.28 mmol, 52%

6.7.6 Synthesis of $SmCl_3(thf)_{1.75}$

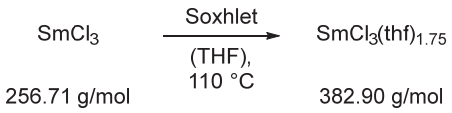

Procedure

A glass thimble is charged inside a glovebox to 2/3 with samarium(III) chloride (approximately 10 g) and is placed in a 30 ml Soxhlet extractor. All glass joints of the reaction setup are diligently sealed using Teflon grease. The Soxhlet extractor is attached to a Schlenk flask with 150 ml THF, a reflux condenser, and a pressure valve using a Schlenk line outside the glovebox. The oil bath is heated at 110 °C and THF is heated to reflux for 1 week under vigorous stirring. After cooling the Schlenk flask to room temperature and detaching it from the reaction setup, THF is removed in vacuo. The product is obtained as a white powder and the amount of coordinating THF is determined by elemental analysis. The yield is nearly quantitative if pure lanthanide (III)chloride is used as a starting material.

EA calculated: C, 21.96; H, 3.69;

found: C, 22.30; H, 3.69.

Yield quantitative

6.7.7 Synthesis of $LaCl_3(thf)$

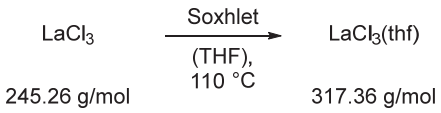

Procedure

A glass thimble is charged inside a glovebox to 2/3 with lanthanum(III) chloride (approximately 10 g) and is placed in a 30 ml Soxhlet extractor. All glass joints of the reaction setup are diligently sealed using Teflon grease. The Soxhlet extractor is attached to a Schlenk flask with 150 ml THF, a reflux condenser, and a pressure valve using a Schlenk line outside the glovebox. The oil bath is heated at 110 °C and THF is heated to reflux for three weeks under vigorous stirring. After cooling the Schlenk flask to room temperature and detaching it from the reaction setup, THF is removed in vacuo. The product is obtained as a white powder and the amount of coordinating THF is determined by elemental analysis. The yield is nearly quantitative if pure lanthanide (III)chloride is used as a starting material.

EA calculated: C, 15.14; H, 2.54;

found: C, 15.13; H, 2.53.

Yield quantitative

6.8 Synthesis of Trimethylsilylmethyl RE Complexes

6.8.1 Synthesis of $(C_5H_5)_2YCH_2TMS(thf)$

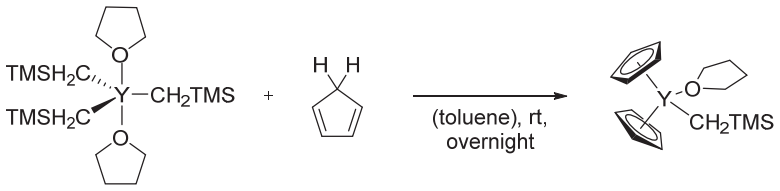

$C_{20}H_{49}O_2Si_3Y$ 494.77 g/mol

C_5H_6 66.10 g/mol

$C_{18}H_{29}OSiY$ 378.42 g/mol

Procedure

$Y(CH_2TMS)_3(thf)_2$ (8.9 g, 22.0 mmol, 1 eq.) is dissolved in toluene (200 ml) and 2.9 g of freshly cracked C_5H_6 (44.0 mmol, 2 eq.) are added dropwise at room temperature. The mixture is stirred overnight. Volatile compounds are removed in vacuo and the product is recrystallized from toluene. The product is obtained as white crystalline needles.

^{1}H NMR	(500 MHz, C_6D_6) δ = 6.12 (s, 10H), 2.95 (m, 4H), 0.92 (m, 4H), 0.43 (s, 9H), -0.67 (d, 2H, $^2J_{YH}$ = 3.5 Hz).
^{13}C NMR	(125 MHz, C_6D_6) δ = 110.4 (s), 71.2 (s), 25.4 (d, ^1J(Y-C) = 42.5 Hz), 24.9 (s), 4.8 (s).
^{29}Si NMR	(100 MHz, C_6D_6) δ = -3.09.
^{1}H NMR	(300 MHz, THF-d_8) δ = 6.06 (s, 10H), 3.61 (m, 4H), 1.77 (m, 4H), -0.06 (s, 9H), -0.94 (d, $^2J_{YH}$ = 3.5 Hz, 2H).
^{13}C NMR	(75 MHz, THF-d_8) δ = 110.5 (s), 68.0 (s), 26.2 (s), 4.4 (s), -0.2 (s).
IR (cm^{-1})	3674, 3559, 3087, 2955, 2893, 2707, 1638, 1459, 1438, 1422, 1368, 1345, 1287, 1248, 1011, 861, 766, 696.
EA	calculated: C 57.13, H 7.72;
	found: C 57.21, H 7.85.
Yield	5.4 g, 14.3 mmol, 65%

6.8.2 Synthesis of $(C_5H_5)_2LuCH_2TMS(thf)$

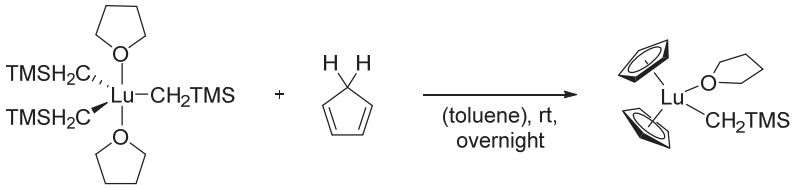

$C_{20}H_{49}O_2LuSi_3$ 580.83 g/mol

C_5H_6 66.10 g/mol

$C_{18}H_{29}OLuSi$ 464.48 g/mol

Procedure

$Lu(CH_2TMS)_3(thf)_2$ (8.9 g, 15.3 mmol, 1 eq.) is dissolved in toluene (140 ml) and 2.05 g of freshly cracked C_5H_6 (30.6 mmol, 2 eq.) are added dropwise at room temperature. The mixture is stirred overnight. Volatile compounds are removed in vacuo and the product is recrystallized from a toluene hexane mixture. The synthesis via salt metathesis and crystallographic characterization was reported by Schumann et al..[319]

^{1}H NMR	(300 MHz, C_6D_6) δ = 6.06 (s, 10H), 2.91 (m, 4H), 0.89 (m, 4H), 0.44 (s, 9H), -0.76 (s, 2H).
^{13}C NMR	(75 MHz, C_6D_6) δ = 109.82 (s), 71.53 (s), 24.89 (s), 5.03 (s), -2.19 (s).
^{29}Si NMR	(100 MHz, C_6D_6) δ = -0.8 (s).
^{1}H NMR	(300 MHz, THF-d_8) δ = 6.00 (s, 10H), 3.61 (m, 4H), 1.77 (m, 4H), -0.04 (s, 9H), −1.00 (s, 2H).
^{13}C NMR	(75 MHz, THF-d_8) δ = 110.0 (s), 68.2 (s), 26.4 (s), 4.7 (s), -0.0 (s).
IR (cm^{-1})	3563, 3091, 2953, 2896, 2710, 1459, 1439, 1420, 1287, 1248, 1122, 1013, 859, 775, 695.
EA	calculated: C 46.55, H 6.29;
	found: C 45.93, H 6.10.
Yield	5.5 g, 11.8 mmol, 77%

6.8.3 Synthesis of $(C_5Me_4)CH_2CH_2NtBuYCH_2TMS(thf)$

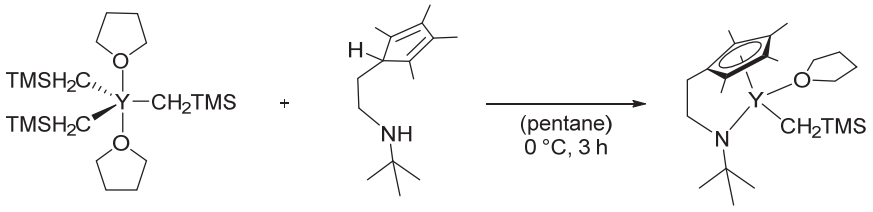

$C_{20}H_{49}O_2Si_3Y$
494.77 g/mol

$C_{15}H_{27}N$
221.39 g/mol

$C_{23}H_{44}NOSiY$
467.60 g/mol

Procedure

$Y(CH_2TMS)_3(thf)_2$ (988 mg, 1.89 mmol, 1 eq.) is dissolved in pentane (18 ml) and the mixture is cooled to 0 °C. A solution of $(C_5Me_4H)CH_2CH_2NHtBu$ (418 mg, 1.89 mmol, 1 eq.) in pentane (7 ml) is added dropwise and the reaction solution is stirred for 2 h at 0 °C. Volatile compounds are removed in vacuo, resulting in a yellow solid. The crude product is washed with cold pentane and dried in vacuo. The product is purified by recrystallization from pentane and is obtained is a slightly yellow crystalline solid.

^{1}H NMR (300 MHz, C_6D_6) δ = 3.89–3.81 (t, 2H), 3.60–3.20 (m, 4H), 3.02 (t, 2H), 2.25–1.96 (m, 12H), 1.34 (s, 9H), 1.08–0.97 (m, 4H), 0.36 (s, 9H), -0.97 (d, 2H).

^{13}C NMR (75 MHz, C_6D_6) δ = 126.4 (s), 126.2 (s), 126.0 (s), 68.5 (s), 53.7 (s), 52.4 (s), 28.2 (s), 25.8 (s), 23.2 (d), 22.7 (s), 9.1 (s), 3.0 (s), -2.0 (s).

^{29}Si NMR (99 MHz, C_6D_6) δ = -2.86.

EA calculated: C 59.08, H 9.48, N 3.00;

found: C 58.70, H 9.43, N 3.17.

Yield 787 mg, 1.68 mmol, 89%

6.8.4 Synthesis of $(C_5Me_4)SiMe_2NtBuYCH_2TMS(thf)$

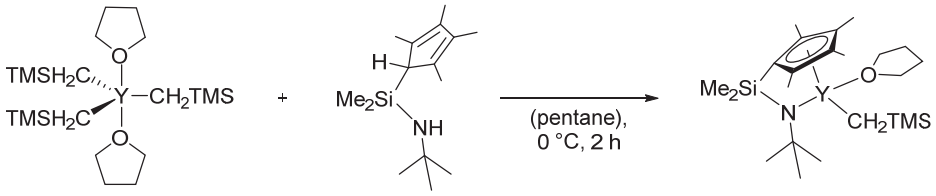

$C_{20}H_{49}O_2Si_3Y$
494.77 g/mol

$C_{15}H_{29}NSi$
251.49 g/mol

$C_{23}H_{46}NOSi_2Y$
497.70 g/mol

Procedure

$(C_5Me_4)SiMe_2NtBuYCH_2TMS(thf)$ was synthesized following an adapted literature procedure.[214] $Y(CH_2TMS)_3(thf)_2$ (4.4 g, 8.9 mmol, 1 eq.) is dissolved in pentane (90 ml) and cooled to 0 °C. A pentane solution (35 ml) of $(C_5Me_4H)SiMe_2NHtBu$ (2.24 g, 8.9 mmol, 1 eq.) is added dropwise and the mixture is stirred under cooling for 2 h. The mixture is filtered and volatile compounds are removed in vacuo. 3.7 g of the yellow crude product $(C_5Me_4)SiMe_2NtBuYCH_2TMS(thf)$ (84%) are obtained and further purified by recrystallization from pentane. The product is obtained as a white powder.

^{1}H NMR (300 MHz, C_6D_6) δ = 3.38–3.15 (m, 4H), 2.21 (s, 12H), 1.39 (s, 9H), 1.03–0.96 (m, 4H), 0.77 (s, 6H), 0.31 (s, 9H), -0.90 (d, J = 3.2 Hz, 2H).

^{1}H NMR (300 MHz, C_6D_{12}) δ = 4.05–3.97 (m, 4H), 2.06–2.00 (m, 12H), 2.00–1.93 (m, 4H), 1.24 (s, 9H), 0.42 (s, 6H), -0.12 (s, 9H), -1.18 (d, J = 3.2 Hz, 2H).

^{13}C NMR (75 MHz, C_6D_6) δ = 4.7, 8.4, 11.5, 14.0, 24.7, 26.2, 36.0, 54.0, 70.7, 106.6, 122.3, 126.4.

^{29}Si NMR (99 MHz, C_6D_6) δ = -2.73, -25.06.

EA calculated: C, 55.51; H, 9.32; N, 2.81;

found: C, 55.77; H, 9.50; N, 2.85.

Yield 2.29 g, 0.38 mmol, 52%

6.8.5 Synthesis of $(C_5Me_4)SiMe_2NtBuLuCH_2TMS(thf)$

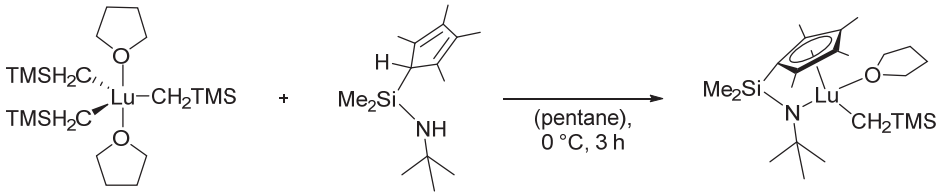

$C_{20}H_{49}O_2LuSi_3$
580.83 g/mol

$C_{15}H_{29}NSi$
251.49 g/mol

$C_{23}H_{46}LuNOSi_2$
583.76 g/mol

Procedure

$Lu(CH_2TMS)_3(thf)_2$ (2.20 g, 3.79 mmol, 1 eq.) is dissolved in 90 ml pentane and cooled to 0 °C. A solution of $(C_5Me_4H)SiMe_2NHtBu$ (953 mg, 3.79 mmol, 1 eq.) in pentane (15 ml) is added dropwise and the combined solutions are stirred for 3 h at 0 °C. The product is removed from an oily byproducts by filtration and volatile compounds are removed in vacuo. The product is obtained as a white solid.

The spectroscopic data are in agreement with ref. 200.

EA calculated: C, 47.32; H, 7.94; N, 2.40;

found: C, 47.30; H, 8.13; N, 2.42.

Yield 1.95 g, 3.34 mmol, 88%

6.8.6 Synthesis of $(C_5Me_4)SiMe_2NtBuScCH_2TMS(thf)$

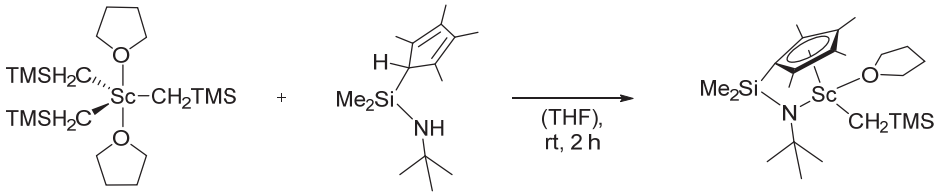

$C_{20}H_{49}O_2ScSi_3$ 450.82 g/mol

$C_{15}H_{29}NSi$ 251.49 g/mol

$C_{23}H_{46}NOScSi_2$ 453.75 g/mol

Procedure

$(C_5Me_4)SiMe_2NtBuScCH_2TMS$ was synthesized following an adapted literature procedure.[320] $Sc(CH_2TMS)_3(thf)_2$ (1.02 g, 2.26 mmol, 1 eq.) is dissolved in 12 ml THF. A solution of $(C_5Me_4H)SiMe_2NHtBu$ (546 mg, 2.26 mmol, 1 eq.) in THF (5 ml) is added dropwise and the combined solutions are stirred for 2 h at room temperature. After volatile compounds are removed in vacuo, the product is purified by lyophilization from a benzene solution and is obtained as a yellow solid.

^{1}H NMR (300 MHz C_6D_6) δ = 3.51–3.35 (m, 4H), 2.38 (s, 3H), 2.27 (s, 3H), 1.96 (s, 3H), 1.74 (s, 3H), 1.38 (s, 9H), 1.15–0.99 (m, 4H), 0.81 (s, 3H), 0.67 (s, 3H), 0.31 (s, 9H), -0.68 (d, 2H).

^{13}C NMR (126 MHz, C_6D_6) δ = 126.8 (s), 124.7 (s), 124.3 (s), 120.8 (s), 105.7 (s), 70.1 (s), 52.6 (s), 33.8 (s), 22.5 (s), 12.9 (s), 12.2 (s), 10.7 (s), 9.30 (s), 6.4 (s), 5.6 (s), 2.8 (s), -2.0 (s).

^{29}Si NMR (99 MHz, C_6D_6) δ = -3.13, -24.02.

EA calculated: C, 60.88; H, 10.22; N, 3.09;

found: C, 59.78; H, 10.21; N, 2.97.

Yield 785 mg, 1.73 mmol, 77%

6.9 Synthesis of Initiating Ligands via C–H Bond Activation

6.9.1 Synthesis of $(C_5H_5)_2Y((CH_2(C_5H_2Me_2N))(thf)_{0.2}$

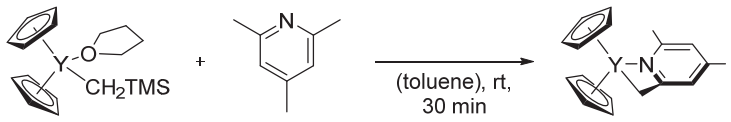

$C_{18}H_{29}OSiY$ 378.42 g/mol | $C_8H_{11}N$ 121.18 g/mol | $C_{18}H_{20}NY$ 339.27 g/mol

Procedure

$Cp_2YCH_2TMS(thf)$ (365 mg, 0.96 mmol, 1 eq.) is dissolved in toluene (7 ml) and *sym*-collidine (117 mg, 0.96 mmol, 1 eq.) is added dropwise to the stirred solution. The mixture is stirred at room temperature for 30 min and volatile compounds are removed in vacuo. The yellow residue is recrystallized from a toluene pentane mixture and the product is obtained as yellow crystals. 0.2 eq. coordinating THF stem from the recrystallization conditions and were verified by ^{1}H NMR.

^{1}H NMR (300 MHz, C_6D_6) δ = 6.41 (s, 1H), 6.05 (s, 10H), 5.80 (s, 1H), 2.83 (s, 3H), 2.44 (s, 2H), 1.79 (s, 3H).

^{13}C NMR (126 MHz, C_6D_6) δ = 167.4 (s), 155.8 (s), 148.0 (s), 118.5 (s), 112.3 (s), 111.2 (s), 40.7 (d), 23.9 (s), 21.1 (s).

EA calculated: C 63.84, H 6.16, N 3.96;

found: C 63.93, H 6.08, N 4.00.

Yield 320 mg, 0.94 mmol, quantitative

6.9.2 Synthesis of $(C_5H_5)_2Lu((CH_2(C_5H_2Me_2N))$

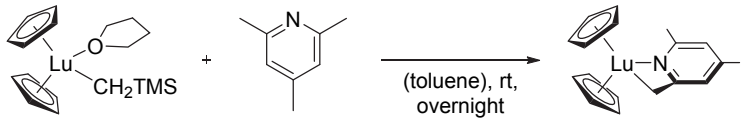

$C_{18}H_{29}LuOSi$
464.48 g/mol

$C_8H_{11}N$
121.18 g/mol

$C_{18}H_{20}LuN$
425.33 g/mol

Procedure

$Cp_2LuCH_2TMS(thf)$ (596 mg, 1.28 mmol, 1 eq.) is dissolved in toluene (11 ml) and *sym*-collidine (163 mg, 1.35 mmol, 1.05 eq.) is added dropwise to the stirred solution. The mixture is stirred at room temperature overnight and a few drops THF are added. Volatile compounds are removed in vacuo, the mixture is dissolved in THF and stirred for 30 min. Volatile compounds are removed in vacuo and impurities are removed as an amorphous precipitate from a toluene pentane mixture at −30 °C. Volatile compounds are removed in vacuo and the product further purified by freeze drying from benzene. The product is obtained as a yellow solid.

^{1}H NMR (300 MHz, C_6D_6) δ = 6.49 (s, 1H), 6.04 (s, 1H), 5.68 (s, 10H), 2.39 (s, 2H), 1.82 (s, 3H), 1.74 (s, 3H).

^{13}C NMR (125 MHz, C_6D_6) δ = 168.5 (s), 156.1 (s), 149.5 (s), 120.2 (s), 114.7 (s), 110.7 (s), 37.8 (s), 23.7 (s), 20.9 (s).

EA calculated: C, 50.83; H, 4.74; N, 3.29;

found: C, 49.18; H, 4.86; N, 2.72.

Yield 174 mg, 0.41 mmol, 32%

6.9.3 Synthesis of $(C_5Me_4)CH_2CH_2NtBuY(CH_2(C_5H_2Me_2N))$

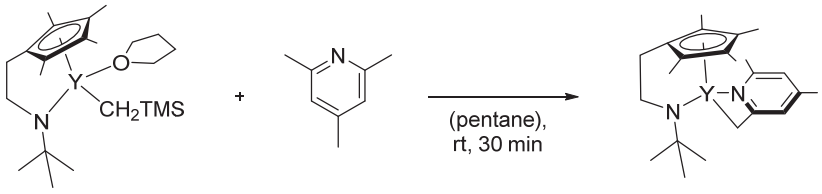

$C_{23}H_{44}NOSiY$ 467.60 g/mol

$C_8H_{11}N$ 121.18 g/mol

$C_{23}H_{35}N_2Y$ 428.45 g/mol

Procedure

$(C_5Me_4)CH_2CH_2NtBuYCH_2TMS(thf)$ (170 mg, 0.36 mmol, 1 eq.) is suspended in pentane (7.5 ml) and sym-collidine (43.5 mg, 0.36 mmol, 1 eq.) is added dropwise. The reaction solution is stirred at room temperature for 30 minutes and volatile compounds are removed in vacuo. The product is obtained as a yellow solid.

^{1}H NMR (300 MHz, C_6D_6) δ = 6.41 (s, 1 H), 6.35 (s, 1 H), 3.58 (m, 2 H), 3.08 (m, 2 H), 2.51 (s, 3 H), 2.44 (s, 2 H), 2.36 (s, 3 H), 2.25 (s, 3 H), 2.04 (s, 3 H), 1.96 (s, 3 H), 1.78 (s, 3 H), 0.97 (s, 9 H).

Yield 139 mg, 0.32 mmol, 90%

6.9.4 Synthesis of $(C_5Me_4)SiMe_2NtBuY(CH_2(C_5H_2Me_2N))$

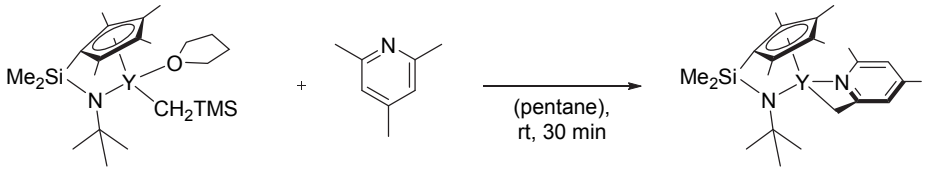

$C_{23}H_{46}NOSi_2Y$ 497.70 g/mol

$C_8H_{11}N$ 121.18 g/mol

$C_{23}H_{37}N_2SiY$ 458.55 g/mol

Procedure

$(C_5Me_4)SiMe_2NtBuYCH_2TMS(thf)$ (2.2 g, 4.4 mmol, 1 eq.) is dissolved in pentane (100 ml) and *sym*-collidine (0.54 g, 4.4 mmol, 1 eq.) in 20 ml pentane is added dropwise to the stirred solution. The mixture is stirred at room temperature for 30 min and volatile compounds are removed in vacuo. The yellow residue (1.85 g, 4.0 mmol, 91%) is washed once with cold pentane and the crude product is recrystallized from toluene. The product is obtained as yellow crystals.

^{1}H NMR (500 MHz, C_6D_6) δ = 6.40 (s, 1H), 5.86 (s, 1H), 2.58 (s, 3H), 2.38 (s, 3H), 2.20 (s, 3H), 2.09 (s, 3H), 1.93 (s, 3H), 1.78 (s, 3H), 1.01 (s, 9H), 0.85 (s, 3H), 0.78 (s, 3H).

^{13}C NMR (126 MHz C_6D_6,) δ = 172.0 (s), 155.0 (s), 150.1 (s), 127.5 (d), 126.9 (d), 123.1 (s), 122.3 (s), 119.3 (s), 116.2 (s), 107.1 (s), 54.8 (s), 41.3 (d), 33.9 (s), 26.1 (s), 20.8 (s), 16.1 (s), 14.6 (s), 11.9 (s), 11.5 (s), 8.8 (s), 7.9 (s).

^{29}Si NMR (99 MHz, C_6D_6) δ = -25.36.

EA calculated: C, 60.24; H, 8.13; N, 6.11;

found: C, 59.66; H, 8.24; N, 5.92.

Yield 1.63 g, 3.6 mmol, 80%

6.9.5 Synthesis of $(C_5Me_4)SiMe_2NtBuY(CH_2(C{\equiv}CTMS)$

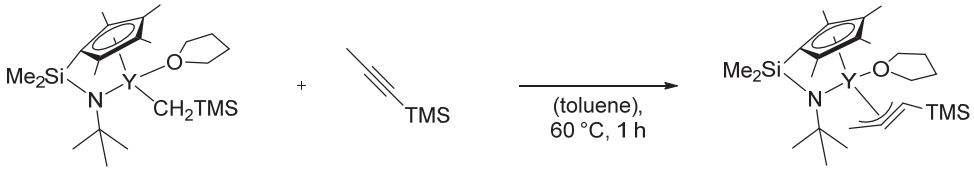

$C_{23}H_{46}NOSi_2Y$
497.70 g/mol

$C_6H_{12}Si$
112.25 g/mol

$C_{25}H_{46}NOSi_2Y$
521.72 g/mol

Procedure

$(C_5Me_4)SiMe_2NtBuYCH_2TMS(thf)$ (1.42 g, 2.9 mmol, 1 eq.) is dissolved in toluene (50 ml) and 1-trimethylsilylprop-1-yne (0.38 g, 3.4 mmol, 1.2 eq.) is added to the mixture. The solution is heated at 60 °C for 1 h and volatile compounds are removed in vacuo. The product is purified by recrystallization from pentane and obtained as a slightly yellow solid.

^{1}H NMR (500 MHz, C_6D_6) δ = 3.63–3.39 (m, 4H), 2.56–1.95 (m, 14H), 1.35 (s, 9H), 1.16–1.07 (m, 4H), 0.92–0.75 (m, 6H), 0.32 (s, 9H).

^{13}C NMR (126 MHz, C_6D_6) δ = 166.6 (s), 127.0 (s), 125.5 (s), 123.9 (s), 120.5 (s), 107.2 (s), 105.8 (d), 72.9 (s), 54.0 (s), 38.3 (d), 35.5 (s), 25.2 (d), 15.3 (s), 14.1 (s), 11.3 (s), 8.9 (s), 8.6 (s), 2.2 (s).

^{29}Si NMR (99 MHz, C_6D_6) δ = -12.65, -25.97.

EA calculated: C, 57.55; H, 8.89; N, 2.68;

found: C, 57.45; H, 9.14; N, 2.77.

Yield 950 mg, 1.82 mmol, 64%

6.9.6 Results of Other NMR Scale C–H Bond Activation Experiments

	2 eq. 2-Methylthiophene[a]	sym-Collidine (room temperature)[a]	Methane (room temperature)[b]	Methane (75 °C)[b]
$(C_5H_5)_2YCH_2TMS(thf)$	Overnight, 60 °C	< 10 min	–	–
$(C_5Me_4)CH_2CH_2NtBuYCH_2TMS(thf)$	–	< 5 min	No reaction	Decomposition
$(C_5Me_4)SiMe_2NtBuYCH_2TMS(thf)$	–	< 5 min	No reaction	Decomposition
$(C_5Me_4)SiMe_2NtBuLuCH_2TMS(thf)$	–	< 30 min	No reaction	Decomposition
$(C_5Me_4)SiMe_2NtBuScCH_2TMS(thf)$	–	Overnight	No reaction	Decomposition

a) Measured in C_6D_6 (full conversion determined by following the decline of the Ln-C*H*$_2$TMS signal). b) Measured in C_6D_{12}

6.10 Syntheses of RE Complexes via Amide Elimination

6.10.1 Synthesis of $(C_5H_5)_2LuNC_4H_4$

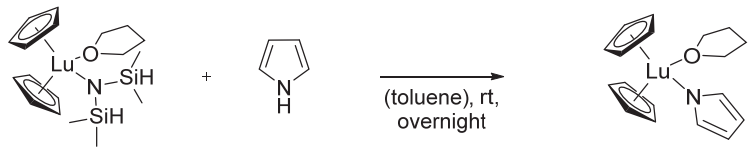

$C_{18}H_{32}LuNOSi_2$ 509.60 g/mol

C_4H_5N 67.09 g/mol

$C_{18}H_{22}LuNO$ 443.35 g/mol

Procedure

$Cp_2Lu(bdsa)(thf)$ (142 mg, 0.278 mmol, 1 eq.) is dissolved in toluene (8 ml) and a toluene solution (2 ml) of pyrrole (18.7 mg, 0.278 mmol, 1 eq.) is added dropwise at room temperature. The reaction is stirred overnight. After removal of volatile compounds, the products is obtained as a white powder.

^{1}H NMR (300 MHz, THF-d_8) δ = 6.81 (t, ^3J= 1.7 Hz, 2H), 6.19 (s, 10H), 5.95 (t, ^3J= 1.7 Hz, 2H), 3.62 (m, 4H), 1.78 (m, 4H).

^{13}C NMR (75 MHz, THF-d_8) δ = 129.5 (s), 111.2 (s), 107.6 (s), 68.5 (s), 26.7 (s).

Yield 115 mg, 0.259 mmol, 93%

6.11 Synthesis of 2-Methoxyethylaminobis(phenolate)yttrium(thiolate)

6.11.1 Synthesis of (ONOO)^{CMe2Ph}YS*t*Bu(thf)

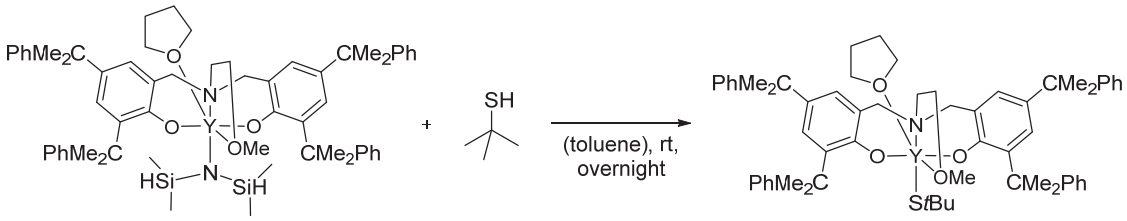

$C_{61}H_{81}N_2O_4Si_2Y$
1051.40 g/mol

$C_4H_{10}S$
90.18 g/mol

$C_{61}H_{76}NO_4SY$
1008.25 g/mol

Procedure

A 3 ml toluene solution of *t*BuSH (43 mg, 0.48 mmol, 1 eq.) is added dropwise to a stirred solution of (ONOO)^{CMe2Ph}Y(bdsa)(thf) (500 mg, 0.48 mmol, 1 eq.) in 7.5 ml toluene at room temperature. The combined solutions are stirred overnight and the volatile compounds are removed in vacuo. The product is obtained as a white crystalline solid after recrystallization from a pentane/toluene solution at −30 °C.

^{1}H NMR (300 MHz, C_6D_6) δ = 7.51 (s, 1H), 7.43–7.27 (m, 10H), 7.25–7.20 (m, 2H), 7.12–6.92 (m, 10H), 6.72 (s, 1H), 4.83 (d, 1H), 4.02 (d, 1H), 3.17–2.74 (m, 4H), 2.58 (s, 4H), 2.38 (d, 2H), 2.11 (s, 3H), 2.04–1.93 (m, 4H), 1.91–1.74 (m, 12H), 1.74–1.59 (m, 12H), 1.48 (s, 9H).

^{13}C NMR (126 MHz, C_6D_6) δ = 152.0 (s), 151.8 (s), 151.1 (s), 150.9 (s), 137.5 (s), 137.3 (s), 136.3 (s), 135.7 (s), 135.1 (s), 129.0 (s), 128.2 (s), 127.9 (s), 127.0 (s), 126.8 (s), 126.7 (s), 126.3 (s), 126.0 (s), 125.4 (s), 125.3 (s), 125.0 (s), 124.6 (s), 124.2 (s), 72.5 (s), 64.0 (s), 60.1 (s), 59.1 (s), 55.5 (s), 46.1 (s), 42.9 (s), 42.4 (s), 42.3 (s), 38.3 (s), 31.2 (s), 30.6 (s), 29.6 (s), 28.9 (s), 21.1 (s).

EA calculated: C, 72.67; H, 7.60; N, 1.39; S, 3.18;

found: C, 73.16; H, 7.48; N, 1.50; S, 3.10.

Yield 383 mg, 0.38 mmol, 79%

6.11 Synthesis of 2-Methoxyethylaminobis(phenolate)yttrium(thiolate)

7 References

(1) Lehn, J.-M. *Angew. Chem. Int. Ed.* **2015**, *54*, 3276-3289.

(2) Lehn, J.-M. *Angew. Chem. Int. Ed.* **2013**, *52*, 2836-2850.

(3) Lehn, J.-M. *Interdisciplinary Science Reviews* **1985**, *10*, 72-85.

(4) Michaelis, A. R. *Interdisciplinary Science Reviews* **1996**, *21*, 130-139.

(5) Lehn, J.-M. *Interdisciplinary Science Reviews* **1996**, *21*, 103-109.

(6) Borman, S.; Ronald, R. "Notable chemists who should have won the Nobel," Chemical & Engineering News, **2016**.

(7) Carr, B.; Gates, M. F.; Mitchell, A.; Shah, R. *The Lancet* **2012**, *380*, 80-82.

(8) Michaelis, A. R. *Interdisciplinary Science Reviews* **2003**, *28*, 280-286.

(9) Wiberg, E.; Holleman, A. F.; Wiberg, N. *Lehrbuch Der Anorganischen Chemie*; De Gruyter, **2007**.

(10) Welter, K. *Chem. unserer Zeit* **2007**, *41*, 422-424.

(11) Ertl, G. *Angew. Chem. Int. Ed.* **2008**, *47*, 3524-3535.

(12) Appl, M. In *Ullmann's Encyclopedia of Industrial Chemistry*; Wiley-VCH Verlag GmbH & Co. KGaA, **2000**.

(13) Erisman, J. W.; Sutton, M. A.; Galloway, J.; Klimont, Z.; Winiwarter, W. *Nature Geosci.* **2008**, *1*, 636-639.

(14) Nations, U. In *Global Challenges for Humanity* www.millennium-project.org, (05/2015).

(15) Kreimeyer, A.; Eckes, P.; Fischer, C.; Lauke, H.; Schuhmacher, P. *Angew. Chem. Int. Ed.* **2015**, *54*, 3178-3195.

(16) Iwata, T. *Angew. Chem. Int. Ed.* **2015**, *54*, 3210-3215.

(17) Whitesides, G. M. *Angew. Chem. Int. Ed.* **2015**, *54*, 3196-3209.

(18) Ertl, J. "Plastics – the Facts 2015," **2015**.

(19) Hapke, W. "Plastics – the Facts 2012," **2012**.

(20) Hapke, W. "Plastics – the Facts 2013," **2013**.

(21) Ertl, J. "Plastics – the Facts 2014/2015," **2015**.

(22) Hoyningen-Huene, J. v.; Forrest, R.; Schulz, O.; Rings, T. "Chemical Industry Vision 2030: A European Perspective," A.T. Kearney, **2012**.

(23) Hansell, G.; Kotzen, J.; Olsen, E.; Plaschke, F.; Stelter, D.; Farag, H. "The 2012 Value Creators Rankings," Boston Consulting Group, **2012**.

(24) Gocke, A.; Willers, Y.-P.; Friese, J.; Gehrlein, S.; Schönberger, H.; Farag, H. "The 2013 Chemical Industry Value Creators Report," Boston Consulting Group, **2014**.

(25) Friese, J.; Gehrlein, S.; Gocke, A.; Plaschke, F.; Schönberger, H.; Willers, Y.-P. "The 2012 Chemical Industry Value Creators Report," Boston Consulting Group, **2013**.

(26) Tullo, A. H. "Dow And DuPont Lay Out Merger Plan," Chemical & Engineering News, **2015**.

(27) Tullo, A. H. "DowDuPont Is C&EN's Company Of The Year," Chemical & Engineering News, **2016**, *1*, 14-15.

(28) King, A. "Dow and DuPont mega-merger heralds break-up of giants," RSC Chemistry World, **2015**.

(29) Broadwith, P. "Is bigger really better?," RSC Chemistry World, **2015**.

(30) Gellrich, T. "Shale gas: Reshaping the US chemicals industry," PricewaterhouseCoopers, **2013**.

(31) Gocke, A.; Lang, N. "How the Global Chemical Industry Has Become a Battle of Equals," Boston Consulting Group, **2015**.

(32) Ringel, M.; Taylor, A.; Zablit, H. "Innovation in 2015," Boston Consulting Group, **2015**.

(33) Monge, S.; Canniccioni, B.; Graillot, A.; Robin, J.-J. *Biomacromolecules* **2011**, *12*, 1973-1982.

(34) Soller, B. S.; Salzinger, S.; Rieger, B. *Chem. Rev.* **2016**, *116*, 1993–2022.

(35) Salzinger, S.; Soller, B. S.; Plikhta, A.; Seemann, U. B.; Herdtweck, E.; Rieger, B. *J. Am. Chem. Soc.* **2013**, *135*, 13030-13040.

(36) Chen, E. Y. X. *Chem. Rev.* **2009**, *109*, 5157-5214.

(37) Miyake, G.; Caporaso, L.; Cavallo, L.; Chen, E. Y. X. *Macromolecules* **2009**, *42*, 1462-1471.

(38) Bock, T.; Möhwald, H.; Mülhaupt, R. *Macromol. Chem. Phys.* **2007**, *208*, 1324-1340.

(39) Allcock, H. R.; Hofmann, M. A.; Ambler, C. M.; Lvov, S. N.; Zhou, X. Y.; Chalkova, E.; Weston, J. *Journal of Membrane Science* **2002**, *201*, 47-54.

(40) Berber, M. R.; Fujigaya, T.; Nakashima, N. *ChemCatChem* **2014**, *6*, 567-571.

(41) Berber, M. R.; Fujigaya, T.; Sasaki, K.; Nakashima, N. *Sci. Rep.* **2013**, *3*.

(42) Yamada, M.; Honma, I. *Polymer* **2005**, *46*, 2986-2992.

(43) Lee, S.-I.; Yoon, K.-H.; Song, M.; Peng, H.; Page, K. A.; Soles, C. L.; Yoon, D. Y. *Chem. Mater.* **2012**, *24*, 115-122.

(44) Dimitrov, I.; Takamuku, S.; Jankova, K.; Jannasch, P.; Hvilsted, S. *Macromol. Rapid Commun.* **2012**, *33*, 1368-1374.

(45) Dimitrov, I.; Takamuku, S.; Jankova, K.; Jannasch, P.; Hvilsted, S. *Journal of Membrane Science* **2014**, *450*, 362-368.

(46) Jiang, F.; Kaltbeitzel, A.; Zhang, J.; Meyer, W. H. *Int. J. Hydrogen Energy* **2014**, *39*, 11157-11164.

(47) Sen, U.; Usta, H.; Acar, O.; Citir, M.; Canlier, A.; Bozkurt, A.; Ata, A. *Macromol. Chem. Phys.* **2015**, *216*, 106-112.

(48) Mizuno, M.; Iwasaki, A.; Umiyama, T.; Ohashi, R.; Ida, T. *Macromolecules* **2014**, *47*, 7469-7476.

(49) Ebdon, J. R.; Price, D.; Hunt, B. J.; Joseph, P.; Gao, F.; Milnes, G. J.; Cunliffe, L. K. *Polym. Degrad. Stab.* **2000**, *69*, 267-277.

(50) Banks, M.; Ebdon, J. R.; Johnson, M. *Polymer* **1993**, *34*, 4547-4556.

(51) Abueva, C. D. G.; Lee, B.-T. *Int. J. Biol. Macromol.* **2014**, *64*, 294-301.

(52) Tan, J.; Gemeinhart, R. A.; Ma, M.; Mark Saltzman, W. *Biomaterials* **2005**, *26*, 3663-3671.

(53) Seo, J.-H.; Matsuno, R.; Takai, M.; Ishihara, K. *Biomaterials* **2009**, *30*, 5330-5340.

(54) Chirila, T. V.; Zainuddin *React. Funct. Polym.* **2007**, *67*, 165-172.

(55) Dalas, E.; Kallitsis, J. K.; Koutsoukos, P. G. *Langmuir* **1991**, *7*, 1822-1826.

(56) Anbar, M.; St John, G. A.; Elward, T. E. *Journal of Dental Research* **1974**, *53*, 1240-1244.

(57) Ellis, J.; Anstice, M.; Wilson, A. D. *Clinical Materials* **1991**, *7*, 341-346.

(58) Ellis, J.; Wilson, A. D. *Dent. Mater.* **1992**, *8*, 79-84.

(59) Braybrook, J. H.; Nicholson, J. W. *J. Mater. Chem.* **1993**, *3*, 361-365.

(60) Khouw-Liu, V. H. W.; Anstice, H. M.; Pearson, G. J. *Journal of Dentistry* **1999**, *27*, 351-357.

(61) Salzinger, S.; Rieger, B. *Macromol. Rapid Commun.* **2012**, *33*, 1327-1345.

(62) Webster, O. W.; Hertler, W. R.; Sogah, D. Y.; Farnham, W. B.; RajanBabu, T. V. *J. Am. Chem. Soc.* **1983**, *105*, 5706-5708.

(63) Webster, O. W. *Science* **1991**, *251*, 887-893.

(64) Webster, O. *Adv. Polym. Sci.* **2004**, *167*, 1-34.

(65) Mai, P. M.; Müller, A. H. E. *Die Makromolekulare Chemie, Rapid Communications* **1987**, *8*, 99-107.

(66) Mai, P. M.; Müller, A. H. E. *Die Makromolekulare Chemie, Rapid Communications* **1987**, *8*, 247-253.

(67) Müller, A. H. E. *Macromolecules* **1994**, *27*, 1685-1690.

(68) Müller, A. H. E.; Litvinenko, G.; Yan, D. *Macromolecules* **1996**, *29*, 2339-2345.

(69) Müller, A. H. E.; Litvinenko, G.; Yan, D. *Macromolecules* **1996**, *29*, 2346-2353.

(70) Quirk, R. P.; Bidinger, G. P. *Polym. Bull.* **1989**, *22*, 63-70.

(71) Quirk, R. P.; Ren, J. *Macromolecules* **1992**, *25*, 6612-6620.

(72) Jenkins, A. D. *Eur. Polym. J.* **1991**, *27*, 649.

(73) Szwarc, M. *Nature* **1956**, *178*, 1168-1169.

(74) Szwarc, M.; Levy, M.; Milkovich, R. *J. Am. Chem. Soc.* **1956**, *78*, 2656-2657.

(75) Asano, S.; Aida, T.; Inoue, S. *J. Chem. Soc., Chem. Commun.* **1985**, 1148-1149.

(76) Inoue, S. *Journal of Macromolecular Science: Part A - Chemistry* **1988**, *25*, 571-582.

(77) Inoue, S. *J. Polym. Sci., Part A: Polym. Chem.* **2000**, *38*, 2861-2871.

(78) Iovu, M. C.; Sheina, E. E.; Gil, R. R.; McCullough, R. D. *Macromolecules* **2005**, *38*, 8649-8656.

(79) Zhang, Y.; Tajima, K.; Hirota, K.; Hashimoto, K. *J. Am. Chem. Soc.* **2008**, *130*, 7812-7813.

(80) Xu, Y.-Q.; Lu, J.-M.; Li, N.-J.; Yan, F.; Xia, X.-W.; Xu, Q.-F. *Eur. Polym. J.* **2008**, *44*, 2404-2411.

(81) Maniruzzaman, M.; Kawaguchi, S.; Ito, K. *Macromolecules* **2000**, *33*, 1583-1592.

(82) Sanda, F.; Fueki, T.; Endo, T. *Macromolecules* **1999**, *32*, 4220-4224.

(83) Stridsberg, K.; Albertsson, A.-C. *J. Polym. Sci., Part A: Polym. Chem.* **2000**, *38*, 1774-1784.

(84) Yao, K.; Tang, C. *Macromolecules* **2013**, *46*, 1689-1712.

(85) Wang, J.-S.; Matyjaszewski, K. *Macromolecules* **1995**, *28*, 7901-7910.

(86) Wang, J.-S.; Matyjaszewski, K. *J. Am. Chem. Soc.* **1995**, *117*, 5614-5615.

(87) Amgoune, A.; Thomas, C. M.; Ilinca, S.; Roisnel, T.; Carpentier, J.-F. *Angew. Chem. Int. Ed.* **2006**, *45*, 2782-2784.

(88) Aida, T.; Inoue, S. *Acc. Chem. Res.* **1996**, *29*, 39-48.

(89) Darling, T. R.; Davis, T. P.; Fryd, M.; Gridnev, A. A.; Haddleton, D. M.; Ittel, S. D.; Matheson, R. R.; Moad, G.; Rizzardo, E. *J. Polym. Sci., Part A: Polym. Chem.* **2000**, *38*, 1706-1708.

(90) Percec, V.; Tirrell, D. A. *J. Polym. Sci., Part A: Polym. Chem.* **2000**, *38*, 1705-1705.

(91) Szwarc, M. *J. Polym. Sci., Part A: Polym. Chem.* **2000**, *38*, 1710-1710.

(92) Inoue, S. *J. Polym. Sci., Part A: Polym. Chem.* **2000**, *38*, 1729-1729.

(93) Matyjaszewski, K. *J. Polym. Sci., Part A: Polym. Chem.* **2000**, *38*, 1738-1739.

(94) Nuyken, O. *J. Polym. Sci., Part A: Polym. Chem.* **2000**, *38*, 1741-1742.

(95) Waymouth, R. M. *J. Polym. Sci., Part A: Polym. Chem.* **2000**, *38*, 1750-1751.

(96) Webster, O. *J. Polym. Sci., Part A: Polym. Chem.* **2000**, *38*, 1751-1751.

(97) Yasuda, H. *J. Polym. Sci., Part A: Polym. Chem.* **2000**, *38*, 1752-1752.

(98) Yasuda, H.; Yamamoto, H.; Yokota, K.; Miyake, S.; Nakamura, A. *J. Am. Chem. Soc.* **1992**, *114*, 4908-4910.

(99) Collins, S.; Ward, D. G. *J. Am. Chem. Soc.* **1992**, *114*, 5460-5462.

(100) Yasuda, H.; Ihara, E. *Adv. Polym. Sci.* **1997**, *133*, 53-101.

(101) Yasuda, H. *Prog. Polym. Sci.* **2000**, *25*, 573-626.

(102) Boffa, L. S.; Novak, B. M. *Chem. Rev.* **2000**, *100*, 1479-1494.

(103) Yasuda, H.; Yamamoto, H.; Yamashita, M.; Yokota, K.; Nakamura, A.; Miyake, S.; Kai, Y.; Kanehisa, N. *Macromolecules* **1993**, *26*, 7134-7143.

(104) Salzinger, S. *PhD Thesis*, TU München, **2013**.

(105) Salzinger, S.; Seemann, U. B.; Plikhta, A.; Rieger, B. *Macromolecules* **2011**, *44*, 5920-5927.

(106) Li, Y.; Ward, D. G.; Reddy, S. S.; Collins, S. *Macromolecules* **1997**, *30*, 1875-1883.

(107) Nguyen, H.; Jarvis, A. P.; Lesley, M. J. G.; Kelly, W. M.; Reddy, S. S.; Taylor, N. J.; Collins, S. *Macromolecules* **2000**, *33*, 1508-1510.

(108) Soller, B. S. *Master's Thesis*, TU München, **2013**.

(109) Evans, W. J.; Dominguez, R.; Hanusa, T. P. *Organometallics* **1986**, *5*, 1291-1296.

(110) Heeres, H. J.; Maters, M.; Teuben, J. H.; Helgesson, G.; Jagner, S. *Organometallics* **1992**, *11*, 350-356.

(111) Nakajima, Y.; Okuda, J. *Organometallics* **2007**, *26*, 1270-1278.

(112) Soller, B. S.; Salzinger, S.; Jandl, C.; Pöthig, A.; Rieger, B. *Organometallics* **2015**, *34*, 2703-2706.

(113) Altenbuchner, P. T.; Soller, B. S.; Kissling, S.; Bachmann, T.; Kronast, A.; Vagin, S. I.; Rieger, B. *Macromolecules* **2014**, *47*, 7742-7749.

(114) Dengler, J. *Diploma Thesis*, TU München, **2007**.

(115) Leute, M. *PhD Thesis*, Universität Ulm, **2007**.

(116) Rabe, G. W.; Komber, H.; Häussler, L.; Kreger, K.; Lattermann, G. *Macromolecules* **2010**, *43*, 1178-1181.

(117) Seemann, U. B.; Dengler, J. E.; Rieger, B. *Angew. Chem.* **2010**, *122*, 3567-3569.

(118) *IUPAC. Compendium of Chemical Terminology, 2nd ed. (the "Gold Book"), electronic version, http://goldbook.iupac.org/S05995.html*; Compiled by A. D. McNaught and A. Wilkinson. Blackwell Scientific Publications.

(119) *IUPAC. Compendium of Chemical Terminology, 2nd ed. (the "Gold Book"), electronic version, http://goldbook.iupac.org/S05989.html*; Compiled by A. D. McNaught and A. Wilkinson. Blackwell Scientific Publications.

(120) Komber, H.; Steinert, V.; Voit, B. *Macromolecules* **2008**, *41*, 2119-2125.

(121) Hans Wedepohl, K. *Geochim. Cosmochim. Acta* **1995**, *59*, 1217-1232.

(122) *Application of rare earths in consumer electronics and challenges for recycling*; Compiled by Oeko-Institut from the sources Jefferies 2010, Oakdene Hollins 2010, Kingsnorth 2010, GWMG 2010, BGR 2009 and Lynas 2010.

(123) Pyykko, P. *Chem. Rev.* **1988**, *88*, 563-594.

(124) Eppinger, J. *PhD Thesis*, Technische Universität München, **1999**.

(125) Anwander, R.; Runte, O.; Eppinger, J.; Gerstberger, G.; Herdtweck, E.; Spiegler, M. *J. Chem. Soc., Dalton Trans.* **1998**, 847-858.

(126) Marçalo, J.; De Matos, A. P. *Polyhedron* **1989**, *8*, 2431-2437.

(127) Edelmann, F. T. *Coord. Chem. Rev.* **2014**, *261*, 73-155.

(128) Edelmann, F. T. *Coord. Chem. Rev.* **2015**, *284*, 124-205.

(129) McClure, D. S.; Kiss, Z. *The Journal of Chemical Physics* **1963**, *39*, 3251-3257.

(130) Ranasinghe, Y. A.; MacMahon, T. J.; Freiser, B. S. *J. Am. Chem. Soc.* **1992**, *114*, 9112-9118.

(131) Marçalo, J.; Santos, M.; Matos, A. P. d.; Gibson, J. K.; Haire, R. G. *The Journal of Physical Chemistry A* **2008**, *112*, 12647-12656.

(132) Evans, W. J.; Ulibarri, T. A.; Ziller, J. W. *J. Am. Chem. Soc.* **1988**, *110*, 6877-6879.

(133) Evans, W. J.; Lee, D. S.; Lie, C.; Ziller, J. W. *Angew. Chem. Int. Ed.* **2004**, *43*, 5517-5519.

(134) Evans, W. J.; Rego, D. B.; Ziller, J. W. *Inorg. Chem.* **2006**, *45*, 10790-10798.

(135) Demir, S.; Lorenz, S. E.; Fang, M.; Furche, F.; Meyer, G.; Ziller, J. W.; Evans, W. J. *J. Am. Chem. Soc.* **2010**, *132*, 11151-11158.

(136) Evans, W. J.; Lee, D. S.; Ziller, J. W. *J. Am. Chem. Soc.* **2004**, *126*, 454-455.

(137) Evans, W. J.; Lee, D. S.; Rego, D. B.; Perotti, J. M.; Kozimor, S. A.; Moore, E. K.; Ziller, J. W. *J. Am. Chem. Soc.* **2004**, *126*, 14574-14582.

(138) Evans, W. J.; Lee, D. S.; Johnston, M. A.; Ziller, J. W. *Organometallics* **2005**, *24*, 6393-6397.

(139) Hitchcock, P. B.; Lappert, M. F.; Maron, L.; Protchenko, A. V. *Angew. Chem. Int. Ed.* **2008**, *47*, 1488-1491.

(140) MacDonald, M. R.; Ziller, J. W.; Evans, W. J. *J. Am. Chem. Soc.* **2011**, *133*, 15914-15917.

(141) MacDonald, M. R.; Bates, J. E.; Fieser, M. E.; Ziller, J. W.; Furche, F.; Evans, W. J. *J. Am. Chem. Soc.* **2012**, *134*, 8420-8423.

(142) MacDonald, M. R.; Bates, J. E.; Ziller, J. W.; Furche, F.; Evans, W. J. *J. Am. Chem. Soc.* **2013**, *135*, 9857-9868.

(143) Evans, W. J.; Gonzales, S. L.; Ziller, J. W. *J. Am. Chem. Soc.* **1991**, *113*, 7423-7424.

(144) Evans, W. J. *Inorg. Chem.* **2007**, *46*, 3435-3449.

(145) White, D.; Taverner, B. C.; Leach, P. G. L.; Coville, N. J. *J. Comput. Chem.* **1993**, *14*, 1042-1049.

(146) Tilley, T. D.; Andersen, R. A. *Inorg. Chem.* **1981**, *20*, 3267-3270.

(147) Evans, W. J.; Forrestal, K. J.; Ziller, J. W. *J. Am. Chem. Soc.* **1998**, *120*, 9273-9282.

(148) Evans, W. J.; Forrestal, K. J.; Ziller, J. W. *Angew. Chem. Int. Ed. Eng.* **1997**, *36*, 774-776.

(149) Evans, W. J.; Nyce, G. W.; Clark, R. D.; Doedens, R. J.; Ziller, J. W. *Angew. Chem. Int. Ed.* **1999**, *38*, 1801-1803.

(150) Recknagel, A.; Noltemeyer, M.; Edelmann, F. T. *J. Organomet. Chem.* **1991**, *410*, 53-61.

(151) Evans, W. J.; Perotti, J. M.; Kozimor, S. A.; Champagne, T. M.; Davis, B. L.; Nyce, G. W.; Fujimoto, C. H.; Clark, R. D.; Johnston, M. A.; Ziller, J. W. *Organometallics* **2005**, *24*, 3916-3931.

(152) Evans, W. J. *Coord. Chem. Rev.* **2000**, *206–207*, 263-283.

(153) Evans, W. J.; Forrestal, K. J.; Ziller, J. W. *J. Am. Chem. Soc.* **1995**, *117*, 12635-12636.

(154) Evans, W. J.; Kozimor, S. A.; Nyce, G. W.; Ziller, J. W. *J. Am. Chem. Soc.* **2003**, *125*, 13831-13835.

(155) Evans, W. J.; Davis, B. L. *Chem. Rev.* **2002**, *102*, 2119-2136.

(156) Wilkinson, G.; Birmingham, J. M. *J. Am. Chem. Soc.* **1954**, *76*, 6210-6210.

(157) Birmingham, J. M.; Wilkinson, G. *J. Am. Chem. Soc.* **1956**, *78*, 42-44.

(158) Schumann, H.; Meese-Marktscheffel, J. A.; Esser, L. *Chem. Rev.* **1995**, *95*, 865-986.

(159) Seemann, U. B. *PhD Thesis*, TU München, **2010**.

(160) Evans, W. J.; Seibel, C. A.; Ziller, J. W. *J. Am. Chem. Soc.* **1998**, *120*, 6745-6752.

(161) Jeske, G.; Lauke, H.; Mauermann, H.; Swepston, P. N.; Schumann, H.; Marks, T. J. *J. Am. Chem. Soc.* **1985**, *107*, 8091-8103.

(162) Rausch, M. D.; Moriarty, K. J.; Atwood, J. L.; Weeks, J. A.; Hunter, W. E.; Brittain, H. G. *Organometallics* **1986**, *5*, 1281-1283.

(163) Haar, C. M.; Stern, C. L.; Marks, T. J. *Organometallics* **1996**, *15*, 1765-1784.

(164) Zimmermann, M.; Anwander, R. *Chem. Rev.* **2010**, *110*, 6194-6259.

(165) Schumann, H.; Glanz, M.; Hemling, H. *J. Organomet. Chem.* **1993**, *445*, C1-C3.

(166) Soller, B. S. *unpublished results*.

(167) Peterson, J. K.; MacDonald, M. R.; Ziller, J. W.; Evans, W. J. *Organometallics* **2013**, *32*, 2625-2631.

(168) Bradley, D. C.; Thomas, I. M. *Proc. Chem. Soc.* **1959**, 225-226.

(169) Bradley, D. C.; Thomas, I. M. *J. Chem. Soc. (Resumed)* **1960**, 3857-3861.

(170) Gibbins, S. G.; Lappert, M. F.; Pedley, J. B.; Sharp, G. J. *J. Chem. Soc., Dalton Trans.* **1975**, 72-76.

(171) Morawietz, M. J. A. *PhD Thesis*, TU München, **1995**.

(172) Chandra, G.; Lappert, M. F. *J. Chem. Soc. A* **1968**, 1940-1945.

(173) Diamond, G. M.; Jordan, R. F.; Petersen, J. L. *Organometallics* **1996**, *15*, 4030-4037.

(174) Vogel, A.; Priermeier, T.; Herrmann, W. A. *J. Organomet. Chem.* **1997**, *527*, 297-300.

(175) Herrmann, W. A.; Morawietz, M. J. A.; Priermeier, T. *Angew. Chem.* **1994**, *106*, 2025-2028.

(176) Christopher, J. N.; Diamond, G. M.; Jordan, R. F.; Petersen, J. L. *Organometallics* **1996**, *15*, 4038-4044.

(177) Diamond, G. M.; Jordan, R. F.; Petersen, J. L. *J. Am. Chem. Soc.* **1996**, *118*, 8024-8033.

(178) Bordwell, F. G. *Acc. Chem. Res.* **1988**, *21*, 456-463.

(179) Bradley, D. C.; Ghotra, J. S.; Hart, F. A. *J. Chem. Soc., Chem. Commun.* **1972**, 349-350.

(180) Alyea, E. C.; Bradley, D. C.; Copperthwaite, R. G. *J. Chem. Soc., Dalton Trans.* **1972**, 1580-1584.

(181) Bradley, D. C.; Ghotra, J. S.; Hart, F. A. *J. Chem. Soc., Dalton Trans.* **1973**, 1021-1023.

(182) Ghotra, J. S.; Hursthouse, M. B.; Welch, A. J. *J. Chem. Soc., Chem. Commun.* **1973**, 669-670.

(183) Eller, P. G.; Bradley, D. C.; Hursthouse, M. B.; Meek, D. W. *Coord. Chem. Rev.* **1977**, *24*, 1-95.

(184) Booij, M.; Kiers, N. H.; Heeres, H. J.; Teuben, J. H. *J. Organomet. Chem.* **1989**, *364*, 79-86.

(185) Stults, S. D.; Andersen, R. A.; Zalkin, A. *Organometallics* **1990**, *9*, 115-122.

(186) Fraser, R. R.; Mansour, T. S.; Savard, S. *The Journal of Organic Chemistry* **1985**, *50*, 3232-3234.

(187) Herrmann, W. A.; Anwander, R.; Munck, F. C.; Scherer, W.; Dufaud, V.; Huber, N. W.; Artus, G. R. J. *Zeitschrift für Naturforschung B* **1994**, *49b*, 1789-1797.

(188) Herrmann, W. A.; Eppinger, J.; Spiegler, M.; Runte, O.; Anwander, R. *Organometallics* **1997**, *16*, 1813-1815.

(189) Eppinger, J.; Herdtweck, E.; Anwander, R. *Polyhedron* **1998**, *17*, 1195-1201.

(190) Eppinger, J.; Spiegler, M.; Hieringer, W.; Herrmann, W. A.; Anwander, R. *J. Am. Chem. Soc.* **2000**, *122*, 3080-3096.

(191) Hieringer, W.; Eppinger, J.; Anwander, R.; Herrmann, W. A. *J. Am. Chem. Soc.* **2000**, *122*, 11983-11994.

(192) Anwander, R. In *Organolanthoid Chemistry: Synthesis, Structure, Catalysis*; Springer Berlin Heidelberg: Berlin, Heidelberg, **1996**, 33-112.

(193) Bordwell, F. G.; Algrim, D. J. *J. Am. Chem. Soc.* **1988**, *110*, 2964-2968.

(194) Lappert, M. F.; Pearce, R. *J. Chem. Soc., Chem. Commun.* **1973**, 126-126.

(195) Davidson, P. J.; Lappert, M. F.; Pearce, R. *Chem. Rev.* **1976**, *76*, 219-242.

(196) Davidson, P. J.; Lappert, M. F.; Pearce, R. *Acc. Chem. Res.* **1974**, *7*, 209-217.

(197) Estler, F. *PhD Thesis*, TU München, **2002**.

(198) Hultzsch, K. C.; Voth, P.; Beckerle, K.; Spaniol, T. P.; Okuda, J. *Organometallics* **2000**, *19*, 228-243.

(199) Evans, W. J.; Brady, J. C.; Ziller, J. W. *J. Am. Chem. Soc.* **2001**, *123*, 7711-7712.

(200) Arndt, S.; Voth, P.; Spaniol, T. P.; Okuda, J. *Organometallics* **2000**, *19*, 4690-4700.

(201) Schumann, H.; Müller, J. *J. Organomet. Chem.* **1979**, *169*, C1-C4.

(202) Schumann, H.; Freckmann, D. M. M.; Dechert, S. *Z. Anorg. Allg. Chem.* **2002**, *628*, 2422-2426.

(203) Niemeyer, M. *Acta Crystallographica Section E* **2001**, *57*, m578-m580.

(204) Atwood, J. L.; Hunter, W. E.; Rogers, R. D.; Holton, J.; McMeeking, J.; Pearce, R.; Lappert, M. F. *J. Chem. Soc., Chem. Commun.* **1978**, 140-142.

(205) Lukešová, L.; Ward, B. D.; Bellemin-Laponnaz, S.; Wadepohl, H.; Gade, L. H. *Dalton Transactions* **2007**, 920-922.

(206) Schumann, H.; Müller, J. *J. Organomet. Chem.* **1978**, *146*, C5-C7.

(207) Rufanov Konstantin, A.; Freckmann Dominique, M. M.; Kroth, H.-J.; Schutte, S.; Schumann, H. In *Zeitschrift für Naturforschung B*, 2005; Vol. 60.

(208) Nishiura, M.; Hou, Z. *Nat Chem* **2010**, *2*, 257-268.

(209) Zeimentz, P. M.; Arndt, S.; Elvidge, B. R.; Okuda, J. *Chem. Rev.* **2006**, *106*, 2404-2433.

(210) Holton, J.; Lappert, M. F.; Ballard, D. G. H.; Pearce, R.; Atwood, J. L.; Hunter, W. E. *J. Chem. Soc., Dalton Trans.* **1979**, 54-61.

(211) Evans, W. J.; Champagne, T. M.; Ziller, J. W.; Kaltsoyannis, N. *J. Am. Chem. Soc.* **2006**, *128*, 16178-16189.

(212) Barker, G. K.; Lappert, M. F. *J. Organomet. Chem.* **1974**, *76*, C45-C46.

(213) Hitchcock, P. B.; Lappert, M. F.; Smith, R. G.; Bartlett, R. A.; Power, P. P. *J. Chem. Soc., Chem. Commun.* **1988**, 1007-1009.

(214) Hultzsch, K. C.; Spaniol, T. P.; Okuda, J. *Angew. Chem. Int. Ed.* **1999**, *38*, 227-230.

(215) McKnight, A. L.; Waymouth, R. M. *Chem. Rev.* **1998**, *98*, 2587-2598.

(216) Hultzsch, K. C. *PhD Thesis*, Universität Mainz, **1999**.

(217) Tian, S.; Arredondo, V. M.; Stern, C. L.; Marks, T. J. *Organometallics* **1999**, *18*, 2568-2570.

(218) Eaborn, C.; Hitchcock, P. B.; Izod, K.; Smith, J. D. *J. Am. Chem. Soc.* **1994**, *116*, 12071-12072.

(219) Eaborn, C.; Hitchcock, P. B.; Izod, K.; Lu, Z.-R.; Smith, J. D. *Organometallics* **1996**, *15*, 4783-4790.

(220) Qi, G.; Nitto, Y.; Saiki, A.; Tomohiro, T.; Nakayama, Y.; Yasuda, H. *Tetrahedron* **2003**, *59*, 10409-10418.

(221) Zhang, N.; Salzinger, S.; Deubel, F.; Jordan, R.; Rieger, B. *J. Am. Chem. Soc.* **2012**, *134*, 7333-7336.

(222) Zhang, N.; Salzinger, S.; Soller, B. S.; Rieger, B. *J. Am. Chem. Soc.* **2013**, *135*, 8810-8813.

(223) Crabtree, R. H. *Chem. Rev.* **1985**, *85*, 245-269.

(224) Blanksby, S. J.; Ellison, G. B. *Acc. Chem. Res.* **2003**, *36*, 255-263.

(225) Shilov, A. E.; Shul'pin, G. B. *Chem. Rev.* **1997**, *97*, 2879-2932.

(226) Bergman, R. G. *Science* **1984**, *223*, 902-908.

(227) Labinger, J. A.; Bercaw, J. E. *Nature* **2002**, *417*, 507-514.

(228) Cavaliere, V. N.; Mindiola, D. J. *Chemical Science* **2012**, *3*, 3356-3365.

(229) Bergman, R. G. *Nature* **2007**, *446*, 391-393.

(230) Konnick, M. M.; Hashiguchi, B. G.; Devarajan, D.; Boaz, N. C.; Gunnoe, T. B.; Groves, J. T.; Gunsalus, N.; Ess, D. H.; Periana, R. A. *Angew. Chem. Int. Ed.* **2014**, *53*, 10490-10494.

(231) Baik, M.-H.; Newcomb, M.; Friesner, R. A.; Lippard, S. J. *Chem. Rev.* **2003**, *103*, 2385-2420.

(232) Ackermann, L. *Chem. Rev.* **2011**, *111*, 1315-1345.

(233) Huang, W.; Diaconescu, P. L. In *Adv. Organomet. Chem.*; Pedro, J. P., Ed.; Academic Press, **2015**; Vol. Volume 64.

(234) Wicker, B. F.; Fan, H.; Hickey, A. K.; Crestani, M. G.; Scott, J.; Pink, M.; Mindiola, D. J. *J. Am. Chem. Soc.* **2012**, *134*, 20081-20096.

(235) Watson, P. L. *J. Chem. Soc., Chem. Commun.* **1983**, 276-277.

(236) Watson, P. L.; Parshall, G. W. *Acc. Chem. Res.* **1985**, *18*, 51-56.

(237) Watson, P. L. *J. Am. Chem. Soc.* **1983**, *105*, 6491-6493.

(238) Thompson, M. E.; Baxter, S. M.; Bulls, A. R.; Burger, B. J.; Nolan, M. C.; Santarsiero, B. D.; Schaefer, W. P.; Bercaw, J. E. *J. Am. Chem. Soc.* **1987**, *109*, 203-219.

(239) Johnson, K. R. D.; Hayes, P. G. *Chem. Soc. Rev.* **2013**, *42*, 1947-1960.

(240) Woodrum, N. L.; Cramer, C. J. *Organometallics* **2005**, *25*, 68-73.

(241) Rabaa, H.; Saillard, J. Y.; Hoffmann, R. *J. Am. Chem. Soc.* **1986**, *108*, 4327-4333.

(242) Ziegler, T.; Folga, E.; Berces, A. *J. Am. Chem. Soc.* **1993**, *115*, 636-646.

(243) Hajela, S.; Schaefer, W. P.; Bercaw, J. E. *Acta Crystallographica Section C* **1992**, *48*, 1771-1773.

(244) Booij, M.; Deelman, B. J.; Duchateau, R.; Postma, D. S.; Meetsma, A.; Teuben, J. H. *Organometallics* **1993**, *12*, 3531-3540.

(245) Evans, W. J.; Champagne, T. M.; Ziller, J. W. *J. Am. Chem. Soc.* **2006**, *128*, 14270-14271.

(246) Evans, W. J.; Ulibarri, T. A.; Ziller, J. W. *Organometallics* **1991**, *10*, 134-142.

(247) Evans, W. J.; Perotti, J. M.; Ziller, J. W. *Inorg. Chem.* **2005**, *44*, 5820-5825.

(248) Evans, W. J.; Davis, B. L.; Champagne, T. M.; Ziller, J. W. *Proceedings of the National Academy of Sciences* **2006**, *103*, 12678-12683.

(249) MacDonald, M. R.; Langeslay, R. R.; Ziller, J. W.; Evans, W. J. *J. Am. Chem. Soc.* **2015**, *137*, 14716–14725.

(250) Roering, A. J.; Davidson, J. J.; MacMillan, S. N.; Tanski, J. M.; Waterman, R. *Dalton Transactions* **2008**, 4488-4498.

(251) Sadow, A. D.; Tilley, T. D. *J. Am. Chem. Soc.* **2003**, *125*, 7971-7977.

(252) Lin, Z.; Marks, T. J. *J. Am. Chem. Soc.* **1987**, *109*, 7979-7985.

(253) Waterman, R. *Organometallics* **2007**, *26*, 2492-2494.

(254) Woo, H. G.; Walzer, J. F.; Tilley, T. D. *J. Am. Chem. Soc.* **1992**, *114*, 7047-7055.

(255) Neale, N. R.; Tilley, T. D. *J. Am. Chem. Soc.* **2002**, *124*, 3802-3803.

(256) Fu, P.-F.; Marks, T. J. *J. Am. Chem. Soc.* **1995**, *117*, 10747-10748.

(257) Koo, K.; Fu, P.-F.; Marks, T. J. *Macromolecules* **1999**, *32*, 981-988.

(258) Perrin, L.; Eisenstein, O.; Maron, L. *New J. Chem.* **2007**, *31*, 549-555.

(259) Sadow, A. D.; Tilley, T. D. *J. Am. Chem. Soc.* **2005**, *127*, 643-656.

(260) Kawaoka, A. M.; Marks, T. J. *J. Am. Chem. Soc.* **2004**, *126*, 12764-12765.

(261) Kawaoka, A. M.; Marks, T. J. *J. Am. Chem. Soc.* **2005**, *127*, 6311-6324.

(262) Amin, S. B.; Marks, T. J. *J. Am. Chem. Soc.* **2007**, *129*, 10102-10103.

(263) Amin, S. B.; Seo, S.; Marks, T. J. *Organometallics* **2008**, *27*, 2411-2420.

(264) Waterman, R. *Organometallics* **2013**, *32*, 7249-7263.

(265) Levine, D. S.; Tilley, T. D.; Andersen, R. A. *Organometallics* **2015**, *34*, 4647-4655.

(266) Arnold, P. L.; McMullon, M. W.; Rieb, J.; Kühn, F. E. *Angew. Chem. Int. Ed.* **2015**, *54*, 82-100.

(267) Deelman, B.-J.; Booij, M.; Meetsma, A.; Teuben, J. H.; Kooijman, H.; Spek, A. L. *Organometallics* **1995**, *14*, 2306-2317.

(268) Ringelberg, S. N.; Meetsma, A.; Troyanov, S. I.; Hessen, B.; Teuben, J. H. *Organometallics* **2002**, *21*, 1759-1765.

(269) Arndt, S.; Spaniol, Thomas P.; Okuda, J. *Eur. J. Inorg. Chem.* **2001**, *2001*, 73-75.

(270) Deelman, B.-J.; Stevels, W. M.; Teuben, J. H.; Lakin, M. T.; Spek, A. L. *Organometallics* **1994**, *13*, 3881-3891.

(271) Den Haan, K. H.; Wielstra, Y.; Teuben, J. H. *Organometallics* **1987**, *6*, 2053-2060.

(272) Duchateau, R.; van Wee, C. T.; Teuben, J. H. *Organometallics* **1996**, *15*, 2291-2302.

(273) Duchateau, R.; Brussee, E. A. C.; Meetsma, A.; Teuben, J. H. *Organometallics* **1997**, *16*, 5506-5516.

(274) Arndt, S.; Elvidge, B. R.; Zeimentz, P. M.; Spaniol, T. P.; Okuda, J. *Organometallics* **2006**, *25*, 793-795.

(275) Jantunen, K. C.; Scott, B. L.; Gordon, J. C.; Kiplinger, J. L. *Organometallics* **2007**, *26*, 2777-2781.

(276) Williams, B. N.; Benitez, D.; Miller, K. L.; Tkatchouk, E.; Goddard, W. A.; Diaconescu, P. L. *J. Am. Chem. Soc.* **2011**, *133*, 4680-4683.

(277) Quiroga Norambuena, V. F.; Heeres, A.; Heeres, H. J.; Meetsma, A.; Teuben, J. H.; Hessen, B. *Organometallics* **2008**, *27*, 5672-5683.

(278) Kaneko, H.; Nagae, H.; Tsurugi, H.; Mashima, K. *J. Am. Chem. Soc.* **2011**, *133*, 19626-19629.

(279) Dimov, D. K.; Hogen-Esch, T. E. *Macromolecules* **1995**, *28*, 7394-7400.

(280) Kronast, A.; Altenbuchner, P. T. *unpublished results*.

(281) Carver, C. T.; Williams, B. N.; Ogilby, K. R.; Diaconescu, P. L. *Organometallics* **2010**, *29*, 835-846.

(282) Jie, S.; Diaconescu, P. L. *Organometallics* **2010**, *29*, 1222-1230.

(283) Ringelberg, S. N.; Meetsma, A.; Hessen, B.; Teuben, J. H. *J. Am. Chem. Soc.* **1999**, *121*, 6082-6083.

(284) Zhang, Y.; Zhang, J.; Hong, J.; Zhang, F.; Weng, L.; Zhou, X. *Organometallics* **2014**, *33*, 7052-7058.

(285) Lyubov, D. M.; Luconi, L.; Rossin, A.; Tuci, G.; Cherkasov, A. V.; Fukin, G. K.; Giambastiani, G.; Trifonov, A. A. *Chemistry – A European Journal* **2014**, *20*, 3487-3499.

(286) Yi, W.; Zhang, J.; Huang, S.; Weng, L.; Zhou, X. *Chemistry – A European Journal* **2014**, *20*, 867-876.

(287) Carver, C. T.; Diaconescu, P. L. *J. Am. Chem. Soc.* **2008**, *130*, 7558-7559.

(288) Miller, K. L.; Carver, C. T.; Williams, B. N.; Diaconescu, P. L. *Organometallics* **2010**, *29*, 2272-2281.

(289) Jian, Z.; Cui, D. *Chemistry – A European Journal* **2011**, *17*, 14578-14585.

(290) Reznichenko, A.; Hultzsch, K. In *Molecular Catalysis of Rare-Earth Elements*; Roesky, P. W., Ed.; Springer Berlin Heidelberg, **2010**; Vol. 137.

(291) Alonso, F.; Beletskaya, I. P.; Yus, M. *Chem. Rev.* **2004**, *104*, 3079-3160.

(292) Hong, S.; Marks, T. J. *Acc. Chem. Res.* **2004**, *37*, 673-686.

(293) Fontaine, F.-G.; Tilley, T. D. *Organometallics* **2005**, *24*, 4340-4342.

(294) Barros, N.; Eisenstein, O.; Maron, L.; Tilley, T. D. *Organometallics* **2006**, *25*, 5699-5708.

(295) Barros, N.; Eisenstein, O.; Maron, L.; Tilley, T. D. *Organometallics* **2008**, *27*, 2252-2257.

(296) Sadow, A. D.; Tilley, T. D. *Angew. Chem. Int. Ed.* **2003**, *42*, 803-805.

(297) Li, C.; Dinoi, C.; Coppel, Y.; Etienne, M. *J. Am. Chem. Soc.* **2015**, *137*, 12450-12453.

(298) Perutz, R. N.; Sabo-Etienne, S. *Angew. Chem. Int. Ed.* **2007**, *46*, 2578-2592.

(299) Rouquet, G.; Chatani, N. *Angew. Chem. Int. Ed.* **2013**, *52*, 11726-11743.

(300) Hunt, P. A. *Dalton Transactions* **2007**, 1743-1754.

(301) Balcells, D.; Clot, E.; Eisenstein, O. *Chem. Rev.* **2010**, *110*, 749-823.

(302) Kefalidis, C. E.; Castro, L.; Perrin, L.; Rosal, I. D.; Maron, L. *Chem. Soc. Rev.* **2016**.

(303) Lin, Z. *Coord. Chem. Rev.* **2007**, *251*, 2280-2291.

(304) Whitesides, G. M. *Adv. Mater.* **2004**, *16*, 1375-1377.

(305) Lin, F.; Wang, X.; Pan, Y.; Wang, M.; Liu, B.; Luo, Y.; Cui, D. *ACS Catalysis* **2016**, *6*, 176-185.

(306) Sun, Q. *unpublished results*.

(307) Satoh, Y.; Ikitake, N.; Nakayama, Y.; Okuno, S.; Yasuda, H. *J. Organomet. Chem.* **2003**, *667*, 42-52.

(308) Soller, B. S.; Sun, Q.; Salzinger, S.; Jandl, C.; Pöthig, A.; Rieger, B. *Macromolecules* **2016**, *49*, 1582-1589.

(309) Fulmer, G. R.; Miller, A. J. M.; Sherden, N. H.; Gottlieb, H. E.; Nudelman, A.; Stoltz, B. M.; Bercaw, J. E.; Goldberg, K. I. *Organometallics* **2010**, *29*, 2176-2179.

(310) Ranganathan, D.; Rao, C. B.; Ranganathan, S.; Mehrotra, A. K.; Iyengar, R. *The Journal of Organic Chemistry* **1980**, *45*, 1185-1189.

(311) Chi, Y.; Guo, L.; Kopf, N. A.; Gellman, S. H. *J. Am. Chem. Soc.* **2008**, *130*, 5608-5609.

(312) Fischer, B.; Boersma, J.; Van, K. G.; Spek, A. L. *New J. Chem.* **1988**, *12*, 613-620.

(313) Fendrick, C. M.; Schertz, L. D.; Mintz, E. A.; Marks, T. J.; Bitterwolf, T. E.; Horine, P. A.; Hubler, T. L.; Sheldon, J. A.; Belin, D. D. *Inorg. Synth.* **2007**, 193-198.

(314) van Leusen, D.; Beetstra, D. J.; Hessen, B.; Teuben, J. H. *Organometallics* **2000**, *19*, 4084-4089.

(315) Carpenetti, D. W.; Kloppenburg, L.; Kupec, J. T.; Petersen, J. L. *Organometallics* **1996**, *15*, 1572-1581.

(316) Evans, W. J.; Meadows, J. H.; Kostka, A. G.; Closs, G. L. *Organometallics* **1985**, *4*, 324-326.

(317) Evans, W. J.; Keyer, R. A.; Ziller, J. W. *J. Organomet. Chem.* **1990**, *394*, 87-97.

(318) Sobota, P.; Utko, J.; Szafert, S. *Inorg. Chem.* **1994**, *33*, 5203-5206.

(319) Schumann, H.; Genthe, W.; Bruncks, N.; Pickardt, J. *Organometallics* **1982**, *1*, 1194-1200.

(320) Oyamada, J.; Nishiura, M.; Hou, Z. *Angew. Chem. Int. Ed.* **2011**, *50*, 10720-10723.

8 Appendix

8.1 Curiculum Vitae

Education:

Since 7/2013	**PhD candidate** at *WACKER-Chair of Macromolecular Chemistry* (TU Munich) Professor Bernhard Rieger (Topic: Poly(vinylphosphonate)s, catalyst design, mechanism, application to new monomers)
	Activities: Planning and execution of experiments, kinetic studies, analysis, evaluation, and optimization of reaction conditions
10/2010 – 2/2013	**Studies Master of Science**, Chemistry TU Munich Major: Organic Chemistry Minor: Macromolecular Chemistry
	Master's thesis student at *WACKER-Chair of Macromolecular Chemistry* (TU Munich) – Professor Bernhard Rieger
10/2011 – 4/2012	**Exchange semester** at *Ateneo de Manila University* in the Philippines
10/2007 – 9/2010	**Bachelor of Science**, Chemistry TU Munich
	Bachelor's Thesis at *WACKER-Chair of Macromolecular Chemistry* (TU Munich) – Professor Bernhard Rieger
11/2006 – 7/2007	Civil service at *München rechts der Isar* hospital Field of work: emergency ambulance and oncology in the pediatric policlinic
9/1997 – 6/2006	**High School**, Allgemeine Hochschulreife – *St.-Anna-Gymnasium*, Munich, Germany

Work Experience and Internships:

5/2012 – 6/2012	**Research internship** at *King Abdullah University of Science and Technology* (KAUST) in Jeddah, Saudi Arabia
	Activities: Artificial amino acid synthesis, analysis, preparation of a written report, final talk
3/2011 – 4/2011	**Industry internship** at *BASF SE* in Ludwigshafen am Rhein, Germany
	Activities: Emulsion polymerization and modifications of silicas, patent literature search, preparation of a written report

8.1 Curiculum Vitae

8.2 Posters and Presentations

8.2.1 Poster 206: Catalytic Precision Polymerization of Polar Monomers: Lanthanide Polymerization Beyond (Meth)Acrylates (ISHC-XIX - International Symposium on Homogeneous Catalysis)

Location: Ottawa Convention Centre, Ottawa, Canada

Event Date: 06 July 2014 – 11 July 2014

Event Type: Conference

Benedikt S. Soller and Bernhard Rieger

Macromolecular Chemistry, Technische Universität München, Garching bei München, Germany

Rare Earth Metal-Mediated Group Transfer Polymerization (REM-GTP) was originally discovered in the early 1990s for the polymerization of methyl methacrylate (MMA). The produced PMMA has a high molecular weight (Mn > 50 kDa) with narrow polydispersities (PDI = 1.02 – 1.05), a high syndiotacticity up to 95% and the propagation proceeds via an eight membered transition state.[1] In the following years REM-GTP was expanded to a variety of different meth(acrylates) and meth(acrylamides). Just recently, interest in this field emerged for the polymerization of different Michael-type acceptor monomers, having new heteroatom functionalities. Beyond the known (meth)acrylates, now a variety of monomers from vinyl phosphonates to *N*-coordinating 2-isopropenyl-2-oxazoline and 2-vinylpyridine monomers can be polymerized with high precision from simple lanthanide complexes using living REM-GTP.[2-4]

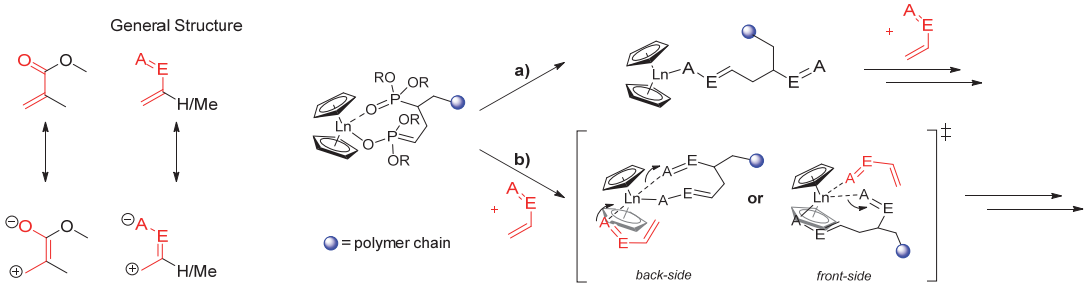

Figure 20. Structure of polar monomers and different reaction pathways for the REM-GTP of polar monomers.

8.2 Posters and Presentations

(1) Yasuda H.; Yamamoto H.; Yokota K.; Miyake S.; Nakamura A. *J. Am. Chem. Soc.* **1992**, *114*, 4908

(2) Kaneko H.; Nagae H.; Tsurugi H.; Mashima K. *J. Am. Chem. Soc.* **2011**, *133*, 19626

(3) Zhang N.; Salzinger S.; Soller B. S.; Rieger B. *J. Am. Chem. Soc.* **2013**, *135*, 8810

(4) Salzinger S.; Soller B. S.; Plikhta A.; Seemann U. B.; Herdtweck E.; Rieger B. *J. Am. Chem. Soc.* **2013**, *135*, 13030

8.2.2 Presentation and Poster at the Pacifichem Conference 2015

Location: Halls I, II, III - Hawaii Convention Center (Poster), Tapa Tower; Suite 1 - Hilton Hawaiian Village (Presentation), Honolulu, USA

Event Date: 15 December 2015 – 20 December 2015

Event Type: Conference

8.2.2.1 Poster INOR 553: Rare earth metal-mediated group transfer polymerization of vinylphosphonates: Tuning the metal ligand interaction via steric crowding at the rare earth center and novel highly efficient initiators from C–H bond activation

Benedikt S. Soller and Bernhard Rieger

Macromolecular Chemistry, Technische Universität München, Garching bei München, Germany

Rare Earth Metal-Mediated Group Transfer Polymerization (REM-GTP) was originally discovered in the early 1990s for the polymerization of methyl methacrylate (MMA). The produced PMMA has a high molecular mass (Mn > 50 kDa) with narrow polydispersities (PDI = 1.02 - 1.05), high syndiotacticities up to 95% and the propagation proceeds via an eight membered transition state. In the following years, REM-GTP was expanded to a variety of different (meth)acrylates and (meth)acrylamides. Recently, interest in this field emerged for the polymerization of different Michael-type acceptor monomers, having new heteroatom functionalities. Beyond the known (meth)acrylates, now a variety of monomers from vinylphosphonates to *N*-coordinating 2-isopropenyl-2-oxazoline and 2-vinylpyridine can be polymerized with high precision from simple lanthanide complexes using living REM-GTP.[1-3]

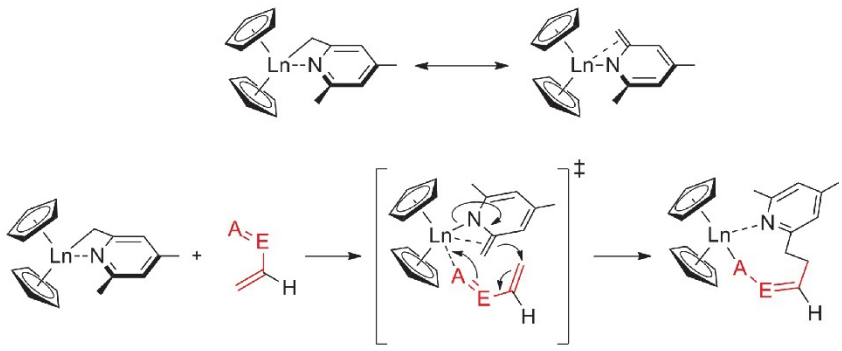

Scheme 25. Initiation of polar monomers via eight membered ring transition state.

8.2 Posters and Presentations

Currently, our research focuses on the application of new, sterically crowded catalyst systems. For a better understanding, the thermodynamic parameters of diethyl vinylphosphonate REM-GTP propagation via substituted tris(cyclopentadienyl) RE complexes were determined with different ionic radii. By further developing this strategy, ligand systems for the first precise stereoregular polymerization of vinylphosphonates are identified. The combination of the thereby established complexes with novel initiators from C–H bond activation via σ-bond metathesis gives access to so far unpresented poly(vinylphosphonate)s with high isotacticities and remarkably narrow polydispersities.[4]

(1) Salzinger, S.; Soller, B. S.; Plikhta, A.; Seemann, U. B.; Herdtweck, E.; Rieger, B. *J. Am. Chem. Soc.* **2013**, *135*, 13030

(2) Zhang, N.; Salzinger, S.; Soller, B. S.; Rieger, B. *J. Am. Chem. Soc.* **2013**, *135*, 8810

(3) Soller, B. S.; Salzinger, S.; Rieger, B. *Chem. Rev.* **2016**, *116*, 1993

(4) Soller, B. S.; Salzinger, S.; Jandl, C.; Pöthig, A.; Rieger B. *Organometallics*. **2015**, *34*, 2703

8.2.2.2 Presentation INOR 1230: Catalytic precision polymerization: From polar monomers to functional materials

Benedikt S. Soller, Alexander Kronast, and Bernhard Rieger

Macromolecular Chemistry, Technische Universität München, Garching bei München, Germany

Materials of the future face ever increasing demands with respect to functionality and complexity, hence polymer chemistry needs to meet these challenges by pushing the boundaries of accessible monomers and high precision polymerization techniques. In 1992, Yasuda et al. used simple lanthanide catalysts for the first metal mediated group transfer polymerization of methyl methacrylate (MMA).[1] Since then rare earth metal-mediated group transfer polymerization (REM-GTP) has evolved into a thriving field which allows the access to a wide variety of functional materials including thermoresponsive or pH-responsive materials (see Scheme 26).[2-3]

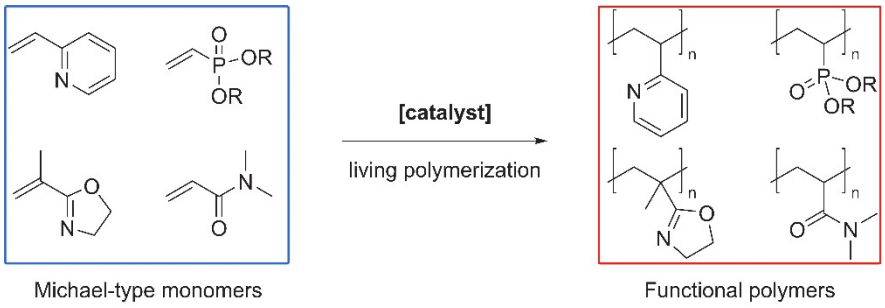

Scheme 26. Overview of different Michael-type monomers and their corresponding homopolymers.

Novel complexes for the polymerization of Michael-type monomers such as dialkyl vinylphosphonates (DAVP) or 2-vinylpyridine (2VP) were developed and in depth mechanistic investigations reveal the initiation and propagation mechanism of REM-GTP of vinylphosphonates.[4] Moreover we developed one of the first examples for non-metallocene based catalyst systems, highly active 2-methoxyethylaminobis(phenolate)yttrium complexes.[5]

Based on these results our current work focuses on the investigation of new ligand systems as well as on the improvement of polymer properties. The utilization of catalytic precision polymerization in combination with new polymer functionalities gives access to highly functional and tunable materials of the future.

8.2 Posters and Presentations

(1) Yasuda H., Yamamoto H., Yokota K., Miyake S., Nakamura A., *J. Am. Chem. Soc.* **1992**, *114*, 4908

(2) Zhang N., Salzinger S., Rieger B., *Macromolecules* **2012**, *45*, 9751

(3) Zhang L., Zhang Z., Wang P., *NPG Asia Materials* **2012**, *4*, e8.

(4) Salzinger S., Soller B. S., Plikhta A., Seemann U. B., Herdtweck E., Rieger B., *J. Am. Chem. Soc.* **2013**, *135*, 13030

(5) Altenbuchner P. T., Soller B. S., Kissling S., Bachmann T., Kronast A., Vagin S. I., Rieger B., *Macromolecules* **2014**, *47*, 7742

8.2.3 Presentation: Rare Earth Metal-mediated Group Transfer Polymerization of Vinylphosphonates (Changchun Institute of Applied Chemistry)

Location: Changchun Institute of Applied Chemistry, Chinese Academy of Sciences, Changchun, P. R. China

Event Date: 26 September 2015

Event Type: Invited Talk

Benedikt S. Soller

Macromolecular Chemistry, Technische Universität München, Garching bei München, Germany

8.3 Declaration

I declare that I have developed and written the enclosed PhD thesis by myself, and have not used sources or means without declaration in the text. Any thoughts from others or literal quotations are clearly marked.

Munich, May 22, 2016 Benedikt Soller